Further titles in this series:

1. G. SANGLERAT, THE PENETROMETER AND SOIL EXPLORATION
2. Q. ZÁRUBA and V. MENCL, LANDSLIDES AND THEIR CONTROL
3. E. E. WAHLSTROM, TUNNELING IN ROCK
4. R. SILVESTER, COASTAL ENGINEERING, I and II
5. R. N. YOUNG and B. P. WARKENTIN, SOIL PROPERTIES AND BEHAVIOUR
6. E. E. WAHLSTROM, DAMS, DAM FOUNDATIONS, AND RESERVOIR SITES
7. W. F. CHEN, LIMIT ANALYSIS AND SOIL PLASTICITY
8. L. N. PERSEN, ROCK DYNAMICS AND GEOPHYSICAL EXPLORATION
   Introduction to Stress Waves in Rocks
9. M. D. GIDIGASU, LATERITE SOIL ENGINEERING
10. Q. ZÁRUBA and V. MENCL, ENGINEERING GEOLOGY
11. H. K. GUPTA and B. K. RASTOGI, DAMS AND EARTHQUAKES
12. F. H. CHEN, FOUNDATIONS ON EXPANSIVE SOILS
13. L. HOBST and J. ZAJÍC, ANCHORING IN ROCK
14. B. VOIGT (Editor), ROCKSLIDES AND AVALANCHES, 1 and 2
15. C. LOMNITZ and E. ROSENBLUETH, SEISMIC RISK AND ENGINEERING DECISIONS
16. C. A. BAAR, APPLIED SALT-ROCK MECHANICS, 1
    The In-Situ Behavior of Salt Rocks
17. A. P. S. SELVADURAI, ELASTIC ANALYSIS OF SOIL-FOUNDATION INTERACTION
18. J. FEDA, STRESS IN SUBSOIL AND METHODS OF FINAL SETTLEMENT CALCULATION
19. Á. KÉZDI, STABILIZED EARTH ROADS
20. E. W. BRAND and R. P. BRENNER (Editors), SOFT-CLAY ENGINEERING
21. A. MYSLIVEC and Z. KYSELA, THE BEARING CAPACITY OF BUILDING FOUNDATIONS
22. R. N. CHOWDHURY, SLOPE ANALYSIS
23. P. BRUUN, STABILITY OF TIDAL INLETS
    Theory and Engineering
24. Z. BAŽANT, METHODS OF FOUNDATION ENGINEERING
25. Á. KÉZDI, SOIL PHYSICS
    Selected Topics
26. H. L. JESSBERGER (Editor), GROUND FREEZING
27. D. STEPHENSON, ROCKFILL IN HYDRAULIC ENGINEERING
28. P. E. FRIVIK, N. JANBU, R. SAETERSDAL and L. I. FINBORUT (Editors), Ground Freezing 1980

Developments in Geotechnical Engineering 29

CANAL AND RIVER LEVÉES

by
PAVOL PETER

Department of Civil Engineering,
Slovak Technical University,
Bratislava, Czechoslovakia

ELSEVIER SCIENTIFIC PUBLISHING COMPANY
Amsterdam – Oxford – New York – 1982

Scientific Editor
Prof. Ing. Dr. Stanislav Kratochvíl, DrSc.

Reviewers
Prof. Ing. Václav Hálek, DrSc.
Prof. Ing. Július Šoltész, CSc.

Published in co-edition with
VEDA, Publishing House of the Slovak Academy of Sciences, Bratislava

Distribution of this book is being handled by the following publishers
for the U.S.A. and Canada
Elsevier/North-Holland, Inc.,
52 Vanderbilt Avenue
New York, New York 10017
for the East European Countries, China, Northern Korea, Cuba, Vietnam and Mongolia
VEDA, Publishing House of the Slovak Academy of Sciences, Bratislava
for all remaining areas
Elsevier Scientific Publishing Company
1, Molenwerf
P.O. Box 211, 1000 AE Amsterdam, The Netherlands

Library of Congress Cataloging in Publication Data

Peter, Pavol
Canal and River Levées
(Developments in Geotechnical Engineering, 29)
Revised and updated translation of: Kanálové a ochranné hrádze.
Bibliography: p. 540
Includes indexes.
1. Earth dams. 2. Levées. 3. Embankments. I. Title. II. Series.
TC543.P4613 627'.42 81-9833
ISBN 0-444-99726-1 (Vol. 29) AACR2
ISBN 0-444-41622-5 (Series)

Printed in Czechoslovakia

PREFACE

The need has arisen for a comprehensive book for civil engineering designers. A few books on canal embankments and levées do exist, but they either give insufficient consideration to the many practical problems, or are limited to special aspects. In this book, we intend to give a clear explanation of the fundamental principles of canal embankments and levées calculation and design. It is assumed that the designer has no prior knowledge of the subject, but has a good understanding of mechanics and fluid dynamics.

The basis of this English version is the Slovak version, augmented in the first, sixth and seventh chapter by recent work on dam design, engineering and maintenance. Some fundamental principles are discussed and illustrated with applications to practical situations. It is intended that the book can also be used as a reference source.

The author is grateful to various contractors, organizations (mainly to Hydroconsult, Bratislava) and individuals who permitted the use of their figures and tables.

Most of all, the author would like to thank Professor S. Kratochvíl, Associated Professor V. Hálek, and Professor J. Šoltész for their valuable comments.

INTRODUCTION

Canal embankments and levées are amongst the world's oldest hydroengineering structures. Their history began many thousands years ago, as is proven by the remains found in all centres of ancient culture, especially in China, India, Egypt and Mesopotamia. This fact often leads to the erroneous supposition that the long history of this type of construction contributes to progress in this particular field of civil engineering, which should logically have a certain superiority over other younger branches of the science, for example, hydroelectric works. However, a thorough study of the present state of the design and construction of levées and canal embankments persuades us that the reverse is true.

This unfavourable situation is evidenced in the fact that neither modern scientific knowledge about soil mechanics, hydrogeology and hydrology, nor even experience in modern construction technology, are taken sufficiently into account when designing levées and embankments. If we consider the profiles of levées planned or constructed over the last ten years, we see that new gains in our knowledge of the functional properties of soils commonly used in earth dams, are ignored both from the point of view of stability and from the possibilities of seepage and uplift control in embankment subsoils.

From a comparison and study of older and newer canal embankment cross-sections, we can see the progress made in perfecting their construction, especially since 1935. At the same time, designers of levées and canal embankments are usually complacent, drawing their knowledge from traditional earth structures alone. The main source of learning is found in the treatment of dams, documented by the international Paris-based organization, Commission Internationale des Grands Barrages. This institution is systematically developing theory and reassessing knowledge in this field, while other international societies, International Commission on Irrigation and Drainage in New Delhi, India and International Central Board of Irrigation and Power devote themselves mainly to questions of hydraulics and the wider aspects of irrigation. Drawing knowledge from traditional structures leads to a simplistic view of planning problems. Drawing knowledge from dam engineering leads, as with most problems, to an excessively perfectionist view of their solution; this results in a substantial increase in construction costs. Even so, many of the problems remain unsolved, because, despite the relatively modest

construction of canal embankments and levées compared with dams, they are not easier to design. One reason for this is that, whereas for dams one profile is usually chosen from a wide range, the choice is much more limited for levées. These have to lie along the direction of water flow where geological conditions are often complicated. This is true of embankments running through regions beset with filtration anomalies, where it is necessary to choose active and passive protecting elements to counter seepage according to totally different criteria from those for dams.

This fact is extremely important for the further development of embankment design. It shows that it is necessary to work through these particular problems and indeed to abandon completely old seepage theories in favour of seeking new ones. We shall not be satisfied with past stability analyses of embankments; we shall rework totally the theory of filtration stability in a subsoil which is based on laws drawn from Darcy's equation, also the basis of the most commonly used criteria of K. S. Bligh and E. W. Lane. Previously, these criteria have very often been used even though they are not really suitable for assessing the real danger in the most critical cases. We must also revise the idea that seepage, and sometimes the quantity of springs along the embankment, comprise the main criteria for judging the threat to the structure and whole surrounding area.

With regard to the inevitability of a reappraisal of our knowledge, we shall concern ourselves fairly thoroughly with the theory of seepage and calculations of stability, and also with examining the difficult geological conditions in the actual subsoil of embankments, not only in completely ideal conditions. From this standpoint, we also wish to analyse sealing methods and embankment-building technology, but without losing sight of the fact that our main concern is with the correct evaluation of dimensions, and solutions to the problems of embankments in unfavourable geological conditions.

Canal embankments entirely define the upper flow profile of the canal, in order for it to fulfil safely its function as an artificial water course. This function is laid down by its basic aim to serve, and according to this we can distinguish between the embankments of power-station supply canals, irrigation canals — supply and distribution for the irrigation of land — and waterway canals.

These all present their own problems, especially in the demands of sealing (protection of the seal in navigation canals) and in the technology of construction. In this respect, the largest functional variation is found in irrigation canals, for which we sometimes require impermeability (usually in supply canals) and elsewhere find that permeability is of little importance (in distribution channels). We avoid the problems of drainage channels since they are usually below level.

River levées (for the prevention of flooding of land and housing) have a varied character which demands their inclusion. From the point of view of functional construction, we can differentiate:

(1) special levées for the protection of housing, towns and land;

(2) control levées by which the flow regime is regulated and directed, and the flow direction controlled, mainly during floods but occasionally also for controlling flows of ice and floating debris:
(3) dykes around reclaimed land (overflowed structures and otherwise) for improving land-usage conditions;
(4) sea walls and dyke embankments — for protection against waves.

We direct our main attention at solving the problems of protecting control levées, which we sometimes call anti-flood (or -inundation) dykes. However, we shall first apply ourselves to common problems closely related to these structures.

SYMBOLS

a	storage capacity of a layer ($a = T/n_0$); coefficient; distance between two objects (plates, layers, etc.)
A	air content
Ar	Archimedean number
b	coefficient
B	width of footing; width of canal water
B, $\bar{B}$	pore pressure coefficients
c	shear strength parameter; coefficient of hydraulic resistance
c_f	coefficient of hydraulic friction
c_u	undrained (total stress) shear strength parameter
c_v	coefficient of consolidation; surface area of dry packing per unit volume
C	constant
C_c	coefficient of curvature
C_D, C_L	coefficient of drag force and lift force
C_u	coefficient of uniformity of soil
d	diameter; thickness of the layer (slab, lining, apron, etc.);
d_c	length od drainage path; diameter of grain which can be carried out by seepage water
d_s	diameter of sediment particle or of particle with characteristic specific surface
D	depth of footing; depth below drains to the impermeable layer; distance; thickness of the layer
D_d, D_r	degree of density and relative density
e	distance; void ratio; expansion
E	energy; Young's modulus
E_a, E_p	total active thrust; total passive resistance of earth
E_H	modulus of elasticity (after Hooke)
ERFC(u)	error function complementary of $u = \frac{2}{\sqrt{\pi}} \int_0^\infty \exp(-z^2)\,dz$
f	factor of mechanical friction
f_H	hydraulic friction factor
F	force; hydrodynamic force
F_D	seepage force

Fr	Froude number
g	acceleration due to gravity 9.81 m s^{-2} (force per unit mass due to gravity)
G	weight of the body
G_s	specific gravity of solid particles; gravity parameter ($G_s = v_s : v$)
G_s^*	gravity parameter; v_s related to fictive velocity
h	water elevation difference between two positions s and s_0 ($H_1 - H_2$)
h_s	water elevation difference between exit free water surface and water table in the well (or ground surface)
H	height; potential energy related to weight of mass — $H = p : (\varrho g + h)$; total elevation difference
i	unit vector in the x coordinate direction
i_m	material commodity index
I	hydraulic gradient; integral value
I_L	index of liquidity
I_p	index of plasticity; pressure gradient
j	unit vector in the y coordinate direction, vertical coordinate
J	integral, seepage force
k	coefficient of permeability; the unit vector in the z coordinate direction
k_D, k_t, k_0	coefficients of permeability according to Darcy (after empirical formulas and other)
k_h, k_v	coefficients of permeability in horizontal and vertical directions
l, L	length; the direct distance between the ends
m	factor of safety (in mechanical stability computation)
M	mass
n	porosity
n_{eff}	effective porosity
N	number of equipotential drops
N_f	number of low channels
p	pressure of the liquid (water); normal load
p^*	piezometric pressure — potential energy related to value $p^* = p + \varrho g h$
P	total pressure
P_a, P_p	total active thrust and total passive resistance (earth pressure)
PI	plasticity index
PL (w_p)	plasticity limit
q	volume of water flowing per unit time (through unit cross-sectional area); volume flux; surface pressure; total foundation pressure of the structure
$\bar{q}$	specific seepage quantity ($\bar{q} = q : kH$)
q^*	superficial (fictive) velocity
Q	total flow per unit time; discharge; surface load
R	resistance

R, r	radius, and radius of the small tube (capillary)
R_H	hydraulic radius
s	path of seepage; settlement; total unit of shear strength; shear strength
S	surface; cross-sectional area; degree of saturation; sand
SF	safety factor
t	time; thickness of the sealing
T	transmissivity of aquifer ($T=kD$)
T_k	tortuosity of pore channels
T_v	time factor of vertical drainage
$\bar{u}$	average velocity
u, u_w	pore water pressure
u_a	pore air pressure
U	potential of volume forces; uplift water force; degree of consolidation
v	discharge velocity
v_f'	seepage velocity
v_s	fall velocity — settling velocity of a solid particle in a fluid due to gravity
V	volume; total velocity vector
w	water content (w_n — natural, w_{opt} — optimum)
w_L, w_P	liquid and plastic limits
X, Y, Z	components of the body force (forces) in the x, y, z axis directions
z	depth coordinate; vertical coordinate; elevation head
α	slope angle; coefficient of drainage effect of a bore hole
β	slope angle
γ	unit weight
γ'	Buoyant unit weight of soil
γ_d	dry unit weight of soil
γ_n	unit weight in natural conditions (in the field)
γ_{sat}	saturated unit weight
γ_w	unit weight of water
δ	angle of friction between two different materials
δ_p	portion of sand filled in pores of gravel
δ_s	heterogeneity coefficient
η	dynamic viscosity
ϑ	function of Youkowski
$\varkappa$	relationship
λ	modulus of eliptic integral
ν	kinematic viscosity
ξ, η, ζ	horizontal (ξ, η) and vertical (ζ) coordinates
ϱ	bulk density
ϱ_d	dry density
ϱ_s	density of solid particles
ϱ_{sat}	saturated soil density

ϱ_w	density of water
σ	total normal stress
σ'	effective normal stress
$\sigma_1, \sigma_2, \sigma_3$	total principal stresses
$\sigma'_1, \sigma'_2, \sigma'_3$	effective principal stresses
τ	shear stress
τ_f	shear strength; peak shear strength
$\varphi\ (h)$	piezometric potential
φ'	potential of seepage water
Φ	potential function; the potential at the given position of mass; shear strength parameter
Φ'	drained (effective stress) shear strength parameter
$\Phi_g\ (gh)$	the potential due to gravity
Φ_s	sheape factor
Φ_u	undrained (total stress) shear strength parameter
χ	seepage casale
Ψ	flow (stream) function
ω	complex (potential) number

Chapter 1
GENERAL PROBLEMS OF DAM DESIGN AND CONSTRUCTION

The *design and construction of dams* and levées forces the civil engineer to encounter various subjects such as water, soils, hydrology, geology, climate, etc., in order to make a structure conform to its requirements — safely and economically. During such a task, the following questions and problems are faced by the civil engineer.

(1) The selection of the best dam structure.
(2) Investigation of ground stability and foundations.
(3) The selection of proper material — type of soil.
(4) The method of excavation location and then control of the actual placement of material.
(5) Changing the design during construction to allow for any difference in the properties of the subsoil or of the constructed fill from those employed at the design stage.
(6) Special problems of an embankment on soft soil.
(7) Assessment of piping or liquefaction.
(8) Earthquake effects, slope failures and foundation failures.
(9) Long-term stability and consolidation.
(10) Hydraulic filling — hydraulic technology and consolidation.

The latter half of the problems mentioned above have to be solved under special or extraordinary conditions and can only be solved in cooperation with specialists in the pertinent field of science. However, it should be noted that the slopes of a dam must always be safe against both shear failure and the effects of moving water. If protection against moving water is not provided, then canal banks may be eroded, requiring continuous removal of eroded earth from the canal and possibly general shear failure of the canal sides.

The Zuider Zee Dyke and other dykes along the coast of Holland and Belgium can be considered as structures which are very well balanced in resisting all the forces acting on them, especially wave action. The shape and composition of these structures can be designated as a successful solution, involving a combination of classical and stone-pitched profiles, with a progressive type of hydraulic structure using modern new material (asphalt lining) and with very efficient modern technology — fill and hydraulic fill within the structure — as can also be seen in the Sigma plan project.

1.1 The Distinction between Dams and Levées

*A canal embankment** is a structure constructed for an artificial watercourse serving one of various purposes (Fig. 1.1a – f), such as transport, irrigation, water power. It guides water as we choose and prevents water loss. Considering their aims, they can be designated as *hydraulic structures* and divided into five groups:

(a) hydroelectric-plant canal embankments — taking water to a power station;
(b) embankments of irrigation canals — agricultural purposes;
(c) waterway embankments — transport purposes;
(d) canals for fish;
(e) multi-purpose canals.

There is usually little difference in *cross-section* between the different canal embankments mentioned above. The embankments differ in size and in the construction of the sealing. The biggest (Fig. 1.2) are to be found along power-station canals, and have the most perfect sealing as well, since water losses have to be held at a low level. Losses along irrigation canals are of little importance — they only raise the irrigation quantities, a harmless effect.

Levées, in operation for only short periods, have in the past been designed to be less watertight and less safe. They lacked any antiseepage measures, because communication between groundwater (Fig. 1.1g) and river water in the dry season is desirable. It is unfortunately difficult to avoid this effect during the flood, when it is less desirable.

With regard to the aims of protection, these structures can be categorized as follows.

(1) Levées for agricultural purposes and development protection.
(2) Levées regulating water or ice flow.
(3) Protective embankments for land in both summer and winter.
(4) Dykes — mainly as protective structures against the sea.

In engineering practice, the first three kinds of structure involve very similar construction and it is not necessary to alter designs. However, very clear thinking has to occur during the period of operation of the designed earthwork: great attention must be given to the stability of the foundation if it lies on sands or soft river deposits.

* The term "embankment" not only implies two dams which limit a canal, but also the support which contains more material than the dam itself sometime.

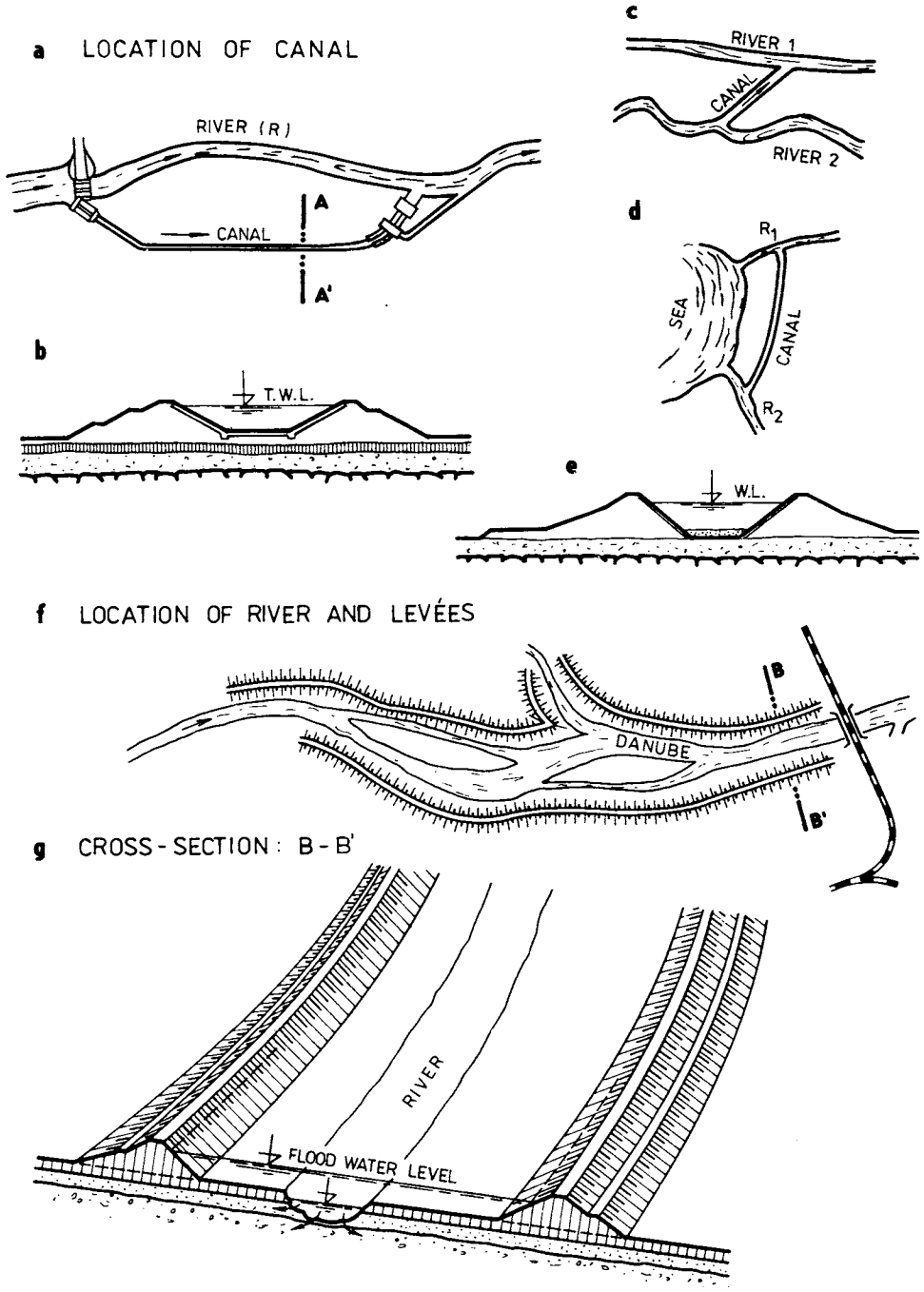

Fig. 1.1. Canal dams and levées. a — diversion canal, b — cross-section, c — connecting two rivers, d — near the sea, e — enabling the navigation (layer for anker), f — levées protecting land but enabling communication of groundwater, g — cross-section of river and levées.

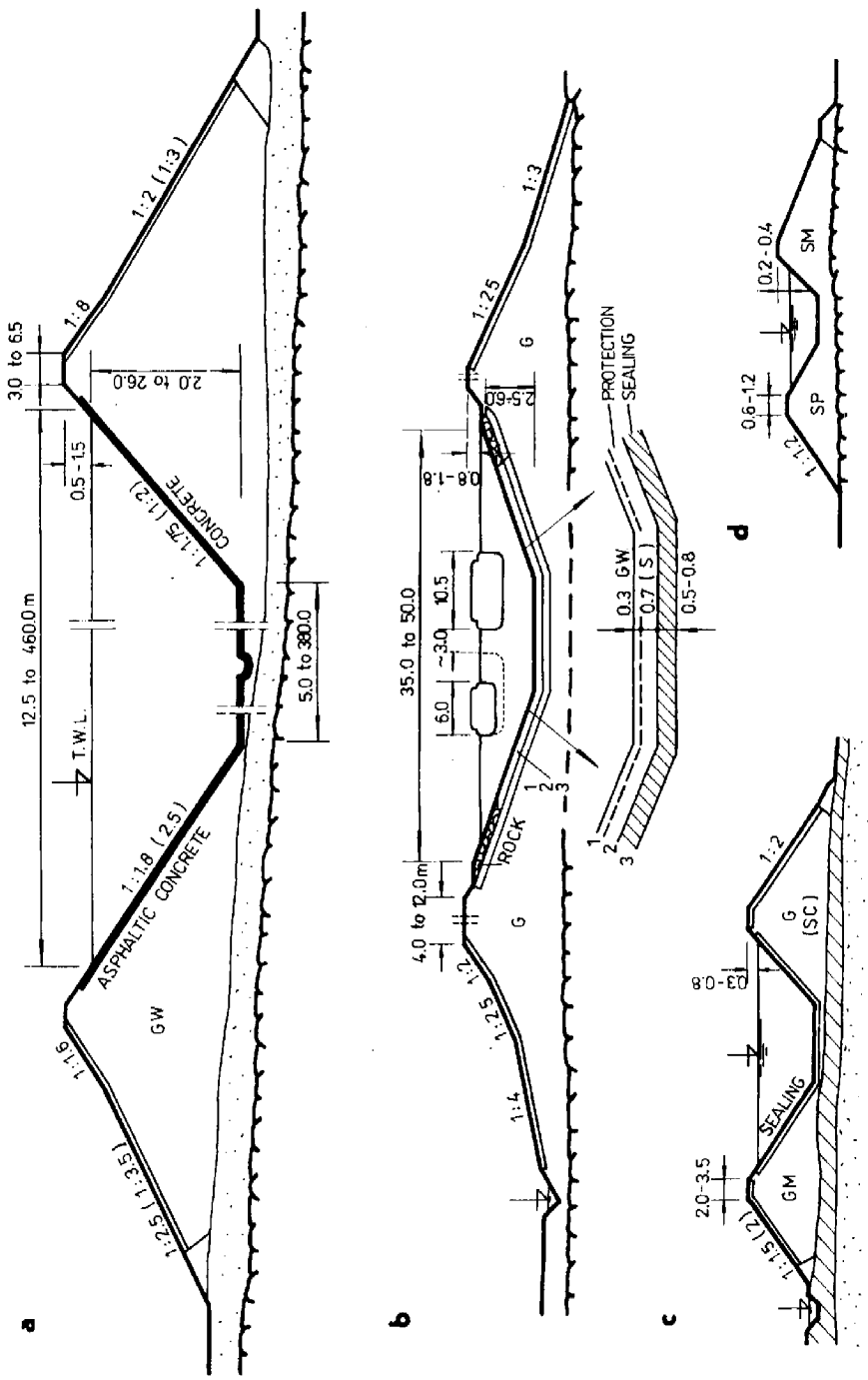

Fig. 1.2. Cross-section of dams. a — canal dams (head-race canal, hydroelectric power station), b — waterway canal with clay sealing and (S + GW) protection, c — irrigation canal, d — fishway canal (homogeneous dams).

1.2 The Situation of Embankments and Related Problems

Canal embankments lie, for the most part, on *river deposits* (gravels, sands) which are permeable, and the banks themselves are made of gravel. This is the case for the Grand Canal of Alsace in the valley of the Rhine, from which water is taken away by means of gates — control barrages, into canals diverting the stream along a length of 53.5 km (Fig. 1.3). A similar solution can be seen on many other hydroelectric schemes in France — in the Rhône valley at Montélimar (Donzère—Mondragon scheme), and also in Czechoslovakia (the river Váh scheme), on the border with Hungary in the Danube valley, where the construction of one of the biggest schemes in Europe, designed to carry 4500 m^3 per second with a water speed of 1.3 m per second, has been started. Construction of dams and large canals, and subsequent maintenance, are usually associated with enormous difficulties.

Special problems connected with *land protection* have to be solved on the northern coast of the European part of the Soviet Union, where a 25.4 km long dam has to be built across the Gulf of Finland to protect Leningrad from spasmodic flooding of the Neva.

Linking Lomonosov on the south coast of the Gulf, with Kronstadt, with Kotlin Island, and then to the settlement of Gorskaya on the north coast, the dam will be 35 m wide and the crest will be 8 m above sea level, nearly 4 m above the highest recorded flood level.

Giant "gates" through the dam will allow access for ships, and the main shipping channel across the Gulf of Finland will be diverted to pass through a 200-m gate to the south of Kronstadt, which will remain open unless there is a flood alarm.

It is estimated that over 40 million m^3 of earth will be moved (and 2 million m^3 reinforced concrete) to complete this dam within ten years, i.e. in 1990 (World Water News, May 1978).

At present, the most important *dykes in Holland* are in operation where the population have fought against the sea for more than four hundred years. The first polder (Alkmaar) in the sixteenth century (1564) was built, followed by eight others in the seventeenth to nineteenth centuries. In the last fifty years, the construction and draining of five of the largest polders: Wieringermeer (1927—1930/41), Noordoostpolder (1937—1942/59), Oostelijk Flevoland (1950—1956/60), Zuidelijk Flevoland (1961—1966), Markerwaard (1966—1978) have been finished. Two dykes are built or are in preparation every ten years to keep out the sea and let fresh water in. More than 300 km of earthen embankments (in total length) have to be built to form a new coastline — containing important hydraulic structures (locks, gates — such as Brouwershavensche Gat and others) enabling operation of the polders, and to keep shipping in active. Problems with these embankments and structures (Fig. 1.4) are often

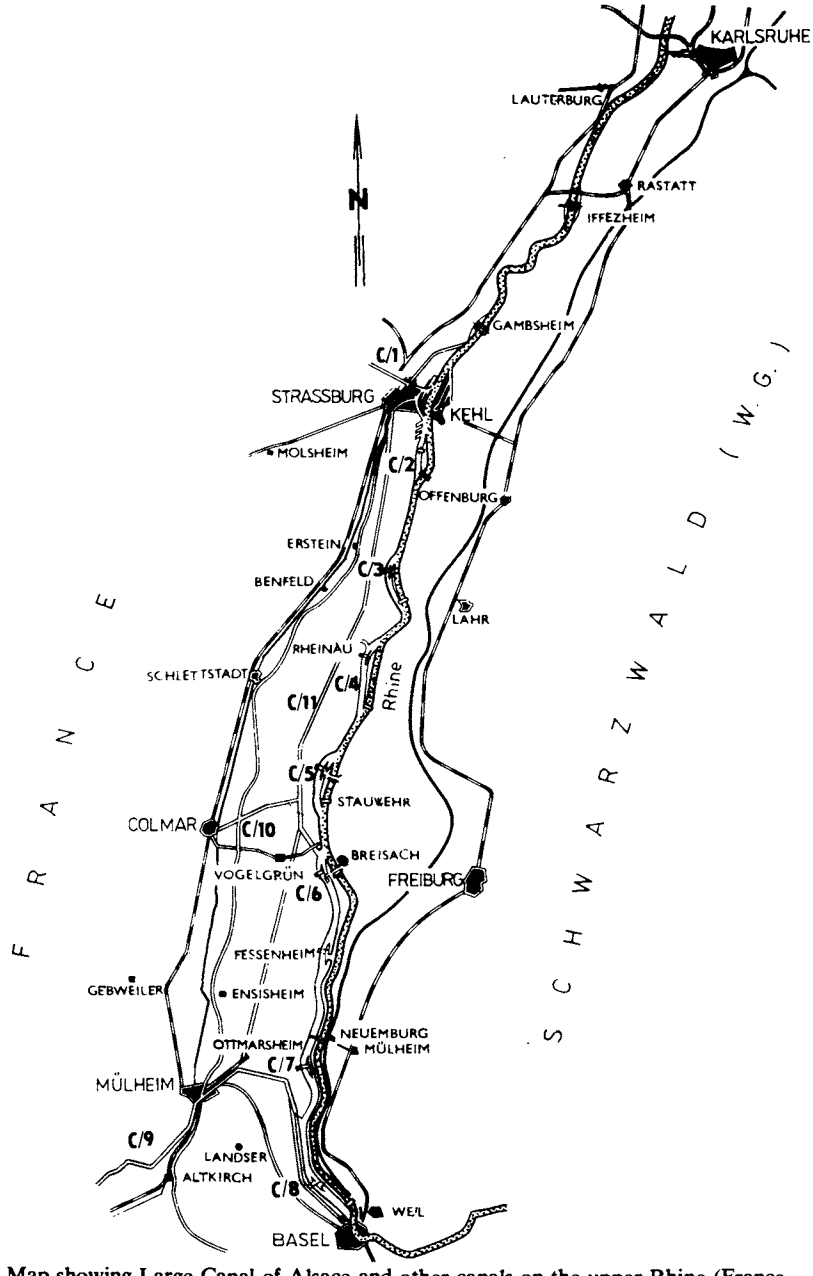

Fig. 1.3. Map showing Large Canal of Alsace and other canals on the upper Rhine (France — FRG). C/1 — Rhine—Marne (waterways), C/2 — hydroelectric power station Strassburg, C/3 — Rhine—Rhône (w.w.), C/4 — Rheinau (h.e.p.), C/5 — Markholsheim (h.e.p.), C/6 — Vogelgrün—Fessenheim (h.e.p.), C/7 — Ottmarsheim (h.e.p.), C/8 — Kembs (h.e.p.), C/9 — upper canal Rhine—Rhône (w.w.), C/10 — conjunction canal Colmar, C/11 — other canals under construction or projected.

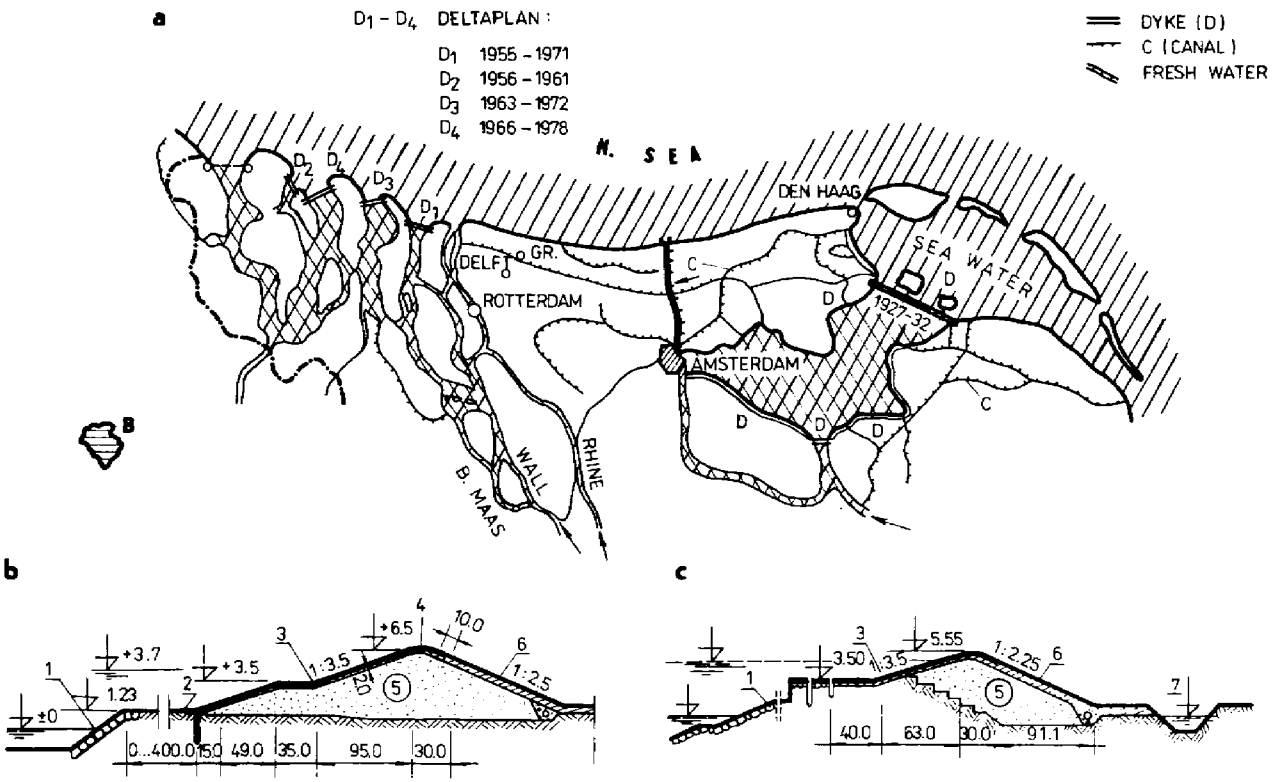

Fig. 1.4. Embankments along coasts in Holland, a — location of the dykes (D) protecting the land, b — cross-section at St Jacob, c — van Pallandpolder; 1 — stone-pitches (pitched with asphalt), 2 — rip-rap stones with asphalt penetration, 3 — asphaltic concrete (10 cm), 4 — bitumen with sand, 5 — sand, 6 — clay layer (80 cm thick), 7 — water canal.

cited, not only in Dutch literature and papers (Nooitgedacht and Ree 1964, Van der Weele 1968), but also in other foreign literature (Walters 1971, Kézdi 1976). Weak foundation problems and building-site protection are stressed in the literature mentioned above.

Large-dyke and polder problems mentioned above are peculiar to coastal countries. We will pay particular attention to inland engineering where both problems — construction and maintenance — are very instructive for an engineer. Completion of the earthwork rarely ends structural problems.

During the operation of canal systems in France, difficulties concerning the stability of dams and the watertightness of canals became a great concern to engineers and geologists. There have been many *failures of dams* arising from the ground on which the structure is built. In some respects, it is easier to design such a structure than to predict its subsequent behaviour and the natural forces which may act if the soils and rocks are subjected to water and hydrodynamic forces (Sherard et al. 1973).

The long-term strength characteristics of soft shales, such as the linings of the Panama Canal, are a perplexing problem to the soil engineer, since the slides along the canal appear to be related to cracks in the rocks. As reported by Lambe and Whitman (1969), the side slopes are currently moving into the canal at a rate exceeding 8 m per year (more than 100 m in fifty years).

In the Soviet Union — in Central Asia, the engineers have to contend with arid soils transported by wind. The reservoir dams constructed in Canada and in the USA, for control of the water which flows at night over the Niagara and is diverted to power-stations during the day, are also remarkable structures. There are also many kilometers of ship canal with earthen embankments in the St Lawrence scheme, where frost danger is a big problem.

In this domain the irrigation canal leading the water from Amu Darya to the Caracum Desert should be mentioned.

Embankment (dyke, canal dam, levée) construction forces the designer overcome many difficulties of a geological, technological and ecological nature. The biggest problems arise in dyke erection — where weak foundations and rough seas complicate every step from the first move.

The *construction of diversion canals* seems much easier at first sight, but it is necessary to remember that by diverting the river from the old course, many problems concerning flooding have to be solved and often unsuitable site geology must be overcome. The location of dams in permeable material leads to the interfering of this structure with the natural underground water levels, which can complicate the dam construction and canal operation (Delattre 1959).

The situation and *construction of old levées* conceal the dangers which lie in our ignorance of the material quality in the embankment structure and its sub-base, and the danger of overflow. They were built at the end of the last century, and at the eginning of this century. These constructions along the big rivers in North

America — along the Mississippi River and in Canada along St Lawrence River — were menaced by the threat of overflow during flood seasons. The danger facing European rivers such as the Rhine, Rhône, Garonne and Loire in France, the Po and Tivere in Italy, the Danube in Czechoslovakia, Hungary and Yugoslavia, the river Chuand-che in China, the Ganges and Jamuna rivers in India and others, has many facets. It is not only the danger of overflow (overtopping), landslides, erosion or "piping" in alluvial deposits, and settlement if the structure is on unconsolidated clay or silt. Settlement of the levées often reaches 10 to 15% of the height of the fill and together with the river-bed deposit reaches, for example, in the Danube valley in Czechoslovakia 1—2 cm per year. Hence we have the danger of overtopping — and hence the danger of structural collapse.

The danger mentioned above must be taken into account when designing all earthen embankments (Fig. 1.5a). It is unreasonable to place the structure (2) on the border of a river-bed where slope sliding (3) can occur. The placement of a dam must be in a position (4) where the stability condition will be satisfied. An embankment lying on organic clays (Fig. 1.5b) can be damaged as a result of a high shear strength near the foot which leads to failure of the sub-base (6). Over the rock base (7), a failure plane (8) can originate: this can be overcome by using moderate slopes (9).

Large settlement (Fig. 1.5c, d) of an embankment (10) can be limited by proper division of dam construction into stages (Fig. 1.5e). It is useful to fill the foot and the bottom of the embankment — in the case of a height exceeding 3 m. We obtain a plateau giving good conditions for laying wells and drains (17) and finally for filling the upper part of the embankment (18).

A theoretical solution to the problems mentioned above can be found in Chapters 3 and 6 and also in the very rich literature on the subject (Bishop 1955, Casagrande and Rivard 1959, Terzaghi 1959, Harr 1962, Skempton 1964, Myslivec 1968, Lambe and Whitman 1969, Lobdell 1969, Kézdi 1976, and others).

1.3 Loading Conditions and the Influence of Water

While the primary loading conditions (during and after construction) of canal embankments and levées are the same (see Chapter 3), during operation the loading conditions and effective loads differ and have to be handled separately. Commonly (but in different time intervals), some *forces operate during loading stages,* i.e.:

I — during construction;
II — after dam, levée erection;
III — during operation of the structure — water loading;
IV — in exceptional conditions during earthquake, slope failures, other catastrophic cases.

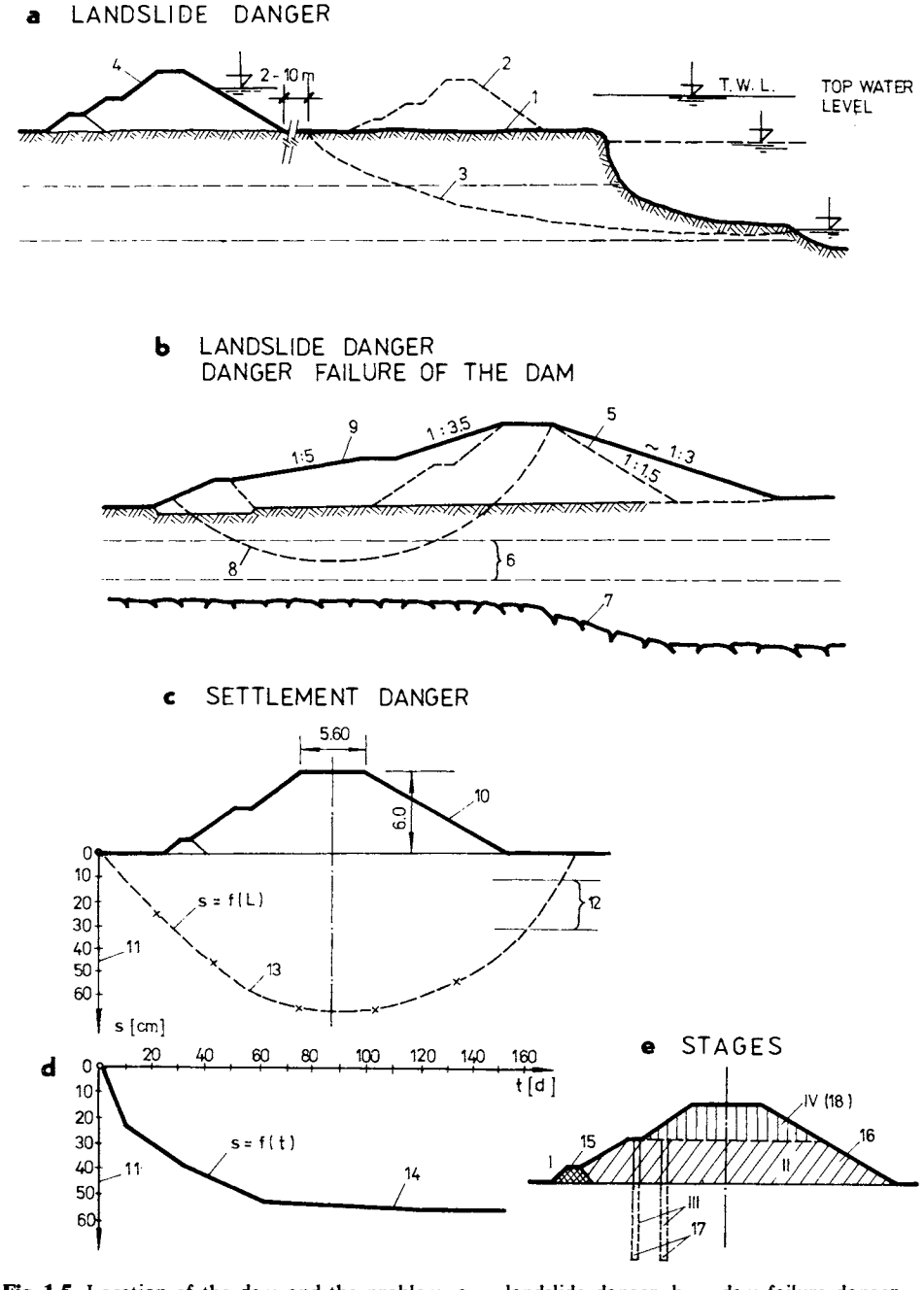

Fig. 1.5. Location of the dam and the problem. a — landslide danger, b — dam-failure danger, c — expected settlement, d — course of settlement, e — stages of material placement; 1 — ground surface, 2 — incorrect position of structure, 3 — assumed failure plane, 4 — correct position, 5 — profile insufficient, 6 — organic clay, 7 — rock surface, 8 — failure surface, 9 — correct

In normal cases, the following *forces* are *in action.*

(1) The weight of the structure.
(2) The water pressure — static and dynamic loading.
(3) Seepage forces and pore pressures.
(4) Wind forces: waves from wind, vessels, etc.
(5) Earth pressures.
(6) Frost effects: expansion of water and soils.
(7) Forces induced by other volume changes — swelling, shrinkage.
(8) Forces leading to internal instability of soils — piping, hydraulic fracturing, liquefaction, for example.
(9) Earthquake and other dynamic loading (vibration).
(10) Man-made forces: prestressed construction.

From the point of view of mechanics, these forces can be divided into surface and volume forces. Most have a variable character and change with water-head. This is a leading factor as a transfer medium working on the structure. At every stage, it is very important to take into account not only the height of the embankment (H) but also the water elevation — head above a chosen datum. Let us define γ_w, unit weight of *water pressure,* by

$$p_a = \gamma_w z \qquad [\text{MPa}]. \tag{1.1}$$

The water-head also determines the potential energy and kinetic energy. In the *Bernoulli equation,* we have

$$E = z + \frac{p}{\gamma_w} + \frac{v^2}{2g} \qquad [\text{m}]. \tag{1.2}$$

Evaluating eqn. (1.2), we obtain the values used for the Newton and also Navier—Stokes equations.

The remaining loading stages can also be characterized by *water-head* or by increase of head Δh. The water pressure from a wave will be caused by water velocity w_{10}, from a run distance D (km), angle of wave α_w, some coefficient k_w — depending on relative depth ($h : \lambda$) which expresses the relation between water depth and wavelength. The *increase in head* can be calculated by the formula

$$\Delta h = k_w \frac{D w_{10}^2}{2gh} \cos \alpha_w \qquad [\text{m}], \tag{1.3}$$

as explained in Section 3.3.

These comments show two things: the change of water-head energy as a first principle, and our attempt to express the influence of water as a "hidden" energy and not in pure static form — neglecting its dynamic aspect.

---

contour, 10 — profile of structure, 11 — scale of settlement, 12 — peat layer, 13 — final settlement, 14 — values of settlement with time, 15 — rocky toe (stage I), 16 — basic part of embankment (stage II), 17 — sand drains (stage III), 18 — final fill (stage IV).

1.4 Construction Materials

The *choice of materials* to be used in dam construction is governed by the extent of local soils and rocks and by the *technological experience* of the contractor. Further assumptions of *climatic conditions* and the possibility of artificial (lining) and man-made materials have to be made. As sealing materials cement concrete, asphaltic concrete, polyethylene, polyvinylchloride foil, ceramic elements and so on, can be taken into consideration. These materials predetermine what kind of cross-section may be designed; this will be treated in Chapter 4. However, in all cases, the main construction material is the soil. This allows us to build many types of dam and levée cross-sections (Middlebrooks 1953, Ringheim 1964, Striegler and Werner 1969, Koster 1975) and a choice of various methods of emplacement and control of work. Manually placed soil is called fill and the most used process of placing is termed filling. An essential part of the engineer's task is to see that the properties of the placed material correspond to those assumed in the design or to *change* the design *during construction* to allow for any differences arising.

If a *homogeneous profile* (Fig. 1.6a) has been chosen, as is very often advantageous in levées, the requirement of impermeability and soil stability is given for the

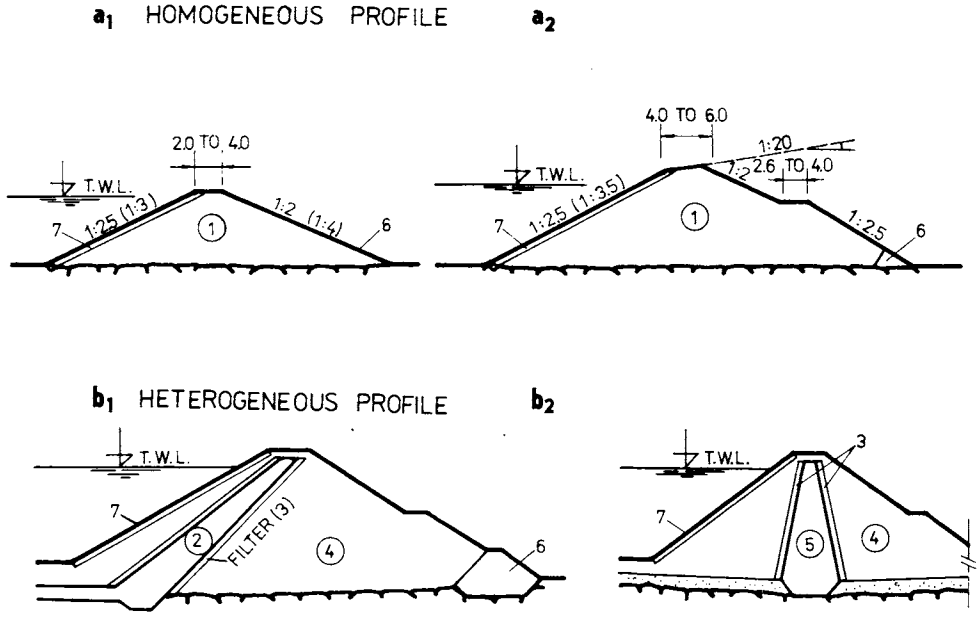

Fig. 1.6. Materials in dam profile. a_1 — uniform (for smaller levées and dams), a_2 — cross-section (with oblique top and shelf), b_1 — heterogeneous profile with inclined profile, b_2 — with clay core; 1 — silt or silty sand, 2 — clay or silty clay, 3 — sand, 4 — gravel or sandy gravel, 5 — clay, 6 — rocky or gravel toe, 7 — rip-rap, pitched stone or pavement with sand seam.

same soil. It may be silt, silty sand (loam) or sandy clay. A portion of sand in such a soil mixture is desirable every time. It does not change its properties. It is easy to compact, little affected by moisture, not subject to frost action. Coarse-grained components increase the stability slightly. *Finer, uniform sand* approaches the characteristic of silt, i.e. a decrease in permeability and a reduction in stability with increase in moisture. Silt itself is inherently unstable, particularly when moisture is increased, with a tendency to become *quick when saturated.* It is relatively impervious, difficult to compact, highly susceptible to frost heave, easily eroded and subject to *piping and boiling.* Bulky grains reduce compressibility; flakey grains, i.e. mica, diatoms, increase compressibility, produce an "elastic" silt (Lambe and Whitman 1969).

Organic matter, present even in moderate amounts, increases the compressibility and reduces the stability of the fine-grained components. It may decay causing voids or by chemical reaction change the properties of a soil, and hence organic soils are not desirable for use in dams and levées. Only a small part (2—5%) is admissible.

Heterogeneous profile and zoned earth dam are not very frequent. In engineering practice of dam or levée construction, dams with a clay core (Fig. 6b) which keeps leakage low, and a heavy, highly permeable rock or gravel toe which adds considerably to stability are common. Between these two main zones there is a sand gravel filter to prevent washing off soil particles from the core into the voids of the gravel or rock toe. Between the core and the reservoir, rock or concrete is laid on a gravel bed. The rock or concrete *facing prevents erosion* of the core by rain or water in the river or in the canal. The gravel bed prevents instability of the facing and any sinking into the clay.

In Czechoslovakia, excellent results with the hydraulic development of "canal cascades" on the Váh valley have been obtained. For example, in the Krpeľany—Sučany—Lipovec scheme (Fig. 1.7), the main structures are the embankments of the head-race canal (Fig. 1.7a), 6.2—18.4 m high (the canal being up to 50.0 m in width), the hydroelectric power house, and the tail-race canal 28.5—62.0 m in width, with up to 10 m of water. The embankments had to be made in variable coarse-grained soils, mostly gravels and sands with a permeability coefficient $k = 6 \times 10^{-5}$—3×10^{-3} m s^{-1}; the structure had to be lined with a concrete pavement 15 cm thick. The construction works on the upper Váh cascade amounted to 9.55×10^6 m^3 excavation work, 6.66×10^6 m^3 levées and back-fill, 5.2×10^5 m^3 concrete and reinforced concrete, 1.35×10^5 m^3 rip-rap and concrete paving, and 1.4×10^5 m^3 rock and levée toes.

Experiences of French builders in *dam construction using local material* on the Rhône valley canal (the hydroelectric plant at Donzère—Mondragon) are remarkable. The use of alluvial gravel compacted into horinzontal layers is well known: it was used on the Montélimar canal. The canal-bed is lined with a mixture of selected mud and gravel laid with particular care. The slopes are formed of gravel, and to

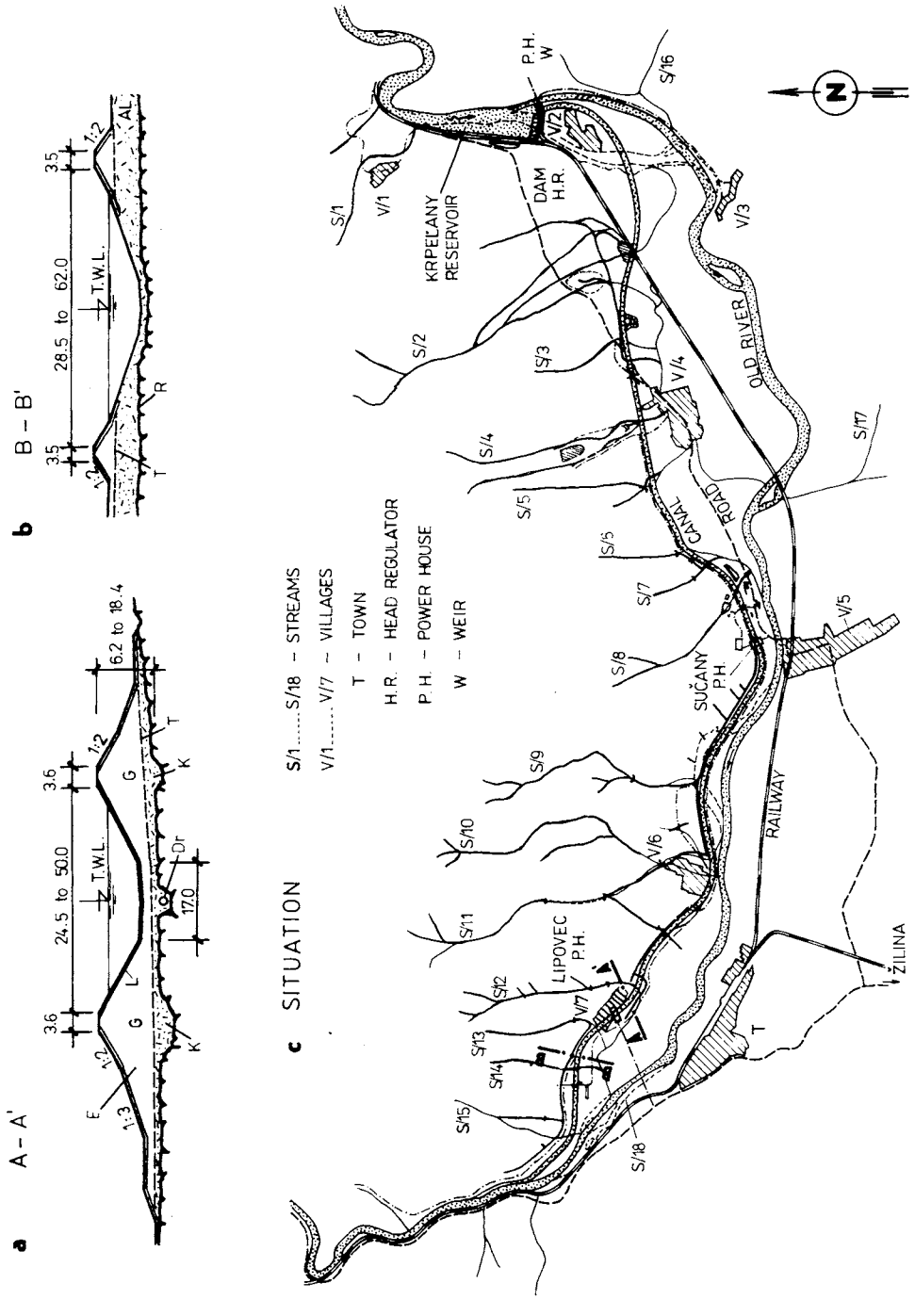
a A – A'
b B – B'
c SITUATION
S/1.....S/18 – STREAMS
V/1.....V/7 – VILLAGES
T – TOWN
H.R. – HEAD REGULATOR
P.H. – POWER HOUSE
W – WEIR
KRPELANY RESERVOIR
DAM H.R.
P.H. W
OLD RIVER
CANAL
ROAD
RAILWAY
SUČANY P.H.
LIPOVEC P.H.
ŽILINA
T.W.L.
AL.
Dr
N

avoid erosion by waves (caused naturally or by boats) have a bituminous lining 6 cm thick on them (Delattre 1959).

In the literature (Walters 1971), we find the coefficient of permeability of the Rhône deposits to be in the range $k = 4.2 \times 10^{-7}$—2.0×10^{-3} m s^{-1}, and the seepage losses 17 m^3 s^{-1}. After 3 years, the losses fell to one quarter of the original value.

This method was also adopted on the Seine scheme of dams where silty materials, "limons" and gravels, are used as construction material (Fig. 1.8).

A *special method* was adopted for the Zuider Zee Dyke, where the bed of the sea under the dam consists of Boulder Clay and other glacial material onto which willow mattresses of brushwood (118 × 26.5 m) were lowered and weighted with stones. Two parallel dams of Boulder Clay, deposited by hopper-bottom barges with sand pumped between them, formed the underwater foundations for the dyke. The Boulder Clay was obtained from the lake. The North Sea embankment was pitched with basalt in the tide range of wind and water, and the toe was protected by brushwood held down by stones.

Sandy materials were incorporated into canal dams of the Volga—Don scheme where hydraulic filling — very popular in the fifties in the Soviet Union — had to be used.

In the choice of construction materials, the civil engineer has a very large spectrum of possibilities, but also has to face *many questions* during the design and construction.

(1) What kind of structure should be chosen?
(2) What are the slopes of the upstream and downstream faces?
(3) How thick a layer of gravel and rock facing is necessary to keep any swelling of the clay core to a tolerable amount?
(4) What should the dimensions of the dam be to give the most economical, safe structure?
(5) What kind of operation will be used in the canal, what are the floods like, what is the duration?
(6) What are the strength and permeability characteristics of the constructed dam?
(7) How would the strength and permeability of the dam vary with time and water level in a canal or river?
(8) How much leakage would occur under and through the dam?
(9) What is the danger of soil instability — liquefaction of soil, piping problem or hydraulic fracturing threat?
(10) What, if any, special restrictions on the operation of the canal are necessary?

Fig. 1.7. Dam profile used in Czechoslovakia in Váh valley. a — head-race canal, b — tail-race canal, c — site of the canal; E — embankment, G — gravel, L — lining (concrete), T — surface of original territory, AL — alluvial deposit, Dr — drainage, K — key of territory against sliding.

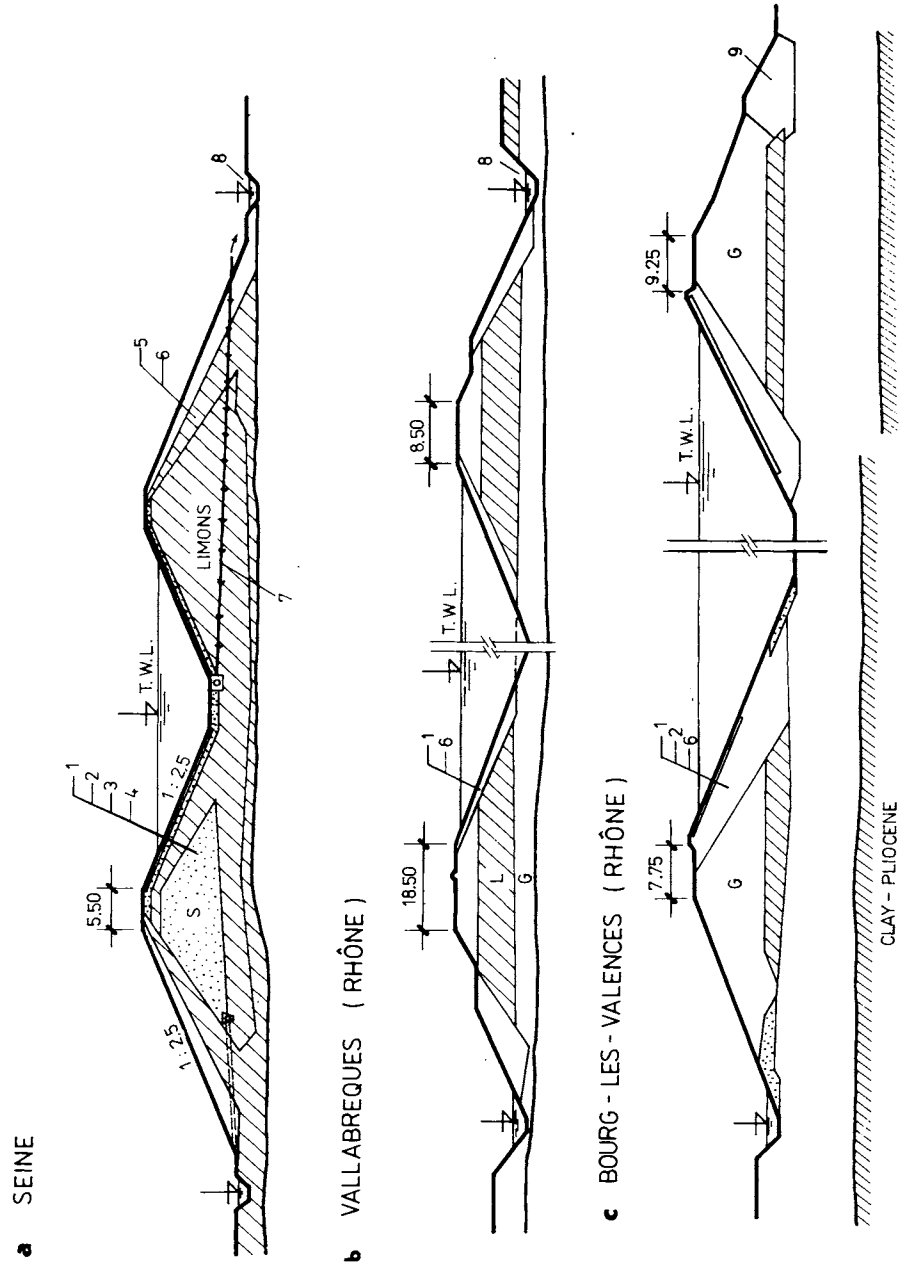
a SEINE
LIMONS
T.W.L.
5.50
1:2.5
1:2.5
S
b VALLABREQUES (RHÔNE)
8.50
18.50
T.W.L.
L
G
c BOURG - LES - VALENCES (RHÔNE)
9.25
7.75
T.W.L.
G
CLAY - PLIOCENE

To answer these and other questions, the properties of materials involved must be known.

Soil classification and soil properties. The direct approach to the solution of the given problem of dam design consists in measuring the soil propertyneeded and in employing this measured value in some rational expression, to determine the structure parameters. During the *investigation and design* period it is necessary:

(a) to determine the *shear and stress parameters* of the soil with regard to the pore pressure;
(b) to determine the *settlement* of the structure, measure the compressibility of the soil and use this value in the settlement equation based on the appropriate theory of consolidation;
(c) to determine the *rate of water* flowing through a sample of soil, measure the permeability of the soil and use this value together with a flow net to determine the seepage quantity;
(d) to evaluate the *stability of a slope,* measure the effective parameters of shear strength of the given soil, and substitute this value into an expression based on the laws of statistics and of plasticity theory (if necessary).

Measurement of some fundamental soil properties such as permeability, compressibility and strength can be difficult and time consuming. In dam design as well as other branches, it is very helpful to use soil classification.

In dam design, many proscriptions and instructions must be respected — as committed for given country. The most popular in use is the *Unified System,* intended for use in all engineering problems involving soils, developed by the *Bureau of Reclamation and the Corps of Engineers* (USA), which is presented in Tables 1.1 and 1.2. For earth dams and canal section use, Table 1.3 is also convenient. As an additional characteristic, the *plasticity index* (PI) (Fig. 1.9) can be used, where

$$\mathrm{PI} = w_{\mathrm{L}} - w_{\mathrm{P}}. \tag{1.4}$$

This characteristic (PI) — soil classification of all other Attenberg's limits w_{opt}, permeability, for example, mentioned later — helps the designer to substitute the results of field experience by giving him a general guidance, making it available in an empirical manner. He must be cautious in the use of soil classification mainly when solving flow and stability problems concerned with the privileged path of the appearance of water on the surface of the path, which changes to a livery consistency and becomes glossy.

Fig. 1.8. Characteristic canal dams in France. a — canal dams of Seine Reservoir, b — water power Rhône scheme near Vallabreques, c — Bourg-les-Valences heterogeneous dams; 1 — canal lining, 2—sand or gravel, 3—limons (L) (fine-grained soils), 4—sands, 5—slope protection (grass, silt, gravelly material), 6 — gravel, 7 — pipeline collecting seepage water, 8 — ditch, 9 — rocky (or gravel) toe.

Table 1.1. Unified soil classification

Description			Group symbols	Laboratory criteria			Notes
				Fines [%]	Grading	Plasticity	
Coarse grained (more than 50% larger than No. 200 BS sieve size). After CSN 73 6850 larger than 0.063 mm	Gravels (more than 50% of coarse fraction of gravel size)	Well graded gravels, sandy gravels, with little or no fines	GW	0—5	$C_u > 4$ $1 < C_c < 3$		Dual symbols if 5—12% fines Dual symbols if above A line and $A < PI < 7$ $C_u = \frac{d_{60}}{d_{10}}$ $C_c = \frac{(d_{30})^2}{d_{10}d_{60}}$
		Poorly graded gravels, sandy gravels, with little or no fines	GP	0—5	Not satisfying GW requirements		
		Silty gravels, silty sandy gravels	GM	> 12		Below A line or $PI < 4$	
		Clayey gravels, clayey sandy gravels	GC	> 12		Above A line and $PI > 7$	
	Sands (more than 50% of coarse fraction of sand size)	Well graded sands, gravelly sands, with little or no fines	SW	0—5	$C_u > 6$ $1 < C_c < 3$		
		Poorly graded sands, gravelly sands with little or no fines	SP	0—5	Not satisfying SW requirements		
		Silty sands	SM	> 12		Below A line or $PI < 4$	
		Clayey sands	SC	> 12		Above A line and $PI > 7$	
Fine grained (more than 50% smaller than No. 200 BS sieve size). After CSN 73 6850 smaller than 0.063 mm	Silts and clays (liquid limit less than 50)	Inorganic silts, silty or clayey fine sands, with slight plasticity	ML	Use plasticity chart (Fig. 1.9); rock flour too			
		Inorganic clays, silty clays, sandy clays of low plasticity	CL	Use plasticity chart (gravelly clays)			
		Organic silts and organic silty clays of low plasticity	OL	Use plasticity chart			
	Silts and clays (liquid limit greater than 50)	Inorganic silts of high plasticity	MH	Use plasticity chart (elastic silts too)			
		Inorganic clays of high plasticity	CH	Use plasticity chart			
		Organic clays of high plasticity	OH	Use plasticity chart			
Highly organic soils		Peat and other highly organic soils	Pt				

Table 1.2. Field identification on fine-grained soils

Group	Dilatancy	Dry strength	Toughness
ML	Quick to slow	None to slight	None
CL	None to very slow	Medium to high	Medium
OL	Slow	Slight to medium	Slight
MH	Slow to none	Slight to medium	Slight to medium
CH	None	High to very high	High
OH	None to very slow	Medium to high	Slight to medium

According to Wagner (1957) and Craig (1974).

Very fine clean sands give very *quick reaction to water* and to shaking. They are very dangerous in dam construction with respect to stability and dilatancy.

Strength characteristics are changed quickly by fine-grained soils. After removing larger particles (sands), mould a pat of soil to the consistency of putty, adding water if necessary. Allow the pat to dry completely by oven, sun or air and then test

Table 1.3. Maximum and minimum void ratio for granular soils

Porosity	Uniform sand	Silty sand	Fine-coarse sand	Silty sand and gravel
e_{max}	1.00	0.90	0.95	0.85
e_{min}	0.40	0.30	0.20	0.14
n_{max}	50% } 40%	47% } 35%	49% } 33%	46% } 30%
n_{min}	29% }	23% }	17% }	12% }

its strength by breaking and crumbling between the fingers. This strength is a measure of the character and quantity of the *colloidal fraction* contained in the soil. The dry strength increases with increasing plasticity. High dry strength is characteristic for clays of the CH group. A typical inorganic silt possesses only very slight dry strength. *Silty fine sands* and *silts* have about the same low dry strength,

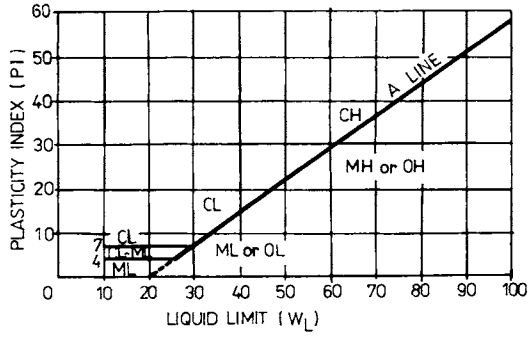

Fig. 1.9. Position of USC soil groups — after Casagrande (1948). Plasticity chart; A line as "border": toughness and dry strength increase with increasing PI, below A line toughness decrease.

but can be distinguished by the feel when powdering the dried specimen. Fine sands feels gritty whereas a typical silt has the smooth feel of flour.

Fine soils change their properties near the plastic limit. By wetting they become weak plastic, on drying they become sticky. Wet soils folded and rerolled gradually lose moisture content and also lose plasticity. Weakness of the thread at the plastic limit and quick loss of coherence of the lump below the plastic limit indicate either inorganic clay of low plasticity or material such as kaolin-type clays and organic clays which occur below the *A* line.

Highly *organic clays* have a very weak and spongy feel at the plastic limit. They are not desirable in dam construction, and are menaced by piping — as reported later (Section 1.9) and in more detail by Lambe and Whitman (1969) and Sherard et al. (1973).

Silts are inherently unstable, particularly when moisture is increased, with a tendency to become quick when saturated. It is relatively impervious which is why in old levée construction, its use was very common despite its inconvenient properties — easily eroded and subject to piping and boiling. Bulky grains reduce compressibility; flakey grains, i.e. mica, diatoms, increase compressibility and produce an "elastic" silt. Work by machine — placing and compaction — can be inconvenient, particularly in rainy seasons.

Gravels and sands have essentially the same engineering properties, and differ only in degree. They are *easy to compact,* little affected by moisture, not subject to frost action. Gravels are generally more perviously stable, resistant to erosion, than sands. With uniform *sand* ($C_u < 3$), there is a danger of liquefaction in the *loose state*, as reported later. Well graded sands and gravels are generally less pervious and more stable than those which are poorly graded. Irregularity of particles increases the stability slightly.

Many of the properties mentioned above can be recognized by physical soil properties expressed as unit weight (γ), porosity (n), water content (w), etc. Their relations must be known.

Phase relationships. The water content (w) is the ratio of the mass of water to the mass of solids in the soil, i.e.

$$w = \frac{M_w}{M_s}. \tag{1.5}$$

Plasticity index (PI) (eqn. 1.4) can be determined from the liquid limit — water content (w_L) and plastic limit (w_P).

Soil characteristics can be expressed quantitatively through the following phase relationships:

— the *degree of saturation* (ratio of the volume)

$$S_r = \frac{V_w}{V_v}, \tag{1.6}$$

— *void ratio*

$$e = \frac{V_v}{V_s}, \tag{1.7}$$

— *porosity*

$$n = \frac{V_v}{V} \quad [\%], \tag{1.8}$$

related as follows

$$n = \frac{e}{1+e}, \qquad e = \frac{n}{1-n}. \tag{1.9}$$

The *bulk density* (ϱ) is

$$\varrho = \frac{M}{V} \quad [\mathrm{kg\ m^{-3}} \text{ or } \mathrm{Mg\ m^{-3}}]. \tag{1.10}$$

The *specific gravity* of the solid soil particles is

$$G_s = \frac{M_s}{V_s \varrho_w}. \tag{1.11}$$

The air content is

$$A = n(1 - S_r) \quad [\%]. \tag{1.12}$$

The *bulk density* — expressed as specific gravity, void ratio, water content and density of water (ϱ_w) is

$$\varrho = \frac{G_s(1+w)}{1+e}\varrho_w, \qquad \varrho = \frac{G_s + S_r e}{1+e}\varrho_w. \tag{1.13}$$

For a completely *dry soil* ($S_r = 0$),

$$\varrho_d = \frac{G_s}{1+e}\varrho_w. \tag{1.14}$$

In the calculations and dam designs, the most frequent characteristics are:

the *unit weight*

$$\gamma = \frac{W}{V} = \frac{Mg}{V} = \frac{\text{total weight}}{\text{total volume}}, \tag{1.15}$$

or

$$\gamma = \frac{G_s(1+w)}{1+e}\gamma_w \quad [\mathrm{kN\ m^{-3}}], \tag{1.16}$$

the *buoyant unit weight*

$$\gamma' = \frac{G_s\gamma_w - \gamma_w}{1+e} = \frac{G_s - 1}{1+e}\gamma_w, \tag{1.17}$$

$$\gamma' = \gamma_{sat} - \gamma_w, \tag{1.18}$$

$$\gamma_{sat} = \varrho_{sat} g, \qquad \varrho_{sat} = \frac{G_s + e}{1+e}\varrho_w, \tag{1.19}$$

where V_v, V_s are the volume of voids and the volume of solids; V is the total volume; M_s, M are the mass of solids and the total mass.

In the description of soils we can further use w_n, *natural water content*; γ_n the unit weight of soil in natural condition in the field; w_{opt}, optimum water content (%).

The density of a natural granular soil, the *relative density* is given by

$$D_r = \frac{e_{max} - e}{e_{max} - e_{min}} 100\% = \frac{\gamma_{d\,max}}{\gamma_d} \frac{\gamma_d - \gamma_{d\,min}}{\gamma_{d\,max} - \gamma_{d\,min}} 100\%, \tag{1.20}$$

where e_{max} is void ratio of soil in loosest condition; e_{min} is void ratio of soil in densest condition; $\gamma_{d\,max}$, $\gamma_{d\,min}$ are dry unit weight in loosest and densest condition; e, γ_d are in-place void ratio and in-place dry unit weight.

In engineering practice, we denote the density of granular soils on the basis of relative density as follows

$D_r =$	0—15%	15—35%	35—65%	65—85%	85—100%
	very loose	loose	medium	dense	very dense

In the field, granular soils with this void ratio (porosity) can usually be found (Table 1.3).

The characteristics mentioned above influence the most important soil characteristic in dam construction, i. e. the permeability characterized by the *coefficient of permeability k* and the factor of resistance to seepage water Φ_n.

1.5 Sealing Materials

In canal-embankment and levées construction, the following *sealing materials* can be used.

(1) Sealing *earth* — very often used in levées and irrigation canals.
(2) *Concrete* or reinforced concrete lining — in embankments of canals, head-race canals and divertion canals.
(3) *Bituminous materials*: asphaltic concrete, bitumen facing.
(4) *Cementation* of strata below canal embankments and levées, grout screen.
(5) *Splash mortar* and "torcrete" lining of the slope.

(6) *Prestressed concrete slabs.*

(7) *Watertight foil* — plastics of polyvinylchloride, for example.

Wooden lining, used in the USA and the Soviet Union in the past, as well as iron and aluminium linings, were not proven satisfactory and have no importance today.

The remaining most important sealing materials — *fine-grained soils*: silt, silty clays and some sandy materials — are semipervious or even impervious. Their properties are influenced by their mineral composition and by the size and shape of minerals. Before use of these soils, soil testing is necessary. In preliminary planning, however, the soil *Identification Code* (Fig. 1.10) has many advantages. It allows us to make an initial estimation of the permeability of the soil, as the decisive property of a sealing material. This can be influenced by compaction. According to Lambe and Whitman (1969), increasing the molding water content results in a decrease in permeability on the dry side of optimum moisture content and — after some lag — a slight increase in permeability on the wet side of optimum. In general, increasing the compactive effort reduces the permeability since it both increases the dry density, thereby reducing the voids available for flow, and increases the orientation of particles.

It can be said that for permeability, the value of *effective porosity* (n_{eff}) is decisive. This can be calculated using empirical formulae — as a function of porosity (n), critical porosity (n_{cr}), water content (w, w_{opt}) (Fig. 1.11a) and an empirical (measured) coefficient (α'), as follows

$$n_{\text{eff}} = n - \Delta n = n\left[1 - \alpha' \frac{w}{w_{\text{opt}}} \left(\frac{n_{\text{cr}}}{n}\right)^2\right]. \tag{1.21}$$

An inverse relation between n_{eff} and a *factor of resistance* against the flow Φ_n is given by formula

$$\Phi_n = \left(\frac{1}{n}\right)^z, \tag{1.22}$$

with values of exponent $z = 2.4$—4.6.

Tests of *cohesive soils* in the Danube deposits (Peter 1977) resulted in the values $\alpha' = 0.65$—0.6, $w_{\text{opt}} = 19.1$ and 27%, respectively, and $n_{\text{cr}} = 0.41$ and 0.46, respectively, for an exponent $z = 3.2$. The value Φ_n (Fig. 1.11b) was determined by computation and then compared with the value of permeability coefficient measured in the laboratory or in the field. Many such experiments with Danube deposits used in levées and dams were made. Silty clays showed a wide range of k for the same soil compacted at various water contents with a high hydraulic gradient ($I = 18.5$—22). The ratio of values determined in the laboratory giving the relationship $k_{\max} : k_{\min} = 236$ and 16.5, respectively, corresponded to the ratio of computed resistance $\Phi_{n\max} : \Phi_{n\min} = 242$ and 20.8, respectively.

Similar results were obtained by Lambe and Whitman (1969) some years ago

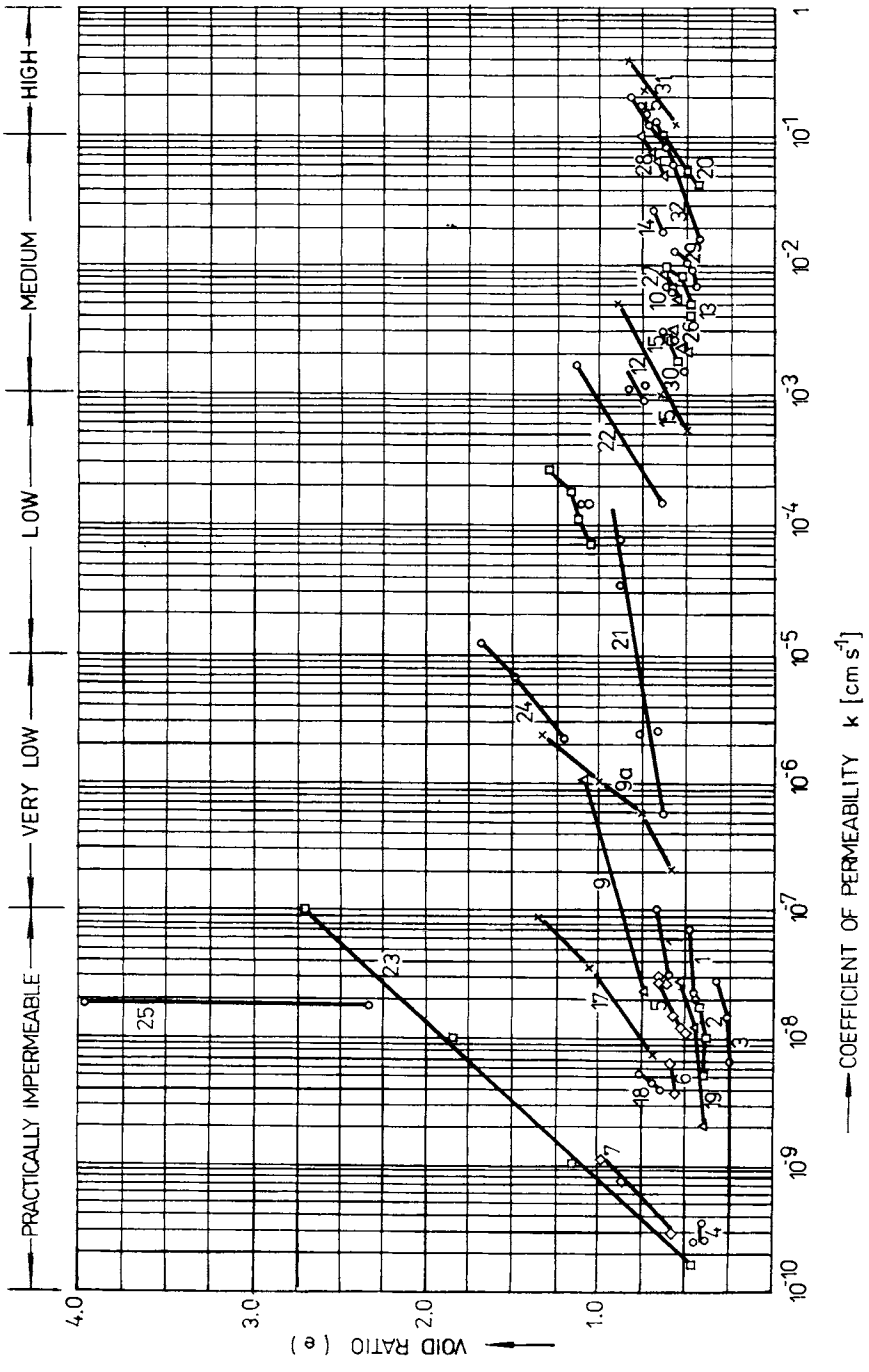
PRACTICALLY IMPERMEABLE
VERY LOW
LOW
MEDIUM
HIGH
VOID RATIO (e)
4.0
3.0
2.0
1.0
COEFFICIENT OF PERMEABILITY k [cm s⁻¹]
1
10⁻¹
10⁻²
10⁻³
10⁻⁴
10⁻⁵
10⁻⁶
10⁻⁷
10⁻⁸
10⁻⁹
10⁻¹⁰

(Fig. 1.12), while investigating the effect on the structure of mixing in a polyphosphate dispersant.

The facts mentioned above show that the coefficient of permeability cannot be given as a constant value for the permeability characteristic. This characteristic expresses *hydraulic resistance* of soil (f_H), with dependence on the *hydraulic radius of pore channels* which changes due to porosity (n), *degree of saturation* (S), state of soil and the viscosity of water. The permeability diminishes through compaction; its dependence can be expressed as a function of the form

$$k = f(d, n, w, w_{opt}, D, \ldots).$$

The concrete and reinforced concrete used for *concrete facing slabs* of canal embankments should have a high actual compressive strength: 25—30 MPa or more, and be watertight enough; for this reason it should be made of a cement of

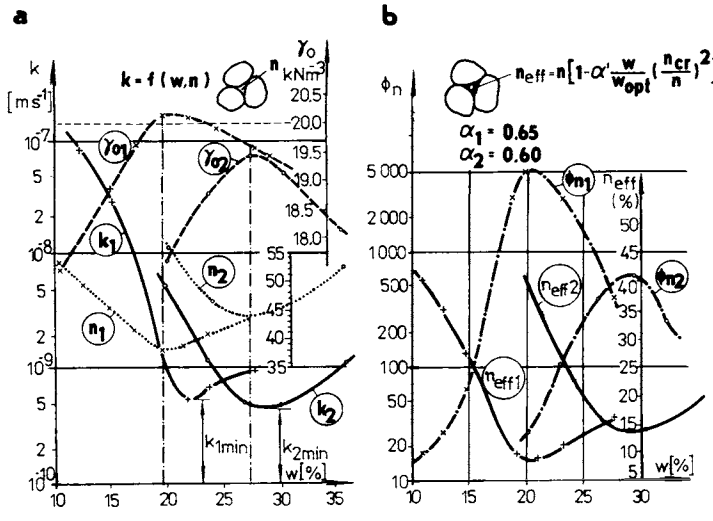

Fig. 1.11. Permeability of partially saturated soils. a — relationship $k = f(w, n)$, permeability, water content and porosity, b — hydraulic resistance Φ_n depending on effective porosity n_{eff} (Peter 1977).

Fig. 1.10. Permeability test data. Soil identification: 1, 2 — compacted caliche, 3 — silty sand, 4 — sandy clay, 5 — beach sand, 6 — compacted Boston blue clay, 7 — Vickburg buckshot clay, 8 — sandy clay, 9 — silt Boston, 9a — silt Danube, 10 — Ottawa sand, 11 — sand Gaspee Point, 12 — sand Franklin Falls, 13 — sand Scituate, 14 — sand Plum Island, 15 — sand Fort Peck, 15a — sand Danube, 16 — silt Boston, 17 — silt Danube, 18 — loess, 19 — lean clay, 20 — sand Union Falls, 21 — silt North Carolina, 22 — sand from dyke, 23 — sodium Boston blue clay, 24 — calcium kaolinite, 25 — sodium montmorillonite, 26—30 — sand (dam filter), 31 — sandy gravel Danube, 32 — sandy gravel Váh.

high quality. This does not involve any volume change. It must withstand water action.

The selection of stone aggregate for concrete mixtures can first be done on the canal site. A further survey will also include other localities. The basic task of technological research consists in securing sufficient gravel and sand from alluvial deposits, or rock material if necessary. This should be suitable not only from the point of view of strength and resistance, but it should allow suitable workability and minimum cement admixture. This depends not only on the *mineralogical composition*, but also on the *petrographic origin*: grafite, diorite, granodiorite, quartz, aplits, sandstone, etc. are usually preferable, while limestone and shale are not recommended. In Europe, continuous grain-size distribution curves of stone aggregate are in use; sand fractions with grain size $d = 0.1$—2 (4) mm and gravels of size $d = 4$—8, 8—16, 16—32 and 32—63 mm.

Many *types of ingredients* for which render concrete mixtures plastic can be added in amounts of 0.2 to 0.5% of the weight of cement. In most countries, composition of mixtures and ingredients are designated in Standards — as a basic prescription which should be kept. The concrete sealing manufactured thus has a coefficient of permeability $k = 10^{-10}$—10^{-8} m s^{-1}.

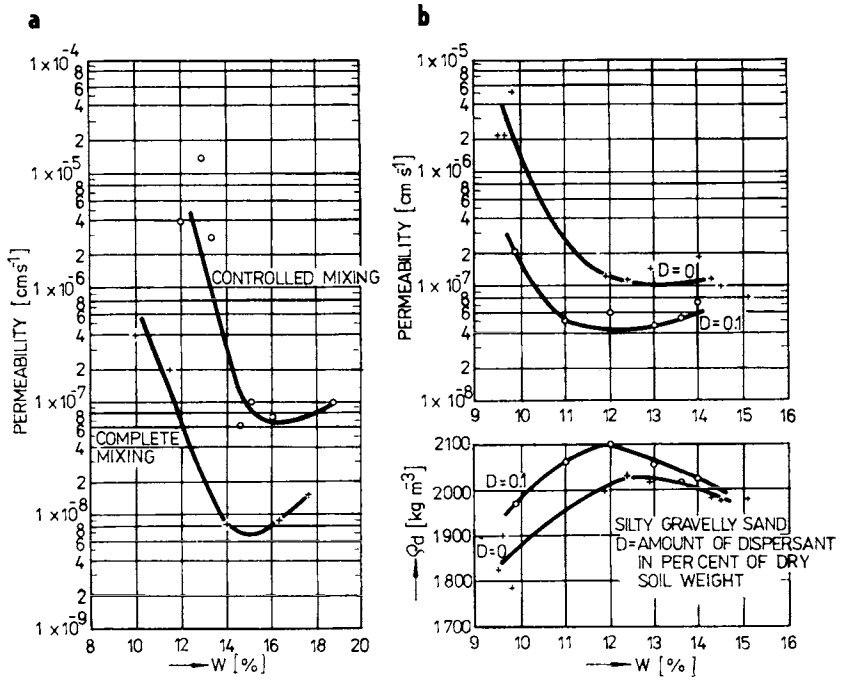

Fig. 1.12. Effect of water content and structure on permeability. a — effect of mixing on permeability, b — effect of dispersion (D) on permeability (from Lambe and Whitman 1969).

Reinforced concrete facing slabs of a size $4.0 \times 4.0/0.08$ m up to $4.0 \times 10.0/0.10$ m are themselves practically impermeable ($k = 10^{-10}$ m s^{-1}), but their chinks are very often sources of leakage: thus it is necessary to reckon on a value of $k = 10^{-8}$—10^{-7} m s^{-1} over the whole surface of the canal lining (see Chapters 2 and 4).

Asphaltic concrete has a good availability as a deck (facing) material. Experience of placing asphaltic concrete canal facing was good ten years ago, at which time good quality of such 6—15 cm thick decks and lower costs were recorded. Maintenance under wind-wave action, rapid drawdown, is referred to by Geier and Morrison (1968). It allowed repair of cracks and cavities which might occur during operation. Eventually, some surface treatment, replacement of oxidized and volatile constituents is also possible. These advantages are not true of cement concrete, whose cracks and surface faults are not so easy removed.

In spite of these favourable characteristics, there are a number of questions that have to be resolved before the final adoption of concrete material. Among these are *durability and watertightness*; effect of freezing and sunshine; behaviour of the material on steep slopes at the temperatures expected. Usually, the bitumen and aggregates chosen are subjected to experimental work in a Bitumen Laboratory.

Usually the *amount of asphalt* used in the design is a mixture of 7.0 to 8.5% of the combined weight of the dried aggregates and filler. If the choice is possible, the requirement is met, that the asphalt is to be a product of the refining of crude petroleum by either steam or vacuum distillation with no air blown, catalytically blown, solvent-extracted or cracked asphalt is permitted. Further specifications are found in the following literature: Kratochvíl (1965), Striegler and Werner (1969), and in Section 5.5.

A basic general condition of a good asphaltic concrete is *good compaction*, minimum of *pore volume* (not more than 3%); it has to have a coefficient of permeability more than $k = 10^{-9}$ m s^{-1}. In the laboratory we measure $k = 10^{-13}$ to 10^{-10} m s^{-1}, but in the actual concrete it is always less.

Such an *asphaltic lining* (Fig. 1.13) consists of two asphalt concrete layers, connecting a layer (binder), filter layer (sand, gravel), and base layer (gravel). In the last ten years, geotextile in the role of filters and sub-base of coatings are in use, with any advantages. The slope of such lining can be 1 : 1.8 to 1 : 2.5, and with a thickness $t = 12$—35 cm for canal dams of 6—30 m height. The pavement of dams can also be replaced by asphaltic concrete, bituminous layer and geotextile on the downstream site.

Sealing tape and synthetic plastics are watertight and in this way convenient for sealing, but their fragility is a problem. The fragility and resistance to damage goes down with a reduction in temperature. Thus they must be protected from harmful work and animals by an earthen layer or concrete (see Chapter 5). The protecting layer of earth should be 0.30—0.95 m thick or, that of concrete 0.10—0.35 m thick. *Watertight synthetics* have some advantageous properties also, i.e. a great

elasticity and extensibility which is favourable in cases where the embankment has to be built on a compressible, weak foundation.

Kézdi (1976) commented on two kinds of watertight synthetics to be used as sealing material; one polyvinylchloride (PVC) and the other polyethylene (PE).

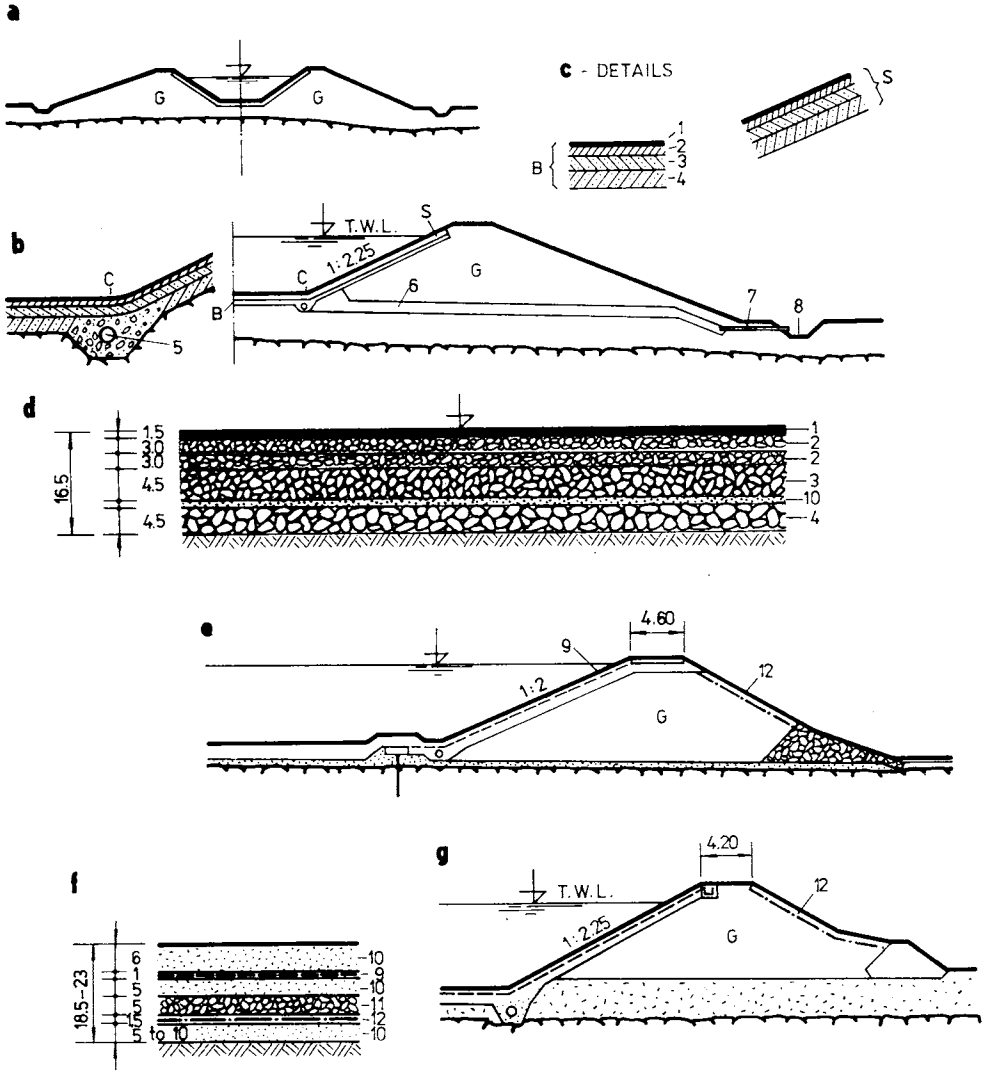

Fig. 1.13. Sealing apron. a — canal embankment and sealing, b — upstream and bottom sealing with drainage, c — bottom and slope details, d — asphalt-concrete layers on the bottom, e — sealing fail, f — details of the bottom, g — fail protecting slope and the bottom; 1 — watertight layer, 2 — bituminous lining, 3 — asphalt concrete, 4 — concrete, 5 — drainage pipe, 6 — gravel, 7 — pipe, 8 — ditch, 9 — watertight (plastic) foil, 10 — sand, 11 — gravel layer, 12 — textile fabric.

Table 1.4 provided a summary of data that can be used in the preliminary design of a watertight membrane.

It is necessary in general to *protect the plastic synthetic membrane by sand* or silty soils which have friction angles $\Phi = 35—40°$ and 19—25°, respectively. For the stability of the sealing, the friction angle between the synthetic and that of the soil (ϑ) is critical and has a value of $\vartheta = 13°30'—24°$. From this fact, it can be concluded that the slope of a dam or levée has to be from 1 in 2.5 to 1 in 4.5, otherwise it is necessary to step at the slope. In the sixties in Czechoslovakia, an attempt was made with synthetic plastic (PVC) at laying it out between two twiddle-shaped concrete slabs as a protecting lining (see Section 5.4). In the last decade, we have been able to undertake experimental *construction of lining,* laying it on a rip-rap or gravel layer, which enables us to increase the angle between the sealing and protective layer to $\vartheta = 25—30°$. In this way, an economy of earthwork can be reached (Sembenelli 1976).

Table 1.4. Data for preliminary design of watertight membranes

Classification	γ [kN m^{-3}]	E [MPa]	Maximal stress, σ [kPa]	Extensibility [%]	Temperature resistance [°C]	Melting point [°C]
Hard PVC	13.8	3.0	55.0	60	60—70	120—150
Soft PVC	9.0	1.1	35.0	650	150	162—167
Hard PE	9.6	1.1	27.0	100—1000	125	130—132
Soft PE	9.2	1.1	15.0	300	100	100—110

Synthetic plastics have many advantages derived from their watertightness and low price, but also some disadvantages, namely their vulnerability — they are easily damaged by man and animals, usually in the dry seasons, which create the prominent problems.

Paccard (1977) has suggested, by using *thin membranes placed on concrete,* an adapted system consisting of a sheet of butyl of 0.75 in thickness, protected on its two faces by a synthetic felt.

In order to be efficient, they must have the following *qualities*:

(1) be *watertight* in the running section and the assemblies;
(2) be sufficiently *resistant to perforation*;
(3) have, on the upper face, *sufficient roughness* to permit the casting, in situ, of the concrete on a slope. This condition does not apply in the case of use of prefabricated blocks, although, in such a case, this surface roughness might facilitate the laying of the blocks;
(4) have characteristics of *friction* (or adhesion) on the support, elongation, tensile strength and creep resistance so that they withstand the opening of a crack in the support;
(5) have *sufficient elongation* to be able to accept, at least temporarily a major

deformation of the foundation, have a minimum life of 40—50 years, taking into account the existing environment.

The membrane laps are performed by a hot-vulcanization process in suitable assemblies. All joints constitute potential weak points, particularly when carried out on the site. Therefore, it would seem to be desirable to produce panels of a large area at the works. However, the prefabrication of large panels is not possible with thick membranes, because of weight constraints. Sizes 3.0×3.0 m to 4.0×6.0 m seem reasonable. The length of the membranes depends on the nature of materials used and on the conditions of utilization. The most successful experiences are with bituminous products and butyls and similar material (Hypaleon, etc.). Also, we should mention PVC plastic and ethylene compounds (polyethylene and chlorinated polyethylenes) used in East Europe since 1960 — as can be found in the literature (Hobst 1962).

1.6 Choice of Material and Placement

Three kinds of material placing are in use in dam construction: *fill, hydraulic fill* and a combination of these two. The first is characterized by placing and compaction in layers; the second consists of the placing of earth material in the embankment by water, and the third can be used as semihydraulic fill — placement usually by trucks and pumps (by water).

The *fill technique* consists of three different technological processes — extraction, haulage (transport), and lay-out (placing) of earth materials. These three processes have to be closely connected to reach a desirable quality and the best economy of fill. They depend on the mechanism of the climate and other factors decisive for dam construction. Climatic conditions have a much greater influence on the placement of fine-grained soils than of cohesionless material. Sand and gravel consistencies are quite independent of the method of excavation, and success of their use rarely depends on the method of placing — on the water content or intensity of compaction. For the earthfill does not develop excess pore pressures during construction is the main requirement in dam construction.

With *fine-grained soils*, excessive *compressibility combined* with *low permeability*, large drainage depths, high initial water contents and rapid construction leads to pore (water) pressure increase. Experience from Czechoslovakian canal embankments and levées indicates that a coefficient of permeability greater than $k = 5 \times 10^{-6}$ m s^{-1} is required to allow the fill to be "free draining" under the rates of construction encountered. In canal-embankment construction in the Váh valley, sandy gravel traces from the tail-race canal were found below groundwater level as is always the case with excess water. This excess of water was most disadvantageous, because with a permeability of sandy gravel of $k = 5 \times 10^{-5}$ to 3×10^{-3} m s^{-1}, "free draining" ensures that the water from the fill is drained under

gravity. A good compaction of fill was assured. The canal embankments have operated safely for more than thirty years, over a length exceeding 42 km.

On the other hand, in the construction of levées in the Danube valley whose fill consisted mainly of silty sand, the initial water content of excavated material was too low to prevent collapse *settlement* on saturation in some cases. It was necessary to add water to the fill. The same procedure — consisting of water spray when placing the silty material during levée construction (in the valley of Laborec and Latorica) — has been in use in East Slovakia.

Dam construction using fine material is always more difficult. It makes placement in layers and *compaction by rollers* (usually vibrating rollers) more difficult. The cost increases because of the required processing (water addition or water drainage — drying). Many problems may arise in disposing of rejected material.

In the USA and many European countries, the engineers handle the fill in such a manner that a water content (w_n) which is near the value of w_{opt} after the Proctor Standard is obtained. If we have to deal with a fine soil having w_n and w_{opt}, it is necessary to add an amount of water Q_w to every cubic meter of soil — with a unit weight γ_n, which can be calculated from the following formula

$$Q_w = \frac{w_{opt} - w_n}{100 - w_n} \quad [m^3]. \tag{1.23}$$

It is evident that the advantages of homogeneous material (silty soils) can be used by a contractor to a certain extent, where the soil possesses an appropriate water content. This is influenced by climate, mainly the rainy season, which makes the placement of fine material unsuitable. If the period of time convenient for placing is shorter than 80 to 100 days, use of these fine materials (silt, silty clays and clayey material) is not usually an attractive proposition in Europe. This fact represents a serious obstacle to the construction of homogeneous dams and levées which have been built of fine material in the past — mainly at the end of the nineteenth century and in the first half of our century, in nearly all countries.

The advances in soil mechanics over the most recent decades of the twentieth century have allowed the introduction of many *heterogeneous profiles* with many technological advantages in engineering practice, as can be seen on French canal embankments (Construction Industry International, 1977, pp. 48—54).

Another direction taken in engineering practice can be observed *in Holland* in the construction of dams built to protect the land against the sea. The massive profiles (Fig. 1.4) require many million cm^3 of earth to be moved. In these cases the *combination of fill placing* in layers and hydraulic fill came into play. *Semihydraulic fill* proved to be most efficient in canal embankment construction in the Volga basin in the USSR.

In moving earth, technological and mechanical principles together with safety aspects must be borne in mind, mainly in cases where the stability of the structure

may be critical (Fig. 1.14). Such structures must be handled individually with increased care.

In *modern canal-embankment* construction techniques, the main factors decisive for performance and profitability are machines of high efficiency. Modern earth-moving machinery for excavation, haulage and placing of soil materials, ensuring high rates of dam erection and for relatively low costs, has contributed proportionally to this. Besides, great experience and advances in the field of soil mechanics has also favoured advances in the design and construction of earth-fill dams.

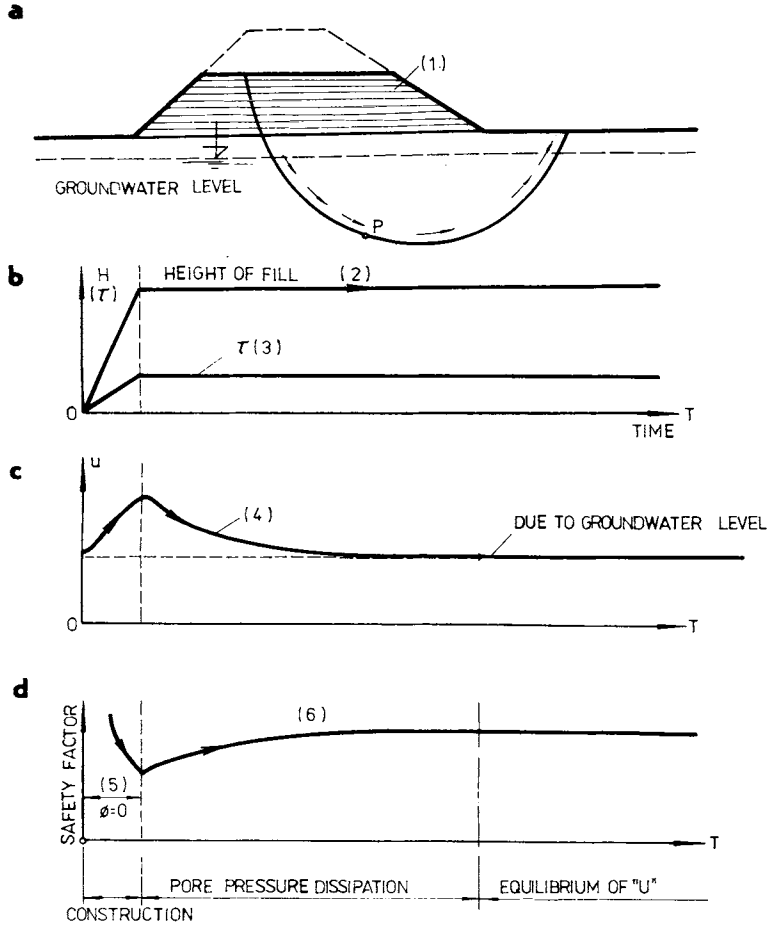

Fig. 1.14. Changes in shear stress, pore pressure and safety factor (from Bishop and Bierrum 1960). a — dam erection, b — increase in dam height (1) and shear-strength increase (2), c — pore-pressure (u) changes (3), d — safety factor with time; 1 — embankment, 2 — height of dam, 3 — shear stress, 4 — pore pressure at point P, 5 — region of small friction ($\Phi = 0$, method applicable), 6 — factor of safety against foundation failure ($\bar{c}$, $\bar{\Phi}$, method applicable).

Erection of such large earthworks such as all "dykes" in Holland, the canal embankments of the Donzère—Mondragon scheme in France, the Danube scheme in Czechoslovakia, the Volga—Don scheme in the Soviet Union or the Bijas Sutlej scheme in India favours further progress in dam-construction techniques with all its advantages.

One of the most important advantages of the earth-fill dams built recently, is the utilization of the material properties — as shown in Fig. 1.8, which represents tions. In constructing the Verkhne Tuĭomskaya dam in the USSR, all embankment material was taken from the canal and underground excavations (Gaziev 1977).

It is a point of great interest that soils previously considered to be unsuitable for incorporation into earth dams on account of their physical and mechanical properties, can now be used. Widening the varieties of soil and rock materials suitable for the construction of dams, allows for economical construction of earth dams in any region in Europe, Asia and America.

At present, practically every kind of soil material can be used, but only in cases where their use assures safety of the structure and justifies the costs, and provided that properties of the material such as shear strength and bearing capacity are not reduced when the structure is in service. The skill of the designer lies in ensuring the reliability and safety of structures erected from such poor-quality soils. This can be achieved first of all by zoning the dam on its cross-section, that is, by a distribution of materials in the dam cross-section which will afford the best utilization of the material properties — as shown in Fig. 1.8, which represents a cross-section of canal dams erected in France in the Seine and Rhône valleys in recent years.

Both laboratory studies and compaction of test fills on a large scale precede the choice of optimum characteristics of embankments made of poor-quality rocks or boulders. The design density of an embankment of low-quality fill material compacted by vibrating rollers has been achieved on most dam projects with a thickness of compacted layer of about 1.0 m. In such a way, it is possible to erect a fill made of gravel and boulder soils.

The use of poor-quality soils for *antiseepage measures* in dams was attempted in the interim period, between the First and Second World Wars, erecting the embankments for the "Bielomorskoĭ kanal". During the last few years, poor-quality soils have found wide application, despite the fact that such soils with higher moisture content involve serious difficulties in their placement and compaction.

Soil filling directly into water is a good method for placing such soils. It can be used most efficiently with soils which are relative easily dewatered, for example, if the permeability coefficient $k = 1 \times 10^{-6}$ m s^{-1}. Engineering practice in the USSR shows that, in these soils, the pore pressure (u) diminishes at the moment the construction loading reaches 20 to 30% of the total pressure (σ).

Another method of *placing overmoistened soils* is to lay such soils in thin layers with slight compaction, usually performed with the help of tractors, followed by

consolidation of the fill under the action of the soil. This method has found its application not only in the USA, but also in the USSR, Poland, Czechoslovakia, and mainly in Scandinavian countries where the use of overmoistened organic soils with low clay content for dam cores offers a number of advantages. This method allows the builders to place the soils during rainy seasons. It is mainly suitable in the *construction of levées* and small dams where the disadvantages of a fill density lower than usual have significant influence on the quality, because as the load proceeds, the Proctor density increases up to 95—98%. Dam-body settlement with this method is higher than that of dams compacted with the help of rollers. However, the soil consolidates during the course of dam construction.

This method of placing *overmoistened organic soils* or materials from excavations required for canals is very economic, but needs more quality control. In European countries, these procedures are connected with a growing use of synthetic membranes as impermeable liners or barriers, in earth dams. These are under test in many laboratories (Sembenelli 1976).

1.7 Laboratory Tests, Field Trials and Control

In dam and levées construction, it is always necessary to make use of the testing of materials and field properties in making the principal decisions and to design the structure. Field testings are preferred to laboratory tests. In alluvial deposits, the time and scale effect must be observed, as well as many differences and discrepancies from the theory, used in calculation (Cambefort 1972).

For example, the coefficient of permeability can be determined in three ways: by *field tests*, by *laboratory tests* on soil samples and from *empirical formulae*. All these methods have as their appropriate field test for evaluation of soil permeability a *pumping test*, which consists of pumping water (at a rate q) from a well and evaluating soil permeability (coefficient of permeability k) from observation of the resulting drawdown surface (Fig. 1.15). The test is carried out using many observation bore holes (piezometers), which enable us to observe the groundwater level at a distance x from the well axis.

Theoretical investigation and calculations are based on the *Dupuit assumptions* as follows.

(1) The water-bearing *stratum is homogeneous*, horizontal and of constant thickness.
(2) The water table is of infinite extent in the *horizontal* direction.
(3) The test well is a *perfect well*. This means that it extends to the bottom of the permeable stratum and is perforated over the section below the water table.
(4) In its original state the *groundwater is at rest*, and there is no flow into or out of the system during the test.

The radial flowing water takes on a curved surface called a drawdown surface at a height h_0 in the well, and z at a distance x from the axis of the well, which has a diameter $2r_0$. In such a case, we can obtain the values enabling us to calculate the coefficient of permeability from the *Dupuit formula*

$$k = \frac{q}{\pi} \frac{\ln x - \ln r_0}{z^2 - h_0^2} . \tag{1.24a}$$

In the vicinity of even the best well, the drawdown surface differs from that assumed by Dupuit, which is why it is more practical to calculate the value of k using heights z_1 and z_2 observed in observation wells (Fig. 1.15) located at some

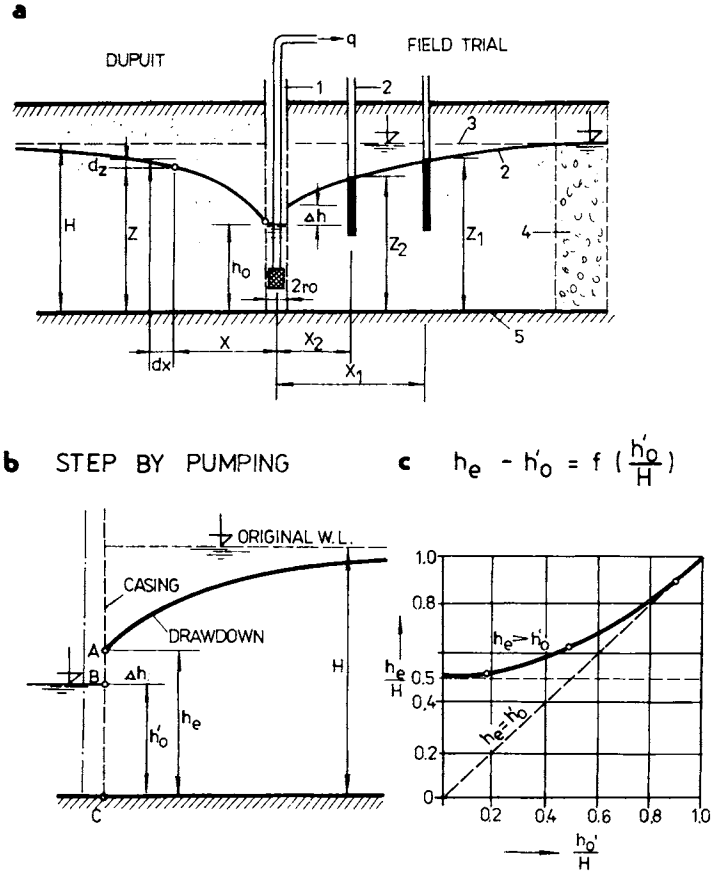

Fig. 1.15. Determination of q and k by means of pumping. a — establishment of the pump and piezometers, b — step by pumping, c — dependence of the step on water height h_0'; 1 — the well, 2 — observation tube (piezometer), 3 — original groundwater table, 4 — permeable layer, 5 — impervious layer.

large distances x_1 and x_2. In this sort of case, we determine the coefficient of permeability k

$$k = \frac{q}{\pi} \frac{\ln x_1 - \ln x_2}{z_1^2 - z_2^2}. \tag{1.24b}$$

The range of applicability of the pumping test can be expressed in terms of k values, approximately 10^{-3}—10^{-6} m s^{-1}. This method is most suitable for sand and sandy gravel. If the permeability of a soil is too low, the flow towards the well is insufficient to permit continuous operation of the pump — one of the fundamental assumptions of the test (Kézdi 1974).

Besides this most extensive field test, many trials can be made at the stage of dam design and preparation of foundation and also dam erection, with the aim of investigating the shear parameters, soil compaction, pore-pressure distribution over the cross-section of the dam, sudden drawdown effect, and wave effect on the embankments of canals, etc. Some of these *trials* help us to choose the most convenient machines and technology, *optimum thickness*, optimum *moisture* content, and *number of passes*, as explained later. Let us now explain some of the most suitable laboratory tests and methods.

Firstly, we shall consider *laboratory methods* serving to determine the coefficient of permeability (k) by a constant-head permeability test. The soil specimen, at the appropriate density, is contained in a perplex cylinder of cross-sectional area A: the specimen rests on a coarse filter or wide mesh. A steady vertical flow of water, under a constant total head, is maintained through the soil and the volume of water flowing per unit time (q) is measured by a stable (constant) hydraulic gradient (H/L) which is used to determine the *coefficient of permeability*

$$k = \frac{qL}{AH} = \frac{q}{AI}. \tag{1.25a}$$

This is in accordance with Darcy's empirical law

$$q = AkI. \tag{1.25b}$$

A series of tests should be run, each at a different flow rate. The water used in the test should be deaired.

For fine-grained soils, the falling-head test should be used, in which the hydraulic gradient changes with changing (falling) head H (from H_1 to H_2) with constant specimen (cylinder) area (A_c) and standpipe area (A_p). The coefficient of permeability (k) can be determined from the formula

$$k = \frac{A_p L}{A_c t_1} \ln \frac{H_1}{H_2} = 2.3 \frac{A_p L}{A_c t_1} \log \frac{H_1}{H_2}, \tag{1.26}$$

if the water level falls from head H_1 to H_2 in time t_1.

The coefficient of permeability (k) of fine-grained soils can also be determined indirectly from the results of consolidation tests (Craig 1974).

On the other hand, the coefficient k of a granular material can be determined from *empirical and experimental formulae* — taking into account the effect of composition of the soil, its porosity, the particle size, effect of structure, grain shape, the fabric-effect of degree of saturation (presence of air) and permeant viscosity (see Section 2.6, and also Lambe and Whitman 1969).

The reliability of the formulae and of permeability determination depends on the agreement of the characteristic with reality, and on the extent to which the test specimens are representative of the in situ soil mass as a whole. For important projects, the *in situ determination of permeability* may be justified.

Other in situ methods include constant-head and variable-head *bore-hole tests.* In one procedure, water is allowed to flow, under constant head, into the stratum under test through the bottom of a bore hole, the sides of which are lined with a pipe casing. In such a case, the flow of water in the horizontal direction is predominant, and horizontal permeability — the coefficient of permeability in the horizontal direction k_h — can be obtained.

Figure 1.16 from Hvorslev (1949) and Lambe and Whitman (1969), respectively, notes a number of arrangements which can be used to measure the permeability of soil in the field by different methods — adopted to measure horizontal (k_h) or vertical (k_v) permeability of the given stratum. The mean coefficient of permeability (k_m) can be determined by appropriate arrangement of the field test (B, C) or calculated by means of k_h and k_v

$$k_m = \sqrt{k_h k_v} .$$

Various *formulae for determination of the permeability of soils* after Hvorslev (1949) are given in Table 1.5. All dimensions of intake (sample) diameter (D), standpipe (d), length (L) and piezometer head (H) are in cm, the time in s, flow of water (v) in cm s^{-1}. Thus the coefficients of permeability, k_h, k_v, k_m (cm s^{-1}) and basic time lag T (s) can be determined by means of a diagram in which the piezometric head H is plotted on a log scale and time t on a linear scale. In this diagram (Lambe and Whitman 1969, p. 285), time $t = T$ for a 0.37 (H) piezometric head. When judging the values of k which can be obtained using the formulae in Table 1.5 and comparing them with k obtained by other laboratory or field tests of indirect calculation, a number of aspects and circumstances must be borne in mind. The young engineer will realize that these values are very different. These differences and discrepancies will be as great as the heterogeneity and faults of soil layer investigated. Stratification of the soil and an uneven distribution of the fine fractions within it influence the value of k and the difference between the horizontal (k_h) and vertical (k_v) permeability of the given stratum. Such effects as those of soil cavities and lack of appropriate compaction can hardly be simulated in normal laboratory testing — using samples of small size. A soil sample has a more

Table 1.5. Formulas for determination of permeability coefficient

Case	Constant head	Variable head	Basic time lag
A	$k_v = \frac{4qL}{\pi D^2 H_c}$	$k_v = \frac{d^2 L}{D^2 (t_2 - t_1)} \ln \frac{H_1}{H_2}$ $k_v = \frac{L}{t_2 - t_1} \ln \frac{H_1}{H_2}$ for $d = D$	$k_v = \frac{d^2 L}{D^2 T}$ $k_v = \frac{L}{T}$ for $d = D$
B	$k_m = \frac{q}{2.0 D H_c}$	$k_m = \frac{\pi d^2}{8D(t_2 - t_1)} \ln \frac{H_1}{H_2}$ $k_m = \frac{\pi D}{8(t_2 - t_1)} \ln \frac{H_1}{H_2}$ for $d = D$	$k_m = \frac{\pi d^2}{8DT}$ $k_m = \frac{\pi D}{8T}$ for $d = D$
C	$k_m = \frac{q}{2.75 D H_c}$	$k_m = \frac{\pi d^2}{11D(t_2 - t_1)} \ln \frac{H_1}{H_2}$ $k_m = \frac{\pi D}{11(t_2 - t_1)} \ln \frac{H_1}{H_2}$ for $d = D$	$k_m = \frac{\pi d^2}{11DT}$ $k_m = \frac{\pi D}{11T}$ for $d = D$
D	$k'_v = \frac{4q\left(\frac{\pi}{8}\frac{k'_v}{k_v}\frac{D}{m} + L\right)}{\pi D^2 H_c}$	$k'_v = \frac{d^2\left(\frac{\pi}{8}\frac{k'_v}{k_v}\frac{D}{m} + L\right)}{D^2(t_2 - t_1)} \ln \frac{H_1}{H_2}$ $k_v = \frac{\frac{\pi}{8}\frac{D}{m} + L}{t_2 - t_1} \ln \frac{H_1}{H_2}$ for $\begin{cases} k'_v = k_v \\ d = D \end{cases}$	$k'_v = \frac{d^2\left(\frac{\pi}{8}\frac{k'_v}{k_v}\frac{D}{m}\right) + L}{D^2 T}$ $k_v = \frac{\frac{\pi}{8}\frac{D}{m} + L}{T}$ for $\begin{cases} k'_v = k_v \\ d = D \end{cases}$

Case	Constant head	Variable head	Basic time lag
E	$k'_v = \dfrac{4q\left(\dfrac{\pi}{11}\dfrac{k'_v}{k_v}\dfrac{D}{m}+L\right)}{\pi D^2 H_c}$	$k'_v = \dfrac{d^2\left(\dfrac{\pi}{11}\dfrac{k'_v}{k_v}\dfrac{D}{m}+L\right)}{D^2(t_2-t_1)}\ln\dfrac{H_1}{H_2}$ $k_v = \dfrac{\dfrac{\pi}{11}\dfrac{D}{m}+L}{t_2-t_1}\ln\dfrac{H_1}{H_2}$ for $\begin{cases}k'_v = k_v\\ d = D\end{cases}$	$k'_v = \dfrac{d^2\dfrac{\pi}{11}\dfrac{k'_v}{k_v}\dfrac{D}{m}+L}{D^2 T}$ $k'_v = \dfrac{\dfrac{\pi}{11}\dfrac{D}{m}+L}{T}$ for $\begin{cases}k'_v = k_v\\ d = D\end{cases}$
F	$k_h = \dfrac{q\ln\left[\dfrac{2mL}{D}+\sqrt{1+\left(\dfrac{2mL}{D}\right)^2}\right]}{2\pi L H_c}$	$k_h = \dfrac{d^2\ln\left[\dfrac{2mL}{D}+\sqrt{1+\left(\dfrac{2mL}{D}\right)^2}\right]}{8L(t_2-t_1)}\ln\dfrac{H_1}{H_2}$ $k_h = \dfrac{d^2\ln\dfrac{4mL}{D}}{8L(t_2-t_1)}\ln\dfrac{H_1}{H_2}$ for $\dfrac{2mL}{D}>4$	$k_h = \dfrac{d^2\ln\left[\dfrac{2mL}{D}+\sqrt{1+\left(\dfrac{2mL}{D}\right)^2}\right]}{8LT}$ $k_h = \dfrac{d^2\ln\left(\dfrac{4mL}{D}\right)}{8LT}$ for $\dfrac{2mL}{D}>4$
G	$k_h = \dfrac{q\ln\left[\dfrac{mL}{D}+\sqrt{1+\left(\dfrac{mL}{D}\right)^2}\right]}{2\pi L H_c}$	$k_h = \dfrac{d^2\ln\left[\dfrac{mL}{D}+\sqrt{1+\left(\dfrac{mL}{D}\right)^2}\right]}{8L(t_2-t_1)}\ln\dfrac{H_1}{H_2}$ $k_h = \dfrac{d^2\ln\left(\dfrac{2mL}{D}\right)}{8L(t_2-t_1)}\ln\dfrac{H_1}{H_2}$ for $\dfrac{mL}{D}>4$	$k_h = \dfrac{d^2\ln\left[\dfrac{mL}{D}+\sqrt{1+\left(\dfrac{mL}{D}\right)^2}\right]}{8LT}$ $k_h = \dfrac{d^2\ln\left(\dfrac{2mL}{D}\right)}{8LT}$ for $\dfrac{mL}{D}>4$

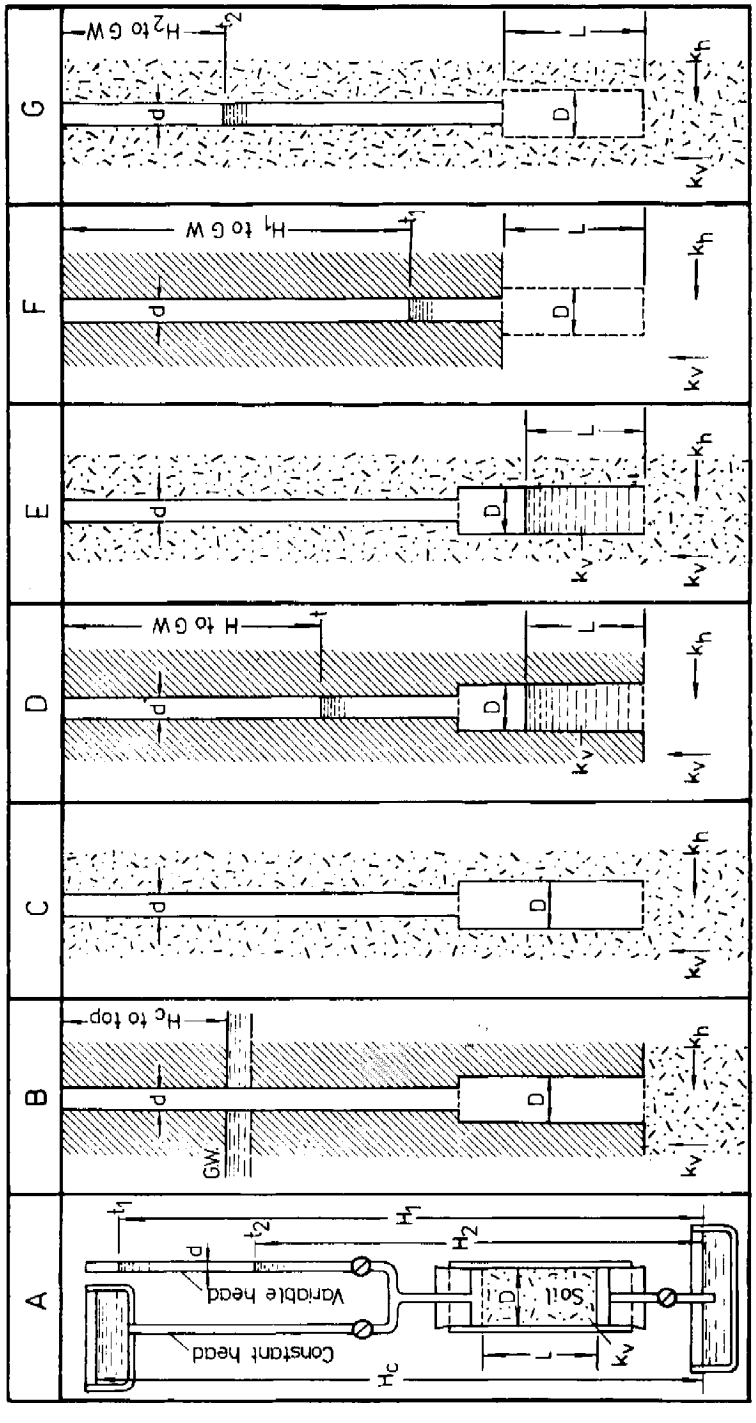

Fig. 1.16. Arrangement of tests for determination of permeability after Hvorslev (1951). A — laboratory test (constant head and variable head), field tests: B — flush bottom at impervious boundary, C — flush bottom in uniform soil, D — soil in casing at impervious boundary, E — casing in uniform soil, F — well point — filter at impervious boundary, G — well point — filter in uniform soil.

homogeneous character than actual soil, and the flow direction should not be a deciding factor for the value of k (Boreli 1978, Dracos 1978).

The importance of the scale effect was emphasized in several papers presented to the IAIRH in Thessaloniki in 1978, where the microscopic, macroscopic and megascopic scale influences were analysed. A definition of the Representative Elementary Volume was given in connection with the flow domain (Bear 1978).

A special case is that of a layered stratum (Fig. 1.17) where many different values of k can be obtained depending on method and scale used. In general, the lowest-value result from laboratory tests (principal directions — inhomogeneity neglected) is used. Pumping tests often reveal these directions. In territory with many piping phenomena, the greatest value of k (calculated from seepage losses) can be obtained. In this way with laboratory testing, the permeability of heterogeneous soil will be underestimated. In cases of major importance, therefore, the coefficient of permeability should be determined by a suitable in situ test.

In the last twenty years, various *isotope methods* for the determination of the basic soil and hydrological characteristics of the dam subsoil and dam body were established. They are used as tracing methods using ^{131}I or ^{24}Na, ^{60}Co, ^{82}Br, ^{32}P and ^{3}H. The samples of tracers (used to count γ-rays or other radiation) in bottles are measured with a conventional scintillation counter or Geiger counter. A Gei-

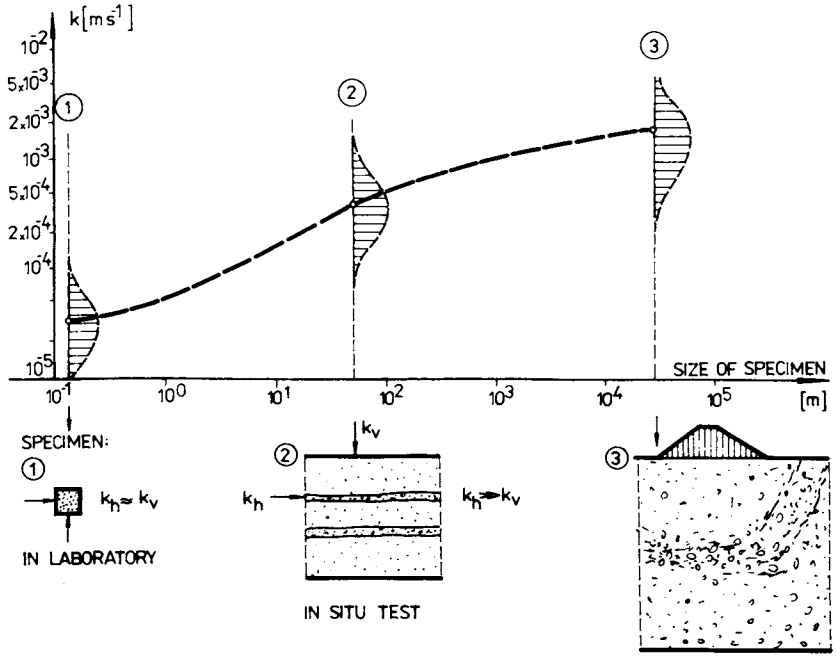

Fig. 1.17. Scale effect in permeability test. 1 — laboratory specimen, 2 — heterogeneous couche in the field, 3 — sub-base in nature (with cracks and faults).

ger—Müller detector can be put in the well as an underwater detector in the one-well technique described in many articles of the Proceedings of Radioisotopes in Hydrology (IAEA, Tokyo—Vienna, 1963).

In the use of the one-well method in a bore hole of diameter d, with a water height h, if a nuclear counter counts an impulse number N_0 at the beginning and N counts during a period t, then from a coefficient of drainage α, the seepage (macroscopic Darcian) velocity v_f can be calculated using the formula

$$v_f = \frac{\pi d^2 h}{4dhat} \ln \frac{N_0}{N} = \frac{\pi d}{4at} \ln \frac{N_0}{N}. \tag{1.27}$$

Groundwater movement can be investigated by three methods: pulse-tracing method, controlled injections or non-controlled artificial injections. The use of isotopes for porosity, permeability, density, direction of flow, velocity of flow, hydraulic-head distribution, storavity in confined aquifer determination is mentioned by Harpaz et al. (1963). Heterogeneous permeability distribution can also be measured by means of radioactive tracers (Nelson and Reisenauer 1963).

Besides permeability measurement, *pore water-pressure measurement* is of great importance in dam design. It enables us to express strain-stress conditions and stability in terms of effective stress. Pore water pressure must be measured under conditions of no flow (either out of or into the specimen). It is recorded using a pressure gauge and manometer. Any change in pore water presssure in the specimen causes a movement of the mercury level in the indicator. The balancing pressure, which equals the pore water pressure in the specimen, is recorded by the pressure gauge or the manometer.

The most frequently used apparatus for pore water-pressure measurement is the triaxial apparatus, which is used to measure shear strength under failure conditions.

Resistance of a soil to failure in shear connected with stability of soil masses, can be investigated in the laboratory or field.

The *shear-strength parameters* for a particular soil can be determined by means of the direct shear test and by the triaxial test. In a shear box, a vertical force (N) is applied to the specimen through a loading plate, and shear stress is gradually applied on a horizontal plane, causing the two halves of the box to move relative to each other, the shear force (T) being measured together with the corresponding shear displacement (ε). The change in thickness (Δh) of the specimen is also measured. The shear stress at failure — using three or more specimens of the soil — is plotted against the normal stress for each test. The shear-strength parameters (cohesion c and angle of shearing resistance τ) are obtained from the best-line fit of the plotted points.

Direct *shear-test results* for sands are represented in Fig. 1.18, showing the difference in behaviour between dense and loose sands. The first shows the dilatancy, the second the contractancy. The sand specimen is said to be at the

critical void ratio if its volume remains unchanged during the shearing process. The shear strength (τ) can be expressed by the simple *Coulomb equation*

$$\tau_f = \sigma_f \tan \Phi \tag{1.28}$$

for cohesionless soils and for cohesion soils by

$$\tau_f = c + \sigma_f \tan \Phi \tag{1.29a}$$

or

$$\tau_f' = c' + \sigma_f' \tan \Phi', \tag{1.29b}$$

if effective shear-strength parameters (c', Φ', σ_f') are used. For fine-grained soils, the triaxial apparatus gives the most reliable values of parameters for engineering practice (Lambe and Whitman 1969). If a dam of cohesive soil is to be constructed, the shear-strength parameters have to be chosen carefully with regard to the conditions in which the structure is to be built and operate.

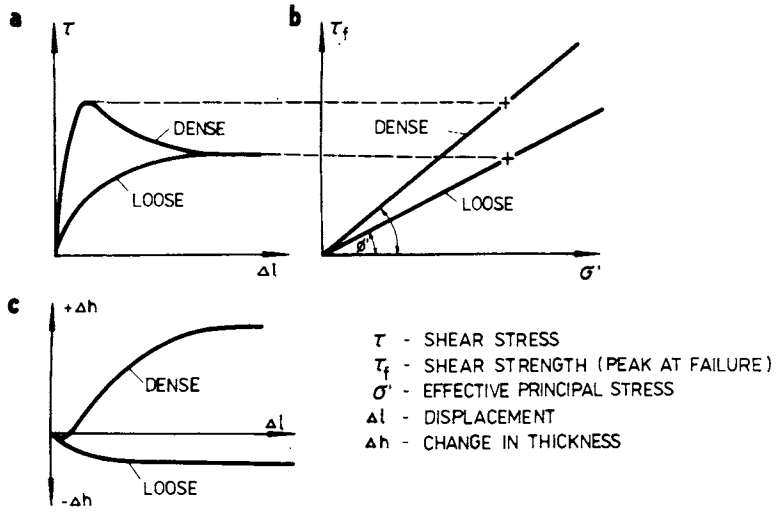

Fig. 1.18. Direct shear-test results for sand. a — relationship between shear stress (τ) and shear displacement (Δl), b — failure envelopes, c — change in specimen thickness.

If sands and gravels are under consideration, values of the *shear-strength parameter* Φ' from Table 1.6 can be used as a basis for calculation.

Table 1.7 provides a summary of data that can be used for preliminary design. However, for final design of an embankment, the actual soil should be tested using the void ratio and stress system with loading conditions and other parameters found in the field. Also important are the composition of materials to be used in man-made fills, the smoothness of the surface, the atmosphere, the water content and the change of water level.

Table 1.6. Friction angle data for sand, gravel and silt

Soil description	Friction angles	
	Loose soil	Dense soil
Uniform sand, rounded particles	27°	35°
Well-graded sand, angular particles	33°	45°
Sandy gravel	35°	50°
Silty sand	(27—30°)	(30—40°)

Table 1.7. Summary of friction-angle data for use in preliminary design

Classification[1]	Friction angles							
	Slope[3] angle of repose		Ultimate strength		Peak strength			
					Medium dense		Dense	
	α	Vert. to hor.	Φ_{cv}[1]	tan Φ_{cv}	Φ	tan Φ	Φ	tan Φ
Silt (non-plastic)	26°	1 on 2	26°	0,488	28°	0.532	30°	0.577
	30°	1 on 1.75	30°	0.577	32°	0.625	34°	0.675
Uniform fine to	26°	1 on 2	26°	0.488	30°	0.577	32°	0.625
medium sand	30°	1 on 1.75	30°	0.577	34°	0.675	36°	0.726
Well-graded sand	30°	1 on 1.75	30°	0.577	34°	0.675	38°	0.781
	34°	1 on 1.50	34°	0.675	40°	0.839	46°	1.030
Sand and gravel	32°	1 on 1.60	32°	0.625	36°	0.726	40°	0.900
	36°	1 on 1.40	36°	0.726	42°	0.900	48°	1.110

According to Lambe (1960) — from B. K. Hough, Basic Soil Engineering. New York, 1957.

[1] Φ_{cv} — angle of shearing resistance (Φ) at constant volume.

[2] Within each range, assign lower values if particles are well rounded or if there is significant soft shale or mica content; higher values for hard, angular particles. Lower values for high normal pressures than for moderate normal pressure were used.

[3] The slopes of canal dams are 1 on 1.50 to 1 on 3.50, and those of levées are even flatter, 1 on 2.00 (3.50) for small levées and usually 1 on 2.00 to 1 on 5 for bigger structures.

The degree of compaction of a soil is measured in terms of dry density, i.e. the mass of solids only per unit volume of soil. The dry density after compaction depends on the type of soil, the water content and the work done by the compaction equipment.

The *compaction characteristics* of a soil can be assessed by means of standard laboratory tests. In general use are in Czechoslovakia, CSN 72 1015, 73 6850 and in Great Britain, BS 1377. In the *standard* (Proctor) test, the volume of the mould is 9.44×10^{-4} m^3 and the soil (free of all particles larger than 20 mm) is compacted by a rammer consisting of a 2.5 kg mass falling freely through 305 mm, the soil is compacted in three equal layers, each layer receiving 25 blows with the rammer. In the *heavy* (Proctor modified) test, the mould is the same as that used in the

standard test, but the rammer consists of a 4.5 kg mass falling through 458 mm. In the *vibrating hammer test,* a vibrating hammer compacts three layers (the volume of the mould is 2.31×10^{-3} m^3) for a period of 60 s each. The process is repeated at least five times with varying water content (w). Each time, the dry density (ϱ_d) of the soil is determined. The result of the test is plotted (Fig. 1.19), and so the *optimum water content* (w_{opt}) can be deduced, as the water content at which a maximum value of dry density (ϱ_d) is obtained (Fig. 1.19a).

The saturation dry density ("zero air voids") can be calculated from the expression

$$\varrho_d = \frac{G_s}{1 + wG_s} \varrho_w. \tag{1.30}$$

In general, the dry density after compaction at water content w to an air content A, can be calculated from the following expression

$$\varrho_d = \frac{G_s(1 - A)}{1 + wG_s} \varrho_w. \tag{1.31}$$

The calculated relationship between the zero-air-voids dry density and water content (for $G_s = 2.65$) is shown in Fig. 1.19b. It shows that the "heavy" test gives a lower value of w_{opt} than the "standard" test. For this reason, optimum water content is relative. It differs mainly in relation to compactive effort, depending on soil type (Fig. 1.19c). In practice, w_{opt} usually varies from $w_{opt} = 8$—28%.

Laboratory compaction tests are not directly applicable to field compaction, since the compactive efforts in the laboratory tests are different from those produced by field equipment. Further, the laboratory tests are carried out only on material smaller than either 20 or 40 mm size. The main value of laboratory tests is in the classification and selection of soils for use in fills and embankments. The dry density achieved after field compaction is defined as the relative compaction of 92—98% of the maximum dry density of the "Proctor standard" (Striegler and Werner 1969). In addition, water-content limits (w) have to be specified in relation to the natural water content. The average natural water content must be measured below the top 0.5 to 2.0 m (usually 1.0 m) of unexcavated soil, provided that the soil at this depth is above the water table.

For major projects, field *compaction trials* should be carried out to determine the best compaction procedure. The performance of different types of field compaction equipment on different soils has been investigated. In the preliminary planning of the Danube canal embankments, many field tests were made (Fig. 1.20). The first (1964—1965) was a combination embankment test. The trial platform was 20.0 m wide and nearly 120 m long, with three fields enabling changes in the number of passes. The soil density after 3, 6, 10 (12) passes of the equipment was investigated by means of specimens of various moisture content. It was 4—12% in gravel and sandy soils, 10—21% in loam and 14—27% in silty clay. The soil density and coefficient of permeability were evaluated (Fig. 1.20b).

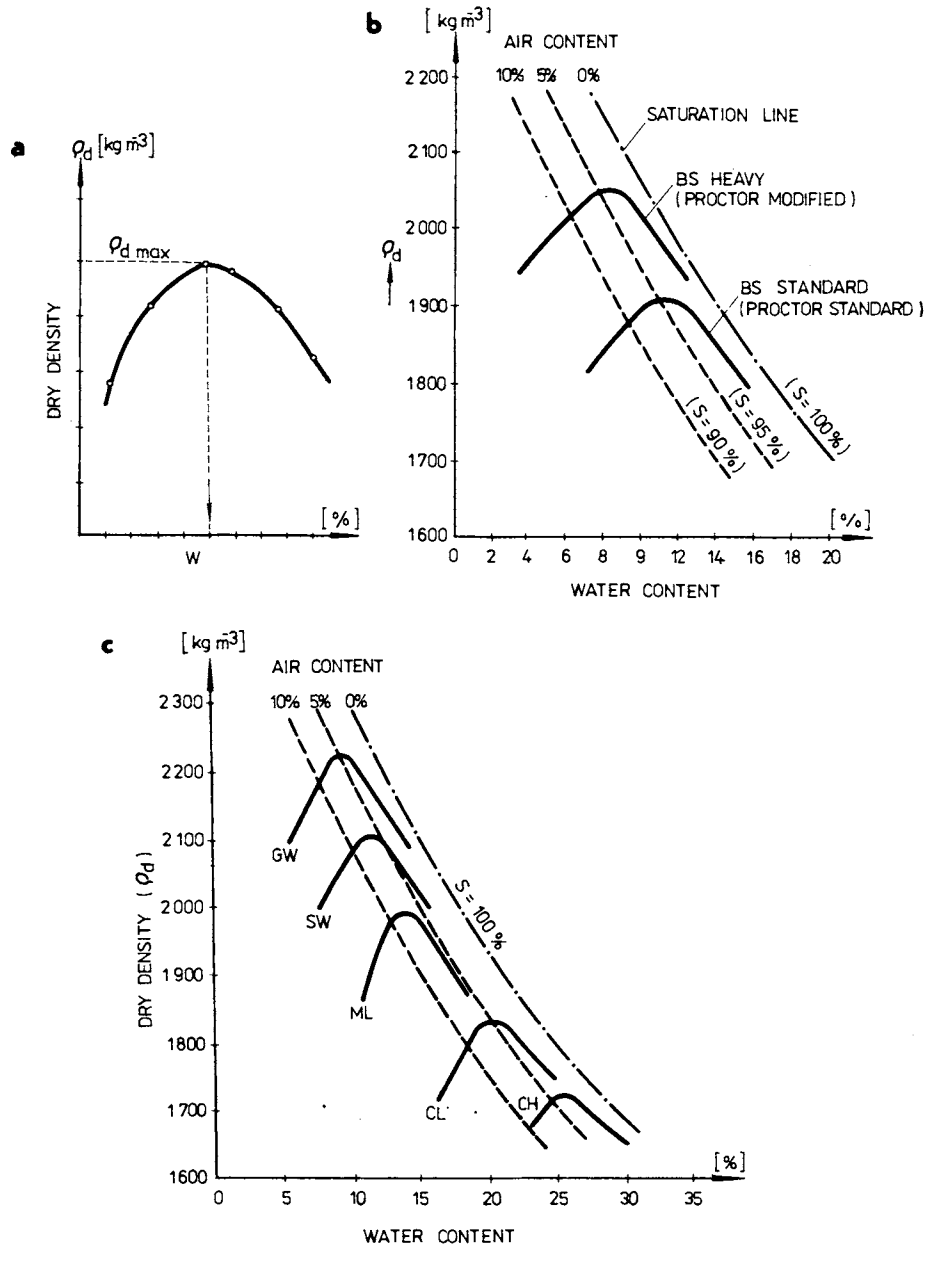

Fig. 1.19. Dry density — water-content curves. a — Proctor standard compaction test results, b — relations $\varrho_d = f(w)$ for different compactive efforts, c — $\varrho_d = f(w)$ for a range of soil types.

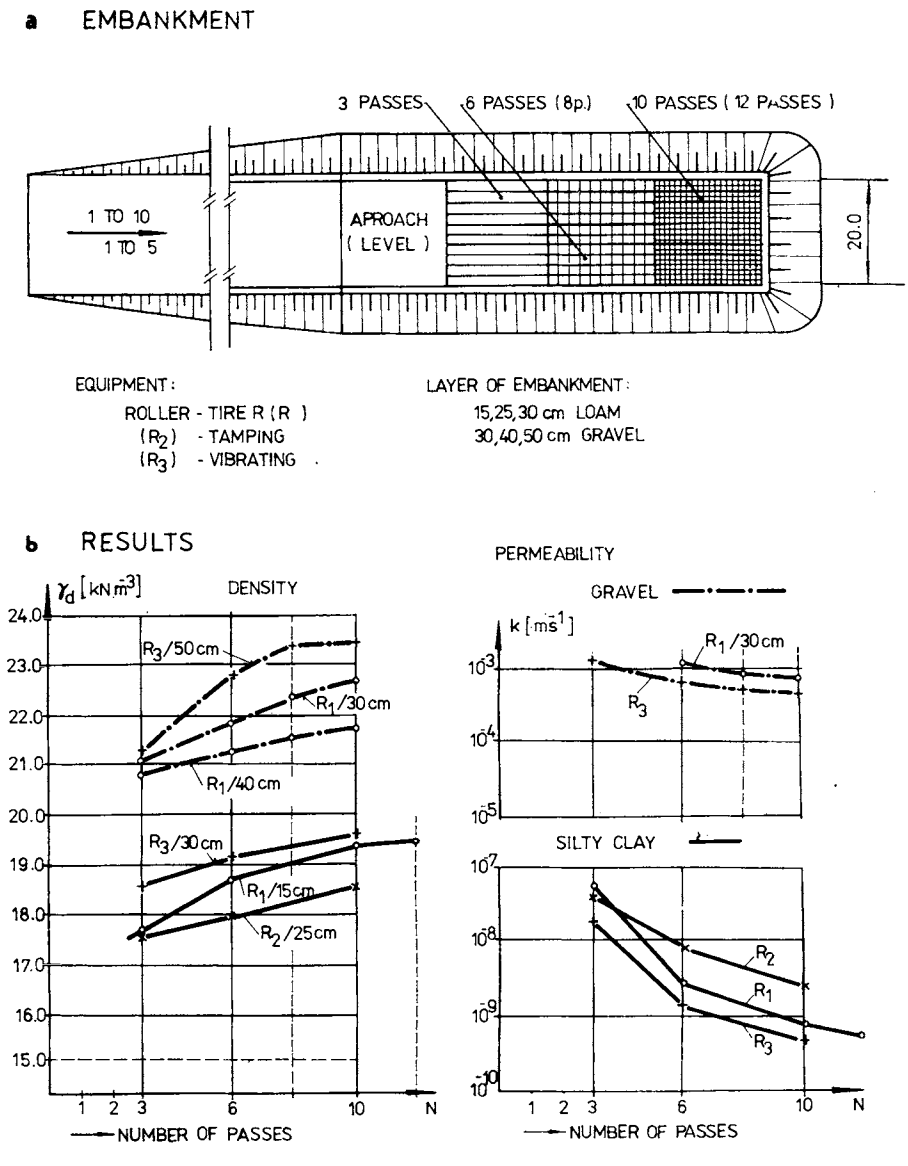

Fig. 1.20. Field embankment test. a — trial silt, b — results in density changes and in changes of permeability coefficient.

The second field tests, performed in 1977 and 1978, were more detailed. They not only had the character of compaction permeability tests, but also stability tests (Fig. 1.21). In the large-scale trial on the line of the channel which needed an embankment, 1 to 4 served as fine-grained soil investigation, 5 for excavation and 6 was a field compaction for gravel and sand. Two basins — divided by a small

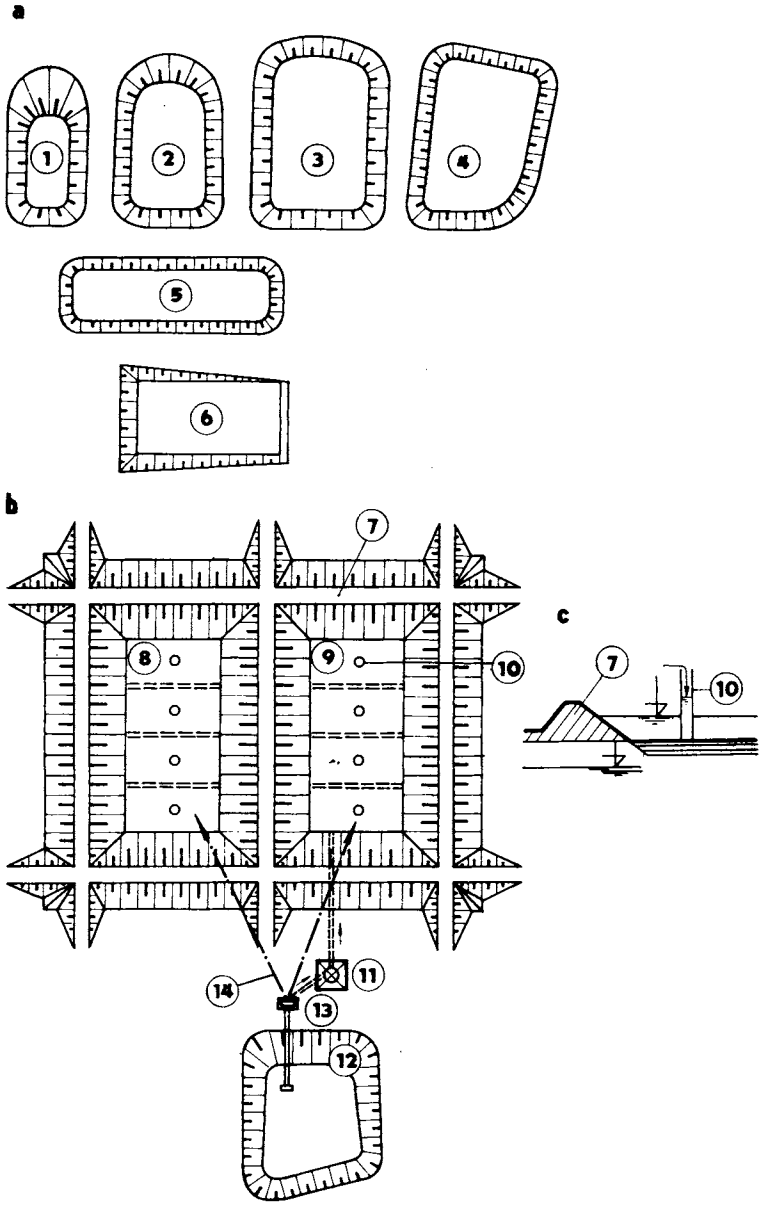

Fig. 1.21. Field tests — the Danube scheme Gabčíkovo. 1—4 — soil tests for fine-grained soils, 5 — gravel excavation, 6 — gravel and sand compaction, 7 — bank bordering the basins, 8 — basin No. 1 (loam in footwall), 9 — basin No. 2 (loam in footwall), 10 — large-dimension casings ∅ 1800 mm, 11 — column, 12 — gravel pit, 13 — pump, 14 — pipeline ∅ 300 mm.

embankment with the bottom covered by sealing soils (silt, silty loam) — were reserved for permeability investigation; critical hydraulic gradient and the conditions of structural collapse were also investigated.

Consolidation tests on large scales are associated with many difficulties. It is very difficult to introduce appropriate boundary conditions in the field. The consolidation curves for various soils can be obtained more easily in the laboratory. Consolidation ratio versus time factor can be evaluated by means of laboratory tests and represented in diagrams for various boundary conditions. The coefficient of consolidation, as an important characteristic, may be calculated with the help of the coefficient of permeability of the soil and its modulus of compressibility, as shown in Chapters 2 and 3.

1.8 Hydraulic Fill Dams

A true hydraulic-fill dam is built by conveying earth materials from the borrow to the embankment as a liquid mixture, and placing them in the embankment using water. This entails continuous pounding.

An alternative to the true *hydraulic fill* is the semihydraulic fill, which has been adopted at some sites where water transportation is not favourable for material transport over longer distances. In this type of construction, transport from the borrow area is accomplished by other means.

A hydraulic-fill dam is composed of silty clay in the core and usually of sands and gravels in the shell. The core material is placed as a muddy mixture which settles out after placement, but if it is of excessively fine — *colloidal material*, it remains in *suspension* for a long time. By contrast, sand and gravel shells tend to stabilize readily and gain strength quickly. In the core, very high pore pressures would be observed over a long period. Thus, hydraulic-fill dams are considered, typically, to have a lower factor of safety during the construction period.

One of the common rules in construction of hydraulic fills has been that the permeability of the shell should by much higher than the permeability of the core. The ratio of these permeabilities has been reported to range up to several hundred times in typical hydraulic fills. In such cases, dams with a slope 1 in 6 to 1 in 4 have been constructed in the Soviet Union on the Volga—Don scheme, and in other schemes in the Volga valley, constructed mainly during the forties and fifties (Popov 1950).

In the Volga—Don canal scheme, the hydraulic fill consisted of sands and sandy soils with effective diameter $d_{\text{eff}} = 0.05$—0.25 mm, which is very suitable for a hydraulic fill. The suspension of such a material can be made very easily. To handle 1 m^3 of sandy deposits and prepare a suspension from it, it is necessary to use between 6 and 15 m^3 of water. Hydraulic transport has economic advantages in energy consumption and in performance. If the conditions of the borrow site,

transport and fill are favourable, some ten thousand m^3 of fill can be achieved.

Good results have been obtained in the Soviet Union, China and the USA, as well as West Europe, mainly Holland, where several million m^3 earth were moved for dyke construction round polders, the bodies of which were filled up with sandy filler.

Considering central Europe, much experience has been gained in FRG and in Poland, while in Austria, Hungary and Czechoslovakia there is little experience in the technology mentioned above. However, experts from the USSR have repeatedly recommended this technology. In these recommendations, the following *advantages* can be seen.

1. *Large volumes* in performance and a great efficiency of machines and transport equipment. Time efficiency extends from 70 to 98% of the working season. The work can proceed in the rainy period, whereas fill in trucks has to stop for several days or even several weeks in autumn — if clay material is used.

2. Hydraulic fill in canal construction requires 0.1—0.2 man-hours per 1 m^3 of material laid out in the embankment; this is nearly half the traditional rate in dam construction.

3. *Energy consumption* is 1.5—4 kWh for sands and for sandy gravel 5—6 kWh, per 1 m^3 of fill. Transport by pumps reduces this still further — in the USSR 3.6—4.8 kWh per 1 m^3 fill.

4. In favourable geological and geographical conditions — a slow slope from the borrow site to the dam — the monetary outlay for hydraulic fill may be a half to a third of the usual amount.

On the other hand, many *disadvantages* have been cited for hydraulic and semihydraulic fills.

(1) Certain deficiencies in performance, serious *sliding* during construction (Calaveras dam) and after construction (Fort Peck dam).
(2) Many uncertainties in the sealing effect caused by intrusions of sand lenses into the core.
(3) A high content of fine colloidal materials would severely inhibit consolidation — *high pore pressure* leads to soil instability.
(4) Typical damage consists of *cracks* extending longitudinally along the embankment of canals.
(5) Many difficulties arise in changing the placement; the pipeline must be transported, resulting in a great deal of cost and trouble.
(6) *Environmental deficiencies.*
(7) A pronounced effect from *seismic activity* in a hydraulic fill — manifested by cracking or settlements. All these effects can be intensified by liquefaction.

Susceptibility to this is highest in saturated low-density soils with uniform gradation of silt to fine sand. Liquefaction is a potential problem in any embankment, such as a hydraulic fill, which may have continuous layers of such materials. Especially vulnerable are poorly compacted saturated layers near the top of the

dam, where amplitudes of seismic vibration are often largest. This danger was very thoroughly investigated by Napetvaridze (1956) in the USSR and Seed et al. (1973).

It can be said that *hydraulic-fill technology is* a hundred years *old,* having enjoyed its greatest popularity in the USA in the period of the 1930s. In the USSR, its peak was in the 1950s, and in China its popularity remains to this day. In the USA, a massive slide (more than 9 million m^3 fill) on the Fort Peck dam in 1938 ensured that the hydraulic-fill concept came under a cloud of suspicion. A few years later, heavy transport machines and perfect compaction equipment brought the rolled embankment to the fore as a competitive alternative to hydraulic fill. In the Soviet Union, the same process can be observed in the decade from 1950 to 1960.

The popularity of this concept with Chinese designers and contractors can be explained by the lack of heavy machinery and mass-man power.

In the developed countries, we observe from time to time a certain interest from engineers responsible for dam design and construction, towards hydraulic fill under favourable conditions (in Holland and FRG) where appropriate soils (sands) and sufficient water make this technology favourable, and disadvantages such as earthquakes and liquefaction are rare.

To all engineers interested in hydraulic-fill construction and its problems, an excellent review of the subject from Jansen et al. (1976) can be recommended.

1.9 Particular Problems in Canal Embankments and Levées

Changing conditions during operation must be respected many times. As mentioned before, embankments and levées have many common aspects of construction, but the conditions of strain and stresses during operation are quite diverse, especially for levées along a river valley with wide variations in flow and even floods. In many cases, they are in operation for only a few days in a given year, and in some cases go years without operation. The time of operation depends on the rate of flow, the magnitude of flood, the weather and so on. As we mentioned earlier, the properties of some soils change with water content, rate of saturation and climatic conditions. A space and time dependence of soil properties can be observed, and that is why the strain and stress conditions are not always the same in two cases, when the water level in a river is the same. In engineering practice, the stress is related to the water level and case history is neglected.

The *loading conditions* are also related to the rate of flow (Q) of the river, and the loading proposed in the calculation is determined for a flow with a frequency of 1% ($Q_{1\%}$) or 0.1% ($Q_{0.1\%}$) as constant in time. However, fresh hydraulic obstacles, such as bed alterations and new river deposits in the valley can change the flow

conditions quite remarkably. In order to have the same *structural safety* (of the embankment), the engineer has to change the profiles of the levées. Thus, it has been necessary to *change the cross-section* of these structures on the Mississippi River three times in a half century, as reported by Middlebrooks (1953). During the last century (over a period of 80 years), it was necessary to raise the profile of levées on the Danube to a magnitude ten times that built in the end of the nineteenth century (Peter 1977).

Similar evolution can be observed in the changes of profile on other European rivers, in Italy (Po), in France (Rhône), in the USSR (Bug, Emba and Kuban), in Hungary (Danube and Tisa), as can be found in literature (Kézdi 1976, pp. 68—70; World Water, May 1978, pp. 36—38). Probably the most remarkable changes to an embankment are on the rivers Huang Ho and Chang Chiang in the Honan Province of China, where river deposits elevated the river bed some meters above the level of surrounding territory. It became necessary to raise the top of the embankment by more than 10 m in a century.

On the other hand, in FRG — near Karlsruhe, considering construction of levées on the river Rhine, the mechanism for the river changing lies in the deeping of the river bed by erosion leading to a fall in water level of over 7 m in a 100-year period, which has made land protection easier (World Water, May 1978).

When designing a new — more massive — profile for an embankment, the engineer must not forget that in this way he has to adapt to a higher water pressure part of the profile, namely that which is over the territory. In Fig. 1.22a, representing the old and new cross-sections of the levées on the Danube near Palkovičovo (in Czechoslovakia), it is evident that the upper layer of loam (of thickness D) has to sustain nearly twice the load in its new situation (Fig. 1.22b), than was previously the case. If we remember that the quality of the substratum of the structure was downgraded by piping, it is evident that the new protecting line is not adapted to withstand the rising forces of groundwater resulting from the new water level (H_2). The substratum is overcharged.

A similar situation can be cited in canal-embankment construction for a head-race canal on any of the older hydroelectric plants, constructed in the thirties in the Váh valley. The profiles of the new dams are bigger and more massive, and the soil stresses higher than before. In most cases, the character of load has changed. It has the features of a dynamic load — the water level changes more quickly and to a greater extent, caused by a new type of power-house operation having to follow the peak-energy-consumption diagram, and not only basic energy consumption, as was previously necessary — before World War II in Czechoslovakia.

The need for dam and levée reconstruction always poses quite a difficult task for the designer, consisting of the problems of water resources, economy and safety of a structure of unknown quality. The material of the dams is heterogeneous — made up of soil whose quality is often very variable. This material is neither uniformly

compacted, nor in the least uncompacted. In consequence, knowledge of the physical properties of the material of the earthworks is rather limited. There are few methods suitable for determining the maximum and minimum values of strength and permeability properties, which are economically feasible. This uncertainty usually grows as regards the subsoil, which shows a tendency to degradation, as is the case in the alluvial deposits of the Mississippi, Jamuna and Danube valleys, among others. It is very difficult to discover how far the process of degradation is advanced. The most frequent tool giving general information is field investigation by means of piezometers, and now also methods based on the use of radionuclear techniques. Tracer methods are suitable for groundwater investigation; the flow velocity and flow rate can be obtained in this way, while research into soil density by the investigation of the compaction of an earthwork or its subsoil using γ-ray treatment, can be useful.

The inconvenience lying in the poor information about dams and levées, especially for large dams, can be partially overcome by a study of the problems of changes in seepage and uplift, and also other phenomena — observed on large dams (Peter 1976).

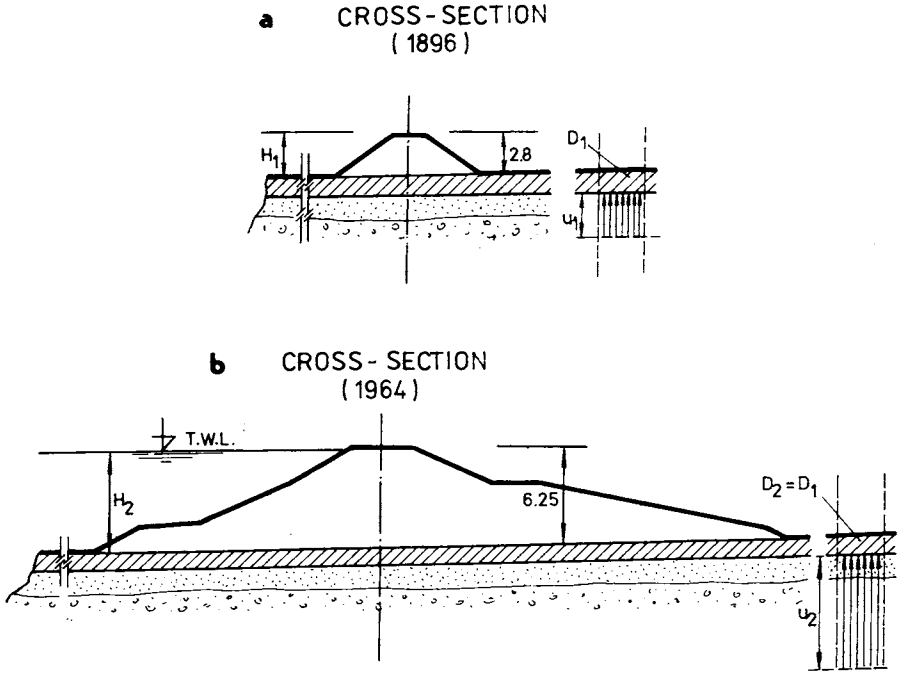

Fig. 1.22. Past and present cross-section of the levées and its loading. H_1, H_2 — water height, U_1, U_2 — uplift pressure.

Unfavourable changes in dams and levées connected with rising hydrodynamic loading can lead to three phenomena:

(a) *liquefaction* — which causes damage mainly in loose sands;
(b) *piping* — in sandy gravel;
(c) *hydraulic fracturing* as a phenomenon connected with the cracking of earth and rock masses.

These cracks, which are very frequent in the homogeneous earthwork of levées built of silts and silty clay, are caused by diminution of water content and shrinkage, or else as a consequence of unequal settlement which is more frequent in canal embankments. In extraordinary cases and with exceptional properties of soil, these cracks and activities may arise as a consequence of soil swelling due to moisture content in combination with a peculiar hydrodynamic loading.

Terzaghi (1948) and Middlebrooks (1948) suggested that dams and levées are menaced by seeping water flowing through the embankment and its subsoil. They divided the failures due to underseepage into three categories:

(a) *rapid discharge* through tunnel-shaped openings in the subsoil of the embankment, preceded by the formation of a large boil or boils on the foreland of the dam, near the toe;
(b) *sloughing* of the downstream slope due to seepage pressure in an upward direction on the underlying soil;
(c) backward *erosion* by springs located at the toe of the embankment.

All the failures mentioned above have some common causes and some common features. They are caused by the rising of water in front of the structure, which leads to *increasing pressures and increasing velocities.* The most dangerous situation is a rapid change of water level, which introduces a wave in the stratified porous medium moving with a varying velocity. In the layer of gravel, which has a greater porosity, the pressure wave reaches furthest in a given time, whilst the overlying layer is still without pressure. In this manner, uplift pressure begins to operate, and involves expansion of the layer and finally induces gradual liquefaction (Fig. 1.23).

The expanded and liquefied layer puts up a decreasing resistance to the water flow which very often changes its original horizontal direction to a vertical one and then breaks through the layer along a shorter course, i.e. a "hydraulic short circuit" originates. The hydraulic gradient increases, and with it the velocity of water flow, which in turn starts to carry away grains of sand through the pores of the gravel skeleton. In this way the second phenomenon "piping" begins. These two phenomena interact with one another. Piping aids the development of liquefaction and vice versa.

A much more detailed analysis of the piping process can be found from Sherard et al. (1973) in connection with the use of dispersive clays having a high liquid limit (most frequently above $w_L = 30—50\%$). These are very common in the USA, and are built-into the levées on the Mississippi River and in arid areas in Australia. In

these cases, a variety of animals such as hamsters are responsible for channeling found in the body of an embankment. This kind of damage must be excluded now from our consideration, which is based on hydraulic laws. It will be mentioned later.

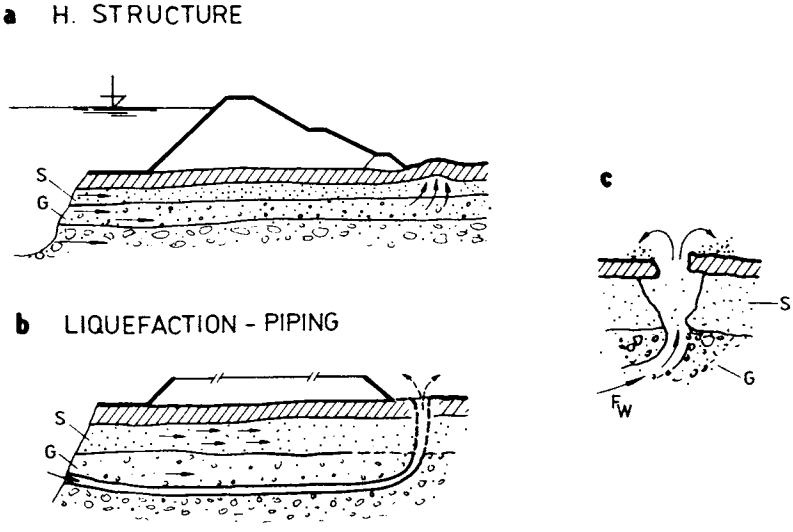

Fig. 1.23. Cross-section of the levées and soil failures. a — hydraulic structure and seepage forces acting on sand (S) and gravel (G) layer in its subsoil, b — gradual liquefaction and channeling in subsoil, c — final soil failure.

Common aspects of hydraulics and soil mechanics should be respected. Seeping water flows through the interconnected pores (characterized by porosity n) between the solid particles [which have a volume $(1-n)$ in unit volume]. In the normal state, total pressure head of water is dissipated as viscous friction producing a frictional drag, acting in the direction of flow, on the solid particles. Seepage forces act on the particles of a soil in addition to gravitational forces (F_g). The combination of these *forces on a soil element* (Fig. 1.24) is called the resultant body force (F_R).

In accordance with this simple connection, the equilibrium of a soil element depends on the density of solid particles (ϱ_s), that of water (ϱ_w), the pressure gradient acting on the solid ($\Delta p/l$) and on the water (H/s). The water moves in the pores of the soil. Its volumetric relation to a unit of soil is expressed by porosity (n) or porosity number $e=n(1-n)^{-1}$, influencing the hydrodynamic force $F_w = e(1+e)^{-1}\,\varrho_w$ grad H. On the other hand, the pressure (F_p) acting on the solid particle can be estimated from the expression: $(1+e)^{-1}$ grad p. Opposing these active forces are resistance forces depending on the magnitude of velocity, grain size, and many other factors — specific surface, shape of grains, shape of pores,

arrangement of grains — very frequently expressed by a global coefficient, the hydraulic friction (f_H), or else the drag coefficient (C_D) if grains in a water stream are being considered.

BOUNDARY AND SEEPAGE FORCES

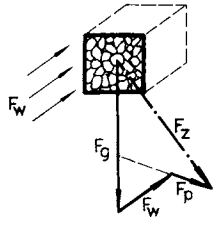

Fig. 1.24. Forces acting on an elementary cube. F_g — gravitational force (acting on an element), F_w — seepage force (acting in pores — n), F_p — pressure force (on soil particles) F_z—resultant body force.

If, as a consequence of exceeding some *critical velocity*, *volume changes* (a low of liquefaction) are to be found, the characteristics mentioned above must be known. To be in a position to determine the typical velocities, the superficial velocity (v_m), the "incipient velocity" (v_0), the flow velocity governing the outflow of solid particles (v_c) and its settling velocity (v_s), some assumption has to be made. The value of the coefficient of hydraulic friction (f_H) depends not only on the flow velocity (v) of water, but also on its viscosity (η), density (ϱ_w), the grain diameter (d_s), shape factor (Φ_s) and other soil characteristics (Peter 1979a).

If we have an expanded sand layer of thickness D_e, its global porosity (n') can be expressed by a relationship

$$n' = 1 - \frac{D_s}{D_e}, \tag{1.32a}$$

where D_s is the thickness of the layer without pores.

Introducing *incipient porosity* n_0 and incipient layer thickness (D_0), we can derive some simple equations for relative porosity (n_r) and D_0:

$$n_r = \frac{n' - n_0}{n - n_0} = \frac{1 - \frac{D_s}{D_e} - 1 - \frac{D_s}{D_0}}{1 - D_s - 1 - \frac{D_s}{D_0}} = \frac{D_e - D_0}{D_e} = 1 - \frac{D_0}{D_e}. \tag{1.32b}$$

In a further step, we can deduce the relationship

$$\frac{n - n_0}{1 - n_0} = \frac{v^{z'} - v_0^{z'}}{v_s^{z'} - v_0^{z'}}; \quad \text{if} \quad z' = \frac{1}{2} \quad \text{and} \quad n_0 = \left(\frac{v_0}{v_s}\right)^{z'}. \tag{1.33}$$

The porosity is a decisive factor for incipient velocity v_0 and is also decisive for the liquefaction of a sand layer. As shown by Beránek and Sokol (1961) or Peter

(1972a), many factors regarding layer stability can be derived from interdependence between porosity (n) and flow velocity (v). The main equation for incipient thickness D_0 of the sand layer in question is

$$D_0 = \frac{D_s}{1-n_0} = \frac{m_c}{\frac{\varrho_s - S_0}{1-n_0}}, \tag{1.34}$$

where m_c is the mass of the given layer, and S_0 is the surface of a pore void which is free for — allowing seepage — water movement. Using Terzaghi's equation for *critical hydraulic gradient*

$$I_{cr} = \frac{(1-n_0)(\varrho_s - \varrho_w)}{\varrho_w} = \frac{\Delta H}{D_0} \tag{1.35}$$

and the well-known Kozeny—Carman equation for seepage velocity, we have an expression

$$\varrho_w \Delta H = D_0(1-n_0)(\varrho_s - \varrho_w) = 180 \frac{\nu \varrho_w}{d_s^2 g} \frac{(1-n_0)^2}{n_0^3} v_0. \tag{1.36a}$$

From eqn. (1.35) derived for the equilibrium condition, we obtain a new equation for *incipient velocity* v_0 in the form

$$v_0 = \frac{g d_s^2}{\alpha^2 K_{KC}} \frac{\varrho_s - \varrho_w}{\nu \varrho_w} \frac{n_0^3}{(1-n_0)} = (30\text{—}350)\, d_s^2 . \tag{1.36b}$$

The grain diameter has to be set in cm, the result v_0 is in cm s^{-1}.

This expresses the dependence between grain diameter (d_s), the incipient porosity (n_0), pore-shape factor (α), Kozeny—Carman resistance coefficient (K_{KC}), density difference ($\varrho_s - \varrho_w$), gravity coefficient (g) and kinematic viscosity (ν), which can be set as a global constant for a given soil (Peter 1975).

If we bear in mind that the liquefaction of sand in an upstream flow occurs near the toe of an embankment, we can use another formula known from fluidization. The *pressure drop* (Δp) can be expressed by a practical formula

$$\frac{\Delta p}{l} = C_D \Phi_n \Phi_s \frac{\gamma_w v^2}{2 g d_s}. \tag{1.37}$$

Taking appropriate values for

drag coefficient

$$C_D = \frac{24}{\mathrm{Re}} \qquad \text{(laminar flow)}, \tag{1.38}$$

porosity factor

$$\Phi_n = \frac{1}{n^z} = \frac{1}{n^{4.5}}, \tag{1.38}$$

*fall velocity**

$$v_s = c_s \frac{g}{\nu}(\varrho_s - \varrho_w) d_s^2, \qquad v = v_0,$$

and *critical gradient*

$$I_{cr} = \frac{(1-n)(\varrho_s - \varrho_w)}{\varrho_w},$$

we obtain

$$v_0 = \frac{2}{24} \frac{n_0^{4.5}}{\Phi_s} \frac{(1-n_0)(\varrho_s - \varrho_w)}{\varrho_w} d_s^2, \tag{1.39}$$

and then, finally, an expression for the critical relation between the fall velocity (v_s) of a given grain (d_s) and incipient velocity (v_0) for a layer having critical porosity $n_{cr} = n_0$, consisting of grains which are characterized by diameter d_s.

The *relation between* these two *velocities* is

$$\frac{v_s}{v_0} = \frac{3}{5} \frac{\Phi_s}{n_0^{4.5}} \frac{1}{(1-n_0)} = 0.6 f_H^*, \tag{1.40}$$

where

$$f_H^* = \frac{\Phi_s}{n_0^{4.5}(1-n_0)}.$$

The values of the ratio of critical velocities $v_s : v_0$ at the boundary of failures in a sandy layer of varied porosity n (from $n = 0.35$ to 0.60) and varied grain shape, characterized by $\Phi_s = 1.5$—2.5 calculated through eqn. (1.40), are given in Table 1.7.

From Table 1.7, it can be seen that in the dense state, and with unfavourably oriented grains, the ratio $v_s : v_0$ can reach the value 260, whereas in the opposite case, in a loose state of rounded (spherical) grains, this ratio can be less than 23. According to this law, loose sands can be damaged much more easily than a well-compacted layer of angular (crushed) material. Also following from this law, the liquefaction of a sandy layer in a hydraulic structure or in its subsoil can be avoided by the choice of a suitable material and by intensive compaction.

The "law" expressed by eqn. (1.40) represents a simple criterion taking into account two extreme velocities v_0 and v_s, which occur on the border of liquefaction in the field and which can be calculated using only a few laboratory tests.

Using data from Table 1.8 and taking into account the fall velocity of fine sand particles ($d_s = 0.06$—0.25 mm), we can say that the sands can be damaged by

* The coefficient c_s depends on the shape of the grain: for spherical grains $c_s = 1/18$ (Stokes), for rounded natural grains $c_s = 1/20$.

Table 1.8

Characteristic of soil	Data of these characteristics					
n_0	0.35	0.40	0.45	0.50	0.55	0.60
$1 - n_0$	0.65	0.60	0.55	0.50	0.45	0.40
$n_p^{4.5}$	0.00888	0.1619	0.02750	0.04419	0.06786	0.10038
$n_p^{4.5}(1 - n_0)$	0.0058	0.0097	0.0151	0.0221	0.0302	0.0402
$0.6f'_H$	103.96	61.73	39.76	27.15	19.90	14.95
	Value of the relationship $v_s : v_0$					
for $\Phi_s = 1.5$	155.94	92.60	59.50	40.72	29.85	22.43
$\Phi_s = 2.0$	207.92	123.43	79.34	54.30	39.80	29.90
$\Phi_s = 2.5$	259.90	154.33	99.18	67.88	49.75	37.38

a seepage velocity of $v = 2 \times 10^{-5}$—1.5×10^{-4} m s^{-1}. This means that the contact between gravels and sands is very often threatened.

From the point of view of dams, levées and other hydraulic structures, there is a difference between *liquefied sand,* explained by the laws of hydraulics and of fluidization theory as developed by Richardson et al. (1961), Aérov and Todes (1968) and others, and "quicksand" caused by the influence of seepage on effective stress, as shown by Terzaghi (1943), Lambe and Whitman (1969) and Craig (1974). We conclude that: "the soil is then said to be in a quick condition (quick — meaning alive) and if the critical gradient ($I_{cr} = 0.8$—1.1) is exceeded, the surface will appear to be *boiling* as the particles are moved around in the upward flow of water". In this case, the *quick condition* is indirectly connected with the free surface of a soil. *Liquefaction* (caused by critical velocity) can also be produced deep in the subsoil of a hydraulic structure. It is usually connected with expansion of the sand layer.

Piping phenomena represent a most important problem in dam and levée constructions. When high hydraulic gradients and high velocities exist in a soil mass — usually sandy gravel — there is a possibility that the seeping water may erode channels within the embankment or its subsoil, especially if the soil is poorly compacted. The stability of the dam may then be impaired. The process of internal erosion is referred to as "piping". In eastern countries (USSR, Czechoslovakia, Hungary, Bulgaria, Poland and GDR), piping phenomena are denoted as "sufosia" (suffosion) and many experts in this field distinguish the different 5 types of this phenomenon (Istomina 1957; Lubochkov 1962) and further in Czechoslovakia (Hálek 1966, Bažant 1967). In the French literature, we have found "piping" as "les renards" (Post and Londe 1955). For many German specialists, it is enough to denote it "innere Erosion".

If we examine all the *conditions of piping* phenomena in the subsoil and near levées in the Mississippi region in the USA, or in the Danube region in

Czechoslovakia, Hungary and Yugoslavia, and those of the Jamuna river, we see that many levées present favourable conditions for the formation of piping in their respective geological conditions (very permeable sandy gravel), as may be seen on the grain-size distribution chart (Fig. 1.25). Sandy gravel has a substantial amount of fine particles ($d = 0.25$ mm, more than 10%), coefficient of uniformity $C_u \geqq 20$, unfavourable coefficient of curvature on the particle-size distribution curves, $C_v \geqq 3$, and there is a lack of grains of size 0.5—2 mm. That is why the grains of fine sand move easily through the pores of the gravels which form their skeleton (Peter 1974c).

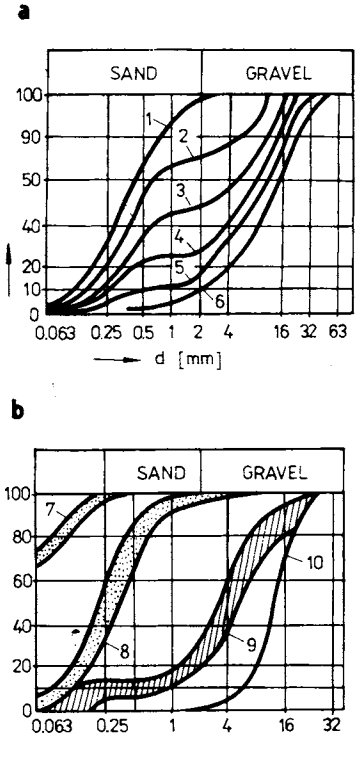

Fig. 1.25. Grain-size distribution of soils from the Danube valley in Czechoslovakia. a — grain-size distribution of unstable soils, b — grain-size distribution of soils in a cross-section of the dam failure; 1 — sand, 2 — sand with gravel, 3 — gravelly sand, 4 — sand gravel, 5 — gravel with sand, 6 — gravel, 7 — overburden, 8 — sands washed away, 9 — unstable soil, 10 — skeleton-stable part of Alluvium.

To investigate the piping problem, it is necessary to bear in mind two different soil grain types — fine sand and silt — which have a small diameter (d_c), and.can therefore be carried away through another more stable soil (diameter d_s). Gravel grains remain stable, despite growing seepage forces and *uplift pressure* (p) induced by a rising water level. *Stream velocity* (v) and effective porosity (n_{eff}) of the soil are also very important parameters, critical in piping failures. Taking into account that the sand grains in a water stream must be lifted, we can express the water pressure by the Archimedean number (Ar), and the forces generated due to inertia by the Froude number (Fr or Fr_M). The following equilibrium equation has

to be investigated

$$\frac{\Delta p}{l}\frac{n_{\text{eff}}^3}{(1-n)\varrho_w v^2} = \varkappa_F \,\text{Ar}\,\text{Fr}_M. \tag{1.41}$$

The left-hand side of eqn. (1.41) represents the modified *Eulerian number* (Eu_M), which can be expressed by a relationship between the hydraulic *friction coefficient* (f_H) and the size (d_c) of the *grain carried away*. From this consideration, we can introduce a new relation for the coefficient f_H

$$f_H = \frac{\Delta p}{l}\frac{2d_c}{\varrho v^2}\frac{n_{\text{eff}}^3}{(1-n)}, \tag{1.42}$$

and derive an equation for the equilibrium condition in the simple form

$$\text{Eu}_M = \varkappa_F \,\text{Ar}\,\text{Fr}_M = \frac{f_H}{2d_c}, \tag{1.43}$$

where $\varkappa_F$ is a coefficient expressing the ratio of pressure and shearing forces to inertia forces.

More than a hundred failure tests were evaluated. They gave good accordance with eqn. (1.43) and confirmed that the hydrodynamic laws proved the exponential tendency to manifest the increasing influence of inertia forces with increasing velocity (v), and decreasing influence of friction forces which almost disappear at $\text{Fr}_M = 25$. The data from a small test series, put together in Table 1.9, give evidence of this tendency.

Table 1.9. Values of stream characteristics and of $\varkappa_F$

Experiment		Ar	Basic characteristics					Coefficient
No.	d_c [mm]		$\frac{v^2}{2gd_c}$	$\frac{1-n}{n_{\text{eff}}^3}$	Fr_M	Ar Fr_M	Eu	$\varkappa_F = \frac{\text{Eu}}{\text{Ar}\,\text{Fr}_M}$
86	0.20	80	0.317	18.0	5.7	456	795	1.745
87	0.20	80	0.477	20.7	9.9	792	582	0.735
89	0.25	158	0.370	21.9	8.1	1279	465	0.363
90	0.25	158	0.416	24.5	10.2	1612	700	0.434
91	0.30	270	0.438	29.0	12.7	3430	490	0.143
92	0.30	270	0.510	32.6	16.6	4482	425	0.094
94	0.30	270	0.698	37.8	26.4	7130	350	0.049

The values of coefficient $\varkappa_F$ prove that by increasing the flow velocity of water over the range $v = 5$ cm s^{-1}, the influence of friction forces ceases to be significant and the movement of solid particles is determined primarily by inertial forces (Peter 1972b). This leads to a practical conclusion: the movement of coarse and medium-size sands is controlled by Newton's law. Thus is not correct to take a scale

model after the simple Reynolds number comparison, in the way often used in hydraulic research (Peter et al. 1978).

Many experiences (Walters 1971, Marsal and Albero 1976) lead to the conclusion that in practical calculations it is more convenient to estimate soil instability phenomenologically. Conventional methods of soil mechanics have allowed us to obtain many of the characteristics needed for the estimation of *soil resistance* under given seepage (water-stream force) conditions. We can introduce into the stability equations and criteria, or into our special mathematical models, the characteristics of the porous medium (if they are useful for design calculation). The magnitude of soil resistance is usually expressed by the *characteristics of the porous medium*: d_s (median size of the skeleton), d_c (effective diameter of fill), δ_s (soil heterogeneity), Φ_s (grain shape) and K (total resistance characteristic). The energy of the water stream is described by water density (ϱ_w), velocity (v) and its relation to the fall velocity v_s of a grain which can be removed (grain size d_c). An appropriate characteristic seems to be the *Froude number* (Fr), which can be replaced by the Reynolds number — raised to an appropriate exponent ξ. This exponent expresses the degree of development of turbulence and the progress of increasing inertial forces in the particular case under consideration. This will be brought out in Chapter 6.

It can be stated that both kinds of damage, liquefaction and piping, occur with a volume change, i.e. expansion with liquefaction (Richardson et al. 1961), or *piping with heave* (Martin 1971). This piping-and-heave mechanism yields a rapid growth in seepage velocity due to the opening up of the pore channels in the gravel skeleton: transportation of sand particles inside the porous medium starts (Wittmann 1978).

Holland and Rothwell (1977) proved in the laboratory, that many other effects manifested with boils can be masked by preferential channeling. It can be stated incidentally that all these effects, in sandy gravel (filter layer), manifest an elevated seepage velocity. The two authors named above give $v_{cr} = 2.5—3.3$ cm s^{-1}.

In a homogeneous embankment, and especially in the body of a levée, channeling by animals is very dangerous. This danger is usually gravest for levées built on silts and clay which are eroded easily.

Sherard et al. (1973) have written about the very real possibility of dispersion and deflocculation of clay. A clay of fine particles can be separated and turned into a suspension.

The solubility of the cations of sodium in pore water leads to *dispersion piping.*

The stability of an embankment built of a fine-grained soil can be damaged by the chemical influence of water. Sodium exchange is very well known in dams in Australia, where this phenomenon leads to *sinkholes and tunnels* within the body of dams, if the fill material consists of clay which has more than 15 SEP in the pore water.

In consequence, a dangerous change in the dam body, characterized by holes and

the transport of fine particles through the sands and gravels in the subsoil, occurs (Fig. 1.26).

It can be said with truth that piping problem is very complicated. After Terzaghi (1948), the designer is obliged to make adequate provisions to prevent *subsurface erosion*: "These provisions do not need to have any static or hydraulic function

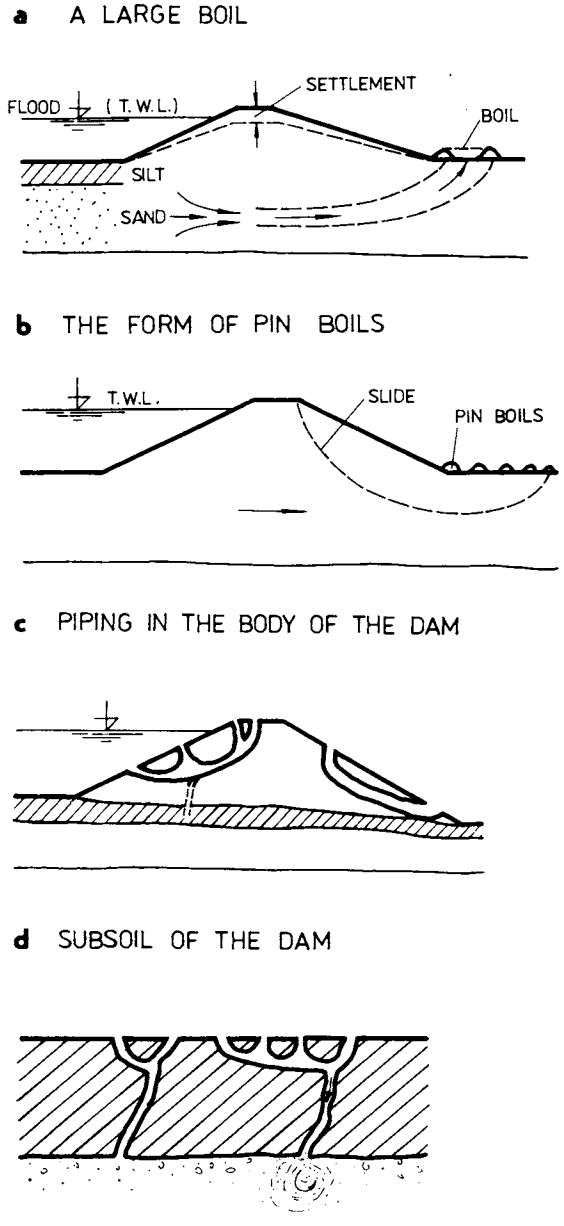

Fig. 1.26. Piping phenomena. a — sand movement, b — slide of soil mass, c — channeling in the structure, d — channeling in the subsoil.

because they are no more than the equivalent of the means for protecting steel against corrosion, or timber against termites or decay."

Hydraulic fracturing menaced the dams in special conditions. Following the disaster of Bear Wallow dam in North Carolina (in February 1976) and especially after the failure of the 90 m high Teton dam in Idaho (in June 1976), breached by piping and hydraulic fracturing as the reservoir was being filled for the first time, greater attention has been given to hydraulic fracturing. There are many causes for this effect (Peter 1979), besides that mentioned above.

Chiefly, they are:

(a) pore water pressure;
(b) pore air (gas) pressure and its movement in the soil;
(c) volume change of fine-grained soils (clays and silts);
(d) the unfavourable combination of negative pressure of water and soil (negative skin friction) and also flowing water.

The pore water pressure (u), being the pressure of the water filling the void space between the solid particles, influences the shear stress and shear resistance of soil. Shear stress can be resisted by the skeleton of solid particles, by means of forces developed at the interparticle contacts. The effective normal stress (σ'), representing the stress transmitted through the soil skeleton alone, is a part of total stress (σ)

$$\sigma = \sigma' + u \qquad \text{or} \qquad \sigma' = \sigma - u. \tag{1.44}$$

Increased pore pressure (u) diminishes the effective stress. In this case, $u > \sigma$ and the value of σ' becomes negative. Such a case cannot be avoided if the water in the river or reservoir drops and the pore water has insufficient time to escape from the voids; pore water pressure cannot be dissipated. The soil structure can then be damaged by growing negative pressure.

The *pore air pressure* (u_a) can also have an unfavourable effect on stability, as has been stated many times by Bishop and others, in the case of partially saturated soils where part of the void space is occupied by water, and part by air. The pore water pressure (u) must always be less than the pore air pressure (u_a) because of tension. Unless the degree of saturation is close to unity, the pore air will form continuous channels through the soil, and the pore water will concentrate in the regions around the interparticle contacts.

Volume change has many features. The volume of the soil skeleton as a whole can change as a result of rearrangement of the solid particles into new positions, mainly by rolling, sliding and flowing, with a corresponding change in the forces acting between particles. The actual compressibility of the soil skeleton will depend on the structural arrangement of the solid particles. In a fully saturated soil, since water is considered to be incompressible, a reduction in volume is possible only if some of the water can escape from the voids.

The absorbed water surrounding clay mineral particles will experience recover-

able compression due to increased interparticle forces, especially when there is face-to-face orientation of the particles. When a decrease in total normal stress takes place in a soil, there will be a tendency for the soil skeleton to expand to a limited extent, especially in soils containing an appreciable proportion of clay mineral particles. As a result, the pore water pressure will be reduced, and the excess of pore water pressure will be negative. The pore water pressure will gradually increase to the steady-state value, flow taking place into the soil, accompanied by a corresponding reduction in effective normal stress and increases in volume. This process is called *swelling* and is characteristic for soils of low permeability (silt, silty clay) used in engineering practice for the construction of levées.

In these hydraulic structures, the reverse process — shrinkage — can be observed in dry seasons. Fine-grained soils subjected to drying lose water and the soil turns into a solid material. The volume diminution and hardness of material are connected with a tension in the soil mass which leads to cracking. The transition between semisolid states occurs at the shrinkage limit, defined as the water content at which the volume of the soil reaches its lowest value as it dries out. It can be said that this moment coincides with the greatest danger of cracking in the dam, which can also lead to hydraulic fracturing.

Summarizing the many dangers threatening embankments, we can see that many can be avoided by appropriate choice of construction material, good compaction and appropriate design and performance of the structure. In accordance with a statement from Sherard et al. (1973), when assessing earth dams and levées the following facts must be considered.

(1) The most *frequent danger* to these structures is *hydraulic fracturing and channeling.*
(2) A heavily *concentrated seepage flow,* breaking through the impervious top strata at the downstream toe of an embankment slope, rapidly develops a channel under the embankment. The embankment settles and failure generally occurs as a result of *overtopping of the structure.*
(3) The danger of *cracks* can be expected in cases where the lateral stress (σ_3) is very small ($\sigma_3 < 0$), the settlement is uneven, and the stress condition moves over the strength limit.
(4) Ultimate bearing capacity is important — large settlements can occur, connected with plastic behaviour and *local shear failure* of the soil.
(5) Piping caused by *erosion* of fine particles is frequent in sandy gravel, and in clays chemical influence and dispersion of fine particles can play an important role.
(6) Underseepage or *seepage* through a previous foundation of different permeability and large porosity can very often damage a structure.
(7) Uniform sandy soil (fine sands) can be destroyed by *liquefaction* caused by high seepage velocity.

Table 1.10. Engineering use chart

Typical names of soil groups	Group symbols	Important properties				Relative desirability of various uses						
						Rolled earth dams			Canal sections		Foundations	
		Permeability when compacted	Shearing strength when compacted and saturated	Compressibility when compacted and saturated	Workability as a construction material	Homogeneous embankment	Core	Shell	Erosion resistance	Compacted earth lining	Seepage important	Seepage not important
Well graded gravels, gravel-sand mixtures, little or no fines	GW	Pervious	Excellent	Negligible	Excellent	—	—	1	1	—	—	1
Poorly graded gravels, gravel-sand mixtures, little or no fines	GP	Very pervious	Good	Negligible	Good	—	—	2	2	—	—	3
Silty gravels, poorly graded gravel-sand-silt mixtures	GM	Semipervious to impervious	Good	Negligible	Good	2	4	—	4	4	1	4
Clayey gravels, poorly graded gravel – sand – clay mixtures	GC	Impervious	Good to fair	Very low	Good	1	1	—	3	1	2	6
Well-graded sands, gravelly sands, little or no fines	SW	Pervious	Excellent	Negligible	Excellent	—	—	3 if gravelly	6	—	—	2
Poorly graded sands, gravelly sands, little or no fines	SP	Pervious	Good	Very low	Fair	—	—	4 if gravelly	7 if gravelly	—	—	5
Silty sands, poorly sand – silt mixtures	SM	Semipervious to impervious	Good	Low	Fair	4	5	—	8 if gravelly	5 erosion critical	3	7
Clayey sands, poorly graded sand – clay mixtures	SC	Impervious	Good to fair	Low	Good	3	2	—	5	2	4	8
Inorganic silts and very fine sands, rock flour, silty of clayey fine sands with slight plasticity	ML	Semipervious to impervious	Fair	Medium	Fair	6	6	—	*	6 erosion critical	6	9
Inorganic clays of low to medium plasticity, gravelly clays, sandy clays, silty clays, lean clays	CL	Impervious	Fair	Medium	Good to fair	5	3	—	9	3	5	10
Organic silts and organic silt-clays of low plasticity	OL	Semipervious to impervious	Poor	Medium	Fair	8	8	—	*	7 erosion critical	7	11
Inorganic silts, micaceous or diatomaceous fine sandy or silty soils, elastic silts	MH	Semipervious to impervious	Fair to poor	High	Poor	9	9	—	*	—	8	12
Inorganic clays of high plasticity, fat clays	CH	Impervious	Poor	High	Poor	7	7	—	10	8 volume change critical	9	13
Organic clays of medium to high plasticity	OH	Impervious	Poor	High	Poor	10	10	—	**	—	10	14
Peat and other highly organic soils	Pt	—	—	—	—	—	—	—	***	—	—	—

Only some of the above dangers can be estimated by calculation. Much more has to be done in appropriate dam construction (compaction, filter layer) and control.

Old dams should be investigated in the field, but as a preliminary estimate, the *Engineering Use Chart* (Table 1.10) from Wagner (1952) can serve us well. In this chart, soils threatened by piping are signified with a danger. In the cases thus signified, care must be taken.

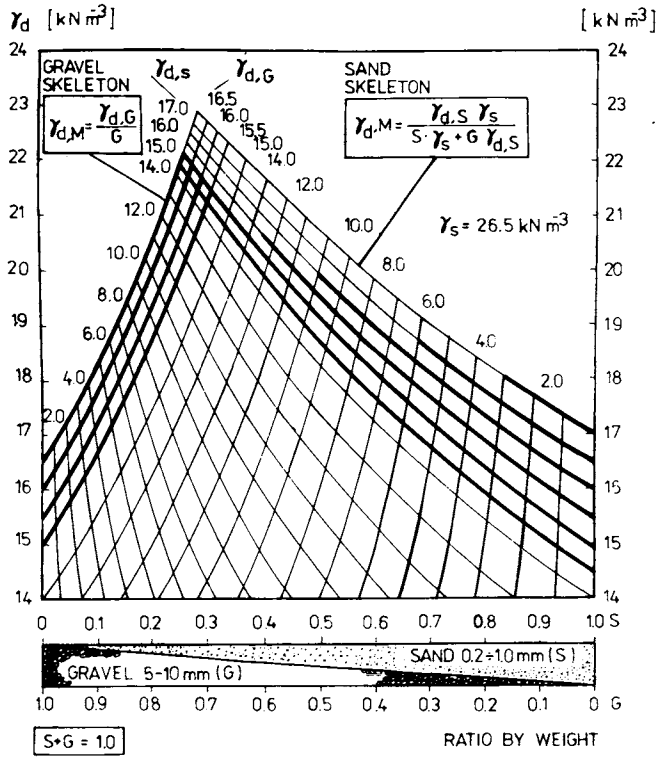

Fig. 1.27. Possible mixtures of two-component soils. G — gravel, S — sand, M — mixture; k_G, k_S ... k_M, γ_G, γ_S ... γ_M — after Wittmann (1978).

Another division can be found in some papers which categorized cohesive soils according to their tensile resistance, taking account of their plasticity index.

Probably, the richest source of stability problems connected with seepage control can be found in Russian literature. Best known are the works of Istomina (1957), Izbash and Khaldre (1959), Lubochkov (1962), Chugaev (1965), Bulatov (1968),

Nosova (1972). Some of this Russian knowledge and experience will be mentioned later (see Chapter 6).

Melioration of soils and techniques for raising the quality of an earthwork and its subsoil is most important for levées. The content and aim of this book do not allow the analysis of many interdependences between properties of soils and their grain-size distribution, groundwater flow and stability of an earthwork and its subsoil. It can be stated, in general, that a mixture of fine-grained soils and granular soils also helps the impermeability and stability. It can be seen in the simplest example of a gravel and sand mixture (Fig. 1.27), that the appropriate percentage of sand both diminishes the danger of piping, suffusion and erosion on the one hand, and makes the sludging more effective on the other, and is manifested by a high unit weight (Wittmann 1978).

In certain special cases, the civil engineer has many other tools at hand for increasing the resistance to erosion and piping and for increasing the quality of a soil in a given situation. Most universal is the compaction of soil — compaction in layers or deep compaction. He can also choose appropriate material to influence the mass transfer (Peter 1974a, c) or else a special technique for sealing or strengthening the soil. In the last decades, using a new technique called vibroflotation, for antiseepage and strengthening measure of levées and its subsoil, good results were obtained (Borowicka 1968). However, best is grouting, whose basic problems have been investigated by many authors, e.g. Cambefort (1964), Brauns and Blinde (1978) and others.

Chapter 2

SEEPAGE

2.1 Basic Characteristics and Relations

The flow conditions of water in a given soil are given by both soil characteristics and by energy of the water. Soil containing water has different conditions for seepage, according to its grain-size distribution; and the influence of the energy of water can be analysed by Bernoulli's equation. Water flow occurs when the energy of water differs at various points within the soil mass. Its *total energy* is the sum of the potential and kinetic energies

$$E = z + \frac{p}{\gamma_w} + \frac{u^2}{2g}. \tag{2.1}$$

The first term is the elevation head, the second the pressure head and the third the velocity head, which is usually the smallest and can therefore be neglected. The potential of the motion related to the mass may be expressed by the first two terms

$$H = z + \frac{p}{\gamma_w}. \tag{2.2}$$

The lines drawn through points of equal potential are called *equipotential lines.* The loss of potential per unit of length is the gradient, which is responsible for water movement in the pores of the soil. The magnitude of the latter can be expressed by the simple Darcy's formula adapted in the form

$$q^* = k\,\frac{\varphi_1^* - \varphi_2^*}{\Delta s} \cong k\,\frac{H_1 - H_2}{\Delta s} = kI, \tag{2.3}$$

where $\varphi^* = z + \frac{p}{\gamma_w} + \frac{u^2}{2g}$, *potential of seepage water* (Fig. 2.1); k is the coefficient of permeability (treated in Chapter 1); I hydraulic gradient.

The coefficient of permeability depends primarily on the average pore size, which in turn is related to the distribution of particle size (see Fig. 1.10) and void ratio.

For a given soil, the coefficient of permeability is a function of void ratio (e) or more exactly of effective porosity n_{eff}. Real (seepage) velocity is

$$u^* = \frac{q^*}{n_{\text{eff}}}, \tag{2.4}$$

or precisely

$$\bar{u} = u^* \sqrt{T_k}, \qquad T_k = \frac{l_0^2}{l^2}, \tag{2.5}$$

if we take into account tortuosity of pore channels T_k, after Scheidegger (1960). In a soil profile (Fig. 2.1a), pore-size variation causes big differences in velocity u; we shall consider an average value $\bar{u}$. Calculating *seepage quantity* Q or q, it is more convenient to express fictive (superficial) velocity (related to the surface S)

$$q^* = \frac{Q}{S} = kI, \tag{2.6}$$

after Darcy (1856), assuming also the presumptions of Dupuit (Fig. 2.1b). In engineering practice, the use of the *Hagen—Poiseuille model* (Fig. 2.1c) is also quite common. The tortuosity concept is used exceptionally as a consequence of macroscopic-scale-model calculation preferred in dam design.

In practical calculations, the consequences of use of different models (Darcy, Dupuit, Scheidegger, etc.) and macroscopic or microscopic scale can be neglected, except in cases where the stability of coarse-grained material should be treated.

In practice, Darcy's and Dupuit's conditions are the same. After *Dupuit*, it is necessary to use

$$I = -\frac{\mathrm{d}H}{\mathrm{d}l} = \text{constant}. \tag{2.7}$$

For a surface S — consisting of elements $\mathrm{d}S$ — seepage Q will be determined by integrating

$$Q = -k \int_S \frac{\mathrm{d}H}{\mathrm{d}l} \mathrm{d}S, \tag{2.8}$$

or

$$Q = -k \frac{\mathrm{d}H}{\mathrm{d}l} \int_S \mathrm{d}S = -kS \frac{\mathrm{d}H}{\mathrm{d}l}. \tag{2.9}$$

The *superficial velocity* will be

$$\bar{q}^* = \frac{Q}{S} = -k \frac{\mathrm{d}H}{\mathrm{d}l}. \tag{2.10}$$

The average superficial velocity depends on the "slope" of the flow path (Fig. 2.1b) given by the differential of height with respect to length.

In practical computation, we use the macroscopic concept, considering the flow path as a straight line and ignoring the fact that water seeping through a soil must

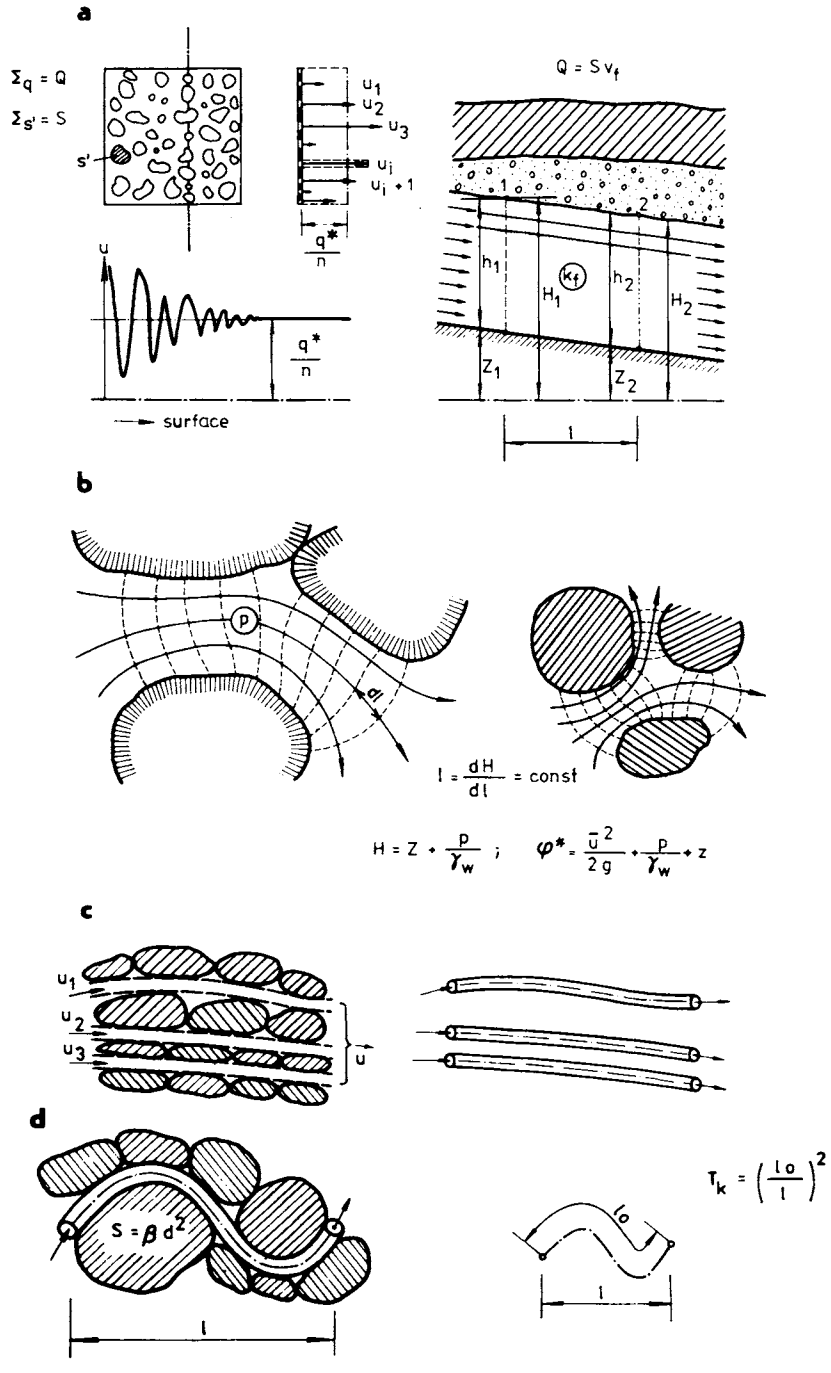

Fig. 2.1. Groundwater movement and soil models. a — after Darcy, b — after Dupuit and Hagen, c — Hagen—Poiseuille model, d — tortuosity concept.

flow in a very tortuous manner between the solid particles. In such a mixed macroscopic and microscopic concept, a new term *seepage velocity* v_f' was introduced, assuming that the water flows per unit time through an average area of voids (A_v) with a velocity

$$v_f' = \frac{q}{A_v} = \frac{q}{nA} = \frac{v}{n}, \tag{2.11a}$$

$$v_f' = \frac{kI}{n}, \tag{2.11b}$$

neglecting the difference between n and n_{eff} and also omitting the tortuosity of pore channels. In coarse-grained soils with small percentages of fines and porosities $n = 26—36\%$, this assumption can be accepted only if the soil layer is "favourably" stratified and if water flows parallel to the direction of stratification.

In heterogeneous soils, the coefficient of permeability k should be treated as a tensor $\bar{\boldsymbol{K}}$ and the velocity of motion as a vector

$$\boldsymbol{V} = \bar{\boldsymbol{K}}\boldsymbol{I}. \tag{2.12}$$

Equation (2.12) will be analysed in Chapter 3 in more detail, in connection with practical programming aspects.

Another approach was made by Forchheimer (1914) and Irmay (1958) in the analysis of flow resistances by means of a two-component formula with two constants (a, b); a for linearly dependent resistances and b for quadratic resistances. Using as a basic formula the relation between the hydraulic gradient (I) and the superficial velocity (q^*), a new form of *resistance equation* can be obtained

$$I = aq^* + bq^{*2} \tag{2.13a}$$

or

$$I = (w + bq^*)\, q^* = w_0 q^*, \tag{2.13b}$$

$$q^* = \boldsymbol{K}\boldsymbol{I}; \qquad \boldsymbol{K} = \frac{1}{w_0} = \frac{1}{w + bq}. \tag{2.14}$$

A very interesting analysis made by Irmay (1967) treating the Dupuit theory, Pavlovskiĭ approximations and Navier—Stokes equation (omitted in our treaty), allows us to write the Bernoulli equation (eqn. 2.1) in a special form

$$g\nabla^2 E = g\nabla^2 \left(h + \frac{V^2}{2g}\right) = (\text{rot } \boldsymbol{V})^2 - (\boldsymbol{V} \text{ rot rot } \boldsymbol{V}). \tag{2.15}$$

Neglecting inertia forces

$$\frac{V^2}{2g} = 0,$$

and by assumptions

$$\nabla^2 E = 0, \tag{2.16}$$

$$\nabla^2 h = 0 \tag{2.17}$$

new equations characterizing water flow in porous media can be obtained.

Introducing velocity components (u, v, w) in three perpendicular directions, the energy E_x in the direction of the x axis can be expressed by the following equation

$$gE_x = \frac{1}{2}(v^2 + w^2 - u^2) + (uv)_y + (uw)_x - u_t + (u_{xx} + u_{yy} + u_{zz}). \tag{2.18}$$

Transverse velocities $\bar{v}$, $\bar{w}$ are omitted in a soil mass in general and thus

$$u\bar{v} = 0, \qquad u\bar{v}_y = 0, \qquad u\bar{w} = 0, \qquad u\bar{w}_z = 0, \tag{2.19}$$

$$\begin{aligned} u_x &= v_y - w_z, \\ u_{xx} &= v_{xy} - w_{xz}, \\ \bar{u}_{xx} &= -\bar{v}_{xy} - \bar{w}_{xz} = 0 - 0 = 0. \end{aligned} \tag{2.20}$$

The motion is influenced by the mean direction in the first row; in most cases it is the horizontal direction or nearly horizontal direction (in groundwater flow), and thus the flow component u will be most interesting for superficial velocity q^*. It can be related to the average velocity ($\bar{u}$), by porosity (n) — in accordance with Fig. 2.2 — as follows

$$q^* = \bar{u}n, \qquad \bar{u} = \frac{q^*}{n}, \tag{2.21}$$

$$n = \frac{e}{e+d} \qquad \text{or} \qquad \frac{e}{d} = \frac{n}{1-n}. \tag{2.22}$$

Related to time, the acceleration velocity $\bar{u}_t$ can be expressed

$$\bar{u}_t = \frac{\bar{q}_t^*}{n}. \tag{2.23}$$

Very often we can set $\bar{u}_t = 0$ (no time influence).

It is evident that in the middle of (between) grains, u will be u_{max} (in meridian profile), and then the curvature of the flow path changes and becomes negative

$$u_{yy} < 0, \qquad u_{zz} < 0.$$

Introducing the curvature (β) of the flow path in two perpendicular directions β_1, β_2

$$\bar{u}_{yy} = -\beta_1 \frac{\bar{u}}{e^2} = -\beta_1 \frac{(1-n)^2}{n^3} \frac{q^*}{d^2}, \tag{2.24a}$$

$$\bar{u}_{zz} = -\beta_2 \frac{\bar{u}}{e^2} = -\beta_2 \frac{(1-n)^2}{n^3} \frac{q^*}{d^2}, \tag{2.24b}$$

$$\bar{u}_{yy} + u_{zz} = \beta \frac{(1-n)^2}{n^3} \frac{q^*}{d^2}. \tag{2.24c}$$

In eqn. (2.24c) valid for laminar flow, β denotes resulting curvature

$$\beta = \beta_1 + \beta_2. \tag{2.25}$$

If velocities are higher, resistances will depend on the square of velocities by a change of curvature

$$(v^2 + w^2)_x = -\alpha \frac{\bar{u}^2}{e} = -\alpha \frac{1-n}{n^3} \frac{q^{*2}}{d}. \tag{2.26}$$

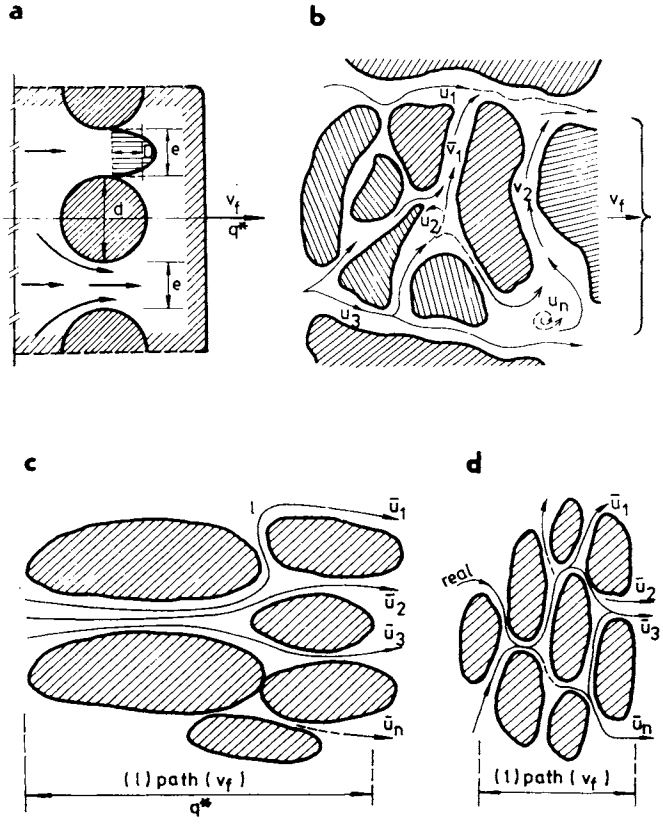

Fig. 2.2. Real (u) and superficial (v_f) or fictive (q^*) velocity and real (l_r) and superficial path of flow (l). a — grains idealized as spheres, b — real irregular grains, c — flat lying grains, d — flat standing grains.

According to the proposals of Polubarinova-Kochina (1952) and Irmay (1967), gradients (I) and energy losses (E) can be analysed in more detail. Neglecting energy losses in $y(E_y)$ and $z(E_z)$ axis directions

$$I_2 = -E_y = 0; \qquad I_3 = -E_z = 0 \tag{2.27}$$

can be written

$$I_1 = -E_x = aq^* + bq^{*2} + cq^*_{(t)}, \tag{2.28}$$

where

$$a = \beta \frac{(1-n)^2}{n^3} \frac{\nu}{gd^2}, \tag{2.29a}$$

$$b = \alpha \frac{1-n}{n^3} \frac{1}{gd}, \tag{2.29b}$$

$$c = \frac{1}{ng}. \tag{2.29c}$$

Equation (2.28) takes into account resistances of laminar flow (through coefficient a — eqn. 2.29a), those of turbulent flow (b) and time-dependent losses (with coefficient c).

It is evident that coefficients a, b (c) replace the coefficient of permeability k introduced in eqns. (2.3), (2.6) and (2.8)—(2.10). More accurately they replace the *absolute coefficient of permeability* K_0 (with unit m^2) related to k through the equation

$$K_0 = \frac{\eta}{\gamma_w} k. \tag{2.30}$$

Using eqn. (2.29a), a resistance coefficient K_0 can be expressed, for laminar flow

$$K_0 = \frac{1}{a} = \frac{gd^2}{\beta\nu} \frac{n^3}{(1-n)^2}. \tag{2.31}$$

The expression for K_0 was deduced theoretically first by Kozeny (1927) and investigated by Lindquist (1933) and Carman (1956). In the literature treating water flow in porous media (Ward 1966), it is called *the Kozeny—Carman resistance constant* and the symbol K_{KC} is introduced to distinguish it from other similar constants (Peter 1972a).

Using the models of Poiseuille and Hagen, for liquid flow in a capillary tube with diameter d_0, the *loss of head* (h) can be expressed in this way

$$h = \frac{p_1 - p_2}{\gamma_w} = 32 \frac{\eta}{\gamma_w} \frac{1}{d_0^2} \bar{u} = 32\nu \frac{1}{gd_0^2} \bar{u}. \tag{2.32}$$

When kinematic viscosity ν are also introduced instead of η and γ_w into eqns.

(2.31) and (2.32), new formulae for superficial velocity (q^*) and coefficient of permeability can be deduced by analogous steps

$$q^* = \frac{g d_0^2}{32\nu} I, \tag{2.33}$$

$$K_0 = \frac{g d_0^2}{32\nu} = \frac{1}{2} R_H^2 \frac{g}{\nu}. \tag{2.34}$$

Through the *hydraulic-radius* (R_H) *concept* many other characteristics and flow regimes can be investigated, remembering the definition of the hydraulic radius — a characteristic of the porous media — as follows

$$R_H = \frac{\text{volume of the soil}}{\text{surface of the grains}} \frac{n}{1-n} = \left(\frac{V}{S}\right) \frac{n}{1-n}. \tag{2.35}$$

Average velocity in a tube (pore channel)

$$u_a = -\frac{R_H^2}{K'\eta} \nabla p_s^*, \tag{2.36}$$

$$p_s^* = \frac{\Delta p^*}{l} \frac{1}{l_0},$$

$$\left[u_s = |\boldsymbol{V}| \frac{1}{l_0} \right]. \tag{2.37}$$

For a curved pore channel, a new expression for flow velocity can be found

$$\bar{u} = -\frac{R_H^2}{S_T \eta \left(\frac{l_0}{l}\right)^2} \frac{\Delta p^*}{l} = \frac{R_H^2}{\eta S_T T_k} \frac{\Delta p^*}{l} = \frac{R_H^2}{\eta K} I_P, \tag{2.38}$$

where pore-shape factor S_T, tortuosity (T_k) of pore channel are expressed by constant K. It can be introduced into eqn. (2.38), deduced through the Poisseuille model concept.

The most widely used Kozeny model of spherical pores leads to the *Kozeny—Carman formula* for superficial velocity

$$q^* = \frac{\Phi_s \gamma_w n^3}{T_k \eta a^2 (1-n)^2} I \cong \frac{\gamma_w}{\eta} \frac{n^3}{5 a_0^2 (1-n)^2} I. \tag{2.39}$$

If the inverse factor of specific surface area $a = \frac{A}{V} = \frac{6(1-n)}{d_e}$ $\left(A = \pi d^2; V = \frac{1}{6}\pi d^3\right)$ is related to equivalent diameter of grain d_e, and to T_k [sett in (2.39) as $T_k = 2$], then

$$d_e = \frac{6(1-n)}{A} V = (1-n) a_0, \tag{2.40}$$

$$q^* = \frac{\Phi_s \gamma_w n^3 d_e^2}{72\eta(1-n)^2} I, \tag{2.41a}$$

$$q^* = \frac{\Phi_s g}{72\nu} \frac{n^3}{(1-n)^2} d_e^2 I \tag{2.41b}$$

or more commonly

$$q^* = \frac{g n^3 d_e^2}{\Phi' T_k \left(\frac{\alpha_0}{\beta_0}\right)^2 \nu(1-n)^2} I. \tag{2.41c}$$

Equation (2.42) can be deduced by comparing eqn. (2.41c) with eqn. (2.3). The coefficient of permeability and superficial velocity can be expressed as

$$k = \frac{g n^3 d_e^2}{\Phi' T_k \left(\frac{\alpha_0}{\beta_0}\right)^2 \nu(1-n)^2}, \tag{2.42a}$$

$$v_f = \frac{d_e^2}{36 K_{KC}} \frac{n^3}{\nu(1-n)^2} gI. \tag{2.41d}$$

For spherical grains

$$k = \frac{g n^3}{\nu(1-n)^2} \frac{d^2}{36 K_{KC}} = \frac{g}{\nu} K_0. \tag{2.42b}$$

From the work of Lenau (1967), Ward (1966) and Lambe and Whitman (1969), a modified form of eqns. (2.41)—(2.42b) is found to be

$$K_0 = \frac{1}{\Phi_0 S^2} \frac{\gamma_w}{\eta} \frac{e^3}{(1-e)^2} d_s^2, \tag{2.42c}$$

where S is specific surface area, ϕ_0 ($= k_0$) is factor depending on pore shape and ratio of length of flow path to soil-bed thickness, d_s is some effective particle diameter (with characteristic specific surface).

In the Kozeny concept, *relative permeability* is

$$K_0 = \frac{n_{eff}^3}{a^2 K_{KC}} = \frac{1}{36 K_{KC}} \frac{n_{eff}^3}{(1-n)^2} d_e^2. \tag{2.42d}$$

In engineering practice, formulae for average values of resistance factor K and d_e expressed by a diameter taken for grain-size distribution curves are preferable. From Terzaghi $d_e = d_{10}$, Bertram $d_e = d_{15}$, Zauberey $d_e = d_{17}$ and Davis $d_e = d_{20}$.

Among some hundred variations of this formula, we have a form due to Terzaghi

$$K_0' = 200 \left(\frac{n}{1-n}\right)^2 d_{10}^2 \tag{2.43a}$$

and one due to Zauberey

$$K_0' = 349 \frac{n^3}{(1-n)^2} d_{17}^2 \tau, \tag{2.43b}$$

with a value of $\tau = 0.64$—1.2 depending on water temperature.

Remembering that soil damage caused by water seepage occurs in nonlinear (transient) water-flow conditions, the relation of velocities and soil resistances (hydraulic gradients) in transient regions may be of interest. The most simple relation was used by Pavlovskiĭ (1930), Escande (1943) and Trebin (1959).

The former derived an expression in the form

$$v = kI^{m_1} \tag{2.44a}$$

and from Trebin we have

$$v = kI^{\frac{1}{m_2}}, \tag{2.44b}$$

where the value of $m_1 = 1$—2 and $m_2 = 1$—0.6, respectively, was proposed as described later.

Schneebeli (1966) built his theory and mathematical expression on the *dynamic equilibrium of the motion* (motoric) forces (F_M) *and friction forces* (E_R) and inertia forces (F_I), with the help of the following equations

$$F_M + F_I + F_R = 0, \tag{2.45a}$$

$$\frac{F_M + F_I}{F_i} + \frac{F_R}{F_I} = 0. \tag{2.45b}$$

Analysing the relations

$$\frac{F_R}{F_I} = f_1 \left(\frac{du}{\eta/\varrho_w} \right)$$

and

$$\frac{F_M + F_I}{F_i} = f_2 \left(\frac{Igd}{u^2} \right) \tag{2.45c}$$

$$\frac{Igd}{u^2} = \mathrm{f}\left(\frac{ud}{\nu} \right) = \mathrm{f(Re)}, \tag{2.45d}$$

he reached the relation for a value of *hydraulic friction*

$$\frac{1}{2} \frac{Igd}{u^2} = f_H,$$

which can be related to Reynolds number, Re.

In practical engineering design, an approach based on the Forchheimer formula (eqn. 2.13a) can be useful. It leads to equations

$$\frac{\Delta p}{l} = \frac{\alpha_s^2 K(1-n)^2 \eta q^*}{n_{eff}^3 d_a^2} + \frac{\alpha_s \sqrt{K}(1-n) c \varrho_w q^{*2}}{n_{eff}^{3/2} d_a}, \tag{2.46a}$$

$$I = a\alpha_s^2 K \frac{q^*}{d_a^2} + b\alpha_s \sqrt{K} \frac{q^{*2}}{d_a}, \tag{2.46b}$$

where α_s is the pore-shape factor depending on the grain-shape factor and porosity; K constant of resistance depending on the shape of grain and its roughness; c constant as a characteristic of resistances in turbulent flow ($c \cong 0.56$); d_a appropiate grain diameter (d_e, d_s).

Values of *resistance factors* (α_s, K, T_k, S_T) are given in Table 2.1, taken from experiments made by the Department of Geotechnique of the Technical University in Bratislava (1971).

Table 2.1. Values of resistance characteristics α_s, T_k, K and S_T for different grain shapes and position relating stream direction

Characteristic	The value for the shape and orientation of the grain							
	(1) sphere	(2) cubic-oriented			(3) flat		(4) angular	
		parallel	across	free	laying	standing	laying	standing
α_s	6.0	7.0	7.2	6.3	5.4	6.5	6.8	7.5
T_k	2.4	1.25	3.5	2.7	1.8	3.7	2.5	2.8
K	5.0	5.8	18.0	17.0	5.5	11.5	9	10.5
S_T	2.1	4.2	4.7	5.2	3.1	3.1	3.6	3.7

Spherical (1) and cubic grains (2) manufactured from glass and novodur respectively; (3) gravel of river deposit; (4) crushed material (sandstone).

Equation (2.46b) can be written more simply using *global resistance characteristics* $A_{T,d}$ and $B_{T,d}$ calculated or measured for a given soil with a characteristic grain diameter d_a. Given a criterion for the limit of laminar (linear) and quadratic flow velocity (first and second parts of eqn. 2.46a), we can calculate the relation between the first and second parts of *flow resistances* in this way

$$q^*(A_{T,d} + B_{T,d} q^*) = I. \tag{2.47a}$$

If

$$100(B_{T,d} q^*) = A_{T,d}, \tag{2.47b}$$

then

$$q^{*1} = \frac{A_{T,d}}{100 B_{T,d}}. \tag{2.47c}$$

Admitting 1% of resistances from other systems (nonlinear resistances), we have

$$q^{*II} = \frac{100 A_{T,d}}{B_{T,d}}, \tag{2.48a}$$

$$q^{*II} = 10{,}000\ q^{*I}, \tag{2.48b}$$

$$Re^{II} = 10{,}000\ Re^{I},$$
$$(Re^{I} = 0.2—0.4).$$

Admitting 10% of linear resitances, Re^{II} exceed above 200—360, as shown in Table 2.2. It is useful to relate all values (Table 2.3) to the modified Reynolds number Re_M

$$Re_M = \frac{4 n_{eff}\, d_a q^*}{\alpha_s (1-n)\, \nu}, \tag{2.49}$$

containing characteristics of the soil (d_a, n, n_{eff}, α_s) flow velocity and shear stress (resistance) of water (ν).

Table 2.2. Values of hydraulic-gradient I^1 limits for linear resistance—velocity relations

Characteristic	Value of hydraulic gradient I^1 for grain diameter [mm]								
Diameter d_a	0.01	0.025	0.05	0.10	0.20	0.40	1.60	8.0	12.5
Gradient I^1	120	6.40	0.80	0.10	0.013	1.56×10^{-3}	240×10^{-3}	20×10^{-6}	510×10^{-9}
	218	14.50	1.75	0.218	0.027	3.4×10^{-3}	530×10^{-3}	43×10^{-6}	1200×10^{-9}

Value I^1 in the second row was obtained for lower porosity.

Table 2.3. Reynolds number for portion (%) of square of resistances of seepage water in soil

Limit (I)	Values for a portion of square of resistances									
	1%	5%	10%	15%	20%	25%	30%	40%	50%	90%
Re_M^1	0.23	1.22	2.58	4.09	5.79	7.73	9.96	15.47	23.20	209
	0.30	1.59	3.63	5.35	7.57	10.20	13.00	20.20	30.30	273
	0.40	2.10	4.42	7.05	9.95	13.30	17.10	26.60	39.80	360

Values in the first row are particularly valid for angular grains.

From the *two-component equation* (laminar and turbulent), the hydraulic friction factor can also be expressed

$$f_H = f_{H,1} + f_{H,2}$$

in other ways. The simplest is

$$f_H = \frac{a}{Re} + b = gd\left(\frac{d}{\nu q^*} + \frac{1}{q^{*2}}\right) \tag{2.50a}$$

or

$$f_H = 8\left(\frac{g}{c_0^2} + \frac{\beta^2}{Re}\right), \text{ after Forchheimer.} \tag{2.50b}$$

The use of the Kozeny—Carman concept of the two-component relation between hydraulic friction and soil resistance and flow velocity leads to an expression which can be written in the form

$$f_H^* = \frac{\alpha_s K_T (1-n)}{2} \frac{\alpha_s \nu (1-n)}{n_{eff}\, d_a q^*} + \frac{1}{2}\alpha_s \sqrt{K_T}(1-n)c, \tag{2.51a}$$

which includes the modified Reynolds number Re_M (after eqn. 2.49). This equation gives, in an open form not only resistance factor K_T with a constant value but also takes account of the shape of the grain. For a given soil and soil characteristics (d, n, Φ_s), the second compound is a constant evalued by Kozeny to have a mean value of 0.48.

Substituting the constant c into the second term, after Richardson (1957), our relation (Peter 1972b) leads to the expression

$$f_H \cong 8K\, Re_M^{-1} + \sqrt{KT_k}\, Re_M^{-2} \tag{2.51b}$$

using a porosity of soil $n = 0.4$. This function shown in Fig. 2.3 for angular (1), oblique (2), flat (3) and spherical (4) grains can be used in soil-stability analyses mentioned in Chapter 1 and treated in more detail in Chapter 6.

A very interesting simple relation between hydraulic friction and Reynolds number was found by Leibenzon (1947)

$$f_H = C_L\, Re^{-b}, \tag{2.52}$$

which takes account of all characteristics (d, n, Φ_s, α_s, T_k) in a unique constant C_L, and various flow regimes (v, ν) in the exponent b. Practical application of eqn. (2.52), used in petroleum engineering, is very limited.

In the analysis of the problems of dam design in Chapter 1, several eqns. (1.35—1.40) expressing the resistance of soil mass in water streams were mentioned. Many other equations deduced from the Forchheimer formula (2.46a) have been developed and completed using soil characteristics responsible for seepage conditions and soil stability. These equations are used in stability analyses in the

loose state, in which the *drag coefficient* C_D is a basic characteristic of soil resistance.

This one can be calculated by following formulae

$$C_D = \frac{4}{3}\frac{\alpha_s^2 S_g(1-n)}{\mathrm{Re}} + \frac{4}{3} c\alpha_s n_{\mathrm{eff}}^{3/2}\sqrt{\frac{S_g}{T_k}}, \qquad (2.53a)$$

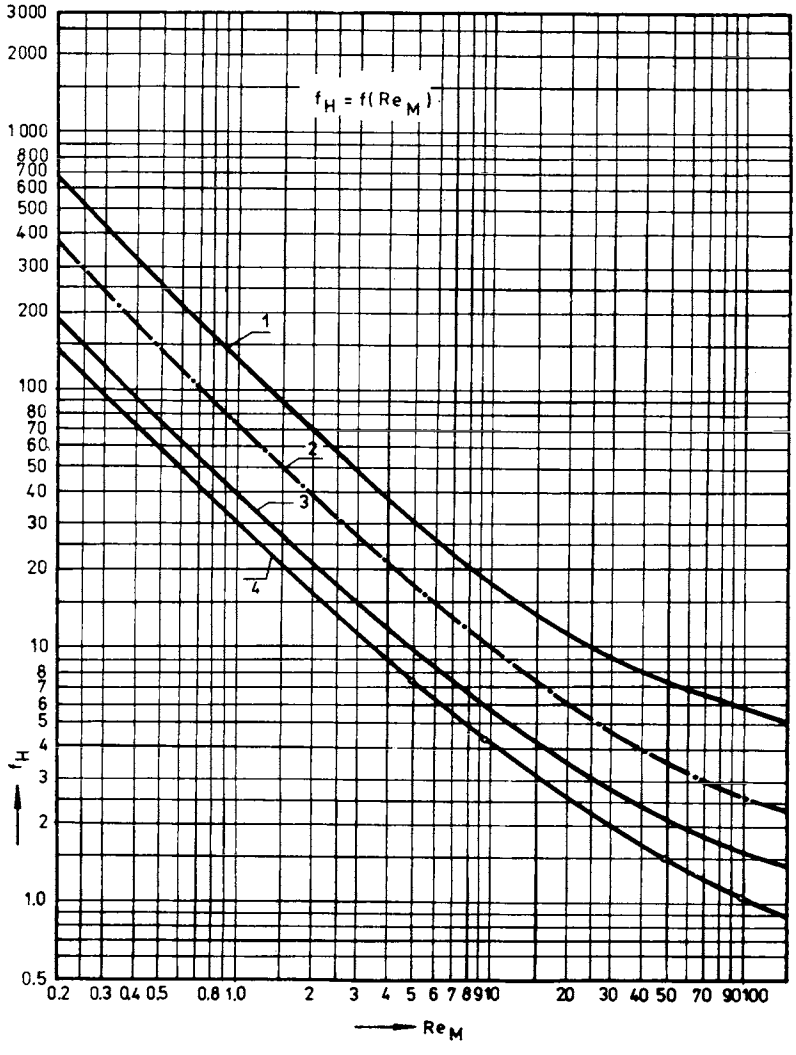

Fig. 2.3. Relationship between hydraulic friction coefficient (f_H) and modified Reynolds number (Re_M) in transitional region. 1 — angular standing grains, 2 — oblique angular grains, 3 — flat, 4 — spherical grains.

$$C_D = \frac{48\, S_g(1-n)}{\mathrm{Re}} + 8cn^{3/2}\sqrt{\frac{\overline{S_g}}{T_k}} \quad \text{(for spheres)}, \tag{2.53b}$$

$$C_D = K_D\, \mathrm{Re}^{-x}. \tag{2.54}$$

Equation (2.53a) takes into account flow velocity (by Re, T_k), shape of the grains (S_g) and of pores (α_s) and soil density (n, n_{eff}) in the whole. The second equation takes spherical and flat-rounded grain into account. The next eqn. (2.54) based on experiment (Peter 1973) has the advantage of covering a wide range of grain shape through the constant K_D, which has a value of $K_D = 30$ to 87 for natural soils (sand and gravel) and crushed rocks, and $K_D = 20$ to 30 for smooth (glass or plexiglass) grains. The exponent x usually varies from $x = 0.35$ to 0.87.

A wide number of values C_D for flat and needle grains are given by Harper (1970).

Finally, a theoretically deduced formula, expressing pressure gradient related to soil and flow characteristics analogous as in eqn. (2.13a), may be introduced in the form

$$\left(\frac{\Delta p}{l}\right) = \left(\frac{\Delta p}{l}\right) 1 + \left(\frac{\Delta p}{l}\right)_2 = C_1 \frac{9}{4}\frac{(1-n)^2}{n^3}\eta\frac{q^*}{d^2} + \\ + C_2 \frac{3}{2}\frac{1-n}{n^3}\varrho_w \frac{q^{*2}}{d}. \tag{2.55a}$$

$$C_1 = 72\text{—}136, \qquad C_1^* = 162\text{—}306,$$
$$C_2 = 1.5\text{—}2.5, \qquad C_2^* = 2.25\text{—}3.75$$

with average, rounded values of constants

$$\frac{\Delta p}{l} = 200\frac{(1-n)^2}{n^3}\eta\frac{q^*}{d^2} + 3\varrho_w\frac{1-n}{n^3}\frac{q^{*2}}{d}. \tag{2.55b}$$

It is in quite good accordance with experimental data obtained for alluvial deposits, and with the Tensdorf equation of the form

$$I_0 = 207\frac{\nu}{g}\frac{1}{n^2\dfrac{1}{1-n}\sqrt{\dfrac{n}{1-n}}}\frac{v}{d_s^2} + 2.97\frac{1}{gn_{eff}^2}\frac{v^2}{d_s}, \tag{2.56}$$

recommended by many authors — Leatherwood and Peterson (1954), Guloti et al. (1970) — as an equilibrium-condition equation.

This short review of formulae and characteristics of seepage represents a wide choice of mathematical expressions which can be used by designers designing a dam structure or levée. Sometimes it is useful to compare values obtained by calculation of various authors; various formulae and data measured in the field and laboratory are mentioned in Chapter 1.

In referring to about 56 formulae treated in this section, it can be mentioned that the first twelve are the most frequently used in classical analysis and calculation, and the remaining come into the consideration if stability problems are treated or if seepage in coarse-grained soils has to be calculated.

2.1.1 Pressures and Forces within the Soil

If we use the normal notation γ for the unit weight of a soil, which we derive from its specific density γ_0' and the porosity n for total σ and effective σ' stresses, we obtain relations at a certain depth z as follows

$$\begin{aligned} \sigma &= \sigma' + p, \\ \sigma_z' &= \gamma_0(1-n)\,z = \gamma_d z. \end{aligned} \tag{2.56}$$

In fully *saturated soil*, the total pressure acts

$$\sigma_z = \gamma_0(1-n)\,z + \gamma_w\, nz = \gamma_n z. \tag{2.57}$$

$$\gamma_{sat} = \gamma_0(1-n) + \gamma_w\, n \text{ — saturated soil,}$$

$$\sigma_z' = (\gamma_0 - \gamma_w)\,z = \gamma' z. \tag{2.58}$$

The *submerget unit weight* $\gamma' = \gamma_{sat} - \gamma_w = (1-n)(\gamma_0 - \gamma_w)$ is a statement of the consequence of the action of Archimedes law, and we can select the term $(1-n)\,\gamma_w$ giving the weight of water displaced by the soil particles.

If we examine the pressure of water flowing through a certain soil element, we obtain these results

in a horizontal direction	$-\dfrac{\partial p}{\partial x}\,dx\,dz,$
in a vertical direction	$-\dfrac{\partial p}{\partial z}\,dx\,dz,$
in total	$-\mathbf{grad}\ \boldsymbol{p}\,dx\,dz.$ (2.59)

We see that the effect is as if the element were subjected to volume forces (**grad** $\boldsymbol{p}$), as well as the gravitational force. After introducing *seepage pressure*, we can say that

$$-\mathbf{grad}\ \boldsymbol{p} = -\gamma_w\ \mathbf{grad}\ \varphi + \gamma_w\ \mathbf{grad}\ z. \tag{2.60}$$

Moreover, we have to consider the expression $(-\gamma_n\ \mathbf{grad}\ z)$, so that in all we obtain three forces acting on the element, as follows

$-\gamma_n\ \mathbf{grad}\ z$	weight,
$\pm\gamma_w\ \mathbf{grad}\ \varphi \rightarrow \gamma_w \dfrac{h}{l} = \gamma_w I$	seepage pressure,
$+\gamma_w\ \mathbf{grad}\ z$	uplift.

The first acts downwards, the second is variable (in the direction of the gradient), and the third acts upwards. The combination of these forces in an embankment or levée can be very undesirable, in particular if with an increase in **grad** φ the resultant volume force is reduced, in accordance with eqn. (2.60), towards or even right down to zero. The grains thus approach a state of weightlessness, familiar to us from the field of liquified sands. In a weightless state, soil cannot support any load since it has no shear strength (Coulomb). A levée or other structure founded on it will inevitably subside. From the condition $(\gamma' - \gamma_w)$ **grad** $\varphi = 0$, it follows that

$$\textbf{grad}\ \varphi_{cr} = \frac{\gamma'}{\gamma_w}, \tag{2.61a}$$

$$I_{cr} = \frac{\gamma'}{\gamma_w}. \tag{2.61b}$$

If we investigate the volume-force potential U, we see that

$$U = \gamma_w \varphi + \gamma' z \tag{2.62}$$

with components

$$\frac{\partial U}{\partial x} = \frac{\partial p}{\partial x}, \tag{2.63a}$$

$$\frac{\partial U}{\partial z} = \gamma_{sat} + \frac{\partial p}{\partial z} = \gamma' + \gamma_w + \frac{\partial p}{\partial z}.$$

Since

$$\sigma'_x = \sigma_x - p, \quad \sigma'_z = \sigma_z - p, \quad \tau = \bar{\tau},$$

then the following apply for *total equilibrium*

$$\begin{aligned} \frac{\partial \sigma'_x}{\partial x} + \frac{\partial \tau}{\partial x} + \frac{\partial U}{\partial x} &= 0, \\ \frac{\partial \sigma'_z}{\partial z} + \frac{\partial \tau}{\partial x} + \frac{\partial U}{\partial z} &= 0. \end{aligned} \tag{2.64a}$$

The *components of potential* are

$$-\frac{\partial U}{\partial x} = -\gamma_w \frac{\partial \varphi}{\partial x},$$

$$-\frac{\partial U}{\partial z} = -\gamma' - \gamma_w \frac{\partial \varphi}{\partial z} = -\gamma_{sat} + \gamma_w - \gamma_w \frac{\partial \varphi}{\partial z}. \tag{2.63b}$$

An important point follows from these relations, that for homogeneous embankments (without a protective apron), water pressures are not concentrated on the upstream slope as is often erroneously assumed, but are dispersed in a system of

volume stresses which act distributively on the entire volume of saturated soil. One of the designer's tasks is to resolve these forces correctly.

We can follow the action of capillary forces from Fig. 2.4. Consider the element dS at a depth h below the water table, where for a weight of dry sand γ_d and wet sand γ_n, the *vertical stress* will be

$$\begin{aligned}
&\sigma_z = \gamma_d e + \gamma_n(\zeta + h),\\
&\sigma'_z = \sigma_z - p\,;\ \textit{if}\ \gamma_{sat} \approx \gamma_n\,;\\
&\sigma'_z = \gamma_d e + \gamma_n(\zeta + h) - \gamma_w h = \gamma_d e + \gamma_n \zeta + \gamma' h,\\
&\sigma'_z = \gamma_d e + \gamma_w \zeta + \gamma'(h + \zeta).
\end{aligned} \tag{2.64b}$$

Above the water table, the following pressures act on the element

$$\begin{aligned}
&\sigma_z = \gamma_d e + \gamma_n(\zeta - h'),\\
&\sigma'_z = \gamma_d e + \gamma_n(\zeta - h') - (-\gamma_w h') = \gamma_d e + \gamma_n \zeta - \gamma' h',\\
&\sigma'_z = \gamma_d e + \gamma_w \zeta + \gamma'(\zeta - h').
\end{aligned} \tag{2.65}$$

The product $\gamma_w \zeta = p_c$ is also termed the *capillary pressure*, and its effect when water flows through an embankment is not necessarily negligible. Between the gravitational water limit described by a phreatic surface and the capillary water limit, σ'_z is greater than σ_z which leads to an increased pressure gradient.

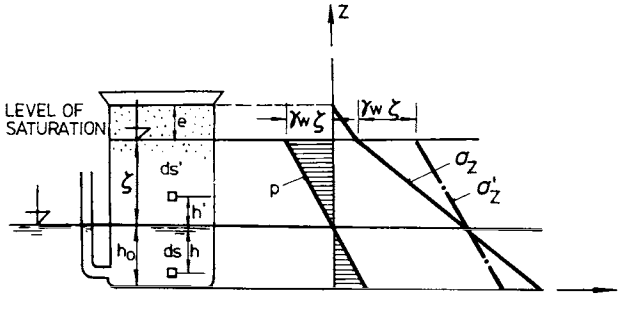

Fig. 2.4. The action of capillary forces.

In soil consolidation, stresses and their variations are determined through the change in effective stress $d\sigma'$. They are connected to volume changes dV by the fundamental equations

$$-\frac{dV}{V} = m_v\, d\sigma', \tag{2.66}$$

where m_v is the coefficient of volume compressibility $[M^{-1}\,T^2\,L^1]$,

$$\begin{aligned}
&dV = d(nV) = V\, dn,\\
&-dn = m_v\, d\sigma',
\end{aligned} \tag{2.67}$$

$$\sigma = \sigma' + p = \text{constant}. \tag{2.68}$$

During the construction of the dam the load ($\gamma_d e$) increases. Since $d\sigma' + dp = 0$, the effective stress increases.

The consolidation process is bound up with the displacement of water from the pores and with pressure changes. According to Terzaghi, the following relations apply with the coefficient of permeability k and volume compressibility of water β

$$\frac{\gamma_w(m_v+n\beta)}{k}\frac{\partial p}{\partial t}=\Delta p \rightarrow \sim \frac{m_v\gamma_w}{k}\frac{\partial p}{\partial t}=\Delta p, \tag{2.69}$$

$$\frac{\partial p}{\partial t}=c_v\Delta p \tag{2.70}$$

if

$$c_v=\frac{k}{\gamma_w m_v}=\textit{coefficient of consolidation}\ [L^2\,T^{-1}].$$

A general equation of consolidation for anisotropic soil and with permeability coefficients in the three principal directions k_x, k_y, k_z, is

$$\frac{\partial p}{\partial t}=\frac{k_x}{m_v\gamma_w}\frac{\partial^2 p}{\partial x^2}+\frac{k_y}{m_v\gamma_w}\frac{\partial^2 p}{\partial y^2}+\frac{k_z}{m_v\gamma_w}\frac{\partial^2 p}{\partial z^2}. \tag{2.71}$$

We use a slightly modified form when we wish to define the total magnitude and variations of pore water pressure according to Florin.

From the standpoint of seepage flow, we must consider whether we are concerned with a seepage-free surface typical of the body of an embankment, or with pressure-potential flow, when dealing with embankment subsoils, etc. and whether we have stationary or unsteady flow.

In calculations involving a free (phreatic) surface, stationary flow is usually assumed, not because stationary flow is in fact more widespread for a critical state, but because the calculations are simpler. It often happens that for specific short periods, we approximate varying flow processes to stationary ones.

2.2 A Homogeneous Embankment on an Impermeable Subsoil

Calculation of seepage for a *homogeneous dam* on an impermeable subsoil is extremely simple, all the more so if we accept further simplifying assumptions, for example an isotropic soil character, and the applicability of Darcy's equation (2.3) and those derived from it (2.6—2.11b). In this case, the region of flow is not affected by peculiarities in conditions at the flow-field extremities. This is especially true if we assume a drainage blanket at the foot of the free slope. We are concerned here with free surface seepage (we assume stationary) and with a clearly defined flow field.

According to the validity of equilibrium and continuity equations, we may assume that in the region marked out in Fig. 2.5b, the Cauchy—Rieman conditions (Dalambert's and Euler's) are fulfilled, and therefore a diagram of potential (φ) and flowlines (ψ) in a plane defines a complex seepage (velocity) potential ω — as

a new function. Polubarinova-Kochina (1952) and Hálek and Švec (1979) start from the idea that $\varphi(x, y)$ and $\psi(x, y)$ are conjugate harmonic functions and express this function

$$\omega = \varphi + i\psi, \tag{2.72}$$

which appears as a function of a complex variable, i.e. $z = x + iy$, which can be expressed by the equation

$$z = A\omega^2. \tag{2.73}$$

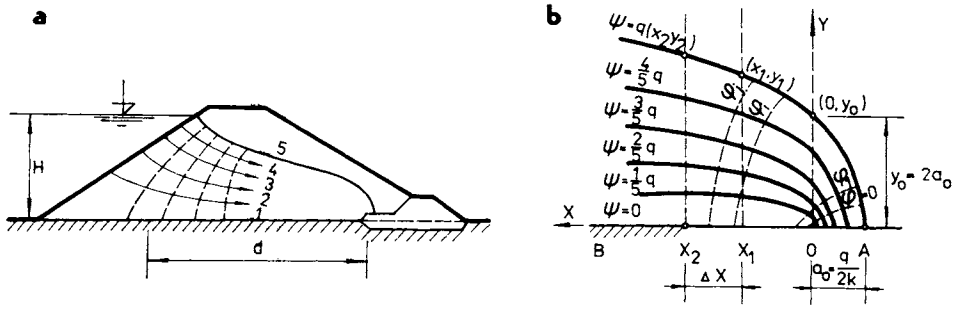

Fig. 2.5. Seepage through a homogeneous dam with a gravel toe-filter. a — phreatic line estimated, b — investigated part of flowlines.

Inflow ($q \to \psi_d$) into the drain at the foot will be limited by the seepage curve ψ_0 on which $p = 0$, and therefore

$$\varphi + ky = 0,$$
$$\varphi = -ky,$$
$$\psi = \psi_d.$$

By substituting into eqns. (2.72) and (2.73) and separating real and imaginary parts, we obtain a relation for the constant A in eqn. (2.73), thus

$$x = iy = A(-ky + i\psi_d)^2, \tag{2.74}$$

$$x = A(k^2y^2 - \psi_d)^2, \tag{2.75}$$
$$y = -2Ak\psi_d y,$$

$$A = -\frac{1}{2k\psi_d}. \tag{2.76}$$

Substituting into eqn. (2.75) we see that

$$x = -\frac{ky^2}{2\psi_d} + \frac{\psi_d}{2k},$$
$$y^2 = -\frac{2\psi_d}{k}\left(x - \frac{\psi_d}{2k}\right). \tag{2.77}$$

With the help of eqn. (2.74), we arrive at the general coordinates

$$x = -\frac{1}{2k\psi_d}(\varphi^2 - \psi^2), \qquad y = -\frac{\varphi\psi}{k\psi_d}. \tag{2.78a}$$

The system of eqn. (2.77) shows that we have here a *system of parabolae*. On the flowline with zero flow $\psi = 0$, we have the positive $y = 0$ axis

$$x = -\frac{\varphi^2}{2k\psi_d}, \tag{2.78b}$$

If we introduce specific values of ψ into eqn. (2.78a), we obtain confocal parabolae. For $\varphi = 0$ we find that

$$x = \frac{\psi^2}{2k\psi_d} \tag{2.78c}$$

which points to the fact that this equipotential is part of the abscissa axis. If we take the section where $0 < x < \psi_0/2k = q/2k$, we obtain three basic characteristics $\psi = 0$, $\psi = \psi_0$, and $\varphi = 0$. At point 0 (at the origin), $\varphi = 0$, $\psi = 0$; at point A (intersection with the seepage curve), $\varphi = 0$, $\psi = \psi_d = q$.

If we take the basic characteristics of a parabola with its focus at the origin of the x_0, y_0 coordinate system to be the coordinates of the points where it crosses the axes, and denote one of these $x_0 = a_0$, then we have

$$y_0 = 2a_0 = \frac{q}{k}, \tag{2.79a}$$

$$\frac{q}{2k} = a_0. \tag{2.79b}$$

Making use of these equations, we can determine seepage, q, so that

$$q = \psi_d = 2ka_0. \tag{2.79c}$$

First to use the above approach were Forchheimer (1914), Pavlovskiĭ (1931) and Polubarinova-Kochina (1952). Through different means, Kozeny (1953) also arrived at the equation of a parabola as the boundary of the flow region, and the final part of the curve is sometimes though not entirely justifiably named after him (the Kozeny parabola).

If we return to our diagram (Fig. 2.5b) where we show two vertical lines at distances x_1, and x_2 from the origin, we can write down the seepage equation for each, and according to eqn. (2.77), we can exclude $\psi_0 = q$. Thus we obtain

$$q = -k\frac{y_2^2 - y_1^2}{2(x_2 - x_1)} = -k\frac{y_2^2 - y_1^2}{2\Delta x}. \tag{2.80}$$

After certain further modifications, we can obtain the approximate equation

$$q = k\frac{H^2}{2d}, \tag{2.81}$$

in which, considering the orientation to the axes, we do not ignore the minus sign. Also, y_2 is taken as H, y_1 as 0, and the distance of an imaginary vertical plane (for the inflow of water into the embankment body) from the focus of the seepage parabola is taken according to Fig. 2.6.

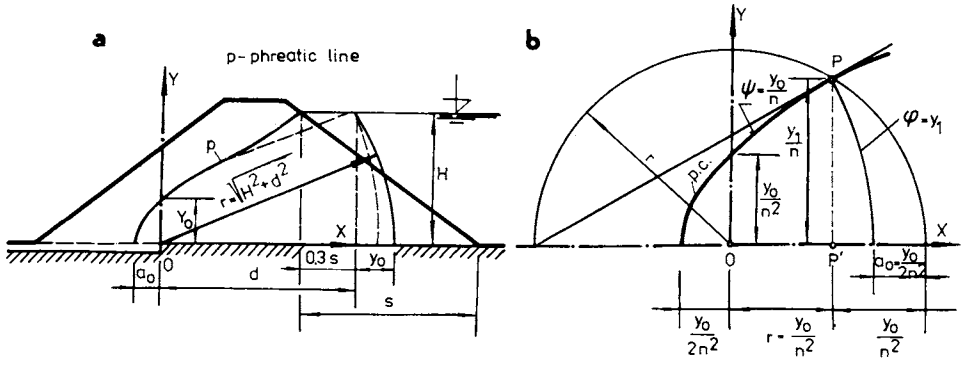

Fig. 2.6. Seepage-parabola construction. a — destination of the parameters y_0, a_0, b — flowline and equipotential line.

The graphical construction in Fig. 2.6a, b follows from geometric and trigonometric relations between confocal parabolae. From these diagrams, y_0 is given by

$$y_0 = \sqrt{H^2 + d^2} - d. \tag{2.82}$$

If we substitute this value of y_0 into eqn. (2.79a) and rearrange slightly, we obtain a *formula for seepage*

$$q = ky_0 = k(\sqrt{H^2 + d^2} - d), \tag{2.83}$$

where H is the head of restrained water, k is the coefficient of permeability, and d is the length of the projection of the line connecting the focus and the intersection point P (the point where the tangent of inflection to the parabola intersects the water surface).

If we evaluate the expression in brackets (eqn. 2.83) by the square root formula we find that

$$q = k(0.398H - 0.040d), \tag{2.84a}$$

because

$$\sqrt{H^2 + d^2} \cong 0.398H + 0.960d,$$

and thus

$$\frac{q}{kH}=0.398-0.040\,\frac{d}{H}. \tag{2.84b}$$

Equations (2.77)—(2.84) are all derived using the assumption that over the final part, the phreatic curve always describes the form of a parabola. Casagrande discovered, however, that for both the slope and also pebble drains at the foot, the phreatic line differs from the presupposed parabola and in fact always remains a certain distance below it (Fig. 2.7). Observing these differences, he formulated

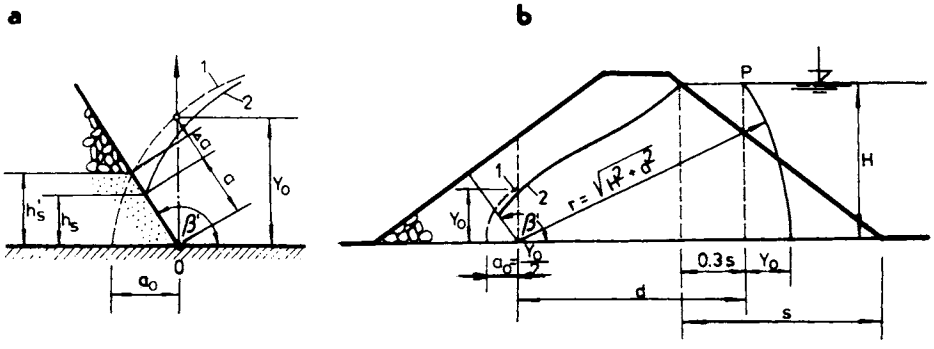

Fig. 2.7. Flowline in the vicinity of gravel drainage. a — basic parameters, b — parameters of the correction; 1 — estimated parabola, 2 — real phreatic line.

a curve which depended on the angle of drainage slope and a coefficient C relating the difference β between the real and assumed points of entry of the phreatic curve into the drainage region (Fig. 2.8a)

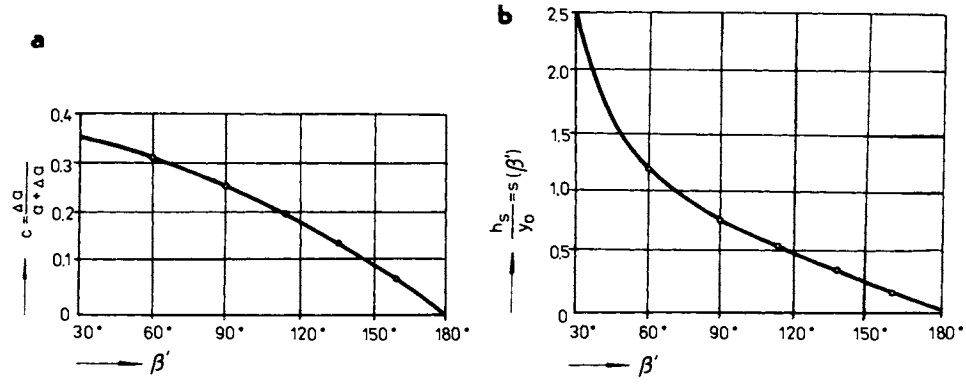

Fig. 2.8. Relationship between parameters $c=\frac{\Delta a}{a+\Delta a}$, $\frac{h_s}{y_0}$ and angle β'. a — basic correction, b — height correction.

$$C=\frac{\Delta a}{a+\Delta a}=1-\frac{h_s}{h'_s}. \tag{2.85}$$

With the help of relations resulting from the parameters of the seepage parabolae, and from the graphical expression of the path of Casagrande's phreatic curve, a further dependence arises as follows

$$\frac{h'_s}{y_0}=\frac{\sin\beta'}{1-\cos\beta'},$$

$$\frac{h'_s}{y_0}=(1-c)\frac{\sin\beta'}{1-\cos\beta'}=m(\beta'). \tag{2.86}$$

Besides these relations allowing relatively exact calculation of seepage flow, Schneebeli (1966) came up with several approximate, experimentally derived equations and graphical constructions. One of these is Huard de la Marre's equation

$$q=k\frac{H^2}{b_1+b_2}, \tag{2.87}$$

which is inadequate since it takes no account of the gradients β_1, β_2 of the embankment slopes. This gives rise to an error in q such that $\Delta q=(10\text{—}15\,\%)\,q$. A rather more precise equation, also experimentally determined, is given by

$$q=k\frac{H^2}{(0.8+0.0045\beta')\,b_1+1.18b_2}. \tag{2.88}$$

We can determine the point at which the seepage surface emerges on the embankment's downstream slope through the following relation

$$\frac{h_s}{H}=\mathrm{f}(\beta)\frac{H}{b_1+b_2}, \tag{2.89}$$

which is represented graphically in Fig. 2.9.

A comparison of equations for the phreatic line and seepage flow according to Casagrande (eqns. 2.85 and 2.86) and Huard de la Marre (eqn. 2.87) gives rise to Schneebeli's graphical analytical relation which is depicted semi-logarithmically in Fig. 2.10, and leads to the equation

$$\log\left(\frac{h_s}{\frac{q}{k}}\right)=0.27\tan\left(\frac{\pi}{2}-\beta\right)-0.15 \tag{2.90}$$

for the range

$$20°\leqq\beta\leqq150°.$$

As for the graphical representation, eqn. (2.90) can be used for embankments without foot drainage, a frequent occurrence in canal embankments and levées, by

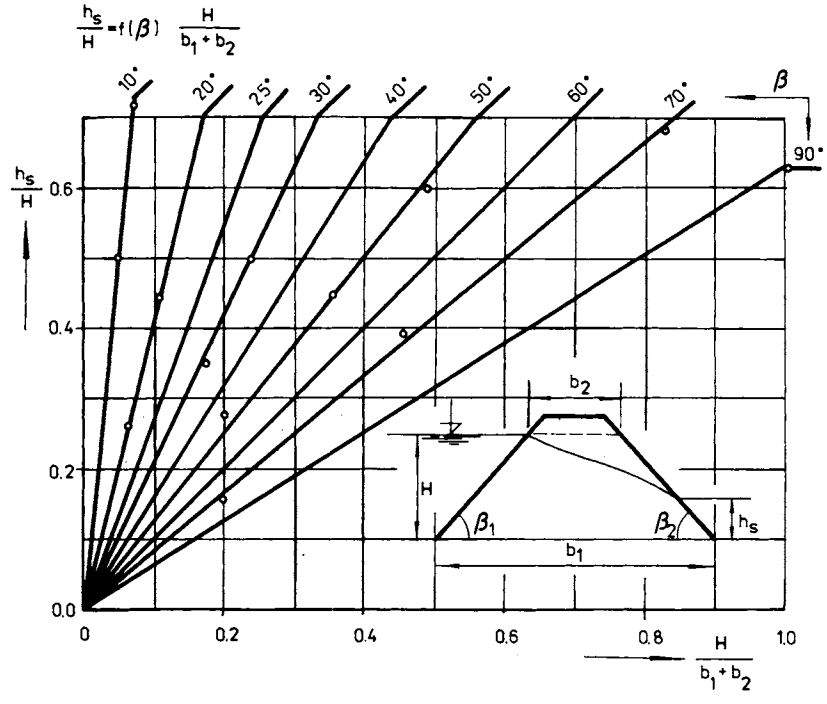

Fig. 2.9. Relationship $\frac{h_s}{H}$ and $\frac{H}{b_1+b_2}$ after Huard de la Marre (Schneebeli 1966).

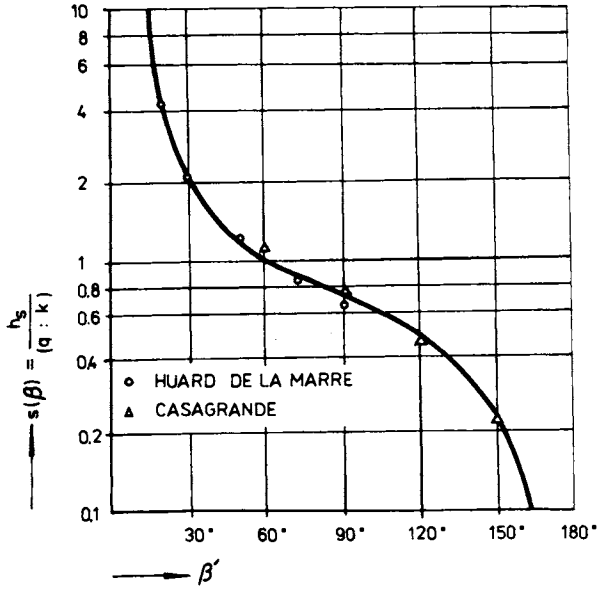

Fig. 2.10. Graph for estimation of the value h_s.

replacing β with β_2, the gradient of the downstream slope, and also for those with a prismatic drain by replacing β with β'.

The data we gain with the help of these equations and graphical constructions is usually sufficient both for finding the seepage flow, and for determining the course of the phreatic curve, at the entry points and also the foot of the downstream slope where our greatest interest lies. If we need to know the path more exactly, we calculate its coordinates using eqns. (2.77) and (2.78a).

We can also use the advantages of the complex potential to express the path of the phreatic line analytically. If we use the Polubarinova-Kochina approach and notation with k becoming $\varkappa$ and heads H_1 and H_2 (see Fig. 2.11a), we can write

$$\omega = \varphi + iq = \frac{1}{2}\varkappa(H_1 + H_2) - \varkappa y + iq,$$

$$x = -\frac{\varkappa y^2}{2q} + \frac{q}{2\varkappa} + \frac{1}{\pi}(\gamma-\xi)^{1-\beta}(-\gamma-\xi)^{\alpha}(1-\xi)^{\beta}(-1-\xi)^{1-\alpha}\times$$

$$\times\left\{\int_{-1}^{-\gamma}\frac{\left(a_0-\frac{a_1}{K'}F-\frac{a_2}{K'^2}F^2\right)\mathrm{d}t}{(\gamma-t)^{1-\beta}(-\gamma-t)^{\alpha}(1-t)^{\beta}(1+t)^{1-\alpha}(t-\xi)} - \right.$$

$$\left. -\int_{1}^{\gamma}\frac{\left(b_0-\frac{b_1}{K'}F-\frac{b_2}{K'^2}F^2\right)\mathrm{d}t}{(t-\gamma)^{1-\beta}(\gamma+t)^{\alpha}(1-t)^{\beta}(1+t)^{1-\alpha}(t-\xi)}\right\}. \qquad (2.91)$$

Using an approximate expression for the integral and values of function F and parameter t

$$t = -\frac{-\xi-\gamma+(1-\gamma)\xi\sin^2\frac{\pi\tau}{2}}{-\xi-\gamma-(1-\gamma)\xi\sin^2\frac{\pi\tau}{2}};\quad \frac{1-t}{1+\gamma}\approx\frac{2}{2}=1,\quad K'\approx\frac{\pi}{2},$$

if $t\approx-1$, $\gamma\approx1$ is taken into account

$$\xi = \gamma\sinh\left[\frac{K'}{q}(\varphi-iq),\,\gamma\right] = \gamma\sinh\left(\frac{K'\varphi}{q}+iK',\,\gamma\right).$$

For the left-hand end of the phreatic line, we obtain immediately the expression (where $y=H$)

$$\frac{\varphi}{q} = \frac{\varkappa(H_1+H_2)}{2q} - \frac{\varkappa y}{q} = \frac{\varkappa(H_1-y)}{q} - \frac{\varkappa H}{2q} = \frac{\varkappa(H_1-y)}{q} - \frac{K}{K'},$$

and in its final form

$$x \approx \frac{\varkappa(H_1^2-y^2)}{2q} + H_1\left[\cot\alpha\pi - F_1\left(\tanh\frac{\varkappa\pi(H_1-y)}{2q},\,\alpha\right)\right] +$$

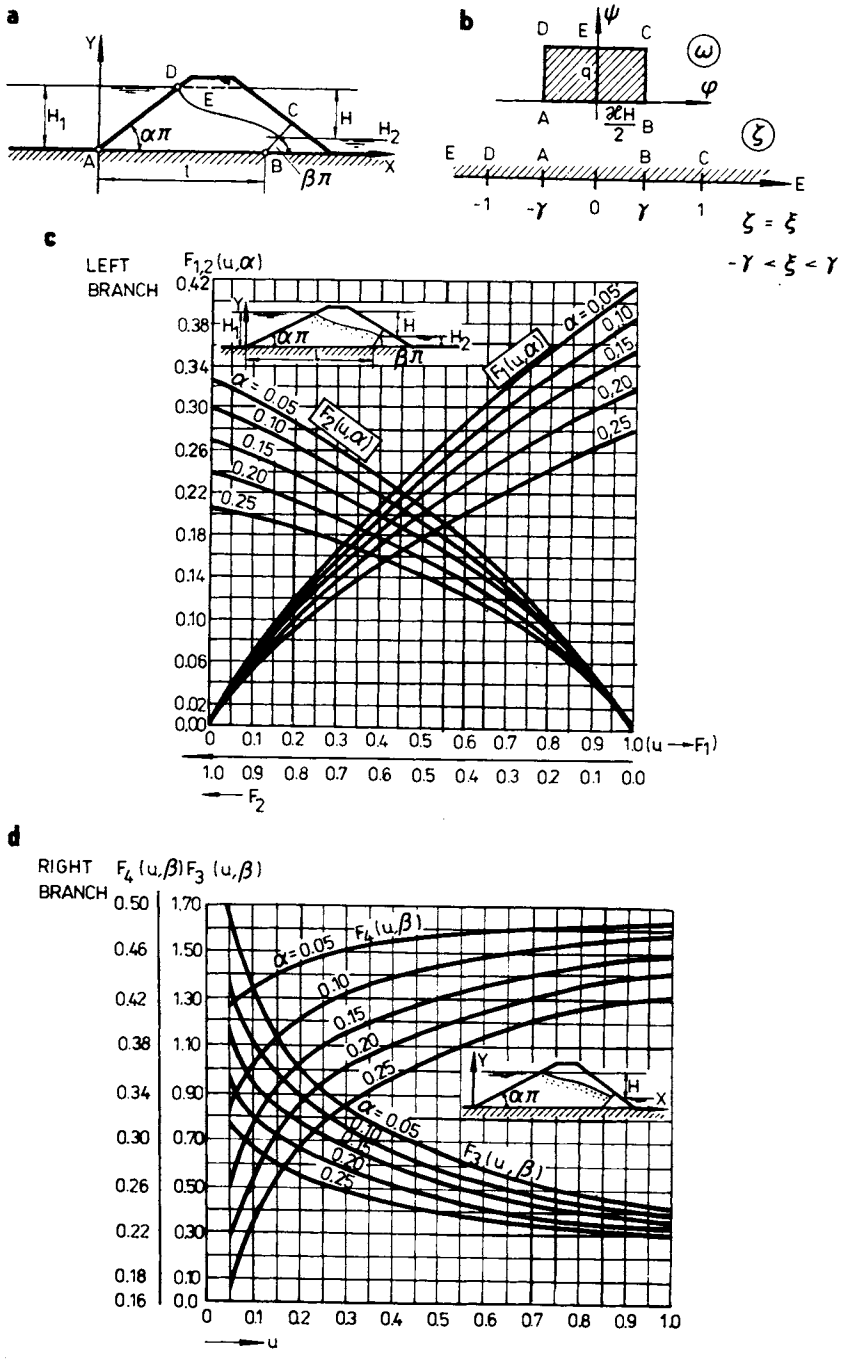

Fig. 2.11. The functionality of the flowline. a — basic scheme, b — transformation of the flow region, c — functions $F_1(u, \alpha)$, $F_2(u, \alpha)$, d — functions $F_1(u, \beta)$, $F_2(u, \beta)$.

$$+\frac{q}{\varkappa}\tan\alpha\pi F_2\left(\tanh\frac{\varkappa\pi(H_1-y)}{2q},\alpha\right). \tag{2.92}$$

Analogously for the right-hand portion of the phreatic curve, we have the expression

$$x\approx l+\frac{\varkappa(H_2^2-y^2)}{2q}+H_2F_3\left(\tanh\frac{\varkappa\pi(y-H_2)}{2q},\beta\right)+$$
$$+\frac{q}{\varkappa}F_4\left(\tanh\frac{\varkappa\pi(y-H_2)}{2q},\beta\right), \tag{2.93}$$

where

$$F_1(u,\alpha)=\frac{2\cos\alpha\pi}{\pi}\int_0^1\cot^{1-2\alpha}\frac{\pi\tau}{2}\tan^{-1}\left(u\tan\frac{\pi\tau}{2}\right)d\tau,$$

$$F_2(u,\alpha)=\frac{2\cos\alpha\pi}{\pi}\int_0^1\cot^{1-2\alpha}\frac{\pi\tau}{2}\tan^{-1}\left(u\tan\frac{\pi\tau}{2}\right)\cdot\left[1-\frac{1}{\pi}\tan^{-1}\left(u\tan\frac{\pi\tau}{2}\right)\right]d\tau,$$

$$F_3(u,\beta)=\frac{2\cos\beta\pi}{\pi}\int_0^1\tan^{1-2\beta}\frac{\pi\tau}{2}\cot^{-1}\left(u\tan\frac{\pi\tau}{2}\right)d\tau,$$

$$F_4(u,\beta)=\frac{1}{2}-\frac{2}{\pi^2}\sin\beta\pi\int_0^1\tan^{1-2\beta}\frac{\pi\tau}{2}\left[\cot^{-1}\left(u\tan\frac{\pi\tau}{2}\right)\right]^2d\tau,$$

$u\cong\tanh\dfrac{\pi x(H_1-y)}{2q}$; $\alpha\pi=\beta_1$; $\beta\pi=\beta_2$ (gradients of up- and downstream slopes).

Values of the functions $F_1(\alpha, u)$, $F_2(\alpha, u)$, $F_3(\beta, u)$, $F_4(\beta, u)$ can be found in Numerov's tables (1947) and are also graphically depicted in Polubarinova-Kochina's work (1952). The phreatic curve for $y=0.2\varkappa H$, $l=3.16H$, $\alpha=\pi/4$ is shown in Fig. 2.12.

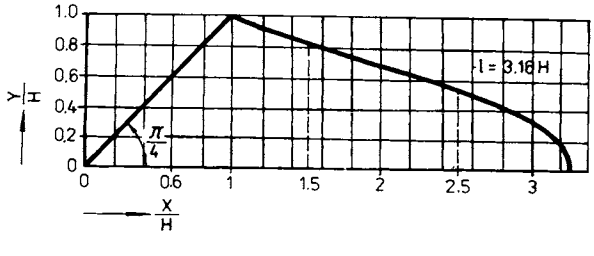

Fig. 2.12. Phreatic line plotted by means of eqns. (2.92) and (2.93).

If we have an *anisotropic embankment*, often the result of treatment technology even when it is being constructed of a homogeneous soil, the simplest method of calculation is to fix a *coefficient of anisotropy* ($\lambda=k_h/k_v$) as the ratio of the horizontal and vertical permeability coefficients, or to determine the square root of the reverse ratio, the so-called *reduction coefficient*

$$\varkappa_r = \sqrt{k_v : k_h}. \tag{2.94}$$

Using this reduction coefficient, we multiply through all the horizontal length dimensions in the embankment profile and redraw it (Fig. 2.13). The coordinates of the individual points (ξ, η) are therefore transformed so that $\xi = \varkappa_r x$ and $\eta = y$.

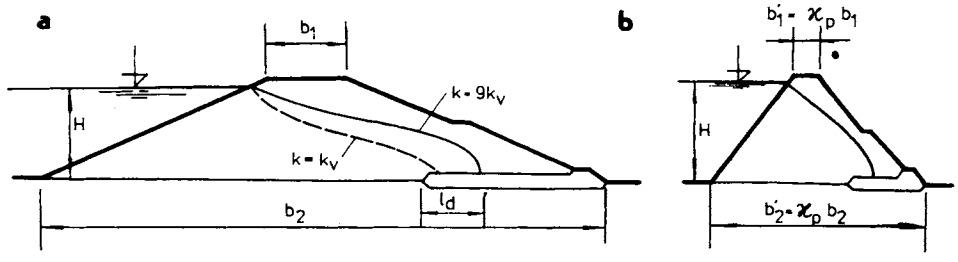

Fig. 2.13. Phreatic line. a — in a normal cross-section, b — in a shortened cross-section.

For further progress, we must add the phreatic curve to the profile we have drawn, as well as the remaining seepage parameters, y'_0, a'_0, d', etc. (for example $d' = \varkappa_r d$), which enables us to proceed using the formulae we have already derived. Thus we can find the seepage flow through eqn. (2.83) which, for the transformed profile, has the form

$$q = k_h(\sqrt{H^2 - d^2} - d),$$

and then

$$q = \sqrt{k_h k_v}\left(\sqrt{H^2 + \frac{k_v}{k_h} d^2} - \sqrt{\frac{k_v}{k_h}}\, d\right). \tag{2.95}$$

This approach can almost always be used for canal embankments and levées, since in general they are never built with the ratio $k_h : k_v \geq 10$.

2.2.1 Calculation of Seepage Flow with Regard to the Capillary Action of Soil

The capillary properties of a soil mean that the pressure gradient across an arbitrary vertical in the profile depends not only on the slope of the phreatic line, which introduces the free gravitational surface path, but also on the depth of a band of capillary water (Fig. 2.14), penetrating up to a height of h_c, so that approximately

$$h_c = \frac{0.3}{d} \cos \alpha \,. \tag{2.96}$$

The volume of capillary water within this height is

$$w_c = \frac{2\sigma_0 a}{h_c \gamma_w} c_w = \frac{2\sigma_0 a}{p_c} c_w, \tag{2.97}$$

where σ_0 is the water surface tension; γ_w the specific unit weight of water; c_w the coefficient of capillary moisture content; $a = S_0/r_{max}$ the coefficient of capillary pressure; S_0 the total surface area of the pores, and r_{max} the maximum pore radius.

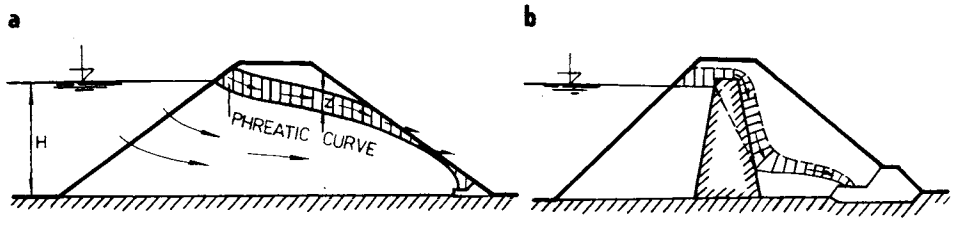

Fig. 2.14. Phreatic line and capillary fringe. a — capillary fringe in a homogeneous dam, b — capillary fringe of a clay core.

If h'_c is the *capillary height* and z the height of the strip above the free surface, then the hydraulic head is $h'_c - z$ and the hydraulic gradient is given by

$$I = \frac{h'_c - z}{z} \,. \tag{2.98}$$

The average speed of capillary rise in a soil of porosity n is

$$v_s = \frac{1}{n} v_k = \frac{1}{n} k \frac{h'_c - z}{z} = \frac{dz}{dt} \,. \tag{2.99}$$

From the equation

$$(h'_c - z) - h_c \ln (h_c - z) = \frac{1}{n} kt + C,$$

through modification, integration and determination of the integration constant C, we obtain the *rise time*

$$t = \frac{nh'_c}{k} \left(\ln \frac{h'_c}{h_c - z} - \frac{z}{h'_c} \right) . \tag{2.100}$$

At times later than this, it is necessary in the case of levées to perform the calculations with an increased gradient and seepage flow, which we determine

through the equation

$$q = k \frac{H^2 - y_0^2}{2d} A_h A_p c_k. \tag{2.101}$$

Here A_h is a coefficient relating to the construction of the levée ($A_h = 1.0$—1.5), A_p is a coefficient taking in the type and depth of the subsoil ($A_p = 0.8$—2.75), and c_k is a coefficient for type of soil in the levée. Some c_k values are given in Table 2.4.

Table 2.4. Values of capillarity coefficient c_k

Soil	Sands	Sandy silts	Loam sands	Silty loam
c_k	1.0—1.5	1.3—1.75	1.5—2.0	1.75—2.5

Capillary action takes noticeable effect, especially in smaller embankments where the height of the capillary film may be as much as several tens of per cent of the total head H. The value of the increase in seepage flow mainly depends on the soil type used, and to a lesser extent on the embankment construction.

As regards capillarity, the value of coefficient c_k is variable. For levées, this is expressed for a state after full soaking (i.e. when it is fully in use). The so-called sweating of an embankment must be attributed largely to the effect of capillary action.

2.3 Embankments with Sealing Elements and those on a Permeable Subsoil

From the point of view of seepage calculations, embankments with sealing elements raise the problem of the shift and variability of water velocity, the water being that which seeps through two different porous media, in which the filtration properties of the less porous material (sealing) are those governing seepage flow. The ratio of the permeability coefficients in the permeable (k_0) and sealing (k_t) soils defines the velocity direction, especially at the boundary, and also the shape of the seepage curve. From the seepage standpoint, we distinguish between two principal cases. In the first case the differences — permeability ratios — vary from one to two or three orders of magnitude, 10—1000, and in the second case are about 1000. In the first case, both soils (materials) have to be considered, and in the second the only criterion is the permeability of the sealing soil or other material (e.g. concrete, asphalt, etc.).

The seepage flow and more particularly the path of the phreatic surface affect the positioning of the sealing, which is usually located aslant near the water-facing

slope, or vertically, sometimes with a slight slope in the centre of the structure. Since the simplest case for calculating seepage is a homogeneous embankment, let us investigate ways in which we can perform the calculations using methods already introduced.

For an *embankment with a vertical seal* (Fig. 2.15) of width t and permeability coefficient k_t, we can obtain the solution by replacing the seal with a strip of soil (called a replacement core) of width j which causes the same head loss as the seal.

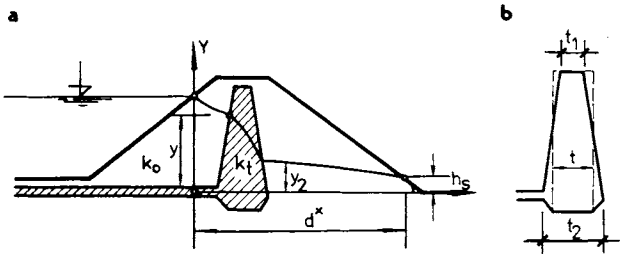

Fig. 2.15. Vertical clay core. a — real phreatic line, b — a compensatory core and phreatic line.

If we denote $\Delta y = y_2 - y_1$, $\Delta x = t$, then we can use eqn. (2.80) to determine the *seepage through the sealing*. Accordingly, we have

$$q_1 = \frac{k_t}{t} \frac{y_2^2 - y_1^2}{2}.$$

For seepage through the replacement core of width j, we have

$$q_2 = \frac{k_0}{j} \frac{y_2^2 - y_1^2}{2}.$$

Then from the condition that these two represent the same seepage

$$\frac{k_t}{t} \frac{y_2^2 - y_1^2}{2} = \frac{k_0}{j} \frac{y_2^2 - y_1^2}{2}, \tag{2.102}$$

$$\frac{j}{t} = \frac{k_0}{k_t}.$$

Thus, if we replace the sealing width by a strip of soil of width

$$j = t \frac{k_0}{k_t}, \tag{2.103}$$

the seepage through the embankment and the profile of the phreatic curve will be the same as for the homogeneous equivalent in Fig. 2.16.

Should the embankment have a thick core with angled sides, the decisive quantity affecting seepage is the permeability of the sealing, most particularly when the permeability difference exceeds three orders of magnitude. We can then use the

calculation and *seepage-curve construction* (Fig. 2.17) given in Section 2.2. With the help of eqn. (2.82), we can evaluate the parameter y_0, and also by substituting the value k_2 into eqn. (2.84), we obtain the seepage flow $q_2 = q$.

If the permeability of the downstream wedge is characterized by coefficient k_3, for the height of the surface of the water flowing through that wedge at the contact face h_2, the following applies

$$h_2 = \sqrt{2ly_0 \frac{k_2}{k_3}} + h_d, \tag{2.104}$$

where h_d is the height of water in the drain.

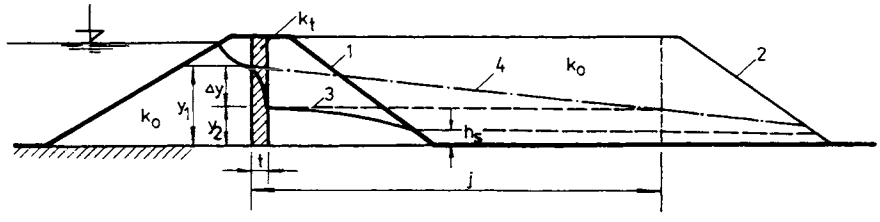

Fig. 2.16. Idealized phreatic line in a compensatory core of a width j. 1 — slope of the real dam, 2 — slope of the idealized dam, 3 — phreatic line of the real dam, 4 — phreatic line in the compensatory, idealized core.

The height at the midpoint of the length l will be $1/2(h_2 + h_d)$ and seepage through the wedge is

$$q_3 = k_3 \frac{h_2^2 - h_d^2}{2l}. \tag{2.105}$$

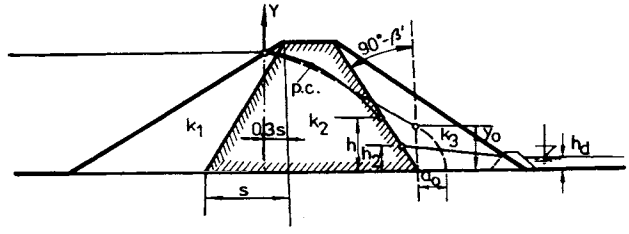

Fig. 2.17. Phreatic line in a wide silty core.

From the stipulation that $q_2 = q_3 = q$, we compute the values of h_2 and h_d, from which we obtain the course of the phreatic curve from its origin, through the water-facing slope down to the drain, out of which the water flows to a seepage well, channel or suitable outlet (see Sections 6.2 and 6.5).

Let us now consider *dams with sloping sealing core.* The simplest calculations arise from assuming two separate principal flow conditions for a slanting core; the

upper part where water seeps directly into the filter, without the larger restraining pressure of water from the downstream side, and the lower part, whence it flows to a saturated stabilization region under the phreatic surface where the pressure is determined by the piezometric height h_3. In this region, it is permissible to assume a seepage curve analogous to that for a heterogeneous embankment (Fig. 2.18). However, in both parts the effect of the sealing core slopes can be seen.

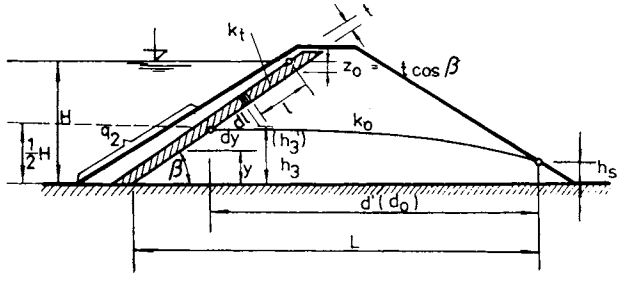

Fig. 2.18. Dam profile with an inclined clay core.

From elementary seepage through a strip of length dy in the upper part, and similarly through a strip of vertical projection dy in the lower part, Uginchus (1960) evaluates the seepage flow q through an embankment with a sloping sealing core, using the equations:

$$\frac{q}{k_t}=\frac{(H^2-h_3'^2\cos\beta)\sqrt{1+\cot^2\beta}-t}{2t} \tag{2.106a}$$

and

$$\frac{q}{k_0}=\frac{h_3'^2}{2d'},$$

where

$$d'=L-\frac{1}{2}H\cot\beta.$$

Therefore

$$\frac{k_t(H^2-h_3'^2-t\cos\beta)\sqrt{1+\cot^2\beta}}{2t}=\frac{k_0h_3'^2}{2d}. \tag{2.106b}$$

The auxiliary height will be

$$h_3'=\sqrt{\frac{\sigma d'\sqrt{1+\cot^2\beta}(H^2-t^2\cos^2\beta)}{\sigma d'\sqrt{1+\cot^2\beta}+t}}, \tag{2.106c}$$

where h_3 is the supposed piezometric height under the centre of the part of the sealing through which water flows.

A relation arises from Dupuit's equation between the depht h_3 and the relative depht h_3' as follows

$$\frac{2q}{k_0}=\frac{h_3^2-h_3'^2}{\frac{H\cot\beta}{2}-h_3\cot\beta}$$

or

$$h_3^2+h_3\frac{2q}{k_0}\cot\beta-\frac{q}{k_0}H\cot\beta-h_3'^2=0, \tag{2.106d}$$

$$h_3=\sqrt{\left(\frac{q}{k_0}\cot\beta\right)^2+\frac{q}{k_0}H\cot\beta+h_3'^2}-\frac{q}{k_0}\cot\beta. \tag{2.106e}$$

Finally, we obtain (through approximation)

$$q=k_t\frac{1}{2t}(H^2-h_3^2)\sqrt{1+\cot^2\beta}. \tag{2.106f}$$

According to Pavlovskiĭ, the total seepage per meter length of embankment will be

$$q_1=\frac{k_t}{2t\sin\beta}(H-h_3)^2-z_0^2+2(H-h_3)h_3=$$

$$=k\frac{H^2-h_3^2-z_0^2}{2t\sin\beta}. \tag{2.107a}$$

If we denote the ratio of permeabilities k_0/k_t as $\varkappa$, then $k_t=k_0/\varkappa$ and

$$q=k_0\frac{H^2-h_3^2-z_0^2}{2t\varkappa\sin\beta}. \tag{2.107b}$$

If to a first approximation we consider the seepage through the upper portion of the sealing, that is above the phreatic curve, as negligibly small ($q_1=0$), then $q=q_0$ and in calculating it we may use a relation analogous to that in eqn. (2.80), which for the section behind the sealing (behind point C) will take the form

$$q'=k_0\frac{h_3^2-y^2}{2l_0}=k_0\frac{h_3^2-h_s^2}{2d_0}. \tag{2.108}$$

After combination with previous equations and modification, we obtain

$$q\cong k_0\frac{h_3^2-h_s^2}{d_0}\ln\frac{H-z_0}{h-z_0-h_2}. \tag{2.109a}$$

The condition for continuity of seepage flow through the sealing and permeable parts of the embankment acts as a control over these approximate expressions, and gives rise to the relation

$$\frac{h_3^2-h_s^2}{d_0}=\frac{(H-h_3)(H+3h_3)}{2t\sin\beta}.$$

We shall use the expression of eqn. (2.107b) to constrain the piezometric heights h_2, h_3 already determined, so that they comply with this expression.

In embankments with a drainage prism or permeable blanket on the free side, we can easily determine the value of y_0, which we then introduce into eqn. (2.105) in place of h_s (the height of the outflow on the downstream slope).

Finally, we also arrive at a formula for an embankment with sloping sealing which extends down into the permeable subsoil as seen in Fig. 2.19

$$q = q_1 + q_2 = \frac{k_1(H^2 - h_3^2)}{2t_1 \sin\beta} + k_2 \frac{H - h_3}{t_2} D. \tag{2.109b}$$

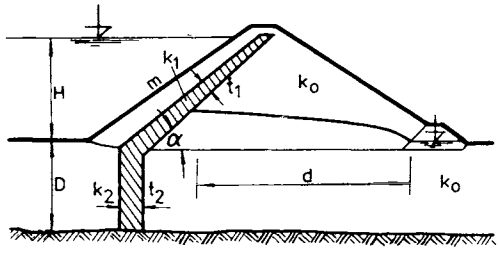

Fig. 2.19. The control of phreatic line.

For the value of piezometric height h_3 behind the sealing, Uginchus states that

$$h_3^3 + ah_3^2 + bh_3 + c = 0,$$

where

$$a = -\left(\frac{d}{m} + \frac{2Dt_1 \sin\beta}{t_2} + \frac{k_1 t_1 \sin\beta}{k_2 m}\right),$$

$$b = -\left(\frac{2D\,\mathrm{d}t_1 \sin\beta}{t_2 m} + H^2 + \frac{2HDt_1 \sin\beta}{t_2} + \frac{2k_1 Dt_1 \sin\beta}{k_2 m}\right),$$

$$c = \frac{H^2 d}{m} + \frac{2HD\,\mathrm{d}t_1 \sin\alpha}{t_2 m}.$$

The advantage of Uginchus' formula is that it is derived from the geometry of the sealing element (t_1, t_2, $\sin\beta$), its permeability k_2, and the head of water H. The coordinate of the seepage line (h_3) behind the sealing is found by evaluating the cubic equation already introduced for h_3.

Let us now consider *homogeneous embankment on a permeable subsoil.* Seepage through an embankment bedded onto a permeable subsoil is most easily evaluated by dividing the seepage into two regions, q_1 (embankment body) and q_2 (subsoil), and then calculating the two seepages separately.

It may also happen, when the same soil exists in both regions, that both the embankment and the subsoil can be treated as one seepage profile (Fig. 2.20).

To determine the characteristic seepage data (y, y_0) for q q_1, it is possible to use eqns. (2.78)—(2.84), and for seepage through a subsoil characterized by permeability k_p we have the approximate expression

$$q_2 = k_p \frac{H}{b_1} \frac{D}{n},$$

where b_1 is the width of the embankment at the foot, n the depth of the permeable underlay, and n a coefficient dependent on the ratio $b_1 : D$ (Table 2.5).

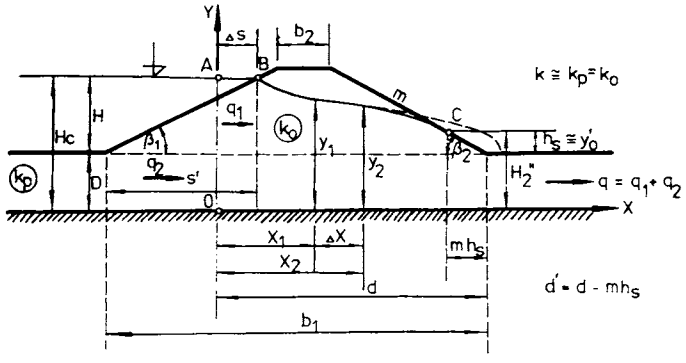

Fig. 2.20. Homogeneous dam lying on a permeable subsoil.

Table 2.5. Values of coefficient n as a function of relationship $b_1 : D$

$\frac{b_1}{D}$	20	5	4	3	2	1
n	1.15	1.18	1.23	1.30	1.44	1.87

The total seepage flow will be

$$q = q_1 + q_2 = k_0 \frac{H^2 - h_s^2}{2d} + k_p \frac{HD}{b_1 n}.$$

Protecting dykes are often constructed from low permeability sandy soils which have approximately the same permeability coefficient as the subsoil $k_0 = k_p$, and the two parts can therefore be considered as a single seepage profile with total height $H + D = H_c$ on the water-facing side and $h_s + D = H_2'$ and $y_0' + D = h_{c2}'$, in the case where there is a drainage element at the free side (Fig. 2.21). For the problem thus conceived, it is necessary to modify the characteristics substituted into eqn. (2.80), so that

$$\Delta s' = (0.3H \cot \beta_1) n = 0.3 n s_1, \qquad (2.110)$$

$$d' = \Delta s' + e_1 + b_2 + H \cot \beta_2 - e \cong s_2 + b_2 + \Delta s, \tag{2.111}$$

$$y_0' = n y_0,$$

in which n is the value of a coefficient arising from the ratio $b_2 : D$.

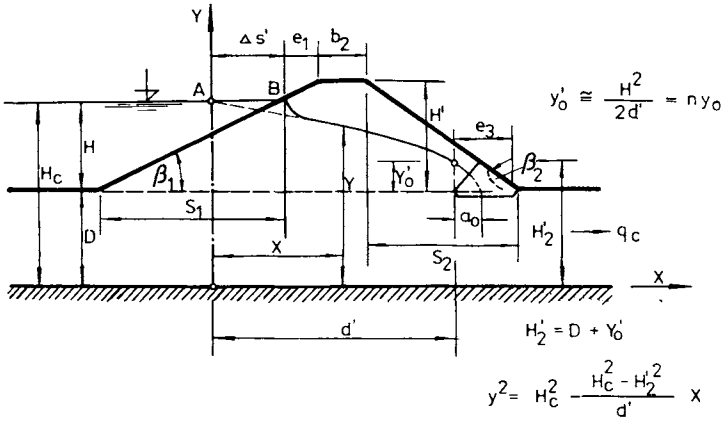

Fig. 2.21. Homogeneous dam with a drainage on the downstream toe lying on permeable subsoil.

Seepage through the embankment and subsoil will be

$$q_c = k_0 \frac{H_c^2 - H_2'^2}{2d'}, \tag{2.112}$$

$$q_c = k_0 y_0', \text{ respectively.} \tag{2.113}$$

The seepage thus calculated may be treated as a maximum since it considers stationary seepage which rarely occurs in protecting dykes.

The indicated computation arises from three simplifying assumptions. These are "uniform flow" of seepage through the embankment and subsoil, with a parabolic boundary to the flow region at the free surface, and a planar boundary along the impermeable substratum at a depth D below the level of the foundation plane. We have assumed that $k_p = k_0$, and in this case the effect of the subsoil will apply in two directions. It will mean an increase in seepage flow and in pressure, and therefore the phreatic curve $(p.l.)_1$ and also the line of piezometric pressures rise above the level of the curve (Voshchinin 1959), $(p.l.)_2$ for a homogeneous embankment bedded directly onto an impermeable subsoil. The phreatic curve begins to be forced upwards (Fig. 2.22).

However, if we trace the seepage through a homogeneous embankment and permeable subsoil, we easily discover that if there are both a preserved stationary flow regime, and the profile of a free surface described by the above eqns. (2.77, 2.78 and 2.91), then we require a constant potential value $\varphi + k_y = \text{constant}$, the

free surface must be given by $\varphi + k_y = 0$ and along the impermeable substratum $\varphi + k_y = -kD$ (Fig. 2.23). For the Zhukovskiĭ function (ϑ) and conforming representations, we obtain the expressions

$$\vartheta = z + \frac{i}{k}\omega = \vartheta_1 + i\vartheta_2, \quad \vartheta_1 = x - \frac{\psi}{k}, \quad \vartheta_2 = y + \frac{\varphi}{k}.$$

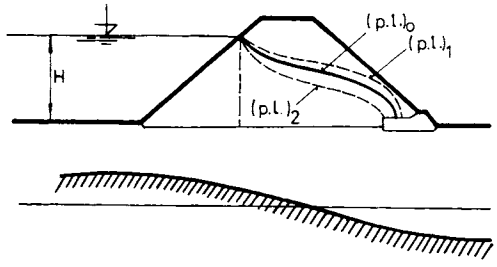

Fig. 2.22. The change in phreatic-line position influenced by subsoil.

For conforming planes there is the expression

$$z = f_1(\xi), \qquad \omega = f_2(\xi), \tag{2.114}$$

where ξ is an auxiliary complex variable,

$$\vartheta = z + \frac{i\omega}{k} = f_1(\xi), \qquad \omega = f_2(\xi). \tag{2.115}$$

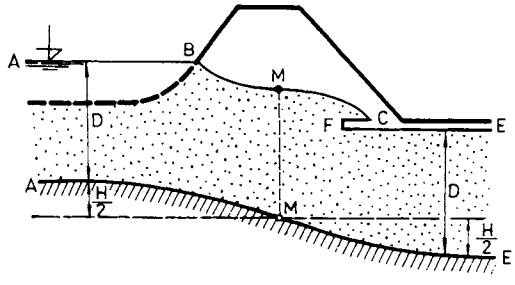

Fig. 2.23. The form of the subsoil surface having fulfilled the requirement of continuity and stationarity of the flow.

In both cases, the seepage flows will be the same only if the same values h, D and length $BC = 2b$ are unchanged, in which case we have

$$q = kH\frac{K'}{2K},$$

where (2.116)

$$K = \tanh\frac{b}{2D}.$$

With regard to the point M, the free surface is rhombosymmetric. The line bounding the impermeable subsoil coming from infinity on either side, should be an even distance from this surface, including both the upper and lower water levels.

In such a case, it is possible to comply with the demands of continuous stationary flow with some sort of rotation (rise) of the plane which divides the permeable and impermeable substrata, on the upstream side in an upward direction (about M) through an amount of $H/2$, and under the foot of the free slope downwards by the same amount $H/2$.

If, following this idea, we place the y axis of a coordinate system such that it runs along the intersection of the upper water surface and the water-facing slope, then for a sheet piling of depth D_s at the centre, we obtain values for ω and ξ

$$\omega = kH - \frac{kH}{K} F\left(\sqrt{\frac{(1+a_2)(\xi-1)}{2(\xi-a_2)}}, \lambda\right),$$

$$\xi = \sqrt{\tanh^2 \frac{\pi x}{2D} + \tan^2 \frac{\pi D_s}{2D}} \cos \frac{\pi D_s}{2D}.$$

The equation of the surface will be

$$y = \frac{H}{K} F\left(\sqrt{\frac{(1+a_2)(\xi-1)}{2(\pm\xi-a_2)}}, \lambda\right). \tag{2.117}$$

For the case introduced above, there are worked graphical representations for practical computation of the unit seepage $\bar{q}$. We have set out one such case in Fig. 2.24. A similar representation can also be constructed and used for determining the coordinates of seepage lines. It is also possible to use the tabulated values (Table 2.6) set up by Voshchinin (1959), which are in fact used in Czechoslovakia.

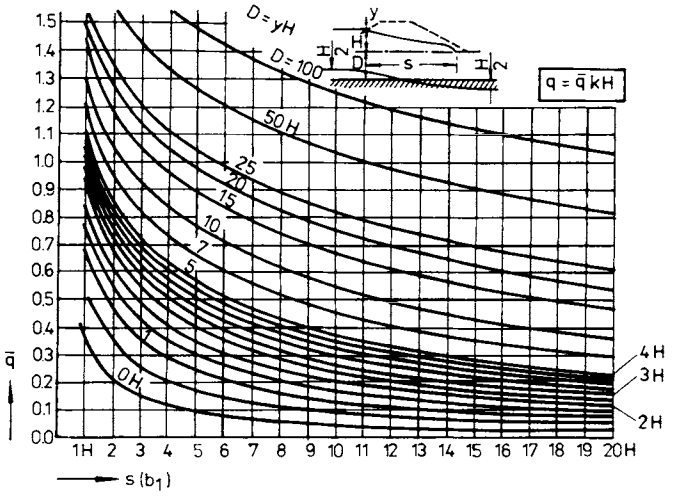

Fig. 2.24. Relationship between unit flow rate ($\bar{q}$) and permeable subsoil thickness (D) for various length of phreatic line (s).

Table 2.6. Ordinate of the phreatic line (after Voshchinin 1959)

$x = \frac{x}{d}$	The ordinate $y = \frac{y}{H}$ for relative depth $\varrho = \frac{D}{d}$														
	0	0.02	0.04	0.1	0.15	0.2	0.3	0.4	0.5	0.65	0.9	1.9	3.9	20	∞
0.01	99.0	98.7	98.4	97.2	96.5	95.7	94.7	94.5	94.3	94.2	94.2	93.8	93.7	93.7	92.2
0.05	95.0	94.0	92.0	91.0	90.0	89.0	89.0	89.0	88.0	88.0	87.0	87.0	86.0	86.0	85.0
0.10	91.0	90.0	89.0	87.0	86.0	85.0	85.0	84.0	84.0	83.0	82.0	81.0	80.0	80.0	78.0
0.20	85.0	84.0	82.0	79.0	78.0	77.0	77.0	76.0	76.0	75.0	74.0	73.0	71.0	71.0	69.0
0.30	78.5	78.0	76.0	73.0	71.0	69.0	69.0	68.0	67.0	66.0	65.0	64.0	63.0	63.0	62.0
0.40	72.0	71.0	69.0	65.0	63.0	62.0	61.0	60.0	60.0	59.0	58.0	57.0	56.0	56.0	55.0
0.50	66.0	64.0	62.0	58.0	56.0	55.0	53.0	52.0	51.0	51.0	51.0	50.0	50.0	49.0	49.0
0.60	60.0	57.0	54.0	50.0	48.0	46.0	45.0	44.0	43.0	43.0	43.0	43.0	43.0	43.0	43.0
0.70	53.0	49.0	45.0	41.0	39.0	38.0	37.0	37.0	36.0	36.0	36.0	36.0	36.0	36.0	36.0
0.80	44.0	39.0	36.0	33.0	33.0	32.0	32.0	31.0	31.0	30.0	29.0	29.0	28.0	28.0	28.0
0.90	32.0	26.0	25.0	23.0	23.0	23.0	22.0	22.0	21.0	21.0	20.0	20.0	19.5	19.0	19.0
0.95	23.0	17.0	16.0	14.0	14.0	14.0	14.0	14.0	14.0	14.0	14.0	14.0	13.5	13.5	13.5
0.99	12.0	7.0	6.0	6.0	6.0	6.0	6.0	6.0	6.0	6.0	6.0	6.0	6.0	6.0	5.8

Graphical techniques of calculation are simple, since from these tables we can read off the value of unit seepage $\bar{q}$, for a certain average length $d_1 = xH$ and depth of subsoil $D = \eta H$. The real seepage flow will then be

$$q = kH\bar{q}. \tag{2.118}$$

A perfunctory glance at the graphical illustration shows that for a relatively permeable embankment set on a subsoil with the same properties, the seepage flow may be up to twenty times the value for one laid on an impermeable subsoil.

The tabulated values show that the shape of the seepage curve barely changes for these two cases, except at the end, where it falls to the extent that its coordinates drop by half from y and y_0, respectively. We must note, however, that in the case we have introduced, the reverse can be true. This is more dangerous, and for dykes we would therefore recommend an investigation into the possibility and extent of seepage increases, and also into phreatic surface rise under the effect of a permeable underlay.

Now let us consider *embankments with* prelaid sealing *blankets.* A precise analytical solution of seepage through an embankment with a prelaid sealing blanket (Fig. 2.25) is extremely hard, and can therefore be avoided by using alternative solutions. From these we obtain the seepage using many degrees of approximation. The easiest approach is one in which we approximate the position of the seepage curve and with it the piezometric height H_3, which is the controlling factor for seepage through the body and subsoil behind the sealing. For seepage through the subsoil under the blanket, the following applies

$$q_2 = k_p SI = k_p \frac{D}{n} \frac{H - h_3}{B + mh_3}, \tag{2.119}$$

where n is a correction factor which takes account of the ratio $2B : D$ or more precisely $(2B + mh_3) : D$.

In the region behind point 0, where the slope of the phreatic curve $(h_3 - h_s) : d$ is determined, the seepage will be

$$q_2' = \frac{h_3 - h_s}{d}\left[Dk_p + \frac{h_3^2 - h_s^2}{2d} k_0\right]. \tag{2.120}$$

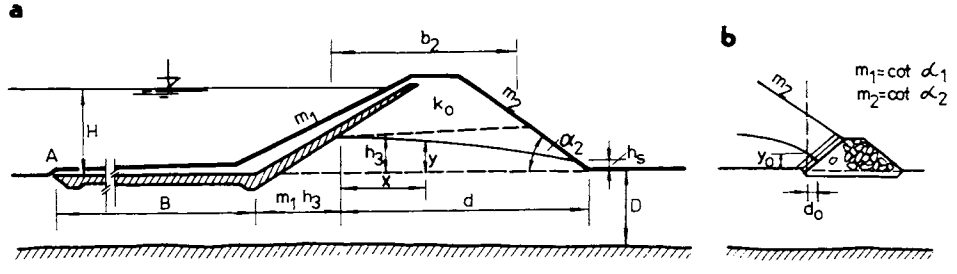

Fig. 2.25. Cross-section of a dam with sealing blanket. a — without drainage, b — with gravel toe drainage.

Neglecting the small quantity h_s, and comparing eqns. (2.119) and (2.120), we obtain

$$\frac{D}{n}\frac{H-h_3}{B+mh_3}=\frac{h_3}{d}\left[D+\frac{h_3^2}{2d}\frac{k_0}{k_p}\right]. \tag{2.121}$$

Through a gradual approximation we find the value of h_3.

We may then evaluate h_s by means of the graphical relation $h_s : H=f(\beta_2)\dfrac{H}{b_1+b_2}$ using the graphical depiction in Fig. 2.9. Thus, we obtain the final seepage equation

$$\frac{q}{k_0}=\frac{h_3^2-h_s^2}{2(d-m_2h_s)}=\frac{H^2-y^2}{2x}. \tag{2.122}$$

We can follow the profile of the phreatic surface using a modification of eqn. (2.77) having the form

$$y^2=2h_sx. \tag{2.123}$$

If the embankment has drainage at the foot, we can determine the shape of the seepage line using the above eqns. (2.122) and (2.123), with the single difference that we must substitute y_0 for h_s. In view of the fact that for protecting dykes y_0 is very small in value, it usually suffices to use a simplified expression analogous to eqn. (2.81), into which we substitute h_3, obtained from the above-mentioned approximations, in place of the H values.

2.4 Seepage from Channels

2.4.1 Geometric Forms of Channels and their Effect on Seepage

The main factor affecting seepage from a channel is the permeability of the soil, and sometimes also the way the profile is sealed, its size and its shape. The most common design shape for a channel is the trapezium. The triangle is more rarely used, and for the smallest channels, and then only exceptionally, a more complicated shape, perhaps with a varying side slope, is used. However, in irrigation and drainage channels, the original geometric form quickly alters, mainly because of carried sediment which rounds off all the corners (Fig. 2.26). It is often not only prudent but even advantageous to account for this change of form, since we avoid singularities at the corners.

In channels on a permeable subsoil and with a curve-linear outline, it is convenient, according to Polubarinova-Kochina, to use the complex Zhukovskii function in this form

$$\vartheta=+iz+\frac{\omega}{k}\pm A\exp\left(\frac{\omega}{\alpha}\right), \tag{2.124}$$

$$-y+\frac{\varphi}{k}=A\exp\left(\frac{\omega}{\alpha}\right)\cos\frac{\psi}{\alpha}, \tag{2.125}$$

$$x+\frac{\psi}{k}=A\exp\left(\frac{\omega}{\alpha}\right)\sin\frac{\psi}{\alpha}.$$

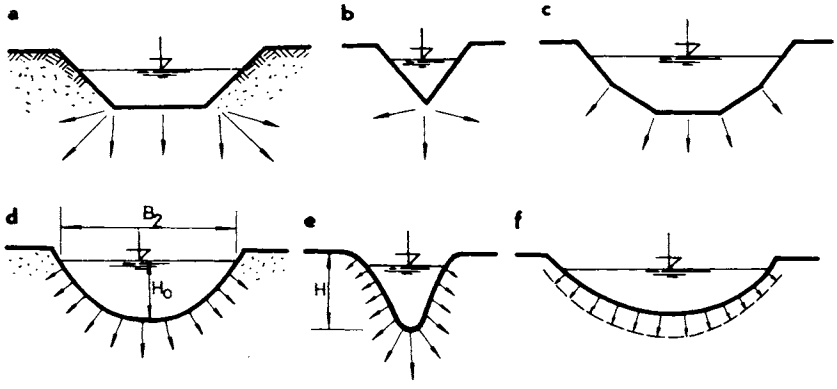

Fig. 2.26. Different shapes of canals and schemes for seepage calculation. a — trapezoidal, b — triangular, c — multi-angled, d, e, f — profiles with rounded bottom.

For the phreatic curve, we have

$$-y+\frac{\varphi}{k}=0,$$

on the free surface $\psi=\psi_0$

$$\cos\frac{\psi_0}{\alpha}=0,$$

$$-q=\psi_0=(2n+1)\frac{\pi\alpha}{2}, \tag{2.126}$$

$$\frac{1}{\alpha}=-\frac{(2n+1)\pi}{2q},$$

$$\vartheta=A\exp-\left(\frac{(2n+1)\pi\omega}{2q}\right). \tag{2.127}$$

Assuming $\varphi=ky$ and $\psi_0=\pi\alpha/2$, we obtain from eqn. (2.125) the equation of the seepage (phreatic) curve as well as its asymptotes

$$x+\frac{\pi\alpha}{2k}=A\exp\left(\frac{ky}{\alpha}\right),$$

$$x = -\frac{\pi\alpha}{2k} = \frac{q}{k} = x_\infty .$$

When $y = 0$, $x = \frac{B}{2} = \frac{q}{k} + A$, and for $\varphi = 0$ (outline of channel), we have

$$-y = A \cos\frac{\psi}{\alpha}, \qquad x + \frac{\psi}{k} = A \sin\frac{\psi}{\alpha}. \tag{2.128}$$

From boundary conditions

$$\psi = 0, \qquad y = -A = H,$$

$$x = -\frac{\psi_0}{k} - H = \frac{B}{2},$$

$$q = -\psi_0 = k\left(H + \frac{B}{2}\right).$$

Together

$$q_t = 2q = k(2H + B). \tag{2.129}$$

The equation for channel characteristics (from eqn. 2.128) for $A = H$ will be

$$\pm x = -\sqrt{H^2 - y^2} + \frac{2H + B}{\pi} \cos^{-1}\left(\frac{y}{H}\right). \tag{2.130}$$

Theoretical investigation shows that water from sealed channels on a permeable subsoil, with a deep underground water table, will seep mainly in a downward direction and without great effect on the surroundings if the level of the water table (D_w) below ground is in the range $D_w \geqslant (2-3)\,H$; for $D_w \geqslant 5\,H$ it practicelly disappears (Fig. 2.27).

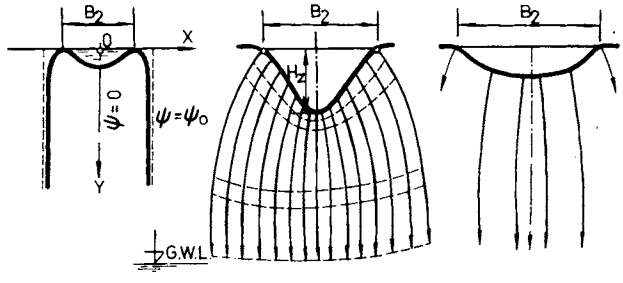

Fig. 2.27. The limitation of the flow region.

Let us next consider *seepage to the underground water.* The region close to the channel bottom can be investigated by means of eqn. (2.124) with the assumption that $n = -1$, $A = -C$. If $\alpha = q_t/\pi$ then

$$-iz=\frac{\omega}{k}+C\exp\left(\frac{\pi\omega}{q_c}\right), \tag{2.131}$$

which with a similar approach and notation to previous equations, leads to one giving the characteristics of this sort of channel (Fig. 2.28). We therefore have

$$\pm x=\sqrt{H^2-y^2}\,\frac{q_c}{k}\cos^{-1}\left(\frac{y}{H}\right) \tag{2.132a}$$

and

$$\pm x=\sqrt{H^2-y^2}+\frac{B-2H}{\pi}\cos^{-1}\left(\frac{y}{H}\right), \text{ respectively.} \tag{2.132b}$$

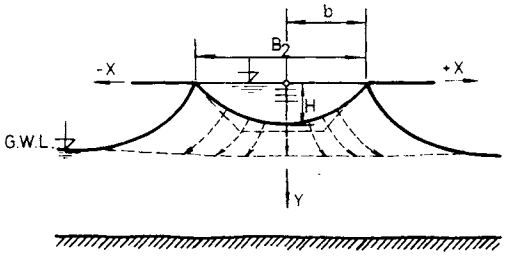

Fig. 2.28. Seepage into the groundwater level.

From an equation similar to eqn. (2.125) for $\psi=-q_c$, $C=H$, $y=\varphi/k$

$$\pm x=H\exp\left(\frac{\pi k y}{2q_c}\right)+\frac{q_c}{k}. \tag{2.133}$$

The + sign applies to the right branch of the phreatic surface and the — sign to the left. The channel will produce more interference as the soil becomes less permeable, which seemingly contradicts ideas about the extent of level changes with pumping or water drainage. The ratio $q:k$ is most important.

For a channel of parabolic profile sealed on the perimeter with a sealing of thickness t, with depth H and surface half-width b, the work of Polubarinova-Kochina (1952, p. 171) for perimeter coordinates x, y and half-section seepage q gives us

$$\begin{aligned} x&=-\psi+\frac{(q-b)(\psi+q)[\psi(H+t)^2+q^3]}{\psi^2(H+t)^2+q^4}-(q-b),\\ y&=-\frac{(q-b)(\psi+q)(H+t)(\psi-q)q}{\psi^2(H+t)^2+q^4}, \end{aligned} \tag{2.134}$$

$$\frac{q'-b}{H}=\frac{q'}{H+t}, \qquad -q\leqq\psi\leqq q,$$

$$q=k\,\frac{b(H+t)}{t}, \qquad q_c=2q. \tag{2.135}$$

Seepage from a channel of trapezoidal cross-section (Fig. 2.29) is evaluated by means of an inverse function given by the relation $z = u + iv$, which for an inverse unit radius will be

$$\frac{1}{\omega} = \frac{1}{u - iv}. \tag{2.136}$$

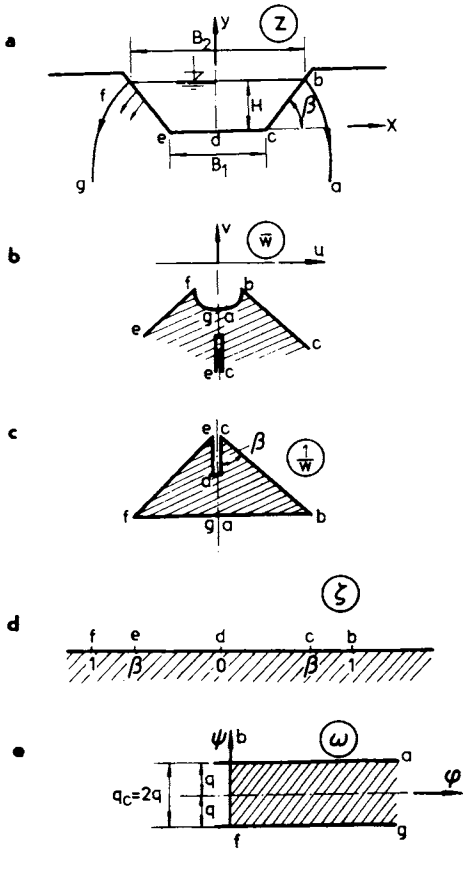

Fig. 2.29. Schemes used for inversion-method application.

The flow region is bounded by straight-line sections *bc*, *cd*, *de*, and *ef*. The slope of the side *bc* to the horizontal axis β' is $\pi\sigma$ characterized on the ζ plane by number

$$\sigma = \frac{\beta'}{\pi}.$$

From the Christoffel—Schwarz equation, we have

$$\frac{1}{\omega} = M \int_0^{\zeta} \frac{\zeta \, d\zeta}{(1-\zeta^2)^{1/2+\sigma}(\beta^2-\zeta^2)^{1/2-\sigma}} + N, \tag{2.137}$$

$$\int_0^{\zeta} \frac{\zeta \, d\zeta}{(1-\zeta^2)^{1/2+\sigma}(\beta^2-\zeta^2)^{1-\sigma}} = \Phi(\zeta), \tag{2.138}$$

$$\frac{1}{w} = M\Phi(\zeta) + N, \tag{2.139}$$

$$\begin{aligned} \int_0^{\beta} \frac{\zeta \, d\zeta}{(1-\zeta^2)^{1/2+\sigma}(\beta^2-\zeta^2)^{1-\sigma}} &= \Phi(\beta) = I_1, \\ \int_{\beta}^{1} \frac{\zeta \, d\zeta}{(1-\zeta^2)^{1/2+\sigma}(\zeta^2-\beta^2)^{1-\sigma}} &= I_2. \end{aligned} \tag{2.140}$$

Finally

$$\Phi(\zeta) = I_1 - \exp(\pi i\sigma) \int_{\beta}^{\zeta} \frac{\zeta \, d\zeta}{(1-\zeta^2)^{1/2+\sigma}(\zeta^2-\beta^2)^{1-\sigma}}.$$

With $\zeta = 1$

$$\Phi(1) = I_1 - \exp(\pi i\sigma) I_2. \tag{2.141}$$

Velocities at point b and other basic quantities are expressed as follows

$$\begin{aligned} u &= k \sin \pi\sigma \cos \pi\sigma, \qquad v = -k \cos^2 \pi\sigma, \\ w &= u - iv = ki \exp(-\pi i\sigma) \cos \pi\sigma, \end{aligned} \tag{2.142}$$

$$M = \frac{i}{kI_2 \cos \pi\sigma},$$

$$\omega = \varphi + i\psi, \qquad \omega = \frac{2qi}{\pi} \sin^{-1} \zeta, \tag{2.143}$$

$$\frac{d\omega}{dz} = w = u - iv,$$

$$\frac{dz}{d\omega} = \frac{1}{w} = \frac{i}{kI_2 \cos \pi\sigma} [\Phi(\zeta) - I_1], \tag{2.144}$$

$$\frac{dz}{d\zeta} = \frac{dz}{d\omega}\frac{d\omega}{d\zeta} = -\frac{2q}{k\pi I_2 \cos \pi\sigma} \frac{1}{\sqrt{1-\zeta^2}} [\Phi(\zeta) - I_1],$$

$$z = -\frac{2q}{k\pi I_2 \cos \pi\sigma} \left\{ \int_0^{\zeta} \frac{\varphi(\zeta) \, d\zeta}{\sqrt{1-\zeta^2}} - I_1 \sin^{-1} \zeta \right\}. \tag{2.145}$$

The final expressions are

$$H = \frac{2q}{k\pi I_2} \tan \pi\sigma \left\{ \frac{\pi}{2} I_2 - f_2(\sigma, \beta) \right\},$$

$$\frac{B_2 - B_1}{2} = \frac{2q}{\pi k I_2} \left\{ \frac{\pi}{2} I_2 - f_2(\sigma, \beta) \right\},$$

$$B_2 = B_1 + \frac{2q}{k}\left[1 - \frac{2f_2(\sigma, \beta)}{\pi I_2}\right], \tag{2.146}$$

$$H = \frac{2q}{k}\tan \sigma\pi \left[1 - \frac{2f_2(\sigma, \beta)}{\pi I_2}\right], \tag{2.147a}$$

$$q = kH \cot \sigma\pi \left[1 - \frac{2f_2(\sigma, \beta)}{\pi I_2}\right]. \tag{2.47b}$$

A very convenient calculation is that according to Vedernikov (1932), in which

$$q_t = 2q = (B_2 + AH), \tag{2.148}$$

where

$$A = \frac{q}{\tan \sigma\pi} \frac{f_2(\sigma, \beta) - \frac{1}{\cos \sigma\pi} f_1(\sigma, \beta)}{\frac{\pi}{2} I_2 - f_2(\delta, \beta)}. \tag{2.149}$$

Seepage through the bottom half of the channel will be

$$q_b = \frac{q}{\pi} \sin^{-1} \beta. \tag{2.150}$$

Through the whole bottom area

$$q_{wb} = 2q_b.$$

Auxiliary quantities for the seepage calculation can be found in Table 2.7. The value of β is clear from Fig. 2.29d.

In estimating seepage from a rectangular channel using eqn. (2.148), we need to know, besides the geometrical characteristics and permeability, the coefficient A whose values are given in greater detail by Polubarinova-Kochina.

2.4.2 The Effect of Capillary Action in the Soil

As shown in Sections 2.1 and 2.2, capillary action in the soil causes an increase in hydraulic gradient, which leads to an increased velocity and seepage flow. In the case of seepage from channels, this can be expressed by an equation similar to eqn. (2.101), or one in which this effect is given by a certain factor $\alpha = \zeta/h_c$ with value $\alpha = 0.1$—0.5 (depending on degree of saturation and type of soil). The general seepage equation is similar then to eqn. (2.80)

$$q' = k \frac{h_2 - h_1}{x_2 - x_1}\left(\frac{h_1 + h_2}{2} + \alpha h_c\right). \tag{2.151}$$

In the same way, we can adjust the above equations for seepage from a trapezoidal channel into a homogeneous subsoil (eqn. 2.147b) into the form

Table 2.7. Values of quantities $\frac{kB_1}{2q}$, $\frac{kB_2}{2q}$, $\frac{kH}{2q}$, $\frac{q_d}{2q}$, A, $\frac{B_2}{H}$

	m	β	$\frac{kB_1}{2q}$	$\frac{kB_2}{2q}$	$\frac{kH}{2q}$	$\frac{q_d}{2q}$	A	$\frac{B_2}{H}$
45°	1	0.0	0.0	0.500	0.250	0	2.00	2.00
	1	0.25	0.167	0.545	0.189	0.333	2.40	2.88
	1	0.50	0.304	0.595	0.146	0.500	2.78	4.08
	1	0.75	0.479	0.676	0.0986	0.667	3.29	6.86
	1	0.875	0.609	0.746	0.0682	0.770	3.73	10.90
	1	0.9375	0.706	0.802	0.0480	0.839	4.12	16.70
	1	1	1	1	0	1	∞	∞
30°	1.732	0	0	0.656	0.189	0	1.82	3.46
	1.732	0.25	0.204	0.684	0.139	0.333	2.28	4.93
	1.732	0.50	0.353	0.720	0.106	0.500	2.63	6.78
	1.732	0.75	0.530	0.777	0.0713	0.667	3.13	12.90
	1.732	0.875	0.653	0.824	0.0494	0.770	3.55	16.65
	1.732	1	1	1	0	1	∞	∞
22°30′	2.414	0	0	0.736	0.152	0	1.74	4.82
	2.414	0.25	0.229	0.757	0.109	0.333	2.22	6.92
	2.414	0.50	0.384	0.786	0.0382	0.500	2.58	9.45
	2.414	0.75	0.559	0.829	0.0559	0.667	3.05	14.80
	2.414	0.875	0.678	0.865	0.0387	0.770	3.48	22.30

$$q' \doteq kH\left[(1+\alpha h_c)-\frac{2f_2(\sigma,\beta)}{\pi I_2}\right]\cot\sigma\pi, \tag{2.152}$$

where H is the depth of water in the channel, h_c the capillary height of the soil concerned $f_2(\sigma, \beta)$, I_2 the values of the functions and integrals in eqns. (2.140) to (2.146).

Modification is also possible after the method of Vedernikov's equation (eqn. 2.148), for which we can choose values of A from Table 2.7.

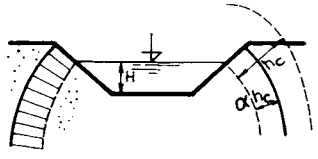

Fig. 2.30. Capillary fringe beneath the phreatic line of seepage water.

Seepage always increases with the effect of capillarity, but not to such a degree that it would significantly alter the ratio $h_c : H$ (Fig. 2.30).

2.5 Collection and Removal of Seepage Water

2.5.1 Types and Uses of Drainage and Relief Structures

Levées and canal embankments act as boundaries between two different potentials, given by the different levels of surface and underground water. The water travels through the boundary and under it in the direction of the hydraulic gradient (and the gradient arising from capillary action, and occasionally other forces affecting the potential). This water has to be controlled both from the seepage point of view (collection and drainage), and also from the point of view of distribution of potential, weakening of uplift forces, stabilization of surfaces, etc. From this standpoint, linear drainage and relief wells comprise an important element of the so-called active protection of the land behind levées, and of the subsoil of the levées, which are referred to in greater detail in Section 6.5.

To this end, we use in part seepage ducts as the simplest arrangement for collecting and disposing of water, and in part pebble drains, various sorts of pipe drain, and wells as relatively demanding and expensive structures with which to control the water even at great depth (Fig. 2.31).

Consider now an *open trench.* Seepage quantity and the effect on the phreatic curve can be calculated by means of the Zhukovskiĭ function, that is by a transformation (see Fig. 2.32) to a plane, for which

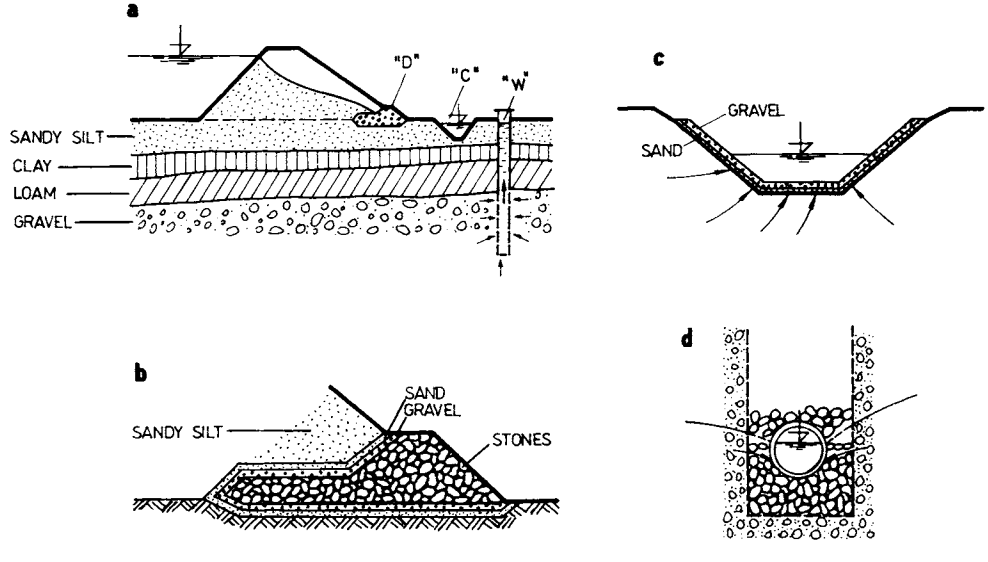

Fig. 2.31. Different kinds of drainage and collectors of the dam. a — the position of the drain "D", b — detail of a rocky drain, c — filter of a ditch, d — pipe drain.

$$\zeta = \xi + i\eta = z - i\omega, \tag{2.153}$$

$$\xi = x + \psi, \qquad \eta = y - \varphi, \tag{2.154}$$

$$u - iv = k\frac{d\omega}{dz}.$$

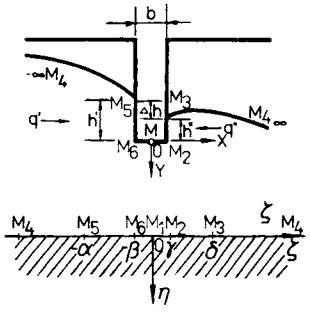

Fig. 2.32. The scheme of calculation of an open ditch.

In the centre of the trench, i.e. at point M_1 (0, 0), we make the assumption that $\psi = 0$ and that the drained quantity q is made up of inflows q' from the left and q'' from the right, where

$$q = q' + q'',$$

Numerov (1951) introduces the further assumption that the water flows into the trench from infinity, and it is therefore possible to express the complex potential (ω) logarithmically as follows

$$\omega = -\frac{\bar{q}}{\pi}\ln\zeta + iq'' + w, \tag{2.155}$$

$$W = U + iV = -i\bar{q}'' + \frac{\bar{q}}{\pi}\ln\zeta + \omega, \tag{2.156}$$

$$U = \frac{q}{\pi}\ln|\zeta| + \varphi, \qquad V = -q'' + \frac{q}{\pi}\arg\zeta + \psi$$

if $\bar{q} = q$: k is the apparent unit seepage quantity, and also if

$$\omega = -i\bar{q}' + C\sqrt{(-\beta-\zeta)(\gamma-\zeta)} + \frac{2}{\pi}(\alpha-\zeta)\tanh^{-1}\frac{A}{f} + \frac{2}{\pi}(\delta-\zeta)\times$$

$$\times\tanh^{-1}(Bf) - \frac{2}{\pi}\bar{q}\tanh^{-1}f, \tag{2.157}$$

$$\alpha = \bar{q}' + \frac{b}{2}, \qquad \delta = \bar{q}'' + \frac{b}{2}, \tag{2.158}$$

$$f=\sqrt{\frac{-\beta-\zeta}{\gamma-\zeta}}, \qquad A=\sqrt{\frac{\alpha-\beta}{\alpha+\gamma}}, \qquad B=\sqrt{\frac{\delta-\gamma}{\delta+\beta}},$$

$$C=-J+\frac{2}{\pi}\tanh^{-1}A-\frac{2}{\pi}\tanh^{-1}B, \quad \tanh^{-1}x=\frac{1}{2}\ln\frac{1+x}{1-x} \tag{2.159}$$

$$\alpha+\delta=b+q.$$

Considering the boundary conditions

$$C=-J+\frac{2}{\pi}\tanh^{-1}A+\frac{2}{\pi}\tanh^{-1}B=0, \tag{2.160}$$

$$q=\sqrt{(\alpha-\beta)(\alpha+\gamma)}+\sqrt{(\delta-\gamma)(\delta+\beta)},$$

after enumerating the sum under the square root and constants A and B (eqn. 2.160), we obtain the equation of the seepage curve from the left $(-\infty<x<-b/2)$ as follows

$$y=\frac{2}{\pi}\left(\frac{b}{2}+x\right)\tanh^{-1}\frac{A}{f}+\frac{2}{\pi}\left(\frac{b}{2}+\bar{q}-x\right)\tanh^{-1}(Bf)-$$

$$-\frac{2}{\pi}\bar{q}\tanh^{-1}f, \tag{2.161}$$

where

$$f^2=\frac{b\left[\exp\left(\frac{\pi J}{2}\right)\sqrt{1+\frac{2\bar{q}}{b}}-1\right]^2-4\exp\left(\frac{\pi J}{2}\right)\left(\frac{b}{2}+x\right)\cosh\frac{\pi J}{2}}{b\left[\exp\left(\frac{\pi J}{2}\right)\sqrt{1+\frac{2\bar{q}}{b}}+1\right]^2-4\exp\left(\frac{\pi J}{2}\right)\left(\frac{b}{2}+x\right)\cosh\frac{\pi J}{2}}. \tag{2.162}$$

For the outflow from the left wall of the trench,

$$\frac{h'}{q}=\frac{J}{2}+\frac{1}{\pi}\left(1+\frac{b}{2\bar{q}}\right)\ln\left(1+\frac{2\bar{q}}{b}\right)+\frac{1}{\pi}\left(1+\frac{b}{\bar{q}}\right)\ln\frac{\cosh\frac{\pi J}{2}}{1+\frac{\bar{q}}{b}}. \tag{2.163}$$

Denoting J as the slope of the seepage curve, all else is as before

$$\frac{y}{\bar{q}}\cong\frac{Jx}{\bar{q}}-\frac{1}{\pi}\ln\left(-\frac{x}{\bar{q}}\right)-\frac{1}{\pi}\left[1+\ln\left(1+\exp\left(\frac{\pi J}{2}\right)\right)+\ln\frac{2\bar{q}}{b}-\right.$$

$$\left.-\left(1+\frac{b}{2\bar{q}}\right)\ln\left(1+\frac{b}{2\bar{q}}\right)\right]. \tag{2.164}$$

For the height of the outflow on the right wall of the trench

$$\frac{h''}{\bar{q}} = -\frac{1}{2}J + \frac{1}{\pi}\left(1+\frac{b}{2\bar{q}}\right)\ln\left(1+\frac{b}{2\bar{q}}\right) + \frac{1}{\pi}\left(1+\frac{b}{\bar{q}}\right)\ln\frac{\cosh\frac{\pi J}{2}}{1+\frac{\bar{q}}{b}}. \quad (2.165)$$

The difference in outflow heights will be

$$\Delta h = h' - h'' = J\bar{q} = J\frac{q_t}{k}, \quad (2.166)$$

$$\Delta\varphi \doteq \varphi_1 - \varphi_2 = h_1 - h_2 = J'\frac{q_t}{k}.$$

For large distances, we can say

$$\frac{y}{\bar{q}} \cong J\frac{x}{\bar{q}} - \frac{1}{\pi}\ln\frac{x}{\bar{q}} - \frac{1}{\pi}\left[1+\ln\left(1+\exp\left(\frac{\pi J}{2}\right)\right)+\ln\frac{2\bar{q}}{b} - \left(1+\frac{b}{2\bar{q}}\right)\ln\left(1+\frac{b}{2\bar{q}}\right)\right] + J. \quad (2.167)$$

In levées, the slope of the phreatic curve is relatively small and we can therefore use the approximate equations

$$\frac{x_{max}}{\bar{q}} \cong \frac{1}{\exp(\pi J - 1)},$$

$$\frac{y_{max}}{\bar{q}} \cong \frac{1}{\pi}\ln\frac{\pi J b}{4\bar{q}} + \frac{1}{\pi}\left(1+\frac{b}{2\bar{q}}\right)\ln\left(1+\frac{2\bar{q}}{b}\right). \quad (2.168)$$

The values of potentials on the two sides of the trench differ. However, it is often possible to take an average value, and thus

$$\varphi = -\frac{q}{\pi k}\ln(2), \qquad \varphi_r = 0.22\frac{q}{k}.$$

At the beginning of the region, the thickness of the water-bearing layer (D) will determine the value of φ_0.

Even though a trench is not a common type of drain, the relations derived for it are significant in principle, since previously, for a seepage duct (a very frequently used drainage element), we have not had the precise analytical expressions with which to describe the seepage flow and profile of the depression curve. These are approximate and derived from expressions formed for seepage through a vertical wall, or are analytical-empirical or directly empirical. One was developed by Muskat (1946).

2.5.2 The Seepage Duct

Vedernikov (1932) and Numerov (1951) derived some very simple formulae by considering the two main cases of seepage from an irrigation channel. In one case,

the bottom was in permeable soil of infinite thickness, and in the other the canal bottom was on a permeable layer thickness D and a duct had been cut down to the impermeable substratum (Fig. 2.33).

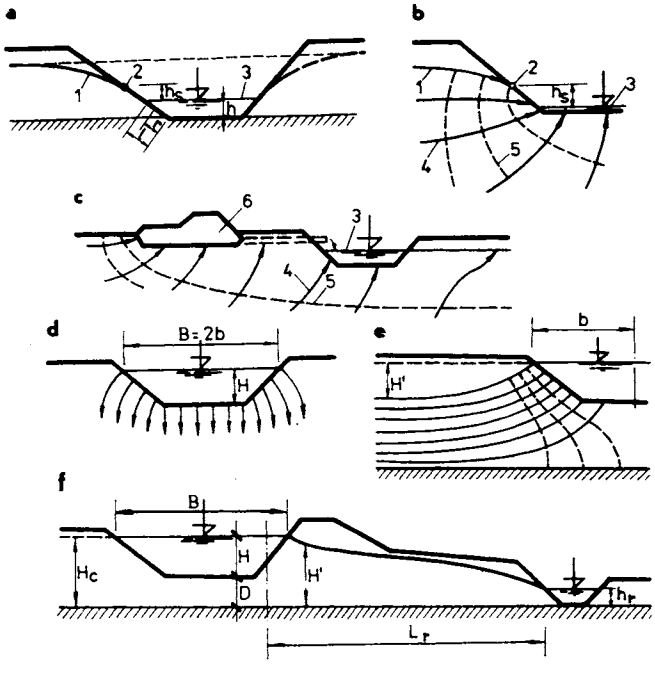

Fig. 2.33. Decantation and irrigation canals. a — drain ditched on an impermeable layer, b — drain in a permeable soil, c — open drain and stone drain, d, e — irrigation canals, f — mean canal and drainage channel; 1 — phreatic line, 2 — step of the water height, 3 — water level in canal, 4 — flowline, 5 — equipotential line, 6 — rocky drain.

In the first case, one can express the losses from the channel using the approximate formula which Uginchus presented in the form

$$q = k(B+2H)\frac{K}{K_1} \quad [\mathrm{m^3\,s^{-1}}], \tag{2.169}$$

where B is the breadth of the channel at the surface ($B=2b$), K and K_1 are elliptical integrals of the first order $2K/K_1 = A = \mathrm{f}(B/H)$, and in final form we have the following for the wetted perimeter P_w

$$q = kP_w\frac{\beta+2m+A}{\beta+m} = kP_w\zeta_k. \tag{2.170}$$

For a given shape of channel described by the slope inclination (m), the ratio of base width to water depth (H), and the value of A, the losses q are dependent on the three above-mentioned factors (k, P_w, ζ_k). From these, it is also possible to derive experimentally a dependence for the duct inflow q_r, thus

$$q_r = f(q).$$

In the second case, the levels above the impermeable layer $H = D + h$ can be determined from the height and water depth in the duct h_r, if the interdependence is known between certain other quantities Φ_1 and Φ_2, which are dependent on the reduced seepage q'_r, the value of H, and on B/h. Thus we can state that

$$\left(\frac{H'}{H}\right)^2 = \Phi_1^2 - \frac{q'_r}{H}\Phi_2,$$

where H is the apparent height of the phreatic surface above the impermeable layer.

If we assume a symmetrical canal, symmetrical embankments, and a duct at a distance L_r from the vertical given by the intersection of the surface with the slope, the flow into the duct will be

$$q = k\frac{(H')^2 - h_r^2}{L_r}. \tag{2.171}$$

Our next case to consider is an absorbing *circular drain*, length $2l$ on a horizontal at depth D.

Schneebeli (1966) suggests that it is necessary to differentiate between the case of finite-length drains ($\pm l$) in a thick water-bearing layer of thickness D, and the case where a relatively thin water-bearing layer (thickness $e \ll l$) supports an infinitely long drain.

If a quantity of water Q is flowing in and leaving a certain circular region $R = 1$, the complex potential for the first case in the ζ, η plane will be

$$\omega = \varphi + i\psi = \frac{Q}{2\pi kD}\ln(\zeta).$$

Making use of the transformation relations between the planes z and ζ from Zhukovskiĭ, we can write (for planes ξ, η and x, y)

$$z = \frac{1}{2}\left(\zeta + \frac{l^2}{\zeta}\right),$$

$$\zeta = z + \sqrt{z^2 - l^2},$$

$$\omega = \varphi + i\psi = \frac{Q}{2\pi kD}\ln\left(z + \sqrt{z^2 - l^2}\right) = \frac{Q}{2\pi kD} \times$$

$$\times\left\{\cosh^{-1}\left(\frac{z}{l}\right) + \ln(l)\right\}. \tag{2.172}$$

Separating real and imaginary parts and denoting $r=\sqrt{x^2+y^2}$, we find that

$$\varphi=\frac{Q}{2\pi kD}\left\{\cosh^{-1}\left[\sqrt{\frac{r^2+l^2+\sqrt{(r^2+l^2)^2-4l^2x^2}}{2l^2}}\right]+\ln(l)\right\}, \quad (2.173)$$

$$\varphi=\frac{Q}{2\pi kD}\cos^{-1}\sqrt{\frac{r^2+l^2+\sqrt{(r^2+l^2)-4l^2x^2}}{2l^2}} \quad (2.174)$$

The equipotentials are confocal ellipses with axial dimensions a and b, for which we have

$$\frac{x^2}{l^2\cosh^2\Phi}+\frac{y^2}{l^2\sinh^2\Phi}=1,$$

where

$$\Phi=\frac{\varphi}{Q/2\pi kD}-\ln(l),$$

half-axes

$$a=l\cosh\left(\frac{\varphi}{\frac{Q}{2}\pi kD}-\ln(l)\right),$$

$$b=l\sinh\left(\frac{\varphi}{\frac{Q}{2}\pi kD}-\ln(l)\right). \quad (2.175)$$

Similarly, we can find the flowline equation which turn out to be hyperbolae with foci at the drain ends $x=\pm l$, $y=0$ (Fig. 2.34).

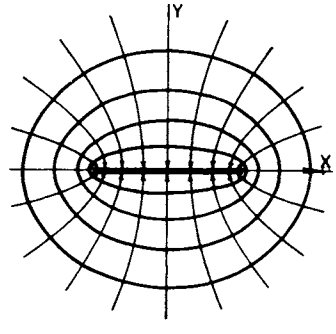

Fig. 2.34. The equipotentials and flowlines for a circular drain of length $2l$.

If we consider that along the drain surface the ellipse degenerates into a line with the length of the longer half-axis $a=l$, it follows that

$$\cosh\Phi=1, \qquad \Phi=0,$$

$$\varphi_d = \frac{Q}{2\pi kD} \ln (l). \tag{2.176}$$

The drain has an effect on the potential up to a distance of the 'active radius' R_a at which the potential equals

$$\varphi_0 = \frac{Q}{2\pi kD} \ln (2R_a). \tag{2.177}$$

It follows from eqns. (2.176) and (2.177) that the total drain inflow is

$$Q = 2\pi kD \frac{\varphi_0 - \varphi_d}{\ln\left(\frac{2R_a}{l}\right)}. \tag{2.178}$$

The specific inflow $q(x)$ at point x will be

$$q(x) = -2kD \frac{\partial \psi}{\partial x} = \frac{Q}{\pi l} \frac{1}{\sqrt{1-\left(\frac{x}{l}\right)^2}} = \frac{2q_{av}}{\pi\sqrt{1-\left(\frac{x}{l}\right)^2}} \tag{2.179}$$

if

$$\psi = \frac{Q}{2\pi kD} \cos^{-1}\left(\frac{x}{l}\right), \tag{2.180}$$

$$q_{av} = \frac{Q}{2l} = \text{average inflow}. \tag{2.181}$$

The inflow at the centre of the drain ($x = 0$) is

$$q(x=0) = \frac{2}{\pi} q_{av} = 0.636 q_{av}. \tag{2.182}$$

The inflow is concentrated in the main at the ends of the drain.

Sometimes Dupuit's simplified conditions (horizontal surface; impermeable subsoil) are accepted as valid, and then the potential difference at the end of the region $\varphi_0 D \rightarrow D^2/2$ is the vital factor affecting inflow, and near the drain $\varphi_d h_d \rightarrow h^2/2$, is substituted into eqn. (2.178).

2.5.3 A Horizontal Drain in a Thin Water-bearing Layer

For a horizontal drain laid in a horizontal water-bearing stratum of thickness D (Fig. 2.35) and height a above a lower impermeable layer, where the coordinate system has its origin at the centre of the drain, the general potential equation is

$$\varphi = \frac{q}{4\pi k} \ln \left\{ \frac{\cosh\left(\frac{\pi x}{D_0}\right) - \cos\left(\frac{\pi(y+a)}{D_0}\right) \cosh\left(\frac{\pi x}{D_0}\right) - \cos\left(\frac{\pi(y-a)}{D_0}\right)}{2} \right\}. \tag{2.183}$$

If q is the specific inflow in the proximity of the drain $x \to 0$, then $y \to a$, and $(y-a) \to 0$, so that

$$\varphi = \frac{q}{2\pi k} \ln \left[\frac{\sqrt{x^2+(y-a)^2}}{2D_0} \sin\left(\frac{\pi a}{D_0}\right) \right]. \tag{2.184}$$

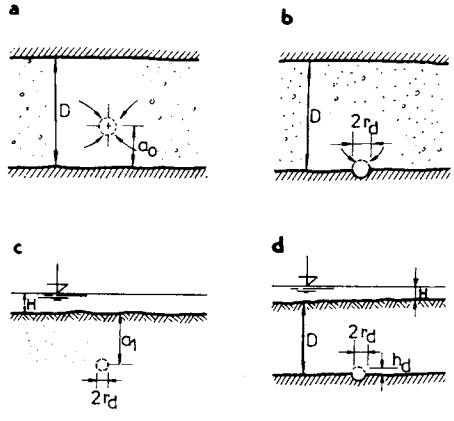

Fig. 2.35. The schemes for calculation of a horizontal relief drain. a—d — different position of drains.

At greater distances $|x| > (l-a)$, we have approximately

$$\varphi = \frac{q}{2\pi k} \left[\frac{\pi x}{D_0} - 2 \ln (2) \right]. \tag{2.185a}$$

The potential on the circumference of a drain (φ_d) of radius r_d will be

$$\varphi_d = \frac{q}{2\pi k} \ln \left(\frac{\pi r_d}{2D_0} \sin \frac{\pi a}{D_0} \right), \tag{2.185b}$$

for an ideal trench

$$\varphi = -\frac{q}{\pi k} \ln (2).$$

A real drain always yields greater resistance. Its value depends on r_d/D_0, a/D_0, and also q/k. The difference is accounted for by inflow losses ($\delta\varphi_a$), given by the equation

$$\delta\varphi = \varphi - \varphi_d = \frac{q}{2\pi k} \ln \left\{ \frac{D_0}{2\pi r_d} \frac{1}{\sin\left(\frac{\pi a}{D_0}\right)} \right\}. \tag{2.186}$$

Minimum losses occur at $a = D_0/2$, giving

$$\delta\varphi_{\min} = \frac{q}{2\pi k} \ln \left(\frac{D_0}{2\pi r_d} \right). \tag{2.187}$$

If the drain is situated on the border between the water-bearing and impermeable strata $a=0$ (Fig. 2.35), then

$$\varphi_d=\frac{q}{2\pi k}2\ln\left(\frac{\pi r_d}{2D_0}\right). \tag{2.188}$$

Comparison with an equivalent trench gives

$$\delta\varphi_{max}=\frac{q}{2\pi k}\left\{2\ln\left(\frac{D_0}{\pi r_d}\right)\right\}. \tag{2.189}$$

Inflow losses are approximately double this value (half the drain is shielded). In an artesian horizontal plane it is most advantageous to place the drain in the centre of the horizontal (see Fig. 2.35a), since its effectiveness falls with depth.

The potential of a sunken drain at depth a_1 below the surface of a permeable soil, on which water stands to a depth of H, with head h_d above the drain, is given by

$$\varphi\cong\frac{q}{2\pi}\ln\frac{2a_1}{r_d}-kH, \tag{2.190}$$

$$q=\frac{2\pi k(H-h_d)}{\ln\dfrac{2a_1}{r_d}}. \tag{2.191}$$

A drain situated on the boundary between the permeable and impermeable layers (Fig. 2.35d) implies an approximate seepage of

$$q\cong\frac{k\pi(H-h_d)}{\ln\dfrac{2D}{r_d}}. \tag{2.192}$$

Relief wells for which we seek a potential φ_w are usually calculated, if they absorb a seepage flow q, by assuming and infinite row of wells, diameter r_w and $2a$ apart, and distance l from an infinite line source (Fig. 2.36). With these assumptions for a direct channel, $q_k=\infty$. Charniĭ (1951) gives a basic relationship for the transformed plane ζ, such that

$$\zeta=\varrho_k\exp\left(\frac{i\pi z}{a}\right). \tag{2.193}$$

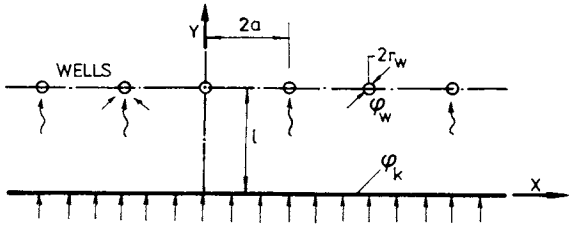

Fig. 2.36. The scheme for capacity computation of wells lying along a river.

Additional equations are

$$\delta = \varrho_n \exp\left(-\frac{i\pi}{a}\right), \qquad \alpha = \frac{\pi x_1}{a}, \tag{2.194}$$

$$\varrho_w = r_w \left|\frac{d\zeta}{dz}\right|_{x=x_1 \pm 2an} = r_w \frac{\pi \varrho_k}{a} \exp\left(-\frac{\pi x_1}{a}\right), \tag{2.195}$$

$$\varrho = \varrho_k \exp\left(-\frac{\pi y}{a}\right), \qquad \vartheta = \frac{\pi x}{a}, \tag{2.196}$$

$$U = \frac{Q}{2\pi} \ln \frac{\exp\left(\frac{\pi}{a} iz\right) - \exp\left(\frac{\pi}{a}(ix_1 - 1)\right)}{\exp\left(\frac{\pi}{a}(iz - 1)\right) - \exp\left(\frac{\pi}{a} ix_1\right)} + C, \tag{2.197}$$

$$\varphi = \frac{Q}{2\pi} \ln \frac{\cosh\frac{\pi}{a}(y - l) - \cos\frac{\pi}{a}(x - x_1)}{\cosh(y + H) - \cos\frac{\pi}{a}(x - x_1)} + C. \tag{2.198}$$

Finally we can derive the equation for flow into a well

$$Q_w = \frac{2\pi(\varphi_k - \varphi_w)}{\ln\left(\frac{2a}{\pi r_w} \sinh\frac{\pi l}{a}\right)} \tag{2.199a}$$

A similar equation was set out by Schneebeli (1966) and Muskat (1949) according to which

$$Q_w = \frac{2\pi(\varphi_k - \varphi_w)}{\ln \dfrac{\sinh\frac{\pi l}{a}}{\sinh\frac{\pi r_w}{2a}}}. \tag{2.199b}$$

Since the well diameter $2r_w$ is negligible compared to their spacing and the head is smaller than the distance from the line of wells to the source line, the equation for potential can therefore be simplified to give

$$\varphi = \frac{Q}{2\pi} \ln\left[\cosh\frac{\pi}{a}(y - l) - \cos\frac{\pi(x - x_1)}{a}\right]. \tag{2.200}$$

If we consider the interference of a row of periodically sited wells of spacing

$$x = \pm 2va, \qquad y = \pm l \pm 2vl,$$

we obtain

$$\varphi = \frac{Q}{4\pi}\left\{\ln \frac{\cosh\frac{\pi}{a}(y + l) - \cos\frac{\pi x}{a}}{\cosh\frac{\pi}{a}(y - l) - \cos\frac{\pi x}{a}} + \right.$$

$$+\sum_{v=1}^{\infty}\ln\frac{\left[\cosh\frac{\pi}{a}(y+l+2vl')-\cos\frac{\pi x}{a}\right]}{\left[\cosh\frac{\pi}{a}(y-l-2vl')-\cos\frac{\pi x}{a}\right]}\times$$

$$\times\frac{\left[\cosh\frac{\pi}{a}(y+l-2l'v)-\cos\frac{\pi x}{a}\right]}{\left[\cosh\frac{\pi}{a}(y-l+2l'v)-\cos\frac{\pi x}{a}\right]}\Bigg\}+C_1y+C_2, \tag{2.201}$$

where C_1 and C_2 are constants: the remaining symbols are as above.

To express the potential at an arbitrary point we need to know the boundary potentials φ_1, φ_2 and therefore the boundary conditions. After modification and contracting equation (2.201), for $y=l'$, we obtain

$$\varphi_2=\frac{Q}{4\pi}\lim_{v\to\infty}\left\{\ln\frac{\cosh\frac{\pi}{a}[(2v+1)l'-l]-\cos\frac{\pi x}{a}}{\cosh\frac{\pi}{a}[(2v+1)l'+l]-\cos\frac{\pi x}{a}}\right\}-$$

$$-C_1l+\varphi_1=\frac{Q}{4\pi}\frac{2\pi l}{a}-C_1l'+\varphi_1,$$

and

$$C_1=\frac{\varphi_1-\varphi_2}{l'}-\frac{Ql}{2al'}. \tag{2.202}$$

Using eqns. (2.201) and (2.202), we can express the potential at the well circumference φ_w, and also the potential difference as follows

$$\varphi_w=\frac{Q}{4\pi}\left\{\ln\frac{\frac{\pi^2r_w^2}{2a^2}}{\cosh\frac{2\pi l}{a}-1}+\right.$$

$$\left.+\sum_{v=1}^{\infty}\ln\frac{\left(\cosh\frac{2\pi l'v}{a}-1\right)^2}{\left[\cosh\frac{2\pi}{a}(l'v+l)-1\right]\left[\cosh\frac{2\pi}{a}(l'v-l)-1\right]}\right\}-C_1l+\varphi_1$$

or

$$\varphi_1\left(1-\frac{l}{l'}\right)+\varphi_2\frac{l}{l'}-\varphi_w\cong Q\left\{\frac{1}{2\pi}\ln\frac{a}{\pi r_w}+\frac{1}{2\pi}\ln 2\sinh\frac{\pi l}{a}-\right.$$

$$\left.-\frac{l^2}{2al'}+\frac{1}{2\pi}\sum_{v=1}^{\infty}\ln\frac{\sinh\frac{\pi(l'v+l')}{a}\sinh\frac{\pi(l'v-l)}{a}}{\sinh^2\frac{\pi lv}{a}}\right\}. \tag{2.203}$$

For $a < l$,

$$\varphi_1\left(1-\frac{l}{l'}\right)+\varphi_2\frac{l}{l'}-\varphi_w=Q\left[\frac{1}{2\pi}\ln\frac{a}{\pi r_w}+\left(1-\frac{l}{l'}\right)\frac{l}{2a}\right]. \qquad (2.203a)$$

If $l' \to \infty$, then we find that

$$\varphi_1-\varphi_w=\frac{Q}{2\pi}\left(\ln\frac{a}{\pi r_w}+\ln 2\sinh\frac{\pi l}{a}\right). \qquad (2.203b)$$

In addition to this precise but relatively tedious calculation, Charniĭ recommends that the effect of ignoring small quantities in eqn. (2.201) should be evaluated, but this is not carried out in practice since there are other more serious inaccuracies which arise from taking values from tests, and these cannot be avoided.

Moreover, cases solved by proposing protective measures are considerably more complicated than Charniĭ reasons, since all the following affect the inflow to a well: extent of embankment front L_1; width of embankment at foot L_2; depth of permeable layer D; its permeability coefficient k; thickness of nearly impermeable soil h_z; length of cover behind the embankment L_3; and other so-called effective data derived from real quantities, e.g. the effective thickness of the layer t_{eff} and effective permeability coefficient k_z. As initial parameters for calculation, we have the distances from the foot of the downstream embankment slope of the intended intersections of the pressure line with the surface a, and of its intersection with the ground y_3 (Fig. 2.37). If H is the height of the water surface above the terrain, the piezometric height recorded in the embankment piezometers for distances

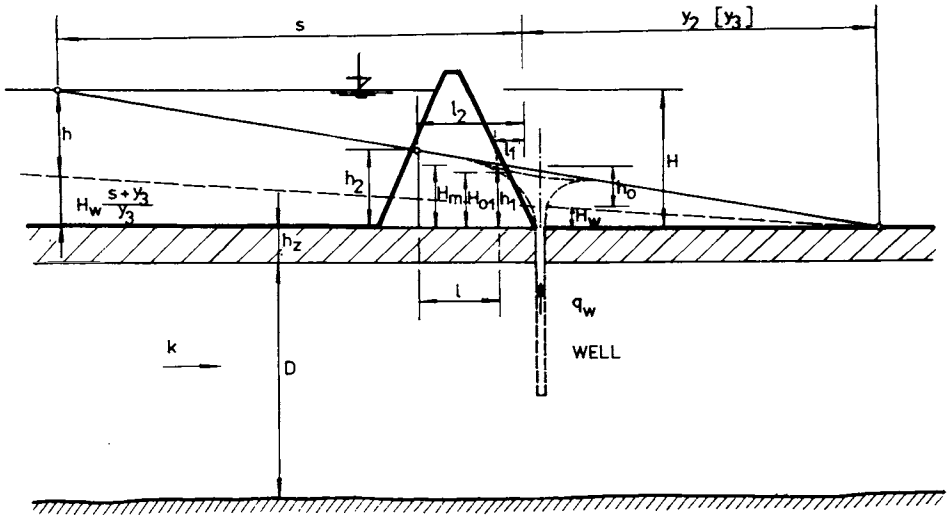

Fig. 2.37. Piezometric height in the vicinity of a well situated near the toe of the dam.

$$l = l_2 - l_1, \qquad h_2,\ h_1$$

will be

$$s = l_1 + (H - h_1)\frac{l_2 - l_1}{h_2 - h_1}, \tag{2.204}$$

$$y_3 = h_1 \frac{l_2 - l_1}{h_2 - h_1} - l_1, \tag{2.205a}$$

whereas Turnbull and Mansur (1954) suggested

$$y_3 = \frac{1}{C \tanh cL_3}, \tag{2.205b}$$

where

$$C = \sqrt{\frac{k_x}{k_p h_z d_c}}.$$

If we know C, we can find how far from the intersection is (y_3), with the help of the graphical representation shown in Fig. 2.38. It is assumed that for pressure losses, $h_x = h_0 = \exp(-cx)$, the above-mentioned authors have their own graphs for them.

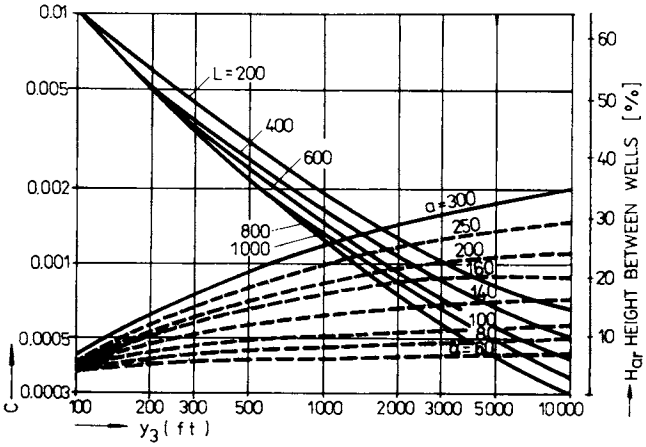

Fig. 2.38. Relationship between blanket parameters L_3, c, x_3 and average piezometric height (H_s) for different distances a, y_3.

For the notation in our picture, the following equations apply

$$h = H - H_w\left(\frac{s + y_3}{y_3}\right), \tag{2.206a}$$

$$H = H_0 + h_0, \tag{2.206b}$$

$$h_{av} = \frac{h\Phi_{av}}{\frac{s}{a} + \left(\frac{s+y_3}{y_3}\right)\Phi_{av}}, \tag{2.207}$$

$$H_{av} = H_w + h_0, \tag{2.208}$$

$$h_0 = h\frac{\Phi_0}{\Phi_{av}} = \frac{h\Phi_0}{\frac{s}{a} + \left(\frac{s+y_3}{y_3}\right)\Phi_{av}}. \tag{2.209}$$

After including uplift factors Φ_0 (on the axis) and Φ_{av} (average) it is possible to evaluate the effectiveness of an individual well, q_w, where

$$q_w = \frac{hk_f D}{\frac{s}{a} + \left(\frac{s+y_3}{y_3}\right)\Phi_{av}}. \tag{2.210}$$

The simplified approach to the calculation indicated, which Turnbull and Mansur derived in 1954 and then successfully used in the design of antiseepage measures on the Mississippi River from 1956 to 1959, is based mainly on theoretical assumptions published after World War II by the Americans (Middlebrooks and Jerris 1947), and taken up with certain modifications by Czechoslovak researchers (Hálek 1966).

Besides this, Hammad's calculation (1960), which is suitable for discovering the extent of seepage and uplift pressures in dams, is sometimes used. Its major use to date has been in the design of the Aswan Dam (Saad el Ali).

Where wells lie along unsealed canals or the embankments of small lakes on some river without an antiseepage carpet or any other protection, it is sufficient to determine the flow lines and potentials according to Schneebeli's formula, for which we have

$$\varphi = \frac{Q}{4\pi kD}\ln\left(\frac{\cosh\frac{2\pi y}{a} - \cos\frac{2\pi x}{a}}{2}\right), \tag{2.211}$$

$$\psi = \frac{Q}{2\pi kD}\tanh^{-1}\left(\frac{\tanh\frac{\pi y}{a}}{\tan\frac{\pi x}{a}}\right). \tag{2.212}$$

The level drop at the i-th well will be

$$\zeta_{wi} = H_0 - \sqrt{D(H_0 + \zeta_d) - \frac{1}{\pi k}\left\{Q_i \ln\left(\frac{2l_i}{r_{wi}}\right) + \sum Q_j \ln\left(\frac{r'_{ij}}{r_{ij}}\right)\right\}}, \tag{2.213}$$

where D is the thickness of the relevant drained layer; H_0 the total active thickness of the layers, $D + \zeta_d$; r_{ij} is the distance between wells w_i and w_j; l_{ij} the distance from

well w_i to the mirrored well w_j; Q_i and Q_j are the quantities pumped out from wells i and j, and the remaining symbols are as before.

2.6 Basic Problems of Unsteady Seepage

Unsteady seepage is a far more common occurrence in canal embankments, and still more so for levées, than the constant seepage we have so far described. During times when levées are in use (during floods), the water level in the river and between levées changes so quickly that a constant flow regime cannot commence. Even so, we very often analyse levées making the assumption of steady seepage flow, usually done for three main reasons.

(a) A steady flow regime — for a certain surface level — gives maximum seepage values and a maximum position for the phreatic (pressure) line.
(b) It is much more convenient to perform calculations for an embankment in an unchanging state than in a state of unsteady seepage flow.
(c) It is difficult to determine seepage parameters with respect to time (t) beforehand, since we do not generally know even a basic relationship between water level and time ($h=\mathrm{f}(t)$).

For these reasons, we frequently retain the fundamental assumptions already introduced, including that of Darcy's seepage, at least for definite time intervals Δt, from which we can progress to unsteady flow.

Here we can start from the basic equations which we have altered for an individual component of velocity, namely the real one

$$u=\frac{\partial \varphi}{\partial x}, \qquad v=\frac{\partial \varphi}{\partial y}, \qquad w=\frac{\partial \varphi}{\partial z},$$

$$\frac{\partial u}{\partial x}+\frac{\partial v}{\partial y}+\frac{\partial w}{\partial z}=0. \tag{2.214}$$

We then introduce the new function F, which records changes in surface position as a function of time $F(x, y, z, t)$, and with the help of which we find, with regard to soil porosity (n_0), that

$$n_0 \frac{\partial F}{\partial t}+\frac{\partial F}{\partial x} u+\frac{\partial F}{\partial y} v+\frac{\partial F}{\partial z} w=0. \tag{2.215}$$

The potential which governs velocity change [or its components, according to eqn. (2.214)] can be written in the form

$$\varphi(x, y, z, t)=\varphi_0(x, y, h, t)+\left.\frac{\partial \varphi}{\partial z}\right|_{z=h}(z-h)+\ldots \approx \varphi(x, y, h, t), \tag{2.216}$$

$$z=\delta(x, y, h, t)=-\frac{\varphi(x, y, h, t)}{k}.$$

A further problem arises in solving nonlinear differential equations (usually solved by approximate or direct substitution methods), where seepage is approximated to the movement of a totally different fluid, e.g. heat flow (according to Fourier).

2.6.1 The Simplest Solutions and Equations

If we use a vector notation for the resultant velocity $\boldsymbol{V}$, with the relevant physical concept of motion and surface movement, we can (as in Section 2.1) state that

$$\boldsymbol{V} = k \,\mathbf{grad}\, \varphi,$$

$$\operatorname{div} \boldsymbol{V} = 0 \qquad \text{(continuity equation)},$$

$$\Delta\varphi = 0 \qquad \text{(Laplace)}.$$

If from eqn. (2.216) we also deduce the expression

$$\varphi = \text{constant} = \varphi_0(t),$$

we obtain

$$\varphi = z \qquad \text{(for a free surface)}.$$

We shall examine the changes which begin at certain instants in time, $t, \ldots, t + \mathrm{d}t$, if the velocity $\boldsymbol{V}$ increases and with it its component in the direction of the normal v_n (see Fig. 2.39). If the inflow volume is $v_n \,\mathrm{d}S\,\mathrm{d}t$, it must follow that

$$v_n \,\mathrm{d}S\,\mathrm{d}t = n_0 \,\mathrm{d}S\,\mathrm{d}n,$$

(n_0 is porosity) and the level rises by

$$\frac{\partial h}{\partial t}\,\mathrm{d}t.$$

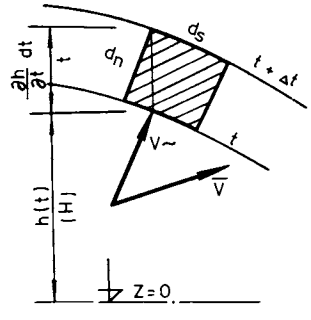

Fig. 2.39. Movement of the free surface as a consequence of velocity change.

It follows from geometrical relations for the velocity components $v_n\mathbf{V}(u, w)$ that

$$\mathrm{d}n = \frac{\partial h}{\partial t}\,\mathrm{d}t \cos\alpha,$$

$$v_n = \mathbf{Vn} = u \sin \alpha + w \cos \alpha,$$

$$n_0 \frac{\partial h}{\partial t} \mathrm{d}t \cos \alpha = (u \sin \alpha + w \cos \alpha)\, \mathrm{d}t,$$

Since

$$\tan \beta = -\frac{\partial h}{\partial x}, \qquad u = -k \frac{\partial \varphi}{\partial y}, \qquad w = -k \frac{\partial \varphi}{\partial z}.$$

we obtain, after some adjustment and generalization, the equation of surface movement

$$\frac{\partial h}{\partial t} = \frac{k}{n_0} \left[\frac{\partial h}{\partial x} \frac{\partial \varphi}{\partial x} + \frac{\partial h}{\partial y} \frac{\partial \varphi}{\partial y} - \frac{\partial \varphi}{\partial z} \right]. \tag{2.217}$$

For small surface inclinations (and large thickness of water-bearing layer) and for small velocities (Darcy), we can assume that the normal is vertical (velocity $w = -k\, \partial\varphi/\partial z = w_0$ is also identified with it), the change in potential will dependent on surface position change, and therefore

$$\frac{\partial h}{\partial t} = \frac{k}{n_0} \left[\frac{\partial}{\partial x} \left(h \frac{\partial h}{\partial x} \right) + \frac{\partial}{\partial y} \left(h \frac{\partial h}{\partial y} \right) \right] + \frac{w_0}{n_0}. \tag{2.218}$$

With further modification and simplification for planar seepage, we can obtain the equation for the small parameter $\lambda = \mathrm{f}(x, t)$, so that

$$\frac{\partial h}{\partial t} = \frac{k}{n_0} \frac{\partial}{\partial x} \left(h \frac{\partial h}{\partial x} \right) + \lambda\, \mathrm{f}(x, t), \tag{2.219}$$

if it is also true that

$$h(x, t) = h_0 + \lambda h^{(1)}(x, t) + \lambda^2 h^{(2)}(x, y). \tag{2.220}$$

Equations with an integral of probability

$$\Phi(\xi) = \frac{2}{\sqrt{\pi}} \int_0^{\xi} \exp(-\xi_1^2)\, \mathrm{d}\xi_1 \tag{2.221}$$

have the form

$$H(x, t) = H_0 + H_1 \left[1 - \Phi \left(\frac{x}{2\sqrt{at}} \right) \right] \tag{2.222}$$

and lead to a simple determination of the coordinate y at the point x and time t (see Fig. 2.40), so that

$$y = H(x, t) - H_0, \tag{2.223}$$

$$\frac{H_1 - y}{H_1} = \Phi \left(\frac{x}{2\sqrt{at}} \right) = \frac{z}{H_1}, \tag{2.224}$$

where $a = kH/n_0$ (transmissivity), H is the average depth of seepage water, and n_0 and k are as before. From eqn. (2.223), it is also easy to obtain the point at which the surface implies a quantity z (or ratio $z: H_1$) or a time

$$t = \mu_1 \frac{x^2}{4a} = \mu \frac{n_0 x^2}{kH}. \tag{2.225}$$

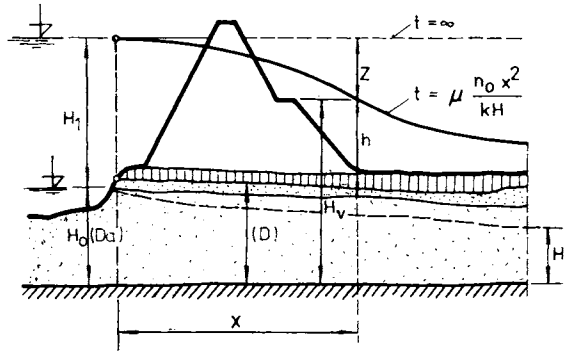

Fig. 2.40. Calculating scheme for estimation of free surface position by means of probability integral.

Table 2.8. Values of coefficient $\mu = f(z/H_1)$

z/H_1	0.01	0.03	0.05	0.10	0.20	0.30	0.40
μ	3190	353	127	31.5	7.69	3.26	1.81
$\log \mu$	3.504	2.548	2.104	1.50	0.886	0.526	0.258

z/H_1	0.50	0.60	0.70	0.80	0.90	0.95	0.99
μ	1.10	0.704	0.463	0.305	0.184	0.130	0.0752
$\log \mu$	0.041	−0.141	−0.334	−0.516	−0.735	−0.886	−1.124

The value or the coefficient μ is usually obtained from tables (Table 2.8).

It is similarly a simple matter to compute from another simplified so-called Fourier heat equation, in which

$$\frac{\partial h}{\partial t} = \frac{kH}{n_0} \Delta h, \tag{2.226}$$

and in a general form

$$\frac{\partial \varphi}{\partial t} = a \Delta \varphi, \tag{2.227}$$

with solution

$$\varphi = \exp\left(-\frac{x^2}{4at}\right) t^{-n/2}. \tag{2.228}$$

Here, the type of flow is governed by the exponent $n = 1, 2, 3$ for one-, two-, or three-dimensional flow.

If we have the simple case of a trench along an embankment into which we take in a quantity w over a distance x, then the lowering is

$$\zeta(x, t) = \frac{w}{2lkH\sqrt{\frac{\pi}{a}}} \frac{\exp\left(-\frac{x^2}{4at}\right)}{\sqrt{t}}. \tag{2.229}$$

If we assume that the water is taken in over a length l, pumping a quantity w in time τ, and considering only elementary quantities $Q\,\mathrm{d}\tau$, then we have

$$\zeta = \frac{Q}{2lkH\sqrt{\frac{\pi}{a}}} \int_0^{\tau=t} \frac{\exp\left(-\frac{x^2}{4a(t-\tau)}\right)}{\sqrt{t-\tau}} \mathrm{d}\tau.$$

Schneebeli solved the equation thus formulated by means of substitution, through which he obtained an expression for the surface lowering (Fig. 2.41)

$$\zeta \cong \frac{Q}{lkH}\left[\sqrt{\frac{at}{\pi}} - \frac{x}{2}\right]. \tag{2.230}$$

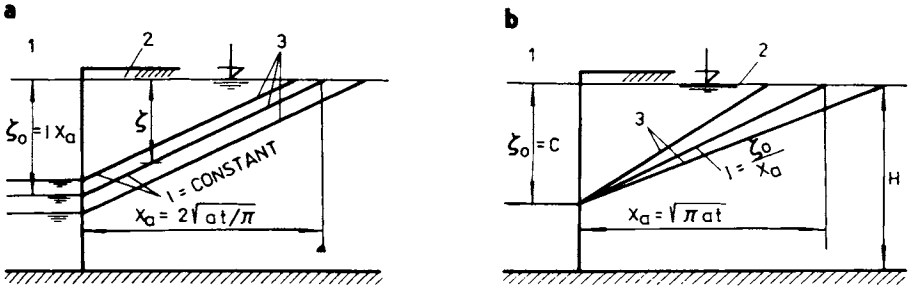

Fig. 2.41. Schemes for the surface lowering and seepage by the trench — calculus uses. a — water-level lowering (for I = constant), b — pumping by constant water level in the trench; 1 — the trench, 2 — original water level, 3 — free water level lowered.

Thus the phreatic curve is replaced by a straight line which enables the pumped volume to be evaluated for a particular relatively constant surface lowering ζ_0, and thus

$$Q = \frac{2lkH\zeta_0}{\sqrt{\pi at}} \cong 2lkHI. \tag{2.231}$$

Equation (2.231) can also be used for more than one well. We find the transmissivity characteristic $k\bar{h}$ (or alternatively kH), and the characteristic of time passage a by means of a pumping experiment

$$kH = \frac{Q}{2\pi\zeta} \ln \frac{R_a}{r_w}, \tag{2.232}$$

$$\sqrt{a} \doteq \frac{R_a}{1.5\sqrt{T_p}}, \tag{2.233}$$

where T_p is the pumping time.

Many more detailed and more exact solutions by Hálek and Švec (1973) can be found.

2.7 Determination of Seepage through Experimental Methods

Using an experimental method, it is possible to determine either the seepage q directly, or several parameters of seepage or seepage field, and then the course of the phreatic line and of equipotentials or flowlines, etc.

Of a large number of experimental methods, the most frequently used are:

— methods of electrical analogy (analogy of two media),
— methods of hydraulic analogy (analogy by replacement of soil),
— methods of membrane analogy, shell models (movement of water in pores replaced by movement in a slot).

These are two-dimensional soil models and arithmetical-experimental methods.

2.7.1 Methods of Electrical Analogy

In methods of electrical analogy, the analogy between electric current in a certain suitable field and water motion in a porous medium is exploited, and furthermore the two fundamental laws describing these movements, Ohm's law and Darcy's law.

In this idea, electrical voltage is analogous to hydraulic gradient; the intensity of flow to the filtration velocity; and the electrical conductivity to the soil permeability. If we denote U as the electric potential, ϱ_E as electrical resistance and γ as the conductivity, then we can write Ohm's law as follows

$$\boldsymbol{i} = -\frac{1}{\varrho_E} \mathbf{grad}\, \boldsymbol{U} = -\gamma\, \mathbf{grad}\, \boldsymbol{U}. \tag{2.234}$$

The analogy with Darcy's law is immediately apparent.

If we consider the most common case, that of planar flow, then for flow-intensity components we can write down the differential equations

$$i_x = -\gamma \frac{\partial U}{\partial x}, \qquad i_y = -\gamma \frac{\partial U}{\partial y}. \tag{2.235}$$

After the introduction of a variable conductor thickness (z) and flow function (ψ), we also have

$$\frac{\partial (z i_x)}{\partial x} + \frac{\partial (z i_y)}{\partial y} = 0,$$

$$\frac{\partial \psi}{\partial x} = -z i_y, \qquad \frac{\partial \psi}{\partial y} = z i_x.$$

For seepage in soil

$$v_x = -k \frac{\partial h}{\partial x}, \quad v_y = -k \frac{\partial h}{\partial y}, \quad \frac{\partial v_x}{\partial x} + \frac{\partial v_y}{\partial y} = 0,$$

$$\frac{\partial h}{\partial x} = -\frac{1}{k} \frac{\partial \psi}{\partial y}, \quad \frac{\partial h}{\partial y} = \frac{1}{k} \frac{\partial \psi}{\partial x}. \tag{2.236}$$

It is clear from the above equations that the flowlines for seepage through soil correspond to the line-of-force equations for an electric field.

The analogous *Laplace equations* also apply

$$\frac{\partial^2 U}{\partial x^2} + \frac{\partial^2 U}{\partial y^2} = 0, \qquad \frac{\partial^2 h}{\partial x^2} + \frac{\partial^2 h}{\partial y^2} = 0. \tag{2.237}$$

In the seepage field, we looked for $h = \text{constant}$, $\partial h / \partial n = 0$ and analogously in our model we shall find $U = \text{constant}$, $\partial U / \partial n = 0$ (Fig. 2.42).

Also, from this analogy, various relations follow for basic quantities. Across area S flows a quantity of current

$$I = \int_s i \, \mathrm{d}s.$$

Across a curve of length l there flows

$$I = \int i \, \mathrm{d}l = -\gamma \int \frac{\partial U}{\partial s} \mathrm{d}l. \tag{2.238}$$

Therefore analogously

$$q = \int v \, \mathrm{d}l = -k \int \frac{\partial h}{\partial s} \mathrm{d}l. \tag{2.239}$$

Electric-network analysers enable this idea to be developed further, starting from equations

$$\frac{U}{U_0} = \frac{\varphi}{\varphi_0},$$

$$\frac{M_E}{U_0}\,\mathbf{grad}\,U=\frac{M_N}{\varphi_0}\,\mathbf{grad}\,\varphi\,, \tag{2.240}$$

$$\frac{M_E}{\gamma U_0}\,i=\frac{M_N}{k\varphi_0}\,\mathbf{V}\,,$$

$$\frac{I}{\gamma U_0}=\frac{q}{k\varphi_0}\,.$$

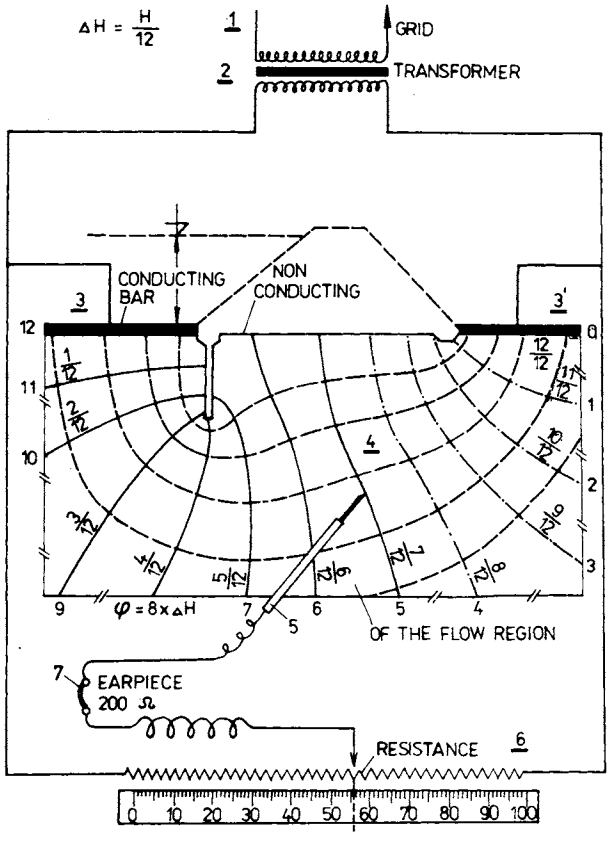

Fig. 2.42. Method of drawing the flow-net using electrical analogy. 1 — current source, transformer, 3 — electrodes, 4 — model of flow region, 5 — probe electrode, 6 — resistance bridge, 7 — aerphone.

We use the principle of Southwell's relaxation method for a square network (Fig. 2.43), in the centre of which (0) we seek a certain, in this case electrical, quantity. According to Kirchhoff's laws for resistance R, with potentials U_0 to U_4, we see that

$$\frac{U_1-U_0}{R}+\frac{U_2-U_0}{R}+\frac{U_3-U_0}{R}+\frac{U_4-U_0}{R}=0\,, \tag{2.241}$$

$$\sum_{i=1}^{4} U_k - 4U_0 = 0.$$

Equation (2.241) in fact incorporates the Laplace equation which is expressed by small differences. For seepage on the x, z plane, this equation for the centre of the square network can be expressed by the equations

$$k_x \frac{\partial^2 \varphi}{\partial x^2} + k_z \frac{\partial^2 \varphi}{\partial z^2} = 0 ,$$

$$k(\varphi_1 + \varphi_3 - 2\varphi_0) + k(\varphi_2 + \varphi_4 - 2\varphi_0) = 0. \tag{2.242}$$

However, the resistances are also dependent on the distances of the considered point (0) from the sides of the square (see Fig. 2.43)

$$R_1 = R_x \frac{2a}{b+b'}, \qquad R_2 = R_z \frac{2b}{a+a'}, \tag{2.243}$$

$$R_3 = R_x \frac{2a'}{b+b'}, \qquad R_4 = R_z \frac{2b'}{a+a'}.$$

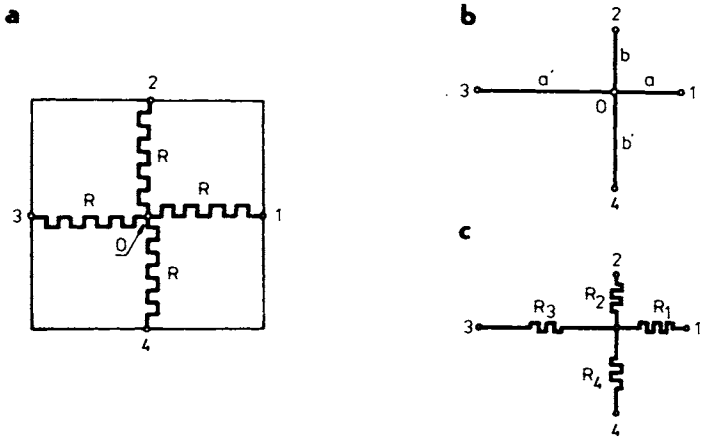

Fig. 2.43. Southwells relaxation method. a — distribution of resistances, b — analogical lengths, c — different resistances.

These equations allow precise setting of the net and also allow us to bring into the calculation the anisotropy of the current field, either directly or indirectly.

In Czechoslovakia, up to 1970, more than 20 analysers (number of nodes 200—2000) have been used, by means of which it has been possible to solve not only hydraulic but also static problems. For solving hydraulic questions, the best equipped centre in Czechoslovakia is the Scientific Research Institute for Hydrau-

lic Engineering at the Technical University in Brno, where Kratochvíl (1961a) was the first scientist who used this device for solution of particular seepage problems, besides of shell models and membrane models.

The great advantages in speed and accuracy of seepage calculations given a homogeneous (continuous) medium, are most manifest when addressing questions concerning unsteady flow.

From the conditions set out in eqn. (2.203), the modeling of a free surface and of variable processes by means of the electrical analogy can proceed with the limiting conditions

$$\varphi = z = h \qquad \text{on the free surface } h(x, t), \tag{2.244}$$

$$\frac{\partial \varphi}{\partial n} = 0 \tag{2.245}$$

at the edge of the region given by the impermeable layer $\varphi = f(t)$, defining the area of seepage at a certain instant.

Into the original equation, by which the level change is defined for a certain free-surface slope $\partial h/\partial x = \tan \alpha$ and for gradients $\partial \varphi/\partial x$ and $\partial \varphi/\partial z$, and which has the form

$$\frac{n_0}{k}\frac{\partial h}{\partial t} = \frac{\partial h}{\partial x}\frac{\partial \varphi}{\partial x} - \frac{\partial \varphi}{\partial z}, \tag{2.246}$$

a new variable is substituted $\tau = \frac{k}{n_0} t$.

Therefore

$$\frac{\partial h}{\partial \tau} = -\frac{\partial \varphi}{\partial z} + \frac{\partial h}{\partial x}\frac{\partial \varphi}{\partial x}. \tag{2.247}$$

After solving and expanding for time instants (1) and (2), (τ and $\tau + d\tau$) on the vertical (see Fig. 2.44), we have

$$h_1 - h_2 = \partial h = \frac{1}{2}\left[\left(\frac{\partial h}{\partial \tau}\right)_1 - \left(\frac{\partial h}{\partial \tau}\right)_2\right] \partial \tau - \frac{1}{12}\left(\frac{\partial^3 h}{\partial \tau^3}\right) \partial \tau^3 + \ldots$$

The average approximate value, which defines the fall (movement) as a function of τ, will be

$$\left(\frac{\partial h}{\partial \tau}\right)_{av} = \frac{1}{2}\left[\left(\frac{\partial h}{\partial \tau}\right)_1 + \left(\frac{\partial h}{\partial \tau}\right)_2\right]. \tag{2.248}$$

From our knowledge of the free surface (phreatic curve K_1), we can construct an analogous model with the conditions mentioned above. At each point on the curve K_1, this model provides us with elements ($\partial \varphi/\partial n$, $\partial \varphi/\partial x$, $\partial h/\partial x$) and $(\partial h/\partial \tau)_1$, ..., $(\partial h/\partial \tau)_2$, which we require in order to determine the value of

$$\frac{\partial h}{\partial \tau} = -\frac{\partial \Phi}{\partial x} \rightarrow -\frac{\partial \varphi}{\partial t} \frac{1}{\cos \alpha} \tag{2.249}$$

for an approximation to the altered surface parameters, and therefore to the curve K_2 at the later instant τ_2

$$\tau_2 = \tau_1 + d\tau.$$

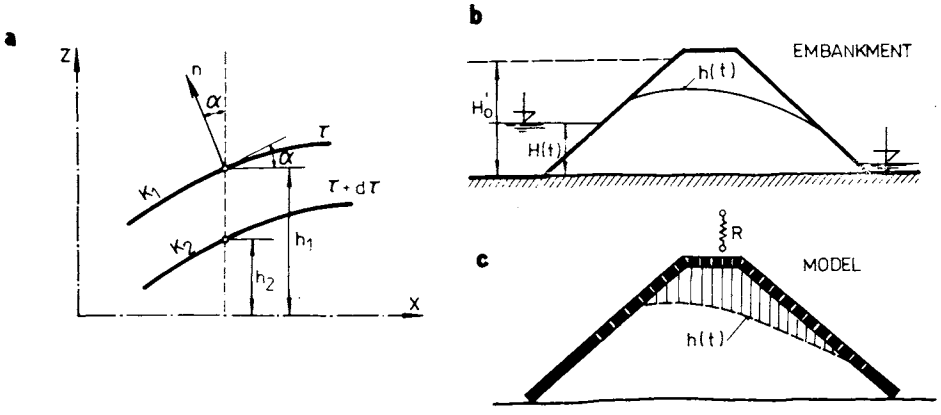

Fig. 2.44. Water-lowering parameters and manifestation by model. a — flowline displacement, b — water level in dam body, c — model of a phreatic curve.

The average speed of surface fall in this further section will be

$$\left(\frac{\partial h}{\partial \tau}\right)_{av} = \frac{1}{2}\left[\left(\frac{\partial h}{\partial \tau}\right)_1 + \left(\frac{\partial h}{\partial \tau}\right)_2\right]. \tag{2.250}$$

In the electrical analogy (Fig. 2.44a, b), the line of the free surface is fed by a certain number of electrodes. Resistance of known value R is inserted between the electrodes and the power source. The potentials are arranged such that on the free surface line, the first of the above conditions ($\varphi = z = h$) is fulfilled. On the edge of the area considered, the intensity $I = (\varphi_a - \varphi_e)/R$ is measured, and is proportional to a current element $\delta\Phi$ according to eqn. (2.239), which gives the value of $\partial h/\partial \tau$ as a function of the measured current intensity.

For modeling with conducting paper, all the electrodes are extended so that their tips describe the free surface. The potentials φ are similarly adjusted.

Correction of the area defined by the line $h(t)$ is done by trimming the conducting paper, a relatively taxing task.

It is more convenient to use an electric-network analyser, in which $\partial h/\partial \tau$ is determined from the values of $\partial \varphi/\partial z$ following the equation

$$\frac{\partial h}{\partial \tau} = -\frac{\partial \varphi}{\partial z} + \left(1 - \frac{\partial \varphi}{\partial z}\right)\left(\frac{\partial h}{\partial x}\right)^2 . \tag{2.251}$$

The surface movement along the normal (n) at a certain 'square' of the network of side a is given by the ratio

$$\frac{\partial \varphi}{\partial n} = \frac{\varphi_2 - \varphi_1}{\overline{12}}, \qquad \cos\alpha = \frac{a}{\overline{12}},$$
$$\frac{\partial h}{\partial \tau} = \frac{\varphi_2 - \varphi_1}{a}, \tag{2.252}$$

if $\overline{12}$ is the length of the lines joining points 1 and 2 on the horizontals defining the square, α is the angle between the normal and verticals of the network.

We can find further details in the relevant specialist literature (Huard de la Marre 1958, Hálek 1963, Bouwer 1965, Schneebeli 1966 and others).

In Fig. 2.45, the solution is illustrated for phreatic-curve movement in a Serre-Ponçon earth embankment with permeability coefficient k, and active porosity n_0 as follows. Core — $k_1 = 1$, $n_{0(1)} = 0.25$; filters — $k_2 = 100\ k_1$, $n_{0(2)} = 0.15$; stabilizing wedges on the up- and downstream sides — $k_3 = 1000\ k_1$; $n_{0(3)} = 0.17$; drain — $k_4 = 10\,000\ k_1$, with zero potential at $\Phi = 0$ in the well and $\Phi = 115$ on the level of retained water, for $t = 0$ to 100.

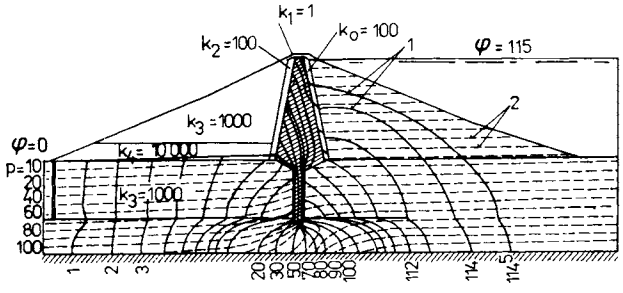

Fig. 2.45. Equipotential lines in Serre-Ponçon dam. 1 — equipotentials, 2 — lines of equal pressures.

2.7.2 Methods of Hydraulic Analogy

If is possible to model the phreatic-surface movement using eqn. (2.217) and the conditions of the analogy, by a relaxation method set out by Southwell. Several models of this type replace flow through a porous medium with a Poiseuille flow,

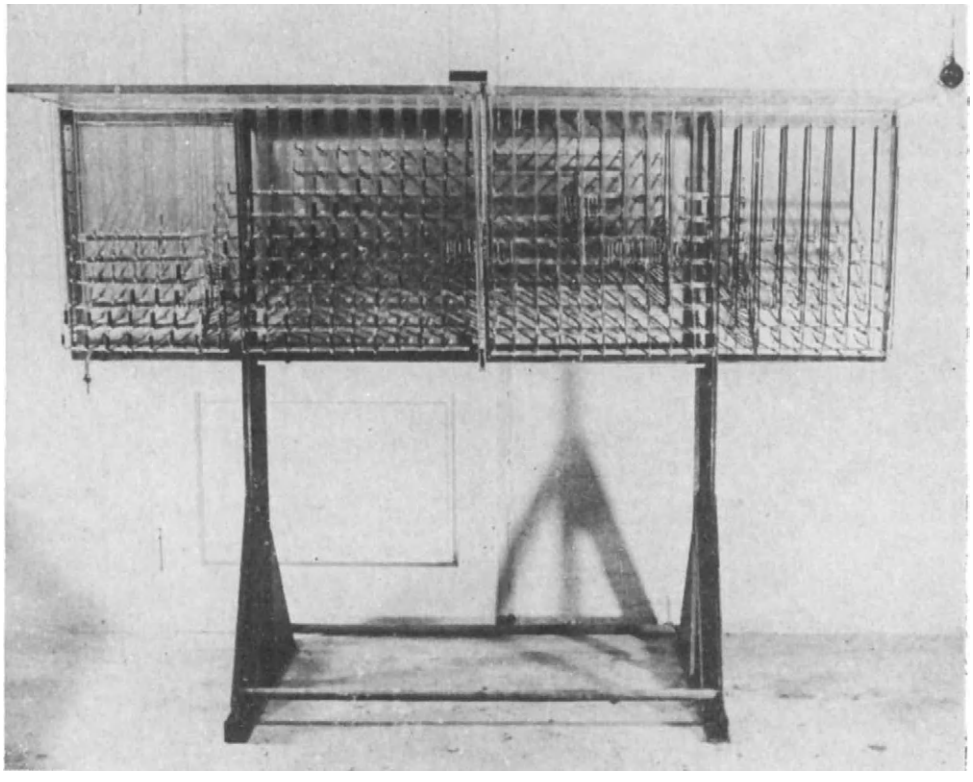

Fig. 2.46. Network model — for hydraulic analogy investigation.

i.e. capillaries, the dimensions of which are fixed in relation to the permeability of the modeled parts of the embankment.

The simple hydraulic-network model which we constructed (Fig. 2.46) involves a square network with grooves set into the aluminium plates. These are covered with plates of plexiglass which close off the groove profiles after the method of closed channels (Poiseuille flowlines), through which, given a pressure distribution, water flows in accordance with the channel profiles (analogous to soil pores). This model renders possible solution of the simple Laplace equation

$$\frac{\partial^2 \varphi}{\partial x^2}+\frac{\partial^2 \varphi}{\partial y^2}=0, \qquad \frac{\partial^2 \psi}{\partial x^2}+\frac{\partial^2 \psi}{\partial y^2}=0,$$

by searching for the function which within the given region satisfies the Laplace equation (Dirichlet's problem). In a square net we seek a certain value ψ_0, if in the centre of the bounding sides we have values ψ_1, ψ_2, ψ_3, ψ_4, and then also ψ_5, ψ_6, ψ_7, ψ_8.

We find the value we seek with an approximation using the equations

$$\psi_0=\frac{1}{4}(\psi_1+\psi_2+\psi_3+\psi_4),$$

$$\psi_0=\frac{1}{4}(\psi_5+\psi_6+\psi_7+\psi_8). \tag{2.253}$$

The calculation is usually continued until Φ_{0-1} (preceding) and Φ_0, calculated at one point, differ by less than one per cent.

On the water-facing slope of a dam and at the lower edge of the drain, we must again solve Neuman's problem, i.e. find the derivative of an applicable function in the direction of the outward normal. Therefore we define

$$\frac{\partial\psi}{\partial n}=\frac{\psi_0+\psi_1}{a} \tag{2.254}$$

and

$$\frac{\partial\psi}{\partial n}=\frac{\sqrt{2}}{2}\left(\frac{\psi_0+\psi_1}{a}+\frac{\psi_0+\psi_2}{a}\right), \text{ respectively.}$$

If we are modeling an anisotropic soil, we define ψ_0 from the formula

$$\psi_0=\frac{k_1\psi_1+k_2\psi_{II}+k_3\psi_{III}+k_4\psi_{IV}}{4(k_1+k_2+k_3+k_4)}, \tag{2.255}$$

where a is the length of a 'side' of the network and k_1, k_2, k_3, k_4 are the values of the permeability coefficient at points 1, 2, 3, 4.

The calculation approach follows from values estimated for evaluating and finally drawing the flowlines. In the model, we determine flowlines for particular surface levels in front of the embankment from which the phreatic surface emerges in the direction of the drain. The hydraulic analogy has certain advantages, especially when modeling anisotropic soils, since it enables us to take into account, using the time scale τ, the differing porosity n_0, n' and soil permeability.

For the distortion which soil anisotropy causes, we can follow eqn. (2.94), and for seepage through an anisotropic soil we can state that

$$\delta_x=\frac{\lambda_x}{\lambda_z}=\sqrt{\frac{k_y}{k_z}}, \qquad \delta_y=\frac{\lambda_y}{\lambda_z}=\sqrt{\frac{k_z}{k_y}},$$
$$\frac{\varkappa_x}{\delta_x^2}=\frac{\varkappa_y}{\delta_y^2}=\varkappa_z. \tag{2.256}$$

For the time scale, it follows that

$$\frac{\lambda_z}{\tau}=\frac{\varkappa_z}{l_0'/l_0}\rightarrow\tau_0=\frac{n_0'}{n_0}\frac{\tau_z}{\varkappa_z}. \tag{2.257}$$

A measure of seepage for stationary flow in the model illustrated will be

$$\chi = \varkappa\lambda^2. \tag{2.258}$$

For the distorted model

$$\chi = \frac{k'}{\sqrt{k_x k_y}}\lambda_z^2 = \varkappa_z\lambda_z^2\delta_x\delta_y. \tag{2.259}$$

It is a distinct advantage here that we are working with real velocities v', because the relations also include the effective porosity n_{eff}

$$v' = \frac{v}{n_{\text{eff}}}. \tag{2.260}$$

It is questionable whether we know the right value to use for it or whether we are modeling it correctly, since Poiseuille flow is different from Darcy flow for which almost all the variable-flow formulae are derived.

The membrane analogy springs from the deformation analogy for a rubber or other elastic membrane, which deforms as a function of the deformation work — the energy used for deformation and movement of the water surface being dependent on pressure (potential). It is possible to derive the simultaneity of the deformation processes — deformation work, and change of level with energy change, and also the applicability of the Laplace equations (Hálek 1963).

The possibilities of the membrane analogy are more limited than those previously mentioned, since this method is one of the least used exprimental modeling methods for seepage and capillary phenomena, which do satisfy the assumptions made, but are accompanied by other effects (soil volume changes, effect of the gaseous phase, etc.) which cannot be considered here.

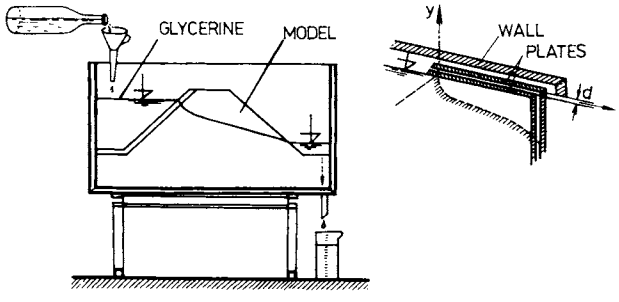

Fig. 2.47. Shell-model analogy.

The *slot analogy* (Fig. 2.47) uses the idea that it is possible to model the soil permeability (k) under the arrangement of a gap of width d between two parallel plates, between which flows a liquid of average unit weight γ_t, and dynamic

viscosity η. Therefore, for seepage q the following equations apply (Schneebeli 1966, Hálek and Švec 1973)

$$q_x = \frac{\gamma_f d^3}{12\eta} \frac{\partial \varphi}{\partial x}, \tag{2.261}$$

$$q_y = \frac{\gamma_f d^3}{12\eta} \frac{\partial \varphi}{\partial y}.$$

The seepage vector for unit length of the slot is

$$\boldsymbol{q} = -C_s \, \mathbf{grad} \, \varphi. \tag{2.262}$$

This relates to the analogous expression for permeability as in eqn. (2.226). It is a simple matter to realize that the coefficient of slot efficiency has the value

$$C_s = \frac{\gamma_f d^3}{12\eta} = \frac{g d^3}{12\nu}. \tag{2.263}$$

From a comparison with Darcy's equation for laminar flow, it follows that

$$C_s = kd. \tag{2.264}$$

The slot analogy is most advantageous in finding the position of the phreatic surface under both static and variable flow. The equation for surface movement here takes the form

$$\frac{\partial h}{\partial t} = C_s \frac{\partial h}{\partial x} \frac{\partial \varphi}{\partial x} - C_s \frac{\partial \varphi}{\partial z}. \tag{2.265}$$

For the time scale, we have that

$$\tau = \lambda_M \frac{k/n_0}{C_s}, \tag{2.266}$$

where λ_M is the scale of the model, k and n_0 are the permeability and porosity coefficients for the modeled soil.

Since modeling the free surface in a slot is the simplest way, the course of the phreatic curve is often derived thus even when another analogy is also to be used (e.g. electric). The free surface determined by the shallow-layer method together with the impermeable sublayer forms the boundary for determining other flowlines, and an auxiliary element in finding the equipotentials.

Earth models are used as aids to calculation if the water movement through the soil and its effect on the solid phase influence the soil properties (volume change, structure, moisture change, etc.), which cannot be introduced into the calculation by known characteristics, only by total effect.

At the Geotechnics Department of the Slovak Technical University in Bratislava, models of this sort have been worked with for more than twenty years. Difficulties have arisen, however, in finding a suitable model-measuring device.

Different phenomena have different relevant similarities, the most commonly used Reynolds' similarity (Re) is only suitable for the motion of a viscous material. To solve soil-stability questions, it is useful to use the Froude similarity (Fr) and also others. Dimensional analysis is a particular problem here, but one which excludes itself from the field of our work.

This also applies — indeed in even greater measure — to computer models, as also to various combined, so-called hybrid models, which have been used more and more in recent years as a progressive element in the planning of earth embankments, but their use is usually denied to the designer.

A wide review of analogous methods and methods of calculator used by Kratochvíl (1961b), Hálek (1963), Martin (1966), Zienkiewicz et al. (1966), Desai and Abel (1972), Kolář et al. (1975) can be found.

2.8 Some Precise and Particular Seepage Calculations

As we indicated in the introductory part of Chapter 1, the most commonly used relations (derived from Darcy's or sometimes Depuit's seepage equations) apply only to seepage through a homogeneous, isotropic soil. For flow through an anisotropic soil, these relations must be adjusted beforehand, which can be done using an anisotropy coefficient or a suitable transformation. It is frequently advantageous to use one of the differential methods, in which it is easy to take account of different ratios and conditions of flow in different directions. One of these methods is the relaxation method.

To understand this method, we must introduce various dimensionless equation of spatial flow, derived by Heinrich and Desoyer (1955). The basic continuity equation, in which flow is described in a space defined by the coordinates ξ, η, ζ, has the form

$$k_\xi \frac{\partial^2 h}{\partial \xi^2} + k_\xi \frac{\partial^2 h}{\partial \eta^2} + k_\xi \frac{\partial^2 h}{\partial \zeta^2} = 0. \tag{2.267}$$

Equation (2.217), adapted for surface movement, will have the form

$$\frac{\partial \zeta_2}{\partial t} = \frac{1}{n_0}\left[k_\xi \frac{\partial \zeta_2}{\partial \xi}\frac{\partial \varphi}{\partial \xi} + k_\xi \frac{\partial \zeta_2}{\partial \eta}\frac{\partial \varphi}{\partial \eta} - k_\xi \frac{\partial \varphi}{\partial \zeta}\right], \tag{2.268}$$

where ζ_2 denotes the ζ-th coordinate on the free surface.

For an *anisotropic medium* we include the transformation equations

$$\xi = \sqrt[3]{\frac{k_\xi}{\sqrt{k_0'}}}\,\bar{\xi}, \quad \eta = \sqrt[3]{\frac{k_\eta}{\sqrt{k_0'}}}\,\bar{\eta}, \quad \zeta = \sqrt[3]{\frac{k_\zeta}{\sqrt{k_0'}}}\,\bar{\zeta}, \tag{2.269}$$

where

$$k_0' = k_\xi k_\eta k_\zeta .$$

In order that the Laplace equation

$$\frac{\partial^2 \varphi}{\partial \xi^2} + \frac{\partial^2 \varphi}{\partial \eta^2} + \frac{\partial^2 \varphi}{\partial \zeta^2} = 0$$

should remain in effect, we introduce the dimensionless quantities

$$\varphi' = H\varphi^+, \quad \xi' = H\xi^+, \quad \eta' = H\eta^+, \quad \zeta' = H\zeta^+, \tag{2.270}$$

where H is an arbitrary constant with the dimensions of length.

After inserting values found through eqns. (2.269) and (2.270) into eqn. (2.267), we find that

$$\frac{\partial^2 \varphi^+}{\partial \xi^{+2}} + \frac{\partial^2 \varphi^+}{\partial \eta^{+2}} + \frac{\partial^2 \varphi^+}{\partial \zeta^{+2}} = 0. \tag{2.271}$$

The equation of the flowline

$$\frac{\partial \zeta^+}{\partial \tau^+} = \left[\frac{\partial \zeta_2^+}{\partial \xi^+} \frac{\partial \varphi^+}{\partial \xi^+} + \frac{\partial \zeta_2^+}{\partial \eta^+} \frac{\partial \varphi^+}{\partial \eta^+} - \frac{\partial \varphi^+}{\partial \zeta^+} \right],$$

where $\tau^+ = t \sqrt[3]{k_0'}/He_0$ is a dimensionless time parameter.

Substitution equations can also be used in evaluating volumes (V_k^+) and seepage (Q) in this way

$$V_k^+ = \iiint n_0 \, d\xi' \, d\eta' \, d\zeta',$$

$$Q = \int_S v \, d\sigma = \int_{S_\xi} v_\xi \, d\eta \, d\zeta + \int_{S_\eta} v_\eta \, d\zeta \, d\xi + \int_{S_\zeta} v_\zeta \, d\xi \, d\eta. \tag{2.272}$$

We shall denote $\boldsymbol{V}$ a velocity vector, $d\sigma$ an element of the area, S the area with flow across it, S_ξ, S_η, S_ζ projections of the area, and v_ξ, v_η, v_ζ projections of velocity.

After substituting the components of velocity

$$v_\xi = -k_\xi \frac{\partial \varphi}{\partial \xi}, \quad v_\eta = -k_\eta \frac{\partial \varphi}{\partial \eta}, \quad v_\zeta = -k_\zeta \frac{\partial \varphi}{\partial \zeta}$$

using the indicated transformation into eqn. (2.272), we have

$$Q = -H^2 \sqrt[3]{k_0'} \left[\int_{S_{\xi^+}} \frac{\partial \varphi^+}{\partial \xi^+} d\eta^+ \, d\zeta^+ + \int_{S_{\eta^+}} \frac{\partial \varphi^+}{\partial \eta^+} d\zeta^+ \, d\xi^+ + \right.$$

$$\left. + \int_{S_{\zeta^+}} \frac{\partial \varphi^+}{\partial \zeta^+} d\xi^+ \, d\eta^+ \right], \tag{2.273}$$

$$Q = -H^2 \sqrt[3]{k_0'} Q^+ .$$

If we introduce the velocity expressed by Darcy's equation into eqn. (2.273), on the x, y plane, with *transformation parameters*

$$\varphi = Hk^+, \quad x' = Hx^+, \quad y' = Hy^+, \quad z' = Hz^+, \tag{2.274}$$

then, after some adjustment, we obtain

$$Q = -H^2 \sqrt{k_x k_y} \left[\iint_{S_{x^+}} \frac{\partial \varphi^+}{\partial x^+} \, dy^+ \, dz^+ + \iint_{S_{y^+}} \frac{\partial \varphi^+}{\partial y^+} \, dx^+ \, dz^+ + \right.$$

$$\left. + \iint_{S_{z^+}} \frac{\partial \varphi^+}{\partial z^+} \, dx^+ \, dy^+ \right],$$

$$Q = H^2 \sqrt{k_x k_y} Q^+, \tag{2.275}$$

where Q^+ is the dimensionless unit seepage.

The potential gradient (φ) is often replaced by the pressure gradient which is defined by the piezometric height; i.e. $\partial\varphi(\partial x \to \partial p)\partial x$. We can therefore easily find all the values required for further computation.

The *relaxation* is an approximate differential method, in which we approach real values by reducing the difference R between actual and calculated values to a figure near zero.

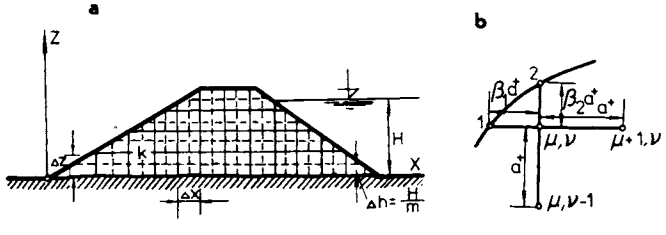

Fig. 2.48. Differential net. a — cross-section and basic net, b — net distortion on the border.

The profile considered is separated into a differential network of unit size Δx, Δy, Δz (Fig. 2.48). In this way we make the transformation from the differentials dx, dy, dz, to finite elements, $dx \to \Delta x$, etc. With a further transformation

$$x = Hx^+, \quad z = Hz^+, \quad h = Hh^+, \tag{2.276}$$

we proceed to the straight-line system

$$x^+ = \mu a^+, \quad z^+ = \nu a^+, \tag{2.277}$$

with values $a^+ = H/a$, and so $a = H/a^+ \rightarrow a = H/m = \Delta h$, where μ, ν are suitable whole numbers, and a is the size of a side of the network.

If we assume isotropic soil ($k_x = k_y = k_z = k$), we may express the equilibrium at a given nodal point (μ, ν) of the network by an equation analogous to eqn. (2.242), thus

$$h^+_{\mu-1,\,\nu} + h^+_{\mu+1,\,\nu} + h^+_{\mu,\,\nu-1} + h^+_{\mu,\,\nu+1} - 4h^+_{\mu,\,\nu} \cong R^+_{\mu,\,\nu} \cong 0, \tag{2.278}$$

which gives us an approximate solution to the Laplace equation

$$\frac{\partial^2 h^+}{\partial x^{+2}} + \frac{\partial^2 h^+}{\partial z^{+2}} = 0$$

at the node (μ, ν), where the second derivatives h^+ are replaced by the quantities

$$\left(\frac{\partial^2 h^+}{\partial x^{+2}}\right)_{(\mu,\,\nu)} = \frac{1}{a^{+2}}\,(h^+_{\mu-1,\,\nu} - 2h^+_{\mu,\,\nu} + h^+_{\mu+1,\,\nu}),$$

$$\left(\frac{\partial^2 h^+}{\partial z^{+2}}\right)_{(\mu,\,\nu)} = \frac{1}{a^{+2}}\,(h^+_{\mu,\,\nu-1} - 2h^+_{\mu,\,\nu} + h^+_{\mu,\,\nu+1}). \tag{2.279}$$

Values of h^+ are placed experimentally into eqn. (2.278) so that with a gradual progression, the value of R^+ should approach zero.

On the *free surface* the squares are deformed in a certain ratio β. For equilibrium at the point (μ, ν), we have that

$$\frac{2}{\beta_1(1+\beta_1)}\,h^+_1 + \frac{2}{1+\beta_1}\,h^+_{(\mu+1,\,\nu)} + \frac{2}{1+\beta_2}\,h^+_{(\mu,\,\nu-1)} +$$

$$+ \frac{2}{\beta_2(1+\beta_2)}\,h^+_2 - \left(\frac{2}{\beta_1} + \frac{2}{\beta_2}\right) h^+_{(\mu,\,\nu)} - R^+_{(\mu,\,\nu)} = 0. \tag{2.280}$$

Therefore, the difference will be

$$\Delta R_{(\mu,\,\nu)} = -\left(\frac{2}{\beta_1} + \frac{2}{\beta_2}\right) \Delta h^+_{(\mu,\,\nu)}. \tag{2.281}$$

Using these approximate equations, a satisfactory accuracy is attained for practical purposes. The least accurate part of the solution will be near the stationary phreatic line (for $\Delta t = \infty$), where it can be improved by means of a graphical check, by drawing out the equipotentials, which we know must be perpendicular to the flowlines (Fig. 2.49).

A great advantage of the relaxation method lies in the ease of programming it for a computer, and also in enabling the simple determination of further quantities (chiefly pressure), which are needed for statistical embankment analysis.

Hydrodynamic pressures are defined from potential differences in the body or on the slope of an embankment. The stress tensor ($\bar{\bar{\sigma}}$) is defined by the equation

$$\Delta\bar{\bar{\sigma}} = s_r \Delta p + \frac{\gamma_0 - n(\gamma_0 - \gamma_w)}{g} \Delta U + p \Delta s_r, \tag{2.282}$$

where s_r is the degree of saturation (in the embankment we are considering); γ_0, γ_w are the unit weights of soil and water; $U = gz$ is the gravitational potential of the volume forces in an element of matter.

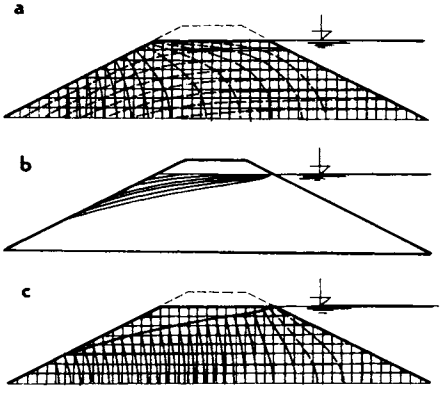

Fig. 2.49. Piezometric height division and the course of water level during the seepage through the earth dam. a — lines $h^+ = \text{constant}$, $p = \text{constant}$, b — change of phreatic curve, c — lines $h^+ = \text{constant}$ for steady flow.

In saturated soil, the *potential function* is given by

$$\Phi = p + (\gamma_0 - n\gamma')\, z\,,$$
$$\Delta\sigma = \Delta\Phi. \tag{2.283}$$

Potential distribution is defined by the equipotentials (constant Φ).

With regard to the piezometric heights $h = p/\gamma_x + z$, it is possible to rewrite eqn. (2.283) in dimensionless form as follows

$$\frac{\Phi}{H\gamma_w} = \Phi^+ = h^+ + (1-n)\left(\frac{\gamma_0}{\gamma_w} - 1\right) z^+ = h^+ + \gamma' z^+. \tag{2.284}$$

For soils under consideration for use in the construction of a homogeneous embankment, the porosity should be $n = 30$—40%, which for $\gamma_0 = 27$ kN m^{-3} and $\gamma_w \cong 10$ kN m^{-3} gives a value of γ' in the range 10.0—12.0 kN m^{-3} (average 11.0).

In Fig. 2.50a, b we illustrate the profiles of potentials in an embankment totally saturated with water and with a depressed phreatic surface. From the point of view of embankment stability, the most dangerous case is when there is high potential at point A on the downstream slope and also a reduced soil shear strength. The danger of embankment failure is therefore great.

It is also possible to develop the flowline network and the distribution of potential according to the finite-difference method in other ways (graphico-analytical, through complex-number expressions, developing differential equations into series, etc.). Jeppson (1968) has described these methods or by finite elements method (Zienkiewicz et al. 1970).

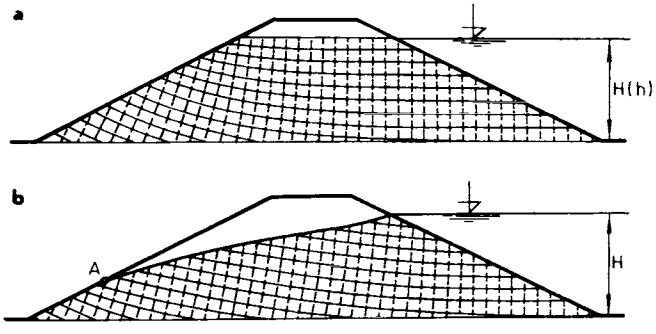

Fig. 2.50. Potential distribution during seepage. a — dam body saturated, b — free water level lowered.

Besides the relatively precise but rather laborious methods of calculating surface movement and determining pressures (piezometric height, potentials) mentioned above, Schnitter and Zeller (1961) consider a simple method, at which they arrive by rewriting Boussinesque's equation for varying flow in the form

$$\frac{\partial h}{\partial t} = \frac{k}{n_0} \frac{\partial^2 (h^2)}{2 \partial x^2} . \tag{2.285a}$$

In this, apart from the known flow characteristics (k, h, t), they take account of the active porosity $n_0 = \alpha_n$ as a certain percentage of the geometrical porosity (n).

After further modification, they obtain the equation

$$\frac{\partial h}{\partial t} = \frac{k\bar{h}}{n_0} \frac{\partial^2 h}{\partial x^2} , \tag{2.285b}$$

a particular solution of which will be

$$\bar{h} = h_u + (h_0 - h_u) \cos \frac{\pi x}{2L'} \exp \left(- \frac{k\bar{h}}{n_0} \frac{\pi^2}{4L'^2} t \right) . \tag{2.286}$$

Evaluation of eqn. (2.286) for discrete time intervals Δt, computing for the instant $t = 0$, is relatively simple because we know (Fig. 2.51) that $h(0) = h_0$ and also h_u, so that

$$h_0(\Delta t) = h_u(\Delta t) + [h_0(0) - h_u(\Delta t)] \exp \left(- \frac{k\bar{h}}{n_0} \frac{\pi^2}{4L'^2} \Delta t \right) .$$

From the quantity $h_0(\Delta t)$, we move to the quantity $h_0(2\Delta t)$, which we can find from the equation

$$h_0(2\Delta t) = h_u(2\Delta t) + [h_0(\Delta t) - h_u(2\Delta t)] \exp\left(\frac{k\bar{h}}{n_0}\frac{\pi^2}{4L'^2}\Delta t\right),$$

where h_0 is the height of the upper surface; h_u the height of the under surface; h the average depth of seeping water; and $L' = L'(\Delta t)$, a measure of the position of the tested point at the instant Δt.

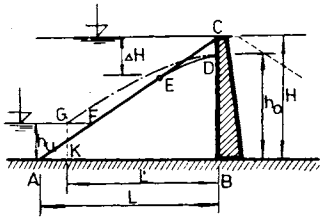

Fig. 2.51. Water lowering calculus scheme after Schnitter and Zeller.

A general expression of eqn. (2.286) will be

$$h_0(i\Delta t) = h_u(i\Delta t) + \{h_0[(i-1)\Delta t] - h_u(i\Delta t)\} \exp\left(\frac{k\bar{h}}{n_0}\frac{\pi^2}{4L'^2}\Delta t\right),$$

where

$$L' = L'(i-1)\Delta t,$$

$$\bar{h} = \frac{1}{L'}\int h(x)\,dx = h + \frac{2}{\pi}(h_0 - h_u). \tag{2.287}$$

The average depth $\bar{h}$ (piezometric height) varies with time, and we therefore introduce a further exponent extracted from eqn. (2.287) for the interval $(i-1)\Delta t$, if we are following the movement of free surface in the permeable part of an embankment containing a sealing core (vertical). Demands on time are reduced especially when helpful graphical representations are used for the dependence (Fig. 2.52)

$$\frac{H - \Delta H}{H} = \left(\frac{k}{n_0 v_z}\right), \tag{2.288}$$

which are evaluated for slope values 1 : 1.5; 1 : 2; 1 : 2.5; 1 : 3 and 1 : 5. In the relation eqn. (2.288), the afore-mentioned velocity of lowering (v_z) is dependent partly on the total height (H) of the reservoir, and partly on the total time (T) for surface lowering, so that

$$v_t = \frac{H}{T}.$$

Besides the Schnitter—Zeller graphs just mentioned, a less precise and less well investigated but similar graph, compiled by Reinius (1955), is sometimes used. It

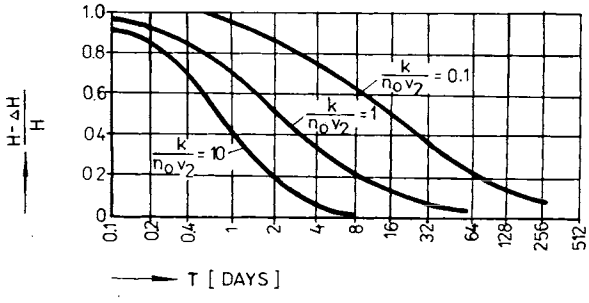

Fig. 2.52. Diagram for the dependence $\frac{H-\Delta H}{H} = f\left(\frac{k}{n_0 v_2}\right)$.

can be used in determining the magnitude of hydrodynamic pressure on the upstream slope of an embankment, for a sudden drop of surface level. It is used in the same way as the Schnitter—Zeller graph.

2.9 Problems and Practical Calculations of Pressures and Seepage out of Canals

2.9.1 The Effect of the Position and Shape of a Canal and Soil Suitability

In practical calculations, problems often arise from a combination of the imperfections in the basis of calculation, and the imperfections in formulae, so that usually there are extreme cases that are solved. It is therefore hard to decide in favour of one particular calculational approach. In this respect, computation of seepage from canals is rather more difficult than that through levées, where we most frequently meet with the two types of homogeneous embankment (with and without sealing). The formulae already given (eqns. 2.77—2.122) exhaust to a sufficient depth all cases which are practically worth considering.

In canals and their embankments, the picture becomes more complicated, the more complex the task imposed by the depth of the subsoil and its permeability, as well as the zone around the canal bottom which is also continually changing (it consolidates or even erodes). Control over the changes in these basic seepage characteristics is rarely kept. Let us consider a certain part of this problem on the schematic basis laid out in Fig. 2.53.

In the first two cases illustrated below (a, b), which are more complicated than cases c and d, we assume a definite functional dependence of seepage (q) on the height of the water surface above the canal bottom (H), on the height difference (D_w) between the water level in the canal and the groundwater (which is at height D_i above the impermeable subsoil), or on the depth of the subsoil below the canal bottom (D_p). In general, in calculations, we ignore any drains or sources in the immediate surroundings since we proceed from the assumption of boundary conditions at infinity. If, however, there are flows and wells, this discrepancy between assumptions and reality may be too large. Interaction between the canal and springs or sources in the neighbourhood may take place up to a distance of 100 B_2. In the Váh valley canals this distance is a matter of several km. This effect is reduced for a smaller thickness of water-bearing layer below the canal bottom, and also with complicated geological relief or an impermeable subsoil.

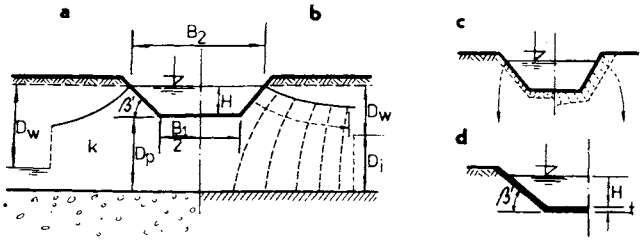

Fig. 2.53. Seepage off the canal. a — groundwater is low, b — in saturated zone, c — influence of capillary fringe, d — sealing apron.

In fulfilling the *boundary conditions* along the x axis, however, the effect of boundary conditions — of an impermeable subsoil — in the z direction disappears relatively quickly. If $D_p : B_1 \geq 5$, the effect of the size of D_p becomes negligible.

In cases c and d, the properties of the solid and gas of the material, which we usually neglect in calculations, may again be a source of discrepancy. Here, it is a case of the effect of air, which is drawn into the soil by the water when there is seepage flow or capillary motion in the subsoil, but which we virtually ignore. Air bubbles increase the water resistance in seepage to such an extent that in some cases — where there are small channels — the water pressure (P) hardly differs from the critical pressure necessary to overcome air resistance. The necessary height for overcoming the critical pressure (P_{cr}) may reach something of the order of 10 to 20 cm for sandy soils and up to 80 to 150 cm for clayey soils (loams, silts, clays). This effect is sometimes governed by the so-called initial gradient I_0, so that $I = I_0 + I'$, but its introduction into practical calculations is difficult, and Bouwer (1965) therefore suggested it to be inserted into formulae for the direct computation of P_{cr}. Thus

$$v = \frac{H + t - P_{cr}}{R_a}, \tag{2.289}$$

where $R_a = t/k_z$ is the resitance (which Bouwer called the hydraulic impendance).

This quantity is also the governing factor for the loss index I_s, which is generally given by a fraction of the specific seepage (q_s) and channel width at surface (B_2), so that

$$\bar{I}_s = \frac{q_s}{B_2}.$$

For a *low permeability* zone of small thickness,

$$\bar{I}_s = \frac{1}{B_2 R_a}\left[(H - h_c)B_1 + (H - 2h_c)\frac{H}{\sin\beta'}\right]. \tag{2.290a}$$

For a small value of $h_c : H$ we can take

$$\bar{I}_s = \frac{H - h_c}{B_2 R_a}\left(\frac{H}{\sin\beta'} + B_1\right). \tag{2.290b}$$

The effect of the water depth on the value of q is to be seen, for canals, mainly in a permeable deposit of large thickness and it can be assessed using the expression

$$\frac{\bar{I}_s B_2 R_a}{B_1^2} = \frac{H}{B_1} - \frac{h_c}{B_1} + 1.4\,\frac{H}{B_1}\left(\frac{H}{B_1} - \frac{2h_c}{B_1}\right), \tag{2.291}$$

which is sufficiently precise for a slope of $\beta' = 45°$.

A further shape factor Φ_k for judging this effect is the ratio

$$\frac{\bar{I}_s B_2 R_a}{H^2} = \Phi_k.$$

Φ_k has values of 1.94 for a triangle, 2.74 for a trapezium, and 4.33 for a rectangle when H is constant. This shows the large losses for a rectangle and the relative advantages of the triangular profile, or furrow on small canals. This ratio is reversed, however, when we consider equal surface width and water depth.

In forming an active seepage zone under a canal, it is not only the basic *canal geometry* (H, B) which has an influence, but also the geometry of the flow region (D_w, D_i) and the degree of soil saturation, which defines a value of P_{cr} — as well as the *basic permeability characteristic* (K). We can follow the effect of degree of saturation on the loss index through the equation

$$\left(\frac{\bar{I}_s}{K}\right)_{P_{cr}} = B\left(1 + \frac{H - h_c}{H + D_i - \frac{1}{2}D_w}\right). \tag{2.292}$$

For canals in permeable deposits with a deep impermeable layer, a rather peculiar sort of seepage originates, caused among other things by the formation of

a less permeable zone under the bottom and along the sides. Water seeps into the unsaturated soil and then proceeds almost vertically towards the water table. In this case, for a given ratio of D_p to B_1, the losses q cease to be dependent on the depth D_p but only on the canal shape $\Phi_k(H, B_1, B_2)$, resistances (R_a) and pressures (P_{cr}), which expressed generally gives us

$$q = f(\Phi_k, R_a, P_{cr}).$$

Specific *losses due to seepage* q are only a minor extent dependent on the canal flow Q (Fig. 2.54) and therefore from the loss point of view, large canals are more economical than small ones. Seepage can increase its influence in small canals to a marked extent through capillary action.

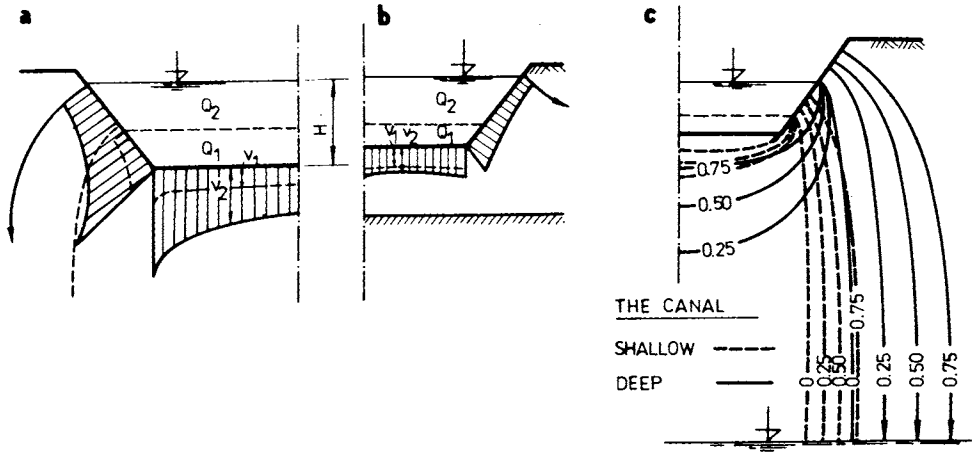

Fig. 2.54. Influence of the thickness of permeable subsoil and flow parameters. a — flow rate (Q) changes by deep foundation, b — seepage velocity v, impermeable subsoil in the proximity of canal bottom, c — unsaturated seepage conditions.

The concept of a collecting drain along the canal gains substance, and has an important function, when the subsoil is fully saturated and the canal profile lies largely below the water table. Its level must be regulated by means of a drain, and clearly some seepage flow must be extracted. Part of the problem connected with this function was explained for a simple case in Section 2.5. We shall now take the case of a canal and drainage system in a permeable layer, as illustrated in Fig. 2.55. From the point of view of the nature of seepage and water movement, we are concerned here with three separate regions. In the first region, the effect of increased potential, caused by raising the water surface in the canal to the level H, above $A - A'$, is dominant; in the second the relief function of the drain is the

more important, and in the third region alternating seepage q_2, q_3 in both directions is typical.

If we suppose that the upper layer (above $A-A'$) has a permeability coefficient k_A and thickness D_A, and that the lower layer has values k_B and D_B, then for laminar water flow in the first section, it must follow that

$$\frac{-\partial k_B D_B \left(\frac{\partial h}{\partial x}\right)}{\partial x} = \frac{H_A - h}{D'_A} k_A, \tag{2.293}$$

$$q_1 = k_B D_B \frac{h_0 - h_1}{B'}. \tag{2.294}$$

By solving the above equations we obtain

$$q_1 = \frac{k_B D_B (H_A - h_1)}{\sqrt{\varkappa_D} \coth \frac{B}{\sqrt{\varkappa_D}} + B}, \tag{2.295}$$

where

$$\varkappa_D = \frac{k_B}{k_A} D_p D_B.$$

In the second section, that with the drain, we can use conform mapping from the Christoffel—Schwarz theorem, which leads to an expression for the complex velocity, using a method of basic transformation parameters, in the form

$$w = \Phi + i\psi = -q\pi \cos^{-1}\left[\left(\frac{\gamma^2 - \zeta^2}{\zeta^2}\right)^{\frac{1}{2}} \left(\frac{\gamma^2 - \beta^2}{\beta^2}\right)^{-\frac{1}{2}}\right] + i\frac{q}{2}. \tag{2.296}$$

The seepage will be

$$q_0 = \frac{\pi k_A H_{av}}{2 \cosh^{-1}\left[\left(\cosh \frac{\pi l_1}{2D_d}\right)\left(\sinh \frac{\pi l_1}{D_d} \sinh \frac{\pi}{4}\frac{d}{D_d}\right)^{-\frac{1}{2}}\right]} \tag{2.297}$$

where apart from those symbols already used, and those in Fig. 2.55, we denote H_{av} as the average pressure height above the drain, and d as the drain diameter. For the pressure height

$$h = h_1 - \frac{2D_d}{\pi k_B D_B} q_0 \, [\bar{x}(\bar{l} - f)], \tag{2.298}$$

where we have values

$$\bar{x} = \frac{\pi x}{2D_d}, \qquad \bar{l} = \frac{\pi l_1}{2D_d}, \qquad f = \frac{2I}{x\pi}. \tag{2.299}$$

The value of integral I is

$$I = \int_0^x \tan^{-1} \frac{\sinh x}{\cosh l} \, dx, \tag{2.300}$$

which is usually obtained by development using series.

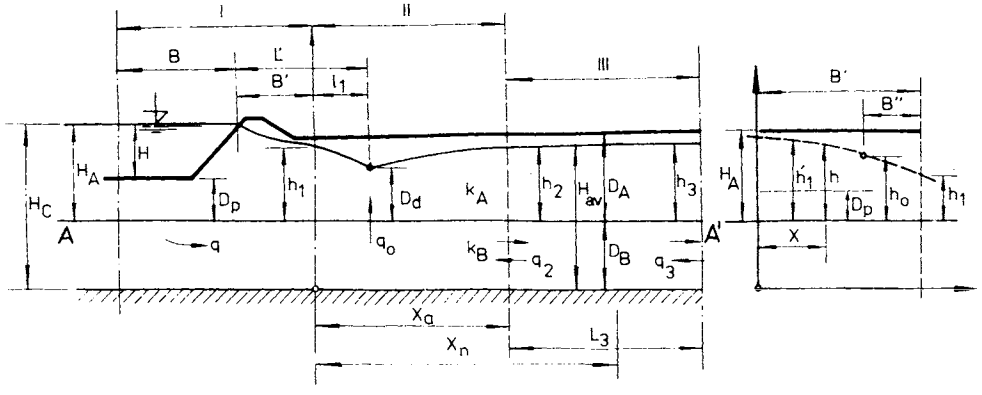

Fig. 2.55. Seepage to the drain — flow parameters.

For small thicknesses of the lower permeable layer (D_B), the following applies for the height above the drain

$$h_0 = h_1 - \frac{l_1}{k_B D_B} q_0. \tag{2.301}$$

In the third section, we consider length L_3; pressure heads h_2 and h_3 at the boundaries; H_{av} at the section centre, and an infiltration w_i per unit length. Then for unit length, for half of L_3, it follows approximately that

$$k_B D_B (H_{av} - h_2) + \frac{k_A}{2} (H_{av}^2 + h_2^2) = \frac{w_i L_3^2}{2}. \tag{2.302}$$

In *practical calculations*, there is the problem that at the beginning of the individual section lengths (1st, 2nd, 3rd), we know neither the average pressure head (H_{av}) nor the extent of the drainage region (x_a). These are usually found by a much used approximation based on the original data, i.e. the total canal depth H, the distance of the drain from the intersection of the surface and the slope L', drain depth D_d, etc. From these quantities, Kirkham (1964a) recommend that we also define

$$\begin{aligned} &\text{distance} && l_1 = 0.6\, L', \\ &\text{head} && H_{av} = h_1 - D_d, \\ &\text{extent of drain} && x_a = 1.18\, D_d + l_1. \end{aligned} \tag{2.303}$$

Finally, these authors give an example, which on account of its instructiveness, we are reproducing here. The following are given: thickness $D_A = 10$ m and $D_B = 300$ m; coefficients $k_A = 0.5$ m/day and $k_B = 50$ m/day; $D_p = 4.0$ m; $B = 30$ m; $H_A = 11$ m — for a drop in water surface; $h_1 = 2.0$ m; $h_2 = 10.0 - 2.0 = 8.0$ m.

A drain of diameter $d = 0.3$ m is entrenched at a depth $z = 6.0$ m, and its height above the soil strata division is $10.0 - 6.0 = 4.0$ m. Also $L' = 30$ m.

According to eqn. (2.303), and also referring to our scheme, we also have $l_1 = 0.6 \times 30 = 18$ m, $B' = L' - l_1 = 30 - 18 = 12$ m, and

$$\sqrt{\varkappa_D} = \sqrt{\frac{50}{0.5}} \times 4.0 \times 300 = 346.$$

The seepages, following from eqn. (2.295), will be

$$q_1 = \frac{50 \times 300(11 - h_1)}{346 \coth \frac{50}{346} + 12} = 3.86(11 - h_1),$$

and from eqn. (2.297),

$$q_0 = \frac{\pi \times 0.5(h_1 - 4.0)}{2 \cosh^{-1} \cosh \frac{18\pi}{2 \times 4.0} \sqrt{\sinh \frac{18\pi}{4} \sinh \frac{0.3\pi}{4 \times 4}}} = 0.446(h_1 - 4.0).$$

The extent of the drain will be

$$x_a = 1.18 \times 4.0 + 18.0 = 22.70 \text{ m}.$$

This leaves us with auxiliary quantities $\bar{l} = 7.0$ and $\bar{x}_a = 8.9$, and correspondingly $f \cong 0.21$. From the equation

$$k_B D_B \frac{h_1 - h}{x_a} = q_1 - f(q_0), \tag{2.304}$$

by substituting $50 \times 300(h_1 - 8) = 22.7(q_1 - 0.21 q_0)$, and using further modified relations, it emerges that

$h_1 = 8.02$ m, $q_1 = 11.5$ m^3/day/m length,

$q_0 = 1.8$ m^3/day/m length, $q_2 = 9.7$ m^3/day/m length.

The figures calculated point to the effect of surface layer permeability.

According to the source cited for tubular drains, a high efficiency is attained especially when the ratio k_B/k_A is around 50 and the ratio of the two layer thicknesses is $D_B/D_A = 5$ (Table 2.9).

Drainage wells are only recommended when there is a really deep permeable horizontal layer under less permeable strata.

Table 2.9. Values of seepage comparison

Characteristics				Seepages [m³/day]		
D_A [m]	k_A [m/day]	D_B [m]	k_B [m/day]	q_0	q_1	q_2
10.0	0.50	300.0	50.0	1.8	11.5	9.7
10.0	5.0	300.0	50.0	17.0	111.2	94.2
20.0	1.0	100.0	50.0	2.7	6.1	3.4

In Fig. 2.56, we lay out schematically the flow net for a similar example.

Seepage and flow pressures at a drain can be seen in Fig. 2.57. If we denote the distance from the drain axis to the peak of the seepage curve as $L/2$, then we can express the value of the potential, using the normal notation, as

$$\Phi = \frac{q}{4\pi k} \ln \left[\sin \frac{2\pi x}{L} \cosh \frac{2\pi y}{L} + \cosh \frac{2\pi D}{L} + \cos^2 \frac{2\pi x}{L} \sinh^2 \frac{2\pi y}{L} \right] + c'. \tag{2.305}$$

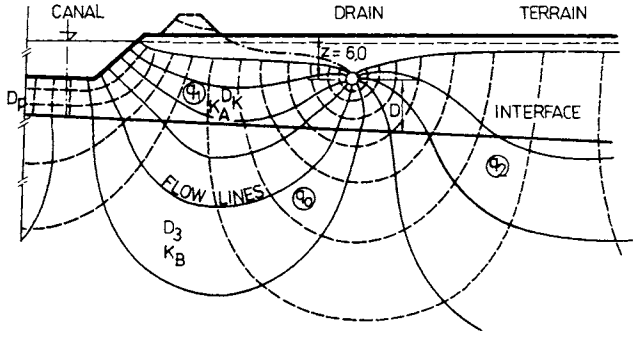

Fig. 2.56. Flow net for seepage conditions influenced by a drain with free water level.

The potential related to the impermeable substratum (Fig. 2.51) is expressed by the pressure head

$$\varphi = \eta + D + h \rightarrow y,$$
$$y = \eta + D + h. \tag{2.306}$$

The potential conceived in this way can be expressed by the y coordinate of the pressure line. This applies to every point on the line and to points on the drain

circumference and within. If, as sometimes happens in rainy periods, the drain is stretched beyond its capacity, then the relation $p_d = 0$ no longer applies.

If we use the data according to our scheme (Fig. 2.57), we obtain a more detailed view of the pressure values acting from plane OE up to plane AG, passing through the drain axis. At the origin, pressure H_c operates, in the plane of the drain $p = \gamma_w h_s$ above the pipe. The potential varies along the pipe, and is determined by the height H. The centre of the gape (of height 2δ) has coordinate $y = a + \delta$.

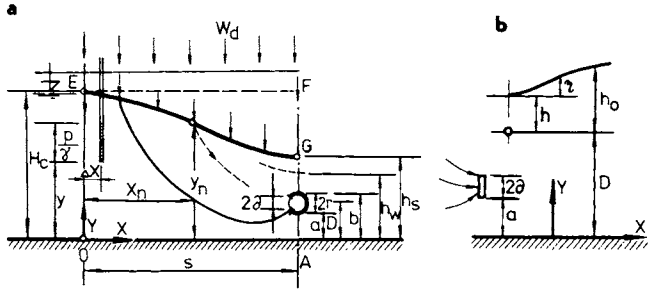

Fig. 2.57. Groundwater surface influenced by infiltration into drain under pressure (full). a — the pressure and inflow conditions — changes near the drain opening, b — detail of the crack and the flowlines.

With regard to the peculiar form and position of the gape relative to the flowlines, we do not yet know an exact solution. We have only approximate solutions, in which the conditions of the Laplace equation with variable relations between flowlines and potentials are also approximated (Cauchy—Rieman relations).

In the case where the proportions of pressure in the drain are determined by the quantity of infiltration w_d (rain) on a strip of width 2 s under conditions given by the Laplace equation, and taking account of boundary conditions, Kirkham (1964b) gives the equation for potential as

$$\varphi = w_0 s \sum_{p=1}^{\infty} A_p \frac{\sinh \frac{p\pi x}{H_c}}{\sinh \frac{p\pi s}{H_c}} \sin \frac{p\pi y}{H_c} + \sum_{n=1,2\ldots}^{N} B_n \sin \frac{n\pi x}{s} \frac{\sinh \frac{n\pi y}{s}}{\sinh \frac{n\pi b_c}{s}}. \quad (2.307)$$

The value of A_p, determined using Fourier series, is given by the expression

$$A_p = (-l) p_1 \frac{2}{p\pi} + \frac{2}{p\pi} \cos \frac{p\pi D}{H_c}, \text{ with } \delta = \frac{b-a}{2} \cong 0. \quad (2.308)$$

In addition, the unknown quantities B_n, H_c, and h_s can be found progressively from other equations and from eqn. (2.308), from which the relation for determining B_n follows, so that

$$\frac{x}{s}=\sum_{p=1}^{\infty} A_p \frac{\sinh \frac{p\pi x_m}{H_c}}{\sinh \frac{p\pi s}{H_c}} \sin \frac{p\pi y}{H_c}+\sum_{n=1}^{N} B_n \sin \frac{n\pi x_n}{s} \frac{\sinh \frac{n\pi y_m}{s}}{\sinh \frac{n\pi H_c}{s}} \pm \Delta. \quad (2.309)$$

The values of y_m, B_n, and N can be gradually discovered by applying the continuity equation for surface infiltration and underground seepage.

From the Cauchy—Rieman conditions, and also from boundary conditions

$$\frac{\partial(k\varphi)}{\partial x}=\frac{\partial \psi}{y}, \qquad \frac{\partial(k\varphi)}{\partial y}=-\frac{\partial \psi}{\partial x}$$

it follows that

$$k\varphi=\sum_{p=1}^{\infty} w_d s A_p \frac{\cosh \frac{p\pi x}{H_c}}{\sinh \frac{p\pi s}{H_c}} \cos \frac{p\pi y}{H_c}-\sum_{n=1}^{N} w_d s B_n \cos \frac{n\pi x}{s} \frac{\cosh \frac{n\pi y}{s}}{\sinh \frac{n\pi H_c}{s}}+C w_d s, \quad (2.310)$$

$$kH=\sum_{p=1}^{\infty} w_d s A_p \coth \left(\frac{p\pi s}{H_c}\right) \cos \frac{p\pi(D+r)}{s}-\sum_{n=1}^{N} w_d s B_n \cos n\pi \times$$

$$\times \frac{\cosh n\pi \frac{D+r}{s}}{\sinh \frac{n\pi H_c}{s}}+CkH_c. \quad (2.311)$$

We obtain the value of potential by subtracting eqn. (2.311) from eqn. (2.310).

$$k(\varphi-H)=\sum_{p=1,2\ldots}^{\infty} w_d s A_p \left(\frac{\cosh \frac{p\pi x}{H_c}}{\sinh \frac{p\pi s}{s}} \cos \frac{p\pi y}{s}-\coth \frac{p\pi s}{H_c} \cos \frac{p\pi(D+r)}{s}\right)-$$

$$-\sum_{n=1}^{N} w_d s B_n \left(\cos \frac{n\pi x}{s} \frac{\cosh \frac{n\pi y}{s}}{\sinh \frac{n\pi H_c}{s}}-\cos n\pi \frac{\cosh \frac{n\pi(D+r)}{s}}{\sinh \frac{\pi H_c}{s}}\right). \quad (2.312)$$

In a similar way, we can obtain the potential at x_m (the point of inflexion of the seepage curve), i.e. $k(y_m-H)$, which is given by an equation analogous to eqn. (2.312). The value of the fraction

$$\frac{x_m}{H_c}=\sum_{p=1}^{\infty}\frac{s}{H_c}A_p\frac{\sinh\frac{p\pi x}{H_c}}{\sinh\frac{p\pi s}{H_c}}\sin\frac{p\pi y_m}{H_c}+\sum_{n=1}^{N}\frac{s}{H_c}B_n\sin\frac{n\pi x_m}{s}\frac{\sinh\frac{n\pi y_m}{s}}{\sinh\frac{n\pi H_c}{s}}\pm\Delta, \tag{2.313}$$

is found by approximation in a similar way to other expressions

$$\frac{y_m}{H_c}=\frac{H}{H_c}-\sum_{p=1}^{\infty}\frac{w_d}{k}\frac{s}{H_c}A_p\coth\frac{p\pi s}{H_c}\cos\frac{p\pi(D+r)}{s}+\sum_{p=1}^{\infty}\frac{w_d}{k}\frac{s}{H_c}A_p\times$$

$$\times\frac{\cosh\frac{p\pi x_m}{H_c}}{\sinh\frac{p\pi s}{H_c}}\cos\frac{p\pi y_m}{s}-\sum_{n=1,2}^{N}\frac{w_0}{k}\frac{s}{H_c}B_n\left(\cos\frac{n\pi x_m}{s}\frac{\cosh\frac{n\pi y_m}{s}}{\sinh\frac{n\pi H_c}{s}}-\right.$$

$$\left.-\cos n\pi\frac{\cosh\frac{n\pi(D+r)}{s}}{\sinh\frac{n\pi H_c}{s}}\right). \tag{2.314}$$

Pressure heights (H_c, H, h_s) at the origin of the region which we are looking at, and above the drain, are determined by the equations

$$k(H_c-H)=\sum_{p=1}^{\infty}w_d s A_p\left(\frac{1}{\sinh\frac{p\pi s}{H_c}}\cos\frac{p\pi H_c}{s}-\coth\frac{p\pi s}{H_c}\times\right.$$

$$\left.\times\cos\frac{p\pi(D+r)}{s}\right)-\sum_{n=1}^{\infty}w_d s B_n\left\{\coth\frac{n\pi H_c}{s}-\cos n\pi\frac{\cosh\frac{n\pi(D+r)}{s}}{\sinh\frac{n\pi H_c}{s}}\right\}, \tag{2.315}$$

$$k(h_s-H)=\sum_{p=1}^{\infty}w_d s A_p\left(\coth\frac{p\pi s}{H_c}\cos\frac{p\pi h_s}{s}-\coth\frac{p\pi s}{H_c}\cos\frac{p\pi(D+r)}{s}\right)-$$

$$-\sum_{n=1}^{N}w_d s B_n\left\{\cos\frac{p\pi s}{s}\frac{\cosh\frac{n\pi h_s}{s}}{\sinh\frac{n\pi H_c}{s}}-\cos n\pi\frac{\cosh\frac{n\pi(D+r)}{s}}{\sinh\frac{n\pi H_c}{s}}\right\}. \tag{2.316}$$

The value of A_p can be determined using eqn. (2.308), and that of B_n with eqn. (2.313). In enumerating these equations, we can use to advantage the properties of hyperbolic functions (for the common case where $s>H_c$), thus

$$\frac{1}{\sinh \frac{p\pi s}{H_c}} = 2 \exp\left(-\frac{p\pi s}{H_c}\right), \qquad \coth \frac{p\pi s}{H_c} \cong 1.$$

The relations we have introduced do show that any precise evaluation of parameters using this method with an oversaturated drain, is a relatively complicated procedure. No less complicated are the calculations leading to elliptical integrals and elliptical functions, which Numerov (1951) and later Numerov and Aravin (1955) set out in their work 'Filtratsionnye raschety gidrotekhnicheskikh sooruzhenii'. It is possible to avoid calculations of this sort by sufficiently generous dimensioning of drains, which can easily take up both seepage and rainfall water, even in sudden storms or persistent rain. Thus we dimension drains according to eqns. (2.179) and (2.185), respectively, or (2.191) and (2.192) depending on the sort of case we are dealing with.

Some special relations apply for a sudden surface drop. Almost all the relations which are derived for water movement when the surface is depressed (in a river or canal) are based on Darcy's linear seepage law. More recent works (Comolet 1969) show that it is possible to derive the equations of motion using Lagrange's (Euler's) equations

$$\frac{\partial^2 X}{\partial T^2} = -\frac{1}{\varrho_w}\frac{\partial P}{\partial X}, \tag{2.317}$$

$$\frac{\partial^2 Y}{\partial T^2} = -\frac{1}{\varrho_w}\frac{P}{Y} - g, \tag{2.318}$$

$$\frac{\partial X}{\partial A}\frac{\partial Y}{\partial B} - \frac{\partial Y}{\partial A}\frac{\partial X}{\partial B} = 1. \tag{2.319}$$

After some rearrangement and the introduction of dimensionless variables for time (T) and pressure (P), and suitable lengths, we obtain

$$x = \frac{X}{H}, \quad y = \frac{Y}{H}, \quad t_0 = \frac{kT}{H}, \quad p = \frac{P}{\varrho_w g H}, \quad a = \frac{A}{H}, \quad l = \frac{B}{H}. \tag{2.320}$$

A series development for time parameters,

$$x = x(a, b, t_0), \quad y = y(a, b, t_0), \quad p = p(a, b, t), \tag{2.321}$$

leads us, using Laplace's equation and following the work cited above, to an *equation for pressure* behaviour

$$\frac{\partial^2 p^{(1)}}{\partial a^2} + \frac{\partial^2 p^{(1)}}{\partial b^2} = -4\left[\left(\frac{\partial y^{(1)}}{\partial a}\right)^2 + \left(\frac{\partial y^{(1)}}{\partial b}\right)^2\right]. \tag{2.322}$$

Through Poisson's equation, we can find the other terms

$$\frac{\partial^2 p^{(1)}}{\partial a^2} + \frac{\partial^2 p^{(1)}}{\partial b^2} = 4(y^{(1)} + 1)\left(\frac{\partial^2 y^{(1)}}{\partial a\,\partial b}\frac{\partial y^{(1)}}{\partial a} - \frac{\partial^2 y^{(1)}}{\partial a^2}\frac{\partial y^{(1)}}{\partial b}\right) -$$

$$-4x^{(1)}\left(\frac{\partial^2 y^{(1)}}{\partial b^2}\frac{\partial y^{(1)}}{\partial a}-\frac{\partial^2 y^{(1)}}{\partial a\,\partial b}\frac{\partial y^{(1)}}{\partial b}\right)-$$

$$-12\frac{\partial y^{(1)}}{\partial b}\left[\left(\frac{\partial y^{(1)}}{\partial a}\right)^2+\left(\frac{\partial y^{(1)}}{\partial b}\right)^2\right]+6\left(\frac{\partial y^{(1)}}{\partial a}\frac{\partial^2 p^{(1)}}{\partial a\,\partial b}-\frac{\partial y^{(1)}}{\partial b}\frac{\partial^2 b^{(1)}}{\partial a^2}\right). \quad (2.323)$$

A final solution of the Laplace's equation using a Fourier series development leads to the resulting pressure equations, and the coordinates of the phreatic surface (x, y) after its displacement due to surface depression, in the form

$$p^{(0)}(a, b)=(1-b)-\frac{8}{2\pi}\sum_{n=1}^{\infty}\frac{1}{(2n-1)^2}\exp\left(-\frac{2n-1}{2}\pi a\right)\times$$

$$\times\cos\left(\frac{2n-1}{2}\pi b\right), \quad (2.324)$$

$$x^{(1)}(a, b)=\frac{4}{\pi}\sum_{n=1}^{\infty}\frac{1}{2n-1}\exp\left(-\frac{2n-1}{2}\pi a\right)\cos\left(\frac{2n-1}{2}\pi b\right), \quad (2.325)$$

$$y^{(1)}(a, b)=-\frac{4}{\pi}\sum_{n=1}^{\infty}\exp\left(-\frac{2n-1}{2}\pi a\right)\sin\left(\frac{2n-1}{2}\pi b\right). \quad (2.326)$$

An advantage of the method given above for enumerating individual points lying on the free surface, is that the calculation is easily programmable for use on a computer, and also that the values of the first series often give us a sufficiently accurate approximation, as is displayed in a comparison of calculated and experimental results (Fig. 2.58).

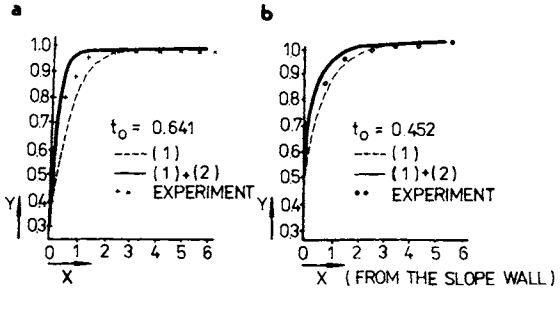

Fig. 2.58. Phreatic curves in suddenly drawdown conditions, dimensionless time: a — $t_0=0.641$, b — $t_0=0.452$.

Concerning notation, it should be mentioned that expressions generally retain the notation of the source material, where A, a and B, b are the horizontal and vertical coordinates of a point (others being in accordance with the system we have so far used).

In model measurements, using the shallow-layer analogy, the average velocity v_m, given by Poiseuille's expression for the movement of a liquid through a gap of width b, comes out as

$$v_m = \frac{b^2 \varrho g}{3\eta} \Delta\varphi, \tag{2.327}$$

which in comparison with Darcy's expression gives

$$k = \frac{b^2 \varrho g}{3\eta}.$$

Notwithstanding the fact that in the calculation a vertical outflow boundary is assumed, and also modeled, the results are most instructive. They show that for an embankment where $H = 15$ m, constructed of sandy soil ($k = 10^{-3}$ cm s^{-1}), then for a value of dimensionless time $t_0 = 0.3$, the actual time for surface depression will be

$$T = t_0 \frac{H}{k} = 0.3 \frac{1500}{0.001} = 4.5 \times 10^5 \text{ s} = 5.2 \text{ days}.$$

In clayey sand, where $k = 10^{-4}$ cm s^{-1}, the depression time will be ten times greater, i.e. 52 days.

Since, however, $t_0 = 0.5$ may be considered as the critical value, the canal would empty itself in a time given by

$$T = 0.5 \frac{1500}{0.0001} = 7.5 \times 10^6 \text{ s} = 87 \text{ days}.$$

In our studies of the homogeneous clayey levées along the Danube (Peter 1964a), we assumed $k = 5 \times 10^{-5}$ cm s^{-1} and $t_0 = 0.7$, and obtained

$$T = 0.7 \frac{1500}{0.00005} = 2.1 \times 10^7 \text{ s} = 243 \text{ days (or 8 months)}.$$

This fact we considered to be a grave disadvantage of homogeneous clayey embankments without any sealing.

For sandy gravel levées ($k = 3 \times 10^{-2}$ cm s^{-1}) with a concrete seal, we calculated using a different method the possible emptying time, using $k = 1 \times 10^{-6}$ cm s^{-1}, as

$$T = 42\text{—}46 \text{ days}.$$

2.9.2 Problems of Emptying in Hydroelectric Canals

In any calculation for the emptying time of a power-station supply canal, whose embankments are composed of sandy gravel, which lies on a sandy gravel subsoil

having a rocky or other (Neogeneous) impermeable base at some depth (as is the case in the Váh cascade canals and also those planned for the Danube hydroelectric system), it is generally necessary to distinguish *three distinct principal cross-sections* (Fig. 2.59).

In the first case, the canal bottom is below the water table. In the second case, it lies characteristically above the water table, and in the third case, typically an outflow canal, it is sunk into the ground a long way below the water table. The first two sections have to be sealed along the canal perimeter — in Czechoslovakia with concrete slope (apron) sealing — whereas the last section is not sealed but the slopes for the most part have to be secured (by paving).

In the *first and third sections,* there is a closer connection between water in the canal and the groundwater regions, which are thus supplied by canal water. Underground water rises, its surface gradually (usually over the course of several years) settling to a new level. In this state, it is characteristic for water to flow from the canal to the surrounding territory, excepting only some cross-sections of outlet canal, where the water level in the canal may be below the original water table, leaving the canal draining its surrounds.

The state described is depicted in diagrams Ia—IIIa of Fig. 2.59, where the conditions of flow are shown for an empty canal. Whilst the canal is being emptied, after a certain time the water surface will fall to below the water table, so that water begins to seep into the canal, and thus to exert a pressure on the bank reinforcement, and sometimes even on the bottom (third case). With conditions of rapid emptying, part of the flow-net twists abruptly towards the slope (reinforcement) of the canal, as shown in diagrams Ib—IIIb. This state is especially dangerous for the first and third cases, where a large proportion of the slope is exposed to hydrodynamic (and hydrostatic) pressure. Water begins to penetrate into the canal under pressure as if from springs (illustrated on Fig. 2.60).

We combat this unwelcome phenomenon in a twofold manner, partly by installing relief wells — near the canal bottom on supply canals — causing pressure drops on the desired section, and partly by lowering the canal level over several days in order to give the seepage water collected in the territory around the canal enough time to dissipate and to form a new, quasi-steady regime with low pressures.

For the *second cross-section,* the best safeguard against the effects of seepage is perfect sealing, not allowing a large amount of water to gather behind the undersurface. As we can see in Fig. 2.59 (IIb), it is only the lower portion of the sealing which is affected by this underground water pressure, and therefore in emptying a supply canal as a whole unit, it is the first section which governs. For the Váh canals which have sandy gravel embankments and concrete sealing, with a water (level) on the first cross-section of 4.5—9.0 m and a pressure head of 2.6—6.5 m, we have calculated the rates of surface lowering to be those given in Table 2.10.

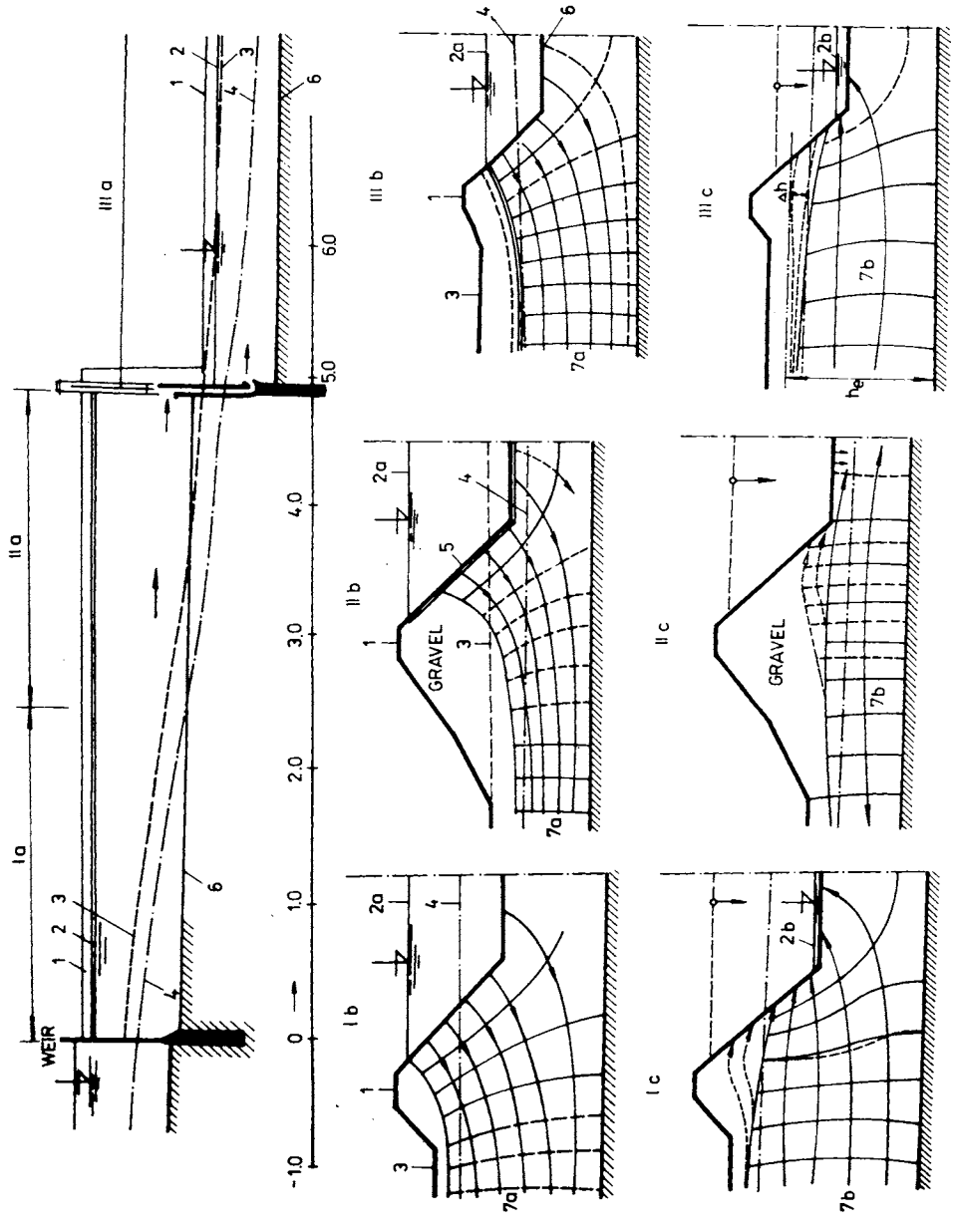
III a
II a
I a
WEIR
III b
II b
I b
GRAVEL
III c
II c
I c
7a
7b
Δh
he

On the last day or days, it is desirable that the surface will be lowered at a rate given by the empirical relation

$$v_z = \frac{1}{D_w} \qquad [\text{m/day}),$$

where D_w is the depth of the depressed surface below the original water table (i.e. that before lowering).

In fact, we can see in reviews of the Váh canals, that the surface has fallen at a rate up to twice as fast as we predicted, but there are always water boils to be seen

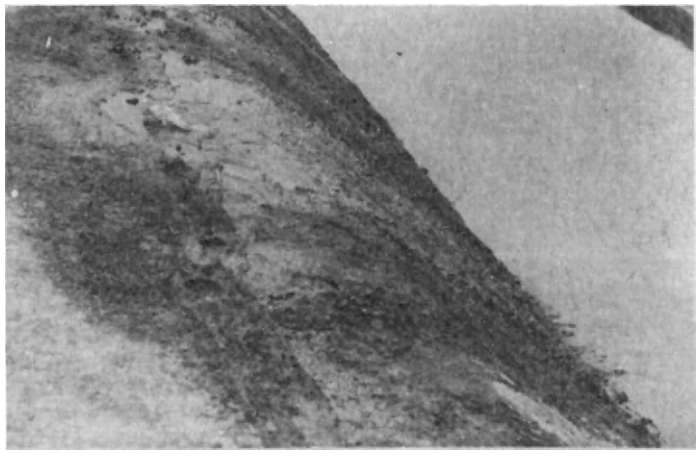

Fig. 2.60. Water boils caused by groundwater pressure.

Table 2.10. Admissible water-level drawdown velocity in canal with respect to groundwater pressure on concrete facing

Day	First	Second	Third	Fourth	Fifth	Sixth	Further
v_z [cm/day]	250—200	200—150	150—100	100—60	60—30	30—20	15—10

Fig. 2.59. Groundwater flow conditions along head-race and tail-race canal. a — oblong profile of the canal, b — cross-sections of the full canal, c — canal empty; 1 — crest of the dam, 2 — T.W.L., 2a — original T.W.L., 2b — lowered T.W.L., 3 — original territory, 4 — G.W.L. (groundwater level), 5 — canal lining, 6 — canal bottom, 7a — full canal flowlines, 7b — empty canal flowlines.

on the bottom, and a certain number on the slopes (near the bottom). A certain risk of damage is justified by the valuable prize of energy gained from the system.

Outlet canals are subjected to water pressure against their sides, frequently even during the normal running of power stations, which 'peak' at certain times, with surface fluctuations of 2—2.5 m, so that for short periods the canal surface drops down to 1.5—2 m below the level of the phreatic surface. However, in spite of this, the slopes' greatest subjection to hydrodynamic pressure from groundwater still occurs when the canal is emptied, since damaged areas are then exposed and failures can be brought to completion (Fig. 2.61).

Fig. 2.61. Canal in empty conditions.

In the case given here, we can calculate these pressures if we investigate the lie of the phreatic curve we determine the fall relative to a mean stationary surface level at individual points (x_i) from the equation

$$\Delta h_e = h_e \left\{ 1 - \left[0.086 + 0.64 \frac{x_i}{\sqrt{4at}} - 0.47 \left(\frac{x_i}{\sqrt{4at^2}} \right)^2 \right] \right\}, \qquad (2.328)$$

where h_e is the height of the original surface above the impermeable layer; a the transmissivity at a given place, as derived earlier and explained in Section 2.6 and eqn. (2.224).

Exact calculations of this sort can be extremely laborious.

Chapter 3
STABILITY CALCULATIONS AND EMBANKMENT SETTLEMENT

In the design of all structures, the problem of construction stability must be considered fundamental. In earth embankments, we often reach a point where safety and therefore stability is at the focus of the whole concept. Even if this approach is not correct, and the embankment overflows by some decimeters and floods hundreds of hectares, there need be no failure in total stability, emphasizing the importance of stability calculations. Stability needs a qualitative and a quantative approach.

We generally divide the *slope stabilities* (up- and downstream) into stability of the protecting layer, stability of the slope covers, stability of the embankment body as a whole, stability of the subsoil, and the total stability of both embankment and subsoil.

Moreover, in general, it is customary to consider only mechanical stability, even though for canal embankments and levées the so-called *filtration stability.* (to which we have already alluded) is no less important, and we shall be returning to it. We should add that both these stabilities are connected with the behaviour of soil under load (mechanical and dynamic). In assessing stability, we shall investigate deformation (seepage failures) and more especially stress, since these are the determining factors regarding stability in the final stages, i.e. at the commencement of failure. *Local deformations* may adversely affect stability of either the embankment or subsoil, before the construction as a whole sustains a critical stress.

Apart from the aspect just mentioned, when considering stability, the time factor emerges as being very important. An embankment or subsoil may bear a short-term loading of as much as twice the long-term load under certain conditions. The time factor often makes the whole design uncertain, mainly because the conditions from which the design arose may change. It is partly the loading conditions which can change, and partly the *internal forces in the soil* — structure, *contact pressure, stress path* (σ) — which govern its ability to withstand loading. It is thus vital to first know the relations between stresses and deformations, and then to turn our attention to actual stability.

3.1 Stress, Deformation and Soil Failure

If we were to extract an element (Δx, Δy, Δz) from a soil mass, as we do in all mechanics problems, we would see that on opposite sides of the element (1, 2), the stress varies by an amount $\Delta\sigma$ relative to the *average stress* σ. Therefore, in the direction of the x axis,

$$\left.\begin{matrix}\sigma x_1\\ \sigma x_2\end{matrix}\right\} = \sigma_x \pm \frac{\Delta\sigma_x}{2}. \tag{3.1}$$

The stability conditions of equilibrium for a planar element in the x, z plane lead to the well known equilibrium equation

$$\left[\left(\sigma_x - \frac{\Delta\sigma_x}{2}\right) - \left(\sigma_x + \frac{\Delta\sigma_x}{2}\right)\right]\Delta z + \left[\left(\tau_{xz} - \frac{\Delta\tau_{xz}}{2}\right) - \left(\tau_{xz} + \frac{\Delta\tau_{xz}}{2}\right)\right]\Delta x = 0. \tag{3.2a}$$

If we consider moment equilibrium about the centre of the element on the edges of which shear stresses τ_{xz} and τ_{zx} act, we obtain

$$\left[\left(\tau_{xz} - \frac{\Delta\tau_{xz}}{2}\right) + \left(\tau_{xz} + \frac{\Delta\tau_{xz}}{2}\right)\right]\Delta z\,\frac{\Delta x}{2} - \left[\left(\tau_{zx} - \frac{\Delta\tau_{zx}}{2}\right) + \left(\tau_{zx} + \frac{\Delta\sigma_{zx}}{2}\right)\right]\Delta x\,\frac{\Delta z}{2} = 0. \tag{3.2b}$$

After rearranging these equations and introducing resultant volume components of force X, Z (and distributing them over the elemental surface), we obtain the *equilibrium equation*

$$\begin{aligned}\frac{\Delta\sigma_x}{\Delta x} + \frac{\Delta\tau_{xz}}{\Delta z} + X = 0,\\ \frac{\Delta\sigma_z}{\Delta z} + \frac{\Delta\tau_{xz}}{\Delta x} + Z = 0.\end{aligned} \tag{3.3a}$$

In differential form, this becomes

$$\begin{aligned}\frac{\partial\sigma_x}{\partial x} + \frac{\partial\tau_{xz}}{\partial z} + X = 0,\\ \frac{\partial\sigma_z}{\partial z} + \frac{\partial\tau_{xz}}{\partial z} + Z = 0.\end{aligned} \tag{3.3b}$$

Under real conditions, when an embankment is complete, there is no horizontal force (in the direction of the x axis) acting on the structure, i.e. $X = 0$, the weight

$Z = \gamma z$ acts vertically and the above equation is therefore often used in a simplified form (no X and $Z = \gamma z$).

By expressing the *relative deformation,* we can find further equation, which for strains u (horizontal) and w (vertical) will be

$$\varepsilon_x = \frac{\partial u}{\partial x}; \qquad \varepsilon_z = \frac{\partial w}{\partial z}, \tag{3.4}$$

$$\Phi_{xz} = \frac{\partial w}{\partial x} + \frac{\partial u}{\partial z}. \tag{3.5}$$

By differentiating eqn. (3.4) and substituting into eqn. (3.5), we obtain an *equation for compatibility* of deformation

$$\frac{\partial^2 \varepsilon_x}{\partial z^2} + \frac{\partial^2 \varepsilon_z}{\partial x^2} + \frac{\partial^2 \Phi_{xz}}{\partial x\, \partial z}. \tag{3.6}$$

This is for a planar transformation, introducing the simplest case, which in general conforms well to mechanical deformation conditions on a long embankment of constant cross-section, in which case the soil behaves as an elastic material, an assumption we have already made.

3.1.1 Stress and Deformation

Arising from the applicability of Hooke's law for the relative deformation $\varepsilon_1 = \Delta l_0 / l_0$, with axial stress as shown in Fig. 3.1a, we have

$$\varepsilon_1 = \frac{\Delta l_0}{l_0} = \frac{\sigma_1}{E_H}. \tag{3.7}$$

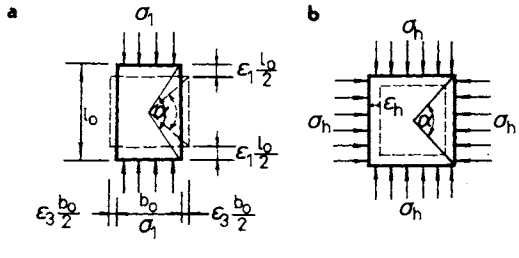

Fig. 3.1. Deformation for different stress conditions. a — axial stress (only vertical), b — all-round equal (hydrostatic) pressure.

Contraction in the z direction causes a linear expansion which is dependent on Poisson's ratio, giving

$$\varepsilon_3 = -\nu\varepsilon_1 = -\frac{\nu\sigma_1}{E_H}. \tag{3.8}$$

However, if the element chosen is subjected to all-round (from three directions) normal pressure (σ_1, σ_2, σ_3), then

$$\varepsilon_1 = \frac{1}{E_H}[\sigma_1 - \nu(\sigma_2 + \sigma_3)],$$

$$\varepsilon_2 = \frac{1}{E_H}[\sigma_2 - \nu(\sigma_1 + \sigma_3)],$$

$$\varepsilon_3 = \frac{1}{E_H}[\sigma_3 - \nu(\sigma_2 + \sigma_1)]. \tag{3.9}$$

If the pressures on each side are equal, i.e. $\sigma_1 = \sigma_2 = \sigma_3 = \sigma_h$, the *pressure* distribution will be *hydrostatic* (see Fig. 3.1b) and the deformations will also be equal

$$\varepsilon_h = \varepsilon_1 = \varepsilon_2 = \varepsilon_3 = \frac{1-2\nu}{E_H}\sigma_h. \tag{3.10}$$

The original volume of the element $V_0 = l_0 b_0 d_0$ changes to

$$V = (1-\varepsilon_1) l_0 (1-\varepsilon_2) b_0 (1-\varepsilon_3) d_0 = (1-\varepsilon_1)(1-\varepsilon_2)(1-\varepsilon_3) V_0. \tag{3.11}$$

Giving the volume change as

$$\delta_0 = \frac{V_0 - V}{V_0} = 1 - (1-\varepsilon_1)(1-\varepsilon_2)(1-\varepsilon_3), \tag{3.12}$$

and ignoring small higher-order terms, we obtain

$$\delta_0 = \varepsilon_1 + \varepsilon_2 + \varepsilon_3 = \frac{3(1-2\nu)}{E_H}\sigma_h = \frac{1}{E}\sigma_h. \tag{3.13}$$

Volume strain depends on stress and on *Young's modulus* for volume deformation E, which has the value

$$E = \frac{E_H}{3(1-2\nu)}.$$

We may also add that for plane stress ($\varepsilon_2 = 0$), we find from eqn. (3.9) that

$$\sigma_2 = \nu(\sigma_1 + \sigma_3) \tag{3.14}$$

and also

$$\varepsilon_1 = \frac{1}{E_H}[\sigma_1(-\nu^2) - \sigma_3(1+\nu^2)],$$

$$\varepsilon_3 = \frac{1}{E_H}[\sigma_3(1-\nu^2) - \sigma_1(1+\nu^2)]. \tag{3.15}$$

There are also the well known expressions following from the *Mohr circle* construction (Fig. 3.2),

$$\sigma = \frac{\sigma_1 + \sigma_3}{2} + \frac{\sigma_1 - \sigma_3}{2} \cos 2\alpha, \tag{3.16}$$

$$\tau = \frac{\sigma_1 - \sigma_3}{2} \sin 2\alpha. \tag{3.17}$$

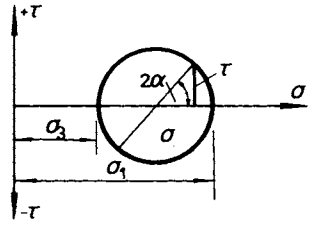

Fig. 3.2. The Mohr stress circle.

After Scott and Schouster (1968), we can use these to obtain analogous transformation equations arising from the relations between *stresses and strains*, as follows

$$\varepsilon = \frac{\varepsilon_1 + \varepsilon_3}{2} + \frac{\varepsilon_1 - \varepsilon_3}{2} \cos 2\alpha, \tag{3.18}$$

$$\frac{\Phi}{2} = \frac{\varepsilon_1 - \varepsilon_3}{2} \sin 2\alpha, \tag{3.19}$$

$$\frac{\Phi}{2} = \frac{1+\nu}{E_H} \left[\frac{\sigma_1 - \sigma_3}{2} \sin 2\alpha \right], \tag{3.20}$$

$$\Phi = \frac{2(1+\nu)}{E_H} \tau = \frac{\tau}{G}, \tag{3.21}$$

where the elastic shear modulus $G = \dfrac{E_H}{2(1+\nu)}$ expresses the transformation properties of the soil, with the assumption that the strains are relatively small (Hooke's law applies).

If we develop Mohr's theory further, and extrapolate its validity to include cohesive soils, where part of the shear stress is taken up by the cohesion c, then from Fig. 3.3 the *limits of failure* will be given by (for σ_{1f}, σ_{3f}, when $\sigma_{1f} = \gamma z + q$)

$$\sin \Phi = \frac{\dfrac{\sigma_{1f} - \sigma_{3f}}{2}}{\dfrac{\sigma_{1f} + \sigma_{3f}}{2} + c \cot \Phi}, \tag{3.22}$$

$$\sigma_{3f}=\frac{1-\sin\Phi}{1+\sin\Phi}\sigma_{1f}-\left(\frac{1-\sin\Phi}{1+\sin\Phi}\right)^2 2c. \tag{3.23}$$

For the two extreme cases ($c=0$ and $\Phi=0$), we can find the value of the coefficient of *active pressure* K_A from eqn. (3.23) as follows

$$K_A=\frac{\sigma_{3f}}{\sigma_{1f}}=\frac{1-\sin\Phi}{1+\sin\Phi}, \tag{3.24}$$

and for $\Phi=0$ we have

$$\sigma_{1f}-\sigma_{3f}=2c, \tag{3.25}$$

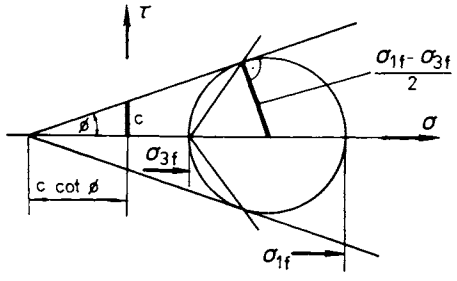

Fig. 3.3. The Mohr failure envelope.

from which it follows that a cohesive soil can withstand some tensile stress, since at the ground surface the vertical stress is zero.

At ground level ($z=0$), the value of the lesser principal stress is given by the expression

$$\sigma_{3f}=\frac{1-\sin\Phi}{1+\sin\Phi}q-\frac{1-\sin\Phi}{1+\sin\Phi}2c. \tag{3.26}$$

By substituting the values $\sigma_{3f}=0$ and $\sigma_{1f}=\gamma_0 z_0+q$ into eqn. (3.23), we obtain the height at which the slope is capable of maintaining itself

$$z_0=\frac{2c}{\gamma_0}\sqrt{\frac{1+\sin\Phi}{1-\sin\Phi}}-\frac{q}{\gamma_0}. \tag{3.27}$$

Equation (3.27) gives the minimum value of height z_0: this is the height up to which a cohesive soil appears stable in a vertical wall. This height may be several meters, but nevertheless in practice we usually ignore any vertical-wall stability. In hydro-engineering structures subjected to the effects of seepage, we never consider it, although many cases are known where such a wall has even remained stable for several years.

To complete the picture, we also need to introduce an expression for the coefficient of *passive pressure* in cohesionless soils

$$K_P = \frac{\sigma_{1f}}{\sigma_{3f}} = \frac{1+\sin \Phi}{1-\sin \Phi}, \tag{3.28}$$

which we can use in stability calculations using the wedge method.

3.2 Calculation of Slope Stability

Many methods of slope-stability calculation are used nowadays which spring from either force and moment equilibrium or else energy equilibrium. The most frequently used are: calculations assuming failure surface; methods assuming definite *boundary-stress values* (Sokolovskiĭ 1942, Tschebotarioff 1949, 1956, Kopacz 1961, etc.); methods based on the various soil characteristics which determine the failure state (Caquot and Kérisel 1956); methods considering the degree of safety for force and *moment equilibrium* (De Beer-Louisberg 1961); methods comparing deformation work with the potential energy of the structure (Clough and Woodward 1967).

To the first group belong methods which assume a *cylindrical failure surface*. Of these, the most important are the solutions by Fellenius (1927), Petterson (1955), Terzaghi (1948), Fröhlich (1955), Zamarin (1950), and Bishop (1955). Then there are methods in which a plane failure surface is assumed. In these we can include the so-called Terzaghi method and also the wedge method. A diagram showing the various surfaces used in these methods is given in Fig. 3.4.

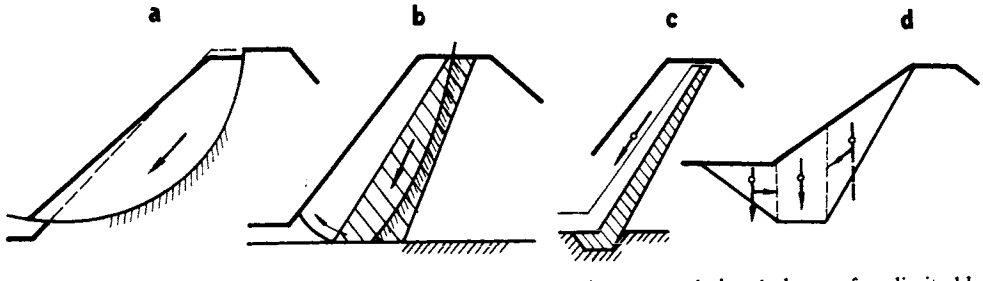

Fig. 3.4. Types of slope failure. a — circular, b — compound, c — translational, d — surface limited by wedges.

The *wedge method* is based on the equilibrium of active (E_A) and passive (E_P) pressures whose values are given by the earth-pressure coefficients (K_A and K_P, respectively), the wedge height (z_A, z_P), and the soil unit weight (γ_0). These quantities can be determined graphically, as shown in Fig. 3.5, where various

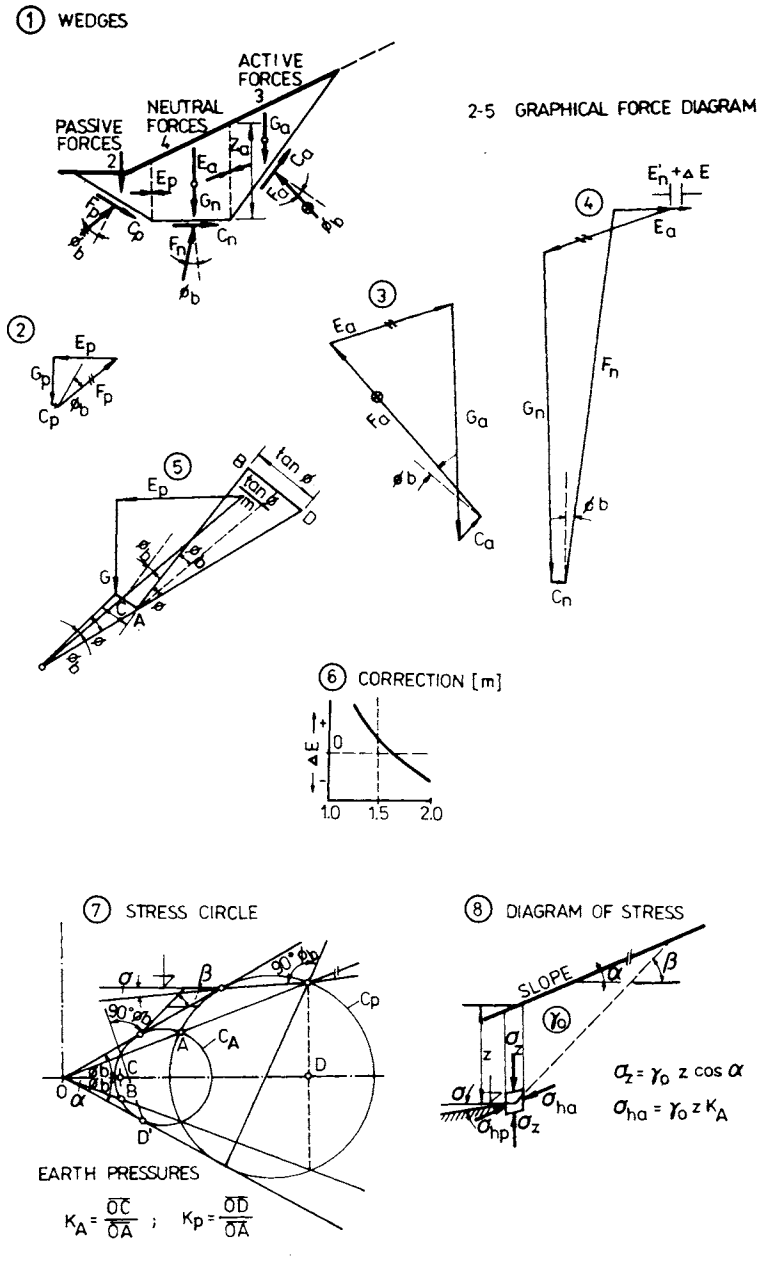

Fig. 3.5. The wedge-method analysis. Φ_b, C_b — values required to maintain equilibrium, C_A — active stress circle, C_P — passive stress circle.

wedges are represented (active, passive and neutral), which determine the sizes of the forces

$$E_A = \frac{1}{2}\gamma_0 z^2 K_A, \tag{3.29}$$

$$E_P = \frac{1}{2}\gamma_0 z^2 K_P \tag{3.30}$$

taking into account their line of action.

In the component diagram (3.5-2), the size of both *passive* (E_P) and *active* (E_A) *pressures* are determined. Figure 3.5-4 shows their composition. In the component and resultant (3.5-5) diagrams, both the cohesion (c_b) and also the angle of internal friction (Φ_b) necessary for the maintenance of equilibrium, are involved. These values are also used in solving the state of stress according to Mohr (Fig. 3.5-7), which is given by the relations

$$\sigma_z = \gamma_0 z \cos\alpha \quad \text{which corresponds to length } OA, \tag{3.31}$$

$$\sigma_{n,a} = \gamma_0 z K_A \quad \text{which corresponds to length } OB. \tag{3.32}$$

If we draw out the values of principal stress σ_1, σ_3 for a passive and an active wedge, then the circles of active (C_A) and passive (C_P) stress allow us to determine the earth-pressure coefficients K_A and K_P, since we know that

$$K_A = \frac{\overline{OC}}{\overline{OA}}; \qquad K_P = \frac{\overline{OD}}{\overline{OA}}. \tag{3.33}$$

Using the above process — observing the principles of force determination — we obtain the values of pressure given in eqns. (3.29) and (3.30). These enable us to construct the component and resultant diagrams (3.5-2, 3, 4), if we introduce into them the wedge weights (G_a, G_p, G_n), the relevant cohesion values (c_a, c_p, c_n) and friction (Φ_b). However, the resultant component diagram (Fig. 3.5-4) will not close when first drawn, since we cannot assume we have chosen the slopes (α) and shear surface gradients (β) to correspond exactly to the required safety factor m (in our example $m = 1.5$). In the quantity for passive earth pressure E_p, we are left with an excess (or sometimes lack) of pressure of magnitude ΔE, which enables us to adjust the values of the safety factor according to the various diagrams given in Figs. 3.5—3.8.

This safety factor m is a sort of *average safety factor,* whose value is considered uniform along all three shear surfaces. Its precise value may be found for individual cases through several approximations using the progression above. Stability is solved here as a planar problem. Those methods which consider a cylindrical shear surface spring from the assumption that when a certain limiting loading is reached (activating the entire possible shear resistance τ, determined from Coulomb's

equation $\tau = f(z, \gamma_0, \Phi, c)$, then the soil fails on some shear surface which can be replaced by a cylinder. Equilibrium is assured while the moment acting on the separated part of the soil mass (given for the most part by the weight G) is smaller than the moment of the forces ensuring stability (Fig. 3.6), i.e. the resistance moment, given largely by the weight of the separated soil, its angle of internal friction, its cohesion and position. The greater the resistance moment with respect to the moment of the disturbing forces, the greater the *stability factor* m. Expressed numerically, we have

$$m = \frac{\text{resisting force moment}}{\text{disturbing force moment}}. \tag{3.34}$$

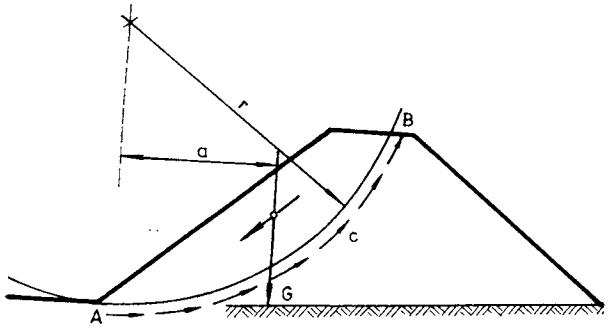

Fig. 3.6. The circle method.

The commonest approach in practical calculations is to divide the soil block above the supposed shear surface into thin slices, for which, by subdividing the weight G, we can determine the size of the *normal* (N) and *tangential* (T) *components* and also the amount of *uplift* (U), which is given by the pore pressure (u). According to *Coulomb's equation* (expressed in effective quantities), the resistance force (shear strength) is given by the expression $(N-U)\tan\Phi' + \Delta l c'$. For all the slices together, we have $\sum_1^n (N-U)\tan\Phi' + \Delta l c'$, and for the analogous disturbing forces we obtain a resultant value in the way shown in Fig. 3.7 $\left(\text{evaluating the sum } \sum_1^n T\right)$. Following eqn. (3.34), we can therefore write the stability factors as

$$m = \frac{r\,\Sigma(N-U)\tan\Phi' + r\,\Sigma c'\Delta l}{r\,\Sigma T}, \tag{3.35}$$

in which we finally omit the moment arm of the various forces acting (r), since it is the same for all terms. The above applies only when we are considering simply the self weight of the soil mass above the supposed separating surface.

If water is seeping through the slope, we must also add to the disturbing tangential components the volume forces of flow pressure (eqn. 2.60). These we take account of by means of the resultant flow pressure force $F_w = S_w I$, which acts on a moment arm r_w, equal to the distance of the resultant volume force from the origin (0). Substituting in the strip width (b), and the differentiated unit weights of

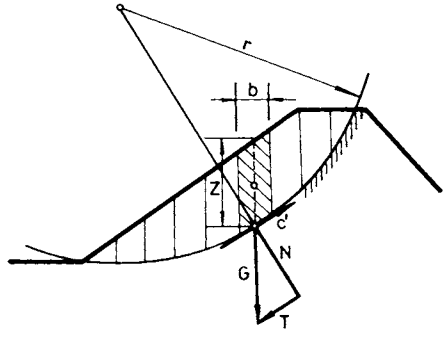

Fig. 3.7. The method of slices.

dry (γ_0) soil at height z and saturated (γ_0') soil at height z' with a variable strip slope α (see Fig. 3.8), we can put eqn. (3.35) into the following form

$$m = \frac{b\,\Sigma[(\gamma_0 z + \gamma_0' z_2)\cos\alpha]\tan\Phi + \Sigma\Delta lc}{b\,\Sigma(\gamma_0 z + \gamma_0' z') + \sin\alpha S_w i\,\frac{r_w}{r}}. \tag{3.36}$$

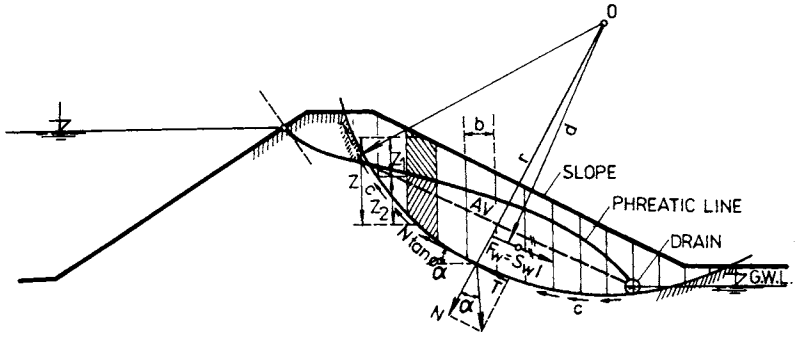

Fig. 3.8. The slices method taking seepage forces into account.

Bishop's solution paves the way for improving the so-called *Swedish methods* (from the first quarter of this century), in that it takes account of lateral pressures (E) between the individual strips (Fig. 3.9a), and also in that it introduces rather

more accurate pore pressures and corresponding stability factor (m). This is set at a value such that the equilibrium state between the normal component (N), the uplift component (U), the cohesion force ($C' = c'\Delta l$), and the weight (G) are rendered safe by an appropriate margin, since we know that

$$N\cos\alpha + (N-U)\frac{\tan\Phi'}{m}\sin\alpha + \frac{c'\Delta l}{m}\sin\alpha = G. \tag{3.37}$$

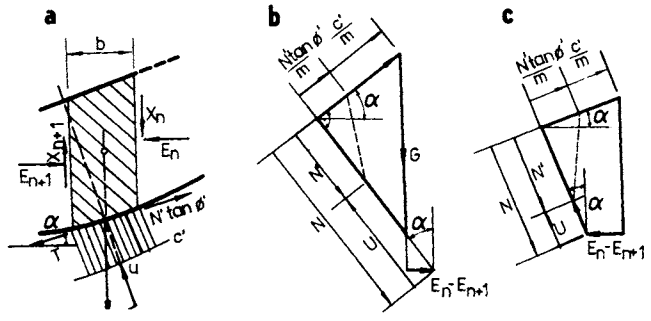

Fig. 3.9. The Bishop solution. a — acting forces, b — the force components in upper part, c — components in lower part of slope failure.

Under these circumstances the component diagram is always closed both in the upper part, where the differences in *lateral pressure* (E) are relatively large (Fig. 3.9b), and the lower part where the differences are small (Fig. 3.9c). Some average stability factor m, determined in a fashion similar to the wedge method, is also reckoned with in this solution, such that this presupposed safety factor m (around 1.2—1.5) fits the equation

$$m = \frac{1}{\Sigma G\sin\alpha}\sum\frac{(G-ub)\tan\Phi' + (X_n - X_{n+1}) + c'b}{\cos\alpha + \dfrac{\tan\Phi'}{m}\sin\alpha}, \tag{3.38}$$

where α (slope angle), b (strip width), u (pore pressure), and shear strength characteristics Φ', c' are inserted.

In original form (Bishop 1955), the pore pressure appears expressed by *Skempton's coefficient* $\bar{B} = \Delta u/\Delta\sigma_1$ and

$$m = \frac{1}{\Sigma G\sin\alpha}\sum\left\{\left[G(1-\bar{B})\tan\Phi' + \right.\right.$$
$$\left.\left. + (X_n - X_{n+1}) + c'b\right]\frac{\sec\alpha}{1 + \dfrac{\tan\Phi'\tan\alpha}{m}}\right\}. \tag{3.39a}$$

Friction forces (X_n, X_{n+1}) between the slices are often neglected, in which case

$$m = \frac{1}{\Sigma G \sin \alpha} \Sigma \left\{ [G(1-\bar{B}) \tan \Phi' + c'b] \frac{\sec \alpha}{1 + \frac{\tan \Phi' \tan \alpha}{m}} \right\}. \tag{3.39b}$$

We can obtain values of the coefficient $\bar{B}$ (0.4 to 0.75) from appropriate tables (Skempton 1954), or else determine it exactly using an appropriate laboratory method (Bishop 1954).

It is not difficult in the above graphical analytical slice methods for determining the stability factor to take account of *earthquake effects*, which are expressed by the addition of an inertia force (Z), depending on the magnitude of *acceleration* (a). This force causes a change in the weight of the soil strip, since it affects gravity and makes up a certain percentage of the acceleration due to earth's gravity. The following values are given in Czechoslovak Standard 73 1310:

$a = 0.025$ g for an earthquake of 7° MCS,
$a = 0.05$ g for an earthquake of 8° MCS,
$a = 0.10$ g for an earthquake of 9° MCS.

The disturbing force increases with the effect of an earthquake from T to a value of $T + \xi N$, and the force resisting shear failure is in turn reduced to a value of $(N_{\text{eff}} - \xi T) \tan \Phi''$. In this expression, the angle of internal friction, denoted thus, takes into account the fact that with fine soils (especially the finer sands) there may be a considerable reduction in the angle. According to Krishann, for an earthquake of 7—9° MCS, the loss of friction angle in sand may be as much as $\Delta\Phi = 1$—5° (Richart et al. 1970).

By introducing revised values into a *modified version* of eqn. (3.35), we obtain

$$m_s = \frac{\Sigma (N - U) \tan \Phi'' + c'' \Delta l}{T + \xi N_{\text{eff}}}. \tag{3.40}$$

Napetvaridze's method of calculation (1956, 1959) is based on an exact expression of earthquake effect, taking account of the fact that with the movement of the earth's crust, an appropriately situated earth dam will also move. If an embankment has elastic shear modulus G (eqn. 3.21) and the horizontal movement of a particular point is x, then the *following differential equation* will give the time variable force $F(t)$

$$\frac{d^2x}{dz^2} - \frac{G\Omega}{\varrho} \left(\frac{d^2x}{dz^2} + \frac{\gamma}{z} \frac{dx}{dz} \right) = u'' \cos pt = F(t). \tag{3.41}$$

The variable seismic coefficient (K_s) derived from it is given by the expression

$$K_s(y) = \frac{a}{\gamma} \mu(y), \tag{3.42}$$

where μ is a function of seismic loading. Introducing and enumerating the expression for this loading, we obtain the general equations

$$\mu(\vartheta) = 1.0 + 1.6 I_0(\vartheta), \tag{3.43}$$

$$K_s(y) = K_s\left(1.0 + \frac{y}{H}\right). \tag{3.44}$$

From these, we have the values of coefficient K_s at the extremities as follows (Fig. 3.10)

$K_s(h) \cong 2.0 K_s$ — at crown level $(y = h)$,
$K_s(0) = K_s$ — at the foot $(y = 0)$.

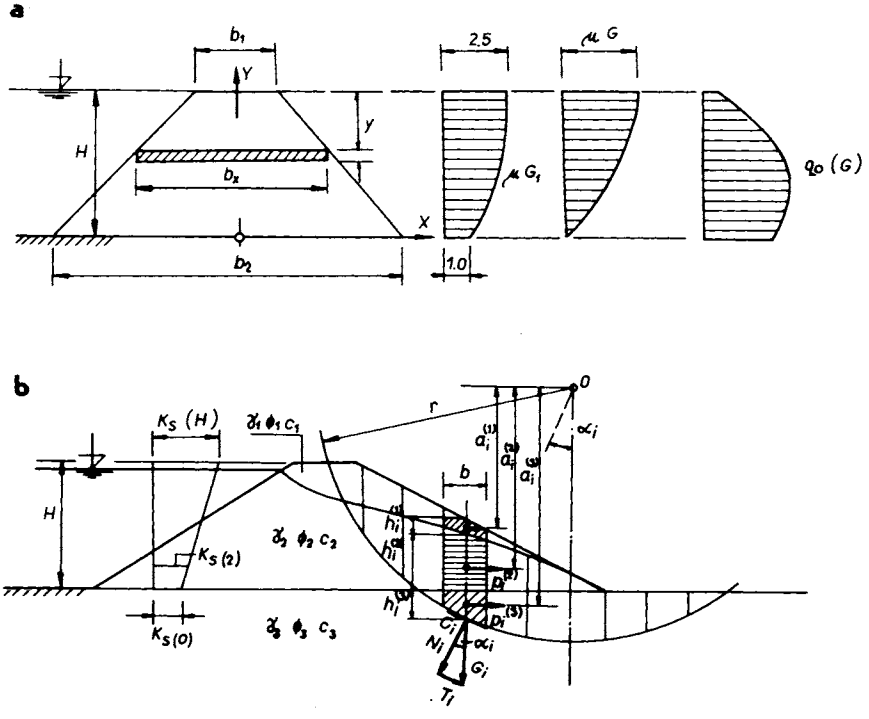

Fig. 3.10. Stability of slopes subject to earthquake. a — distribution of forces, b — by slices method.

The inertia forces P_i acting in the direction of acceleration will be

$$P_i^{(1)} = K_{si}^{(1)} \gamma_{is} b h_i^{(1)}; \quad P_i^{(2)} = K_{si}^{(2)} \gamma_{is} b h_i^{(2)} \ \ldots \text{ etc.}$$

These forces produce moments about the origin (0) given by the product $p_i A_i$. The seismic-force moment arm must be related to the radius (r) or the above-mentioned circle (see Fig. 3.10b), through which, for a moment arm r_i, we find that

$$a_i = rA_i$$

and also

$$A_i^{(1)} = \cos \alpha_i - \frac{1}{r}(0.5h_i^{(1)} + h_i^{(2)} + h_i^{(3)}),$$

$$A_i^{(2)} = \cos \alpha_i - \frac{1}{r}(0.5h_i^{(2)} + h_i^{(3)} + h_i^{(4)}).$$

In this way, the moment effect of *seismic forces* is *related to the centre* of the shear circle considered. If we also relate the seepage Q_w with attendant gradient I to this centre, then we can also include the volume forces caused by flow in the resultant equation for slope *stability factors during an earthquake* (m_s), in a similar way to that of eqn. (3.36). We therefore obtain the expression

$$m_s = \frac{\Sigma N' \tan \Phi'' + c'' \Sigma \Delta l}{\Sigma T + \Sigma(p_i^{(1)} A_i^{(1)} + p_i^{(2)} A_i^{(2)} p_i^{(3)} A_i^{(3)}) + Q_w I \frac{r_w}{r}}. \tag{3.45}$$

A rather different approach is found in the slope stability calculations for earthquakes which Seed et al. (1966) and Ambraseys (1960) have proposed, and which are mainly suitable for earthquake zones with a degree of seismicity exceeds 9° MCS, and are therefore not relevant to Czechoslovakia and central Europe, where Maslov's (1958) recommendations are important.

The methods of slope-stability calculation we have considered for earth embankments generally cover every case occurring in levées and canal embankments, avoiding recourse to other more rarely used solutions. One of these is Ehrenberg's (1927), which is similar to the wedge method we have already looked at. Others include graphical solution of Felleniu's; the so-called "banner" graphical solution (1927, 1936), which is not very precise; Lomize's solution where certain dubious older graphs are used; Taylor's solution of 1948 which has been much used in the past; Trollope's solution of 1957, and the Caquot—Kérisel solution (1956) which is still in common use in France (with modifications taking account of pore pressures). The relevance of slope-stability calculation was analysed by Bishop and Bjerrum (1960).

When we consider *concrete or asphalt sealing,* which is often used in canal embankments constructed of clean sandy gravel (for example, the embankments on the Váh irrigation canals or those proposed for the Danube hydroelectric system), then the safety factor need at first only be determined from the simple ratio of the natural *slope angle of the material* (Φ) and the proposed *slope gradient* (α).

Values of the stability factor for various Φ' (angle of internal friction) are laid out in Table 3.1. In a more precise calculation, we should investigate the danger of the ap. on sliding down the slope.

Table 3.1. Safety factor m for various values Φ and tan α

Angle of internal friction	Value m for a slope tan α				
	1 : 1.75	1 : 2	1 : 2.25	1 : 2.5	1 : 2.8
32°	1.10	1.25	1.41	1.56	1.75
35°	1.23	1.40	1.57	1.75	1.96
37°	1.32	1.50	1.70	1.88	2.11
40°	1.47	1.68	1.89	2.10	2.35

3.3 Calculating the Stability of Protecting Layers and Covers

Protective strengthening layers and slope covers for earth embankments are subject not only to the effect of surface-flow water, but also to that of pore water, and often to large-scale attack from the weather — mainly in winter — during which they are exposed to both *mechanical and thermal strains*. The first of these strains is caused by dynamic effects, for the second the water pressure at rest is the determining factor, whereas for the third we are concerned with a scarcely definable thermal strain, and the mechanical strain of the sealing apron under a moment caused by ice upon the protective element in question.

If we consider all these factors, we observe that in this respect levées and canal embankments are just as troublesome as large dams.

3.3.1 The Dynamic Action of Waves and the Stability of Pavement and Strengthening Elements

The stability of *strengthening elements* and protective layers is affected above all by the dynamic action of waves resulting either from wind or the general running of the system. This second case applies mainly to power station head-race or tail-race canals where shock waves have to be considered (Kratochvíl 1975). In navigation canals, waves are caused by the movement of vessels (Fig. 3.11). The height (h) of these waves can be deduced from the canal width (b_0) from the depth of water (H), from the vessel dimensions (B, L), from the draught (T) and from its driving — respected by coefficient β_1 (having the value 0.85 for drive gearing and $\beta_1 = 1.0$ for drive screw). The vessel speed (v) has the decisive influence — as it follows from the equation of Shankhin introduced by Kratochvíl (1979) in the form

$$h = \beta_1 \left(0.65 + 3.2 \frac{BT}{b_0 H}\right)^2 \left(1 + 0.85 \sqrt{\frac{L}{b_0}} - 0.15 \frac{L}{b_0}\right) \frac{v^2}{2g} \quad [\text{m}]. \quad (3.46)$$

According to Fig. 3.11c the *wave height* (h) has two components

$$h = \Delta h_{z_1} + \Delta h_s.$$

The Czechoslovak and USSR Standards give a simplified relation for h

$$h = \beta \frac{v^2}{2g}, \tag{3.47}$$

where

$$\beta = 2.5\left[1 - \left(1 - \frac{1}{\sqrt{4.2+n}}\right)\left(\frac{n-1}{n}\right)^2\right], \tag{3.48}$$

$$n = \frac{S_c}{S_v} = \frac{\text{cross-section area of the canal}}{\text{cross-section area of submerged part of the vessel}}.$$

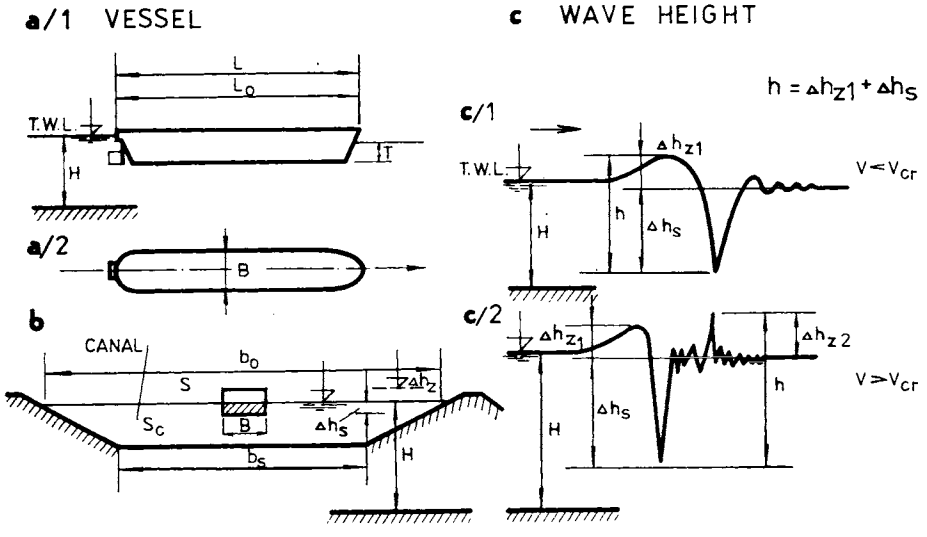

Fig. 3.11. The surf by a ship. a — vessel dimensions in a canal, b — canal dimensions, c — waves characteristics.

The eqn. (3.47) is valid for subcritical region of the vessel velocity v and $n>4$. The dimensions of the vessel (b_0, L) should be considered in the calculation of the wave height caused by the vessel on the slope toe (h') in the relation

$$h' = \frac{2+\sqrt{\frac{b_0}{L}}}{1+\sqrt{\frac{b_0}{L}}} h \quad [\text{m}]. \tag{3.49}$$

The German Institute for Waterway and Water Works — Römisch (1969) and Kratochvíl (1979) emphasized the influence of the eccentric position of the vessel

in the canal profile which caused the increase of the wave height in the slope vicinity by a value h_m

$$h_m = \psi h \qquad [\mathrm{m}], \tag{3.50}$$

where $\psi = 1 + m$ is a coefficient of excentricity (can be taken from the special diagram); $a = \frac{s_v}{b_s/2}$ eccentricity with the positive sign; s_v the distance of the vessel axis of pitch from the canal axis [m]; $m = 0.0086\, n^{2.5}$.

The other formulae introduced by Kratochvíl (1979) take into account the technical limit speed (v_{max}) and the content of the vessel (δ) in the relation

$$h = 2.5 \sqrt{\frac{\delta T}{L}} \frac{v_{max}^2}{g} \exp\left(-\frac{gH}{4v_{max}^2}\right), \tag{3.51}$$

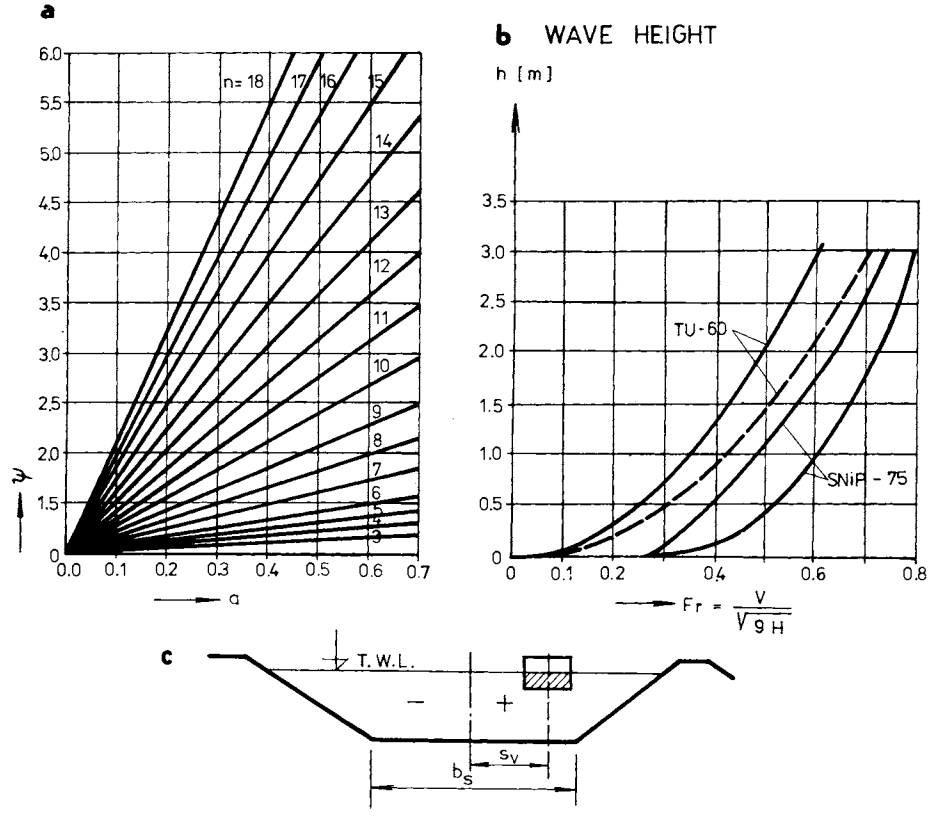

Fig. 3.12. Wave parameters. a — dependence between coefficient of eccentricity ψ and relative value of eccentricity a ($\psi = f(a)$), b — wave height dependence on Froude number, c — vessel eccentricity designation.

with foregoing symbols: (H) water height, (L) the length and (T) the draught of the vessel are recommended by the USSR Standards (1975) too.

Rough values of the wave height caused by the vessel can be obtained from the diagram published in the literature (Kratochvíl 1979) and represented in Fig. 3.12b.

The wave height caused by wind is derived from wind velocity V [km s^{-1}] and its running-length L_v [km] is introduced in the expression in the form

$$h = f(V^{\xi 1} L^{\xi 2}). \tag{3.52}$$

In the USSR Standard (GIDEP) is the following equation

$$h = 0.008\ V^{5/6}(L^{1/2} + L^{1/4}) \qquad [\text{m}] \tag{3.53}$$

is the one most frequently used.

The wind wave heights are of the same order as those caused by vessels, which are more frequent in waterway canals and thus decisive for the design of the strengthening element of the slope embankment that can be destroyed by its shock. Evaluating the wave effect, its augmentation and the shape change should be kept in mind. The wave reaches its maximum height on the slope near the dam top where the "throw parabola" is generated. The crest of the wave breaks down at point B (Fig. 3.13). It is useful (Führböter 1966, Kratochvíl 1977) to take this point as the reference point of the coordinate system (Fig. 3.13). At point A, the wave pressure is assumed to be a maximum. The coordinates of this point (x_A, y_A) depend on the depth of the water under the wave crest — determined as the vertical distance — y_B; the other distance from B to the slope surface, and of the slope inclination (m) is

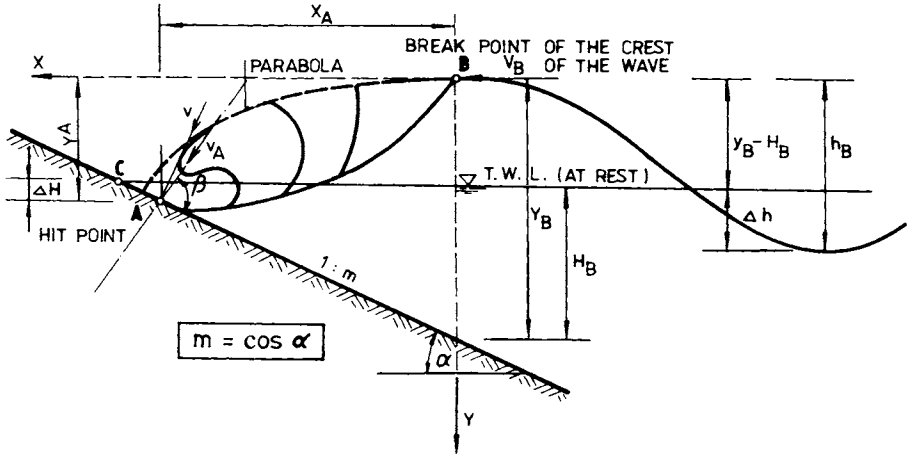

Fig. 3.13. Wave characteristics for slope attack. A (hit), B (crest) as mean relation points.

$$x_A = y_B \frac{1}{m} (\sqrt{1+2m^2} - 1), \tag{3.54a}$$

$$x_A = \frac{y_B}{2} \frac{1}{m^2} (\sqrt{1+2m^2} - 1)^2. \tag{3.54b}$$

Considering the value $y_B = 2 - 10$ m and a slope inclination 1:2 ($m = 2$) we get approximately $x_A = 2$—10 m; ratio $x_A : x_B \cong 1.0$ and $y_A = 0.6$—4.0 m, e.g. $y_A : y_B = 0.3$—0.48 and the depths ratio $y_B : H_B \cong 1.2$. The water depth H_B — in the *point of break* beneath the water level is decisive for the depth (ΔH) of the point of concentrated slope hit. It can be obtained from equation

$$\Delta H = y_B - H_B - y_A. \tag{3.55}$$

Kratochvíl (1976) gives the relation to the wave height; $\Delta H : h$ for different slope inclination (m) in a diagram (Fig. 3.14) which can be used for the determination of some characteristics of primary wave in the relation to the crest-wave break (to the point B) and to the quiet water level. From the original drawing (shown in Fig. 3.13) it follows: $h_B = y_B - H_B + \Delta h$.

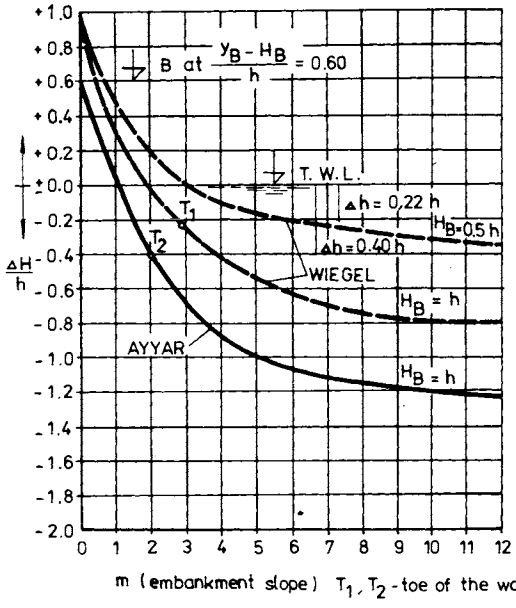

Fig. 3.14. Dependence relation of wave height $\Delta H : h$ for different slope inclination m at different crest heights H_3 — according to Wiegel and Ayyar (after Kratochvíl 1977).

According to this picture, it is possible to determine the characteristic wave velocity at the points A and B. We get

$$v_B = \sqrt{g y_B} \text{ horizontal component of the wave velocity at the crest } B. \tag{3.56}$$

The *wave velocity* at the point of incidence

$$v_A = \sqrt{gy_B\left[1+\frac{1}{m^2}\left(\sqrt{1+2m^2}-1\right)^2\right]}. \tag{3.57}$$

The *velocity component* of the wave shock perpendicular to the slope, the fall velocity, can be calculated

$$v = \sqrt{gy_B}\sqrt{\frac{1+2m^2}{1+m^2}}. \tag{3.58}$$

In the design of slope protection (the pavement, sealing element) e.g., the magnitude of a wave shock of excessive magnitudes with the biggest frequency appearance is decisive. Kratochvíl recommended taking a maximum wave with a 50% appearance into consideration as a fundamental parameter from which the magnitude of the pressure shock with another frequency appearance can be derived. For the *average pressure* wave shock on a dry slope with an inclination 1:1 (and more moderate) he gives the expression

$$p_{max(50)} = 42.0\gamma_w h_B \sqrt[3]{\frac{y_B}{h_B}\frac{d^2}{h_B^2}}\sqrt[3]{\frac{1+2m^2}{1+m^2}}, \tag{3.59a}$$

where $d = 0.1h_B$ is the thickness of the overturned crest tongue of the wave on the slope hit by a wave.

For the magnitude of a pressure shock on the slope inclined 1:3, values of the pressures (F_p) at different heights (h_B) of an overturned wave with various probability appearances P (10, 50, 90, 99 and 99.9%) are given (see Fig. 3.15).

Taking into consideration the facts and analysis mentioned above, it follows

$$\max p_{max} = (1.0—2.1)\,p_{max(50)} \tag{3.59b}$$

should be recommended as design characteristics.

The decisive value can be reached by means of the eqn. (3.59) respecting the wave height (h) and its length (λ) near the slope of the given inclination (1 : n). In a first approximation it is possible to take $h = h_B$ to calculate $d \cong 0.1h_B$ and for the given steepness of the wave (h: λ) by means of diagrams (Kratochvíl 1977) and to determine the relation y_B/h.

This calculation can be done quite exactly, but it is not so easy to choose the appropriate construction measures without a risk of small destructions. That is why the exact calculation by simple estimation of slope protection is preferred sometimes. If the stones of the floor have to withstand the attacks of waves of height h (in meters), their weight W has to be

$$W \geq 1.6(h)^3 \quad [\text{kN}]. \tag{3.60}$$

In engineering practice, we have to use a rip-rap or pavement with stones of a weight of $W = 2.5$ to 6.5 kN.

At other times it is preferable to dimension the strengthening elements with regard to the amount of *energy in the wave* E_v, given by its magnitude (h, λ) in the formula

$$E_v = \frac{1}{8}\gamma_w h^2 \lambda \qquad [\mathrm{kN\ m^{-1}}]. \tag{3.61}$$

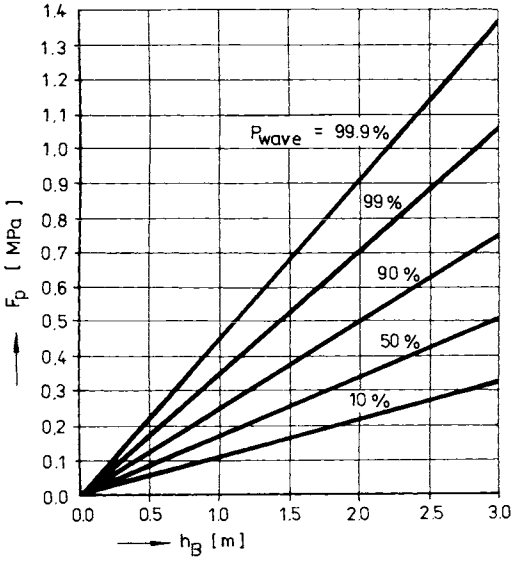

Fig. 3.15. Magnitude of pressure shock F_p for different heights h_B with various probability appearance P.

In the latest Soviet literature, it is recommended that *the thickness* of strengthening material (d_0) be determined by way of the so-called reduced thickness (d_{red}). This is dependent on the slope and a coefficient η ($\eta = 1.3$—1.5) taking into account the safety of the stone positioning and local dimensions, and with due regard to the wave height (h), the unit weight of water (γ_w) and of stone (γ_k) expressed in the formula

$$d_0 = \eta d_{red} h \frac{\gamma_w}{\gamma_k - \gamma_w}. \tag{3.62}$$

If we examine the strengthening against wind produced waves of Czechoslovak canal embankments and levées, then using the fact that the wind speed can reach up to $v = 100$—$120\ \mathrm{km\ s^{-1}}$ (27.8—33.0 m s^{-1}), we find that in canals waves of height $h = 1.5$ m can form, and on the Danube they can reach up to $h_{max} = 2.35$ m. A stone floor of thickness 50—65 cm could withstand these waves, or alternatively a concrete or asphalt sealing of thickness around 20 cm.

When we look at the strengthening material on the sides of earth embankments and reservoirs, for example at Drahovce on the Váh or on the Vihorlat reservoir (Fig. 3.16), we can perceive some quite large deformations. We approach these failures and deformations by easing the angle of slope α thereby lessening the wave pressure (viz. eqn. 3.52), and preventing the extraction of individual grains, rocks and stones into the reservoir on the wave's retreat.

Fig. 3.16. Rip-rap failure of a dam.

With a sandy-gravel rip-rap layer we have to remember that after several years, the sand will be totally washed away and the slope can begin to deform in a similar way to reservoirs bank deformation. Examples from slope strengthening on the Váh hydroelectric complex bear witness to the fact that with light concrete floors, the sandy-gravel sub-base is also sucked away by the effect of waves. The floor therefore cracks and subsides (Fig. 3.17). These cracks are dangerous since the failure does not end with floor degradation. *Instability* in the strengthening leads to the *slope stability failures and sliding* (Fig. 3.18), which can lead in turn to serious disasters.

The problem of ensuring the stability of protective layers and strengthening elements on levées and reservoir banks can be seen from three standpoints:

technical, safety and economic. The first would lead to designing technically perfect protective measures for maximum wave size. However, in the minds of most experts this would be economically disanvantageous, and from the point of view of safety it is unnecessary to strive after technical perfection. Between the times when the protective covering is suffering its worst batterings, and failures are being initiated, there are long periods for repair and rendering the failures harmless. In many cases it is economically more viable to repair the entire slope in the intervals provided by surface fluctuation, than to lay along a length of several km a heavy rock floor with dimensions determined from the above calculations. We can only arrive at the correct solution when we take full account of all three aspects mentioned.

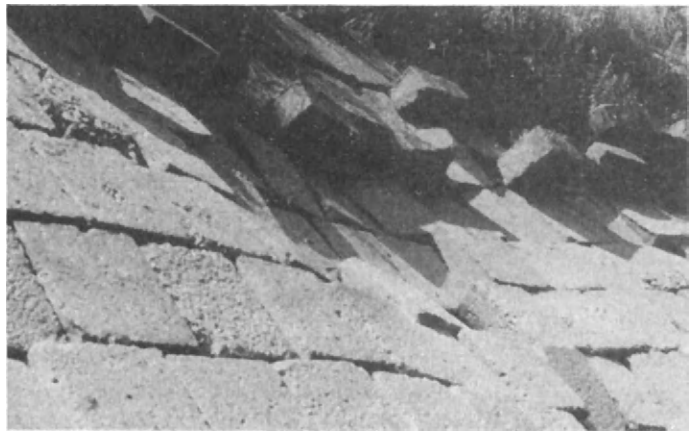

Fig. 3.17. Floor deformation.

Over the last two decades, *stability of cover layers* under seepage pressure has been the subject of extensive study at the research institute VODGEO in Moscow and Kiev. In Czechoslovakia, Myslivec (1964) suggested a relatively simple way of determining the depth of a cover layer. In his opinion, we should start from the magnitude of effective stress, which depends on the weight of the *protecting layer* with material unit weight γ, and on the seepage pressure $P_w = \gamma_w I z$. Therefore

$$\sigma' = z\gamma' + \gamma_w I z = z(\gamma' + I\gamma_w) = z\gamma^+. \tag{3.63}$$

The *effective specific weight* of the soil directed vertically downwards is

$$\gamma^+ = \gamma' + I\gamma_w.$$

With rapid fluctuations, the hydraulic gradient may suddenly increase substantially, so that the covering layer above the earth sealing or homogeneous

embankment is often subjected to pressure forces many times greater than that corresponding to the cover weight. On the other hand, however, the uplift (u) can cause sudden relief to the layer above the sealing. Pore pressure (u) is dependent on the sealing thickness (h_t), as well as on the thickness of the stone layer (h_k), the porosity (n), and the water depth (h) above the point under consideration. Skempton's pore-pressure coefficient is $\bar{B} = \Delta u / \Delta \sigma_1$, using which we have

$$u = \gamma_w [h_t + h_k(1 - \bar{B}n) + h(1 - \bar{B}) - h_w], \tag{3.64}$$

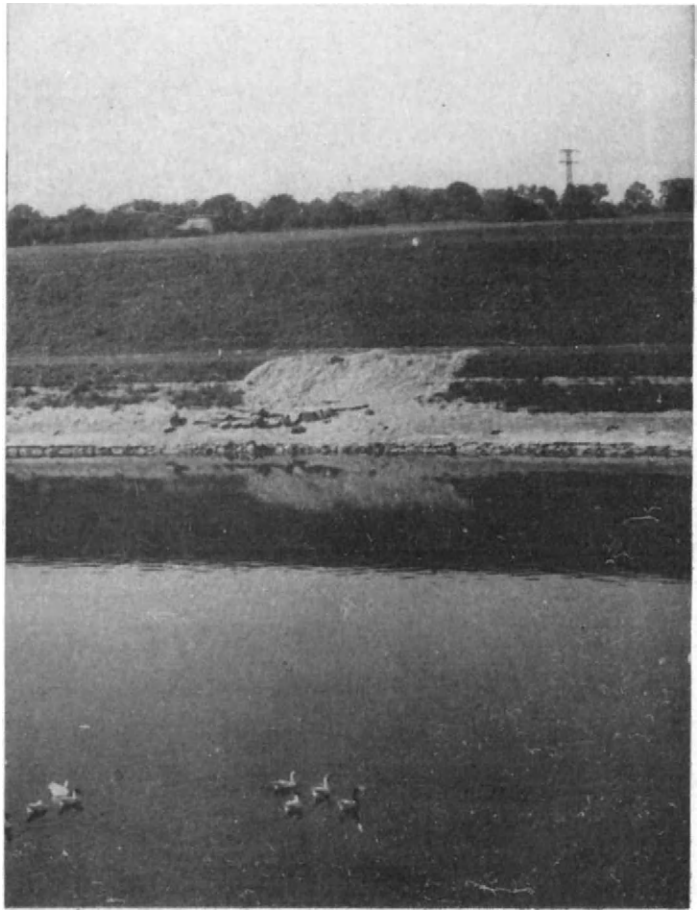

Fig. 3.18. Slide of a slope caused by floor failure.

from which one can determine the thickness of the *stone layer* h_k corresponding to the stability conditions. Myslivec (1964) assumes that for a sudden surface drop, $\bar{B} = 1$, and stipulates that the pore pressure be zero ($u = 0$). Using these assump-

tions, we obtain, through substitution into eqn. (3.64) (in accordance with Fig. 3.19),

$$0 = \gamma_w[h_t + h_k(1-n) - h_v],$$

$$h_k = \frac{h_v - h_t}{1-n}. \tag{3.65a}$$

After substituting in the average porosity $n = 0.34$

$$h_k = \frac{h_v - h_t}{1-0.34} = 1.52(h_v - h_t). \tag{3.65b}$$

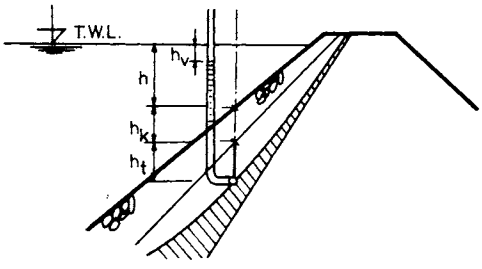

Fig. 3.19. Quantities needed for destination of thickness of rip-rap — after Myslivec (1964).

For a typical case, where the embankment has height $h = 5$—6 m, we find that $h_k = 0.5$—2.0 m. For canal embankments ($h = 10$—20 m) with slope sealing, we find that $h_k = 3$—6 m, but in reality we would need to effect an instantaneous emptying of the canal which is a practical impossibility. With regard to this fact, we can consider the cover layer as having half the above thickness, but never less than 0.5 m, and in this context we should not confuse the floor thickness (d_0) with the thickness of the cover layer (h_k), by which we understand the thickness of the floor and bed, and sometimes an intervening layer, so that h_k is always $> d_0$.

Finally, it should be noted that the problem of pore pressure is not really a deciding factor in dimensioning covers for levées nor even for canal embankments. Their stability is governed by the wave effects of surface water flow, to which we have already partially referred.

3.3.2 The Stability of a Humus Covering

The stability of a humus covering is, from the technical point of view, a far greater problem than it would seem at first glance (Peter 1965). It results from the complicated stress conditions mainly caused by various effects arising from long periods of rain, when rain-water seeps into the humus, very quickly at first, since capillary forces and the thermal gradient are added to the effect of gravity. However, the air trapped in the pores acts as a brake on this movement. In the final

analysis there are usually five distinct sorts of rain-water movement, viz.; gravitational water flow down the slope surface; seepage into the ground caused by a *potential difference*; capillary motion caused by *capillary forces*; thermo-capillary motion caused by a *thermal gradient*; gravitational seepage in the contact layer caused by the height difference. Since humus layers are formed of fine soil (clay, silt) with low permeability, usually characterized by permeability coefficient $k = 10^{-4}$—10^{-6} cm s^{-1} average order of magnitude 10^{-5} cm s^{-1}, then in long periods of rain (intensity more than 1 mm h^{-1}), the surface layer becomes saturated with water flowing under gravity down the slope. The layer of surface water and its movement, accompanied not only by known erosion effects, but also by the formation of a potential difference, have the effect of causing water seepage into the humus. Capillary forces cause a further movement leading in the general direction from the slope surface into the embankment body (approximately perpendicular to the layer). In the spring and summer months, when the surface layer temperature reaches 25—30°C or more, and the internal soil temperature is 10—15°C, a relatively intense thermocapillary motion begins.

In the initial phase of water movement in a direction approximately perpendicular to the surface (Fig. 3.20a), an important action is performed by the *capillary forces*, whose value is approximately in the range

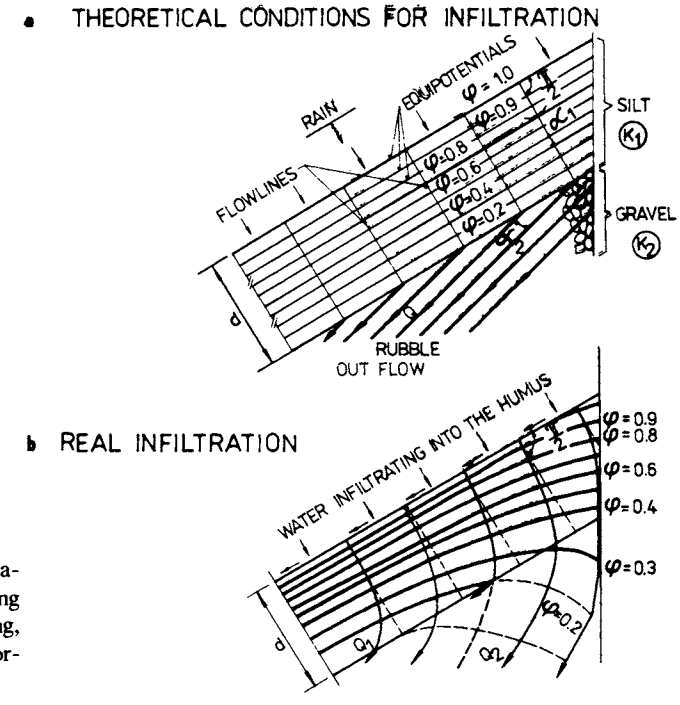

Fig. 3.20. Flowlines for infiltration of water into the protecting layer. a — at the beginning, b — in the stage of contact deformation.

$$P_c = \gamma_w n h_c = 10.0 \times 0.3\ (0.1—0.6) = 0.3 \text{ to } 1.8 \text{ kN m}^{-2}.$$

The *inertia forces*, given by the expression

$$P_i = \varrho z v_s \frac{\Delta v_s}{\Delta z} \tag{3.66}$$

are relatively small. We can usually ignore them without introducing greater errors. This we do partly because they are rather small, but also because *air resistance* (R_{air}) acts against them, and is generally of the same order of magnitude. This resistance can be found from the following formula

$$R_{air} = A \frac{h_w}{h_a - h}. \tag{3.67}$$

In eqns. (3.66) and (3.67), apart from $\gamma_w n$, we have: h_c the capillary height (we assume $h_c = 10—60$ cm); z the depth to which infiltrates; v_i the mean velocity of infiltration; $\Delta v_i/\Delta z$ the relative increase in infiltration velocity; A atmospheric pressure (expressed by the height of a water column); h_w the final infiltration depth; h_a the depth of the air zone.

If, in future, we bring in the coefficient (k_v) and the effective capillary height of the soil (h_c), then with a slope gradient (α) we can obtain the equation for *infiltration velocity* at a certain depth z below the surface

$$v_i = k_v \frac{z \cos \alpha + h_c}{z} = k_v \left(\cos \alpha + \frac{h_c}{z} \right). \tag{3.68}$$

This velocity is not only vital for flow quantities, but also, as we shall be indicating, for changes in stability conditions in the humus layer. With regard to the fact that the protecting layer thickness d is generally small (usually $d = \frac{1}{3}$ to $\frac{2}{3}$ of h_c), a supercritical velocity arises at the interface between the permeable and less permeable soils, i.e. $z = d$, as a consequence of which fine particles are washed out of the protecting layer and gradually settle into the surface of the permeable soil. With flooding the humus permeability increases, and the gravel permeability in the contact zone decreases accordingly. Thus a kind of transition layer is formed where complicated water-flow conditions arise, with flow not only perpendicular to the layer as in the humus, but also in a direction governed in the main by the geometry of the contact face, and the transition layer in general (Fig. 3.20b).

These flow conditions were investigated using a model (Fig. 3.21) which incorporated a sunken trough, in which a gravel layer of thickness 20 cm and a sandy silt layer of thickness 10—20 cm were laid out (Mencl et al. 1965).

Detailed examinations and investigations showed that the humus passes through four distinct phases, distinguished from each other by the action of mechanical forces and the size of hydrodynamic pressures. In the first phase we deal with dry

humus spread out over the embankment slope, and this almost always appears as stable. In the second phase, with the infiltration of water into the protective layer, stability conditions hardly change at first, since the unfavourable effects of hydrodynamic pressure are eliminated by the increasing weight of the layer, which causes an increase in the friction force on the contact between the two soils. Conditions markedly worsen in the third stage as uplift forces begin to act on the slope reinforcement, and to an even greater extent in the fourth stage when the humus is fully saturated.

For these states we can write down *basic equilibrium conditions.* In the first state when the soil is still dry and retains its natural cohesion (c), the following equilibrium equation applies (in accordance with Fig. 3.21)

$$\gamma d \cos \alpha \tan \Phi = \gamma_0 d \sin \alpha - c. \tag{3.69}$$

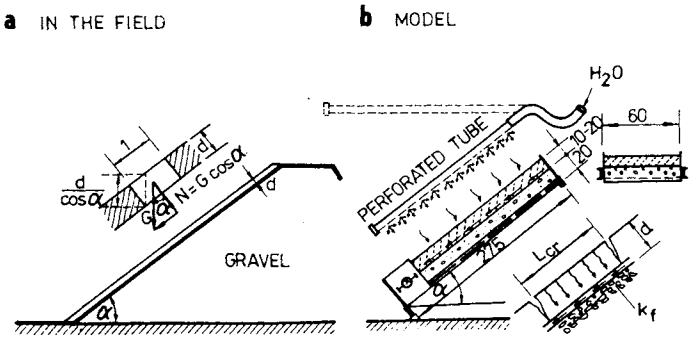

Fig. 3.21. Stability measurements. a — in nature, b — in the laboratory.

In the second state, with infiltration into the humus, which is formed from a soil of porosity n

$$d(\gamma_0 - n\gamma_w) \cos \alpha \tan \Phi = (\gamma_0 - n\gamma_w) d \sin \alpha - c. \tag{3.70}$$

If water penetrates the protective layer over its whole thickness, and in the lower layer we have *uplift and hydrodynamic pressure*, then the third stage begins, for which we obtain the equation

$$d(\gamma_0 - 0.2) \cos \alpha \tan \Phi = (\gamma_0 - 0.2) d \sin \alpha + 0.2 d\gamma_w \sin \alpha - c.$$

In the fourth state the whole humus layer is saturated by continuous rainfall, so that according to Archimedes law the soil becomes 'lighter'. If we denote the unit weight of lightened soil by $\gamma' = \gamma_0 - \gamma_w$, we can write an equilibrium equation in the form

$$\gamma' d \cos \alpha \tan \Phi = \gamma' d \sin \alpha + \gamma_w d \sin \alpha - c. \tag{3.71}$$

This equilibrium state is particularly important, since it is connected with cover-layer failure (Fig. 3.21c). Investigations both in the field and in the laboratory show that as large deformation sets in, the humus does not slide as a coherent carpet of material, but breaks up. In order for the carpet to break up, the cohesive forces must first be overcome on certain cross-sections, and at intervals depending on the thickness d. The equation for the *critical length* l determining the interval of the fissures, into which the carpet is broken in tension, takes the form

$$l_{cr} = \frac{c \cot \Phi (1 - K_A)}{\gamma' \sin \alpha + \gamma_w \sin \alpha - \frac{c}{d} - \gamma' \cos \alpha \tan \Phi}, \tag{3.72}$$

where K_A is the coefficient of active earth pressure.

In our model measurements, we found the critical interval at which fissures were formed, for a slope of $\alpha = 30°$, to be $l_{cr} = 65$—85 cm, which agrees with the values we obtain by substituting the shear-strength characteristics and weight of the soil used into the above equations.

From the equation we have given it is simple to deduce the slope angle at which a humus layer with a certain thickness and certain soil properties is stable. Vice versa, for a certain slope angle, we could determine the necessary characteristics of shear strength for which the stability of the slope reinforcement is ensured. We usually determine the angle of internal friction, which is the governing factor for cover stability For instance, in the fourth stage, where we need to have the largest value of internal friction in order to maintain equilibrium, we find its value from the equation

$$\tan \Phi_b^{IV} = \left(1 + \frac{\gamma_w}{\gamma'}\right) \tan \alpha - \frac{c}{\gamma' d \cos \alpha}. \tag{3.73}$$

To see how the *necessary angle of internal friction* (Φ_b) of the soil changes for different layer thicknesses, and over the four stages (I—IV), we present some figures in Fig. 3.22. Taking the often used slope angle of 30° and protective-silt-layer thickness $d = 0.1$—0.3 m, and with $c = 5.0$ kPa, we obtain the values for Φ_b.

Silty soil with organic impurities such as those we might use in a strengthening layer of humus, have an internal friction angle of $\Phi = 18$—$27°$, and therefore slope reinforcing elements using them tend to be a gradient of around 30°, and have an assumed minimal cohesion of about $c = 0.5$ kPa. When saturated without any reinforcement they are unstable. The actual moment of failure is largely a function of the intensity and duration of the rain and the speed of infiltration.

We can determine the *time* required *for infiltration* (t_i) from the equation

$$t_i = \int_0^d \frac{(w - w_0) z}{k_v (z \cos \alpha) + h_c} \cos \alpha \, dz. \tag{3.74}$$

In practice we often calculate with a simple approximate expression given by the relation

$$t_i = \frac{l}{k2D}(w - w_0)\,d^2, \tag{3.75a}$$

where w_0 and w are unit moisture contents for the soil before and after saturation, and $D = \frac{d}{2}\cos\alpha + h_c$ is the effective pressure height.

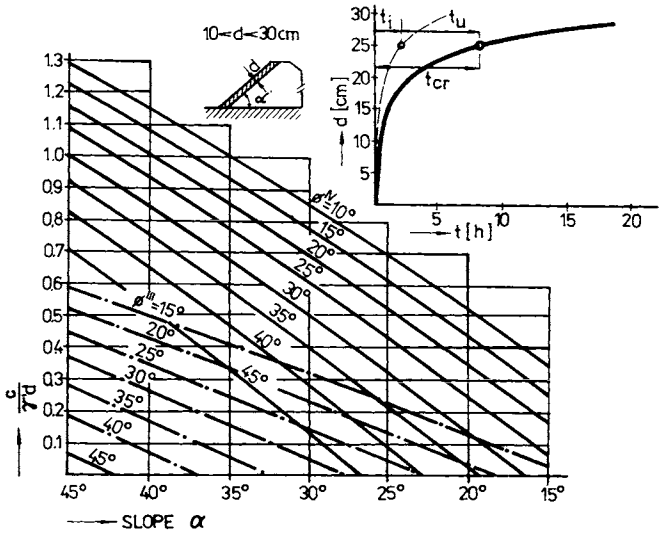

Fig. 3.22. Relationship between value of $c/\gamma' d$ and slope angle α.

After this time interval, the second stage, from the stability point of view, commences, and then, making assumptions as above, it progresses gradually on to the third stage, characterized by the development of uplift forces and water flow on the interface between the protective layer and embankment body, where hydrodynamic forces also act. From the assumption of the progressive formation of fissure and interval l_{cr}, we can also approximately determine the *critical time* for the onset of a change in stability conditions as follows

$$t_{cr} = t_i + \frac{n_e l_{cr}}{k_f \sin\alpha}, \tag{3.75b}$$

where t_i is the duration of infiltration; n_{eff} the effective soil porosity; k_f the permeability coefficient on the contact face in the direction of the slope.

In our case, with values $w=0.38$; $w_0=0.18$; $\alpha=30°$; $b_k=40$ cm; $k_v=4\times10^{-3}$—8.5×10^{-5} cm s^{-1}; and $k_f=10^{-3}$ cm s^{-1}, we obtain the quantities laid out in Table 3.3.

If we take a look at the values given in Table 3.2 and 3.3, we arrive at the conclusion that one disadvantage of thin humus-strengthening layers is the high speed at which the soil becomes saturated, but their advantage is that a grassy covering easily penetrates across the layer interface, and takes root in the embankment body, thus increasing the stability of the strengthening element, and to a much greater extent than would appear from our calculations, in which we take no account of shear-strength enhancement due to the effects of a grassy surface growth. A thick humus layer would become saturated after about one day of steady heavy rain, which seems rather more favourable. However, the fourth stage. when it comes, is then still more awkward for such a layer. For the first and several succeeding years after construction, slipping in thick humus reinforcing layers on gravel slopes is a much more frequent occurrence than in thin layers, and brings more dangerous results.

Table 3.2. Angle Φ_b necessary for different stages

Stage	I	II	III	IV
Necessary angle Φ_b	10°20′—23°50′	13°45′—25°	16°30′—28°50′	36°—44°50′

Table 3.3. Critical time t_{cr} for thickness d = 10 — 30 cm

For a thickness d [cm]	10	15	20	25	30
Critical time t_{cr} [h]	0.45	0.86	2.62	8.34	26.40

These facts have to be realized in *humus-layer design.* In these designs it makes sense to start off from the fourth loading stage, for which one can write down the equilibrium equation in the form

$$\frac{c}{\gamma_d}=\left(1+\frac{\gamma_w}{\gamma'}\right)\sin\alpha+\tan\Phi\cos\alpha\cong2\sin\alpha+\tan\Phi\cos\alpha. \qquad (3.76)$$

This equation has the advantage that it is easily possible to tabulate the values or put them in graphical form. One can use such a graph (Fig. 3.22) to design these humus slope reinforcements, and for the soil characteristics given and planned humus thickness, the slope for limiting equilibrium can be read off, and the necessary shear-strength characteristics for construction data of both embankment

and reinforcement established. The values for the third stage are also recorded on the graph, as well as the graphical relation

$$t_{cr} = f(t_i, d)$$

for values which we have already seen.

On the subject of stability calculations, we should add that rain or flowing water has a markedly varying effect on cover stability in the fourth stage; stability conditions tend to be worst in the years immediately following construction; stability of earth body and cover must be treated separately; wooden fences, hedge rows, pegging, and other stabilizing agents used in the past as downstream slope reinforcement, have substantial usage on precipitous slopes as far as details, stiffener distances, etc., are concerned. Humus covers behave very differently on homogeneous clayey slopes compared with slopes of more heterogeneous earth structures, a fact which must always be borne in mind; at all time the cover has to be designed with sufficient support at the foot. Measurements have shown that pressures acting at the foot are by no means insubstantial. Even on small embankments they can reach values of 10—30 kPa. Theoretical studies, measurements and observations have indicated that a cover thickness of around 20 cm (15—25 cm) is suitable for the conditions prevailing in central Europe.

If we design a humus cover on the downstream bank of any water-retaining embankment, and take due account of rain, then that cover will be stable.

3.4 Stability with Changing Pore Water Pressures

During *persistent rain*, the stability of the downstream part of a homogeneous embankment changes according to distinct laws as we have seen, and principally for two reasons: in clays built into the body of an embankment, a capillary effect comes into play above the free surface level (above the phreatic surface), and after a time rain-water also permeates into this part of the embankment. While the first of these has an almost negligible effect on total stability, the second can affect matters to a very substantial degree (Havlíček 1964).

As shown in Fig. 3.23a, in times of persistent rain it is not only the lower regions of an embankment which are soaked, but also the entire downstream side, with intense water flow down the slope over the humus layer, breaking through towards the bottom. The *embankment* becomes *saturated* and springs appear at the foot which must be dealt with (this will be mentioned later). If the embankment is supported by stones at the foot (Fig. 3.23b), the position is rather better, but when persistent rain lasts for a matter of weeks (as was the case on the Danube in May and June 1965), it is difficult to prevent outflows of water at the foot. In the end, it may be necessary to weigh down the foot area with sandbags (Fig. 3.24) to ensure continuing stability of the structure, which is of course reduced, partly as a result of

an increase in uplift (pore pressure), and also as a result of growth in *disruptive flow pressure forces* ($F_w = z\gamma_w I$) as we said in Chapter 2.

From simple solutions which we meet in soil mechanics (Myslivec 1968), it follows that the stability of a saturated slope in this state can drop locally at the foot to a half of its dry value.

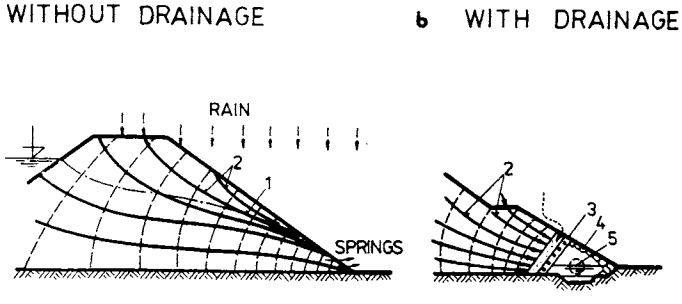

Fig. 3.23. Flowlines for a homogeneous dam during rain. 1 — phreatic line, 2 — seepage caused by rain, 3 — filter, 4 — floor, 5 — drainage pipe.

To test the effect of heavy rain, a combined comparison method can be used to advantage, together with the electro-hydrodynamic analogy described in Chapter 2, with suitable positioning of resistance electrodes over the model cross-section. Using this analogy, we can find the value of pore pressure in every case. If we were to put into the cross-section a shear circle which we wish to investigate, we could discover, for example, by the slice method, the value of total stresses all around this circle and indeed their normal and tangential components, just as for all the methods so far described where cylindrical (circular arc) shear stress is considered (see Fig. 3.7). The degree of stability is defined here as the moment ratio of resisting and disrupting forces (eqn. 3.34). Equation (3.35) expresses this mathematically. The equations for calculating the quantity show that from this same determination of pore pressure, we can deduce the way in which stability changes for a given case.

In 1963, Havlíček and Fiedler tested a low dam profile for ten different cases as follows.

(1) Steady seepage through a homogeneous structure with a planar foot drain.
(2) Seepage and cross-section as in (1), but taking account of the effect of soil capillarity.
(3) Seepage and cross-section as before, but covered by rain water.
(4) Steady seepage through a homogeneous structure, where the foot drain is wider than in (1).
(5) As in (4), but considering capillary effects.

(6) The structure as in (4), but with the effect of persistent rain.
(7) The structure as above, but including four horizontal drains one above the other.
(8) As in (7), but with the effect of persistent rain.
(9) As in (4), but supplemented by a pipe drain.
(10) As in (9), but with the effect of persistent rain.

Fig. 3.24. Slope and toe loaded by bags filled in with sand.

In Table 3.4, we present values of pore pressure found at the two points indicated on the cross-section (Fig. 3.25), approximately at the centre of the embankment, and under the intersection of the horizontal plane of the water surface and the downstream slope.

Comparing data from the above, one of the first things we discover is the *favourable influence of the angled pipe drain* in the centre of the cross-section in conjunction with a drainage blanket under the downstream part of the profile (Fig. 3.26). When comparing data from the first case with the third, in which we considered persistent rain which produced for the given profile a pore-pressure increase of 25% in the first piezometer and about 15% in the second, note that we are concerned with a comparison with a cross-section containing a very active protective antiseepage element.

Table 3.4. Pore-pressure values (u) for various cases

Pore pressure in piezometric tube 1 and 2	Case									
	1	2	3	4	5	6	7	8	9	10
u_1 [kPa]	64	60	80	49	39	68	43	55	37	55
[%]	100	94	125	76	61	105	67	86	58	86
u_2 [kPa]	88	78	100	53	41	75	42	47	25	27
[%]	100	89	115	60	47	85	48	53	28	31

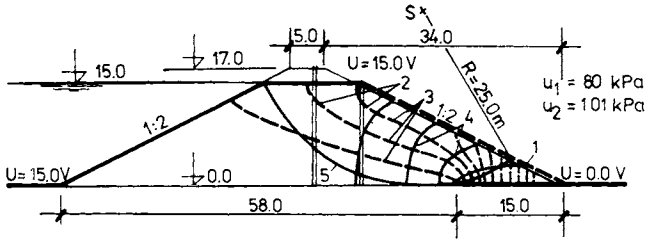

Fig. 3.25. Stability computation using EHDA method — after Havlíček and Fiedler. 1 — electrode, 2 — piezometer pipe, 3 — flowlines, 4 — equipotentials, 5 — slope failure.

However, even such imperfect protective elements are usually lacking in levées, and the degree of slope stability during heavy rain in a loess embankment is often practically unity ($m = 1$). An unstable embankment subsoil renders the situation still worse by virtue of the fact that an even greater pressure acts at the slope foot and its surroundings (Bertram 1967). This will be discussed in Chapter 6.

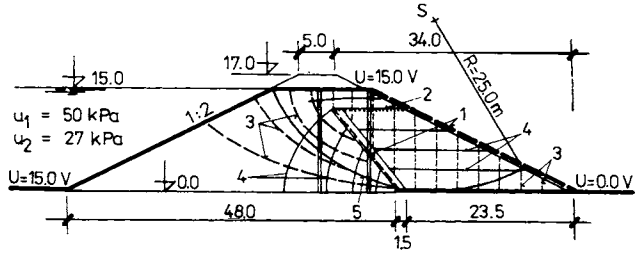

Fig. 3.26. Flow conditions in a dam with oblique chimney drain. 1 — electrode, 2 — piezometer pipe, 3 — flowlines, 4 — equipotentials, 5 — potential failures surface assumed.

3.4.1 Pore-pressure Changes during Embankment Construction

As we know from soil mechanics and also from the work done in Chapters 1 and 2, changes in pore pressure within an embankment do not commence merely in response to external stimuli, i.e. the saturation of either side by rain water as already discussed, but also in response to stress changes, i.e. consolidation of the soil. With *consolidation*, water is forced out from the pores, thereby bringing about a redistribution of total stress σ between the effective stress (σ_{eff}, σ') taken up by the grains, and the neutral stress borne by the water (pore pressure u). The self weight of the soil in the embankment also contributes to water being squeezed out, and means that the effective stress $\sigma' = (\sigma - u)$ increases with time, and therefore with it the stability of the structure (Scott 1963). We can see from the following equation expressing the relation between change in void ratio $\Delta e = e_0 - e$ and change in *effective stress*: $\sigma' - \sigma_0'$ which controls consolidation process — expressed by *degree of consolidation* $U_z = \dfrac{e_0 - e}{e_0 - e_1}$ or $U_z = \dfrac{\sigma' - \sigma_0'}{\sigma_1' - \sigma_0'}$, if $\sigma_1' = \sigma_z' = \sigma' + u_i = \sigma' + u$.

During consolidation $\Delta\sigma' = -\Delta u$ and

$$\frac{\partial u}{\partial t} = c_v \frac{\partial^2 u}{\partial z^2} \tag{3.77a}$$

that by knowing the value of the *consolidation coefficient* c_v which we can find in the laboratory, we can determine the change in pore pressure u in a certain time in a soil layer of thickness Δz. We must of course know the pressure u at the centre of the layer, as well as at the centres of the layers above and below (u_2, u_4). Where *unidirectional consolidation* is involved, we have (Craig 1974)

$$u_3 = \frac{\Delta t c_v}{(\Delta z)^2}(u_2 + u_4 - 2u_0), \tag{3.77b}$$

where $c_v = \dfrac{k}{m_v \gamma_w}$ having units of $m^2\ s^{-1}$; depends on permeability (k), coefficient of volume change (m_v) of soil and unit weight of water (γ_w).

This introduces at the same time the solution to the consolidation equation, which, through the finite-element method, gives us the dependence of changes of stress and porosity. The use of the Terzaghi consolidation theory (Terzaghi and Peck 1948) comes mainly with the results of laboratory measurements, which are then applied to the body of a homogeneous embankment divided into individual elements (Fig. 3.27).

Florin's theory (1948) is based largely on the hydraulic principle of consolidation, whose progress we can trace through piezometric height changes, determined with permeability coefficient k (Fig. 3.28). An *approximate solution* would therefore be

$$\frac{\partial^2 H}{\partial z^2} = \frac{1}{(\Delta z)^2}\,(H_{t,i,k+1} + H_{t,i,k-1} - 2H_{t,i,k}), \tag{3.78}$$

where the nodal points of the net are denoted using Florin's notation (see Fig. 3.28, right-hand side). In this, apart from position indices i and k, the equation also includes t and $t+1$, representing the time at which the relevant steps take place.

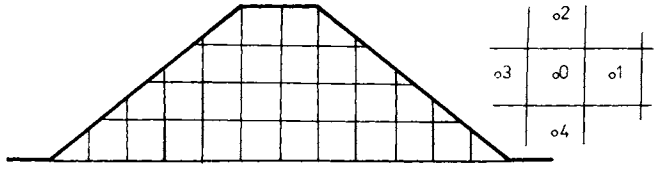

Fig. 3.27. Differential net.

The Laplace equation, which we can solve by the differences methods, makes possible a transformation to the form

$$\frac{\partial^2 H}{\partial x^2} + \frac{\partial^2 H}{\partial z^2} = \frac{1}{\Delta h^2}\,(H_{t,i+1,k} + H_{t,i-1,k} + H_{t,i,k+1} + H_{t,i,k-1} - 4H_{t,i,k}). \tag{3.79}$$

If we introduce yet another of Florin's symbols

$$\Diamond_{t,i,k} = H_{t,i+1,k} + H_{t,i-1,k} + H_{t,i,k+1} + H_{t,i,k-1},$$

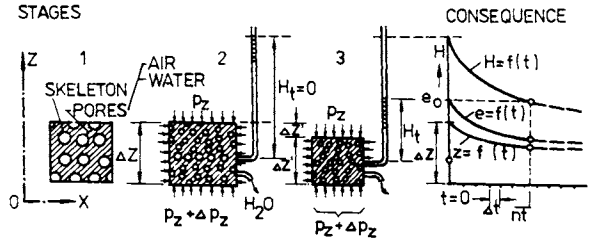

Fig. 3.28. Consolidation with time and its consequence — after Florin (1948): stages of consolidation processes.

the equation of consolidation then becomes

$$\frac{H_{t+1,i,k} - H_{t,i,k}}{\Delta t} = \frac{\Delta\Theta_{t+1,t,i,k}}{2\gamma_w \Delta t} + \frac{k(1+e_{av})(1+\xi)}{2\gamma_w a h^2} \times$$

$$\times (\Diamond_{t,i,k} - 4H_{t,i,k}). \tag{3.80}$$

Multiplying through by Δt and introducing symbols for average void ratio (e_{av}) and ratio change and stress increment ($\Delta e = a_v \Delta \sigma_z'$); expressing

$$\alpha = \frac{k(1+e_{av})}{\gamma_w a_1} \frac{\Delta t}{\Delta h^2}, \qquad a_1 = \frac{2}{1+\xi} a, \tag{3.81}$$

and after modifying eqn. (3.80), we obtain a final equation for calculating piezometric pore-pressure heights on a square differential network

$$H_{t+1,i,k} = (1-4\alpha) H_{t,i,k} + \frac{1}{2\gamma_w} \Delta\Theta_{t+1,t,i,k} + \alpha \Diamond_{t,i,k}, \tag{3.82}$$

for a rectangular network with side dimension $\Delta = m\ \zeta\ z$, we can derive the equation

$$H_{t+1,i,k} = \frac{1}{2\gamma_w} \Delta\Theta_{t+1,t,i,k} \frac{1}{2(1+m^2)} (H_{t,i+1,k} + H_{t,i,k-1}). \tag{3.83}$$

Equation (3.83) is suitable for obtaining pore pressures in an embankment whose sealing element has a slope angle given by $\cot \alpha = m$, because in this case, since the sealing elements, have an inclinative of 1:1 ($m=1$), the rectangular newtork becomes square. Comparing eqn. (3.82) and (3.83) for a value of $m=1$ results in the following

$$\alpha = \frac{m^2}{2(1+m^2)} = 0.25\,. \tag{3.84}$$

The equations then coincide and take the form

$$H_{t+1,i,k} \cong \frac{1}{2\gamma_w} \Delta\Theta_{t+1,i,k} + \frac{1}{4} \Diamond_{t,i,k}\,. \tag{3.85a}$$

It is always convenient to chose a value of 0.25 for α when using eqn. (3.82), since the first term on the right-hand side is then equal to zero.

If we consider a non-consolidated saturated soil of unit weight γ and submerged unit weight γ', then

$$\gamma' = \gamma_0 - \gamma_w\,,$$

where γ_w is the unit weight of water, and we obtain the equation

$$\frac{1}{2\gamma_w} \Delta\Theta_{t+1,i,k} = \frac{1}{2\gamma_w} (\gamma' 2\Delta h) = \frac{\gamma'}{\gamma_w} \Delta h. \tag{3.85b}$$

The results of pore-pressure investigation during the course of construction can be collected to show that the *magnitude of pore pressure depends mainly on soil permeability,* or more exactly on the degree of stiffening, the embankment dimensions, position of drains, sealing element and filters. Drains and filters are especially important in the body of a homogeneous embankment formed from low permeability soils, which will consolidate rapidly — more detailed explanations may be found in various technical works (Lambe and Whitman 1969, Peter 1964a). The problem of consolidation during the process of construction has a place of primary importance for several types of earth dams especially homogeneous ones, but only secondary significance for large canal embankments. For levées, this problem has even less importance, and we shall therefore not be analysing any calculations, nor the consequence to stability of pore pressure changes, in any greater detail. We shall merely be alluding to the results of work in Czechoslovakia regarding research into suitable embankment profiles for the Danube waterway system from 1961 to 1964 (Peter 1964b), where the problem of consolidation in loamy subsoil is serious. The thickness of loam cover on the section we are considering varies from 4 to 6 m. The permeability of loamy or clayey soils varies in the range $k = 5 \times 10^{-6}$ to 3×10^{-7} cm s^{-1}. The values of the unit weights are $\gamma_0 = 17$—21 kN m^{-3}, $\gamma_s = 27.0$ kN m^{-3}, and $\gamma' \cong 11.0$ kN m^{-3}. To build the embankments of height 8—16 m, we had at our disposal tens of millions of cubic meters of this soil as well as very permeable gravel ($k = 0.1$ cm s^{-1}) in inexhaustable quantities. The total volume of soil used is from 28—36 million cubic meters.

In the case outlined, it would seem to be economically advantageous to use the loam on either the upstream part of the cross-section (Fig. 3.29a), or the downstream part, where a simpler technology of construction should be possible (Fig. 3.29b). For similar reasons the profile in Fig. 3.29c, where loam is laid in the

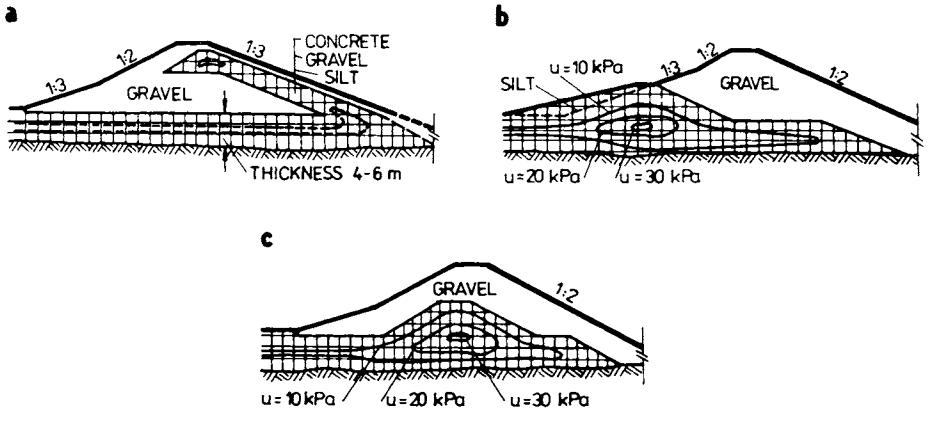

Fig. 3.29. Pore pressures in a canal dam. a — dam with an inclined silty core, b — silt on the downstream side, c — silty core.

centre of the *gravel cross-section*, is favoured. This last profile should at the same time involve the least quantity of material, since soil of high shear resistance is used in those areas governing slope stability, on both upstream and downstream slopes.

Studies have shown that smallest pore pressures over the construction period, some 20 months, occur using variant (*a*) where these pressures are generally less than $u = 10$ kPa at completion of the structure. In the other two profiles, pore pressure of around $u = 30$ kPa maximum have been found. However, to build an embankment according to variant (*a*) would involve an upstream slope of 1 : 3. For an angle $\Phi = 21°$ and cohesion $c = 30$ kPa, we obtain $m = 1.52$, while using the other two designs, slopes of 1 : 2 appeared to be satisfactory for the upstream side, since taking shear-strength characteristics $\gamma_0 = 23.0$ kN m^{-3}, $\Phi' = 38°30'$, a degree of stability against shearing of $m = 1.55$ is obtained, because the shear surfaces do not pass through regions where the soils show a definite pore pressure.

When considering embankment cross-sections, we must not forget that slope stability is only one of the criteria relevant to such evaluation and design investigation. In such structures, we must minimize all threat to the surrounding country. If we consider functional safety (in operation) when the canal is full and the destructive potential is at a maximum, then we see that profile variant (*a*) gives the best results, because seepage can be countermeasured by both a concrete and a loam sealing.

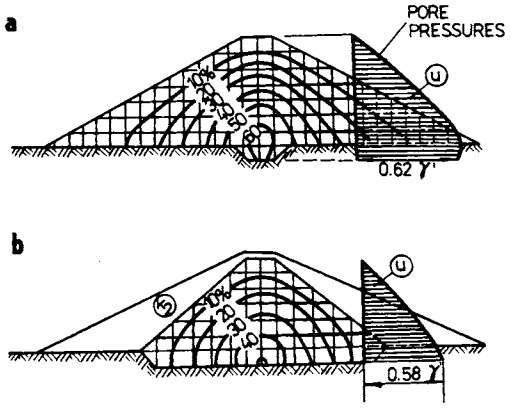

Fig. 3.30. Pore pressures in a homogeneous dam and in a loam dam core. a — homogeneous (silty) profile, b — profile with loam core and pervious (gravel) zone.

If we turn our attention to some other possible solutions (Fig. 3.30), we see that for a homogeneous loam profile we have to reckon with unsatisfactorily large pore pressures, in a similar way to a profile with a thick sealing core. Functional safety is not therefore proportional to the quantity of sealing material used, since besides high pore pressures there are grave technological disadvantages involved, so that an objective evaluation of the various profiles requires other technological and economic considerations to be examined. We shall consider these in next chapters.

3.5 Assessing Stability Using Deformations and Stresses across the Whole Embankment Profile

Over the past twenty years, there has been a growing endeavour to determine the state of stress, and hence the stability of an entire embankment profile as perfectly as possible, as in the methods already described assuming a certain plane of failure. Sokolovskii's attempt in 1942 to discover analytically the path of the principal stresses and failure planes remained as unsuccessful as the attempt to scan an embankment profile by means of intersecting lines made in Czechoslovakia in 1959, or certain attempts to use as a criterion the minimum deformation work in a given half-space.

We move on to work through integral and differential methods based on the use of finite elements making use of high-performance computers capable of processing large quantities of numerical data characterizing the structure, and forming a block system for the entire local stress calculation, as set out by Zienkiewicz (1970). This author is considered to be one of the originators of the method of stability assessment by means of dislocation potential. Relative deformation of the structure is made up by the deformation of individual elements of triangular or tetrahedral shape, according to whether we are dealing with a planar or three-dimensional situation, represented for a certain stage in the proceedings as constants $u(x, y)$ and $v(x, y)$, from which stress can be derived.

The relationship between stress and deformation is found progressively by investigating various *load increments*. The resulting solution is obtained as a component of the solutions of individual linearized steps. For each of these steps the effect of the load increment is found. The elastic deformation moduli and Poisson's numbers change in a manner corresponding to the state of stress in the individual elements reached in the previous step. *Displacement and stress components* are added to the values found for the previous steps. For anisotropic structures, a solution can be reached using a transformed diagram system (Eisenstein 1974).

According to Kratochvíl and Hanzlian (1969), who researched this method in Czechoslovakia, an analysis based on mechanics principles of such a structure consists of three fundamental steps, when looking at the matrix through the method of finite elements. These are: expressing the elemental stiffness matrix, compiling the resultant stiffness matrix of the structure, transforming the external loading into statically equivalent point forces; solving the matrix system, whose resulting stiffness matrix is regular, symmetrical, positively deformed, and of band form; analysing the results of the solution.

The approach to be used for a heterogeneous embankment profile is set out in Figs. 3.31 and 3.32. The former represents a way of dividing the profile into individual layers and triangular elements, and into points on which the individual forces act, satisfying the demands of equilibrium. Solving the problem, we obtain

the deformation and stress in the embankment by means of iteration, whereby we can at the same time verify whether or not a tensile stress occurs in certain elements. Exclusion of all tensile stress makes the assumption that none of the soil incorporated into the embankment can withstand it, and is one of the basic conditions of solution. In the event of tension still occurring in certain elements, the procedure would have to be repeated. According to proofs from the various authors cited, when the structure is subject to loading without resulting tension and formation of fissures, the process is convergent and the structure is stable. If the reverse is true it is conversely unstable.

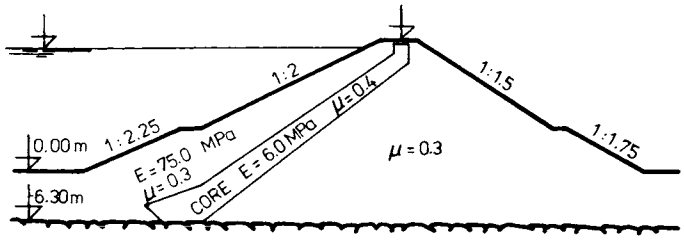

Fig. 3.31. Cross-section of investigated dam.

In effect, we are concerned here with seeking an equilibrium between equivalent forces acting within the elements and the potential energy of the system when it is subject to a certain deformation. A statistical equivalent is found by looking at virtual work.

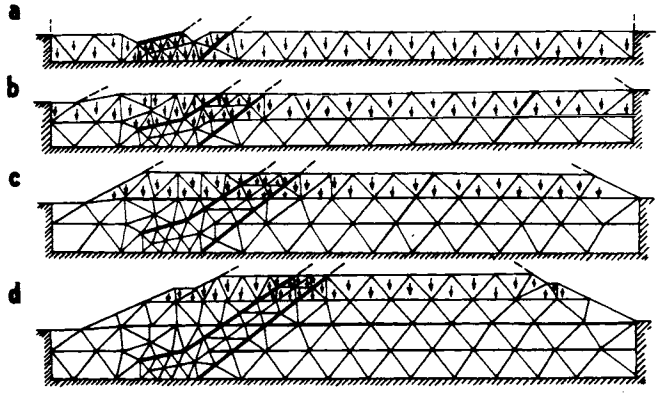

Fig. 3.32. The advance of dam construction and its laying — after Kratochvíl (1969). a — first "layer" of gravel and two layers of clay, b — two layers, c — advanced construction, d — for layers of gravel compacted.

If we denote the column vector for virtual peak displacement by $\boldsymbol{\Delta}^*$, then the column vector for virtual relative principal deformation, corresponding to *virtual displacement* $\boldsymbol{\varepsilon}^*$, is given by

$$(\boldsymbol{\Delta}^*)^T\boldsymbol{F}=\iiint_{V_k}(\boldsymbol{\varepsilon}^*)\boldsymbol{\sigma}\,\mathrm{d}V, \tag{3.86}$$

where $\boldsymbol{F}$ is the column vector of peak elemental forces, V_k the volume of the k-th element, $\boldsymbol{\sigma}$ the principal stress column vector, and T represents the transposed matrix form.

After rewriting eqn. (3.86) in the form

$$(\boldsymbol{\Delta}^*)^T\boldsymbol{F}=(\boldsymbol{\Delta}^*)^T(\boldsymbol{C}^{-1})\iiint_{V_k}\boldsymbol{B}^T\boldsymbol{\sigma}\,\mathrm{d}V, \tag{3.87}$$

we obtain

$$\boldsymbol{F}=(\boldsymbol{C}^{-1})^T\iiint_{V_k}\boldsymbol{B}^T\boldsymbol{\sigma}\,\mathrm{d}V, \tag{3.88}$$

where $\boldsymbol{C}$ and $\boldsymbol{B}$ are matrices from the relations $\boldsymbol{\Delta}=\boldsymbol{Ca}$, $\boldsymbol{\varepsilon}=\boldsymbol{Ba}$, in which $\boldsymbol{a}$ is the column vector of the polynomial coefficient for u and v in the element concerned.

With a plane triangular element with linear polynomial $p(x, y)$, and for $u(x, y)$, the above expression takes the form

$$\boldsymbol{F}=\frac{t}{2}\begin{bmatrix} x_{jk} & 0 & x_{kj} \\ 0 & x_{kj} & y_{jk} \\ y_{ki} & 0 & x_{ik} \\ 0 & x_{ik} & y_{ki} \\ y_{ij} & 0 & x_{ji} \\ 0 & x_{ji} & y_{ij} \end{bmatrix}\begin{Bmatrix}\sigma_1\\ \sigma_2\\ 0\end{Bmatrix}, \tag{3.89}$$

where t is the element thickness and x_{ji} indicates $x_j - x_i$ in the (σ_1, σ_2) coordinate system.

Indices i, j and k indicate the tops of the triangular element, moving anti-clockwise around it. The forces with which the structure is loaded have the same value as those given in the expression of eqn. (3.89), but have opposite sign. Before being introduced into the right-hand side, these are transformed into the basic system in which the geometry was expressed.

In the column vector of eqn. (3.89), only elements with sharply positive values occur. In transforming them to a basic coordinate system, it is necessary to distinguish between the two cases, $\sigma_x > \sigma_y$ and $\sigma_y > \sigma_x$.

If the deformation fields of an embankment are solved (Figs. 3.33 and 3.34), tension excluded, it is possible to discover its stability. Considering the plane

$(x, y; \sigma_1, \sigma_2)$, Kratochvíl and Hanzlian (1969) introduces an equation of *limiting equilibrium* (eqn. 3.22) for cohesive soils, in the form

$$[\sigma_1 - \sigma_2 - (\sigma_1 + \sigma_2) \sin \Phi] < 2c' \cos \Phi. \tag{3.90}$$

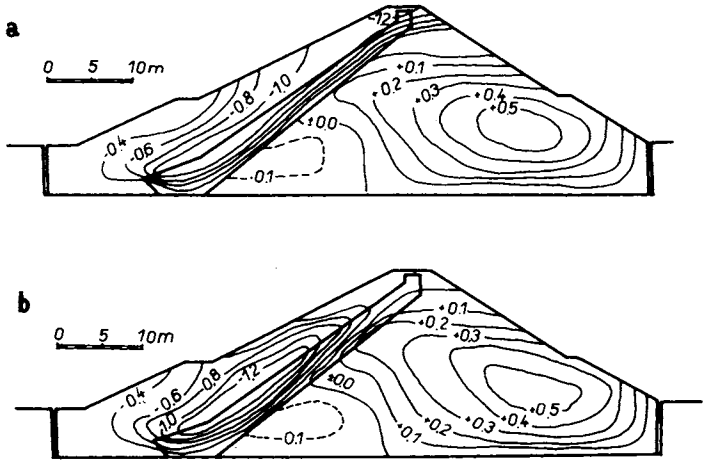

Fig. 3.33. Lines of equal horizontal displacements. a — sudden load through over-weight, b — slowly loaded by over-weight.

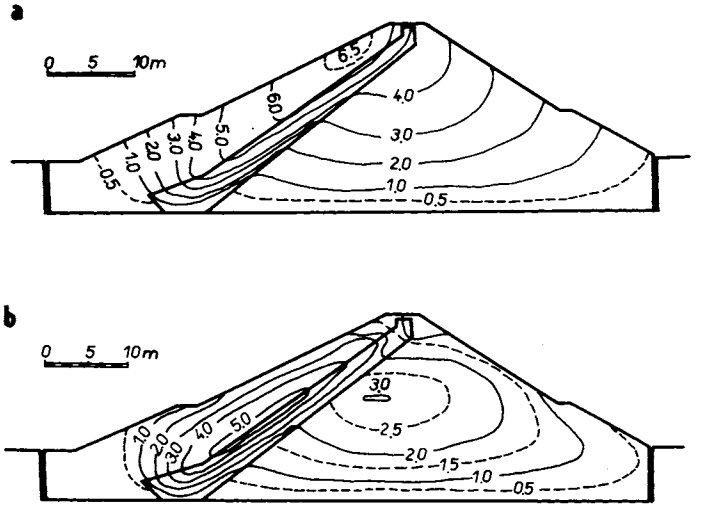

Fig. 3.34. Lines of equal vertical displacements. a — abrupt loading, b — successive loading.

Stability conditions are given by the straight inequality ($\tau < c$), and also by the fact that τ_{max} values are compressed in the direction $\alpha_{eff,\,max} = \pm(\pi/4 + \Phi/2)$. With coarse-grained soils the inequality

$$\frac{\sigma_1 - \sigma_2}{\sigma_1 + \sigma_2} < \sin \Phi \tag{3.91}$$

has to be satisfied.

The above method displays large advantages only when computers are used, giving us information about the fulfilment or otherwise of the inequalities in eqns. (3.90) and (3.91) for each separate element, and producing at the same time a degree of stability against shear failure for the soil element, everywhere across the embankment profile. If we know the deformation properties of the soil, and the stresses (including components σ^1, u), we can model all the stresses and deformations in the structure and indeed its foundation, and then analyse its total and local stability.

3.6 The Stability of Embankment Foundations

The stability of earth embankment foundations can be investigated and calculated using the *finite-element method*, which is based on *dislocation potential theory*, and has already been described. There is, however, a certain danger associated with this method, in that the dependence of stresses and deformations is not entirely linear. Even so, use of this method provides the most reliable results in the majority of cases (Terzaghi Lectures 1974).

Foundation stability can also be ascertained *by* more old-fashioned *elasticity methods*, as well as by other methods arising from the assumption of definite failure planes. These planes must pass through the soil with the least shear resistance. If we have soil beneath the embankment foundation plane (Fig. 3.35), it is reasonable that the shear surface, in this case circular, will pass through the foundation material. This will then involve application of eqn. (3.35) or (3.38) for the given conditions. In the case outlined, we can obtain values relatively simply for shear strength $\tau = (N - U) \tan \Phi + c' \Delta l$. This we determine for individual slices, summing the results, as may be seen in Fig. 3.35 for a medium height embankment with a chimney-pipe drain, where the summation lines for ΣN and ΣT are also shown. These enable us to reach a conclusion as regards the safety factor by a simple visual comparison of the areas under the two curves. A more precise expression of the degree of stability can always be found numerically.

In the construction of levées, we often come across cases where the structure is put directly into an unconsolidated clay — a dead river arm, containing flaked grains — which is caught between a bearing subsoil and the body of the levées, displaying substantially greater shear strength than would a rather less stable layer.

In such a case, one can assume that the failure surface lies at the contact of soils with differing shear-strength properties (Fig. 3.36). The principal factors giving the structure sturdiness to withstand this sort of failure are the weight of the soil above $\gamma_0 D$, and the cohesion of the unconsolidated clay layer concerned. If the width of a levée at its foot is b_2 and its soil unit weight is γ_0, then for an *average contact stress* q_0 on a layer of thickness a, we have

$$q_0 = \gamma_0 D + \left(\frac{2D}{a} + \frac{b_2}{2a} + \pi - \frac{4}{3}\right) c. \tag{3.92}$$

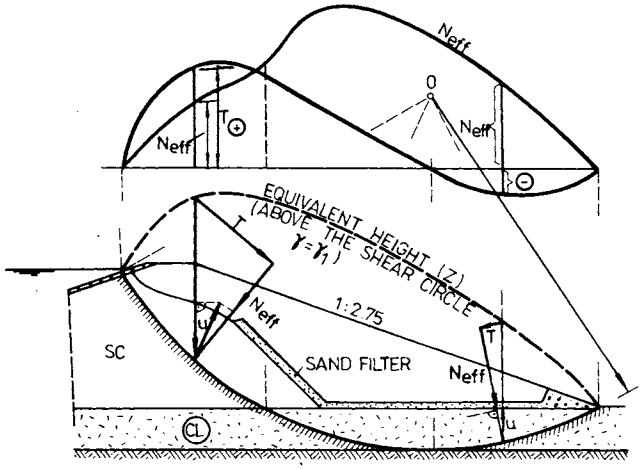

Fig. 3.35. Subsoil-stability investigation by means of circle-failure method.

It is apparent from this formula where the angle of internal friction is neglected, that non-consolidated layers are more dangerous the nearer they are to the surface. All non-consolidated clays and flakey soil beneath the surface should be removed.

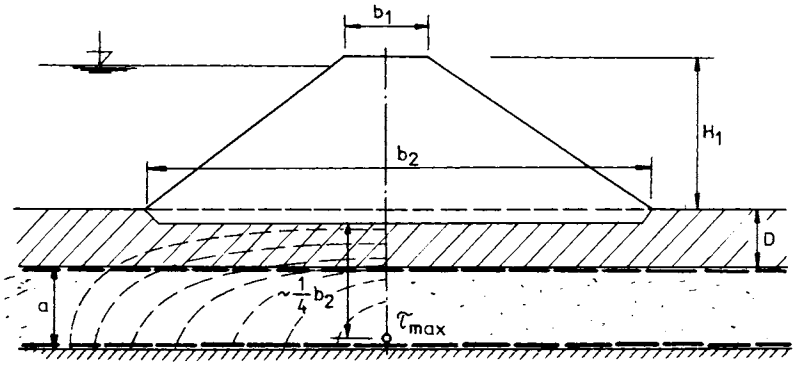

Fig. 3.36. Stability computation of an unconsolidated layer.

One further particular problem can arise in the construction of irrigation channels in areas of loess, with regard to possible *volume changes in the subsoil* after saturation. Because of the peculiar property of loess, deformations in a saturated layer can be as much as 10% of the thickness: in absolute terms they can be up to 1 or 2 m.

The behaviour of these types of soil is chiefly dependent on their mechanical and mineralogical chemical properties, and on the natural and *actual water content* of *the saturated loess* (Fig. 3.37). Using these characteristics we can assess not only the behaviour but also the stability of embankments. It generally emerges that even for quite large deformations, the stability of levée foundations is preserved, since the deformations caused by loading are generally less than those caused by the behaviour of loess.

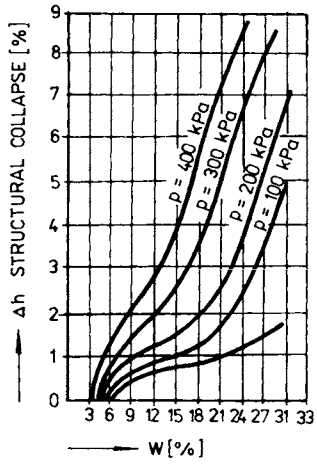

Fig. 3.37. Relationship between sacking (Δh) and moisture content (w) — after Frey (1963).

In Table 3.5, we have set out the values of *deformation in loess subsoil* for 6-m-high irrigation embankments where the loess layer is around 19 m thick. They have been in operation for 4 months.

Table 3.5. Subsoil deformation

Deformation caused by	Settlement [cm]			
	in dam axis		in canal axis	
	calculated	observed	calculated	observed
Irrigation	85.5	80.0	85.5	80.0
Own weight	19.2	23.9	0	−2.9
Canal fill	25.3	15.0	15.3	17.0
Total deformation	130.0	118.9	100.8	94.1

According to Rubinstein, negative deformations in a subsoil occur because of soil expansion. In Czechoslovakia the main causes of these deformations are soil-volume changes, which are commonest in cases where clay flakes comprise a part of the subsoil. These types of deformation which have been documented for canals on the Šaľa—Kolárovo irrigation system, and for embankments on similar canals in the East Slovakian lowlands (as much as 3 cm at Latorica and Beš), are not at all dangerous as regards stability, but are considering watertightness.

One problem concerning stability in a subsoil results from deformations caused by *filtration failures*, which lead on to a problem of hydrodynamics and dynamics rather than of the mechanics and statics we have talked about in this chapter, and we shall therefore be discussing it in greater detail in Chapter 6.

3.7 Settlement and Bearing Capacity of Soil Beneath Embankments

As already indicated, settlement, by which we mean any vertical movement of the embankment, is of interest to us partly because it frequently provides a picture of the bearing capacity and stability of a subsoil, and partly because it enables us to assess the interaction of the structure with its sealing element. The *magnitude of settlement depends* mainly *on the stress* (σ, τ) in the underlay, and *its deformation properties*, i.e. on the compressibility coefficient C or deformation modulus M, according to which calculation method we choose.

An embankment of height h, width $2a$ at crown and $2b$ at foot, gives rise to a loading distribution (Fig. 3.38), which causes *vertical stress* of magnitude

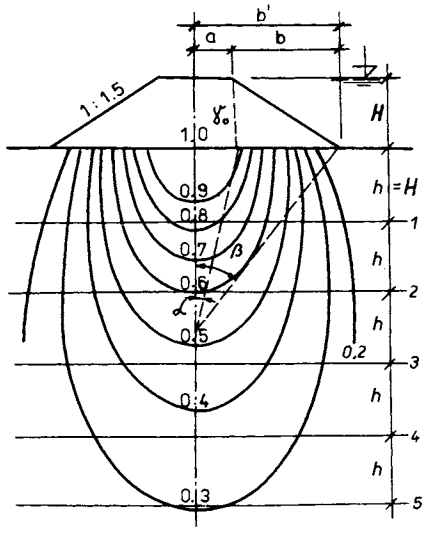

Fig. 3.38. Isobars under a trapezoidal load — after Myslivec (1968).

$$\sigma_1 = \sigma_z = \frac{2\gamma_0 h}{\pi}(\beta + ab). \tag{3.93}$$

Horizontal stress at depth z will be

$$\sigma_3 = \sigma_x = \frac{2\gamma_0 h}{\pi}\left(\beta + \frac{a}{b}\delta - 2\frac{z}{b}\ln\frac{\cos\alpha}{\cos\beta}\right).$$

If we state deformation characteristics, i.e. the modulus of deformation M or the compressibility coefficient, for individual layers of thickness h, we can then determine the *total settlement* s_t. This we do using stress values σ_z and the corresponding loading $\Delta\sigma_z$, and by adding the compressions together. Thus

$$s_t = \sum_{i=1}^{n} \sigma_z h_i \frac{K}{M_{oed}} \tag{3.94}$$

or in an alternative form

$$s_t = \sum_{i=1}^{n} \frac{h_i}{C}\ln\frac{\sigma_z + \Delta\sigma_z}{\sigma_z} \cong \sum_{i=1}^{n} \frac{h_i}{C}\ln\left(1 + \frac{\Delta p_i}{p_i}\right). \tag{3.95}$$

In eqn. (3.94), K is a factor taking account of the degree of consolidation of the soil.

This integration summation method for determining settlement can also be advantageously employed in calculating its time dependence, for which in general we can write

$$s_t = \sum_{i=1}^{n} \eta_i s_{fi}, \tag{3.96}$$

where η_i is the time coefficient of settlement in the i-th layer (is time-dependent), and s_{fi} is the final settlement value.

In most calculations of settlement and bearing capacity, we usually pay regard to vertical stresses and determine the final settlement value. If we wish to take a more exact view of the whole problem of stability in a subsoil, we should take account of some further facts, for instance the way in which vertical, horizontal and shear stresses are actually distributed. As can be seen in Fig. 3.39, in which the paths of *isobars and shear stresses* are illustrated, the local stress paths are quite distinct. Normal stresses are concentrated at the ground surface, whilst shear stresses attain a maximum at a certain distance below. It is worth noticing as well that even with large foot widths, often 20—100 m, this depth is still relatively large. We are talking about concrete examples of 5—30 m depth. This underlines the point that it is an error merely to carry out shallow-ground investigation for levées and canal embankments. Bore depths should in fact be no less than 10—15 m, with at least every fifth bore 3 times as deep. In places where dead river arms intersect, borings shoold always be denser and deeper so as to locate less stable areas, which require

particular attention in embankment foundations, perhaps leading to a change in design of cross-section.

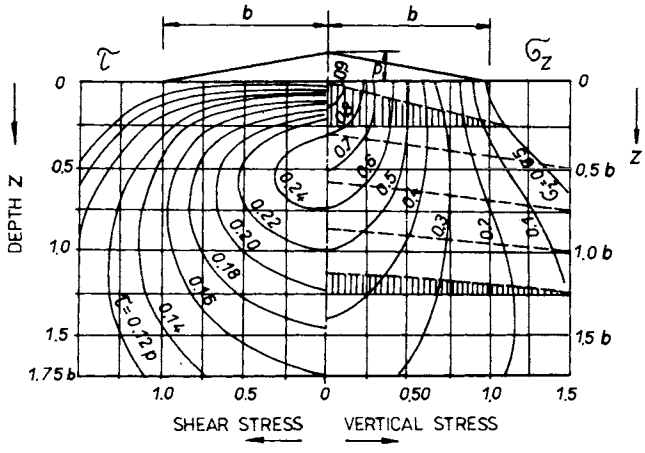

Fig. 3.39. Shear and normal stress under a triangular load — after Jürgenson (1934).

When designing embankments we must make a distinction between *initial settlement*, usually a quite rapid effect, and so-called *consolidation settlement* which often takes many years or even decades to be complete. Initial settlement, most of which takes place during construction, is mainly accounted for by gravels and sandy gravels, and consolidation settlement by fine (usually clayey) soils (Fig. 3.40).

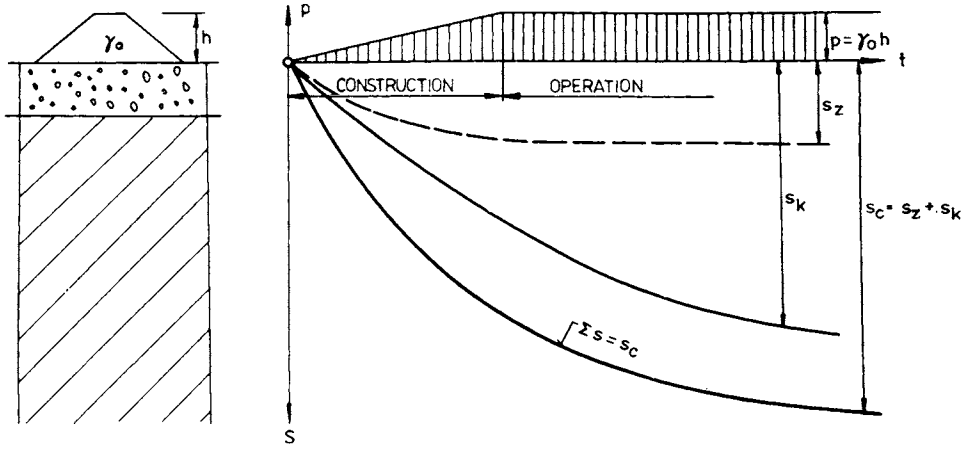

Fig. 3.40. Components of settlement with time of dam construction and operation.

In some cases, values of limiting settlement (s_{max}) and loading (q_{max} or p_{max}) are involved, and a functional dependence is evaluated

$$\frac{s}{s_{max}} = f\left(\frac{p}{p_{max}}\right). \tag{3.97}$$

In the specialist works of Hansen-Brinch and Lundgren (1960), we find relations for principal stress ratios, derived from the Mohr circle of *limiting stress*, as well as a total limit load P. Simplest of all we find

$$\sigma_1 - \sigma_3 = \frac{P}{P_f}(\sigma_1 - \sigma_3)_f. \tag{3.98}$$

From the formulae we already have in eqn. (3.10)—(3.22), and in the settlement equations, it is possible to derive several more interesting and practically applicable expressions for the relation between shear stress τ and the principal stresses. Taking into account the relations between the *stresses*, we can obtain

$$\tau_{max} = \frac{1}{2}\max(\sigma_1 - \sigma_3). \tag{3.99}$$

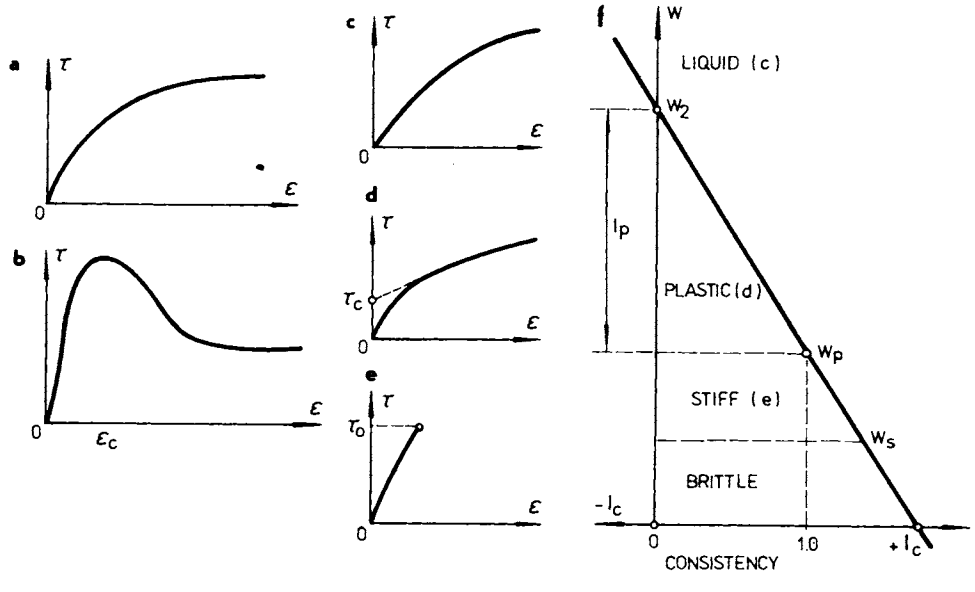

Fig. 3.41. Shear displacement curves and behaviour of cohesive soils. a — normal, b — after critical displacement (peak and residual shearing stress), c — elastic, d — plastic, e — stiff soil, f — behaviour for different consistencies.

In the plastic range, *for plastic loading*, we have

$$\tau_{max} = \frac{p_m}{2+\pi} \cong 0.2 p_m, \tag{3.100}$$

and for a stiff foundation in the *elastic region*

$$\tau_{max} = (0.25 - 0.33) p_m. \tag{3.101}$$

In this connection, we once more have to study the relations between *shear stress* τ *and deformation* ε (Fig. 3.41). Practically, it follows that we cannot guarantee that a subsoil or embankment, which has withstood a certain loading in the past, will be able to do so again. In order to determine this, we must remember the dependence evaluated in Chapters 1 and 2.

Finally, we must recall that with embankment settlement, already discussed, both surface water and pore water have important functions. This applies not only to loams, as discussed in Chapters 3—6, but also to any other soil where the levels of these two regions of water, in the soil and in front of the embankment, both play important roles. Both these effects frequently give rise to such large irregularities in the relations $s = f(p)$ and $s = f(t)$, that they can barely be investigated mathematically (Fig. 3.42).

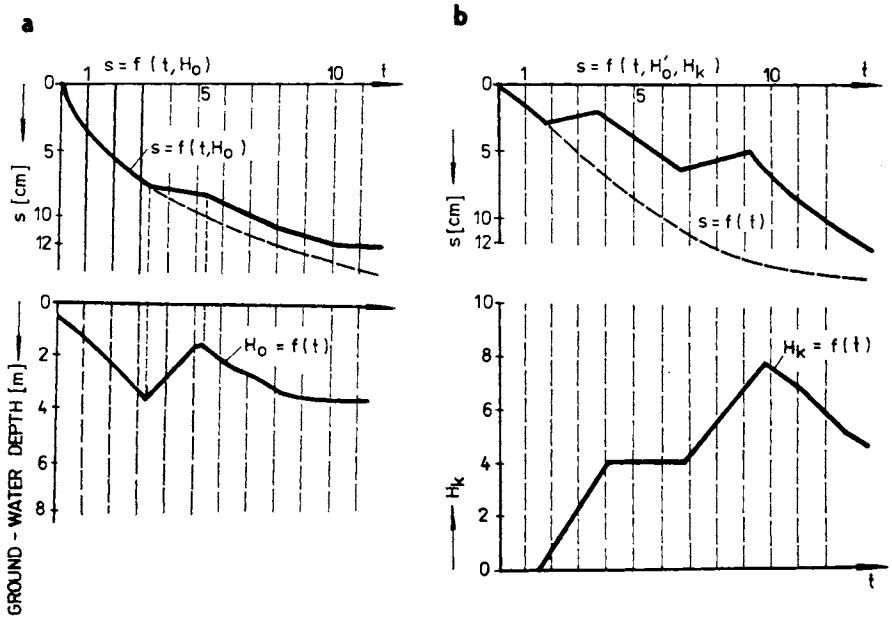

Fig. 3.42. Groundwater (H_0) movement elevation (H_e) and settlement with time. a — influence of groundwater movement, b — changes of water elevation in canal.

Bearing in mind what we have said, it is not possible when calculating an embankment settlement to deduce any absolute applicability. Instead it is the need to keep track of its deformations in every case which should be emphasized, especially on the more suspicious looking cross-sections (crossing dead arms of the river). We occasionally have to make a settlement analysis, studying the causes of the various anomalies which may warn us of dangers from the functional and safety aspects.

3.8 Programming for Computers and New Design Procedures

One common factor in these settlement and stability calculations is that they comprise a large number of simple arithmetic functions. In the past, the tedium of these computations has worked against the application of more precise methods, or any other deeper stability study dealing with various structural details such as sealing layers, filters, drains, etc. Quite often graphical methods have been used and simple elastic solutions, in particular the Petterson method, by which a so-called normal cross-section can be solved. Detailed solutions, paying attention to profiles and subsoil, could only be considered for the design of the largest embankments, for example the earth dam at Nechranice, Digue de la Morge, etc. For such a case, more than 2500 possible shear surfaces were solved, requiring more than 10,000 man-hours for the drawing and arithmetic involved in the design and additional survey of stability.

If we were to progress thus in the various stages of investigation, design and computation for the Danube embankments on a 86-km stretch, the work would keep a single planning and design centre with a personnel of 40 fully occupied for at least two years. Nowadays, with computers coming to the aid of designers, a work group of 6 using "library" programs for solving earth dam stability would suffice. At present there is a library of about 30 different programs already worked out in Czechoslovakia. The simplest are those processing data according to eqns. (3.35) and (3.38), since with this method (Petterson) we have a statistically determinate solution with only a small number of steps (Figs. 3.43, 3.44), and comparatively little demand on computer time. Nowadays, such methods mainly used in the design of canal embankments and levées.

In *computer techniques*, the Petterson and Bishop methods and many other *limiting-equilibrium methods* are used in the analysis of slope stability in principle. Here we consider that failure is about to occur along an assumed circular, non-circular (rotational slip), translational- or compound-slip wedge surface respectively — as the uniform failure surface. It was shown (in Section 3.2) that the shear strength required to maintain a condition of limiting equilibrium is compared with the available shear strength of the soil, giving the average safety factor along

the failure surface. The problem is considered in two dimensions, assuming conditions of plane strain. It has been shown that a two-dimensional analysis gives a conservative result for a failure on a three-dimensional surface, which is why "three-dimensional methods" have also been developed for stability computations.

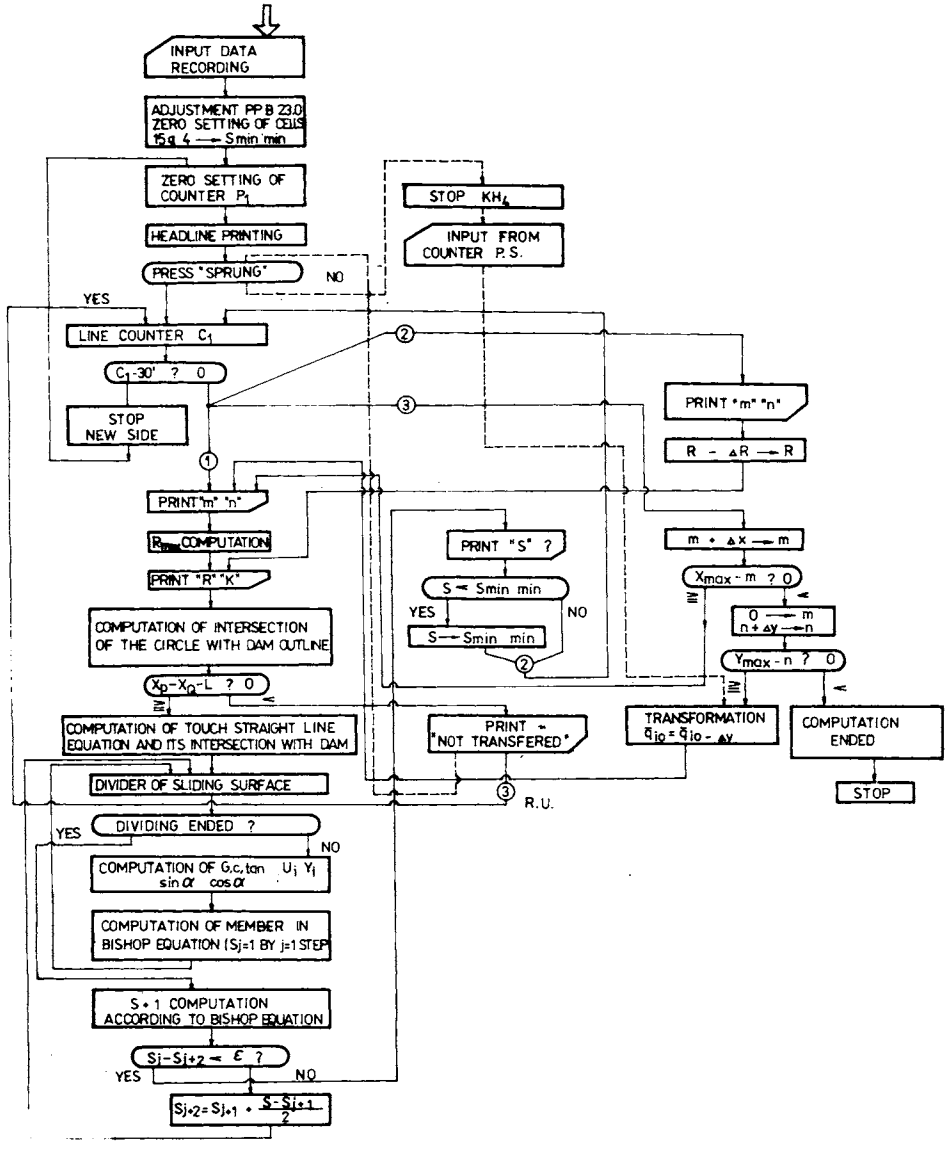

Fig. 3.43. The program of stability computation — after Bishop (1955).

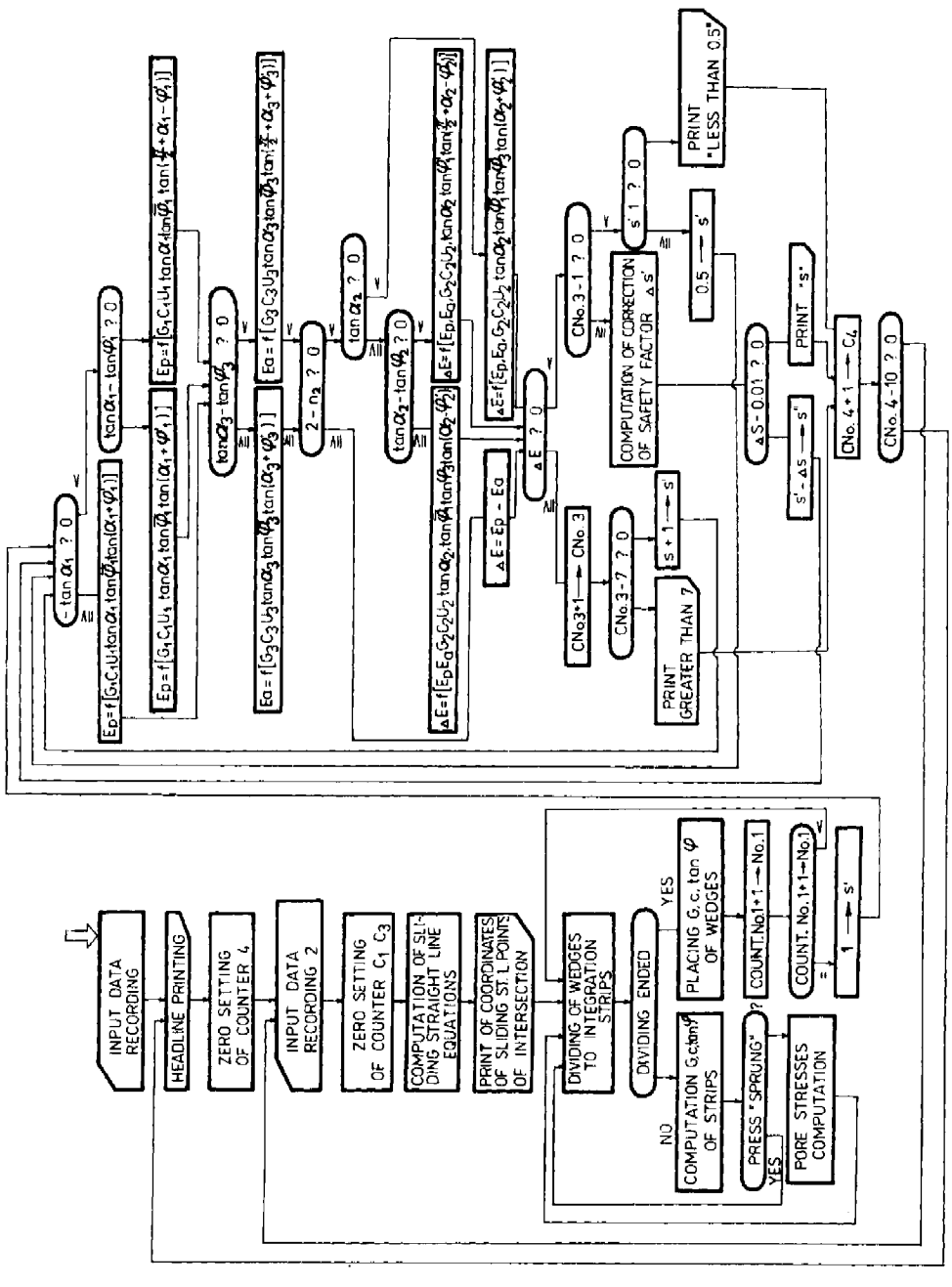

Fig. 3.44. The program of stability computation using the wedge method.

The same can be used with respect to the *static and dynamic load* which can be introduced as a static force too in the plan or in real space.

Stability computation by finite-element methods was mentioned in Section 3.5 and some results of stability computation with respect to the displacement of triangle-nodes-of-points net investigated was given. In this analysis, the classical Hook deformation principle and Mohr—Coulomb failure criterion are the basis of stability computation. At present, nonlinear analysis of stress and strain in soil is more valid in dam design because the load of dams are much higher than before when all nonlinear theories were omitted. Laborious, time-consuming calculations were the main obstacle of introducing nonlinear assumptions in calculation and engineering practice. Duncan and Chang (1970) showed many ways to introduce new progressive methods into earth-structures design. This tendency was stressed by ICOLD — Committee on Analysis and Design of Dams (1977). In Czechoslovakia, an important step in this direction was made by Kratochvíl (1978).

Parallel to this evolution of theoretical mechanics, soil mechanics and calculation methods of strain — stress computation, a large-scale process of nonlinear theory introduction in seepage analysis took place (Bear 1978).

Nonlinear flow in porous media can be solved by finite-element methods by computer, introducing field equations for nonlinear flow assuming that **grad** h and $\boldsymbol{V}$ are opposite vectors (in accordance with Section 2.1). In vector form, the *Forchheimer equation* can be written

$$-\mathbf{grad}\, h = (a + b\,|V|)\,\boldsymbol{V}, \tag{3.102}$$

with unit vector $\mathbf{s}$ normal to the surface of constant h

$$-\mathbf{grad}\, h = -\frac{\partial h}{\partial s}\,\mathbf{s}, \tag{3.103}$$

$$-h_s\mathbf{s} = -h_x i - h_y j, \tag{3.104}$$

$$-h_s\mathbf{s} = (a + b\,|V|)\,\boldsymbol{V} = (a + b\,|V|)\,\boldsymbol{V}_s = (a + b\,|V|)\,(u_i + v_j). \tag{3.105}$$

Here

$$h_s = \frac{\partial h}{\partial \mathbf{s}}, \quad h_x = \frac{\partial h}{\partial x} \text{ and } h_y = \frac{\partial h}{\partial y}, \tag{3.106}$$

$$\mathbf{s} = \frac{h_x}{h_s} i + \frac{h_y}{h_s} j, \tag{3.107}$$

$$u_i + v_j = V_s = \boldsymbol{V}\frac{h_x}{h_s} i + \boldsymbol{V}\frac{h_y}{h_s} j. \tag{3.108}$$

Starting from Forchheimer assumptions, using relations (3.102—3.108), Volker (1969) wrote equation for the *continuity condition*

$$\frac{\partial}{\partial x}\left\{\left[-\frac{a}{2b}+\sqrt{\left(\frac{a}{2b}\right)^2+\frac{|h_s|}{b}}\right]\frac{(-h_x)}{|h_s|}\right\}+$$

$$+\frac{\partial}{\partial y}\left\{\left[-\frac{a}{2b}+\sqrt{\left(\frac{a}{2b}\right)^2+\frac{|h_s|}{b}}\right]\frac{(-h_y)}{|h_s|}\right\}=0. \tag{3.109}$$

With *nonlinear loss* assumpted in the general form

$$I=cV^m, \tag{3.110}$$

the vector form will be

$$-h_s\boldsymbol{s}=(C|\boldsymbol{V}|^{m-1})\,\boldsymbol{V}=(C|\boldsymbol{V}|^{m-1})\,\boldsymbol{V}\boldsymbol{s} \tag{3.111}$$

$$-h_x=(C|\boldsymbol{V}|^{m-1})\,u; \qquad h_y=(C|\boldsymbol{V}|^{m-1})\,v, \tag{3.112}$$

and the *continuity relation* gives

$$\frac{\partial}{\partial x}\left[\left(\frac{|h_s|}{c}\right)^{\frac{1}{m}}\frac{(-h_x)}{|h_s|}\right]+\frac{\partial}{\partial y}\left[\left(\frac{|h_s|}{c}\right)^{\frac{1}{m}}\frac{(-h_y)}{|h_s|}\right]=0. \tag{3.113}$$

Finite-element formulation needs discretization, mathematical expression for boundary conditions and formulation of general variational problem in flow region R.

The boundary conditions for self-adjoint problems are given by

$$\alpha h+\lambda+\beta\frac{\partial h}{\partial n}+\delta\frac{\partial h}{\partial s}=0, \tag{3.114}$$

when α, λ, β, δ are continuously differentiable functions of s on the boundary; $\frac{\partial h}{\partial n}$ is the normal and $\frac{\partial h}{\partial s}$ the tangential derivative on the boundary. Further assumptions are

$$E(h)=\int\int_R G(h, h_x, h_y, x, y)\,dx\,dy \text{ variational problem,} \tag{3.115}$$

$$\frac{\partial G}{\partial h}-\frac{\partial}{\partial x}\left(\frac{\partial G}{\partial h_x}\right)-\frac{\partial}{\partial y}\left(\frac{\partial G}{\partial h_y}\right)=0 \text{ Euler equation for the minimization of } E. \tag{3.116}$$

In *nonlinear flow conditions*, the following requirements must be made

$$\frac{\partial G}{\partial h}=0, \tag{3.117a}$$

$$\frac{\partial G}{\partial h_x} = u = C_1 \left[-\frac{a}{2b} + \sqrt{\left(\frac{a}{2b}\right)^2 + \frac{|h_s|}{b}} \right] \frac{(-h_x)}{|h_s|}, \tag{3.117b}$$

$$\frac{\partial G}{\partial h_y} = v = C_1 \left[-\frac{a}{2b} + \sqrt{\left(\frac{a}{2b}\right)^2 + \frac{|h_s|}{b}} \right] \frac{(-h_y)}{|h_s|}. \tag{3.117c}$$

If the constant C_1 is put equal to -1, these requirements are fulfilled by the function

$$G = -\frac{a}{2b} |h_s| + \frac{2}{3} b \left[\left(\frac{a}{2b}\right)^2 + \frac{|h_s|}{b} \right]^{\frac{3}{2}}, \tag{3.118}$$

and the integral to be minimized is

$$E(h) = \iint \left\{ -\frac{a}{2b} |h_s| + \frac{2}{3} b \left[\left(\frac{a}{2b}\right)^2 + \frac{|h_s|}{b} \right]^{\frac{3}{2}} \right\} dx\, dy \tag{3.119}$$

or

$$E(h) = \iint \left[\frac{1}{C^m} \frac{m}{m+1} |h_s|^{\frac{m+1}{m}} \right] dx\, dy. \tag{3.120}$$

In the finite-element method, using triangular elements with one particular element denoted by nodes I, J, M, the piezometric head h of a particular element IJM may be expressed as

$$h = (a_I + b_I x + c_I y) h_I + (a_J + b_J x + c_J y) h_J + (a_M + b_M x + c_M y) h_M, \tag{3.121}$$

where

$$a_I = \frac{x_J y_M - x_M y_J}{2\Delta}, \quad b_I = \frac{y_J - y_M}{2\Delta}, \quad c_I = \frac{x_M - x_J}{2\Delta}. \tag{3.122}$$

The remaining coefficients (a, b, c with subscripts J, M) are obtained by cyclic permutation of subscripts; Δ denotes the area of triangle IJM.*

By the use of eqn. (3.119) for an element (E^e), after integration and differentiating, we have

$$\frac{\partial E^e}{\partial h_I} \iint \left\{ -\frac{a}{2b} + \left[\left(\frac{a}{2b}\right)^2 + \frac{|h_s|}{b} \right]^{\frac{1}{2}} \frac{\partial |h_s|}{\partial h_I} \right\} dx\, dy \tag{3.123}$$

with

$$|h_s| = (h_x^2 + h_y^2)^{\frac{1}{2}}; \quad \frac{\partial |h_s|}{\partial h_I} = \frac{1}{|h_s|} (h_x b_I + h_y c_I), \tag{3.124}$$

* In contrast to expression (3.89), the triangle nodes are denoted IJM (not i, j, k) to avoid confusion with gradient component i, j (eqns. 3.104—3.108).

$$\frac{\partial E^e}{\partial h_I}=\left\{-\frac{a}{2b}+\left[\left(\frac{a}{2b}\right)^2+\frac{|h_s|}{b}\right]^{\frac{1}{2}}\right\}\frac{1}{h_s}(h_x b_I+h_y c_I)\iint \mathrm{d}x\,\mathrm{d}y. \tag{3.125}$$

By setting the expression for

$$h_x=\frac{\partial h}{\partial x}=\left(b_I h_I+b_J h_J+b_M h_M\right),$$

$$h_y=\frac{\partial h}{\partial y}=\left(c_I h_I+c_J h_J+c_M h_M\right),$$

and

$$\iint \mathrm{d}x\,\mathrm{d}y=\Delta$$

in

$$\frac{\partial E^e}{\partial h_I}=Ab_I(b_I h_I+b_J h_J+b_M h_M)+Ac_I(c_I h_I+c_J h_J+c_M h_M), \tag{3.126}$$

where

$$A=\frac{\Delta}{|h_s|}\left\{-\frac{a}{2b}+\left[\left(\frac{a}{2b}\right)^2+\frac{|h_s|}{b}\right]^{\frac{1}{2}}\right\}, \tag{3.127}$$

eqn. (3.126) is evaluable for node I.

Three differentials associated in an element characterize its potential (potential gradient)

$$\left\{\frac{\partial E^e}{\partial h}\right\}=\begin{Bmatrix}\dfrac{\partial E^e}{\partial h_I}\\[2ex]\dfrac{\partial E^e}{\partial h_J}\\[2ex]\dfrac{\partial E^e}{\partial h_M}\end{Bmatrix}. \tag{3.128}$$

$$\left\{\frac{\partial E^e}{\partial h}\right\}=[S]\,\{h^e\}. \qquad S_{IJ}=Ab_I b_J+Ac_I c_J. \tag{3.129}$$

The final equations are obtained by adding all parts of a differential such as $\dfrac{\partial E}{\partial h_I}$ for all elements connected at node I and equating to zero

$$\frac{\partial E}{\partial h_I}=\sum\frac{\partial E^e}{\partial h_I}=0, \tag{3.130}$$

$$\Sigma[S]\,\{h^e\}=0. \tag{3.131}$$

A narrow band width set of simultaneous equations, which may be solved by an iterative method for all nodes is the result of a finite-element method of calculation. The procedure consists of calculating the $\boldsymbol{S}$ matrix in terms of these

initial (optional) values and then solving for more accurate values of (h_I, h_J, h_M) by iteration.

Hundreds to thousands of equations must be solved to allow us to evaluate and plot seepage characteristics in the flow region—needed to evaluate flow net, pore-water pressures (u), effective stresses (σ') if stability computation is desired. Seepage quantity, hydraulic gradients and velocity magnitudes are the product of such investigation. The danger of internal erosion (piping) within the dam can be shown. This is not the case in classical (slope) stability computations.

An *effective stress analysis* is relevant for all conditions with the value of pore-water pressure (u) being obtained from the static water-table level or the appropriate flow-net. Pore water pressure may thus be an independent variable, determined from the static water-table level or from the flow net for condition of steady seepage, or may be dependent on the total stress changes tending to cause failure.

In the past laborious graphical methods are used in such investigation, over and above analytical methods which are very limited. *Stability charts* enable us to find seepage forces and safety factors of the dam under *special load conditions*, such as rapid drawdown (Morgenstern 1963).

In dam design, many load conditions must be investigated. Including the *construction period*, the most important are:

(a) the *end of construction* — with high water content and a high u value;
(b) *steady seepage* — flowline in the fully saturated state;
(c) *drawdown of* the reservoir level will result in a change in pore water-pressure distribution (equivalent to a change of stability conditions).

Variable load conditions can be observed by appropriate computer programming.

A special stability analysis and computation, appropriate for use of computer, and for a multishaped failure surface (circular, non-circular or compound) was presented by Morgenstern and Price (1967). In this method the soil mass above the failure plane is divided into sections by a number of vertical planes and the *problem* is rendered *statistically determinate* by assuming relationship between the force E and X on the vertical boundaries between each section. This assumption is of the form

$$X = \lambda\, \mathrm{f}(X)\, E, \tag{3.132}$$

where $\mathrm{f}(X)$ is an arbitrary function describing the pattern in which the X: E varies across the soil mass and λ is a scaling factor. The value of λ is obtained as a part of the solution, along with the safety factor m. The values of the forces E and X and the point of application of E can be determined at each vertical boundary.

The wave propagation in saturated soils is of interest, and can be investigated by computer calculation. According to Biot theory, the fluid can be assumed to be

a compressible liquid free to flow through the pores. Assuming a conservative physical system which is statistically isotropic, some simplifications can be made. Disregarding the dissipative forces, the *dynamic equations* of equilibrium in the x direction are

$$\frac{\partial \sigma_x}{\partial x}+\frac{\partial \tau_{xy}}{\partial y}+\frac{\partial \tau_{xz}}{\partial z}=\frac{\partial^2}{\partial t^2}\left[\bar{\varrho} u_x+\varrho_A(u_x-U_x)\right], \tag{3.133a}$$

$$-\frac{\partial p}{\partial x}=\frac{\partial^2}{\partial t^2}\left[\varrho^* U_x+\varrho_A(U_x-u_x)\right], \tag{3.133b}$$

in which ϱ_A is the mass density of an apparent mass, U_x is the displacement of the fluid, u_x is displacement of particles. These equations are treated by Richart et al. (1970). Practical aspects and calculation methods can be found in Seed (1973) and Seed et al. (1966).

In some cases, static and dynamic analysis must be made. In such a case, many more characteristics of the soil are needed, such as deviator stress and pore pressure versus axial strain. Also the stress paths of a great number of test performed are required to evaluate the dynamic reponse of the dam. A comparison with the cyclic shear stress necessary to produce liquefaction can be carried out when the testing program is available (Casagrande 1959, 1974).

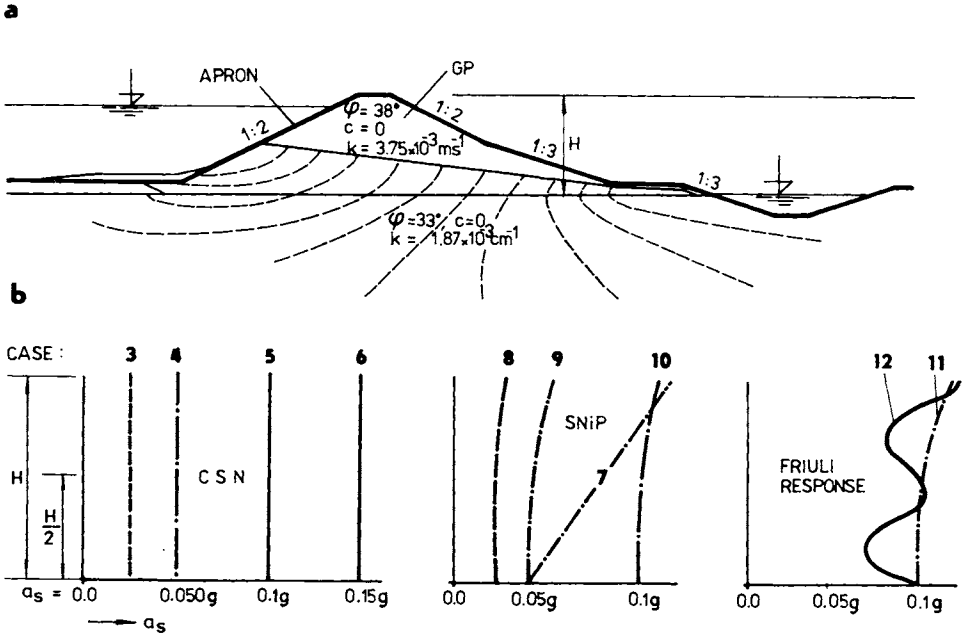

Fig. 3.45. Stability computation. a — cross-section, b — assumptions made in different programs.

Let us present some results obtained from computing — using the *program of Polko and Hobst* (1978) devised for stability computation of dams of head-race canal of the hydroelectric station Gabčíkovo in the Danube valley (Fig. 3.45). A homogeneous earth (sandy gravel) dam with a permeable body ($k = 3.75 \times 10^{-3}$ m s^{-1}, $\gamma = 20.0$—23.0 kN m^{-3}, $\Phi = 38°$, $C = 0$) with concrete apron sealing (slope 1 : 2), lying on permeable alluvium ($k = 1.87 \times 10^{-3}$ m s^{-1}, $\Phi = 33°$, $c = 0$) was investigated by computer which allowed a variety of possibilities for the analysis of slope stability. Two cases using classical methods of slices (Petterson and Bishop) and ten incorporating seismic effects of earthquakes — were analysed and calculated in detail. Different values of acceleration in cases 3 to 6 were used taking the Czechoslovak Standard (CSN) ($a = 0.025$ g, 0.05 g, 0.1 g, 0.15 g) and the USSR standard (SNiP). Also the special calculation method of Napetvaridze and harmonic accelerogram response and real accelerogram response of Friulu earthquake were used. The differences were not considerable ($m = 1.53$—1.74) except in the seismic cases.

In the seventh case, the seismic coefficient K_s increased by 2.5 (shown in Section 3.2, eqns. 3.41—3.44 and Fig. 3.10a) from the toe to the top.

A new approach was made by Polko and Hobst (1978) using a discontinuity model with multiple mass centres governing its movement after following equilibrium conditions by proper vibration

$$\frac{\partial}{\partial x}\left(GS(x)\frac{\partial \bar{w}(x,t)}{\partial x}\right)=0,$$

$$\lim_{x\to x^+}\frac{\partial \bar{w}(x,t)^+}{\partial x}-\lim_{x\to x^-}\frac{\partial \bar{w}(x,t)^-}{\partial x}=\Delta\bar{\psi}_i=\frac{m_i}{G_iS_i}\frac{\partial^2\bar{w}(x,t)}{\partial t^2}\bigg|_{x=x_i}. \tag{3.134}$$

We assume G_i constant shear modulus, S_i (surface) at node i with mass m_i and total displacement $\bar{w}$ in horizontal direction. The profile of the function $F(x)$, $G(x)$ allows us to take into account the supple state of the subsoil expressed by the matrix relation

$$\begin{Bmatrix} w_N \\ \varphi_N \end{Bmatrix}=\begin{bmatrix} \bar{w}_M & \bar{w}_T \\ \varphi_M & \varphi_T \end{bmatrix}\begin{Bmatrix} M_N \\ T_N \end{Bmatrix}, \tag{3.135}$$

where w_N, φ_N are displacement and rotation, M_N, T_N are the moment and shear forces acting in the dams footing base.

The value of T_N will be obtained as the second component of the state vector

$$w_N=\begin{Bmatrix} w_N \\ \psi_N \end{Bmatrix} \text{ giving } T_N=G_NS_N\psi_N, \tag{3.136}$$

if $\Delta\psi_N$ denotes the discontinuity of shear angle at node i and in the footing bottom ($\Delta\psi_N$).

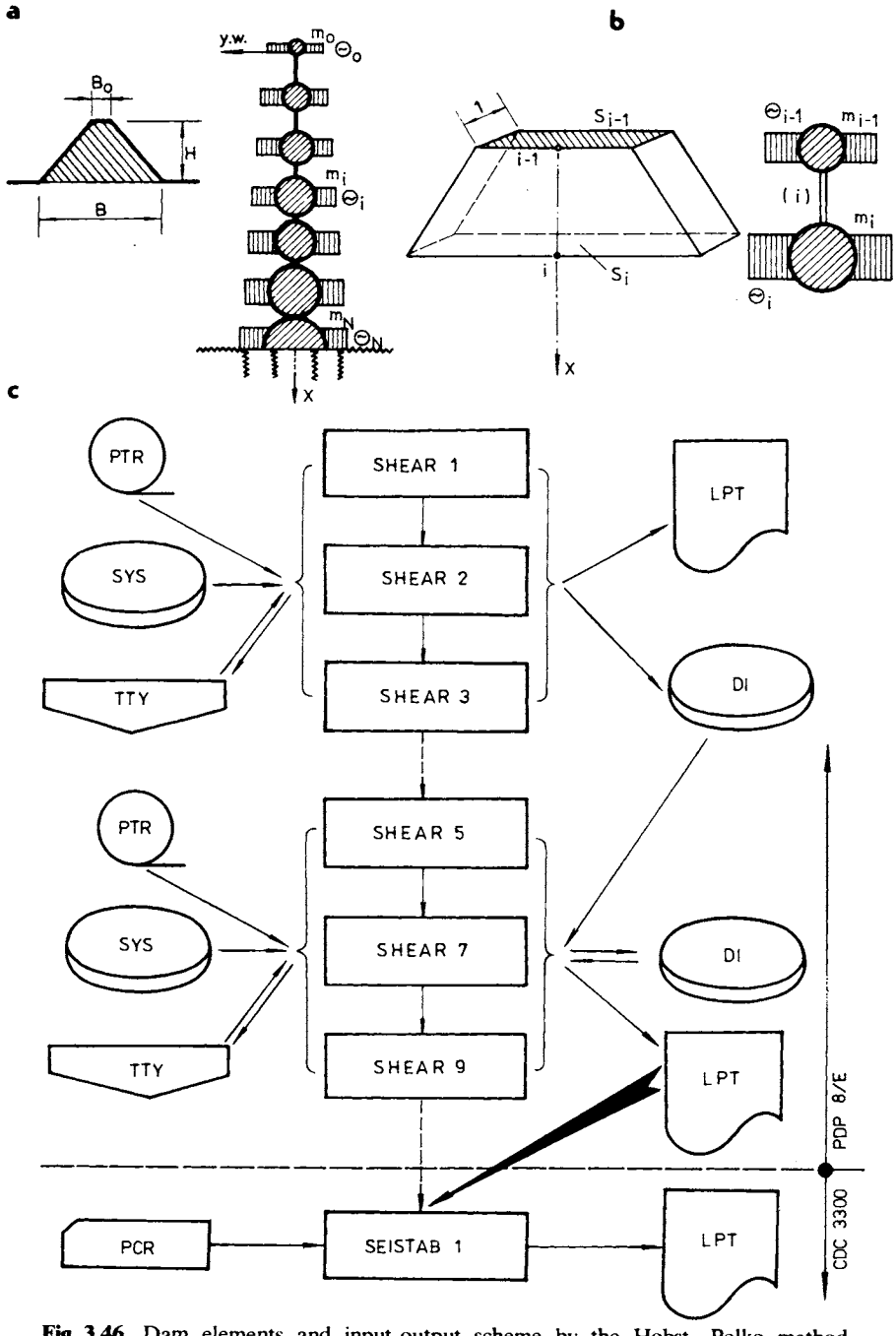

Fig. 3.46. Dam elements and input-output scheme by the Hobst—Polko method. a — cross-section and discretization of the profile, b — m_i element of the "wall", c — programming scheme.

The rotational moment of the body related to the footing bottom is

$$M_N = \omega^2 \sum_{i=0}^{N} [\varphi_N \Theta_i + w_i m_i (H - x_i)] , \tag{3.137}$$

and depends on the frequency a and rotational moment of inertia Θ.

Models of the "dam elements" and input-output scheme of the programming using this method are shown in Fig. 3.46.

The results of detailed analysis made for 365 failure surfaces (rotational slips) and numerical seismic stability analysis of the Danube canal dams have been evaluated by Hobst and Polko. They are expressed by the value of the safety factor (m_s) and are given in Table 3.6 and can be useful in design criteria. Of these criteria (Richart et al. 1970), we limiting mention dynamic conditions (vibration amplitude at operating frequency, velocity, acceleration), possible modes of vibration — coupling effects, fatigue failures, environmental demands, limiting displacement.

Table 3.6. Safety factor m_s calculated for various loading conditions, following different methods

Case number	State of load following	Value of seismic acceleration a [g]	Safety factor m_s
1	Petterson	0	1.56
2	Bishop	0	1.56
3	CSN 73 6503	0.025	1.47
4	CSN 73 6503	0.05	1.39
5	CSN 73 6503	0.1	1.19
6	CSN 73 6503	0.15	1.02
7	Napetvaridze	0.05	1.21
8	SNiP II-A.12-69	0.025	1.46
9	SNiP II-A.12-69	0.05	1.37
10	SNiP II-A.12-69	0.1	1.18
11	Harmonic accelero-gram response	0.05	1.19
12	Friuli accelero-gram response	0.086 (max)	1.26

It is worth mentioning that in designing the canal embankments of the hydroelectric station in Gabčíkovo, the *probability of structure destruction by earthquake*, as an extreme rare loading phenomenon was calculated. The author of this calculation method (Mistéth 1967) made the assumption that the seismic load $S(t)$, as the *bearing capacity* of the stucture $R(t)$, is a random variable which is related to the *permitted risk* $P\mu(t)$. It follows

$$PR(t) \times PS(t) = P\mu(t).$$

In this case — for $P\mu(t) = 1 \times 10^{-4}$ $(m = 1)$ and assumed life-time of 2000 years is

$$PR(t) = \frac{1 \times 10^{-4}}{PS(t)} = \frac{1 \times 10^{-4}}{5 \times 10^{-2}} = 2 \times 10^{-3}.$$

Taking into consideration the factors of safety m_s, obtained by calculation in designing the canal embankments, he concludes that it was designed for a load with a probable occurrence of $P\mu_s(t) = 2 \times 10^{-5}$ to 1.2×10^{-4}.

All these special demands can be found in new design procedures using new analysis methods of soil mechanics and soil dynamics with the help of computers. Also old canal embankments and levées can be investigated in this way, but the insufficiency of appropriate soil characteristics (both of dams and their subsoil) will limit the use of detailed computer analysis mentioned above.

Chapter 4

CONSTRUCTION OF EMBANKMENTS AND THEIR VARIOUS CONCRETE STRUCTURES

Embankment construction is obviously governed primarily by the purpose it is designed to serve, and the sort of material which can be used.

Local conditions and demands relating to the volume of transported water affect construction design. In hydroelectric canals, relatively large quantities are usually transported across flat areas (Fig. 4.1a). When smaller quantities have to be coped

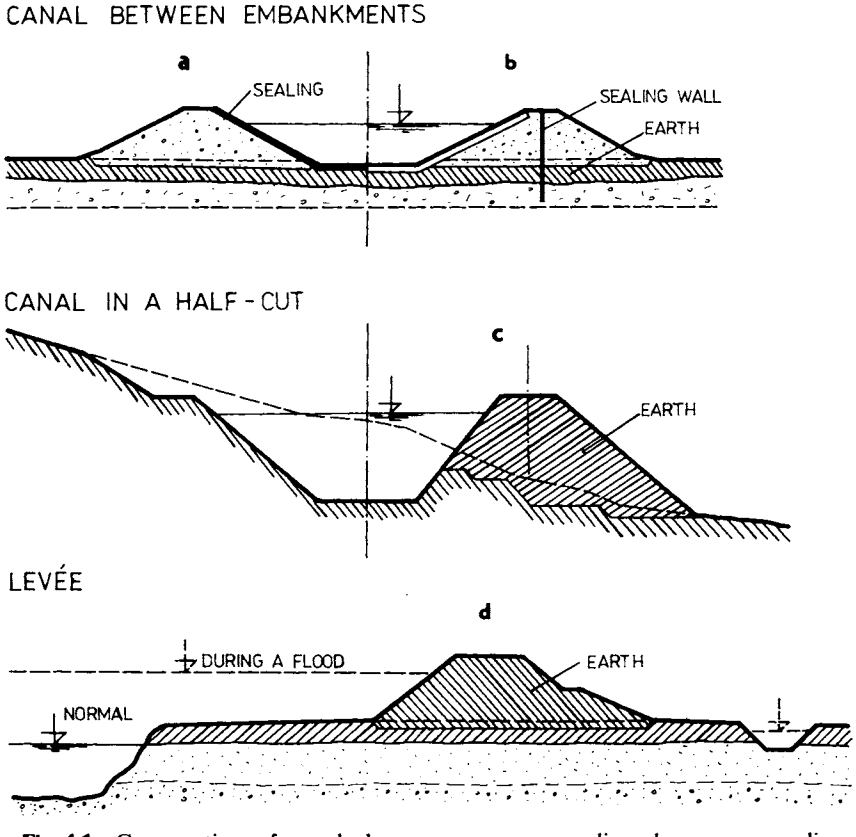

Fig. 4.1. Cross-section of canal dams. a — apron sealing, b — core sealing, c — homogeneous dam, d — homogeneous dam with a "berm".

with in hilly terrain, shafts are most frequently used. For irrigation canals (Fig. 4.1b), the embankments are usually formed by transverse excavation, and the channel is therefore mainly contained within a trench and only partially lined by an embankment (Fig. 4.1c). A solution of this type is also often conditioned by the *demands imposed by the lie of the land* (i.e. gravitational water supply to the appropriate sectors), which can frequently be satisfied by setting out the path of the canal along a contour line. When an embankment has to be built on sloping ground, there are attendant increased problems in forming a junction with the subsoil, i.e. forming a binding or specially graded junction area. Assuming the canal to be sealed, as is the case with larger canals, there are high demands made in this respect on the subsoil interface.

Generally, levées cause fewest problems (Fig. 4.1d) as far as sealing is concerned, and none at all in embankment formation (subsoil binding). Experience drawn from the construction and maintenance of the world's best-known levée systems (on the Mississippi in the USA, the Jamuna in India, the Yellow River in China, and the Danube in Europe) shows that most of the difficulties met in functional construction occur at a certain depth below the soil surface, where layers of high and low permeability alternate, a problem which we shall deal with further in Chapter 6.

These facts support the conclusion that we should be considering levées and canal embankments separately.

4.1 Cross-section and Structural Details of Canal Embankments

4.1.1 Embankment Dimensions

The basic dimensions of embankments are usually derived straight from the height of water above the ground surface which has to be held back (Fig. 4.2). To this height a certain excess h_p must also be added, ensuring that no overspill occurs even in extreme circumstances (due to very strong winds or canal-transport waves). The danger to examine is therefore that a wave may appear above the static or hydrodynamic surfaces, which then spills over the embankment lip. Three components to this added *freeboard height*

$$h_p = \Sigma \Delta h = \Delta h_1 + \Delta h_2 + \Delta h_b. \tag{4.1}$$

The value of Δh_1 can be found arithmetically using eqn. (3.48b), and the upwash Δh_2 using eqn. (3.55), or alternatively we can treat them according to certain standards, but there must be some reservations, as when determining the additional safety margin, which is not differentiated.

Furthermore, some instructions recommend the inclusion of the possibility of an ice barrier forming of height Δh_b.

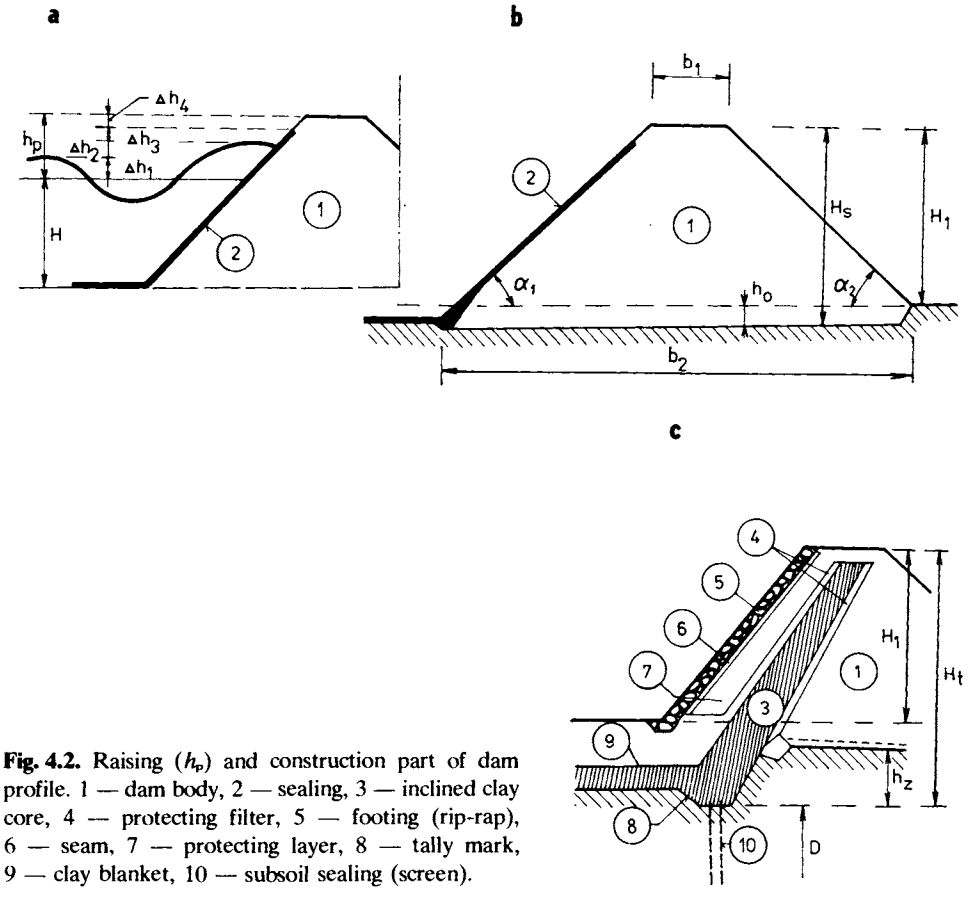

Fig. 4.2. Raising (h_p) and construction part of dam profile. 1 — dam body, 2 — sealing, 3 — inclined clay core, 4 — protecting filter, 5 — footing (rip-rap), 6 — seam, 7 — protecting layer, 8 — tally mark, 9 — clay blanket, 10 — subsoil sealing (screen).

Nowadays, the opinion prevailing is that large and important hydroelectric canals pose a much greater threat to person and property than smaller ones, and therefore it is necessary in canal design to make a distinction between large ($Q \geq 100$ m^3 s^{-1}) and small ($Q \leq 30$ m^3 s^{-1}) canals. In this connection, Table 4.1 gives the minimum safety margins found in various literature (Korolev 1956).

Reinforcement (sealing) of type A means mainly plastic (i.e. earth) sealing, stabilization using bitumen and stone backfill, whereas those of type B are concrete or asphaltic concrete, large area prefabricates, etc.

We generally obtain the vertical *height above ground level* from the depth of water to be retained H and the freeboard h_p, i.e. as in Fig. 4.2b. Thus

$$H_1 = H + h_p.$$

The *structure's actual height* H_s is usually greater still. It is simply the previous figure H_1 with the addition of the vegetation (humus) cover h_0; i.e.

$$H_s = H_1 + h_0.$$

Table 4.1. The raising of the structure in relation to water discharge

Raising with respect to safety (total)		Values of raising for various Q		
		$Q \geqq 100$ [$m^3 s^{-1}$]	$Q = 30—100$ [$m^3 s^{-1}$]	$Q \leqq 30$ [$m^3 s^{-1}$]
Δh_H [cm]	Pavement A	45—60	35—45	25—30
	Pavement B	40—55	30—40	20—25
min h_p [cm]	Pavement A	70—90	40—50	40—45
	Pavement B	60—80	50—65	30—35

In such earthen structures we also include a further embedding depth into the subsoil, which we shall call h_e. The *total height* of the embankment H_t is therefore given by the sum of all these components,

$$H_t = h_e + h_0 + H_1. \tag{4.2}$$

Since a 'tooth' of sealing can be as high as several meters and h_0 is between 0.3 and 1.0 or even more, giving the freeboard h_p as greater than 1 m, the total height may be up to twice as large as the depth of water to be retained H, from which the remaining heights are derived. Thence we also derive the length of the sealing carpet (L), assuming that the bottom is not completely sealed, and the depth of the sealing diaphragm or equivalent vertical element (D).

To fix the amount of material to be used on a cross-section, we need of course the widths of the embankment at the crown ($b_1 = 2—10$ m, usually 3—6 m) and *the foot* b_2. For a trapezoidal shape, we have (see Fig. 4.2b)

$$b_2 = b_1 + H_1 (\cot \alpha_1 + \cot \alpha_2). \tag{4.3}$$

From the basic relations for volume we know that the mass of an embankment increases approximately quadratically with height.

As regards the composition of levée cross-sections, there are usually three basic types of profile: homogeneous low permeability soils without sealing; heterogeneous with both fine and coarse grains in the soil; homogeneous but permeable soil with a sealing apron.

4.1.2 Typical Embankment Sections

Homogeneous embankments (Fig. 4.3a), built of low permeability soils (clay) are usually considered when they are constructed on impermeable soil or a rocky base. If there is enough suitable clay, a uniform body can be formed, bonded

directly onto the underlying soil. In this case, there is no need to seal the canal bottom. For the most part, this solution can only be considered when the water table is deep enough for construction with the clay (soil type ML, CL, OL or MH — see Table 1.1) not to hit on any serious difficulty. The profile which is used when we need to construct an embankment on a permeable foundation soil is that shown in Fig. 4.3b. As explained in the previous chapter, if we talk of pore pressure during

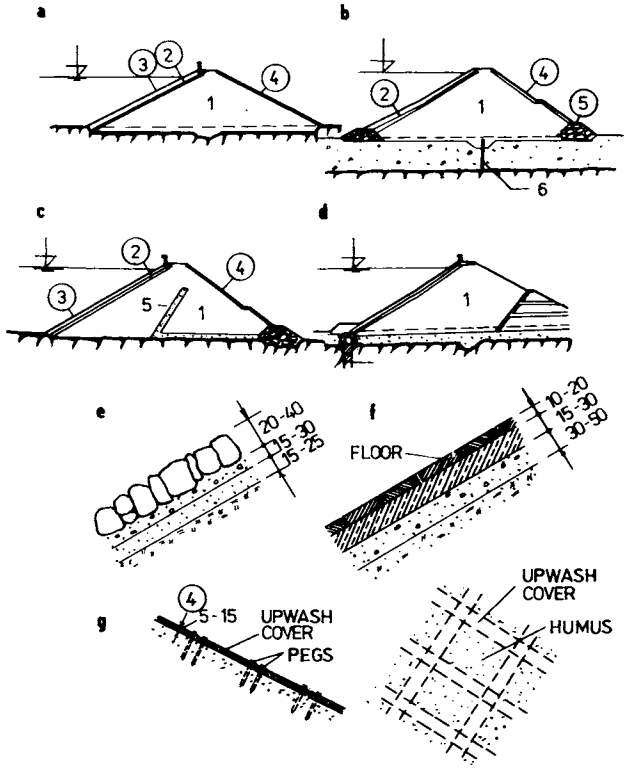

Fig. 4.3. Cross-section and slope protection. a — homogeneous dam on impermeable sub-base with protecting pavement, b — dam on permeable sub-base sealed by sheet piling, c — with inside filter-drain, d — with sandwich filter layers on the downstream toe, e — upstream rocky pavement with filter layers, f — articulated concrete pavement, g — downstream slope protection by humus cover; 1 — dam body, 2 — gravel seam, 3 — pavement of upper slope, 4 — protection of downstream slope, 5 — filter (drain), 6 — sheet piling.

normal operation and during heavy and persistent rain in connection with total stability, then for the higher embankments, formed from soils having a coefficient of permeability less than $k = 10^{-6}$ cm s^{-1}, it is advisable to design the cross-section as in Fig. 4.3c or 4.3d.

4.1.3 Embankment Slopes and Details

The remaining sections shown indicate the arrangement of slope reinforcement on the upstream and downstream sides. It is worth adding that *protection* using a *concrete flooring* laid on top of a concrete layer is relatively complicated and therefore also expensive.

Under certain conditions, the use of aerated hexagonal blocks, as in Fig. 4.4, gives good results. For levées, semi-hollow *reinforcement blocks* have been found to be very satisfactory. The shape of a levée profile is also complicated by subsoil conditions. If, below the level of the interface of embankment body and subsoil,

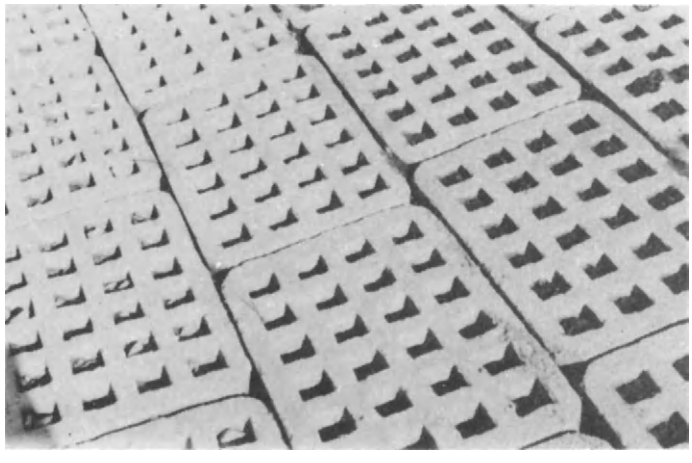

Fig. 4.4. The pavement as upstreamslope protection.

there is a layer of permeable gravel overlying a rock foundation, which simultaneously comprises the canal bottom, the solutions shown in Figs. 4.5a or 4.5b may be suitable. In one case a locking tooth, holds the whole canal profile watertight and in the other a low underground wall (Fig. 4.5c).

Closing off the canal with vertical elements is mainly done on large canals of wide cross-section, the width being at least five times greater than the length of the corresponding vertical sealing elements, since this is always many times more costly than *horizontal sealing.*

Korolev (1956) cites examples of embankments on large canals with flows of over 1000 $m^3 s^{-1}$, which have the peculiarity of not being bonded to the subsoil in a watertight fashion and indeed have permeable subsoils. Looking at the degree of permeability of sandy clays incorporated into the cross-section, these profiles are relatively large and massive with very shallow slopes. Erosion of the slopes is

limited by means of a thick *stone covering*, which at the same time increases the stability (Fig. 4.6a). The reasoning behind this additional allowance of cross-section *mass* with *index of material* used is

$$i_m = G/F_w = 38,$$

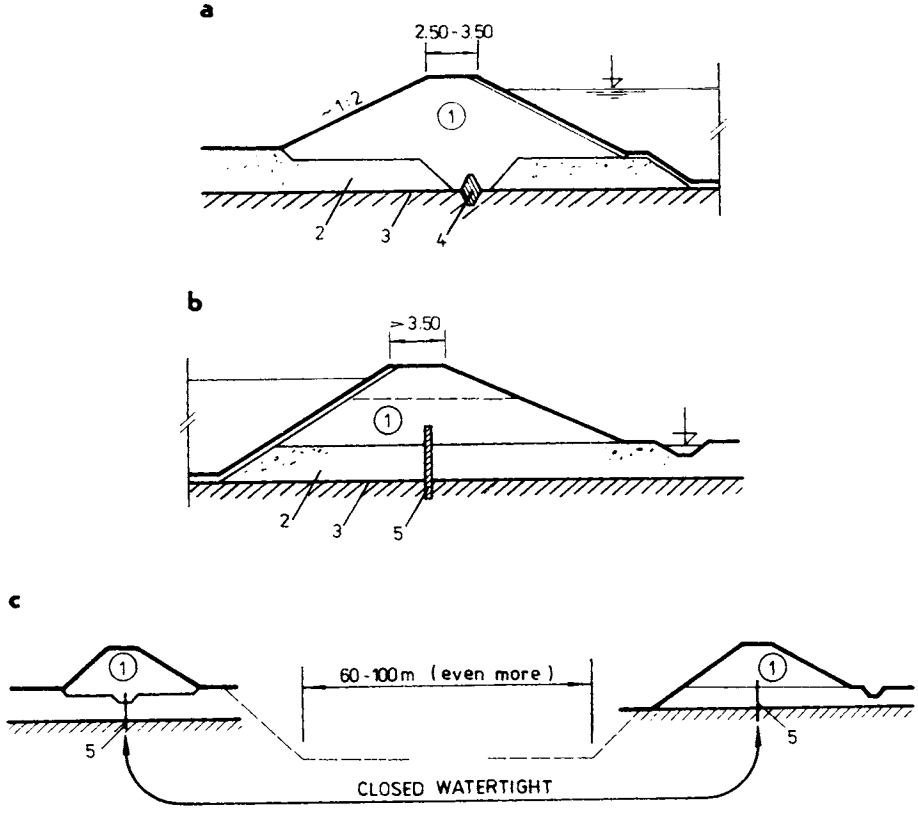

Fig. 4.5. The binding possibility of a dam built on alluvial layer. 1 — dam body, 2 — gravel, 3 — impermeable sub-base, 4 — tally mark of concrete, 5 — slurry trench wall.

where

$$i_m = \frac{\text{weight of soil used on 1-m length of embankment}}{\text{water pressure on that length}},$$

which is more than three times the massivity of gravel embankments ($i_m = 8—12$). Such a cross-section has many advantages if resources of material in the immediate locality are being fully used, since it is not only transportation costs that drop, but also there is no storage problem and ground upheaval is therefore reduced.

However, the solution indicated is only of any technical and economic advantage when the earth along the line of a canal has relatively constant soil-mechanics properties (Fig. 4.6b). Soil heterogeneity which usually means alternating cohesive (clays) and non-cohesive (sand, gravel) soils can complicate matters, mainly as regards soil compaction and may occasionally lead to an inevitable grading, so that all advantage is lost. Thus the above solution becomes unattractive, although from the point of view of haulage and general neatness it would seem desirable. An alternative studied for the Danube canal was of this type and would have been built in part by transverse soil transposition into the embankment (Fig. 4.6c, d).

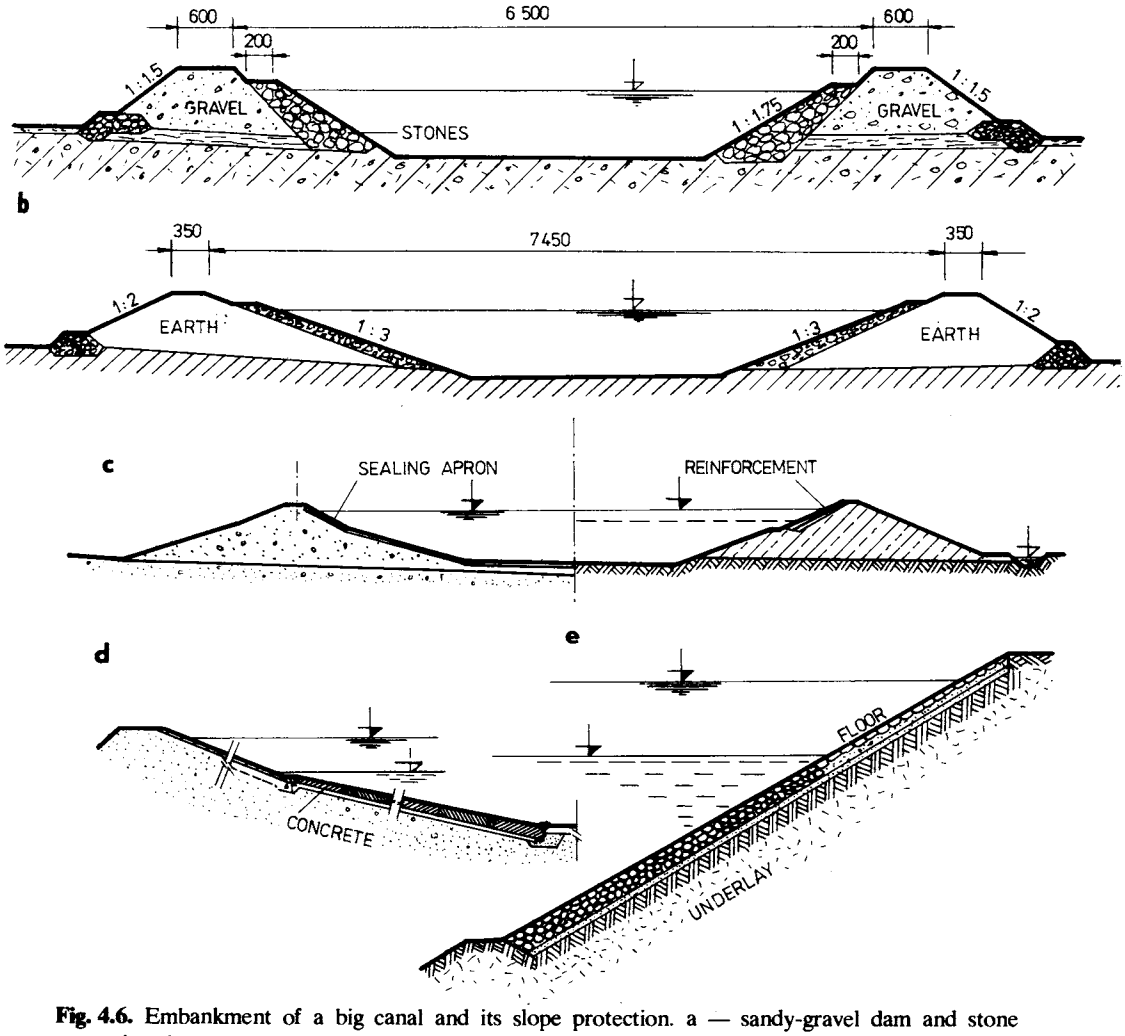

Fig. 4.6. Embankment of a big canal and its slope protection. a — sandy-gravel dam and stone protection, b — earth dam, c — total arrangement of sealing and protection, d — concrete plates, e — rip-rap.

4.1.4 Heterogeneous Embankments

Heterogeneous embankments have cross-sections built of several different sorts of soil. According to this definition, we could also consider the embankments depicted in the previous figure to be heterogeneous. In this type of case, however, the profile is made up with stoney material forming a protection for the slope. In heterogeneous embankments we usually put *coarse-grained* soil and stones *into the body* (stabilizing part), and *finer soil makes up the sealing section.*

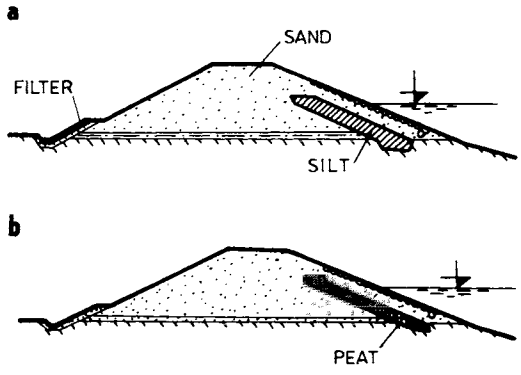

Fig. 4.7. Heterogeneous dam profile filled with sand — after Uginchus (1953). a — inclined silt core, b — peat sealing.

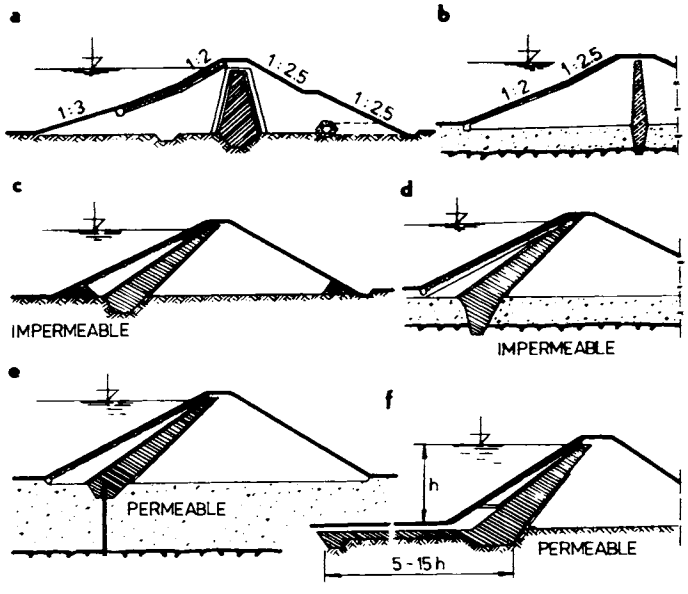

Fig. 4.8. Heterogeneous dam profiles with clay and concrete core. a — clay core, b — concrete core, c, d — inclined clay core, e — clay core and wall, f — inclined clay core and clay blanket.

As Uginchus (1953) demonstrates, it is also possible occasionally to use sand in the stabilizing part of an embankment and to compose the *sealing element of clay* (Fig. 4.7a) or even peat (Fig. 4.7b), which with perfect treatment (compaction and mixing with sandy particles or silt) yields a very good sealing material. Embankments of this sort have been very successful on the White Sea — Baltic canal, and also the Moscow canal.

Besides this, it is possible to shape the profile of a heterogeneous levée as for a larger dam. Such types of profile would normally be considered only for the high banks necessary for hydroelectric canals, and even then when they support water transport only. One advantage of these profiles (Fig. 4.8) is that they have a sealing element which is amply protected by a thick *protective layer*, which even if anchors have to be instituted, cannot be penetrated. However, a definite disadvantage is the almost general tendency (with the exception of those with hard cores) to failure as a result of large and sudden swings in surface level, which are rather frequent on hydroelectric canals when the volume of transportation tends to peak.

Apart from this drawback, heterogeneous embankments have certain further technical disadvantages, mainly because in construction various different technologies come into play, complicating the organization of the work and raising costs as we shall discuss later. For this reason, heterogeneous embankments are much rarer on canals than when used as dams.

4.1.5 Homogeneous but Permeable Embankments with Sealing Aprons

Embankments *built of sandy gravel*, protected by a suitable *sealing apron*, are always preferred for both hydroelectric and major arterial canals. In this sort of canal the natural technological benefits of permeable soil, simple construction as well as static advantages (high shear strength), are used to the full. Any lack of structural material is made up by quality material (concrete, asphalt, plastic sheeting, etc., and even reinforced concrete).

As already emphasized, in this sort of case (Fig. 4.9) the cross-section is the simplest and in general the massivity is least. Usually $i_m < 10$.

With this type of embankment, it is never difficult to form an asymmetrical profile (as we indicate in Fig. 4.10a), which is a relatively common requirement for irrigation channels and hydroelectric supply canals. Forming a profile from fine-grained soil is awkward in this case for two reasons. Such soil has a small angle of internal friction and the embankment must therefore have very shallow bank angles thus increasing the massivity of section substantially. Also, the water has a marked effect on the stability of such soils. In canals which load along a hillside, we must always reckon that water flowing down the slope may saturate the embankments, as it were, from below. *Embankments built of fine-grained material* (clay) not only have the problem that when saturated they tend to break up, but

also that they have an *unfavourable effect on the stability* of the whole region through which they pass. The water moving down the slopes comes to a halt at the embankment, and may rise to the surface, rendering the groundwater logged. An

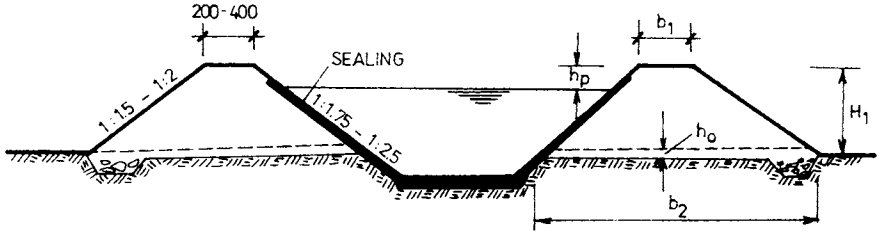

Fig. 4.9. Permeable dam profile with concrete sealing apron.

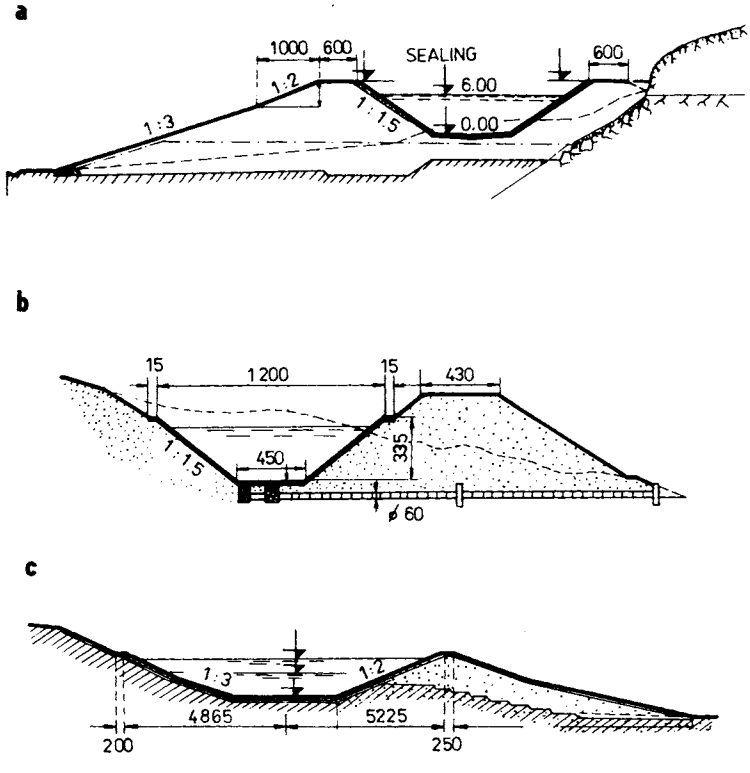

Fig. 4.10. Canal-dam profiles in an inclined territory. a — asymmetrical profile with shallow tally mark, b — dam with parallel and cross drainage, c — stepwise footing bottom of dam.

appropriately shaped and drained permeable embankment acts as a sort of large slope drain. As Fig. 4.10b shows, a homogeneous structure can easily be equipped with *transverse drains* and stone ribs. Also, such embankments can be more easily prevented from sliding at the junction with the subsoil (Fig. 4.10c).

The above facts and the advantages displayed by a homogeneous structure of permeable material persuaded those responsible for the Váh hydroelectric canals to select this type of profile (Fig. 4.11). It gives very good results in practice, and has therefore, with certain variations (in *slopes, sealing, footing reinforcement,* etc.), been repeated on practically all the cascade steps above and below Žilina, and above and below Trenčín.

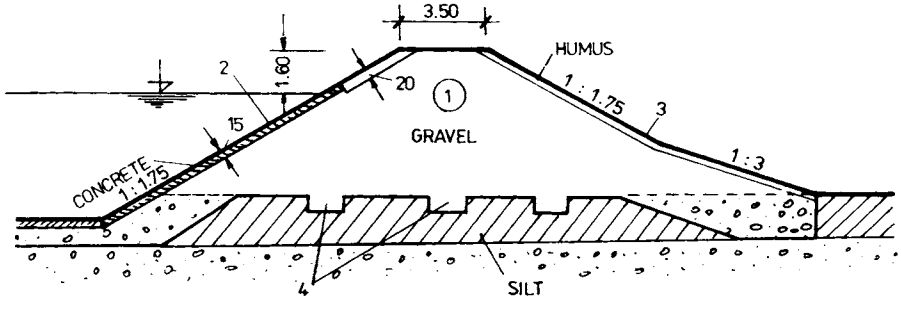

Fig. 4.11. Cross-section of head-race canal of hydroelectric plant in Ladce. 1 — dam body, 2 — concrete apron, 3 — downstream slope protection, 4 — stabilizing "tooths".

On a purely empirical basis, we have chosen the width of the *stabilizing insertion* or 'tooth' in the base under the free slope as being 3.5 m. In fact on the first levées of this type the teeth under the embankments were two to three times smaller, and they were supposed to increase the degree of stability against slip on the subsoil interface. In order to improve shear resistance, and to improve conditions for extracting seepage water, a tooth under the water side of the embankment was also brought into service, always cutting through the layer of covering loam. It is worth noting that for the tooth under the free slope, the wall of loam against which it is supported is vertical. A better support should be ensured for the tooth by a vertical wall like this, as well as for the foot and entire free slope.

As already mentioned, a homogeneous cross-section made of gravel, which was proposed nearly 40 years ago for the first of the hydroelectric head-race canals to one of the river Váh cascades above Trenčín, has given such good performance that it has also been used in subsequent decades in the construction of all other hydroelectric head-race canals.

In Fig. 4.12a, it can be seen that on the Hričov—Mikšová—Považská Bystrica section, on the cascade below Žilina, it was necessary to adapt the embankment

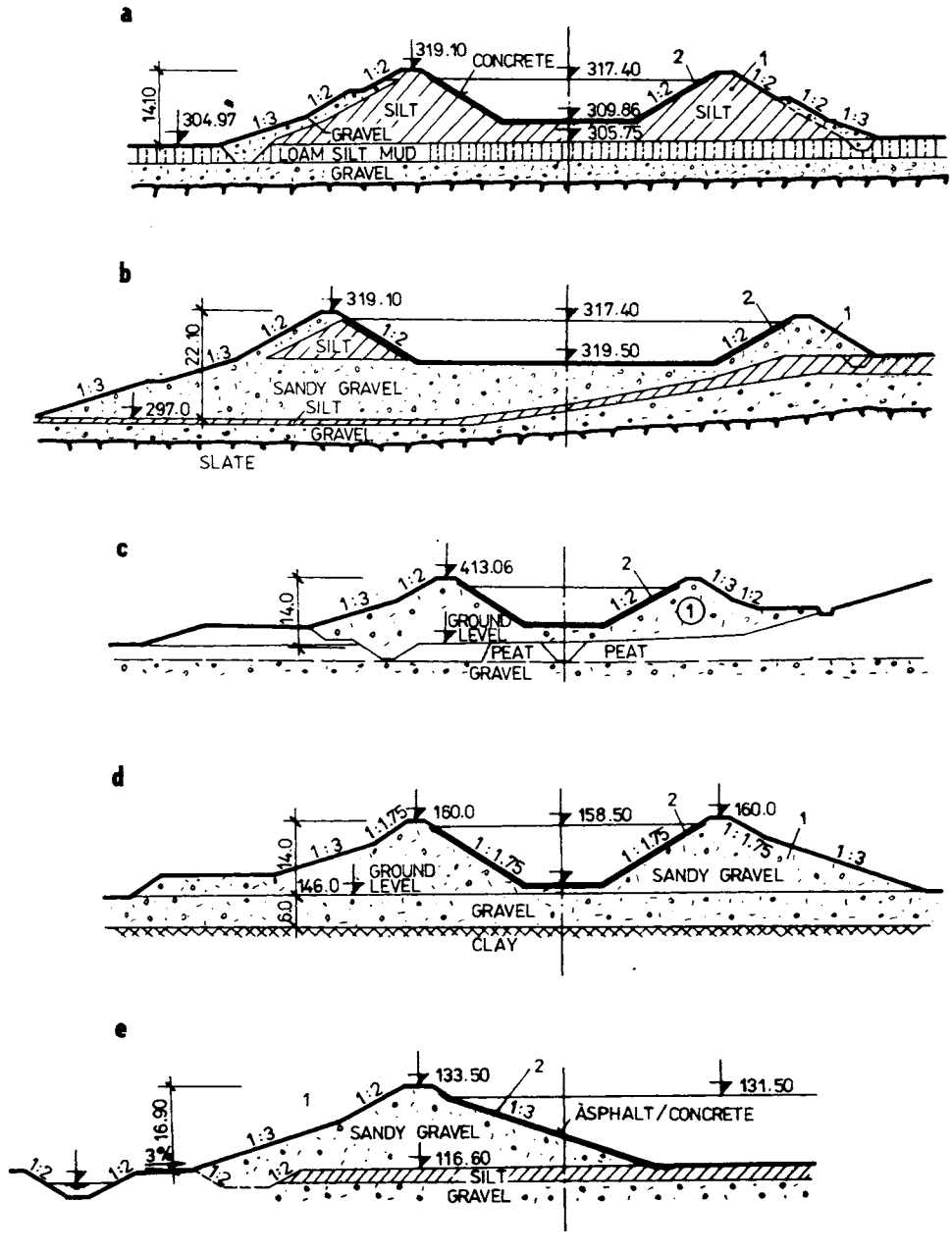

Fig. 4.12. Cross-section of canal dams in Váh valley and of the Danube. a — homogeneous earth dams, b — heterogeneous dams, c — of gravel — on compressible soil, d — on gravel layer, e — on rock with a drainage mark; 1 — dam body, 2 — apron.

slopes to the soil available, which was of rather poorer quality than the alluvial gravels used to construct the canals of the first Váh cascade. Use of the very loamy Váh-*terrace gravels* necessitated the shallowing of both slopes of the embankments, and on the free side pure gravel was also incorporated in a 2—3-m-thick layer for reasons already discussed under slope-stability (Section 3.6). In principle, a tooth was also retained under the foot of the free slope, with the small difference that its slope was slightly altered. This slope was in principle also possible to use on even the highest embankments on the canal above the Mikšová hydroelectric plant. These embankments, built under relatively unfavourable geological conditions (loam and slate with a small angle of internal friction), as well as morphological conditions (sub-seepage into the canal, which is on a slope), reach up to as much as 22 m (Fig. 4.12b).

This profile was again repeated in the late fifties on the Krpeľany—Sučany—Lipovec cascade (Fig. 4.12c), on the head-race canal of the Madunice hydroelectric plant (Fig. 4.12d), and is currently the shape being suggested for the head-race canal on the Danube power plant near Gabčíkovo (Fig. 4.12e).

We could list numerous examples of the use of a homogeneous cross-section for hydroelectric canal embankments, not only from the USSR, but also West Europe (England, France, FRG, Austria, Switzerland and Italy).

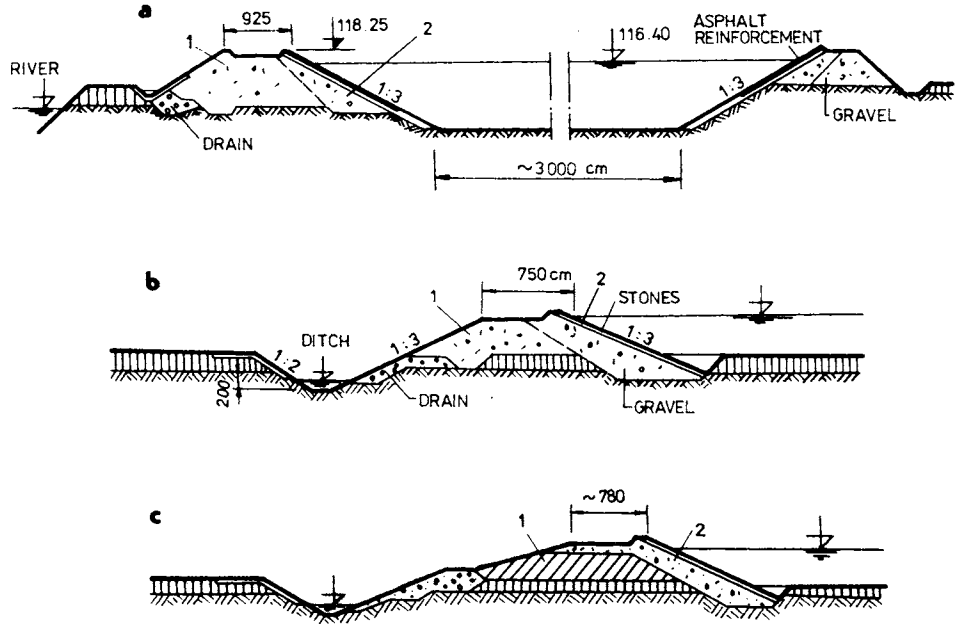

Fig. 4.13. Cross-section of canal dams and levées of the Bourg les Valence water plant. a — canal dams, b — sandy-gravel profile of dyke, c — silty profile ; 1 — dam body, 2 — upstream slope protection.

The profiles of the *canal embankments* used on the water plant at Bourg-les-Valence in France show that those of fine gravel, stiffened by a light *asphalt covering*, together with some using a stoney carpet (Fig. 4.13), built in the development of the river Rhône, hold immense technological benefits and are therefore being ever more widely used (Fig. 4.13a—c).

4.1.6 Some Peculiarities of Irrigation Canal Embankments

A general mark of irrigation-canal embankments is that they have smaller dimensions and so mass. There are certain exceptions on some canals on the large *irrigation complexes* of India and the USA, where embankment cross-sections may reach up to 20 m. This is the case on one of the largest of these systems (Bhakra—Nangal), including a main arterial canal of 178-km length and subsidiaries totalling 4662 km. Such canal embankments are almost always used on some sections as convenient sites for main roads (Fig. 4.14). On the Indian canal

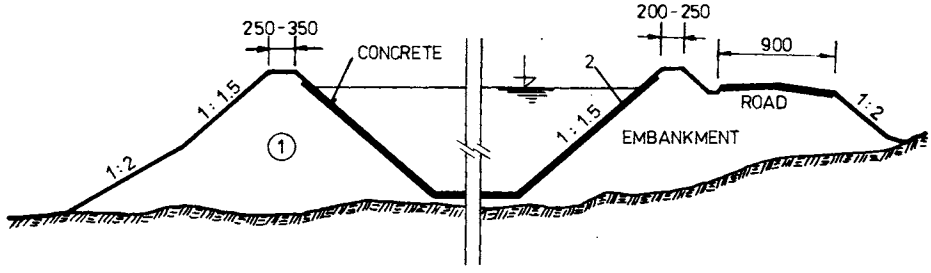

Fig. 4.14. Cross-section of irrigation canal (mean canal of Bhakra—Nangal scheme). 1 — loess, coarse sand (stony material), 2 — apron.

mentioned above, on the sections between Nangal and Ganga and from Ganga to Kozla, the body of the embankment is combined with the roadway, although the actual lie of the road is not situated on the crown of the embankment, which overtops the road by 1.2—2.0 m. With this arrangement the safety of operation of both canal and road is increased, since there is no chance of a vehicle slipping into a deep canal. Because of the variety of applications of embankments they tend to be asymmetrical. The actual embankment top without the roadway is 0.5—1.0 m wider, although the *freeboard remains at 1.2 m.* The embankments (homogeneous) are mainly built up of loess, partly of *stoney material and coarse sand*, and contain a *concrete sealing apron.* The original intention to construct even the main canal without any sealing on certain sections, has to be abandoned because of extremely variable soil properties in some localities.

The embankments on one of the world's best known canals, from Gangar to Hardwar, still dating largely from the first half of the last century, are also

homogeneous, built on loess, unsealed, but very thoroughly reinforced (with stones and more recently concrete), and have a roadway located directly on the crown. The homogeneous unsealed cross-section has given extraordinarily good results, since for a period of more than 120 years of operation, it has served its intended purpose well.

Irrigation canal embankments in Czechoslovakia are generally marked by a lower height, only exceptionally reaching above 2 meters. The average water level in the canals is never more than 1.0 m above the surrounding subsoil level, and consequently hydrostatic and hydrodynamic forces are small. In their design, the functional viewpoint takes precedence over the static one. In the latest irrigation and other similar projects, such as those on the lower river Váh, static considerations fade into the background.

Embankments (Fig. 4.15) almost always have a slope of 1 : 1.5, and are reinforced over the lower half of the slope with a concrete apron (as far as necessary). They are also protected by humus and seeding. The concrete, which

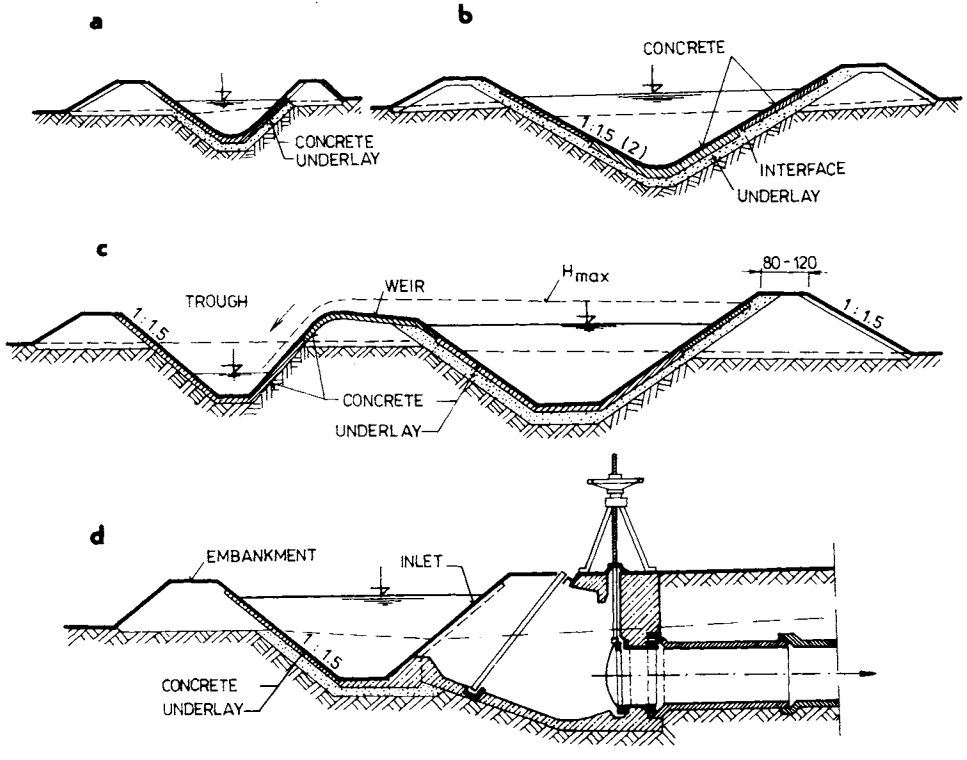

Fig. 4.15. Dams of small irrigation canals: a prefabricated profile (1 piece). a — small canal, b — canal with articulated concrete pavement, c — combined profile with spillway and safety trough, d — near the inlet.

links onto the sealing for the rest of the cross-section is 10—15 cm thick, and sits on a gravel bed of approximately equal thickness. Almost always, the banks are built of materials taken from the canal excavation. These are most frequently loame or sandy soils or more rarely gravels. *Smaller canals* tend to have a *continuous apron*, whereas for those of larger cross-section it is usually divided. At present the dominant type of sealing element for irrigation canals is the *concrete apron*, as is also the case for auxiliary structures (mill-races, sidearms, small holding lakes, and stilling basins). It is only in the last few years that such effort has been devoted to other artificial materials (asbestos or asbestos cement) and plastic cladding, for irrigation structures.

4.1.7 A Technical Comparison and Economic Assessment of Profiles

It is a characteristic of all canal embankments that the chosen profile will repeat itself on innumerable occasions over a length of several kilometers (or tens of kilometers), and therefore every excess cubic meter gives rise to large wastage (maybe $1,000,000). At the same time, any lack of material may mean a substantial increase in the risk of damage to the embankment and the functioning of the canal. In the same way, laying one sort of soil sealing and stabilizing elements in the wrong place may have dire consequences. In assessing a profile, the technology of construction comes out to be no less important, being closely dependent on the choice and distribution of fine-grained (cohesive) and coarse-grained (cohesionless) soils.

Therefore in any technical and economic assessment of a profile, we cannot be content with just one or two aspects, as in the past (usually a simple comparison of soil mass and costs), but must consider a number of points of view. On the Danube scheme, the quantities taken into account are: the mass of cross-section (i_m); the embankment safety factor (m) under loast favourable loading (on the Danube canal this meant for an earthquake of 8° MCS); the *functional reliability* (f) during all possible aspects of canal use (waterway, hydroelectricity, agriculture, recreation, etc.); the cost. Also, due regard was also taken of physical and mechanical working efficiencies, *energy consumption* in kWh, *transportation efficiency (th),* and other factor making a certain profile attractive to construct, or else excluding it from the choice of profile and *technology available.*

In the particular case of the Danube embankments, where over the course of two years more than twenty different variants were thoroughly studied, from which only twelve were finally chosen for comparison (shown in Fig. 4.16), it was usually necessary to compare homogeneous profiles, in which the first assumed construction from loamy soil, and the second used hydraulic filling. In this case, where the volume of soil built-in the embankment body varied from 28×10^6 to 45×10^6 m^3 (according to soil type and the sort of technology chosen), it seemed very appropriate to use hydraulic filling as an extremely efficient construction method

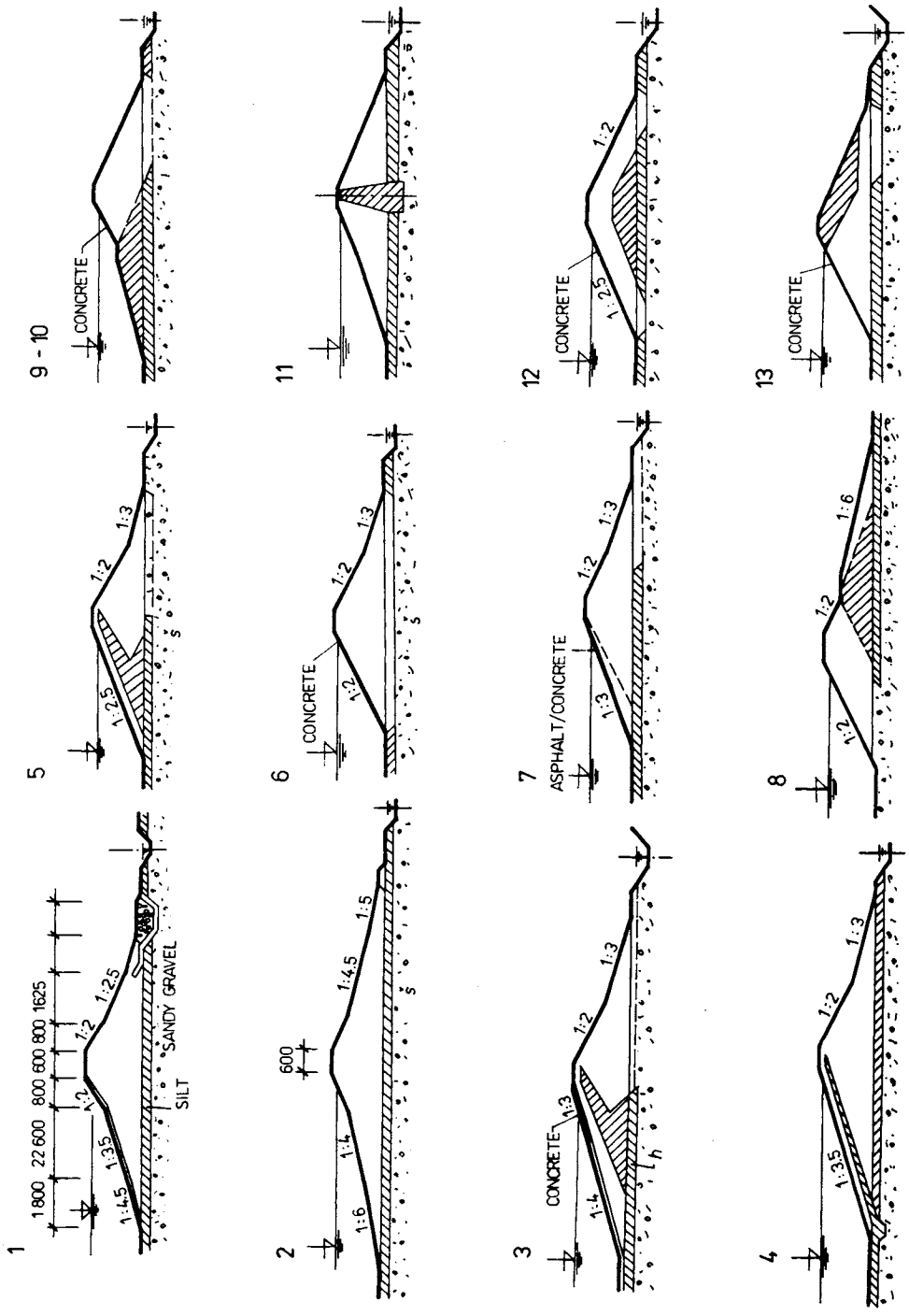
1
1800 22600 800 600 800 1625
1:2
1:2
1:2.5
1:3.5
1:4.5
SANDY GRAVEL
SILT
2
600
1:4.5
1:5
1:4
1:6
3
CONCRETE
1:3
1:2
1:3
1:4
4
1:2
1:3
1:3.5
5
1:2
1:3
1:2.5
6
CONCRETE
1:2
1:3
1:2
7
ASPHALT/CONCRETE
1:2
1:3
1:3
8
1:6
1:2
1:2
9 - 10
CONCRETE
11
12
CONCRETE
1:2
1:2.5
13
CONCRETE

Table 4.2. Head-race canal Gabčíkovo — variants of dams and its volumes

Notation	Cross-section of the dam	Volume [10^6 million m^3]		Material quantity $i_m = \frac{G \text{ of earth}}{P_s}$	Safety factor	Profile reliability	Costs* [million dollars]
		Total	Dam body				
1	Homogeneous, fill of earth	34.25	27.61	9.94	1.20	2.6	101.7
2	Homogeneous, hydraulic fill	44.88	37.41	13.68	1.2	1.4	85.3
3	Heterogeneous with inclined silty core (1 : 3, 1 : 4)	35.67	29.19	10.42	1.25	3.0	94.8
4	Heterogeneous with "hydra-ton" sealing	35.16	28.52	10.20	1.0	1.8	132.3
5	Heterogeneous-like 3 but slope 1 : 2.5	28.04	21.40	8.83	1.05	2.7	89.2
6	Gravelly with concrete apron (1 : 2)	31.82	24.90	8.88	1.03	2.2	68.3
7	Gravelly with asphalt concrete apron	33.44	26.80	9.76	1.24	2.0	75.7
8	— like 7 but slope 1 : 2.5	31.35	24.71	8.84	1.07	1.8	73.2
9	Heterogeneous with prismatic downstream part of earth	33.61	28.79	10.30	1.03	1.2	90.6
10	Heterogeneous with upstream earth (silty) prisms	30.14	23.96	8.48	0.95	2.4	87.5
11	Heterogeneous with central earth core	31.66	25.02	8.46	1.03	2.8	94.8
12	Heterogeneous with special profile (9) adjustment	33.31	26.67	9.70	1.03	2.0	91.9
13	Heterogeneous with special profile (10) adjustment	30.25	23.61	8.42	1.03	1.8	87.2

* Costs (in dollars) deduced from costs in Kčs, in 1969.

Fig. 4.16. Variants of dam profiles of the head-race canal of the Danube scheme near Gabčíkovo. 1 — homogeneous silty loam, 2 — hydraulic fill, 3 — inclined clay core, 4 — hydraton inclined sealing, 5 — modified inclined core, 6 — gravel-pervious embankment with concrete apron, 7 — detto with asphalt-concrete apron, 8 — combined profile with downstream dumped loam prism, 8, 10 — dumped loam prism upstream, 11 — with vertical loam core, 12 — with internal loam prism, 13 — dumped loam material downstream.

Table 4.3. Consumption of energy, costs and efficiency of the Danube diversion canal dams

Consumption			Index values reduced and compared with a gravelly fill with concrete apron profile-multiplied by a weighting coefficient						Overall evaluation	
Profile notation*	of energy [million kWh]	work of machinery [million th]	Safety $1/m \times m' \times 25$	Reliability $1/f \times f' \times 22.5$	Costs $1/C_6 \times 25$	Energy $1/E_6 \times 17.5$	Works $1/(WM)_6 \times 5$	Quantitative $(i_m : i_{m_0}) \times 5$	In per cent [%]	Order of profile
1	895	272.56	0.859 21.50	0.845 19.02	1.469 36.72	1.805 31.60	0.818 4.09	1.12 5.60	118.50	8
2	536	293.91	1.03 25.80	1.570 35.30	1.232 30.80	1.084 19.99	0.883 4.42	1.54 7.70	123.0	11
3	808	262.49	0.824 20.60	0.733 16.50	1.370 34.25	1.630 28.52	0.790 3.95	1.175 5.88	109.7	5
4	744	509.27	1.03 25.80	1.222 27.50	1.913 47.80	1.50 26.25	1.532 7.66	1.148 5.74	140.8	13
5	706	242.05	0.936 23.40	0.815 18.34	1.220 30.48	1.422 24.88	0.727 364	0.993 496	105.7	3
6	496	332.89	1.0 25.0	1.0 22.5	1.0 25.0	1.0 17.50	1.0 5.0	1.0 5.0	100.0	1
7	582	379.88	0.831 20.80	1.10 24.75	1.093 27.35	1.158 20.28	1.142 5.71	1.100 5.50	104.39	2
8	593	394.82	0.962 24.05	1.468 27.50	1.057 26.40	1.160 20.30	1.187 5.93	0.995 4.98	109.2	4
9	716	256.99	1.0 25.0	1.834 41.25	1.310 32.75	1.443 25.24	0.772 3.86	1.158 5.79	133.9	12
10	736	247.97	1.085 27.10	0.917 20.65	1.263 31.57	1.483 25.98	0.745 3.73	0.955 4.78	113.81	7
11	776	256.16	1.0 25.0	0.785 17.67	1.371 34.26	1.569 27.44	0.768 3.84	0.953 4.77	113.0	6
12	724	257.57	1.0 25.0	1.10 24.75	1.328 33.20	1.563 27.34	0.773 3.87	1.091 5.46	119.6	9
13	783	250.43	1.0 25.0	1.222 27.5	1.262 31.52	1.580 27.64	0.752 3.76	0.948 4.76	120.2	10

* Profile notation see Fig. 4.16.

for large volumes of soil (Sherard et al. 1963). In the past, it has been well proven in the construction of large embankments in the USA (Fort Peck, Garza, Saluda, etc.) and in the USSR (near Kuibyshev, the Volga hydroelectric plant, the Volga—Don canal, etc.). It has been shown that, despite the large soil masses used,

these embankments have very little *static safety* margin (Akhutin 1951), mainly in the initial years immediately following construction, when the rather permeable soils used in the body of the structure are still unconsolidated. On the other hand, the embankment profile containing hydroton sealing, at that time very popular in both East and West Germany, appeared to have technological disadvantages (awkward installation). The *most attractive ideas* appeared to be mainly homogeneous *cross-sections built of sandy gravel*, since they give relatively good static and functional realiability and are very easily built and maintained.

We must add to our final evaluation, presented in Tables 4.2 and 4.3, that it is not possible to give equal weight to all the criteria used in the choice of profile. In the comparison we gave pride of place to static safety, functional reliability, and overall economic viability. The variant to emerge as the most advantageous was the sixth, composed of coarse sand with a concrete apron sealing element 20 cm thick on the upstream side, joined to an asphaltic concrete base 50 m wide and sitting on a layer of treated and stabilized soil (binder layer).

As shown by works relating to the reappraisal of the Danube embankment profiles in the Soviet Union (Glavtekhstroĭproekt, 1966) and Hungary (VISITERV, 1966) which concluded the same order of suitability. The trend in embankment and dam development is wherever possible (in the developed countries) to give *priority to homogeneous gravelly structures with apron sealing.*

4.2 Typical Sections of Levées

4.2.1 Slopes and Dimensions

One characteristic of levée profiles is that they are lower than canal embankments and more massive. In Europe their heights rarely exceed 10 meters, seldom even more than 5—6 meters. The material consumption index is usually higher, $i_m \geq 10$—12.

The remaining bases of construction are more indeterminate than for canal embankments, since the fundamental determining factor, the head of water is front of the structure H, which for canal embankments or dams can be given to the nearest centimeter or so, is barely known to the nearest decimeter in the case of levées. The governing situation of course is the water state during flood. Even today there are no precise criteria determining the quantity of water for which a levée has to be designed. While the *older levées gave protection against an* approximate *50-year flood* (Q_{50}), the general opinion *nowadays* is that the profile design should be based on a *100-year flood* (Q_{100}). This quantity was taken as the basic design parameter for the Danube levées in all the states along the Danube (FRG, Austria, Czechoslovakia, Hungary, Yugoslavia, Bulgaria, Rumania), and was ratified by the so-called Danube Commission as *standard data of embankment*

height, with the notation STK ($= Q_{100}$). In discussions over the concept of joint Danube water-usage schemes, which in some cases (navigation, protection) affect not only the participating states but others through which the Danube flows, the opinion was reached that the embankments of stilling basins, for which protection governs the height along most of the length, should be designed with respect to their category of importance. The value of threatened industrial plant and housing area should be determined, and not only that of the land, as was previously the case (Glavtekhstroĭproekt — Moscow 1966). With regard to the *freeboard height* of embankments h_p above the level of a flood, it should have the value

$$h_p = \Sigma \Delta h,$$

as is given by Fig. 4.2a. According to Kratochvíl (1969), Soviet methods give an unnecessarily conservative value.

With the freeboard given thus, it generally turns out that h_p exceeds 1.5 m. If, however, we take a look at levées around the world, designed and constructed in the last ten years, we see that the excess height is usually less. The *height of embankment* above ground level is around

$$H_1 = H + (0.5—1.5). \tag{4.4}$$

The structural height is then $H_s = H_1 + h_0$ as we have shown for canal embankments.

The top thickness b_1 is generally fixed at 2—6 m, which in Czechoslovak conditions gives relatively good agreement with Altunin's empirical formula

$$b_1 = \beta_1 H, \tag{4.5}$$

where β_1 is the coefficient of crown width with a value 1.0—1.2.

The remaining levée dimensions are determined on similar lines to those formulated for canal embankments (Section 4.1). It should be added that in levée-profile design, empirical quantities find rather greater use than for canal embankments. According to one such formula, it is recommended that *the width* of the embankment *at the foot be given* by

$$b_2 = \beta_2 H, \tag{4.6}$$

where β_2 is the slimness ratio of the embankment and is 5.5—7.0.

In accordance with this formula, together with Fig. 4.5, it follows indirectly that the average bank slope should on either side be shallower than 1 : 2.5. In most cases it is between 1 : 2 and 1 : 3. The embankment top has to exceed the water level by 0.4—1.0 m depending on water flow and surface breadth, as well as the fact that a levée without complete protection can possess no overflow spillway. The top of the embankment will then be at nearly the level of the water surface for the design flow, or else the embankment will be protected by a spillway. In this case the

freeboard height has to be above the calculated surface for a 100-year flood, after relief through the spillway (40 cm minimum).

The top thickness has to be 2.0 m minimum for embankments up to 2.0 m in height, and 3.0 m for higher ones. Also, where we have to accommodate a line of communication, the embankment width is determined by it, the bank slopes being calculated in accordance, but no steeper than 1 : 2, and if it is neccessary to design a berm this should be a minimum of 2 m wide. With two-directional transport, the berm should be extended to at least three meters for protection from flood, and also for maintenance reason. The berm arrangement must ensure the backflow of surface water from the embankment slope.

4.2.2 Homogeneous Levées

In the past, an embankment profile was designed with regard both to slope angles already shown to be reasonable — and to the line of the phreatic surface — where it was assumed that an average value of free-surface slope within the embankment body could be taken. This average slope was suggested above 10° (tan $\alpha = 0.176$), or at least in the range 8—13° (Fig. 4.17a) (tan $\alpha = 0.14$—0.23). This view arose from the idea that since the embankment is built of clayey sand, it cannot be permitted to encroach on the protecting berm on the downstream side (Fig. 4.17b) which has to remain dry during a flood to avoid interference with traffic.

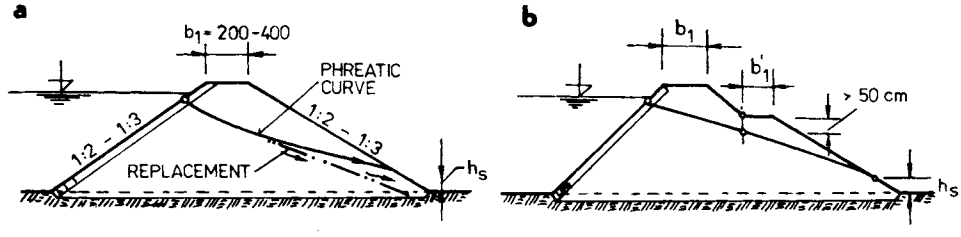

Fig. 4.17. Conservative cross-section of a levée — without antiseepage measures. a — with uniform upstream slope, b — with shelf.

Nowadays, these primitive concepts and associated principles have been abandoned, because, following from the analysis of seepage in Chapter 2 and of slope stability in Chapter 3, the phreatic curve and slope stability can be controlled by *incorporating filters and drains* and by a suitable choice of soil (Fig. 4.18a, b).

When *choosing* an embankment *cross-section*, we must take due regard of the following: the physical and mechanical *properties of materials* used in construction; the *hydrogeological condition* of the subsoil and its physical and mechanical properties; *control of seepage* in the body of the embankment, and especially in the subsoil; the *method of drainage* at the downstream foot; and finally the period

during which embankment and subsoil might be subjected to loading from the design through-flow, and whatever results originate from this (seepage, uplift, drainage of surrounding land, etc.).

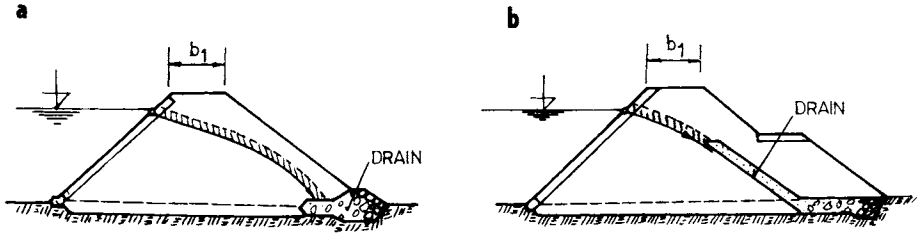

Fig. 4.18. Cross-section with protecting elements — in homogeneous profile. a — uniform profile with toe drain, b — with inclined and blanket drain.

The embankment is usually protected by a *grass covering* seeded into a minimum of 10 cm of topsoil in the appropriate season, or if necessary by sod on the upstream slope. Any sod with improperly developed roots, insufficiently matured, afflicted by grass diseases or weeds, and those taken from a wet environment are not suitable for protecting levées.

As regards slope reinforcement by grass cover or sod, the principle is the same for all embankment types we have been considering.

4.2.3 Heterogeneous Levées

Heterogeneous profiles are not common in levées, but the same principles apply in their construction as for canal embankments. One difference is the fact that when dimensioning levées, it is the technological rather than purely functional viewpoint which dominates. This is particularly true when determining the *dimensions of earth sealing*, whose *thickness t*, found according to the relevant criteria, should be

$$t = \left(\frac{1}{5} - \frac{1}{3}\right) H.$$

For an average head $H = 5$ m, this gives a maximum thickness at the subsoil surface $t = 1.0$—1.7 m. Technologically, however, this thickness should be considered a minimum. The sealing thickness is generally $t = 2$—3 m (measured horizontally), because only at such thicknesses is adequate machining of the soil possible.

The situation is similar for a sealing mat which is a common continuation of sealing (Fig. 4.19a) for this type of embankment, while the *tooth*, as the construc-

tional and functional extension of sealing on the so-called Rhine type of embankment, has a width determined mainly by that of the excavation which has to be carried out for this sort of sealing (Fig. 4.19b).

Some further *similarities between sealing elements* and various active *seepage elements* will be analysed in Chapter 6.

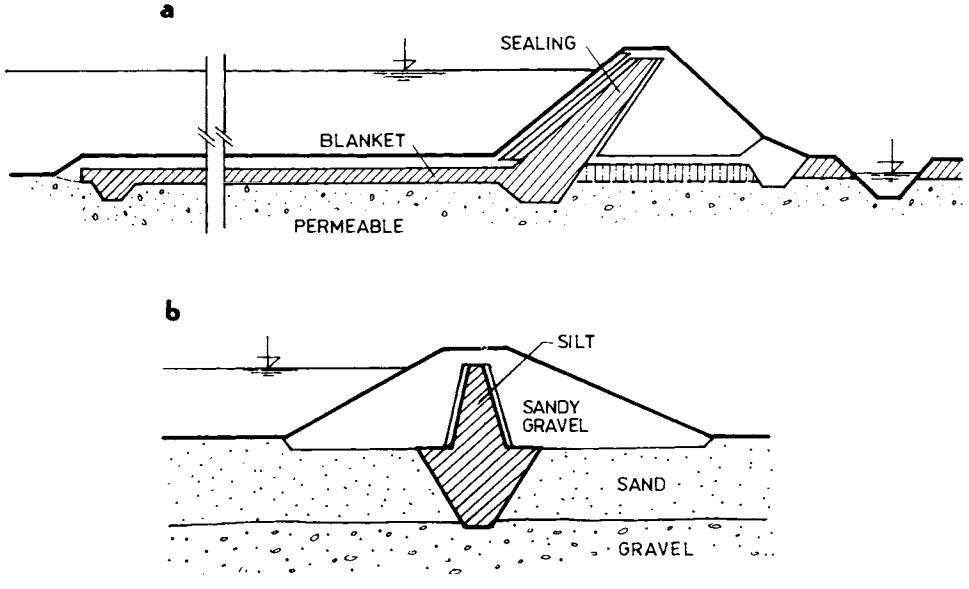

Fig. 4.19. Cross-section of levées — heterogeneous profile. a — inclined core and clay blanket, b — clay core in permeable subsoil.

In choosing the thickness of reinforcement, we make use of principles described in Chapter 3, where certain simple formulae were introduced for use in determining the thickness of flooring or other types of reinforcements.

4.2.4 Examples of Different Levée Cross-sections

Up till now, in Czechoslovakia and elsewhere, the homogeneous levée profile constructed of clayey sand or sandy gravel with a strong loamy element has predominated. The former is common on the lower reaches of a river (the Danube in Hungary and Yugoslavia, the Rhine in Holland, and the Oder in Poland and the German Democratic Republic), and the latter in the upper regions (the Rhine and Danube in FRG and Austria).

As regards the shape of *cross-section*, some have *simple slopes* (Fig. 4.20-1) and others *including berms* of various *widths* from *2.0 to 8.0 m* (Fig. 4.20-8). One

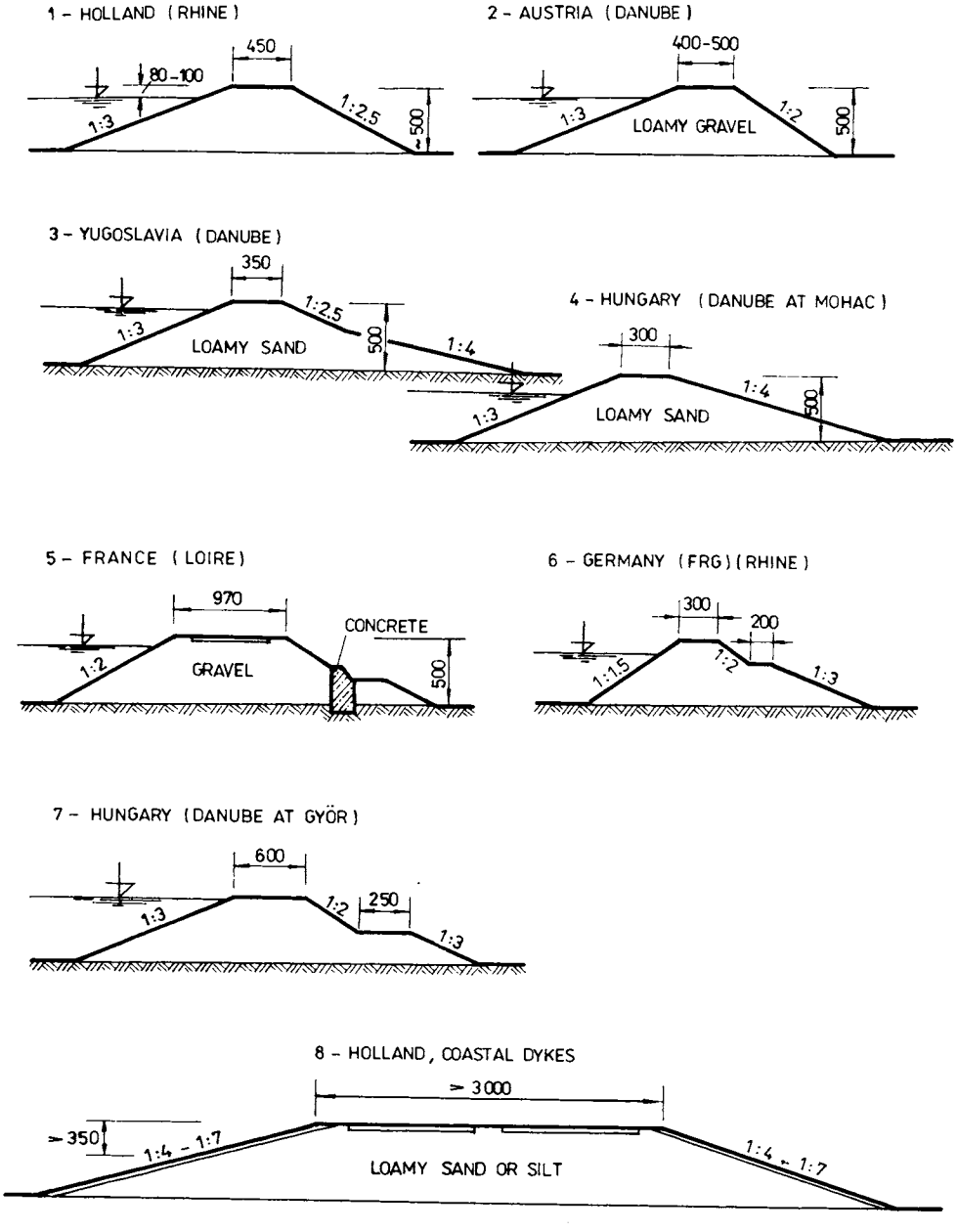

Fig. 4.20. Cross-section of levées and dykes in Europe. 1—4 — uniform profile, 5 — profile with safety wall, 6 — most economical profile, 7 — strengthening profile with respect to soft subsoil, 8 — strong multipurpose profile.

complete exception is the profile of the Dutch sea-defence dykes, which protect dry land from the sea. The massive cross-section which these structures have is justified by three facts. These embankments defend territory of extraordinarily large worth against flooding by a continually attacking sea. Generally, they also serve as channels, a variety of forms of communication. For the *most part*, they are *constructed by tipping* (hydraulic fill), which always leads to shallower slopes then when embanking (rolled fill) is employed. For these reasons, they have a slope of less than one in four and a width at the top thickness of more than 20 m. At sea level when the tide is in, the width is 80—100 m (average 90 m), and the remaining height above water is 3.5 m as described in Chapter 1.

The diagrams given in Figs. 4.20-1 to 4.21-8 show that levée profiles on all the larger European rivers barely differ, with the exception of these where the crown of the levée is used as a line of communication or fulfils some other function (e.g. levées on the Loire). Slopes of 1 : 1.5 (for gravels) down to 1 : 4 (sandy material) have proved suitable in practice.

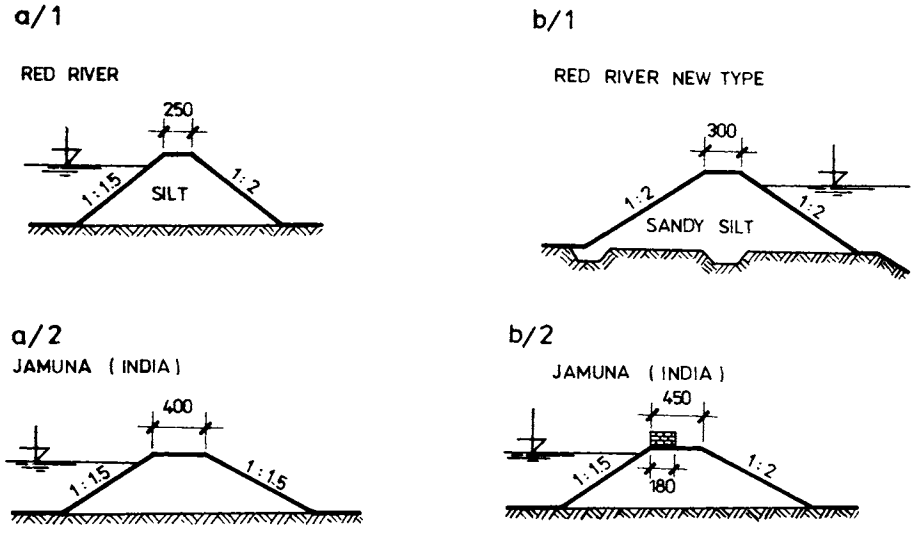

Fig. 4.21. Cross-section of levées on the Red River and the river Jamuna. a/1, a/2 — uniform (original) profile, b/1, b/2 — adapted dam profile.

A somewhat greater divergence of profiles is provided by levées in other continents (see Fig. 4.21). Some fairly general characteristics are a lower massivity, a simple profile, and in most cases a lower static safety factor. In China and India it is common to find the embankment top raised by hand-laid walls of cut stone.

In general, levées in Czechoslovakia retain the *traditional profile with simple slopes* on either side (Fig. 4.22). Because these homogeneous levées are usually

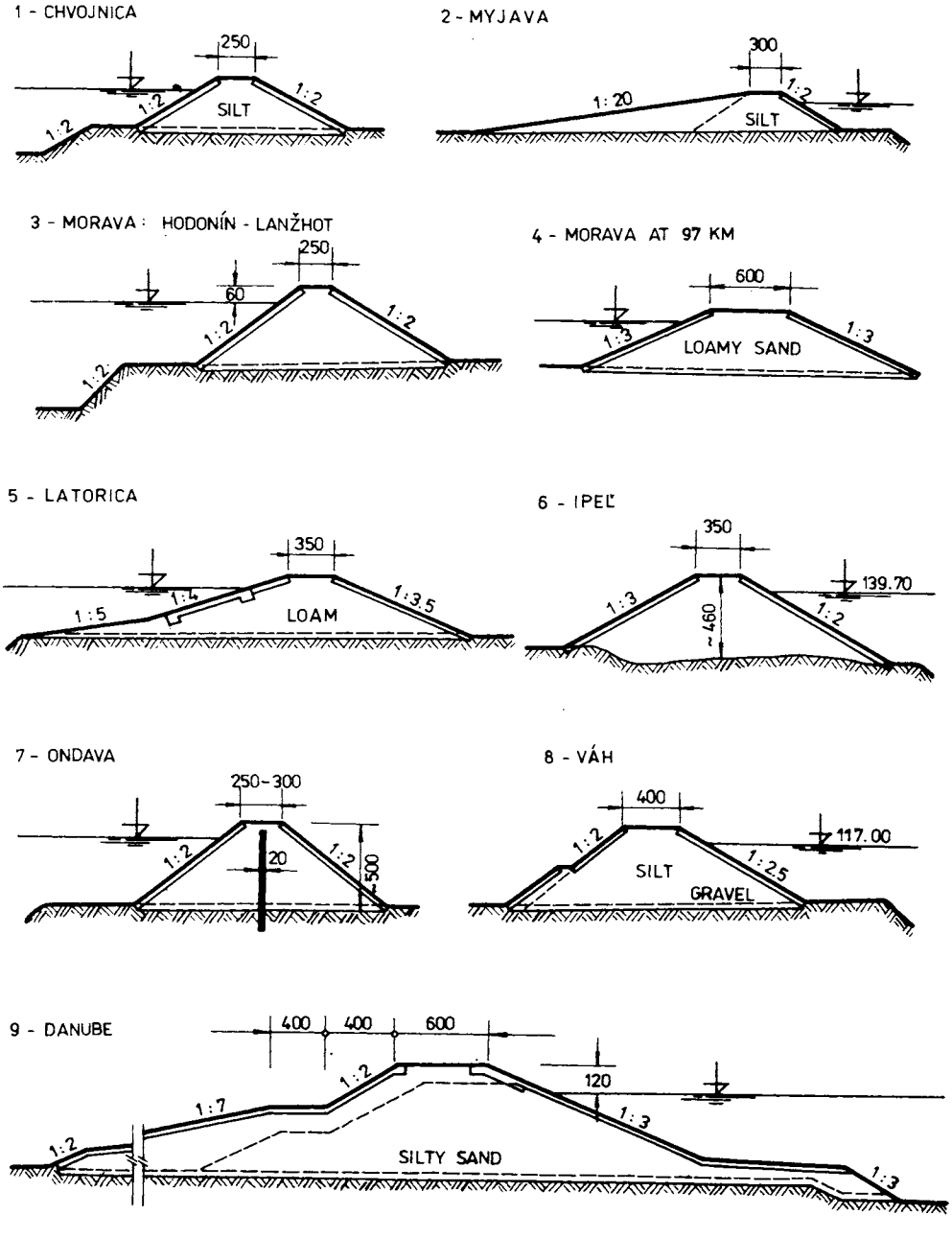

Fig. 4.22. Cross-section of levées in Czechoslovakia. 1—4 — uniform profile, 5, 6 — with upstream random rock zone, 7 — with concrete core membrane, 8 — combined silty-gravel profile, 9 — with short blanket upstream and supporting (compacted) fill downstream.

formed from sandy loam, 1 : 2 appears to be a sufficiently stable slope and practically all levées on the smaller rivers are based on this angle, provided they exceed 3.5 m high. One exception is found in parts of the river Morava levée system, where the embankments are made of sandy soil.

Parts of the relatively low Myjava levées are a total exception, having a slope of 1 : 10 (generally less than 2 m). This shallow slope was chosen for two reasons. Firstly there was a surplus of soil because the river bed had to be deepened, and secondly an effort was made to enable cultivation of the downstream slope, forgetting the principles mentioned above (a safety strip along the downstream foot of the levée).

The shallow slopes and relatively heavy and cumbersome reinforcement on the downstream side of the Latorica embankments were imposed by the awkward properties of the materials used (loess and wind-strewn sand). One unique peculiarity in levée construction on some rivers is the concrete core used in the body of levées. According to expert views (Hanuškin 1924), this thin core of thickness 20 cm grounded only 30 cm below the subsoil surface is not just an antiseepage element, but also must provide strong protection against rodent damage.

The top thickness on Czechoslovak levées varies from 2.5 to 6.0 m, being in the range 2.5 to 3.0 m for small rivers and only wider than 4.0 m on large watercourses such as the Danube, Morava and Váh.

The *cross-section of Danube levées* differs from the others both in their proportions and shape. They *contain berms* used mainly for lines of communication, and *shallow slope angles*. The old profiles had this characteristic outline, and are retained by the current ones which are still more massive. The shallow extension on the downstream side has a basically static purpose of increasing slope stability.

The slopes of these levées are reinforced mainly by sod. *Stone flooring* is usually used on the *upstream side* only *on concave sections*, but on the downstream and sometimes either sides, it is also used at the foot. As a rule, these levées do not have their own active antiseepage elements: exceptions are those newly designed and built after about 1965. Of these are the low Váh levées section, and those on the middle Danube.

4.3 Subsidiary Structures on Canal Embankments and Levées

Canals are basically linear constructions which affect the interests of many parties in the regions they pass through. The embankments do not merely affect the topography of the land, where they alter and influence lines of communication and smaller watercourses, but also the positioning of various engineering systems, the structures of which have to be designed in accordance with the interests of

numerous parties and the general public. These interests cannot always be easily harmonized, and thus conflict can arise.

In order to minimize conflict, it should be realized early in the study, that in building any canal (power-station, irrigation, waterway, or multipurpose) it is necessary to enumerate the objects on and around the canal as well as the embankments themselves. These generally fall into three categries: *objects enabling operation* of the canal (of-takes, locks, sieving walls, gravel traps, etc.); *objects distributing and channeling flow* (inlets, distributors); *objects enabling the crossing* of other watercourses or lines of communication (aqueducts, viaducts, syphons, etc.).

We cannot exhaust the field of problems presented by these objects in this work, particularly since every canal gives rise to different problems. We merely wish to draw attention to some of the chief difficulties most common in designing canal embankments.

4.3.1 Structures Concerned with the Operation of a Canal

One fundamental assumption for proper functioning of a canal and safe maintenance of its embankments is an in-take, which exists just to allow the removal of the appropriate quantities of water: it therefore contains *regulating gates*. It is also required of a correctly functioning gate system that only water is admitted to the canal, i.e. *impurities of floating matter* such as tree trunks, branches, leaves, ice, dead animals, etc. are be excluded, and thus at any inflow to the canal we must construct *sieving walls*, rectifiers, *angled reflectors*, etc., in order to check, deflect and guide this excess along the river. After a period of spate has subsided, these objects which are always brought in by high water flows, have to be removed. They can usually be passed under weirs at *suitable points*, below which there is direct *access to the river*.

Sieving walls are commonly built across *power-station canals* as rigid *bridges* with reinforced *concrete walling*, protected by a fine screen of netting. However, Fig. 4.23 shows a simpler solution suitable for medium to large off-takes (in the case shown $Q_{max} = 50\ m^3\ s^{-1}$), where a light *bridging wall* serves the purpose.

The in-take device itself (1) has four regulating sluice gates, which can be moved along the concrete pillars (2), or up and down. In front of the sluice gates is set a row of rakes (3), preventing the intrusion of smaller matter into the canal, while larger objects, mainly floating debris, are trapped by the raised threshold of *the weir* (4) or as a final resort the *sieving wall* (5), which, although it floats, is secured by cables to a couple of pillars (6, 6'). The pillars are *wall anchored* (7) to remain firm under collision with any floating matter. Further devices also prevent any clogging up of the inflow, the main one being a *catching trench* (8) in front of the inlets where these objects have to descend in order to be able to pass easily through the *movable sluices* (9) under the weir. An especially *large gate* (10), which is

rather harder to manipulate, opens to allow the passage of flood water, ice, and very large floating obstacles.

From the functional point of view, it is important to orientate the off-take device correctly with respect to the main flow. The laws of river hydraulics demand that it be located on a concave stretch of bank (11).

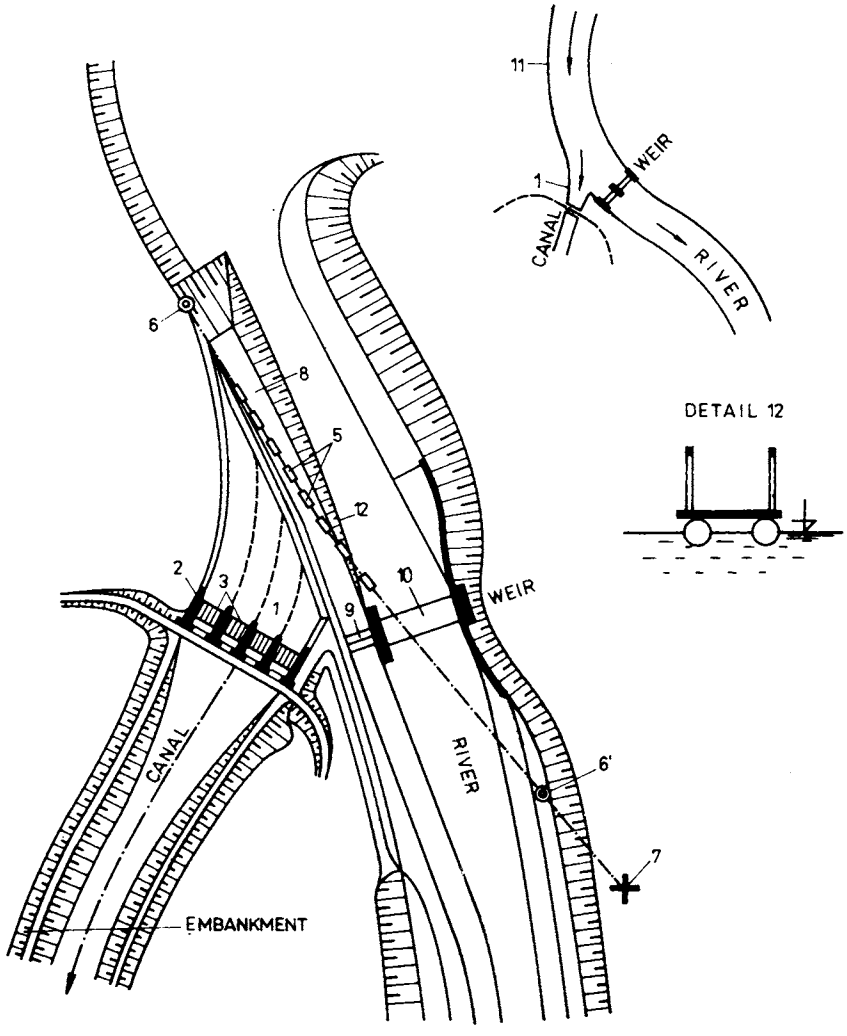

Fig. 4.23. Inlet structure of a canal and weir and auxiliary structures on the river. 1 — inlet structure, 2 — pier, 3 — grill, 4 — limiting threshold, 5 — foot-bridge, 6, 6′ — column, 7 — anchorage of suspended foot-bridge, 8 — ditch, 9 — sector closure, 10 — roof shutter, 11 — location of intake, 12 — cross-section of floating foot-bridge.

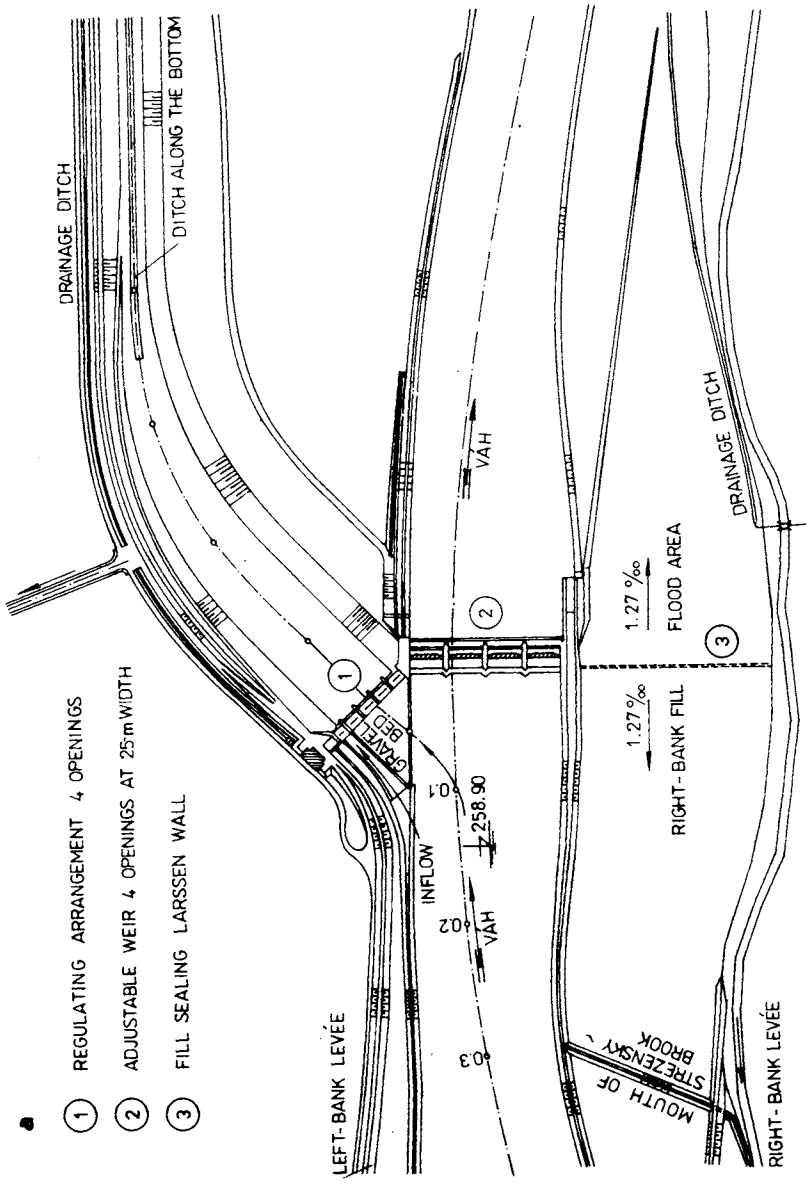
DRAINAGE DITCH
DITCH ALONG THE BOTTOM
1 REGULATING ARRANGEMENT 4 OPENINGS
2 ADJUSTABLE WEIR 4 OPENINGS AT 25m WIDTH
3 FILL SEALING LARSSEN WALL
GRAVEL BED
INFLOW
258.90
VAH
VAH
1.27 ‰
1.27 ‰
FLOOD AREA
RIGHT-BANK FILL
DRAINAGE DITCH
LEFT-BANK LEVÉE
MOUTH OF STREZENSKY BROOK
RIGHT-BANK LEVÉE

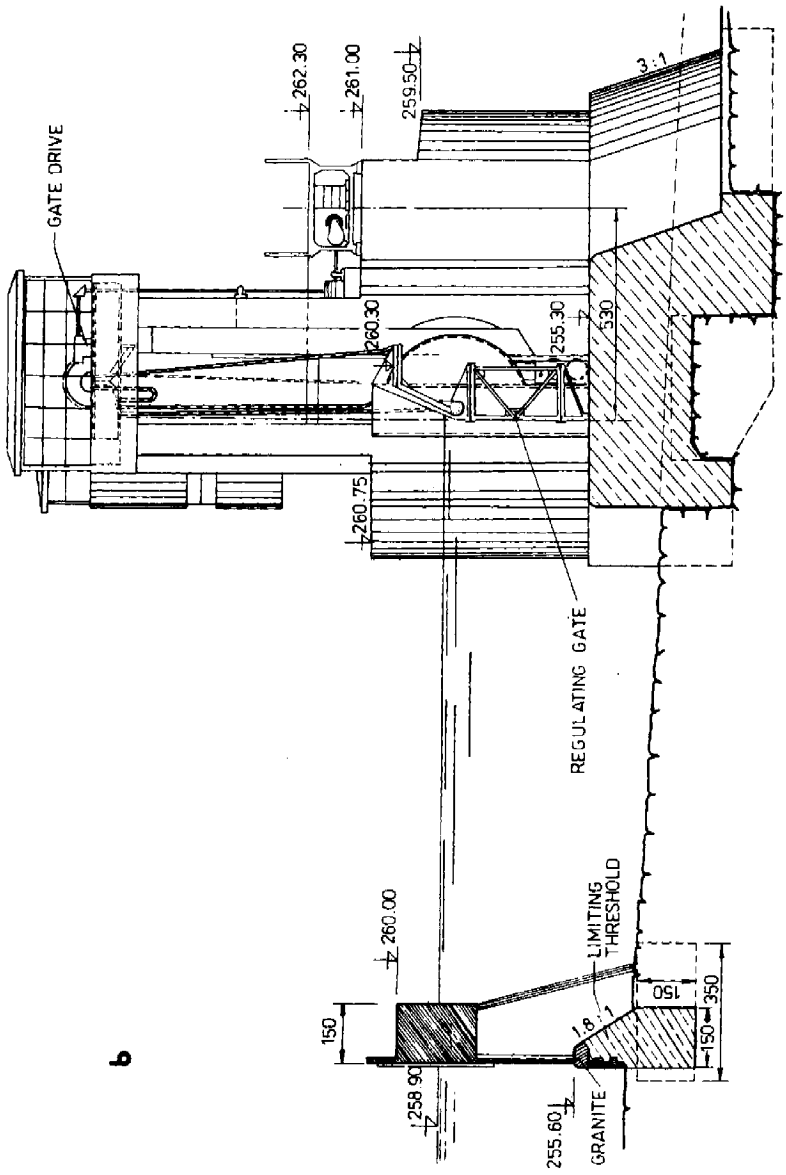

Fig. 4.24. Canal and river structures. a — lay-out of head-race canal of power-plant, b — head-race canal regulator and submerged wall — after Smrček (1958).

In connecting the in-take control structure to the earth levées, it must be emphasized that great attention must be devoted to the contact between the earthen core (sealing) and the concrete structure. The walls must be smooth and angled at between 10 : 1 and 5 : 1, in order to compact the soil at the contact, and also when consolidation of the levée takes place, the soil presses down onto the concrete face. With a vertical joint, there is the possible danger of the contact parting and cracks appearing.

This principle should be adhered to in all joints between a concrete structure and the body of the embankment. It is also necessary to include some cohesive 'expansive' soil at the contact with the concrete, so that when the water reaches it, it swells, sealing the contact even more tightly.

The off-take described serves as an example of an *off-take/inlet device* on power-station and irrigation canals. Figure 4.24a shows a particular solution for an off-take on what is clearly a power-station feeder canal. It depicts the arrangement of canal embankments and protective levées. Also typical is the location of a protecting dumping ground, which we frequently meet on canal embankments with a non-counter-balanced excess of material — usually the case along out-flow canals.

A cross-section through the *regulating equipment*, with the above-mentioned submerged concrete walling, rakes, and threshold at the inlet, is shown in Fig. 4.24b.

4.3.2 Power Stations

Power *stations are* rather *special engineering structure* and always require through study and consideration from all aspects (hydrotechnical, energy flow and static) because they are so rare. It represents a special problem of performance and control of the whole power-plant system, which differs from that of weir or regulating structure constructions. The last structures usually have a stable function. The turbines, governors, upstream and downstream gates and other machinery in a power house are more complicated — mainly Kaplan and bulb unit. One of the features of the *special installation* is the facility *to sluice the discharge* through the unit without power production under the *combined control of the governor* and the *downstream gate.*

Modernization of the station every 20—50 years should take place in accordance with the latest hydroenergetics research. This new concept imposes new problems to canal embankment designers, because such a *power house must be constructed with* a view to *future reconstruction.* In the last decade, two tendencies in power-station design can be observed in Europe: power-house sets are even bigger now, and turbines and their control-mechanism are being rapidly modernized. For general reconstruction of a power-house structure, *20—30 years is the time limit we set*, or for total rebuilding should take place within 40—50 years.

Canal enlargement (over a 1.5—2.0 km length) for power-house inlet facilitates such a scheme.

It is possible to design a *double-canal scheme* (lower part of canal doubled at a later date) in extremely special cases. Such projects currently originate in the USSR.

4.3.3 Shipping Locks and Waterway

Concerning *navigable canals*, which in Czechoslovakia may later include smaller canals (for agricultural transportation), we should add that the demands connected with inflow into the canal differ from these mentioned above. Many of the devices shown in Fig. 4.23 would disrupt any attempted navigation (submerged walling, floating bridge, restricted opening), and it is therefore often necessary to construct separate inflow to *power-station* supply and *waterway canals* (Fig. 4.25), including the case where a *common canal* is in use (multipurpose). A lock can also operate as an inlet to a canal.

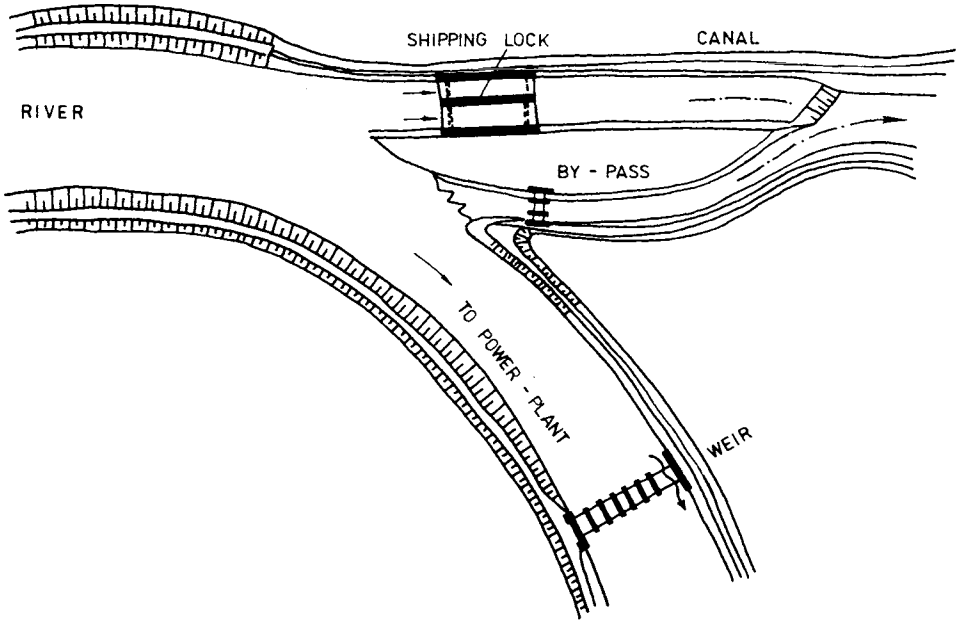

Fig. 4.25. Inlet structure of a multipurpose canal.

The commonest feature to find on a navigable canal is the shipping lock, which rarely poses any special problems in bonding into an embankment core. In the classic method of lock construction (Fig. 4.26), the *contact between it and* the

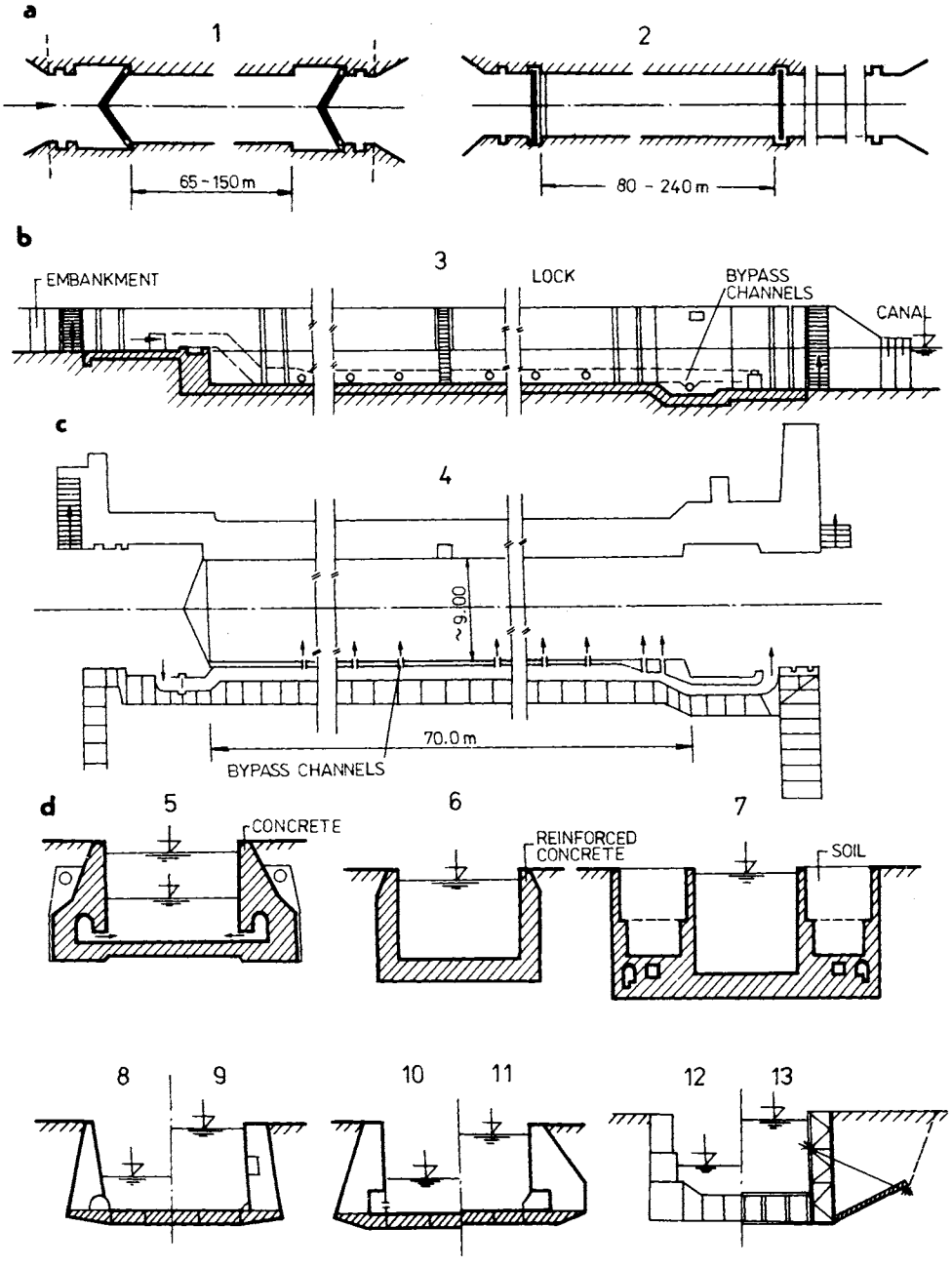

Fig. 4.26. Various types of shipping locks. a — horizontal section, b — longitudinal section, c — horizontal and longitudinal sections, d — cross-section of different types of locks; 1 — lock gate, 2 — lock bay and fall gate, 3 — lock bay head with long flow round, 4 — lock bay and flow round, 5—13 — cross-section of locks of concrete and reinforced concrete.

embankment core is long, the gradients for seepage into the soil through the boundaries of the object are small, and it is thus rare that any damage be caused by flow pressures. As has been demonstrated by the performance of certain locks at the Donzère-Mondragon hydroelectric works, thin *reinforced concrete walls* have a certain disadvantage in comparison with the more massive classic structures.

The rather greater difficulties in ensuring watertightness and stability are an impediment to wide application of the various types of *prefabricated lock*. With these types of lock, we cannot really guarantee to have the same *interaction between the concrete of the structure* and the soil mass, and we therefore have to ensure a more complete control over embankment behaviour around them than for the more massive design.

4.3.4 Intake Structures of Irrigation Canals

It is almost a general rule that for irrigation canals, the problem of structures along the canal is less serious in individual cases, although there may be as many difficulties considering the whole length of embankment. *Irrigation-linked structures* are very common on such canals. It is sufficient here simply to take note of the off-takes from the river (Fig. 4.27), which often come in tandem, i.e. from either

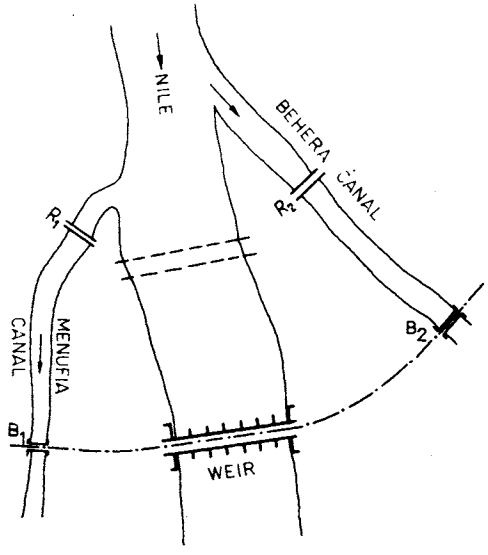

Fig. 4.27. Bilateral-intake structure for irrigation. R_1, R_2 — regulators, B_1, B_2 — bridges.

side of the flow. In this connection, Leliavsky (1957) draws special attention to the functional difficulties involved in irrigation canals and their embankments during a flood, when the off-take structures become *flow regulators*, controlling any flow restrictions, and at the same time regulating the degree of embankment safety.

Considering the various sorts of *settling basins* and *mud traps*, which are only used under special circumstances and are therefore the subject of specialized works (Bouward 1960), this set of features needs chief attention from both functional and constructional viewpoints.

4.3.5 Objects for Distributing and Directing Flow

Such objects have a very varied nature and method of construction, depending on what distribution system is being used with respect to the main channel (Fig. 4.28a). *Distribution canals* may be branched like a fan (Fig. 4.28b), or may have branches jutting out approximately perpendicularly (Fig. 4.28c). The first method has advantages from the point of view of the distribution of water and also of the necessary services (concentration of locks), whereas the second has the edge as regards the excavation required, since its geometry is so much simpler. The occasionally used integrated ditch system is even simpler.

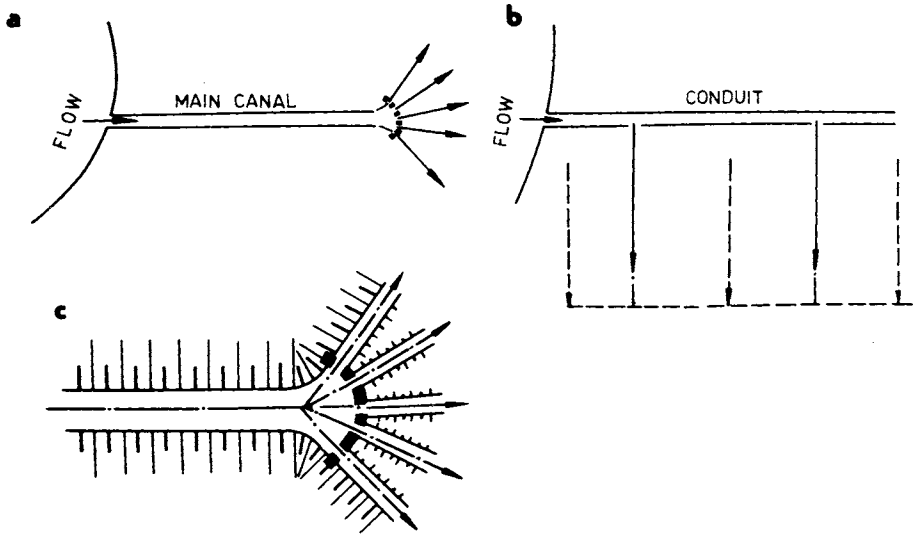

Fig. 4.28. Scheme of a structure for water distribution. a — star arrangement, b — perpendicular arrangement, c — detail of the star.

In the first case, the concrete structure required is centralized, which alleviates the amount of construction work needed. Greater concern can then be devoted to binding the concrete feature to the surrounding earth. However, on the other hand, the joining of these two different media is more complicated in that hydraulic pressures are greater. The factor of static safety is smaller.

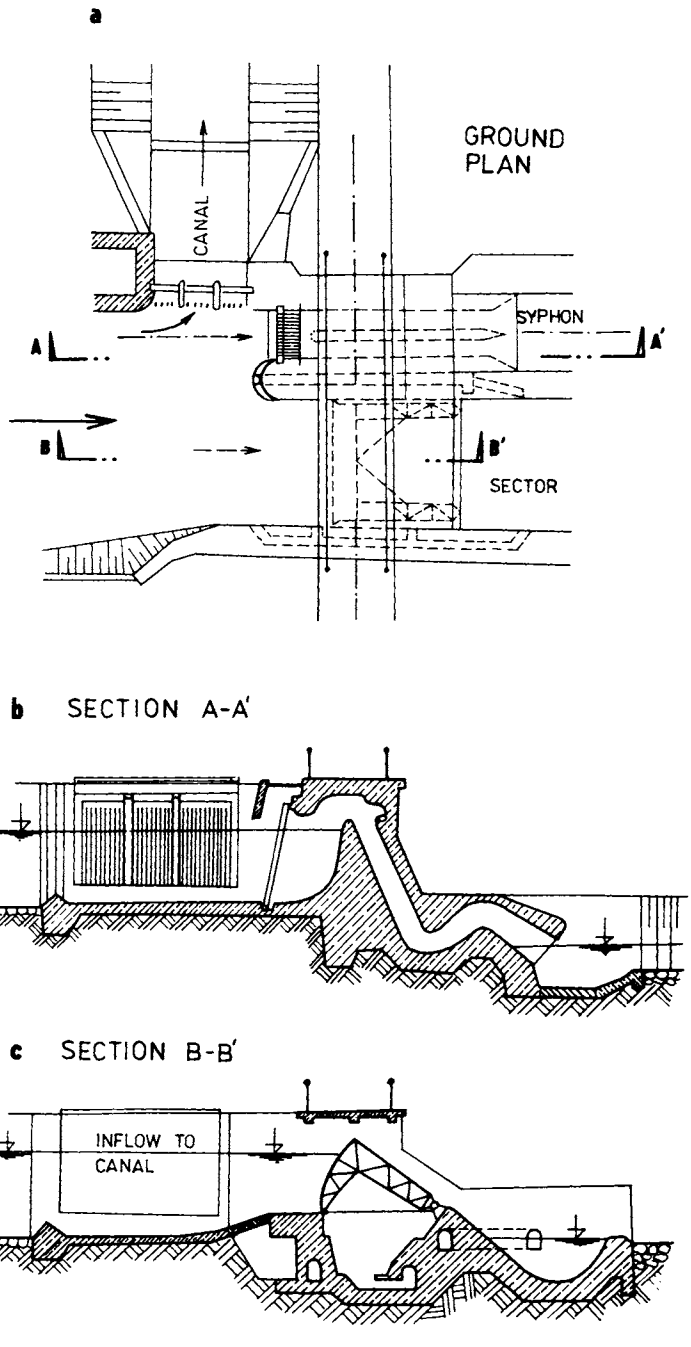

Fig. 4.29. Structure for water distribution and overflow section. a — lay-out, b — cross-section of the syphon, c — sector or weir, cross-section.

Certain functional drawbacks to the second solution can be removed if an automatically functioning safety syphon is built in (Fig. 4.29). In this case, the safety of the earth levées against overspill in times of flood is markedly heightened. The *contact between the earth core and the concrete structure* is indeed somewhat more complicated, but the amount of soil used in the contact region in proportion to the amount of concrete is reduced.

Figure 4.30 depicts the three types of *distribution device* most commonly used nowadays. In the first, the embankment is completely severed by the concrete

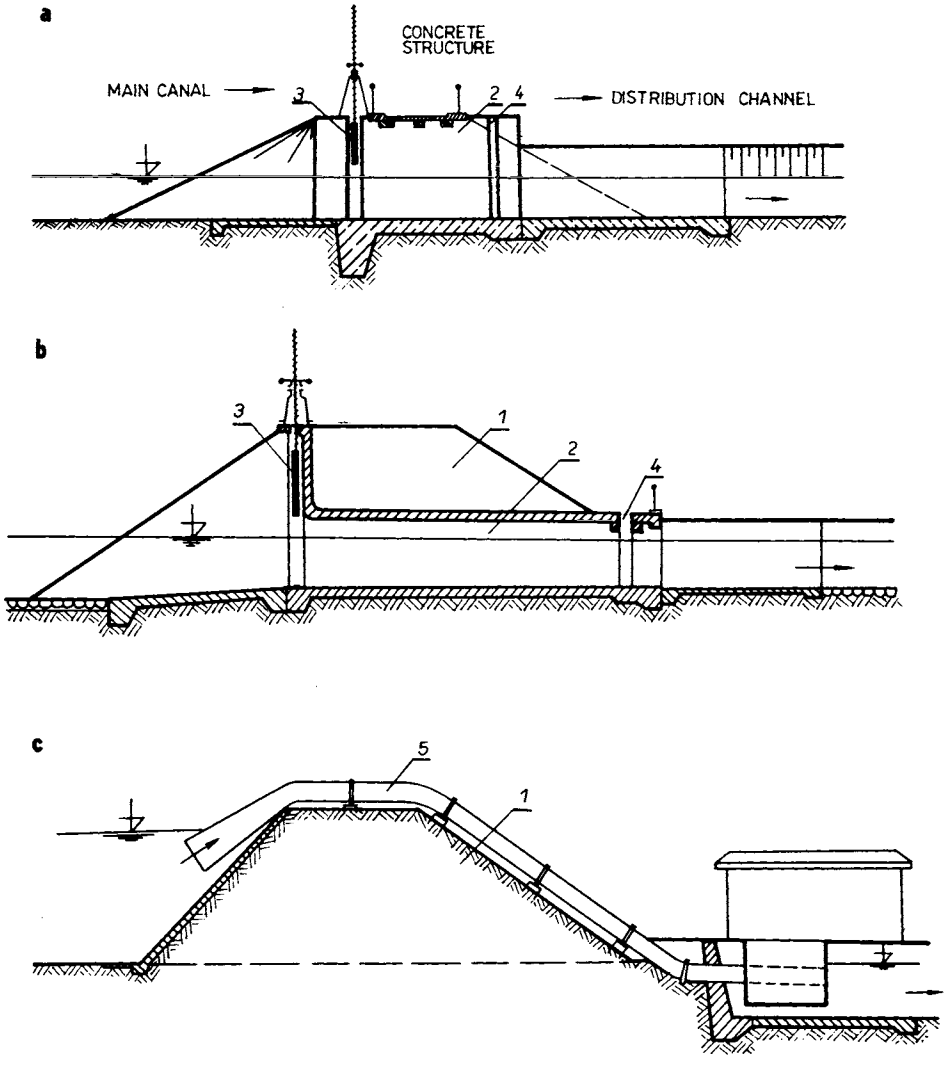

Fig. 4.30. Various types of water-distribution structure. a — bridge and shutter, b — inlet pipe c — syphon; 1 — dam, 2 — concrete structure, 3 — shutter, 4 — groove for a wall, 5 — syphon pipe.

structure (Fig. 4.30a), but the length of concrete face in co' ct with the soil is reduced relative to the second case, since it drops off abov the structures where the soil is hard to work with. The natural bridging created by the presence of a *regulating device* may serve both communication needs and also as a *footbridge* for use when operating the locks. At this juncture, note that a thorough static and hydrodynamical analysis of the central part where the lock is located is vital, since the uplift pressures can fluctuate wildly here. Apart from the relatively large hydrodynamic demands, vibration problems can also occur.

These facts also apply to the solution in Fig. 4.30b, with the sole difference that it is not only soil around and beneath the concrete structure which is subject to shock, but also that above. This danger is considerable, especially with sandy soil. Hence, the question of binding such a structure to the earth core is sometimes tackled by building into the surrounding cohesive soil, which is not so readily transformed to a liquefied state, and at a certain distance is bonded to the sandy embankment core.

On the Váh canals, in the large irrigated areas around Madunice, the third method has proved very satisfactory (Fig. 4.30c). The embankments are of minimal volume, since there are syphons of steel piping lying almost on the top, and the embankments only give and damage slightly.

Canal outlets are structures serving to empty the canal and sometimes merely to relieve the volume of water flow. Usually they are made of reinforced concrete ducting, passing beneath the embankment, and an inlet (Fig. 4.31), generally chimney shaped, rising from the foot of the embankment and joined by a foot-bridge to the top. Sometimes the role of a *safety overflow* is also assigned.

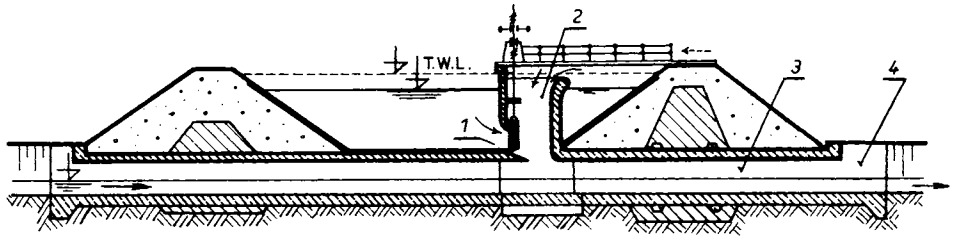

Fig. 4.31. Canal inlet and safety overflow. 1 — inlet, 2 — overflow, 3 — pipeline, 4 — tail-race canal.

A portion of the rim is designed to facilitate the inflow of water at that point. The structure then has a section rather like a small shaft overflow, a subject known in detail from dam engineering (Kratochvíl 1961b). On the other side, there is an *inlet gate* which is very similar to those found at the entry points of dam-overflow tunnels.

In such a structure, the difficult to build but having the most important function is the part passing under the embankment, since there is considerable danger of

inducing seepage along the *reinforced-concrete work.* In order to reduce this threat the concrete ducting is laid in a kind of clay bed, thus acting within the embankment as a sealing core, effective whether homogeneous or heterogeneous.

Since a canal outlet has to lead to yet another auxiliary channel or smaller flow, carried by the piping beneath the canal, this construction may simultaneously take on the character of our next category of structures, those traversing the canal.

4.4 Structures Allowing the Crossing of Flows and Communication Linkage

The commonest structures requiring passage across canals are bridges, aqueducts, gas conduits, inverted syphons, walkways, and more rarely tunnels and culverts.

4.4.1 Bridges and Foot Bridges

Bridges impinge on canal embankments in two main areas, where pillars are needed and on the approach slopes. In the first instance, the earth may be affected by uneven settlement and also imperfect treatment of the soil around the pillars.

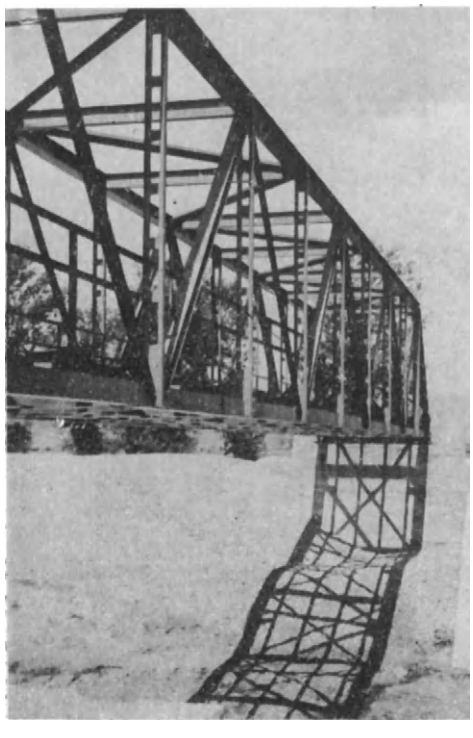

Fig. 4.32. Canal bridge.

The chief danger is avoided by basing *the pillars* at a sufficient depth and if possible on incompressible ground. Besides this, it is useful to be able to lay the *bridge foundations before the embankment is formed.*

Since the embankments will suffer from both the operation of a bridge and also from the required maintenance, it is judicious to choose a type of construction require the smallest and easiest of maintenance while conforming to certain aesthetic criteria. According to current opinion, these requirements are best met by arched structures. In West Europe (especially in France), steel or prefabricated reinforced concrete bridges are commonest. In Czechoslovakia, priority is given to steel bridges (Fig. 4.32), which, when well founded and integrated into the countryside satisfy the given demands adequately.

For foot bridges, the commonest type of construction is generally a *suspension bridge*, since this makes the smallest demands on the foundations. Because the span of this type of foot bridge has a comparatively small effect on constructional requirements, they are often built with their towers set at the foots of the embankments or even totally outside them. Such a structure, as regards both construction and technology, is thus virtually independent.

4.4.2 Syphons

Inverted syphons, which take rather smaller flows under embankments (Fig. 4.33), conceal a significant *danger* arising from *unbalanced deformation* in both structure and subsoil. In this case, the danger is large because unbalanced deformations may cause damage to the structure of the syphon without it being visible on the surface. When the syphon is full, which at the critical point can only be occasionally, watercourse across the foundation plane into the body of the embankment, which may then fail. Since this sort of failure can happen first at a plane of *dilation*, more attention should be devoted to the formation of such planes on syphons under embankments. Below the bottom of the canal they are less dangerous.

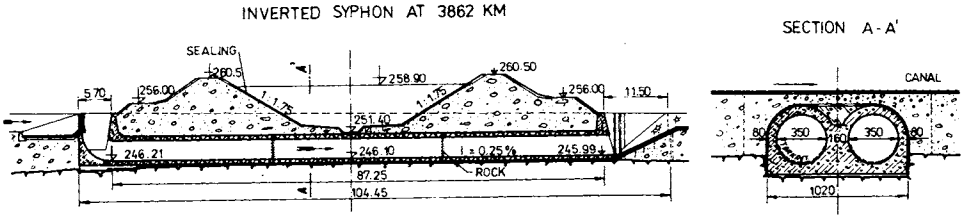

Fig. 4.33. The syphon which brings the stream (below) the canal longitudinal section and cross-section.

4.4.3 Aqueducts

Aqueducts usually present the most complicated problems for canals, where they either have to cross above some natural watercourse, or alternatively allow a river to pass beneath. The greatest complications appear in the second case, particularly if the structure is linked with some safety-relief system. These are generally included in front of or at the end of the aqueduct, in an endeavour to reduce its cross-section. Dimensioning an aqueduct to cope with flows of a catastrophic scale (100—500 times average) would not be economic. On large canals it is possible to bleed off peak flows (of clean water) into the canal, always assuming that the spillway mouth, as far as possible, is some distance from the embankment, i.e. in principle not near the top.

The largest complications are introduced by *expansion of the supporting bridge* in relation to the head of the aqueduct. Expansion must be catered for in such a way that it takes place above some concrete object — away from the line of an

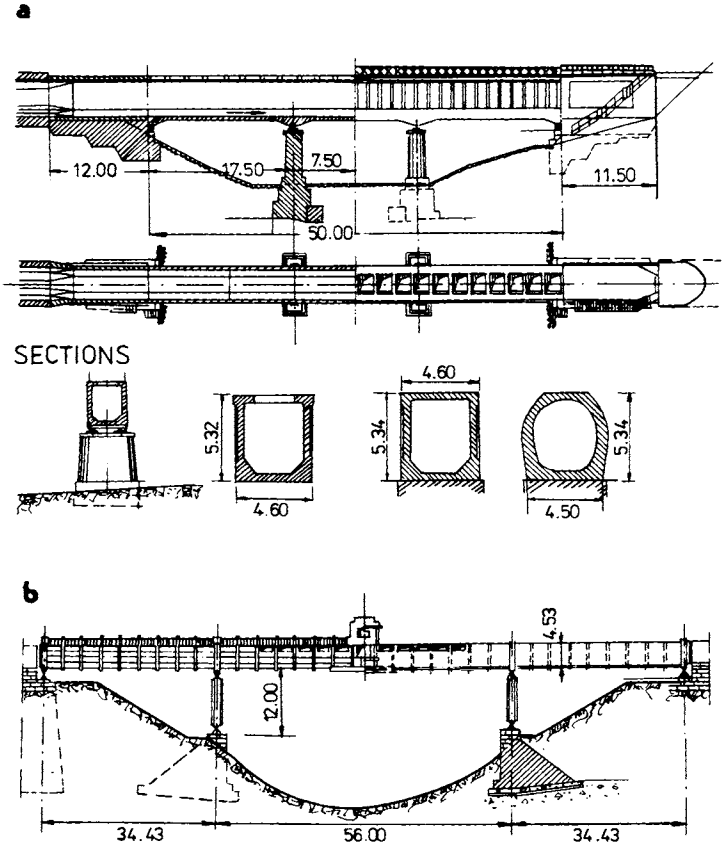

Fig. 4.34. Aqueduct. a — reinforced concrete, b — steel.

embankment, in order that *no escaping water should interfere* with the upper third of the embankment.

The actual construction of the aqueduct (Fig. 4.34) can be steel or reinforced concrete, always separated from the rest of the watercourse because of expansion. In the two cases indicated, an aqueduct brings a canal across a valley, down which a river is flowing. Although the cross-section is apportioned for maximum flow, *openings* (in the upper part of the side walls or in the roof) are made *to enable the overflow to escape.*

The above structures in the body, or crossing of earthen embankments are the most common, but by no means unique, since the variety of purposes which canals and other flows serve makes it inevitable that some extreme structures are constructed, often considerably affecting the structure of the embankments and surroundings. This is the case, for instance, on the embankments of waterway canals where there are ship hoists and lifting apparatus, and also at the junctions of

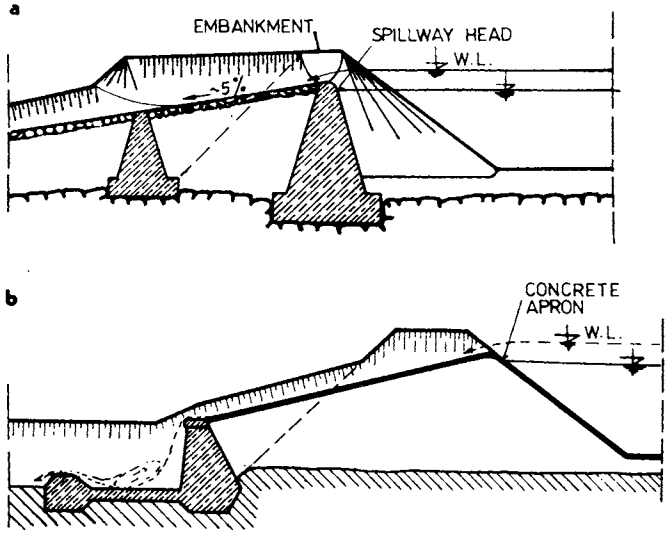

Fig. 4.35. The side overflow with concrete structures. a — concrete wall, b — concrete lining.

multipurpose canals, etc. As regards the structural safety of embankments, one problem is to make possible the various *deformations of concrete and soil* and simultaneously guarantee the watertightness of planes of contact, and where there is seepage to prevent fine particles being washed away. It is often wise to replace a portion of the earth embankment with a concrete structure, or else include a concrete section as a core, with the advantage that it resists watercourse (Fig. 4.35a). Similarly, one can use a *concrete sealing apron* (Fig. 4.35b), which forms a safety overspill, occasionally carried out on levées.

4.4.4 Other Crossings

The protective guards allow foreign flow to pass through the body of an earth embankment so as not to affect its function adversely, not to restrict the operative capability of the flow concerned too much, and also maintaining the safety of both structures. These guards, usually steel or reinforced concrete, are built-in the body of the embankment, either directly while they are under construction or subsequently using special apparatus for pushing them through or drawing them up prepared bore holes.

It must be noted that these flow crossings with the body of an embankment, whether of a canal or levée, are very often the cause of failure, inundation or disaster. Such crossings should be avoided whenever possible. It is almost always safer and cheaper to construct aerial crossings (cables, gas conduits, oil pipelines) above the embankments. These aerial crossings *using suspension-bridge* techniques or just piping, a common sight in mining districts, are unfortunately unsightly.

4.5 The Line taken by Embankments

As with levées, the line taken by canal embankments is determined mainly by the natural, or required, artificial flow and by the needs of the waterway they are accompanying. Waterway canals are usually taken along valley floors, whilst *irrigation canals* are generally set on a hillside, to be raised if possible above the ground to be irrigated.

Other governing factors here are the topographical conditions which constrain the movement of material and the distribution of the various structures required; the geological situation which influences embankment foundations and protection against seepage; the location of inhabited areas, towns, housing estates and factories, larger structures and lines of communication.

The effect of all these factors is very obvious in the path chosen for the Váh diverting canals (Fig. 4.36). Topographical considerations forced the planners to choose a valley path where the transportation of material for canal construction was a minimum, since the haulage routes — the embankments of supply channels — had to be built from material taken from waste canals and were relatively short.

There were also geological advantages to be had from this path, because the sandy gravel deposits there (with few exceptions) formed a good foundation soil for the embankments, and also a useful source of construction material. Housing areas

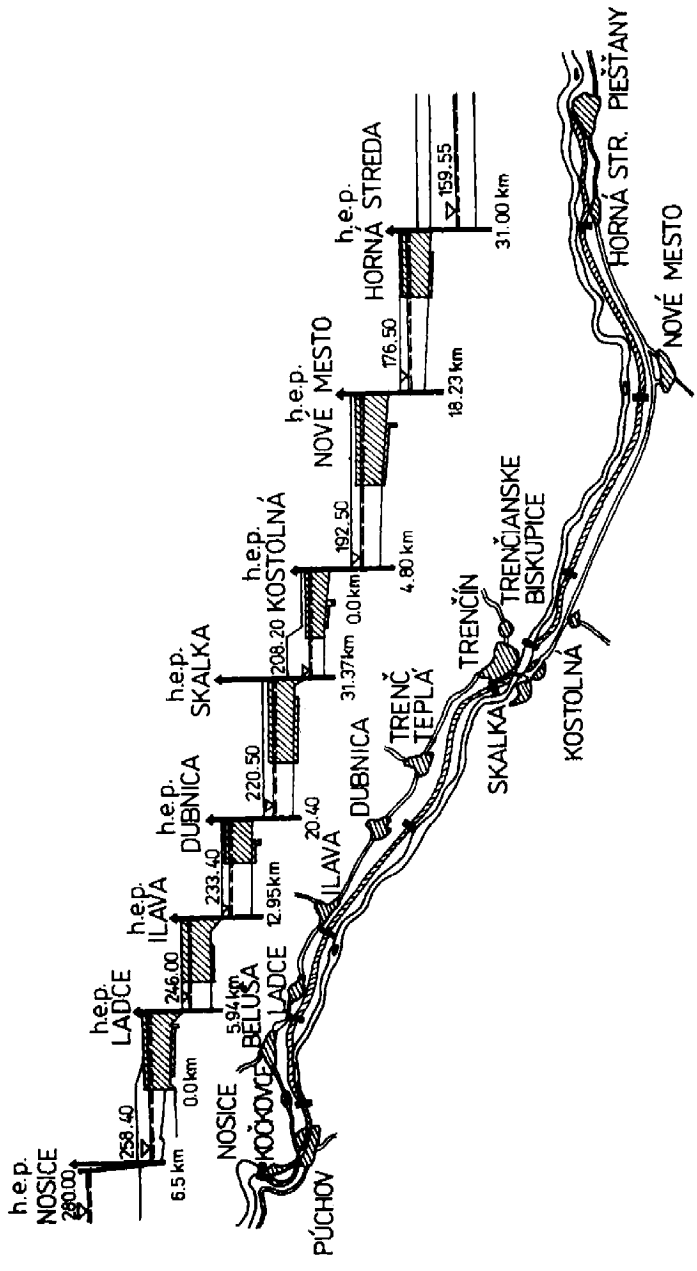

Fig. 4.36. The lay-out of diverting canals in the Váh valley from Nosice to Piešťany. h.e.p. — hydroelectric power station.

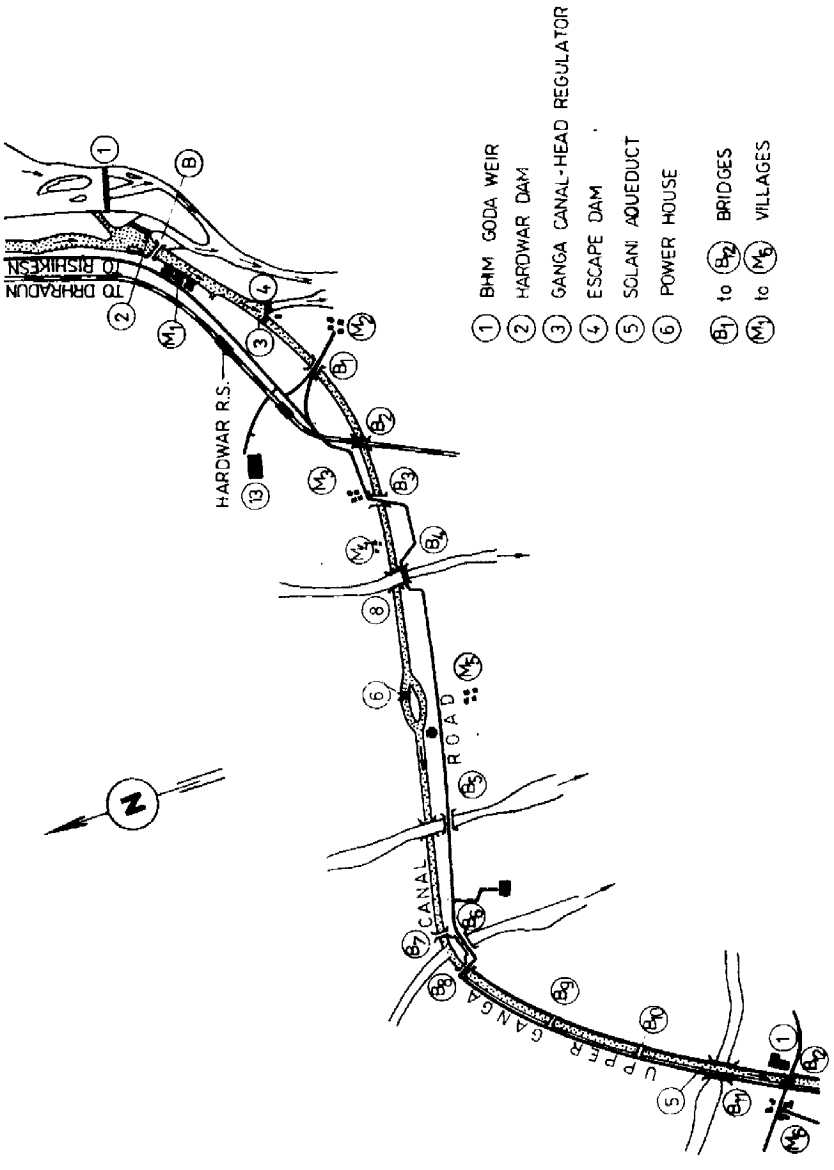

Fig. 4.37. The lay-out of the Ganga canal in India. 1 — Bhin Goda weir, 2 — Hardwar dam, 3 — Ganga canal — head regulator, 4 — Mayapur escape dam, 5 — Solani aqueduct, 6 — Pathri power house; B_1—B_{12} — bridges, M_1—M_6 — villages.

built up along the highway there forced the line of the canal and the embankments between the Váh itself and the highway.

Because of the actual purpose of irrigation canals, the line taken is bound to achieve some height above the general ground level. As an example consider one of the best known canals of this type, the Ganga canal in India (Fig. 4.37). On a length of around 20 km, we see that it crosses four rivers: it passes beneath three flows over one on an aqueduct. The routes taken by roads are adjusted in accordance with the path of the canal, which is only influenced by the sites of five small development areas. On our diagram, we see the various types of structures mentioned in the previous section.

Finally, we show a 20-km-long stretch of the Danube, showing the river levées (Fig. 4.38) and also one of the larger structures, the bridge (at Medveďov), which emphasizes some rather different criteria for siting these levées. The line is mainly determined by natural conditions and the quantity of flow in the Danube. If we were to compare the two sides [left bank (Czechoslovak) and right bank (Hungarian)], we would notice that the area in front of the embankment is rather more expansive on the right bank, the embankment following a path behind various old loops of river and blind arms, leaving a swampy area almost always submerged. On the left bank, much of these swampy patches remain behind the levée. As far as geological factors are concerned, the conditions are equally unfavourable on the two sides. Levées can barely have their paths altered to conform with geological conditions, and are thus at a considerable disadvantage compared with canal embankments. It was once a characteristic of levées that no special measures were taken to face dangers threatening these structures. The most serious threat to levées is always that of cracking, the cause of an extraordinarily large number of disastrous failures.

If we compare the last three diagrams, the Váh power-station diverting canals, an irrigation canal (the Ganga) and the stretch of Danube levées, we see that the greatest number of structures are found on the irrigation canal, and its embankments. The embankments to power-station canals are generally highest, and levées usually present most problems with regard to the subsoil. Although these embankments are the lowest type, the problems connected with their foundations frequently exceed those of other earthen embankments as seen in Chapter 6.

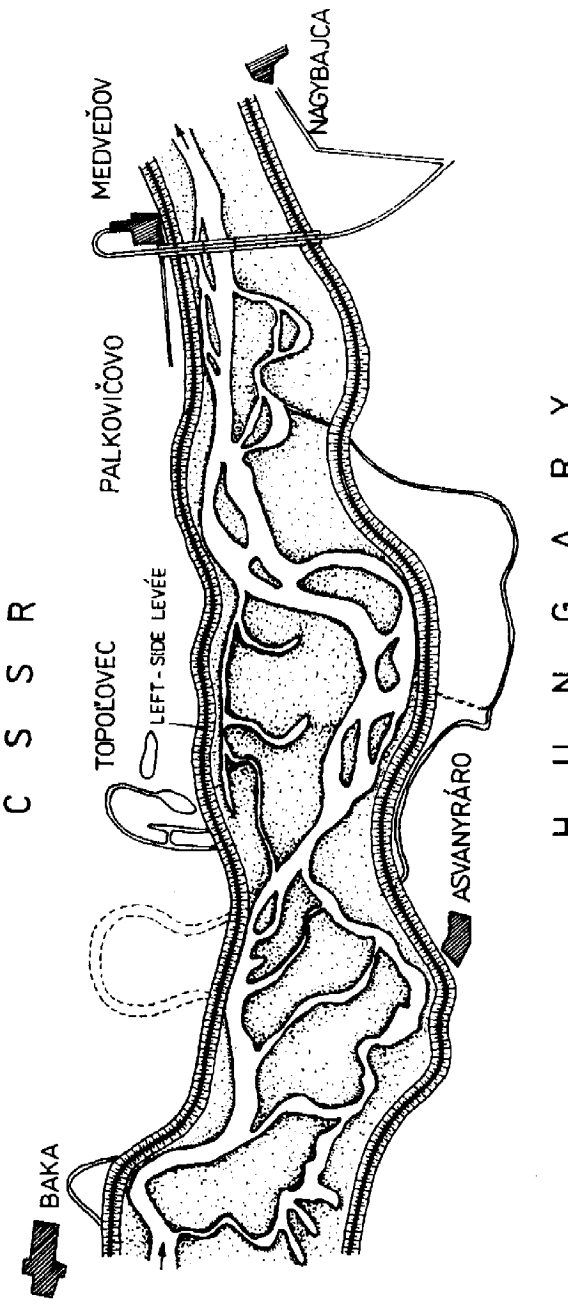

Fig. 4.38. The lay-out of the levée in the Danube valley between the 1805th and 1827th river km.

Chapter 5
POWER- AND IRRIGATION-CANAL SEALING

5.1 Requirements of Sealing

Antiseepage precautions are still vitally important to designers and hydraulic engineers, because observations of canal dams have shown that the sealings are usually the source of defects, and the water losses from canals are rather high. Sealed canals have priority over unsealed canals even in agricultural contexts. In bringing water to sand-steppe terrain — e.g. the Karakum Desert — the main canals must be sealed. Nor is the irrigation of such terrain the only problem. Similar problems are found in loess terrain, e.g. in the Asian Republics of the USSR, as well as in the North Caucasus. In Czechoslovakia, some areas (Záhorie — southwest Slovakia and east Slovakia) are similar to these, and the problems of *canal sealings* are again of prime importance.

As we know, for power and *waterway canals*, appropriate attention was given to this problem at the beginning of this century, to try to *reduce filtration-water losses* and decrease flow resistances. In the construction of irrigation canals, economy comes first. Operation of large irrigation canals in India (canal on the Ganges), in North Africa and in many areas of the USSR have shown that this point of view was wrong, because it worsened the whole economic effect, as well as causing operation difficulties and endangering the safety of water constructions. Filtration water of canals not only increases the underground water level, but often worsens both the filtration characteristics and the shearing strength of soils (especially sand soils). A dam is not made watertight by soil colloids usually considered, but the permeability is raised (often only locally) and it renders dam heels muddy, reduces the stability and results in eventual landslides.

According to Kostyakov (1951), for canals which pass through soils with low permeability, we can assume *filtration-water losses* in accordance with Table 5.1.

The water losses can locally reach up to a factor of ten times these values.

According to experience gathered in large irrigation-canal systems in India, it is generally recommended that canals be sealed only if the filtration losses exceed $1\ l\ s^{-1}\ km^{-1}$ from a delivered $m^3\ s^{-1}$ for main canals and $5\ l\ s^{-1}\ km^{-1}$ from $m^3\ s^{-1}$ for distribution canals, where half of the water from filtration losses can be taken as irrigation water — i.e. used water and not lost.

If we compare the watertightness requirements of irrigation canals, according to modern views, we see that these requirements are similar to those of power canal dams. Further requirements, mainly against mechanical damage and that caused by

Table 5.1. Seepage losses of unsealed canals for various rates of flow Q

Discharge Q [$m^3 s^{-1}$]	5—10	50—100	100—200	200—300
Losses per km [%]	1.1—0.6	0.20—0.15	0.15—0.05	0.05—0.005

the atmosphere are substantially greater for power dams and waterway canals (year-round operation, greater losses from fall-out loss of canal) than in irrigation canals, and are most necessary when there are sealing aprons.

According to Van Asbeck (1968), the *sealing aprons of canals* must comply with general requirements, namely mechanical resilience against impact (ships, ice), as well as erosion resistance, sufficient impermeability, conformability to deformation of dams and their subsoil, and surface smoothness, which guarantees minimal hydraulic losses.

These requirements are met by earth sealings, which always require certain protection, as well as by solid or elastic sealing aprons (if necessary, various types of synthetic sheets with a variety of protection elements).

5.2 Earth Sealing

Earth sealings have been widely used in the past, usually when dams are poured from gravel sand or coarse debris materials on a different compressible subsoil (gravel-sand fluvial deposits with clay components, karst formations, etc.). In such cases, deformations in the subsoil could cause defects in solid sealings. These are also used in waterway canals, where anchors can break the sealing apron. This case is shown in Fig. 5.1, where the clay sealing is placed on a 15-cm-thick sand layer. The sealing is protected against defect by a 95-cm-thick protective gravel-sand layer and a 25-cm-thick pavement.

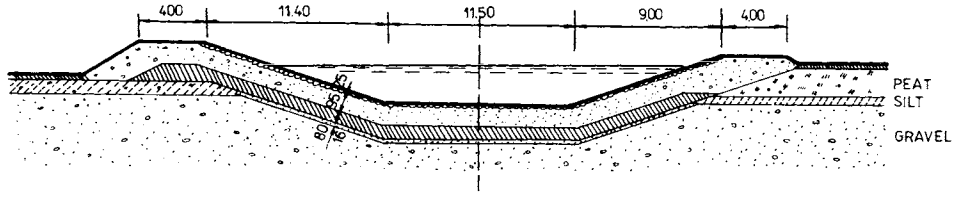

Fig. 5.1. Earth sealing of canal embankment in permeable soils.

In this type of dam and *subsoil sealing*, certainly successful in waterway canals, the sealing-layer thickness (clay, clay sand or loess) is 60—120 cm. The *slope sealing* is laid together with the *canal-bottom sealing*, but this can then be unsymmetrical, if it is sealed to a sufficiently impermeable layer, as shown on the right of Fig. 5.1.

In cases where we can bind the sealing to impermeable subsoil of the dam, it is not necessary to seal the bottom. We bury the oblique sealing in impermeable subsoil by means of clay (Fig. 5.2) and thus the dam sealing is sealed with subsoil. In this case, illustrating the dam of the White Sea — Baltic Waterway Canal, the dam body is built from sandy soils and the sealing, which in the upper part is 1.0 m thick and in the lower part 3.0 m, is built from sandy clays. The whole profile can be formed with relative economy, because the sealing earth in the dam body is not protected by filtering (grading variations in the stabilization part and in sealing are not high) and the rocky pavement, which forms the slope protection (placed on a 15-cm-thick bed) is built-in only at the level of water-oscillation angle. As regards sealing effect, a *clay sealing* is most effective and has a *durability* of several hundred years.

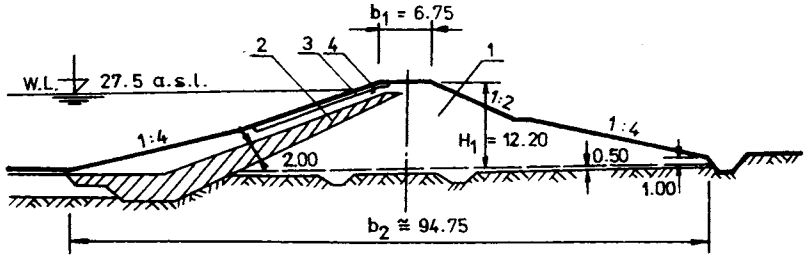

Fig. 5.2. Inclined clay core with tally marks. 1 — silty sand, 2 — silt, 3 — rip-rap, 4 — seam.

As well as this problem, Popov (1950) describes other dam profiles of this canal, which are soil sealed. The most interesting of these profiles is that sealed with two turf layers 0.5 m thick, with a sandy interlayer 0.5 m thick (Fig. 5.3).

In the USSR, these dams are built with two-layer and three-layer oblique turf sealing with sandy interlayers 0.25 and 1.0 m thick, which are not consolidated. In accordance with literature data, turf sealings have proved good both in use (sufficiently watertight) and from the point of view of statics.

In Czechoslovakia, the *swamp soils* and *turfs* have been examined not only as sealing soils, but also as filtration material. They showed advantage in being quite workable and in enabling filters to be made by pressing the soil into plates, which are relatively light and easily built-in. Some verifying research has been done by

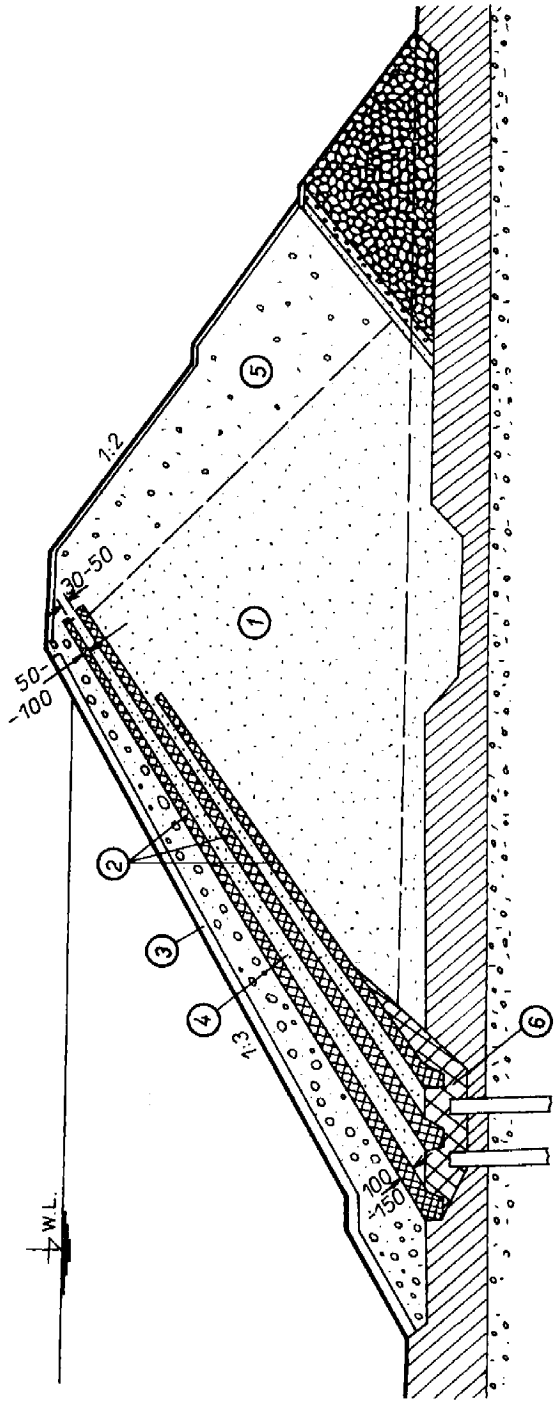

Fig. 5.3. Profile with peat sealing. 1 — sand, 2 — peat, 3 — pavement, 4 — layered filter, 5 — rocky toe, 6 — tally mark.

Myslivec from the Czech Technical University (ČVUT), but realization of dams provided with these elements has not yet been carried out.

5.3 Concrete Sealing

The advantages of concrete sealing, usually employed as the *apron sealing*, could be used mainly when canal dams are built of gravel sand or other permeable materials whose permeability could endanger the canal, but which could be used in a concrete mixture as rocky components. These cases occur in power- and irrigation-canal constructions in the valleys of many bigger European rivers. In these cases, more advantages of apron sealings appear, chiefly in the great *simplification* of dam construction and *technology*. Simplification arises since it is unnecessary to put any special antifiltration and protection elements (filters, drains) in the dam construction. If these elements are used, they can be placed on the finished slope or near the heel of dam, so that the dam body can be created with a uniformly thick profile, on which the concrete apron is placed as a separate sealing element (Hodgson 1977).

Concrete sealing aprons, which are concreted in situ are 5—25 cm thick (in accordance with the height of dam and canal size) and are usually laid on the slope so that they are suitably connected with canal *bottom sealing*, and so they can cover the complete construction, covering both upstream slopes of the dams and the

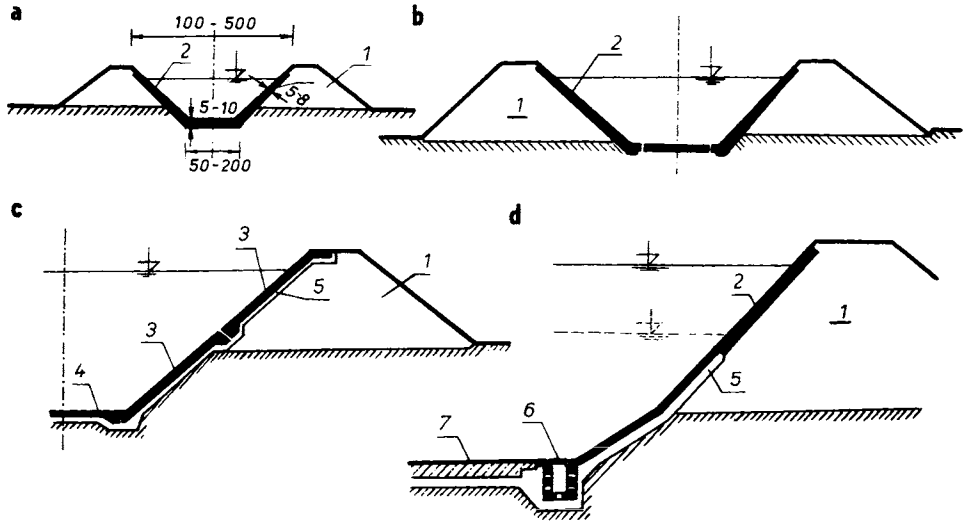

Fig. 5.4. Concrete apron manufactured in situ. a — sealing in one piece, b — sealing divided between bottom and the slope, c — inclined apron divided by a horizontal gap, d — with lifting well; 1 — dam, 2 — concrete apron, 3 — inclined apron divided, 4 — sealing of the bottom, 5 — seam and filter, 6 — uplift well, 7 — sealing.

canal bottom (Fig. 5.4). As shown in Fig. 5.4a, connection of the aprons in one antifiltration element (Fig. 5.4b) in the canal bottom and on the dam slopes has two advantages. The main advantage is that we can neglect the *filtration joints*, which can give rise to unsealings. The second advantage is the improved slope-stability safety, resulting from greater shearing forces and some moments which can be transferred to the slope surface. This occurs mainly in smaller dams of melioration canals. Even if we do not consider these forces, which improve the slope stability, our in-situ observations and measurements show that the increase in safety against local defect rise on the slope is considerable.

In larger dams these advantages are lost, because concrete plates cannot be placed across sharp breaks, if their length measured upright to the break (heel of dam) exceeds 15—20 cm. In these cases, we must remember the development of deformation breaches and of breaches arising from heat stresses of construction (thermal differences on the slope and in the canal bottom). As observations on the Váh canals showed, the thermal stresses produced defects more often than we had assumed (in homogeneous subsoil and in well constructed dams, 60—80% of breaches were due to different heat strains — solar radiation and others).

Although *joints* and breaches considerably *decrease the advantages* of concrete aprons, they still have advantages in slope protection, i.e. very good protection with a small coefficient of roughness. A further advantage is easy control and repair of sealing elements.

Stresses caused by thermal differences Δt and by contraction and swelling of concrete can be obtained from the relation

$$\sigma_{t,2} = (\alpha_T \Delta t + \alpha_z) E_c. \tag{5.1}$$

When canal is filled, the concrete swells, the stress in the concrete being given by

$$\sigma_{t,2} = (\alpha_T \Delta t + \alpha_z - \alpha_p) E_c, \tag{5.2}$$

where α_T is the temperature extensibility coefficient of concrete; α_z coefficient of concrete contraction; α_p coefficient of concrete swelling; E_c modulus of elasticity for concrete in tension.

Stress differences arise in the zone of level variation and thus breaches are created (Fig. 5.5).

Friction hinders the free motion of the concrete apron, and the tensile strength $\sigma^{(t)}$ of concrete prevents the failure of this apron. These characteristics together with thickness and weight determine the *allowed length* l_p of concrete plate (in the direction of longitudinal axis of the canal). According to Gubin (1950), we can determine this length through equation

$$l_p = \frac{2d\sigma_{al}^{(t)}}{k_n(d\gamma_b + H\gamma_w)f}, \tag{5.3}$$

where d is the thickness of concrete apron; γ_b, γ_w volume weight (unit weight) of

concrete and water; H watertight on the apron (pressure height difference); f coefficient of friction of concrete apron in butt joint (joint gap) between subsoil and apron, k_n coefficient accounting for unevenness of resistances to length unit.

Where the sealing thickness is 10—20 cm, the band lengths of non-reinforced concrete sealing are 4—12 m; most frequently they are 6—9 m wide and the *apron thickness* is about 15 cm. For these relations Smrček (1958) gives the concrete expansion for one year, for a temperature variation $\Sigma \Delta t = 26—40.5°C$ and for concrete sealing of the water inlet canal of the Ladce power station (measured in 1944) as $\Delta l_p = 1.46—2.34$ mm. For 1 running meter (linear meter) of apron, this gives an average expansion of $\Delta l_{av} = 0.325$ mm and a temperature extensibility coefficient $\alpha_T = 4.1 \times 10^{-6}$.

Fig. 5.5. Crack in the concrete apron.

We mention these data to emphasize the necessity of dilatation joints in concrete aprons. The arrangements of dilatation joints of concrete sealings are shown in Fig. 5.6. We should also mention that the basic requirement in joint arrangement is watertightness and also elimination of excessive stresses in the apron, which arise when there are large openings due to dilatation. Asphalt joint filling satisfies both requirements until it ages. Arrangements 1 to 4 are the cheapest. Arrangement 9 is most expensive but most reliable, because the copper sheet satisfies the requirements of elasticity, watertightness and has sufficient durability. The last three designs (10, 11, 12) show functional and economic requirement compromise.

Certain compromising designs of *dilatation joints* were accepted in the construction of sealing apron joints in the diverting canals of the river Váh (Fig. 5.7) on which many fillings of dilatation joints were tested over two years. The fillings are

made of impregnated hemp strand with reinforcing steel bar of 7-mm diameter, filled with cement. The first was a rubber angular band and an asphalt filling. Emphasis is on the rubber sealing band, made especially with a high percentage of para-rubber (90%). For these rubber bands, we are given the modulus of elasticity 400 kN cm^{-1}, the proportional limit 250 kN cm^{-1}, the limit of compressibility 17 600 kN cm^{-1}, the breaking strength 20 000 kN cm^{-1}. After 20—45 years' operation of the river Váh diverting canals, the rubber sealing has proved good. Reinforcing steel bar was poor, and therefore in maintenance of concrete aprons, the steel bars are extracted from joints and broken cement filling is supplied by asphalt filling, as we shall mention later.

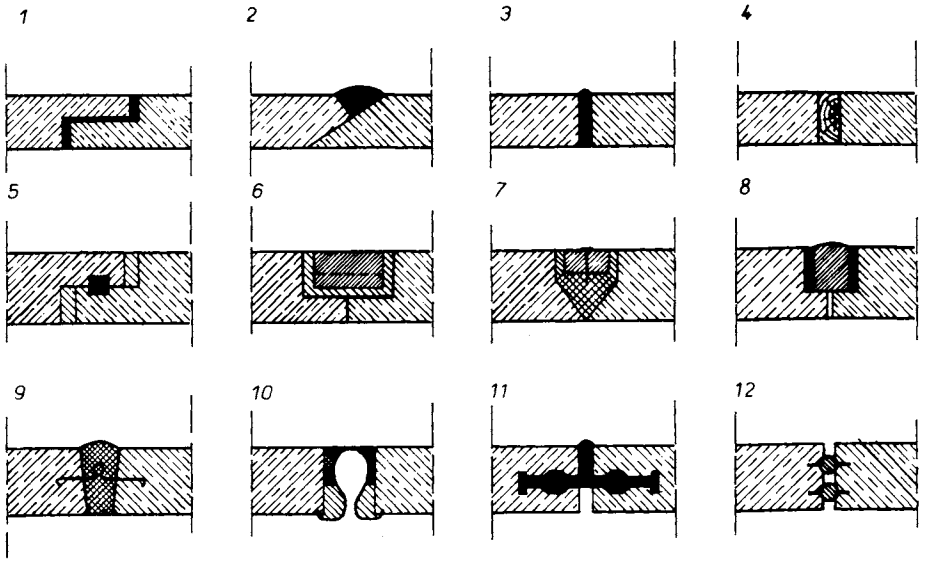

Fig. 5.6. The most frequent types of dilatancy joints of concrete sealing. 1 — joint Z-shaped, 2 — V-shaped with asphalt, 3 — perpendicular with asphalt, 4 — with wooden slating, 5 — Z-shaped with asphalt, 6 — U-shaped with mortar, 7, 8 — bitumen and wood, 9 — asphalt and copper, 10 — aluminium, 11 — rubber stopper, 12 — plastic pipes.

The *heel joint*, mechanically and hydraulically most exposed (loaded) underwent some redesign over three decades of operation. First it was shown that this joint is the source of the worst unsealings, and therefore it was covered (in canals below Trenčín) by three 10—12 cm wide and 5—6 cm thick steel bars. This batten was to serve as a safety element of the joint under pressure of water. This sealing has not been successful and therefore the batten was replaced by an asphalt filling, which fulfils the function of complementary joint sealing element much better.

In characteristic problems of concrete sealing aprons, we should advise on two important design points, connected with improving the stability of aprons. This is

made easier by uplift. When the concrete sealing is made easier, *friction* due to the weight $(N-U)$ tan Φ on the slope decreases its stability (Fig. 5.8). It may be done such a way that it satisfies the condition

$$(T+P_w)<(N-U)\tan\Phi$$

and in this case the sliding should not be done on the slope.

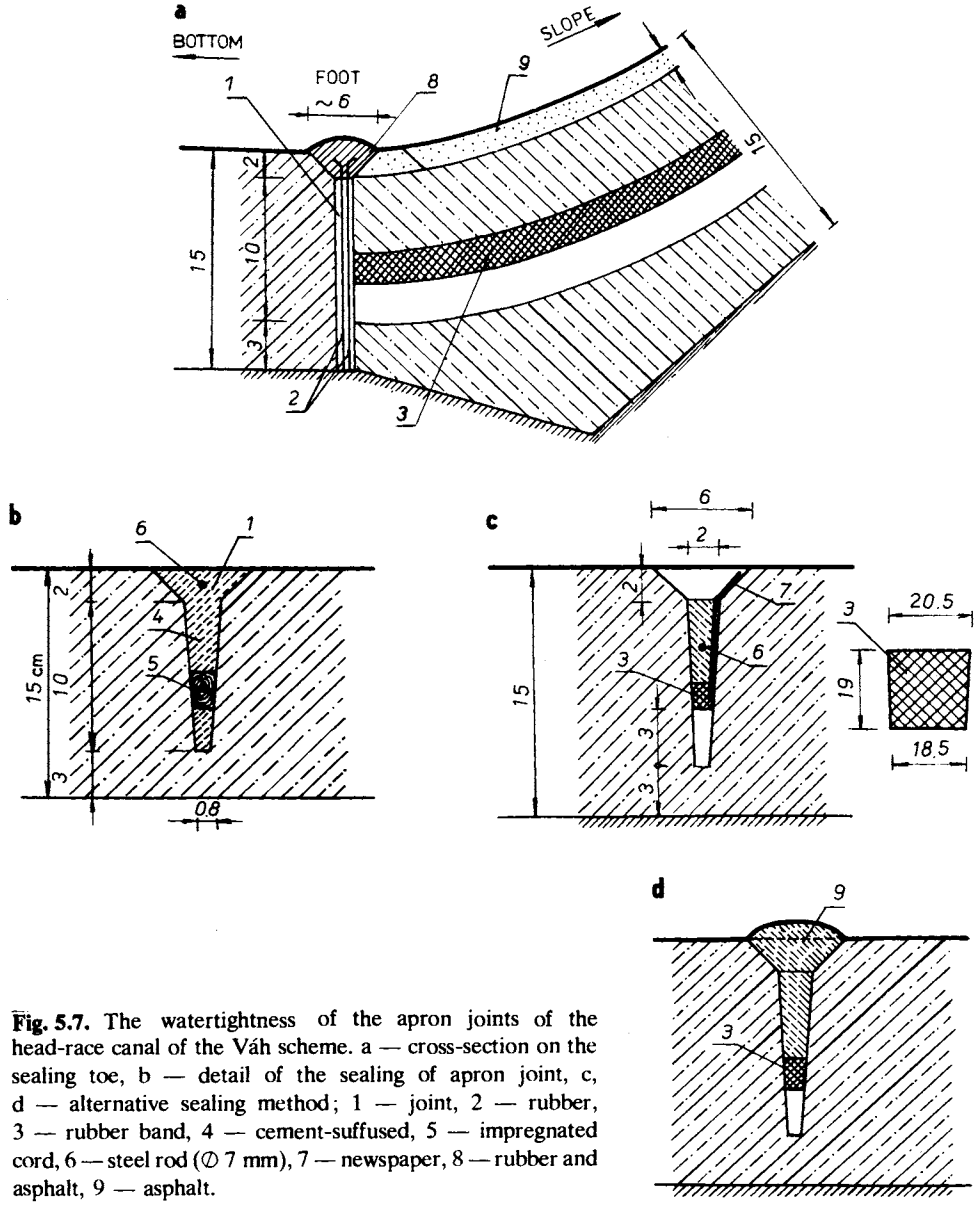

Fig. 5.7. The watertightness of the apron joints of the head-race canal of the Váh scheme. a — cross-section on the sealing toe, b — detail of the sealing of apron joint, c, d — alternative sealing method; 1 — joint, 2 — rubber, 3 — rubber band, 4 — cement-suffused, 5 — impregnated cord, 6 — steel rod (∅ 7 mm), 7 — newspaper, 8 — rubber and asphalt, 9 — asphalt.

In the second phase, we can have $(N-U)$ negative; the water pressure is directed away from the slope and the apron breaks. Both these cases of apron breakage have been observed in canal-dam construction, mainly in irrigation canals, which are unused during non-vegetation seasons.

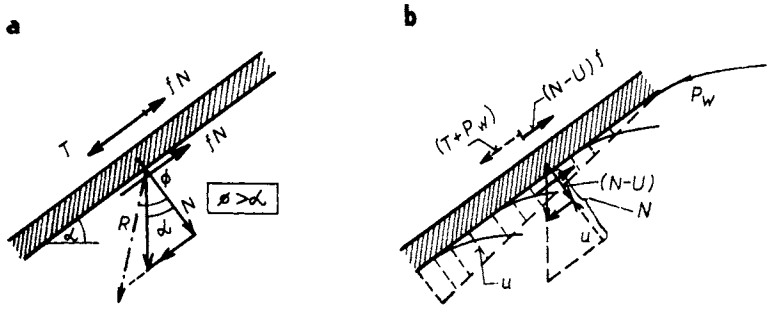

Fig. 5.8. Forces acting on an inclined slab. a — without uplift, b — with uplift.

To protect against the first of these dangers, we build the *supporting footing* (Fig. 5.9a), activate the earth passive resistance against the insecure part of the force, obtained from the difference $(N-U)\tan\Phi-(T+P_w)\leqq 0$. From this point of view, the method shown in Fig. 5.9c is most effective, because it influences all forces and this affects the negative stability of sealing; it also partially solves the problem of the second danger. By *sudden discharging* of the canal, when the ground and filtration waters press against the sealing back, the drain must reduce both the uplifts (U) and the pressure of watercourse (P_w) and it can cause damage.

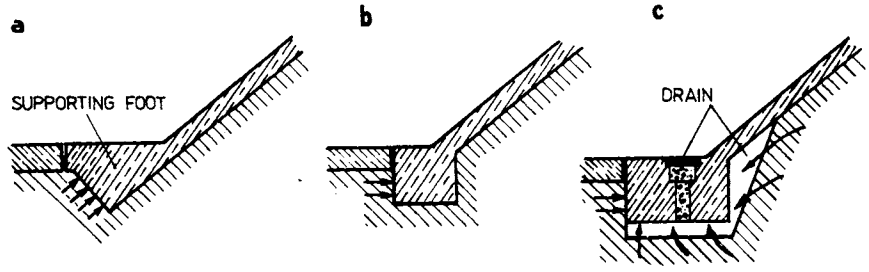

Fig. 5.9. Supporting foot. a — in a form of wedge, b — form of prism, c — with uplift drain; 1 — drain, 2 — covering, 3 — rubber sealing, 4 — perforated pipe, 5 — valve.

A black-coloured plate, which prevents water penetration from canal to drain, raises the amount of groundwater flowing into the canal and so we have a reduction in load. For this reason, the unloading open caissons are sometimes

made directly (Fig. 5.10), mainly in the shape of *circular wells* or *sand drains*, closed by a flap or other closure, which is opened after discharging of the canal. Another latent question is that of soil stability during filtration. Each *drain* or *well decreases* the *uplift* so that it drains water anywhere. At this site of water drainage, the filtration is concentrated and the velocity increases. If we want to reduce the

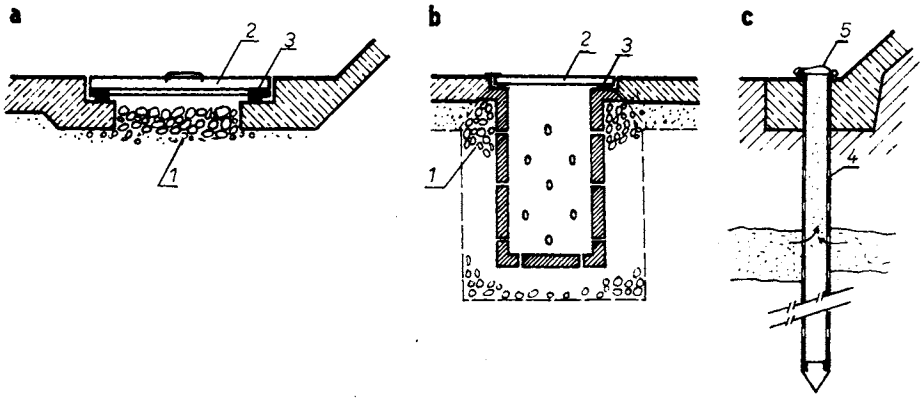

Fig. 5.10. Relief wells. a — with surface effect, b — sub-surface effect, c — deep effect.

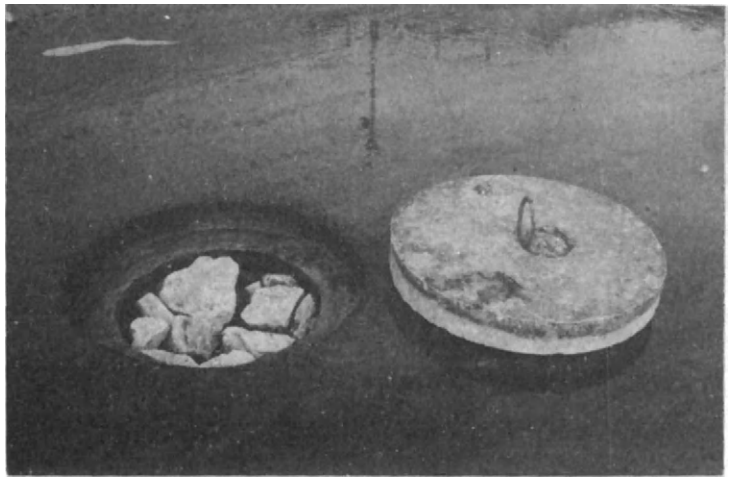

Fig. 5.11. Shallow relief wells on the bottom of canal.

flow pressures we make a stony filling near or in the well, but we cannot prevent replacement of fine sandy grains at larger distances from well or drain. Hence we have the objection to unloading open caissons, and, since they are bult near the

footing (heel) of the dam, they can worsen the sealing stability at this site, because of their local bad influence on the stability of sandy soils, which can drift.

Such a case indicates that in the *diverting canals* in the river Váh, situated partially in a cutting, we should build-in the unloading open caissons on the canal bottom at a minimum of 1.5—2.0 m from the heel of dam (Fig. 5.11). The filtration waters are led to the caisson by means of stony drainage ribs of size 50×50 cm. This type of relief hole, sealing apron security and bottom of canal stability have proved successful.

5.4 Reinforced and Prefabricated Sealing

There are no principal differences between the antifiltration function of sealing, concrete, reinforced and *prefabricated sealings*. However, these two types of sealings differ in apron strength and substantially in technology.

Higher strength of sealing aprons is mainly necessary when the canal dams and the canal itself are built under unfavourable geological conditions. In soils with *different compressibilities*, it is not possible to prevent the uneven deformation of dams and sealing apron. Reinforced concrete cannot transfer these deformations and therefore it cracks at locations of uneven deformation. The breaches appear and the filtration increases, and thus reinforced aprons are particularly found in cases (Fig. 5.12) where we have to take these different deformations into account.

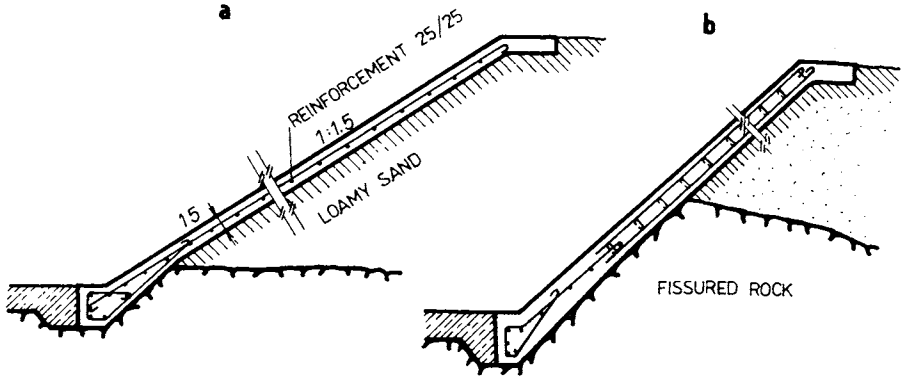

Fig. 5.12. Reinforced-concrete apron. a — reinforcement in one plane, b — reinforcement in two planes in the place of expected deformations.

Distribution of reinforcement is done in accordance with the magnitude of expected deformations. Where we expect uniform deformations, simple steel reinforcement is sufficient (Fig. 5.12a) but where any part of the sealing is under extreme strain (exposed), we apply double reinforcement (Fig. 5.12b). The advan-

tage of *reinforced concrete aprons* lies in the transfer of smaller moments and two-sided pressures, and therefore it is possible to make slopes steeper than in earth sealings and other sorts of sealing aprons.

The thickness of ferroconcrete aprons concreted in situ usually varies from 10 to 15 cm. The dilatation-joint distance is 15—20 m. Steel reinforcement bars have a 8—12 mm diameter and their spacing is 20—30 cm. The same conditions holds in weld reinforcement, which in principle has the function of distribution reinforcement. If the bottom of a canal and part of it is reinforced, reinforcements of these parts are connected by means of an *overhang* (Fig. 5.13). In the case of prefabricated weld reinforcement, the reinforcement is most frequently made in the shape of a net with modul equal to quotients of the joint distance. Most frequent spacings are 3, 6, 9 for a joint distance of 18 m.

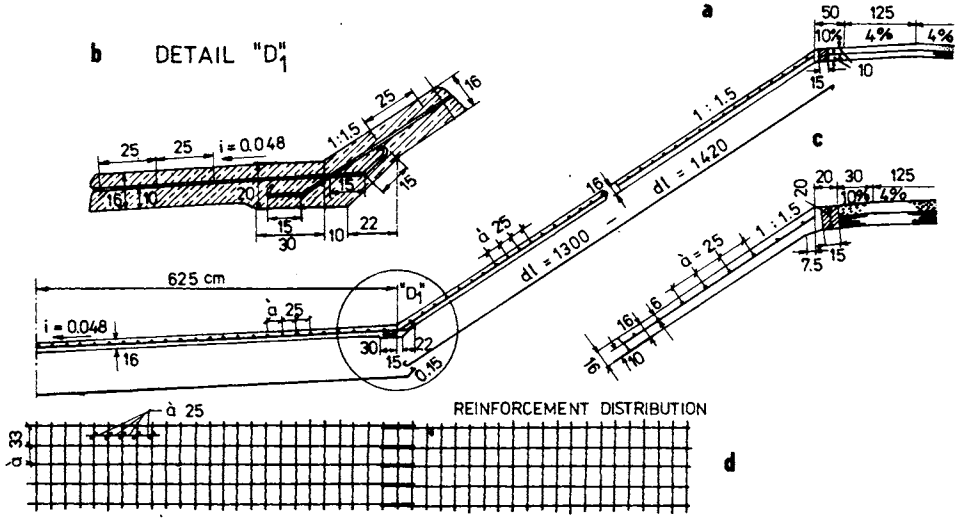

Fig. 5.13. Reinforcement distribution of a lining after Korolev (1956). a — reinforcement distribution, b — reinforcement in the corner D_1, c — detail of the reinforcement near the top of the dam, d — distribution plan.

The demands made of water-construction concretes are valid for stone details and filling into concrete, but we have to follow the requirements of reinforced concretes. Generally more cement (250—400 kg) is prescribed than for unreinforced *concretes*, together with strictly assorted aggregates with maximum grain size 50 mm. Generally the prime task is concrete *watertightness* and therefore concrete mixtures with a relatively high water coefficient, over $w/c = 0.55$, are used. In addition, additives for increasing watertightness and improving concrete-mixture processing are used. If we want to increase the watertightness of the sealing apron, we must make various adjustments before its setting (placing). *Adjustments* made *before placing* have the characteristics of insulations, and are made from a directly

placed layer of gravel of some centimeters, a 2—3 cm thick layer of mortar, 2—3 layers of impregnated cardboard, adjusted and placed as for insulating against water pressure.

The above adjustment causes a desirable *increase in impermeability*, but at the same time it can cause an undesirable increase in uplifting in the back area of sealing during the period of canal discharge. Therefore, the requirement of drainage of the back apron is still more important than that of non-reinforced-concrete aprons. A drainage facility usually has longitudinal and transverse stone ribs, bring the water to the heel, where the pipe drainage leads into the canal (Fig. 5.14). Stiff apron connection on the slope and on the bottom enables the unloading drainage to be removed through the slope sealing near its heel without danger, as mentioned for non-reinforced-concrete aprons.

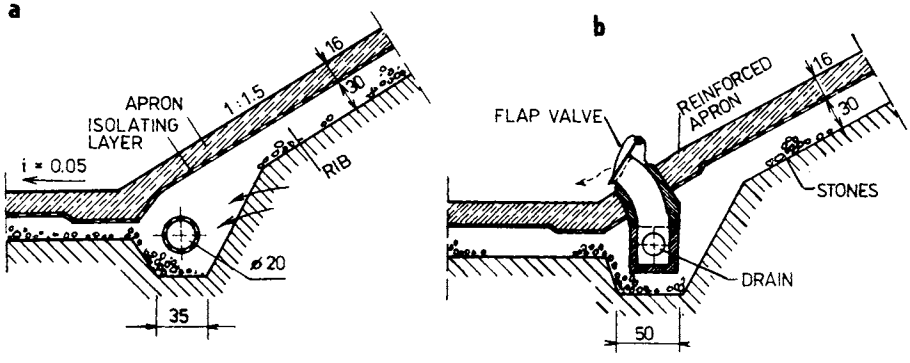

Fig. 5.14. Relief drainage beneath the reinforced apron. a — cross-section. b — section in the place of the flap.

When we expect greater *apron deformation*, a reinforced apron cannot stand over the whole range, it is advantageous to make the apron from reinforced *prefabricated units*, the smaller sizes (compared with the bands of reinforced sealings). *Small plates* make possible the distribution of deformations along the joints so that the construction element will not be damaged. The possibility of large deformation transfer is one of the advantages of prefabricated sealing aprons, which offer other technological advantages. The possibility of industrial production in covered manufacturing plants which are closed and protected from the weather, and the possibility of a wider application of tools in production (welding, handling with reinforcement and others) are among the most important. This results in a further advantage, that of more efficient working time, longer working periods and being able to establish more work-shifts, etc.

When single boards of sizes 2×2, 2×4, 3×3, 3×6 ... 4×8 m are laid,

travelling cranes are usually used, on which the plates are fastened by means of connecting ends, connected with reinforcement. The boards are securely fastened by means of stick grips, so that the air in contact with the smooth apron is exhausted and thus the *prefabricated element* is fastened (usually in 6—12 places). The bending moments and danger of fall decrease, and the fastened prefabricated element is transported to its eventual location. Single prefabricated elements are laid so that no running crevices (joints) appear along the slope line. Continuous *horizontal joints* are often desirable from the point of view of expected deformation. Adjustment of joints must be made to the requirements of expected deformation.

Prefabricated prestressed elements of a width of 2—4 m and thickness of only 3—6 cm and length up to 26 m have a special position among sealing aprons. They are placed on efficiently consolidated subsoil, which is filled with cement mortar, filling the joints. Thin *prefabricated linings* are suitable mainly in the sealing of smaller canal dams, where a single prefabricated element can cover both the dam slopes and the canal bottom: in this case the sealing of *longitudinal joints* is not necessary.

Already by 1950, *prefabricated aprons* were widely used in France, especially in dam sealing of water structures *on the river Rhine*, where prefabricated elements of 750 × 300 cm and with thickness 9 cm (area 22.5 m^2, and mass 5000 kg) were used. These plates were placed with joints of 3—4 cm, in which hemp strand was inserted. Finally, the joints were filled with asphalt.

In Czechoslovakia, the three-layer sealing apron, developed and described by Hobst (1962), is used and consists of *two layers* of wave *prefabricated elements* (with the same form), between which a third sealing layer is located. This layer is made of weldable *PVC foil* with a thickness of 0.9 mm. Isofol BB foils (produced in Fatra, Napajedla) are 140 cm wide and 20 m long. They were applied in one of the smaller dams in Central Slovakia and had a minimum tensile strength 1200 kN cm^{-2}, mass 1.24—1.30 g cm^{-1} (280/2000), placed on the lower layer of wave prefabricated elements which are covered with cardboard without sand. Three-layer sealing aprons, thus placed, were welded to the continuous apron on transverse joints (change in the slope line) using high-frequency welding equipment. The foil was protected by cardboard without sand.

Near the upstream heel of the dam, the apron thus created is attached to a concrete footing, in which the foil is set in concrete, and thus simultaneously covers the footing joint, which is the most dangerous element in all solid sealing aprons — mainly in concrete aprons. This apron also provides two further advantages: it is well *adapted to deformations* and easily repairable, because we can replace defective prefabricated elements. A patch is made from PVC foil and welded to the sealing apron. The hole is covered with a new prefabricated element and filled with concrete.

5.5 Asphalt-Concrete Sealing

In dam structures, *asphalt-concrete aprons* used as antiseepage measures were first applied in the nineteen thirties. For two decades, these initial experiments of the French (which emphasized elasticity and adaptability to deformations) were considered with scepticism. They fasted to demonstrate further advantages, such as impermeability and apron stability, because dams with asphalt-concrete sealing built in North Africa discharged as much as 1—3 l/s per 100 m^2 of sealed surface, even although these aprons had 3—5 layers, a relatively complicated state of affairs. Difficulties in apron maintenance (apron overgrowing with vegetation, local instabilities) gave more evidence to opponents of such aprons, among whom there were many eminent soil-mechanics specialists, for example, Terzaghi. These difficulties were aggravated by the war and post-war situation, since there was a shortage of *natural asphalt* once imported from Trinidad island. Thus, development of this progressive sealing element was retarded.

In the fifties *asphalt-sealing* was put into practice for the first time *in the construction of canal dams* and levées in France and The Netherlands. In the subsequent period the Germans contributed to the perfection of watertight asphalt-concrete composition and to the perfection of special machinery and technological processes. After many years of development, scientists have achieved a satisfactory method of constructing asphalt concrete aprons consisting of a *basic layer* (which can be a drainage layer too) and one (or more) *sealing layer*(s). This concrete is made from earthenware-crushed materials of 0—5 mm size (over 50%), of natural sand (15—20%), stone calcite powder (15—25%), coarse aggregates (12—20%) with ingredient of asphalt (5—9%). A greater addition of asphalt (to 20%) can be used in asphalt-concrete by shower proofing of stone aggregates. The method of production and that of placing as well as the procedure of manufacturing are decisive for a different kind and quality of watertight asphalt-concrete. From this point of view we can distinguish:

(a) compacted asphalt-concrete placed and rolled on the slope;
(b) compacted asphalt-concrete with inserted stones (a rare method);
(c) asphalt-concrete prepared in the formwork (a not frequently used method).

The first kind of asphalt-concrete apron is performed in various modifications which differ in the number of layers (single or double layer) and mainly in the *position of the drainage layer* (Fig. 5.15). The basic layer of asphalt-concrete apron is prepared by perfect compaction of gravel sand, crushed stones or by treated soil stabilizing treatment by cement. The sealing layer has a thickness of 8—10 cm (single layer) or two layers 4—5 cm each. Both layers should be watertight and joined perfectly. If a drainage layer between two sealing layers is inserted, it should have a thickness ($\geqq$6 cm) sufficient to allow it to accumulate and take away the seepage water.

Looking through the *cross-section* of asphalt-concrete apron (Fig. 5.15b, d) in its whole thickness (25—40 cm), we can see that it consists of 5 to 6 layers:

1 — watertight asphalt-concrete layer — AC (eventually 2 × AC),
2 — asphalt macadam — smoothed layer — AM,
3 — binding layer — covered crushed material — BL,
4 — coarse penetrated macadam — PM,
5 — sprinkled hot asphalt ("latex") suspension layer — AP.

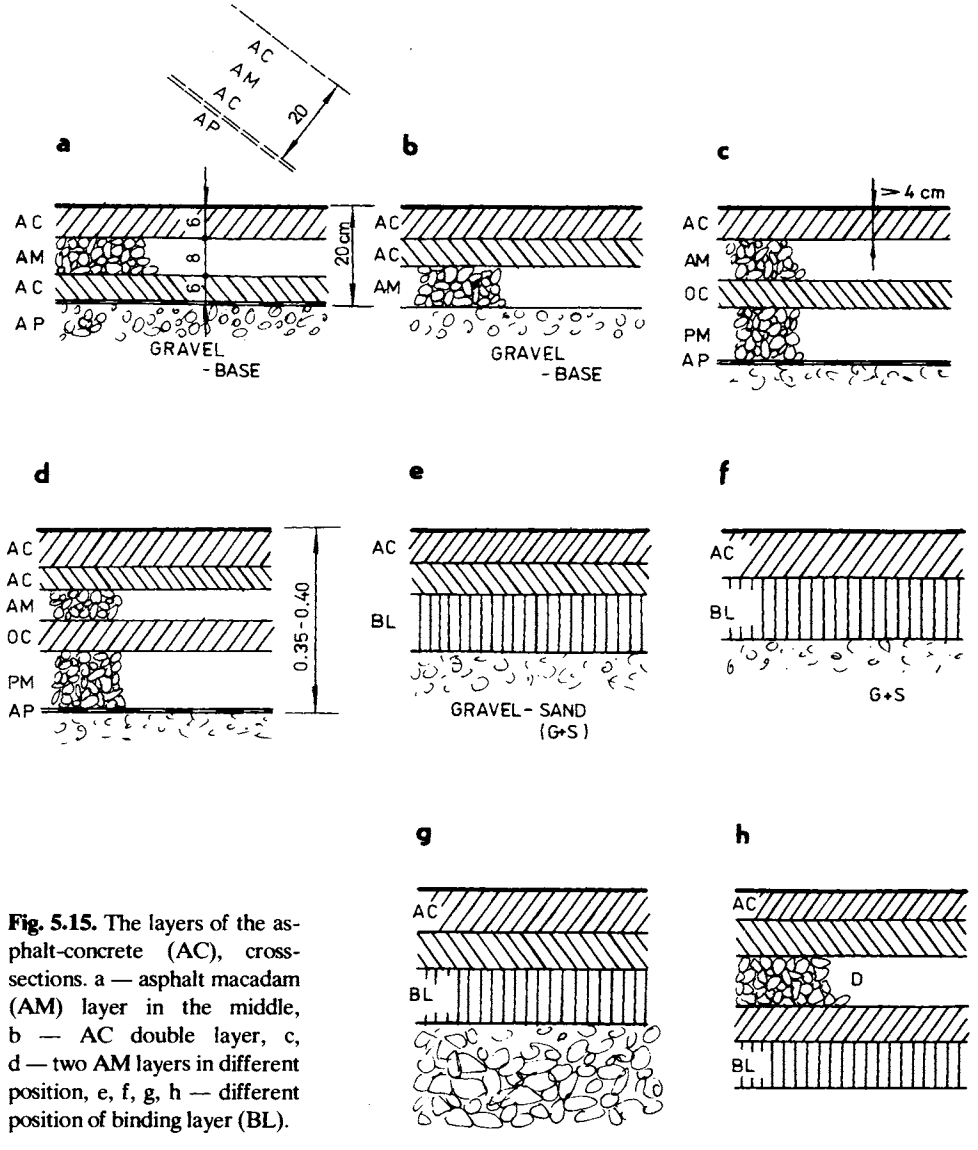

Fig. 5.15. The layers of the asphalt-concrete (AC), cross-sections. a — asphalt macadam (AM) layer in the middle, b — AC double layer, c, d — two AM layers in different position, e, f, g, h — different position of binding layer (BL).

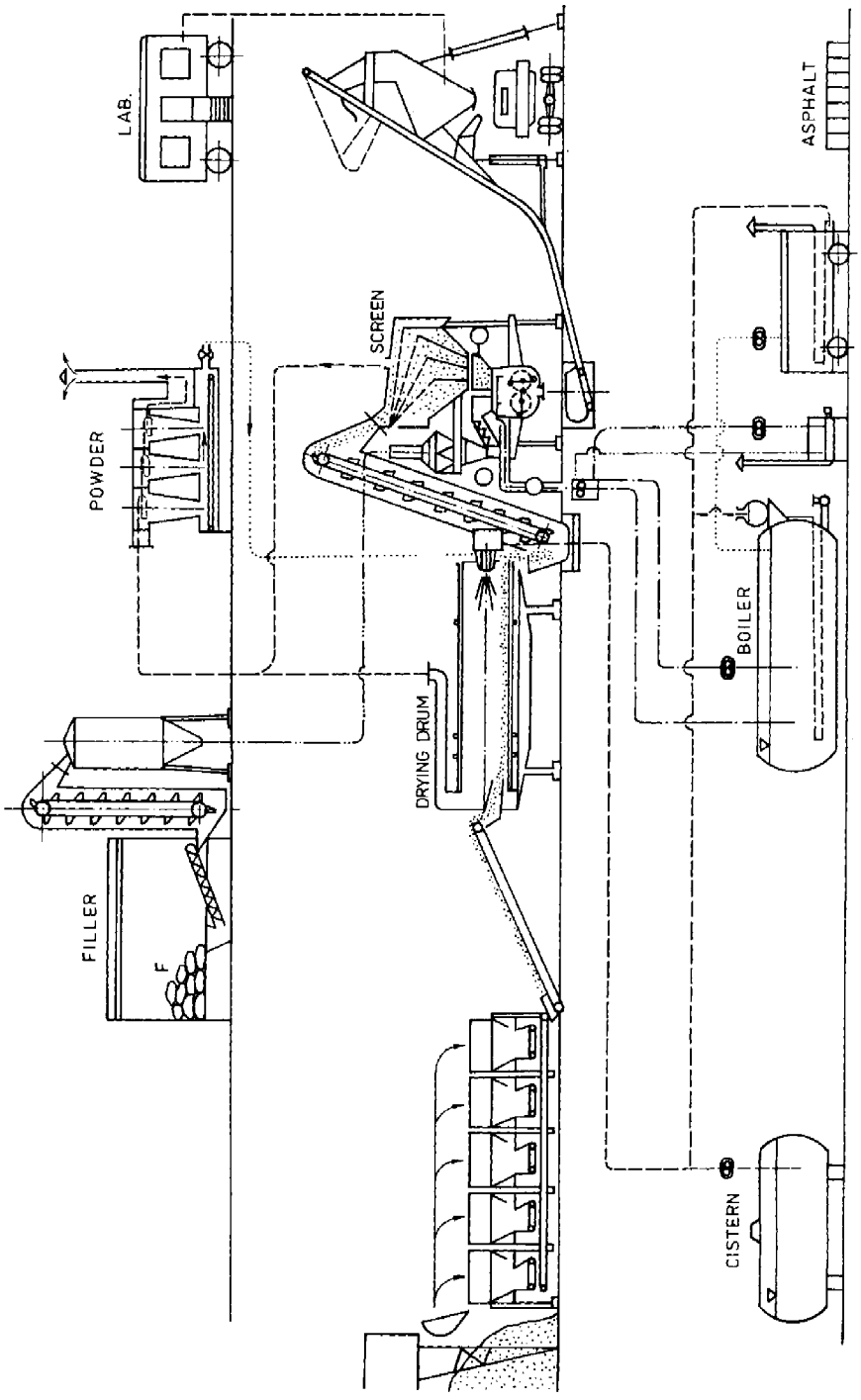

Rig. 5.16. The equipment in the production line and the accessories.

All layers mentioned above are designed with respect to the aim of sealing, taking the construction operation into consideration. The grain size of the stone mixture, its mineral composition and special requirements for the sealing aprons are respected too. It is very important to watch the temperature of the aggregates and of the whole *equipment* (Fig. 5.16) in the production line; beginning with the mixer and storage bins of hot fractions occurring in the storage bins of prepared mixture, transport machinery (conveyor belts, screw grader, trucks) and ending with placing the machinery and compaction means-rollers which usually close the production-placing line.

The quality of the asphalt-concrete aprons is affected by the quality of the mixture, the method of transportation and placing, but especially by compaction of layers and their joints (they should be perfectly sealed). Ludewig (1974) calls attention to the perfect compaction of the base layer (and eventually sub-base) which effects the deformation of the apron (Ludewig and Thieme 1978).

With respect to the workability of the *asphalt mixture* it is necessary to adapt the whole *concrete processing*. The asphalt-concrete mixture prepared hot (T= 170—180°C) in the covering plant is transported to the placing area in isolated thermic bins, from which it is unloaded into the *placing line*. This consists of finisher and very effective compacting machinery (Fig. 5.17). The plant for placing is mounted on a mobile platform with *winches commanded* from the top of the dam. The platform has its own winches by means of which the finisher and skipcar with container move up and down the slope (perpendicularly to the dam axis). The moving container supplies the finisher which spreads the *hot mixture* and usually compacts it by means of a *vibratory beam*. The mixture processing ends with final compacting by means of the roller (Fig. 5.18).

The modern *covering plant* and the plant for placing work continuously by continuous control of the hot mixture temperature which is transported by container from the covering plant to the finisher basket (without its unloading). The placing and processing method used for the sealing layer on the canal bottom is nearly the same as the method mentioned above. In principle, the equipment and its work are more simple; the simple road finisher and vibratory roller can be used for this processing.

The asphalt-concrete sealing layers are placed in single bands 8—12 m wide, the joints of which should be processed most carefully, perfectly consolidated and smoothed, sprinkled with a specially adapted hot or cold asphalt "suspension", and coated with asphalt paint or cement mortar — containing stone powder (filler) or aeolian sands (Kratochvíl 1975).

The main *advantage* of the asphalt-concrete sealing lies in its *adaptability to deformation* and different settlements of the structure and its support. It withstands easily the break crossing between oblique slope and bottom sealing. Using cement concrete sealing it is necessary to arrange a joint in that place which remains a place of increasing water losses and destruction germ. It allowed a good

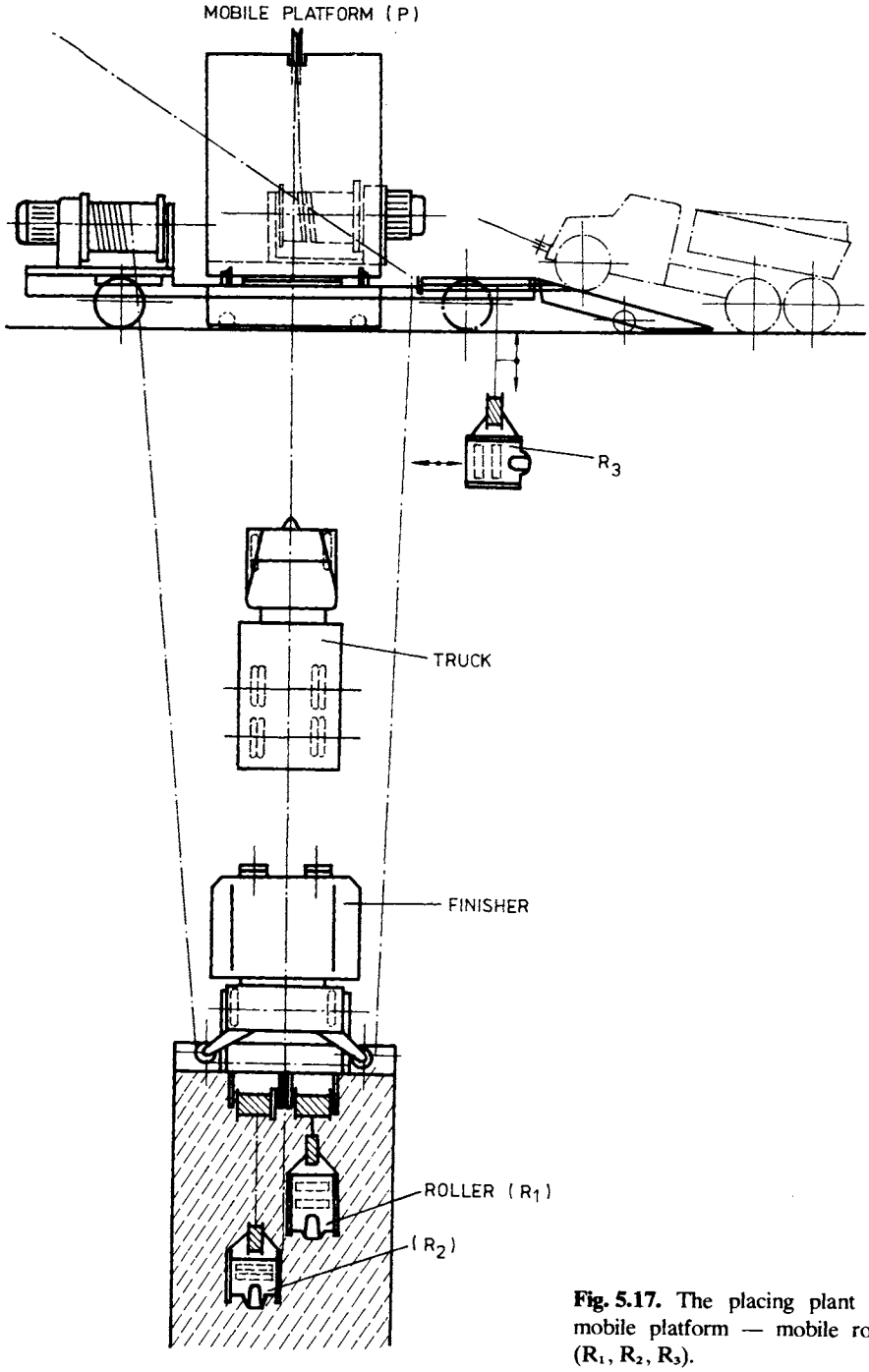

Fig. 5.17. The placing plant with mobile platform — mobile rollers (R_1, R_2, R_3).

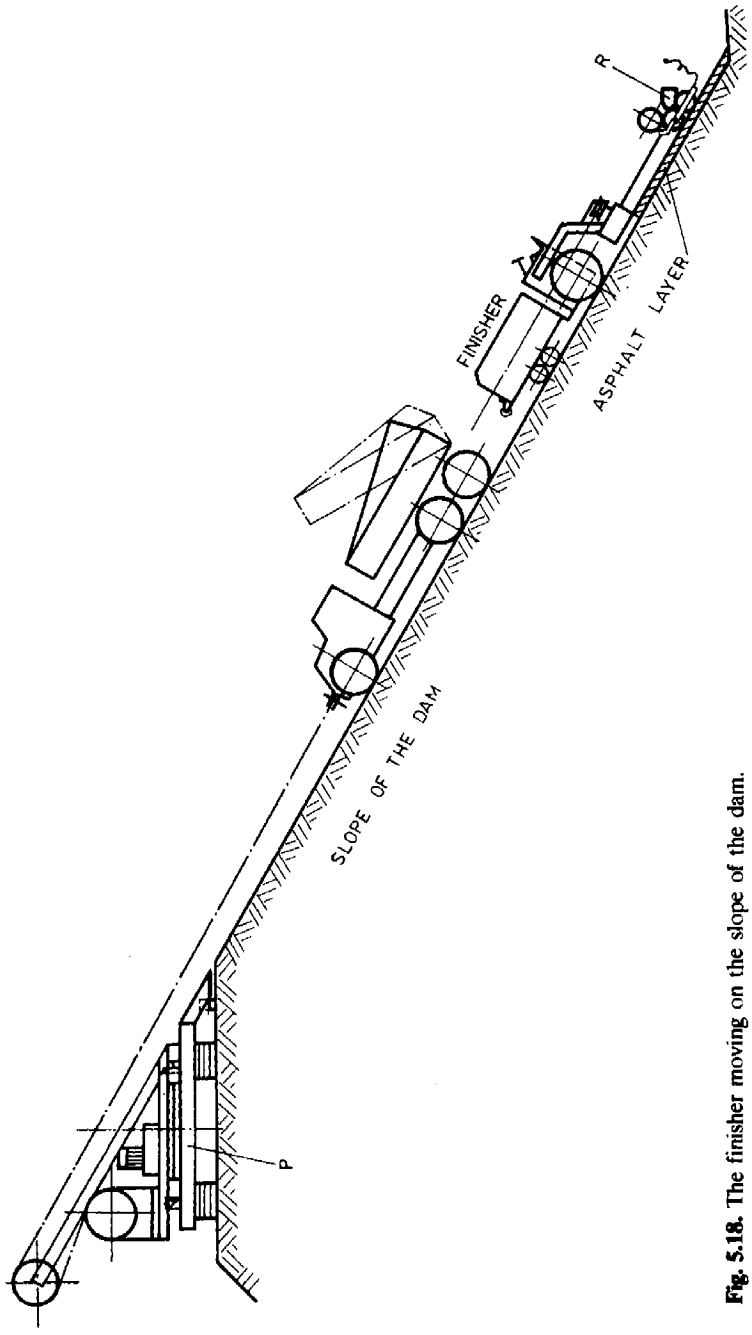

Fig. 5.18. The finisher moving on the slope of the dam.

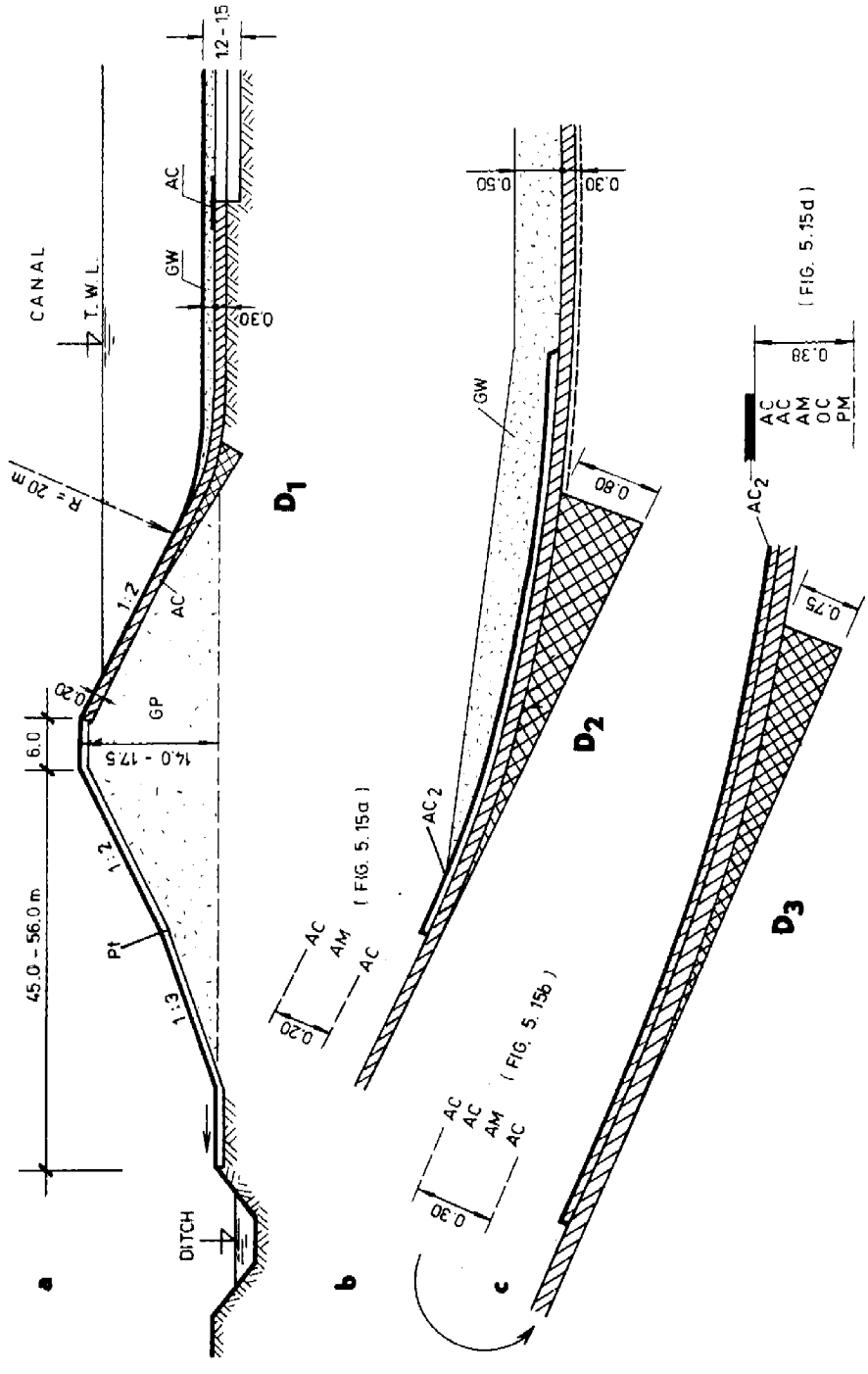

Fig. 5.19. Asphalt-concrete apron and its protection. a — arrangement in cross-section, b — details; D_1, D_2, D_3 — protections for sleading and for anchor lanched by a vessel (Kratochvíl 1974a).

protection (if necessary) for an anchor dropped by a vessel. This can be done by protecting the layer gravel. It facilitates the connection of two various sealings, e.g. *stabilized earth* and asphalt-concrete, as it was in the case of the head-race canal of the Danube water plant near Gabčíkovo — in accordance with the project by Professor Kratochvíl (1974b) (Fig. 5.19). According to his prescription, the following *mixture composition* is used: fine sandy material (0—4 mm) 30%, granulated coarse-crushed material (4—8 mm) 15%, sand-stone powder 10%, powdered material (0—4 mm) 20% and river gravel as a supplement to the mixture.

For *head-race canal embankments* the asphalt-concrete apron prepared from native raw material based on asphalt extracted from oil imported from the USSR, with a designation shower proofing asphalt mark P45, UB50 or A-P80 is designed. This satisfies the following criteria: bitumen content 99%, penetration (at 25°C) 70—100, soften point 44—49 K, fragility point at 10°C, the 100% ductility at 25°C, maximum ash content 0.5%; the inflammation point at 270°C, asphaltene content 11% and the maximum paraffin content 2.0%. The lowered values are given: the penetration — maximally 35% (at 25°C), the ductility "80" at 25°C and the fragility point at −8°C (as the maximum limit). In accordance with the instructions valid for this structure, the portion of asphalt should be 8—9% (on the average 8.5%).

The *binding layer* consists of coarse-crushed material with the addition of 5% of shower proofing asphalt P80. The *asphalt-concrete apron* made of components already mentioned will be placed on the slope of canal embankments in a whole *thickness* of 20 cm (in accordance with the preceding Figs. 5.15a and 5.19a, b) laid on the gravel-sandy layer and will receive a spraying layer of 2 kg m^{-2} asphalt.

On the *canal bottom*, the asphalt-concrete bands 20—50 m wide have a *thickness* of 30 or 38 cm, having the layer composition shown in Fig. 5.15c and 5.15d. The remaining part of the canal bottom will be made watertight by means of stabilized soils (the width of the bottom 340—600 m). The joint of these different parts will be covered by an asphalt-concrete band 3.0 m wide.

In accordance with the engineering practice in large dams and canal embankment sealing well known abroad (Bell 1977) (France, The Netherlands, GFR and Austria) and in Czechoslovakia, the designer supposes the asphalt-concrete density $\varrho = 2300$—2450 kg m^{-3}, porosity $n = 0.5$—2.5% (in the average $n \leqq 1.5\%$) and permeability coefficient $k = 10^{-6}$—10^{-8} m s^{-1}.

Effort towards utilizing many advantages of asphalt and asphalt-concrete aprons caused a new trend in the use of asphaltic sealing elements.

In France, Italy and German Democratic Republic a combined sealing apron from prefabricated elements has been developed. These elements were covered with an asphalt membrane (Fig. 5.20). This consists of concrete square prefabricated elements of 2×2 m and thickness 8—20 cm, placed in cement mortar, spread on the smoothed upstream dam slope. The asphalt layer of thickness 1—1.5 cm is laid on the prefabricated elements, placed with vertical joints. This layer ensures

the *watertightness* of the apron. In order to have good adaptability to deformations, the prefabricated elements are bound as "tongue and groove" in the longitudinal joint, and as a simple cut-off "empty" square joint in the vertical direction. Watertightness of the first joint is secured by a trough-shaped aluminium plate with asphalt filling. The joint surfaces of vertical joints are covered with tar or asphalt and set in cement mortar. Only the top part of the joint is painted with special *sealing binder*, which simultaneously connects the surface fibrous *asphalt membrane*. Added asbestos or other fibres increase the watertightness, elasticity and tensile strength of the membrane.

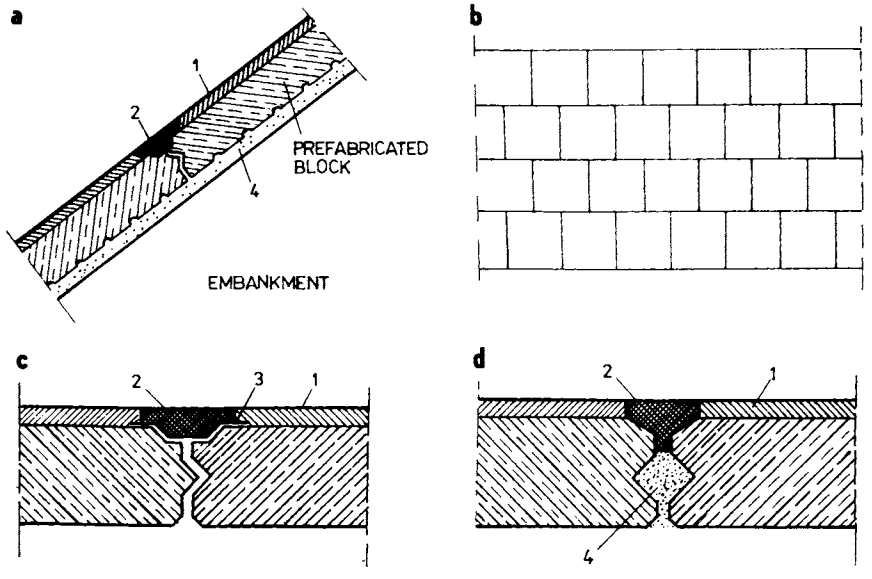

Fig. 5.20. Combined precast apron and its joints. a — lay-out of slabs, b — division of joints, c — form of the horizontal joint, d — form of perpendicular joint; 1 — asphalt membrane, 2 — mortar, 3 — aluminium, 4 — cement mortar.

This briefly described combined prefabricated apron with asphalt membrane, built-in one small dam (Kerngrund in GDR), has proved successful.

A second possibility, on the basis of which we can apply the advantages of asphalts and resins as the proper sealing material, leads to the use of asphalt and resin-stable covers and aprons. Asphalt and *cement stabilizations* are very promising mainly in irrigation-canal structures, where the simplicity in processing and easy maintenance are of prime importance when introducing new sealing materials.

Resin-stabilized covers are made so that a layer of gravel some centimeters thick is placed on a well arranged, consolidated and *resin-sprinkled slope* and which is then sprinkled with resin (4—5 kg m^{-2}) and are reconsolidated. Resin stabilization

is the simplest and cheapest method of surface sealing, though not as good as sealing aprons of cement concrete and asphalt concrete.

Thus asphalt-concrete *aprons*, placed on a *drainage layer* of thickness 12—15 cm, appear — according to French hydrotechnical practice — as safe as concrete and reinforced aprons. However, they overtake the former aprons mainly in that there are few problems with the unsealing of joints, which can anyway be repaired and maintained easily. The fact that many unsealed concrete aprons have been replaced by asphalt-concrete aprons testifies their advantages. For example, Kratochvíl (1965, 1968a) describes the reconstruction of the inlet canal of the water structure on the river Iller near Mosshausen (Federal Republic of Germany), where in 1964 the concrete apron was replaced by an asphalt-concrete apron in two parts. In these cases, the concrete apron with the gravel and resin-sprinkled filling was defective. Such an example is the basis of our own asphalt-concrete layer of thickness 6—7 cm (Kratochvíl 1968b).

There are more successful examples concerning the use of asphalt-concrete aprons, mainly in *France*.

A famous structure in *Austria* is the inlet canal of the St Pantaleon water structure on the river Enz, which was built to $Q = 280\ m^3\ s^{-1}$.

At the present time, it seems that in West Europe asphalt-concrete sealing aprons are popular in power-canal dams, but in irrigation canals concrete aprons have priority.

5.6 Sealings with Foils of Synthetic Materials

In the last twenty years, there has been an attempt to seal the permeable soils in the subsoil of structures, and very obviously in dam constructions (Fig. 5.21).

Some of their advantageous features are used, chiefly the impermeability and elasticity of polymer foils. The problem of utilizing these foils in operation is not as simple as was assumed, because they require protection against heat, ultraviolet radiation and chemicals as well as mechanical damage.

For these reasons, there are *foils* which are protected by soils or specially shaped *prefabricated elements* (Fig. 5.22). The foils can be built-in together with protection from concrete prefabricated elements or earths. The protection methods in accordance with alternatives a, c, d in this figure are assumed from dam engineering, where foil (1) is put in a sandy bed, adjusted to have the shape of steps, covered with protection concrete prefabricated elements (5) or with specially shaped prefabricated elements (6). This method is one of the oldest and most perfected, but it is also most expensive. Thus the Soviet research of VNIIGIM is more directed towards design according to the alternative in Fig. 5.22b, in which the isofoil is placed directly on arranged sandy soil (in gravels there is the danger of defects, in clays and loams there is the danger of foil shear), by means of which it is

also protected. Foil shear is prevented by anchorage in a horizontally placed double small concrete beam (3), from which the foil is led on an adjusted slope to its footing, where it is connected with the bottom foil. The foils can be connected by covering and surcharge (7) or foils (1) and (8) can be welded. Welding into the shape of bands with a length of some tens of meters raises no difficulties, but the foil placing and earth build-in is difficult.

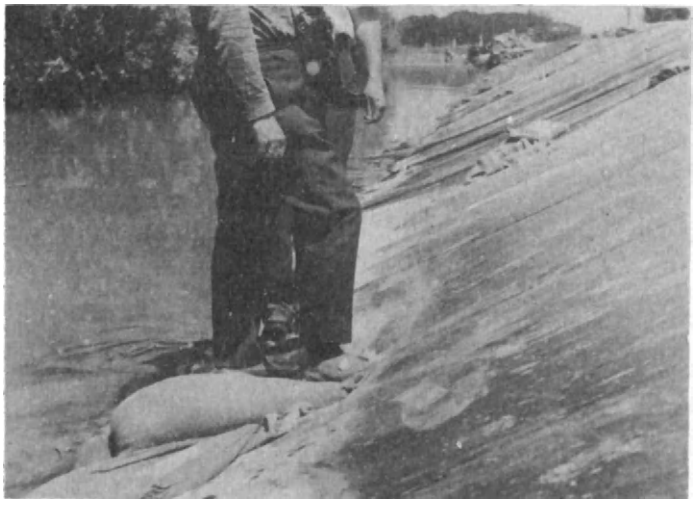

Fig. 5.21. Watertight plastic foil in the slope of a dam.

At present, the *foils* delivered in *the form of bands* with a width of 120, 150 ... 200 cm and with a length of 800—1000 cm, are used. In Czechoslovakia, foils are used as insulation in the foundations of some water and industrial structures, where foils of softened PVC (trade mark Isofol BB, tensile strength $\sigma = 11.7$ MPa, and yield point up to 250%) are used. They are delivered as rolls with a length 10.0 cm and a width 145 cm. The advantage of foils of thickness 0.6—0.9 or 1.1 mm is that they are easily welded by high-frequency heating (compression between two electrodes).

Polyethylene foils were used successfully in the sealing of some part of the sandy-gravel dam in the river Karas in the USSR. Here the foils were placed in a sandy bed and covered with silt and coarse sand. This sand was swept to the foil using a bulldozer, so that the building-in was very easy. In other cases (e.g. in construction of the equalization basin near Port Augusta in Africa), polyethylene foils (with a thickness of 0.15 mm) were built-in between concrete plates with great care. However, there were cases when the foil was placed directly on a rough base of sandy gravel and bush; without incurring damage.

In Czechoslovakia isofoils have been used for dam sealing in more than ten cases. In most cases, the foil was protected by means of cardboard without sand (E500) and by means of concrete. In the first case, the protection was in the form of shaped prefabricated elements, in the second case the concrete layer with a thickness of 5 cm was made in situ. The sealing proved good in all cases. The costs of these sealings are, however, high.

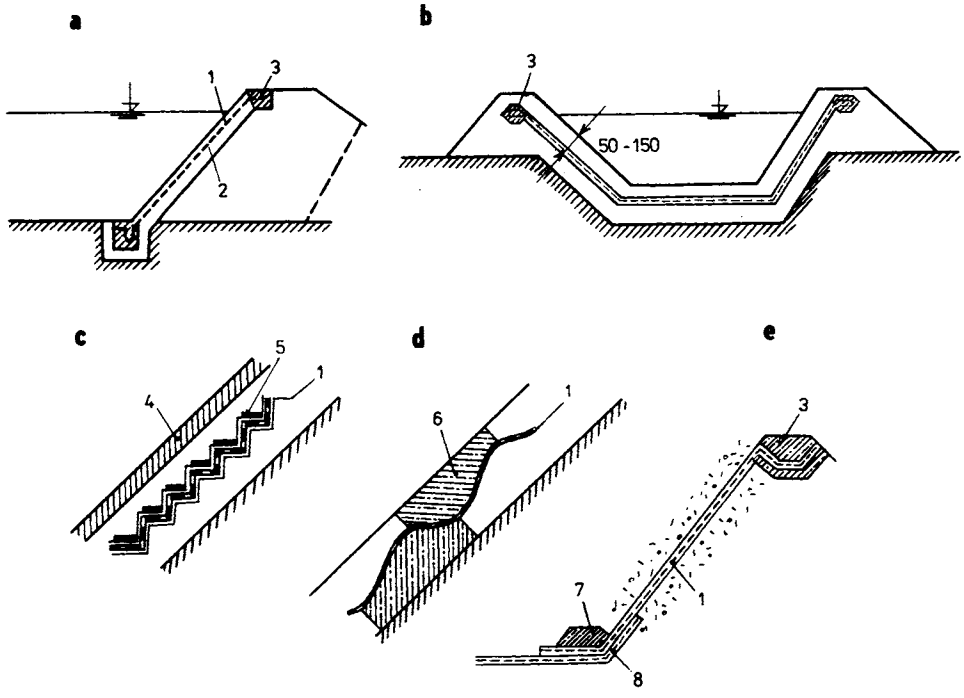

Fig. 5.22. Watertight plastic foil in the cross-section of the dam. a — foil under protecting apron, b — foil protected by a layer of earth, c, d, e — sealing and protecting element position; 1 — foil, 2 — sublayer seam, 3 — anchorage, 4 — protecting apron of concrete, 5 — protecting slab, 6 — S-shaped piece, 7 — ballast piece, 8 — foil on canal bottom.

Sealings with *synthetic-plastic foils* as the basic sealing element (without special protection) are usually more economical than other sorts of sealings and the sealing effect is better than in other classic sealings. However, the durability of these cheap sealings is still a problem. In general, it is assumed that the durability of PVC foils is 25—50 years, but these soft foils are damaged by rodents. At present, research results into the durability and breach danger of plastic foils performed at the Technical University in Dresden contradicts these observations. According to information from Hoffmann (1968) even in cases where the rodents attacked the earth loess dams, the foils in the dam were not damaged. Rodents and other

animals do not attack the foils, because they are repelled by the foil smell of polyvinylchloride.

The sealing foils have a *common disadvantage*; they have a smooth surface and in consequence of this fact a *small friction* angle between the foil and the soil (δ) becomes also small, which results in a small safety of the sealing against sliding. The effort to increase the stability of the sealing and adjacent protecting layer leads to the necessity of moderating the slope angle (β) or increasing the thickness of the protecting layer (d). The precaution is needed by an abrupt canal emptying. In this case the water level goes down rapidly not only inside the canal, but also behind the sealing. Supposing — in accordance with Franke (1972) and Kézdi (1976) — the protecting layer thickness d and water level drop Δh, we get the relation

$$\frac{d}{\Delta h} = \frac{1}{\cos\beta} \frac{\gamma_w \tan\delta}{(\gamma - \gamma_w)(\tan\delta - \tan\beta - \gamma_w \tan\beta)}. \tag{5.5}$$

Equation (5.5) can be used in the design of layer thickness d if unit weight difference $(\gamma - \gamma_w)$ and the values of β, δ are known. In extraordinary conditions it is necessary to put the sealing foil on a slope with moderate (1 : 4 and less) inclination or to insure the stability of sealing elements in an other way.

Constructing the *small irrigation* canals there is no problem of placing the sealing foil as an anchored element without necessity of choosing a flat slope of the embankment. That is why the advantages of the cheap sealing foils (made of PVC, PE, etc.) are here more evident as in power canal with more elevated earthworks and with greater claims to the structure stability.

These sealing foils can be used particularly in irrigation canals where they will be sludged within 10—15 years and the earth is made watertight by soil colloids.

5.7 Evaluation and Construction of Canal Sealing

As mentioned in the previous chapter (mainly in Section 4.1), in the choice of dam profile and sealing we must consider the functional, technical and technological views. In canal dam sealings, we usually give preference to the functional and technological views, because the sealing often determines the economy of the whole canal. If the sealing is faulty, the water losses from canal will be large and, mainly in small canals, even some tens of per cent, though the dams are technically well designed. *Good sealing* enables us to decrease the profile of a canal whose size is dependent on the coefficient of roughness, i.e. on the *smoothness* of the *canal lining* or sealing.

The *technological view* is important, because technological demands recur. In sealing construction, each process increases the *costs*.

If we observe the *flow resistances* (coefficient of roughness), we see that for sealing aprons, the flow resistances in canals is about half the flow resistances of

canals with a pavement or overgrown profile. The sealing aprons in general lead to economy of throughflow profile and simultaneously to the economy of dam profile, because they make possible the construction of *steeper* inclination of *dam slopes* than in earth sealings, which in larger canals require inclination smaller than 1 : 1.8 (1 : 2). In sealing aprons, concrete aprons allow the shearest slope gradients (to 1 : 1.5), in which the filtration losses are relatively small, as verified by observations in our canals and literature data (summary in Table 5.2).

Table 5.2. Seepage losses of canals with different sealing, for various slopes

Type of sealing	Slope tan α	Seepage losses in % Q for a discharge [$m^3 s^{-1}$]				
		1—5	10—30	30—50	50—100	100—200
Concrete apron	1 : 1.5	0.8—0.5	1.2—0.6	0.60—0.30	0.20—0.10	0.15—0.01
Asphalt-concrete apron	1 : 1.75	0.6—0.2	0.3—0.15	0.20—0.10	0.15—0.08	0.05—0.005
Earth sealing	1 : 2	0.5—0.3	0.4—0.2	0.20—0.10	0.10—0.05	—
Watertight foil	1 : 2	0.2—0.18	0.1—0.05	0.15—0.02	—	—

In small canals with a discharge up to $Q = 5—6\ m^3 s^{-1}$, there is usually no difference between canals sealed with concrete or asphalt-concrete and earth sealings, because concrete aprons have no longitudinal joints. The losses increase very fast when longitudinal joints are created. These latter are the source of the greatest losses, because they have little covering.

According to data we have investigated foil sealing and concrete sealing aprons (prefabricated troughs) are for small canals most economical. For dams with height 2—3 m and canal depth 3.5 m ($Q = 10—30\ m^3 s^{-1}$), asphalt-concrete sealings are advantageous. For large canals with dams built from sandy gravel in Europe, concrete or asphalt-concrete sealing aprons can usually be compared. In dams with *earth sealing*, the dam size increases and *construction is complicated.* Dams with plastic-foil sealing have so far been considered sufficiently able to resist the danger of dam burst (break), where there are tens of millions cubic meters of water. To render this sealing very safe certainly would exceed the price of the sealing apron.

The measures needed for stability assurance of different "light" canal sealings are not only expensive but often complicated and their effect is usually quite dubious. The stability and safety of larger waterway and hydroelectric canals must be able to withstand the *wave shock* and water-level changes in great extent. The sealing foils are not usually capable to safeguarde design requirements on the whole and that is why they are refused from the part of designers. Inclined clay core and new kinds of *stabilized earths* (e.g. "hydraton" for example) are refused in

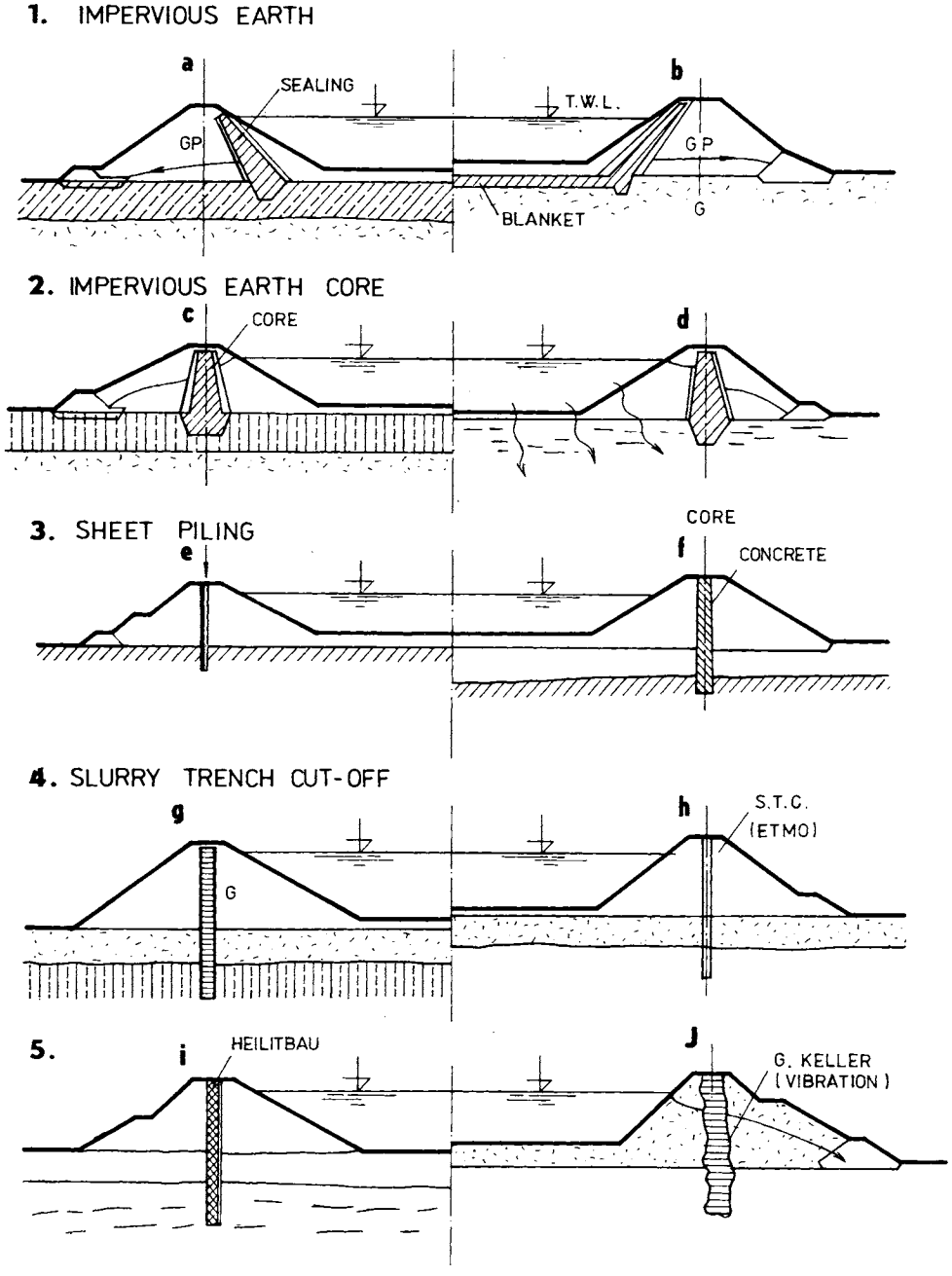

Fig. 5.23. Sealing variants respecting the sub-base permeability. a — impermeable sub-base, b — permeable sub-base, c, e, g, i — low permeability, d, f, g, h, j — sub-base permeability more evident; 1 — inclined clay core sealing, 2 — earth core vertical, 3 — core membrane, 4 — cut-off sealing, 5 — sealing elements bound to a special machinery (German methods).

Europe by contractors as they are weather dependent and complicated in operation and maintenance.

The progress in geotechnics augmented the *choice of canal sealings* — mainly in respect to the special geological conditions as it can be seen in Fig. 5.23a—k representing some variant:

(1) inclined clay core of the dam and canal bottom sealing;
(2) earth-core bonded in the impermeable substratum;
(3) core membrane performed by means of sheet pilling or concrete wall;
(4a) slurry cut-off wall;
(4b) cut-off made in a trench (hole) by an appropriate beam;
(5) cut-off wall combined with folio, after Heilitbau Co. Munich;
(6) the wall made by deep vibration (patented by J. Keller Co., Bauer Co. and others).

A great part of *sealing element* mentioned above is *bound to a special machinery*. The performance of these equipments does not surmount that one of equipment used by placing of asphalt-concrete apron which seems to be the most effective one in large canal constructions. The first three variants have many disadvantages from technological aspects. They do not assure a quick advance of embankment fill, profile of which is interrupted many times. Along the embankment we have to do with 5 to 10 technological bands (parts): gravel in static functional part, sealing, filters, gravel bed protecting part, pavement, drainage elements, etc. A part of them should be performed by hand. The last three variants must be estimated as evolutionary types. In the new construction technique with respect to the quality, performance and operation reliability, experience with both types of asphalt and cement concrete sealing has shown a favourable evolution during the last forty years. In European canal construction the Dingler concrete producing machines from the FRG have proved their worth in the years 1930—1950. It was probably the first moving concrete producing and facing machine with the mixer attached to the chassis, which can move on the canal bottom.

In the last decades the technology and *equipment evolution* on the canal with asphalt-concrete sealing *advanced most rapidly*, mainly in France in the waterway canal — Canal du Nord (1960—1965) construction and in Germany (Mohan—Danube canal construction). According to Kratochvíl (1968, 1975) many other canals as examples of modern technique can be found, e.g. the lateral canal along the river Rhône (connecting Lyon and Marseille), Canal du Centre, Canal du Nord, Canal Rhine—Rhône (in Elsace), the lateral canal of the river Garonne, the lateral canal of the river Marne (by Vitry-le-François), Canal Dunkirque—Valenciennes. Further on the canals in Benelux region: Canal Amsterdam—Rhine, Canal Juliana (Netherlands), Canal Nîmes—Blaton—Péronnes and Canal Gent—Terneuzen (in Belgium). Finally the head-race canal of the water-plant constructed on the rivers

Iller and Enze in Austria and the canal in the Po valley (Milan—Cremona) are mentioned.

Experiences and instructions reached of West Europe canals were adapted in the design of head-race canal of hydroelectric plant on the Danube near Gabčíkovo. This canal replaces the waterway of the Danube in the leg Bratislava and Komárno. Here the use of asphalt-concrete sealing seems to be very suitable. The fear of the damage of the sealing layer by anchors was overcome. A thin (30—80 cm) layer of gravel on the canal bottom is sufficient to protect the sealing from damage, as showed many experiments.

The most remarkable advantage of *asphalt-concrete sealing* apron is in its *easiness to control* and repair besides of perfection in performance by using new modern equipment which safeguard good quality. It is very attractive mainly in the case where gravel embankments are built and the sealing surface exceeds 5000—10,000 m^2.

The *earthen sealing*, slurry cut-off, sealings with foils and other sealings mentioned above can be taken into consideration in construction of *irrigation canals* and power canals which have other sealing material in great store in the vicinity and where the sealing of canal bottom can be overcome, or if the reliability in operation of the sealing element can be omitted as is sometimes the case with foil sealing.

Chapter 6
THE SEALING AND SUBSOIL PROTECTION OF LEVÉE

6.1 Design

The sealing performation and subsoil protection of levées represent a special problem. The reason is that watertight is not the most important property of antiseepage elements. More critical is their regulating and protecting functions in relation to subsoil stability and deformation as well as to filtration failures. This function is more important than that of the seepage barrier. It is wrong to close the soil profile with a levée structure as in the case of the diverting canal of a power-plant. Such a closure would considerably limit the supply of the groundwater basin near the river.

In general, an exchange of river water and groundwater is required, and thus it is not desirable to close the watercourse during minimum water-flow discharge. A ventilating sealing element, operating (closed) only during a flood, would be the ideal antiseepage element. Such elements have been unknown until today, which explains the importance of active protection elements such as seepage ditches, drains, wells, filters and the like, which drain off the seepage water and draw down the uplifts in the footing bottom subsoil as well as in the vicinity of the structure.

In engineering practice, it is thought that old dams and levées function well enough without sealing and protecting elements. This is true only in the case of a homogeneous silty profile situated on an impermeable subsoil — here it is possible to omit the protective elements completely.

Protective elements do not actually increase cost. Use of protective and control elements (filters, drains) can save 15—25% of the construction material, but keeping the same safety factor of the structure. Many levée disasters highlighted the weakness of the profiles, which had structural mass but lacked seepage control elements.

The design of antiseepage and control measures (Fig. 6.1) is based on a detailed analysis of seepage under given geological conditions (Cambefort 1967). Where high hydraulic gradients exist, there is a possibility that the seeping water may erode channels within the dam or in its subsoil especially if the soil (sands, sandy soils) is loose. The control drain (Fig. 6.1a) designed as a filter to provide a barrier to soil particles carried out from the dam body and its subsoil is also an interceptor,

keeping the downstream slope in an unsaturated state. With the subsoil more permeable, deep compaction and a ditch collecting seepage water can be useful (Fig. 6.1b).

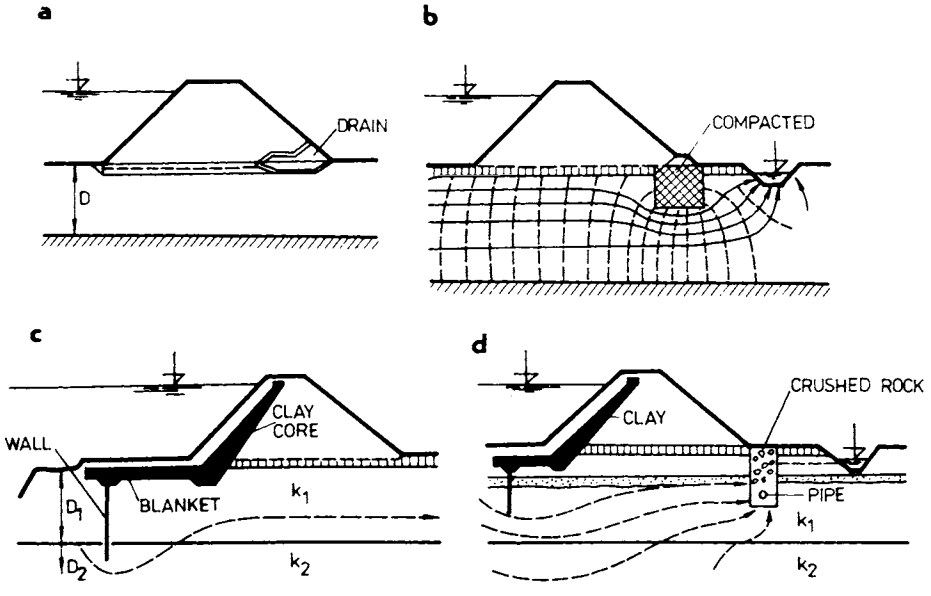

Fig. 6.1. Elements of active and passive protection of levées sub-base. a — gravel toe drain, b — drain and compacted subsoil on the toe, c — clay blanket and deep slurry trench wall, d — shallow wall and seepage channel.

If the demand on the permeability of the subsoil is emphasized and if heterogeneous strata form the sub-base of the structure, more complex antiseepage measures should be considered, e.g. claycore with blanket and cut-off wall with a deep drain or pipe drain (Fig. 6.1c, d). In alluvial deposits, an extensive loam blanket ($L = 5—20H$) combined with a deep perforated relief well can solve the problems of the antiseepage and control measures. In the case of the foundation soil which is more permeable than the dam, underseepage control is always essential. Underseepage can really be eliminated using a blanket and an "impermeable" cut-off. The design and calculation of such a complicated system ("impermeable" structure, permeable subsoil, less permeable blanket and impermeable wall) are sometimes more difficult than for a large earth dam. This is true for complicated boundary and flow conditions. In the dry period, the earth in the profile of the levée becomes dry and a number of changes (shrinkage, cracking) can appear in the soil character and in the flow regime. In the case of an unexpected rise of the water table, the seepage in the unsteady regime is predominant. The

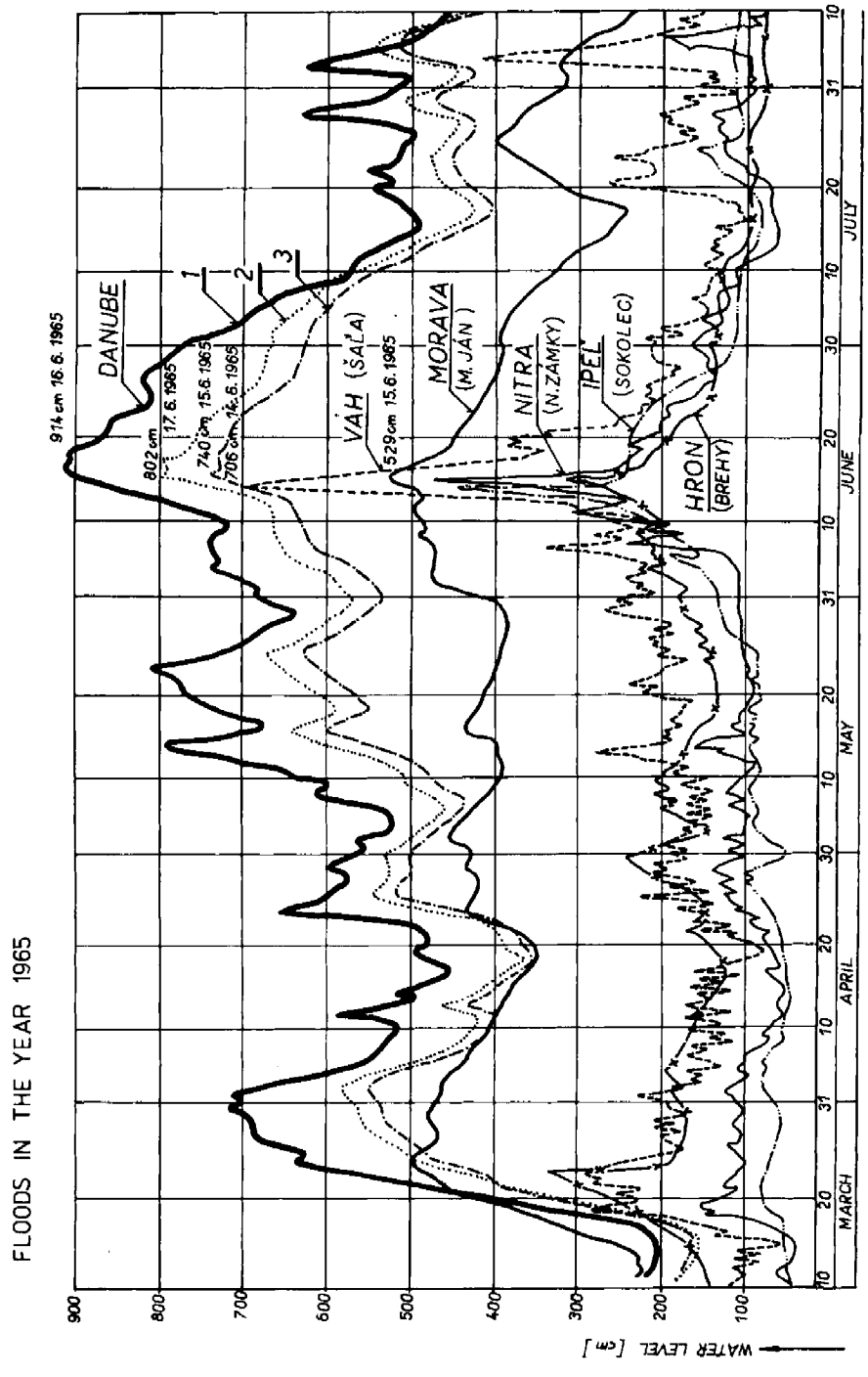

Fig. 6.2. Flood on the Danube in 1965. 1 — at Bratislava, 2 — at Komárno, 3 — at Štúrovo.

hydrodynamic load of the structure varies. The flood duration is very different — from several hours to several months (in the case of big rivers such as the Danube, Mississippi, Rhine, Volga). The flow discharge of the river and its flood regime (Fig. 6.2) are very important factors in the design procedure.

The quality of the materials in the subsoil and near the dam is vital.

6.1.1 Heterogeneous River Deposits and Wave Propagation

Alluvial deposits result in much anisotropy in soil permeability. Natural soil deposits of the Mississippi River, the Jamuna, the Danube and others are anisotropic with a maximum value of permeability coefficient in the direction of stratification (horizontal k_h) and a minimum value in the direction normal to that of stratification (k_v). These directions are denoted by h and v, respectively, i.e.

$$k_h = k_{max}, \qquad k_v = k_{min}.$$

The anisotropy of the above-mentioned soils is connected with the heterogeneity of deposits which have layers of different permeabilities k_A and k_B. If the thickness stet of the first layer is a (k_A) and the second layer is b (k_B) then the relationship of the permeability coefficients k_h, k_v is as follows

$$\frac{k_h}{k_v} = 1 + ab\,\frac{k_A^2 + k_B^2}{k_A k_B} \tag{6.1}$$

The values of the relations calculated through eqn. (6.1) for different ratios $b : a$ and $k_A : k_B$ are given in Table 6.1.

Table 6.1. Values of the permeability coefficient ratio $k_h : k_v$ for different layer thicknesses a, b and different k_A, k_B

Relationship $k_A : k_B$	Ratio of the thickness of less permeable layer (a) to permeable layer (b)						
	0.001	0.01 (1%)	0.05 (~ 5%)	0.1 (~ 9%)	0.2 (17%)	0.3 (~ 23%)	0.5 (~ 33%)
100	1.1	2.0	5.5	9.2	14.9	18.7	23.0
1 000	2.0	10.8	45.8	83.0	140.0	178.0	222.8
10 000	10.9	99.0	449.0	821.0	1391.0	1771.0	2219.0

From this table, it can be seen that in alluvial deposits of very permeable gravels ($k_A = 10^{-3}$ m s^{-1}) and loams ($k_B = 10^{-6}$ m s^{-1}), in continuous layers with more than 5% of the material mentioned, the horizontal sealing elements (blanket) will be less efficient than the vertical ones. When considering the horizontal formation, the gravel layer represents a preferential path enabling a large flow by which the pressure can reach a distance of several 100 m from the river bank within a short time.

The pressure propagation in a layered subsoil of the embankment can be investigated by means of the relations resulting from the flow conditions given in Chapter 2. The use of eqns. (2.205) and (2.212) can be convenient. Assuming a flow in space with velocity components u, v, w, the continuity equation will be as follows

$$\frac{\partial u}{\partial x}+\frac{\partial v}{\partial y}+\frac{\partial w}{\partial z}=0 \tag{6.2}$$

where

$$u=\frac{\partial \varphi}{\partial x}, \qquad v=\frac{\partial \varphi}{\partial y}, \qquad w=\frac{\partial \varphi}{\partial z}. \tag{6.3}$$

Noting that the change of horizontal velocities (u, v) as a function of water height (H) is insignificant, the average velocities (u_{av}, v_{av} in the layer z_n) in accordance with (Fig. 6.3) can be expressed as follows

$$\begin{aligned} u_{av}(x, y)&=\frac{1}{z_n}\int_0^{z_n} u(x, y, z)\,\mathrm{d}z, \\ v_{av}(x, y)&=\frac{1}{z_n}\int_0^{z_n} v(x, y, z)\,\mathrm{d}z. \end{aligned} \tag{6.4}$$

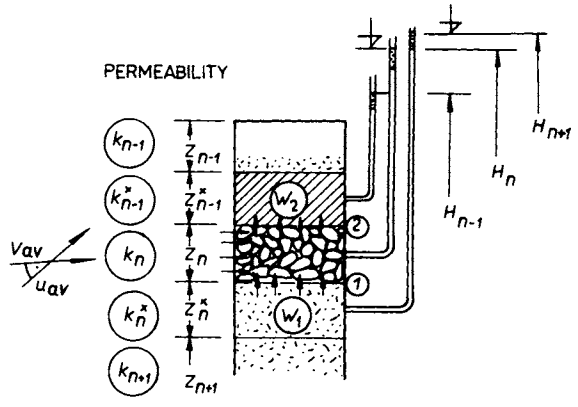

Fig. 6.3. The scheme for velocity determination in a layered soil of different permeabilities.

Integrating eqn. (6.2) over height z, the following equations are obtained

$$\int_0^{z_n}\frac{\partial u}{\partial x}\,\mathrm{d}z=\frac{\partial}{\partial x}\int_0^{z_n} u\,\mathrm{d}z=z_n\frac{\partial u}{\partial x},$$

$$\int_0^{z_n}\frac{\partial v}{\partial x}\,\mathrm{d}z=\frac{\partial}{\partial y}\int_0^{z_n} v\,\mathrm{d}z=z_n\frac{\partial v}{\partial y},$$

$$\int_1^2 \frac{\partial w}{\partial z}\,dz = w_2 - w_1,$$

where w_1 is the vertical velocity on the upper border of the layer and w_2 is the vertical velocity on the lower border. Using these symbols, the *continuity equation* for the layer of thickness z_n has the form*

$$z_n\left(\frac{\partial u_{av}}{\partial x}+\frac{\partial v_{av}}{\partial y}\right)+(w_2-w_1)=0. \tag{6.5}$$

Into the equations expressing the velocity components the potential with a given pressure height h can be introduced in the form obtained from the following equations

$$\varphi = -kh(x, y, z) = -k\left(\frac{p}{\varrho_w g}+z\right),$$

$$u=-k\frac{\partial h}{\partial x}, \qquad v=-k\frac{\partial h}{\partial y}, \qquad w=-k\frac{\partial h}{\partial z}.$$

The average pressure (piezometric) height and the *average velocities* are expressed as follows

$$\bar{H}_{(x,y)}=\frac{1}{z_n}\int_0^{z_n} h(x, y, z)\,dz, \tag{6.6}$$

$$u_{av}=-k\frac{\partial H}{\partial x}, \qquad v_{av}=-k\frac{\partial H}{\partial y}. \tag{6.7a}$$

Analogically, in the n-th layer (of gravel), it will be

$$u_{av}=-k_n\frac{\partial H_n}{\partial x}, \qquad v_{av}=-k_n\frac{\partial H_n}{\partial y}. \tag{6.7b}$$

The *vertical velocity* in the adjacent layers will be as follows

$$w_2=k_{n-1}\frac{H_n-H_{n-1}}{z_{n-1}}, \qquad w_1=k_n\frac{H_{n+1}-H_n}{z_n}. \tag{6.8}$$

By substituting eqns. (6.7) and (6.8) into eqn. (6.2), the following expressions are obtained

$$-z_n k_n\left(\frac{\partial^2 H_n}{\partial x^2}+\frac{\partial^2 H_n}{\partial y^2}\right)+k_{n-1}^{+}\frac{H_n-H_{n-1}}{z_{n-1}^{+}}-k_n^{+}\frac{H_{n+1}-H_n}{z_n^{+}}=0, \tag{6.9a}$$

$$z_n k_n\,\nabla^2 H_n-\frac{k_{n-1}^{+}}{z_{n-1}^{+}}(H_n-H_{n-1})+\frac{k_n^{+}}{z_n^{+}}(H_{n+1}-H_n)=0. \tag{6.9b}$$

* In Chapter 2, another approach was taken (eqns. 2.214 to 2.227).

Into eqn. (6.9a) the symbol of *permeability characteristics* ζ and the averaged pressure height $\bar{H}$ can be introduced, these being given by the following relations

$$\zeta = \left(\frac{k_n^+}{z_n^+} + \frac{k_{n-1}^+}{z_{n-1}^+}\right) \frac{1}{z_n k_n}, \tag{6.10}$$

$$\bar{H} = \frac{H_{n-1}\dfrac{k_{n-1}^+}{z_{n-1}^+} + H_{n+1}\dfrac{k_n^+}{z_n^+}}{\dfrac{k_{n-1}^+}{z_{n-1}^+} + \dfrac{k_n^+}{z_n^+}}. \tag{6.11}$$

For small changes in heights H_{n-1} and H_{n+1}, H = constant and eqn. (6.9) can be written as

$$\frac{\partial^2 H_n}{\partial x^2} + \frac{\partial^2 H_n}{\partial y^2} - \zeta(H_n - \bar{H}_n) = 0. \tag{6.9c}$$

Supposing the motion of water is in the horizontal direction in one permeable layer, a further simplification of the equation is possible

$$\frac{\partial^2 H}{\partial x^2} - \zeta(H - \bar{H}) = 0, \tag{6.9d}$$

with the solution

$$H = \bar{H} + C_1 \exp(-x\sqrt{\zeta}) + C_2 \exp(x\sqrt{\zeta}), \tag{6.12a}$$

provided that the roots are given by the expressions

$$r^2 - \zeta = 0, \qquad r_{1,2} = \pm\sqrt{\zeta}.$$

From the values given by the limiting conditions $r = \infty$, it results that

$$H = \bar{H} + \frac{C_1}{e^{\infty}} + C_2 e^{\infty}.$$

The values of constants are as follows

$$C_2 = 0,$$

$$C_1 = H_0 - \bar{H}.$$

Substituting the constants C_1, C_2 into eqn. (6.12a), we have eqn. (6.12b) for the *pressure height* H at a distance x

$$H = \bar{H} + (H_0 - H)\exp(-x\sqrt{\zeta}). \tag{6.12b}$$

Equations (6.10)—(6.12b) were useful in dam design when marking out the axis of the levée (Fig. 6.4) with the advantage of computer programming. In the computer program, the equilibrium condition between the top-soil-layer weight and uplift forces can be involved. The simplest condition is the fulfillment of the

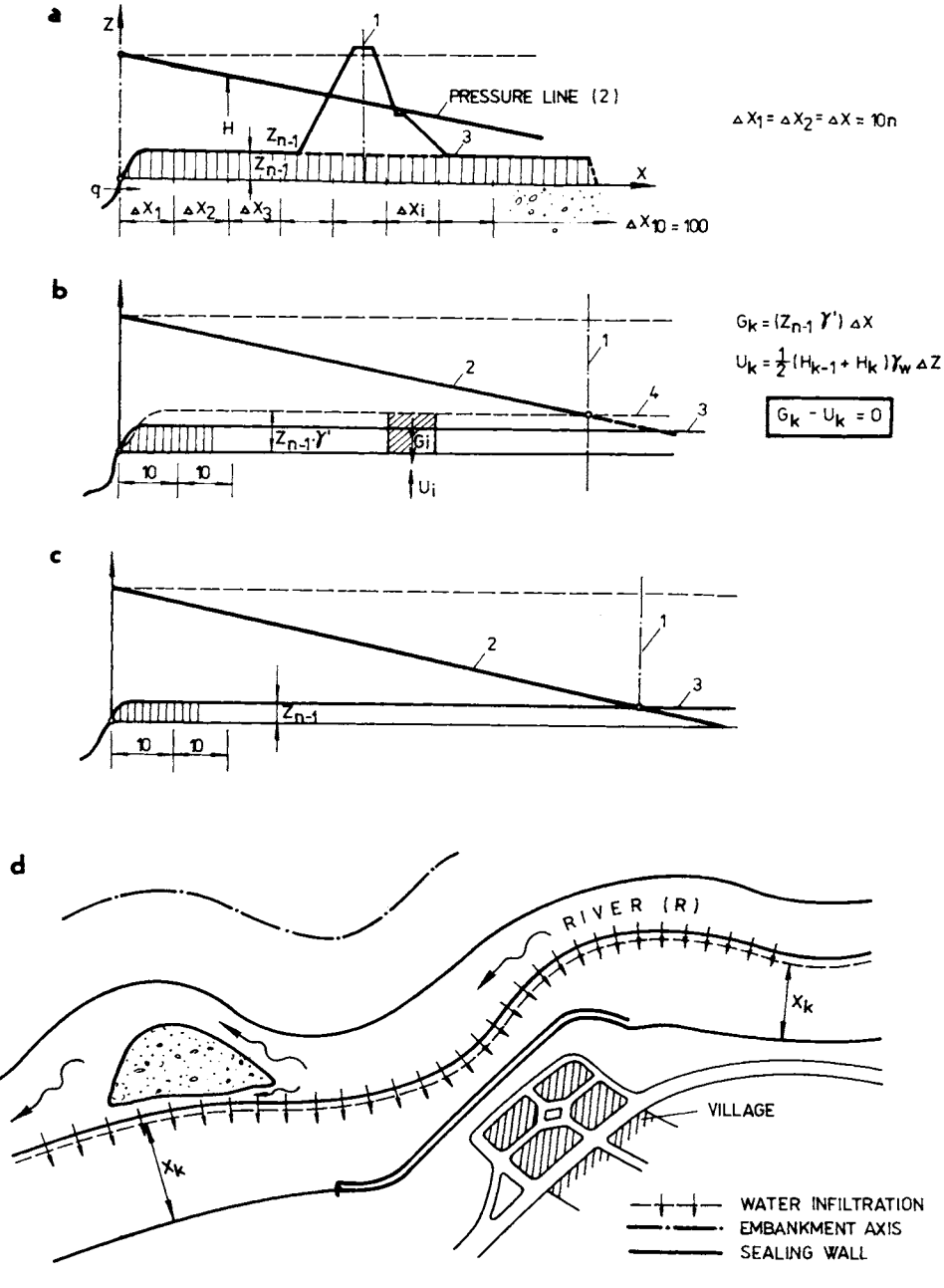

Fig. 6.4. The scheme for design of an embankment location taking into account groundwater pressure in the sub-base. a — axis of the structure at high pressure, b, c, d — corrected.

requirement of a "covered" pressure line behind the downstream toe of the dam (Fig. 6.4b).

The *uplift water force* (U) and the load due to the structure (G) for the given element (k) with a width Δx are given by

$$U_k = \frac{1}{2}(H_{k-1} + H_k)\gamma_w \Delta x, \tag{6.13}$$

$$G_k = G = (Z_{n-1}\gamma')\Delta x,$$

$$G_k - U_k = 0.$$

Hence, values in the following sequence are obtained

(1) k_n^+	(15) z_{n-1}	(16) $\gamma = \gamma'_{n+1}$
(2) k_{n-1}^+	(3) z_{n-1}^+	(4) H_{n-1}
(5) k_n	(6) z_n	(7) H_n
(8) z_n^+	(9) H_{n+1}	(10) $\bar{H}$
(11) $\sqrt{\xi}$	(12) $H_n = 0$	
(13) e = 2.71828		
(14) H		

Constants	Auxiliary values	
$A = 1$	S	$A = H_0$
$B = 2$	T	$B = k_{n-1}^+$
$C = 3$	U	$C = z_{n-1}^+$
$D = 4$	Z	$D = H_{n-1}$
$E = 5$	Q	$E = k_n$
$F = 8$		$F = z_n$
$G = 9$		$G = k_n^+$
$H = 5$		$H = z_n^+$
$Q = 6$		$Q = H_{n+1}$
$P = 15$		$A = Z_{n-1}$
$R = 16$		$R = \gamma_n - 1 = \gamma'$

Analysing eqns. (6.10)—(6.12b) just derived, we can state that with the increasing permeability of the layer the pressure line will also reach above the ground level.

With respect to the low permeability of loam (silty) layers ($k = 10^{-5}$—10^{-7} m s^{-1}) which form the upper layers of the alluvial deposits — encountered most frequently as subsoil of levées — and taking into account a short flood duration, even the aspects of the dam design analysed can be ignored in most case. Levées far enough from the river bed seldom need any subsoil sealing. The requirement of protective measures near the downstream toe of the structure will be evident everywhere.

An *example* taken from the Danube valley reveals a picture of the wave-pressure propagation during a flood at the water heights: $H_0 = 6.0$ m, $H_{n+1} = 2.6$ m, $H_{n-1} = 1.5$ m. In the subsoil of the levée, there are permeable damaged gravels with $k_n = 5 \times 10^{-2}$ m s^{-1}, $z_n = 0.3$ m, the sand layers $k_n^+ = 6 \times 10^{-5}$ m s^{-1}, $z_n^+ = 20.0$ m. Permeable alluvium is covered by loam ($k_{n-1}^+ = 2 \times 10^{-6}$ m s^{-1}, $z_{n-1} = 1.5$ m). Substituting these values into eqns. (6.10)—(6.12b), the following expressions are obtained

Table 6.2. Values of head (H) determined through eqn. (6.14) for various distances x

Values	In a distance x [m]					
	10	50	100	300	500	1000
$x\sqrt{\zeta_n}$	0.17	0.85	1.7	5.1	8.5	17.0
$\exp(-x\sqrt{\zeta_n})$	0.845	0.425	0.179	0.006	2×10^{-3}	1.75×10^{-3}
$c_1 \exp(-x\sqrt{\zeta_n})$	3.16	1.59	0.67	0.02	0	0
Head H of W.T. [m]	5.42	3.85	2.93	2.8	2.26	2.26

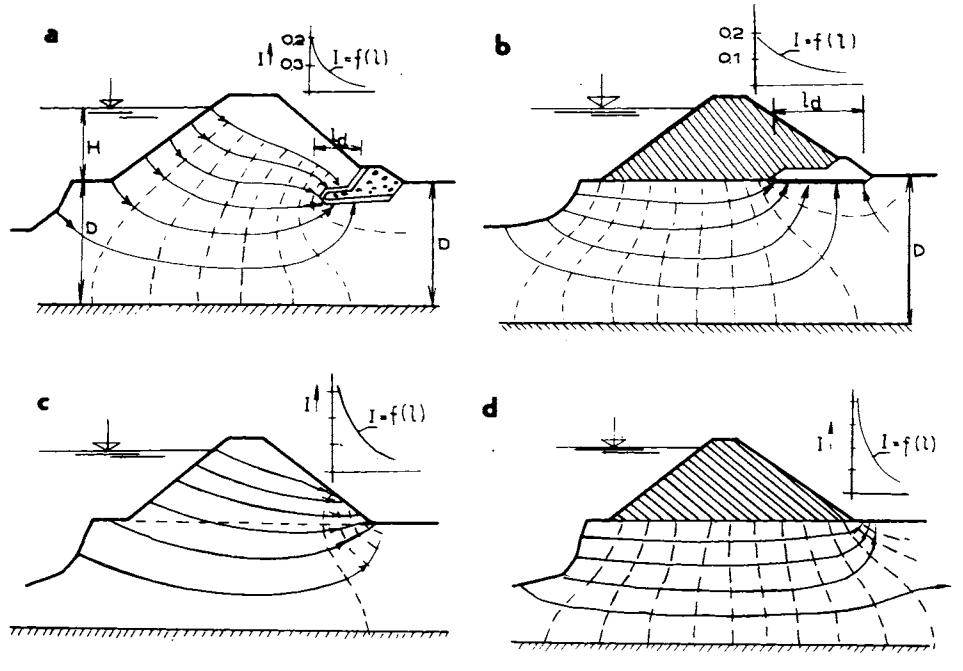

Fig. 6.5. Dam with a protecting element on the downstream toe and without it. a — permeable structure with gravel toe drain, b — impermeable structure with toe drain, c — structure of low permeability without drain, d — impermeable structure without drain.

$$\tilde{H}=\frac{1.5\,\dfrac{2\times10^{-6}}{1.5}+2.6\,\dfrac{6\times10^{-5}}{20.0}}{\dfrac{2\times10^{-6}}{1.5}+\dfrac{6\times10^{-5}}{20.0}}=2.26\text{ m},$$

$$C_1=6.0-2.26=3.74\text{ m},$$

$$\zeta_n=\frac{\dfrac{6\times10^{-5}}{20.0}+\dfrac{2\times10^{-6}}{1.5}}{0.3\times5\times10^{-2}}=2.89\times10^{-4}\qquad[\text{m}^{-2}],$$

$$\sqrt{\zeta_n}=1.7\times10^{-2}\qquad[\text{m}^{-1}].$$

The equation for the *pressure* of the water *height* will be

$$H=2.26+3.74\,\mathrm{e}^{-0.017x}. \tag{6.14}$$

This enables us to calculate the water height at distances x as shown in Table 6.2. It is evident that a water pressure should be observed at a distance $x=300$—400 m. During the flood in 1965, piping phenomena at 350 m were registered (Jakubec 1966).

Cultural land, villages and towns are situated in almost all European countries close to levées. Therefore land protection and levées with efficient seepage control (Fig. 6.5a, b) are necessary. Classical cross-section of a levée with a downstream toe (Fig. 6.5c, d) menaced by seepage water will be quite sufficient.

6.2 Active Subsoil Protection

In the *case of low permeability* of soils in the subsoil of the dam, it is not necessary to provide a passive antiseepage element. The high hydraulic gradients shown in the previous picture represent a particular danger of erosion at the boundary between two soils of different permeability. A high exit gradient near the toe can be avoided by a drain representing the commonest active soil protection. It maintain the toe and the adjacent soil dry and stable. The rocky prismatic element is an appropriate protective measure. Sometimes it can be replaced by a filter drain of sufficient length, keeping the exit gradient within the given limits. The limit value of the exit gradient can be calculated using the empirical equation of Voshchinin (1959)

$$I=\frac{cn\left(\dfrac{2K\psi}{h},x'\right)}{\left[sn\left(\dfrac{2K\psi}{h},x'\right)-cn\left(\dfrac{2K\psi}{h},x'\right)\right]}, \tag{6.15}$$

where *cn* and *sn* are elliptic functions, ψ denotes the stream function, x' represents

the conjugate modulus of the elliptic integral, K is the full elliptic integral of first-order at modulus x_E with the following auxiliary values

$$b = \frac{4KD_c x}{\pi h}, \qquad x_E = \tanh \frac{\pi d'}{4D_c}.$$

$D_c = D + h/2$ are the depth of permeable subsoil; d' is horizontal projection of the length of phreatic line, usually d' is $(0.7—0.8)\,b_1$; D the actual thickness of permeable strata in the subsoil; D_c the calculated thickness.

In engineering practice, the value $I = 0.3$ is considered as the exit-gradient limit. However, this is an approximate value which should be investigated more exactly in some cases in accordance to Voshchinin's proposals or according to the exit velocities with respect to grain size and grain-size distribution. Equation (6.15) shows that the exit gradient depends on both the structure geometry and the subsoil geometry.

A detailed analysis of eqn. (6.15) and the values of the contact-line length given by Voshchinin in Table 6.3 has shown that seepage in the deep permeable strata endangers the earth structure more then the shallow permeable layer in its subsoil.

Table 6.3. Contact-line length (l_d) required by various gradients (after Voshchinin 1959)

d'	$D_c = D + \frac{h}{2}$	Value $l_d = xH$ for a gradient				$D' : l_d$ by $I \leqq 0.1$
		$I > 0.8$	$I \geqq 0.3$	$I \geqq 0.2$	$I \geqq 0.1$	
$4H$	$10H = 2.5d'$	$0.045H$	$0.24H$	$0.45H$	$1.50H$	50
	$20H = 5d'$	0.025	0.26	0.52	1.70	40
	$2H = 0.4d'$	0.02	0.12	0.24	0.65	65
	$4H = 0.8d'$	0.025	0.16	0.31	1.00	60
$5H$	$10H = 2d'$	0.03	0.18	0.37	1.20	47
	$20H = 4d'$	0.03	0.20	0.42	1.50	38
	$4H = 0.5d'$	0.01	0.10	0.21	0.70	50
$8H$	$10H = 1.25d'$	0.01	0.12	0.26	0.90	38
	$20H = 2.5d'$	0.01	0.13	0.30	1.0	30
	$4H = 0.4d'$	—	0.06	0.16	0.56	44
$10H$	$8H = 0.8d'$	—	0.08	0.19	0.68	36
	$20H = 2d'$	—	0.09	0.20	0.78	27

Given favourable levée conditions ($H = 3—4$ m), a length of drain $l_d = 0.4—1.5$ m would be sufficient. When considering the levées on deep permeable strata as is the case for the Danube valley (maximum $H = 5.0—6.0$ m), a length of $l_d = 1.2—4.5$ m is necessary.

The most dangerous stability conditions occur in the case of an impermeable dam founded on permeable deep strata. Assuming *homogeneous porous media* in the

subsoil (depth $D=\infty$) of the structure, the assumption made in Chapter 2 for a *complex velocity*, the following relations

$$w = u - iv,$$

$$w = \frac{d\omega}{dz} = \frac{M}{\sqrt{b^2 - z^2}}, \tag{6.16}$$

$$\omega = \varphi + i\psi = M \sin^{-1} \frac{z}{b} + N, \tag{6.17}$$

$$\varphi = -k \left[\frac{p}{\varrho g} + (y - H_2) \right],$$

or

$$\varphi = -k(H_1 - H_2) = -kH$$

can be determined, because $H_1 - H_2 = H$.

Using extreme values of stream flow, then for $z = \pm b$, $\psi = 0$; $\varphi = 0$ and with $\varphi = -kH$

$$\omega = \frac{kH}{\pi} \sin^{-1} \frac{z}{b} - \frac{kH}{2} = -\frac{kH}{\pi} \cos^{-1} \frac{z}{b}, \tag{6.18}$$

$$z = b \cos \frac{\pi\omega}{kH}. \tag{6.19}$$

Using an analogy for complex velocity (w) and analytic function z, the following equations are obtained

$$z = x + iy, \qquad w = u - iv = \frac{kH}{\pi \sqrt{b^2 - z^2}}. \tag{6.20}$$

Velocity components depending on the position of a given point (x, y) related to (half) footing-bottom length ($2b$) are

$$u = \frac{kH}{\pi \sqrt{2}} \frac{\sqrt{\sqrt{(b^2 - x^2 + y^2)^2 + 4x^2y^2} + b^2 - x^2 + y^2}}{\sqrt{(b^2 - x^2 + y^2)^2 + 4x^2y^2}}, \tag{6.21a}$$

$$v = \pm \frac{kH}{\pi \sqrt{2}} \frac{\sqrt{\sqrt{(b^2 - x^2 + y^2)^2 + 4x^2y^2} - b^2 + x^2 - y^2}}{\sqrt{(b^2 - x^2 + y^2)^2 + 4x^2y^2}}. \tag{6.21b}$$

The relation between point distance and the height H_x in point x

$$x = b \cos \frac{\pi\varphi}{kH} = b \cos \frac{\pi H_x}{H} \tag{6.22}$$

gives possibility to calculate

$$H_x = \frac{H}{\pi} \cos^{-1} \frac{x}{b}$$

and then the uplift (pore) pressure at point x will be

$$p_x = \varrho g_w H_x = \frac{\varrho g_w H}{\pi} \cos^{-1} \frac{x}{b}. \tag{6.23}$$

Our system takes an origin in the centre of the footing length (2b). At the footing bottom $y = 0$, the velocities will be

$$u = \frac{kH}{\pi \sqrt{b^2 - x^2}}, \qquad v = \pm \frac{kH}{\pi \sqrt{x^2 - b^2}}. \tag{6.21c}$$

Equation (6.21c) proves that in the vicinity of the downstream toe where $x = b$ a maximum in flow velocity should be expected (theoretically $v = \infty$) and thus the danger of failure will be maximum. This is in good agreement with the observations after the floods in the Danube valley in 1954 and 1965, where as many as 2320 pipings were registered over a distance of 0 to 350 m, of which 82% occurred over a distance up to 10 m from the downstream toe (Fig. 6.6).

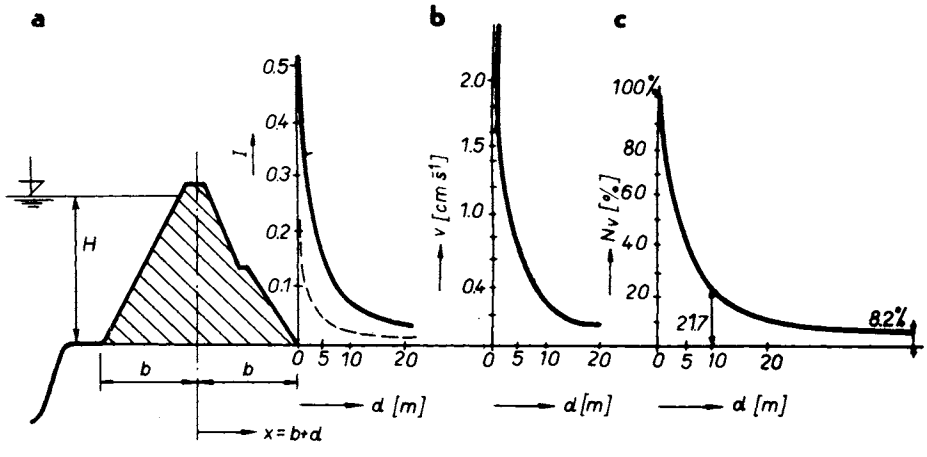

Fig. 6.6. Functionality for $I = f(d)$, $v = f(d)$ and number of boils $N_v = f(d)$ near the levées in the Danube valley. a — gradients, b — velocities, c — number of boils.

On the basis of theoretical knowledge and practical experiences, we can state that the toe of the embankment (levée or dam) laid on a permeable stratum is under heaviest load, as is the subsoil. Thus it must be protected carefully, as must all hydraulic structures including large dams. In Fig. 6.7, many types of downstream

toe drains are shown. The downstream gravel drains (Fig. 6.7a, b) are so far most popular. Toe drains without a fall pipe (Fig. 6.7c) and with a relief well have to take off the permeable (artesian) horizon to a great depth (Fig. 6.7d). Sometimes a series of deep wells, dealt with in Chapter 2, can be applied as described in Sections 6.5 and 6.6. The wells which should relieve the hydrostatic pressure under the natural impervious blanket, can also be connected to the pervious drainage layer.

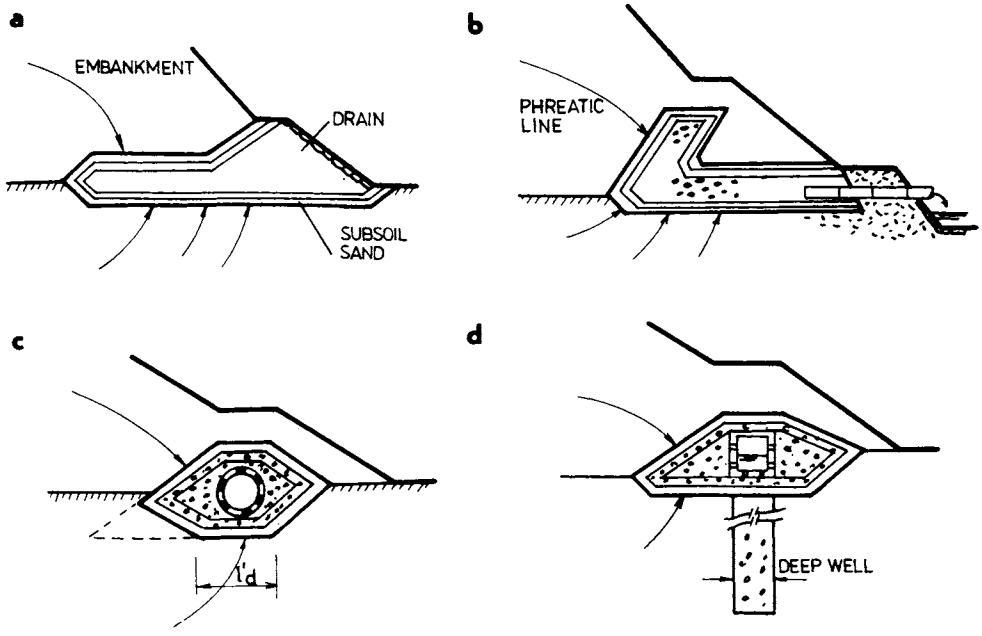

Fig. 6.7. Protecting drains. a — rocky toe with filter, b, c, d — with water collector.

In special cases, a chimney drain can be combined with a drainage blanket and wells. This type of solution is very complicated, and is only acceptable in cases of very large structures (e.g. profiles with a clay core).

6.3 Vertical Sealing and Passive Protection Elements

Vertical sealing elements are not only the most common but also the most efficient antiseepage elements of dams and hydraulic structures where there is subsoil sealing. There are many kinds of examples of such watertight systems, details depending on the conditions, uses and purpose of the antiseepage system concerned. Steel piles, grout curtain, concrete wall, concrete core wall and slurry

trench cut-off are currently the most common vertical sealing elements. It is possible to construct a safe levée as an earth dam on almost any foundation on the ground level. The sealing elements employed should, first of all, prevent the free passage of water from the upstream to the downstream face. Water which passes through and under the structure should have such a low pressure and velocity when reaching the surface (ditch, drain, etc.), so that it cannot shift the material of which the dam foundation is composed. These requirements can be satisfactorily net by means of wooden and steel sheet piling.

All these vertical elements are sufficiently watertight; their permeabilities are 3—5 orders lower than those of gravel and sand foundations. Their efficiencies are determined in particular by the depth and the position on the footing bottom.

6.3.1 The Position of Vertical Sealing Elements

Vertical sealing elements used in levée construction are located near the centre or near the upstream toe of the dam especially in cases where the sealing element is connected to an impervious blanket.

With a vertical sealing (wall) in the central part of the dam body founded on a permeable subsoil of thickness D, bounded in this layer at depth D_s, using a conform mapping in the z- and ζ-planes, along with the following transformation relations

$$\zeta = \pm\cos\frac{\pi D_s}{2D}\sqrt{\tanh^2\frac{\pi z}{2D}+\tan^2\frac{\pi D_s}{2D}},$$

we can obtain equations expressing the complex potential (ω) and flow rate (q)

$$\omega = \frac{A}{\mu}(K+iK'),$$

$$\omega = -kH - q_i,$$

$$q = \frac{kHK'}{K_e} = \frac{kHK'(\beta)}{2K},$$

where A, μ are auxiliary values; K, $K'(K_e)$ elliptic integrals after Polubarinova-Kochina (1952).

If the steel piling is in the centre, the parameter of the elliptic integral will be: $\beta_1 = \beta_2 = \beta$,

$$\beta = \cos\frac{\pi D_s}{2D}\sqrt{\tanh^2\frac{\pi b}{2D}+\tan^2\frac{\pi D_s}{2D}}, \tag{6.24}$$

assuming that the value of the modulus K_e of the elliptic integral is given by the following relation

$$K_e = \frac{2\sqrt{\beta}}{1+\beta}.$$

If unit rate is given by the expression $\bar{q} = q/kH$, we can obtain a common parameter for estimating a relative depth of the sheet piling $D_s : D$ and for the influence of a relative length $b : D$ at unit rate q, as shown in Fig. 6.8.

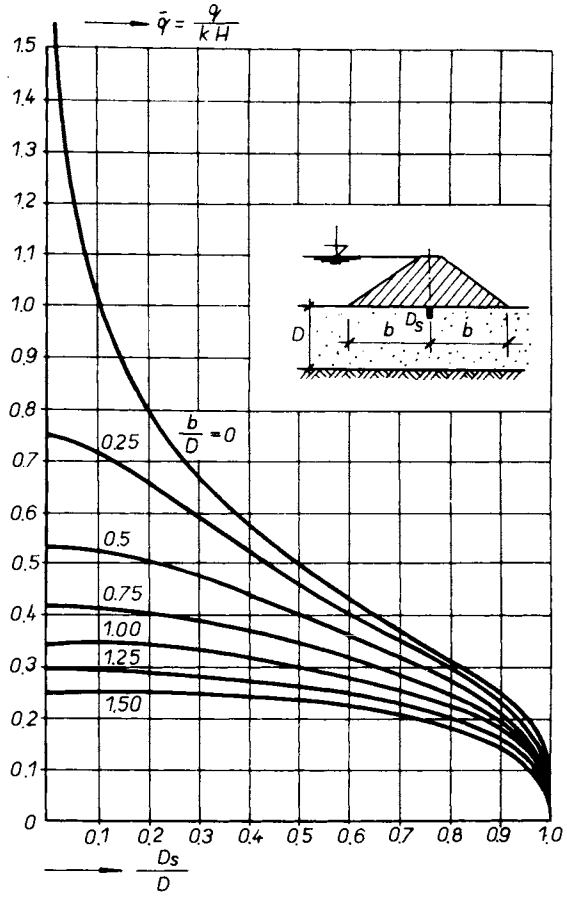

Fig. 6.8. The amount of seepage depending on the size of the structure and of the permeable sub-base thickness.

6.3.2 Watertight Walls

In Fig. 6.9, we plot values of relative pressure height $h : H$ with respect to the relative distance $(x : l)$ from the middle, for different depths $D_s : D$ assuming an impermeable dam body.

Figure 6.10 shows the curves with plotted values of uplift in the footing bottom for a wall made in the line of the upstream toe. All these diagrams (Figs.6.8—6.10)

show that in the case of homogeneous subsoil strata the length of the footing bottom (seepage path) contributes to reduction in both seepage and uplift. If the permeable strata are not deep and the seepage path is relatively long, the depth of sealing element D_s reduces the seepage minimally. This effect is not substantially increased, providing that the element reaches a depth of 90% of the permeable layer thickness. In this case, the flow velocities of water around the end of the wall are substantially increased.

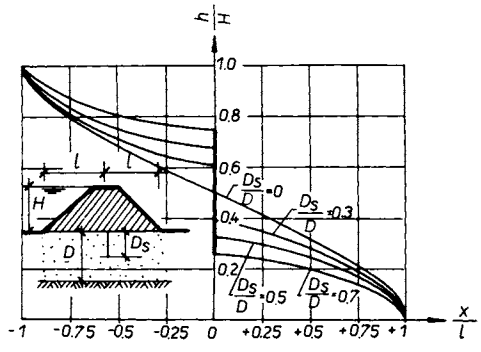

Fig. 6.9. The pressure-line ordinates as a function of wall depth.

It is necessary to cut the permeable layer by a wall, or to cut it off through the whole thickness thus to prevent seepage and to reduce entirely the uplift pressure, unless the free groundwater communication requires an open water-bearing layer. If the foundation consists of gravel or any material resistant to hydrodynamic forces, it is possible to allow the passage of seepage water through a "window"

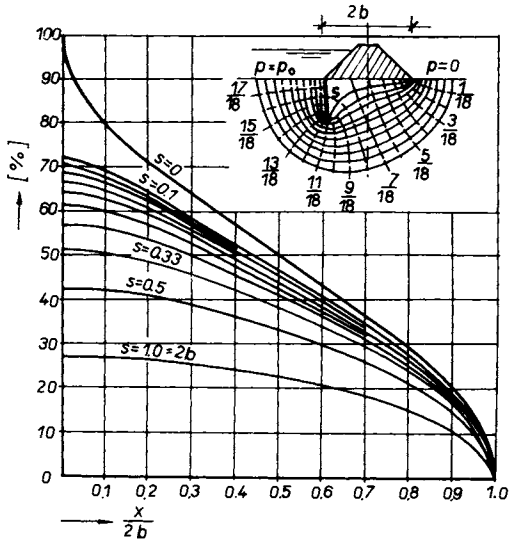

Fig. 6.10. Uplift pressures for various depths (x) of the diaphragm walls at the upstream toe of the dam.

below the wall or in the wall. In special cases, it is possible to ensure the stability of sandy gravel endangered by piping so as to employ grouting or deep vibration.

Our conclusions are valid for a homogeneous permeable layer. In a permeable double layer (Fig. 6.11) or multilayer strata, the seepage is concentrated in the upper layers. Being in the vicinity of the ground level, great uplift forces result in overburden damage. Piping or similar phenomena occur when seepage water issues from the embankment or ground surface under sufficient pressure and at a sufficient velocity that the particles comprising the material are swept away. It is obviously desirable to stop this phenomenon. Sheet pill or a several meters long cut-off wall is preferred for an upstream impermeable blanket several hundred meters long.

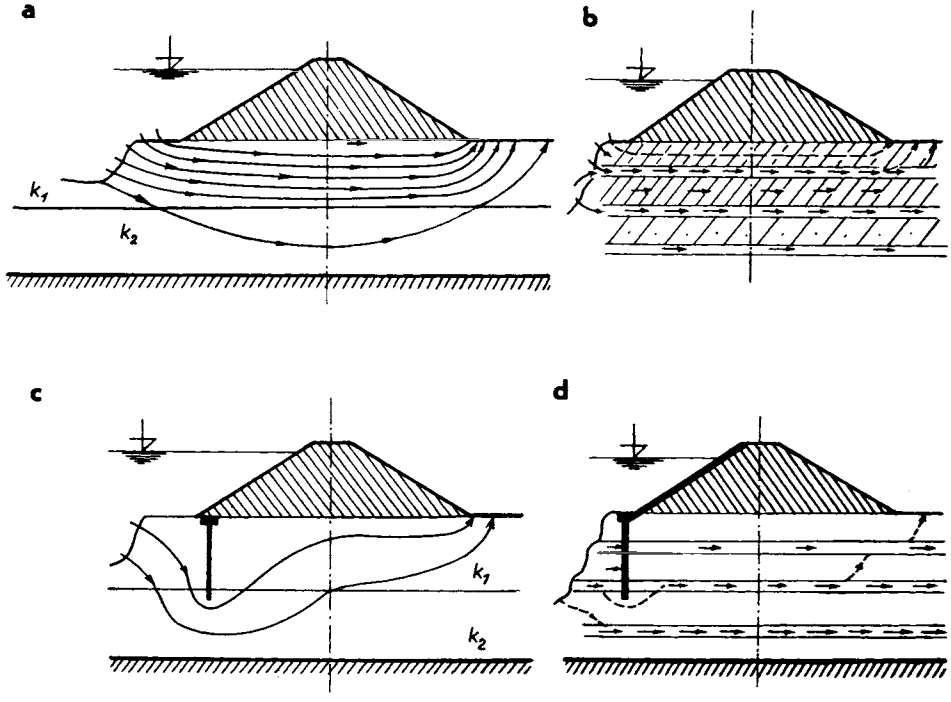

Fig. 6.11. Leakage through a layered subsoil before and after a short wall erection. a, b — without antiseepage measures, c, d — with a wall on the upstream side.

Numerical analysis of seepage and sealing problems of heterogeneous subsoil is rather difficult. The problem can be solved by three approximate methods; these are analogy, the finite-element method and idealization of multilayer strata by two (three) strata. The most convenient idealization (Fig. 6.12) assumes two layers of thickness $D_1 = D_2 = D$, and permeability coefficients k_1, k_2. This idealization

enables us to divide the seepage potential into two parts (φ_1, φ_2), and we obtain the conditions of transformation (Polubarinova-Kochina, 1952) from the z-plane to the ζ-plane as follows

$$\varphi_1 = -k_1 \frac{H}{2}, \qquad \varphi_2 = -k_2 \frac{H}{2}, \tag{6.25}$$

$$\frac{\varphi_1}{k_1} = \frac{\varphi_2}{k_2}, \qquad \psi_1 = \psi_2, \tag{6.26}$$

$$\zeta = \frac{1+a}{2} + \frac{1-a}{2} \cosh \frac{\pi z}{D}, \tag{6.27}$$

$$a = \tanh^2 \frac{\pi b}{2D}, \tag{6.28}$$

$$\omega_1 = \varphi_1 + i\psi_1, \qquad \omega_2 = \varphi_2 + i\psi_2.$$

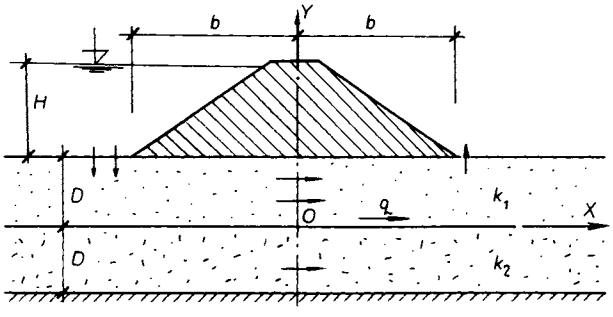

Fig. 6.12. Scheme for a double-layer seepage computation.

At the border, new functions (F_1, F_2) can be introduced

$$F_1 = \frac{d\omega_1}{d\zeta}, \qquad F_2 = \frac{d\omega_2}{d\zeta},$$

which can be determined from the border conditions and from the transformation conditions. These may be simplified and the following equations are obtained

$$\omega_1(\zeta) = \sqrt{\zeta - a}\,[a_0 + a_1(\zeta - a) + \ldots],$$

$$\omega_2(\zeta) = \sqrt{\zeta - a}\,[b_0 + b_1(\zeta - a) + \ldots],$$

$$F_1(\zeta) = \frac{c_0 - c_1(\zeta - a) + \ldots}{\sqrt{\zeta - a}} = \frac{\Phi_1(\zeta)}{\sqrt{\zeta - a}},$$

$$F_2(\zeta) = \frac{d_0 + d_1(\zeta - a) + \ldots}{\sqrt{\zeta - a}} = \frac{\Phi_2(\zeta)}{\sqrt{\zeta - a}}. \tag{6.29}$$

In the vicinity of $\zeta=0$, it will be

$$\omega_1(\zeta)=\sqrt{\zeta}(a_1+a_1+\ldots),$$

$$F_1(\zeta)=\frac{1}{\sqrt{\zeta}}(a_0'+\ldots).$$

In accordance with the Polubarinova-Kochina theory, it is possible to introduce conjugate potential functions, with the help of which we obtain characteristic equations

$$\begin{vmatrix} \dfrac{k_2+k_1}{k_2-k_1}-\lambda & -\dfrac{2k_1}{k_2-k_1} \\ \dfrac{2k_2}{k_2-k_1} & -\dfrac{k_2+k_1}{k_2-k_1}-\lambda \end{vmatrix}=0$$

with roots $\lambda=1$, $\lambda'=-1$, for which — with respect to the initial border conditions of ω_1, ω_2 — it is valid that

$$\gamma=\frac{\ln\lambda}{2\pi i}=0, \qquad \gamma'=\frac{\ln\lambda'}{2\pi i}=-\frac{1}{2}.$$

The *complex velocity* and the components of reduced velocity $(\bar{u}, \bar{v})$ are related by the equation

$$u-iv=\frac{k_1H}{2D}(\bar{u}-i\bar{v}).$$

The latter is the most interesting in the vicinity of the footing bottom, where we have

$$\bar{v}_1=0, \qquad \bar{u}=\frac{\pi}{J}\frac{(\cosh\lambda b)^{2\varepsilon}\cos 2\varepsilon\vartheta}{\sqrt{\cosh^2\lambda b-\cosh^2\lambda x}} \tag{6.30}$$

$$J=\int_0^{\pi/2}\frac{\cos(2\sin^{-1}K\sin\alpha)\,d\alpha}{\sqrt{1-K^2\sin^2\alpha}}=\int_0^{\sin^{-1}K}\frac{\cos 2\varepsilon\alpha\,d\alpha}{\sqrt{K^2-\sin^2\alpha}} \tag{6.31}$$

where

$$\vartheta=\cos^{-1}\frac{\cosh\lambda x}{\cosh\lambda b}, \quad \left(\lambda=\frac{\pi}{2D}, \quad 0\leqq x\leqq b\right),$$

$$\tanh\frac{\pi b}{2D}=K, \quad \cosh\frac{\pi b}{2D}=\frac{1}{K}, \quad a=K^2, \tag{6.32}$$

$$\varepsilon=\frac{1}{2}\tan^{-1}\sqrt{\frac{k_2}{k_1}}.$$

Behind the downstream toe at ground level, we have

$$\bar{u}_1 = 0, \quad v_1 = \frac{\pi}{J} \frac{\cosh 2\varepsilon\vartheta}{(\cosh \lambda b)^{1-2\varepsilon} \sinh \vartheta}, \tag{6.33}$$

where

$$\cosh \vartheta = \frac{\cosh \lambda x}{\cosh \lambda b}, \qquad \left(\lambda = \frac{\pi}{2D}\right).$$

In the middle of the footing bottom (where $x = 0$, $z = y_i$) we obtain

$$\bar{v}_1 = 0, \quad \bar{u}_1 = \frac{\pi}{J} \frac{\cosh \lambda b \cos 2\varepsilon\vartheta}{\sqrt{\cosh^2 \lambda b - \sin^2 \alpha_i}}, \tag{6.34}$$

where

$$\vartheta = \tan^{-1} \frac{\sqrt{\cosh^2 \lambda b - \sin^2 \lambda y}}{\sin \lambda y}, \quad \left(\lambda = \frac{\pi}{2D}\right).$$

In the centre of the less permeable layer (at the same λ, ϑ) we obtain

$$\bar{v}_2 = 0, \quad \bar{u}_2 = \frac{\tan \varepsilon\pi}{J} \frac{\cos \lambda b \sin 2\varepsilon\vartheta}{\sqrt{\cosh^2 \lambda b - \sin^2 \lambda y}}. \tag{6.35}$$

On the contact zone of the second layer and impermeable subsoil, the following expressions are valid

$$\bar{v}_2 = 0, \quad \bar{u}_2 = \frac{\tan \pi\varepsilon}{J} \frac{\cosh \lambda b \sin 2\varepsilon\vartheta}{\sqrt{\cosh^2 \lambda b - \cosh^2 \lambda x}}, \tag{6.36}$$

where

$$\vartheta = \tan^{-1} \frac{\sqrt{\cosh^2 \lambda b - \cosh^2 \lambda x}}{\cosh \lambda x}, \quad \left(\lambda = \frac{\pi}{2D}\right).$$

The *flow rate* through a double layer can be determined from unit rate $\bar{q}$

$$q = k_1 H \bar{q}.$$

Unit rate $\bar{q}$ of a double layer can be determined from Fig. 6.13 if

$$\varepsilon = \frac{1}{\pi} \tan^{-1} \sqrt{\frac{k_2}{k_1}}.$$

Assuming $\varepsilon = 0.25$ we should analyse the limiting case $k_1 = k_2$. This is the case of a homogeneous substratum with a thickness $2D$ and a footing-bottom length $2b$. Assuming $\varepsilon = 0$, e.g. $k_2 = 0$, the seepage passes through the upper permeable layer only. When $k_2 \gg k_1$, the values beneath the curve $\varepsilon = 0.25$ are valid. Analysing the

given expressions and graphical plotting $\bar{q} = f(b : D, \varepsilon)$ we can confirm that the seepage quantity depends on the permeability of the upper layer. Providing that the ratio of permeability is $k_1 : k_2 = 100$, the seepage through the substratum can be judged according to the seepage of the upper layer. In this case, the influence of the ratio $b : D$ can be estimated according to the curve $\varepsilon = 0$.

If the lower layer is stable enough we can bound the cut-off sheet pill at the second less permeable layer; it is not necessary to cut both layers and bound at the impermeable subsoil strata. Such a solution can save 40—60% of the costs needed

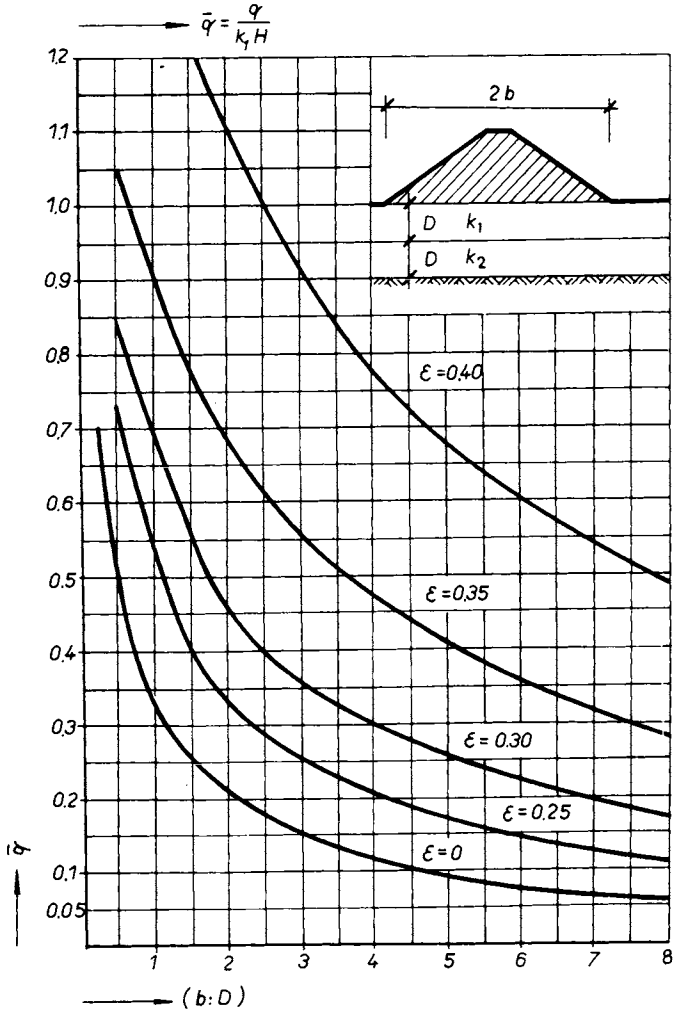

Fig. 6.13. Graph used for calculating unit seepage: $\bar{q} = f\left(\frac{b}{D}\right)$.

for antiseepage measures when increasing the seepage losses which can be a few per cent only.

This case can be exemplified by the protection of the town Freistritz in Austria (Demmer and Grolitsch 1968), where alluvial deposits of the Drava in the upper part where gravel laying on sands was interrupted and the cut-off wall was bounded to a less permeable dense sand (Fig. 6.14).

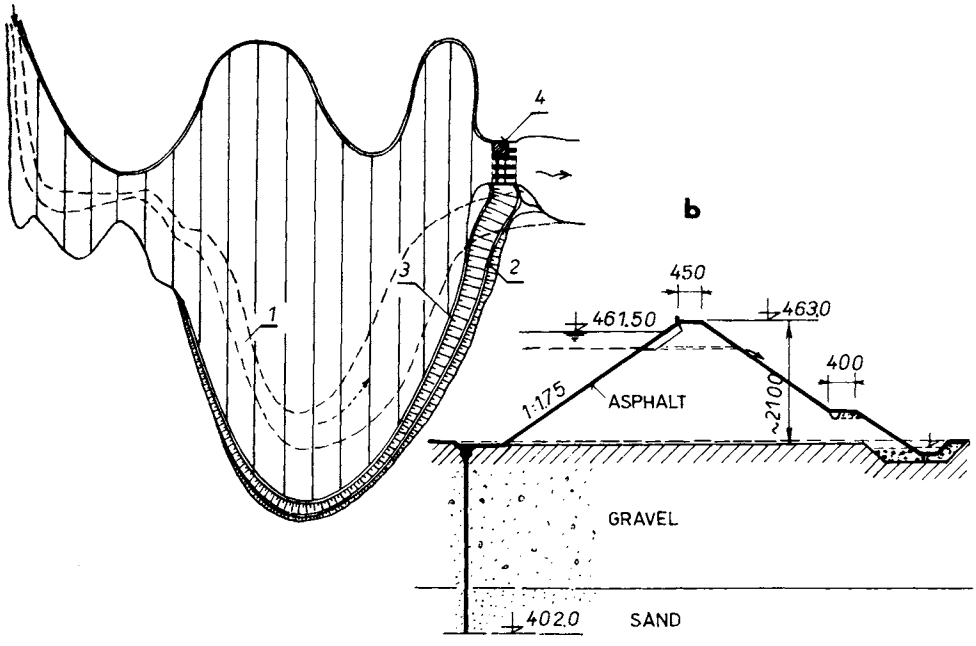

Fig. 6.14. Antiseepage measures on the earth dam Freistritz. a — lay-out, b — cross-section; 1 — river-bed, 2 — earth dam, 3 — cut-off wall, 4 — power-house.

This solution was accepted after a very thorough analysis of permeability coefficient k according to the Dupuit—Thiem method followed by the Gilg—Gavard method.

By the first method, the permeability determination according to the formula

$$k_h = \frac{Q}{\pi} \frac{\ln x_2 - \ln x_1}{(y_2^2 - y_1^2)}$$

gives a value of $k = 5 \times 10^{-3}$ m s^{-1} by a pumping test.

The Gilg—Gavard formula

$$k_h = \frac{Q}{2\pi H} \frac{\ln x_2 - \ln x_1}{\left[D_f - \frac{L - \frac{D_f}{2}}{\ln (2R_a - D_f)} \right]}$$

leads to a value $k = 3 \times 10^{-3}$ m s^{-1} for the average permeability of the upper strata.

The maximum permeability coefficient was calculated for the gravel deposit as $k = 2 \times 10^{-2}$ m s^{-1} in a layer reaching a depth of 42 m. Permeable strata were made watertight by means of a cut-off wall with a surface of 32,400 m^2 reaching a depth of 4—5 m in sands and not rocks as proposed previously. Seepage control has shown the antiseepage measures to be quite sufficient. At a water height of 12.5 m the seepage losses are above 2.0 m^3 s^{-1} per 1-km length and the subsoil strata are stable.

The *grout curtain* is the next antiseepage measure which differs from those above as regards efficiency. It cannot be said to be impermeable. It lowers the permeability of sandy-gravel subsoil by several orders. In engineering practice, one can expect a decrease in the permeability coefficients to one tenth or even one hundredth of their original k_0 value.

In alluvial deposits, the range of k_0 is from 10^{-4} to 3×10^{-3} m s^{-1}. After grouting, this value drops to a value of $k = 10^{-4}$ to 5×10^{-6} m s^{-1}. A permeability of $k = 5 \times 10^{-5}$ m s^{-1} can be used. This value is quite satisfactory for the designer, and thus a grout curtain can be considered as a proper antiseepage measure.

As regards the grout-curtain *location*, this is determined by the technology and the possibility of its repairing. The position behind the upstream toe is preferred (Fig. 6.15). The sealing effect of the curtain is estimated by its efficiency, expressed by the following formula

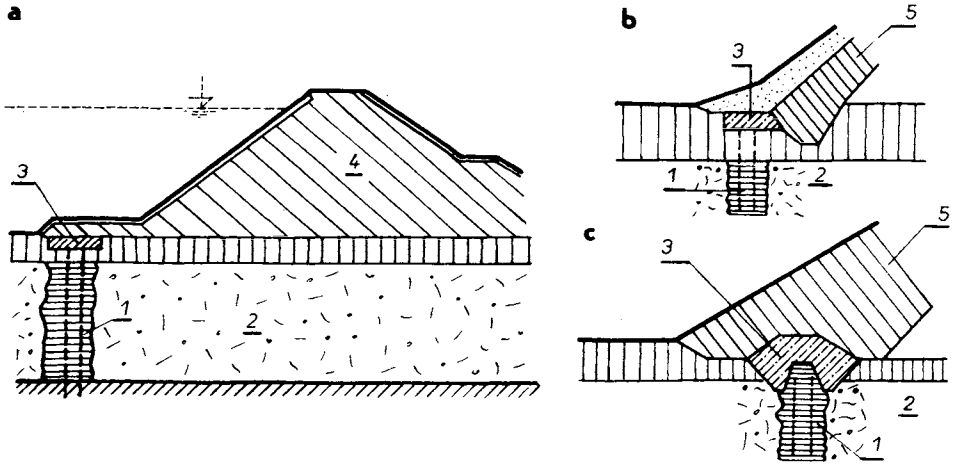

Fig. 6.15. The grout curtain and its position. a — in front of the dam, b — for the sealing, c — below the sealing element; 1 — grout curtain, 2 — Alluvium, 3 — concrete, 4 — dam, 5 — sealing element (clay core).

$$\eta = 1 - \frac{q + q'}{q_0}, \tag{6.37}$$

where q_0 is the rate without the antiseepage element; q rate with antiseepage element; q' losses caused by drainage. Rate q at a given water height H depends on the ratio of permeability coefficients $k_0 : k$, on the ratio between the length of footing bottom and the thickness of permeable strata D, $2b : D$. These effects are involved in the formula of Dachler (1936), modified by Cambefort (1967), as follows

$$\frac{q}{k_0 H} = \frac{1}{0.88 + \frac{2b}{D} + \left(\frac{k_0}{k} - 1\right)\frac{\eta}{D}}. \tag{6.38}$$

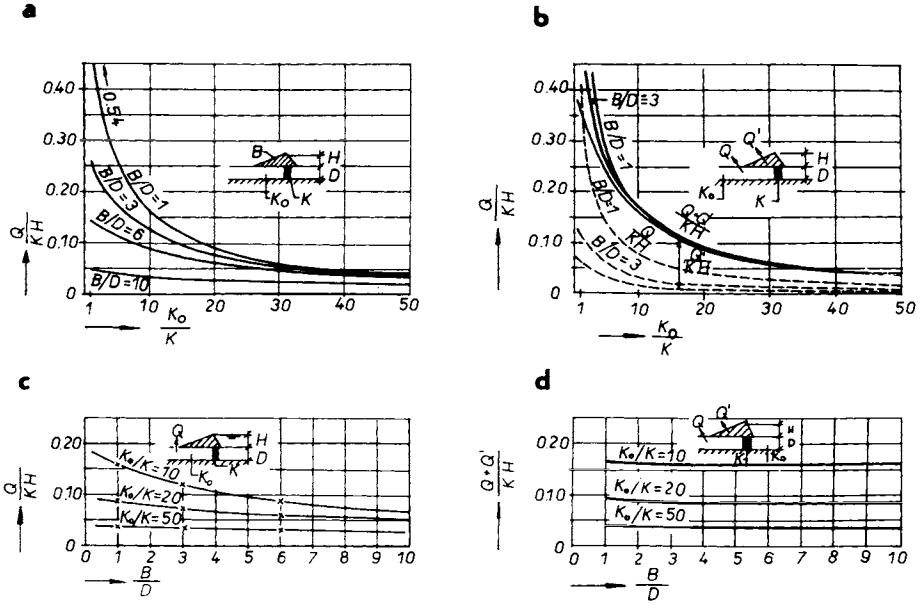

Fig. 6.16. Functionality $\bar{q} = f\left(\frac{2b}{D}, \frac{k_0}{k}\right)$ after Cambefort (1967). a — grout curtain without drain, b — with drain, c — seepage by different permeability ratio, d — seepage and water losses caused by drainage.

The diagrams in Fig. 6.16 plotted for various ratios of footing length, different permeability ($k_0 : k$) ratios and drain position demonstrate the influence of the above parameters as well as the influence of the drain position. The most remarkable influence of drain on rate $q(Q)$ is found in the case when this is located near the grout curtain at the upstream blanket. This disadvantage is compensated by the favourable influence on exit gradients which are reduced by such a drain.

6.4 Horizontal Sealing Elements

Horizontal *impervious blankets* have become the favourite antiseepage elements of levées, not only in the USA where they occur mostly in the Mississippi River valley, but also in Europe and in the USSR. In contrast with vertical sealing elements which stop seepage almost completely, impervious blankets reduce it only as a function of blanket length. This smaller sealing effect of the blanket is seldom considered a disadvantage. Its permeability is an advantage in dry periods. One of the advantages of this element is that the performance of the blanket can be enhanced by using the natural top-soil of the ground as a part of the antiseepage measure. For repairing the blanket, local raw materials such as silt, loam, silty clay, etc., can be used.

At present there are many types of blankets available: earthen (from natural soils), stabilized-soil, bituminous, asphaltic or asphalt-concrete and concrete or reinforced-concrete which can be anchored in the subsoil in special cases. However, in the case of levée protection, the first three of these construction materials are usually used and the remainder can be used for the protection of subsoil of the concrete structures.

The calculations for these three types of blankets — with respect to seepage (see Section 2.3, eqns. 2.119—2.121) — are in fact the same. The *unit rate* depends on the length of the bottom (b_1), the blanket (B) and the permeable subsoil depth (D), which can be expressed as follows (see Fig. 6.17)

$$\bar{q} = \frac{q}{kH} f\left(\frac{b_1}{D}, \frac{B}{b_1}\right). \tag{6.39}$$

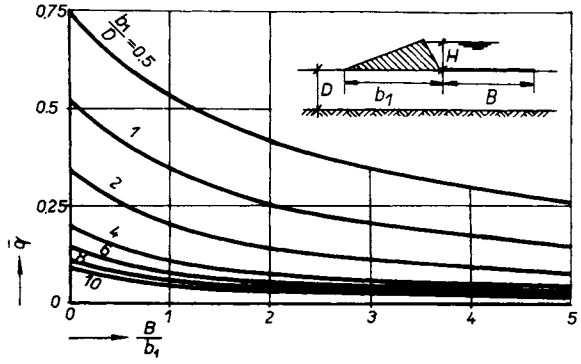

Fig. 6.17. Functionality $\bar{q} = f\left(\frac{b_1}{D}, \frac{B}{b_1}\right)$ for a blanket.

It shows that the influence of the blanket on seepage becomes evident if the length of the footing bottom ($b_0 : D$) and the length of the blanket are large enough. A total length $B^+ = b_1 + B = (5—10)\,D$, and at the same time $B^+ = (10—30)\,H$ are required.

Other rules are valid if we have to protect a subsoil consisting of many layers of different permeabilities, as they are if the subsoil is damaged by filtration deformation. In such cases, a larger length (as much as twice the original) is required, or it should be calculated by the Bažant—Hálek method (Hálek 1966). Their method takes into account the compensated thickness of permeable subsoil D_n, and a replacement length L_n should be added to the length of blanket B. In such a way, we have half the width of the river-bed B_k and the thickness of subsoil (D_n) as the increasing inflow resistances of water the subsoil (Fig. 6.18). For the flow conditions in the subsoil, the soil transmissivity expressed by the product kD and transmissivity of lower layers (k_1D_1) and upper layers (k_2D_2) is responsible. In

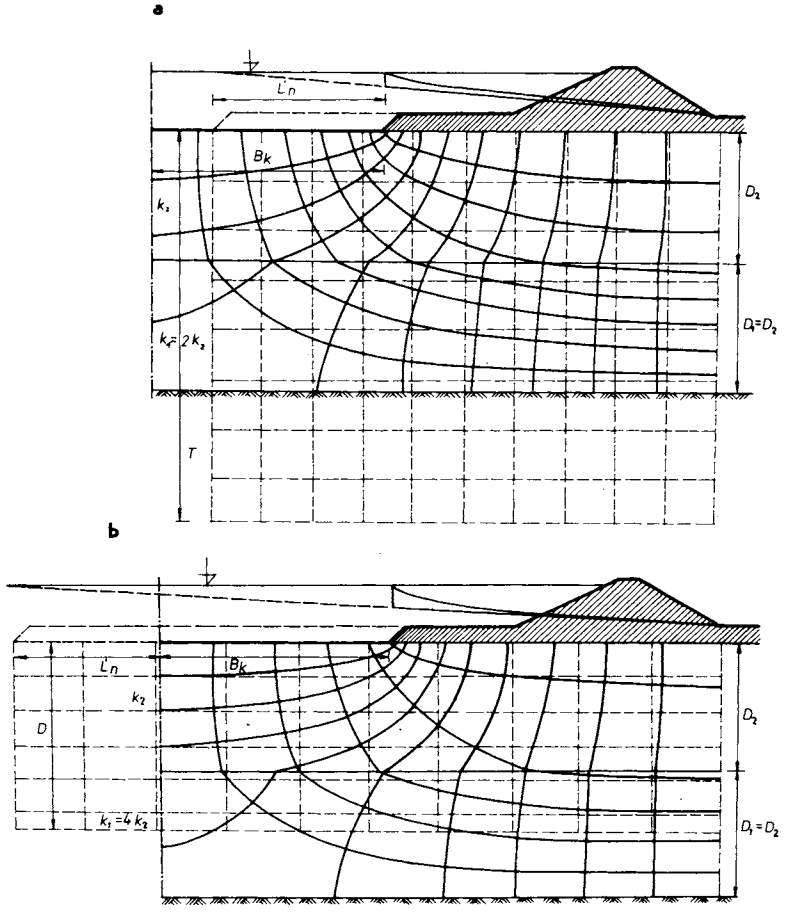

Fig. 6.18. Flow-net and its characteristics (D, D_1, D_2, L'_n, L_n) in an anisotropic media — after Hálek (1966). a — anisotrope subsoil with replaceable depth, b — with replaceable length.

Bažant and Hálek (1966), the multilayer subsoil is idealized by two transmissivities (k_1D_1); (k_2D_2) considering just two cases.

In the first, if $k_1D_1/k_2D_2 \leqq 3$, replacement thickness D_n and length L'_n are calculated from the formulae

$$D_n = D_2 + \frac{k_1 D_1}{k_2}, \tag{6.40}$$

$$L'_n = \frac{B_k}{D} - \frac{2}{\pi} \ln \sinh \frac{\pi B_k}{2D_n}. \tag{6.41}$$

In the second case, if $k_1D_1/k_2D_2 > 3$, another auxiliary value (anisotropy coefficient) is used

$$\beta_0 = \sqrt{\frac{k_2}{k_1 D_1 D_2}}, \tag{6.42}$$

and the following equations are obtained

$$D_n = D_1 + \frac{k_2 D_2}{k_1}, \tag{6.43}$$

$$L'_n = \frac{1}{\beta_0 \tanh \beta_0 B_k}. \tag{6.44}$$

The flow conditions and seepage quantities are influenced by top-soil permeability (k_p), thickness (d_p) and length in front of the blanket with permeability coefficient k_m and thickness d_m. Using these notations — in accordance with Fig. 6.19 — a value of deduced *anisotropy coefficient* of the top-soil (β_p) can be calculated as

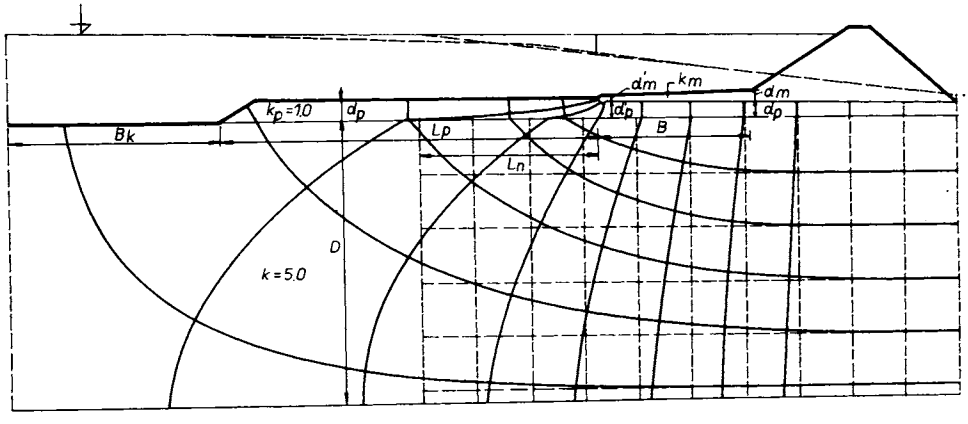

Fig. 6.19. Flow net: seepage through subsoil and permeable overburden in the front of a blanket — after Hálek (1966).

$$\beta_p = \sqrt{\frac{k_p}{kDd_p}}. \tag{6.45}$$

The next criterion is the product $\beta_p L'_n \gtrless 1.0$.
If

$$\beta_p L'_n = 1.0,$$

then

$$L'_n = \frac{1}{\beta_p} \tanh\left(\tanh^{-1} \beta L'_n + \beta_p L_p\right), \tag{6.46a}$$

$$\beta_p L'_n > 1.0,$$

$$L_n = \frac{1}{\beta_p} \frac{1}{\tanh\left(\tanh^{-1} \dfrac{1}{\beta_p L'_n} + \beta_p L_p\right)}. \tag{6.46b}$$

Further criteria derived are blanket thickness d_k and top-soil permeability k_p related to the actual lengths L_n, B. Then, we obtain expressions as follows

$$\frac{d_k}{k_p} = \frac{16(L_n + B)^2}{kD}, \tag{6.47}$$

$$d_k = d_p + \frac{k_p d_m}{k_m}, \tag{6.48}$$

$$\frac{k_k}{k_p} = \frac{16L_n^2}{kD}. \tag{6.49}$$

Using the diagram in Fig. 6.20 it is possible to determine the replacement length of blanket L_n which should be added to blanket length B, to the width of the levée b and to the width of berm b'. The *total length* L_t determining the pressure line gradient I will be

$$L_t = L_n + B + b + b'. \tag{6.50}$$

With total height H_t, the gradient will be

$$I = \frac{H_t}{L_t} = \frac{H + h}{L_n + B + b + b'}. \tag{6.51}$$

Assuming average allowed gradient I_{al}, it is possible to determine how far the drainage element should be from the downstream toe of the embankment. In another case, the width of berm b' can be calculated as follows

$$b' = \frac{H_t}{I_{al}} - (L_n + B + b). \tag{6.52}$$

Since flood duration t_p is smaller than that assumed in our calculations (eqns. 2.222—2.225), the gradients over the flood period will be generally smaller. Thus we can consider a smaller gradient in the drainage zone

$$I_{al} = I - \Delta I,$$

when

$$I = \frac{H}{\sqrt{at_p}} \pm I_l, \tag{6.53}$$

$a = kD/n_0$ being the coefficient of active transmissivity (storage capacity); I_l hydraulic gradient of the groundwater behind the levée. The *seepage through the subsoil* of the levée will be

$$Q_{al} = kDI_{al}. \tag{6.54}$$

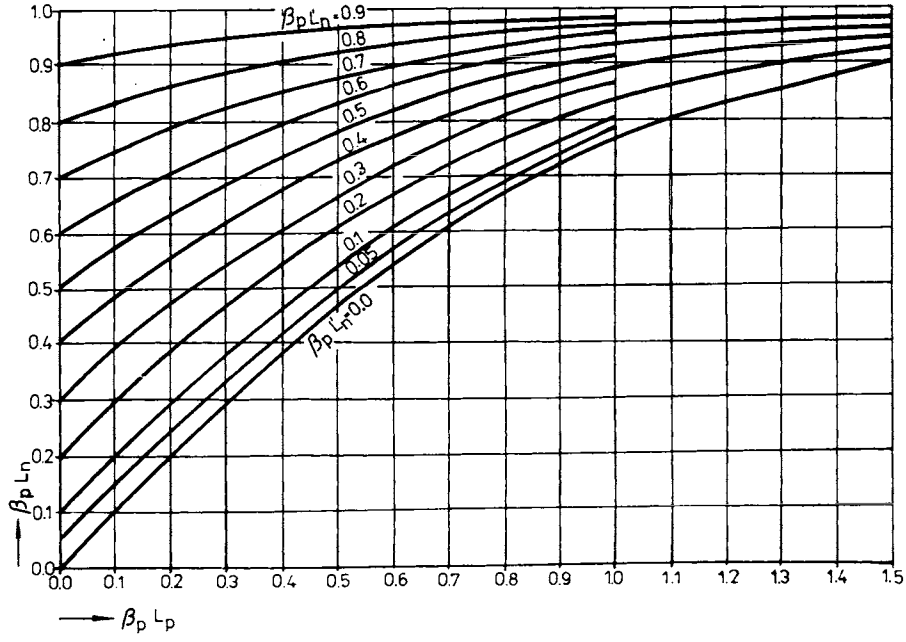

Fig. 6.20. Graph used for determination of a replaceable length (L') of the blanket.

If there are two permeable layers in the subsoil, characterized by k_1, D_1 in the lower layer, and k_2, D_2 in the upper layer, we consider the following depth

$$D = D_c + \frac{k_2 D_2}{k_1}, \tag{6.55}$$

provided that $k_2D_2/k_1D_1 < 1/3$, and

$$D_c = \frac{k_2(D_c)_2}{k_1}, \tag{6.56}$$

having the curtain in the upper layer.

If the *grout curtain* cuts the upper layer with thickness D_2 and if it is deepened in the lower layer at a depth of $(D_c)_1$, then

$$D_c = (D_c)_1 + \frac{k_2 D_2}{k_1}. \tag{6.57}$$

When using a *relief well* as a model of the deep drainage element (in the seepage well), analogically derived formulae are considered. In the first case

$$D = D_w + \frac{k_1 D_1}{k_2}, \tag{6.58}$$

$$D_w = (D_c)_2.$$

If there is a deep well of a depth $(D_w)_2 + (D_w)_1$, we can determine

$$D_w = (D_w)_2 + \frac{k_1(D_w)}{k_2}. \tag{6.59}$$

In the second case, the following expressions are obtained

$$D_c = D_2 + \frac{k_1(D_c)_1}{k_2}, \tag{6.60}$$

$$D_w = (D_w)_2 + \frac{k_1(D_w)_1}{k_2}, \tag{6.61}$$

provided the geological conditions given by the relation

$$\frac{D_2 k_2}{D_1 k_1} \geqq \frac{1}{3}$$

are valid.

6.5 Drain Operation and its Influence

Rocky drains are one of the main components of drainage systems. They control seepage and prevent damage by the flow of particles swept by water; they also prevent land sliding in certain cases.

One of the main roles of drains was treated in Sections 2.5 and 6.2 in association with the problems of subsoil protection. If we consider the role of the drains in more detail, we can draw up four groups: drains for water drainage, drains for

uplift reduction, drains lowering exit gradients and drains which have to stabilize the groundwater level.

As regards special drain types and location, there are drainage blankets (single or double layers), rock-toe drains, rock prisms, pipe drains, etc., and several kinds of wells (hollow or sand drains). All drains have their own purpose and position in relation to the dam structure. The problem of drain location can cause difficulties especially in cases where there are many design requirements and if the fulfillment of one function unfavourably affects another function. A drain reducing uplift and protecting the footing bottom results in increased seepage.

The most common drains are shown in Fig. 6.21 giving a picture of the above drain locations as well as their functions. Ditch-drains (Fig. 6.21c, d, e) are used as collectors, often very important in urban areas.

Drains can have twin functions, very useful in seepage control and diversion unless it reduces the uplift pressure; the relief of the sealing element (blankets in Fig. 6.21a, b) influences the amount of seepage unfavourably. In the majority of cases, the critical role is not played by the quantity of the seepage but by the gradients. This should be considered by the designer.

The *criterion gradients* I_b at water height H and blanket thickness d are determined by the upstream blanket. The values of this gradient are given within a large scale. For silty and clayey blankets, a value of $I_b = 5—50$ has been set by Terzaghi (1948). In the case of the Danube alluvial deposits, a higher value $I_b = 9.2—96$ has been found and thus the consulting bureau IGHP (Jakubec 1966) recommends $I_b = 20$ as an allowable value.

Allowed gradients I_b can be calculated from laboratory test data (k, k_0) or through theoretical formulae. The downstream water flow through a silty blanket into sand and gravel subsoils is given by a simple formula

$$I_{b\,al} = \frac{H}{d_k} \leqq \left(6 - \log \frac{k_0}{k}\right) \tag{6.62a}$$

and for sand and gravel the following expression

$$I_{b\,al} = 3 - \log \frac{k_0}{k} \tag{6.62b}$$

can be recommended, in which k_0 and k are the permeability coefficients of the subsoil and blanket.

Patrashev (1952) recommends that (by filtration deformation) the exit gradients be estimated by the following formula

$$I_{al} = 1.78 \sin\left(25 + \frac{\vartheta}{8}\right) \frac{\xi_p}{(0.7 + \xi_p)^2 (1 - \xi_p)}, \tag{6.63}$$

in which ϑ is the angle of the stream direction to the perpendicular; $\xi_p = d_c / d_{0.50}$ ratio of the diameter of particles carried out to the pore diameter of mean grains, usually, $\xi_p = 0.1—0.7$.

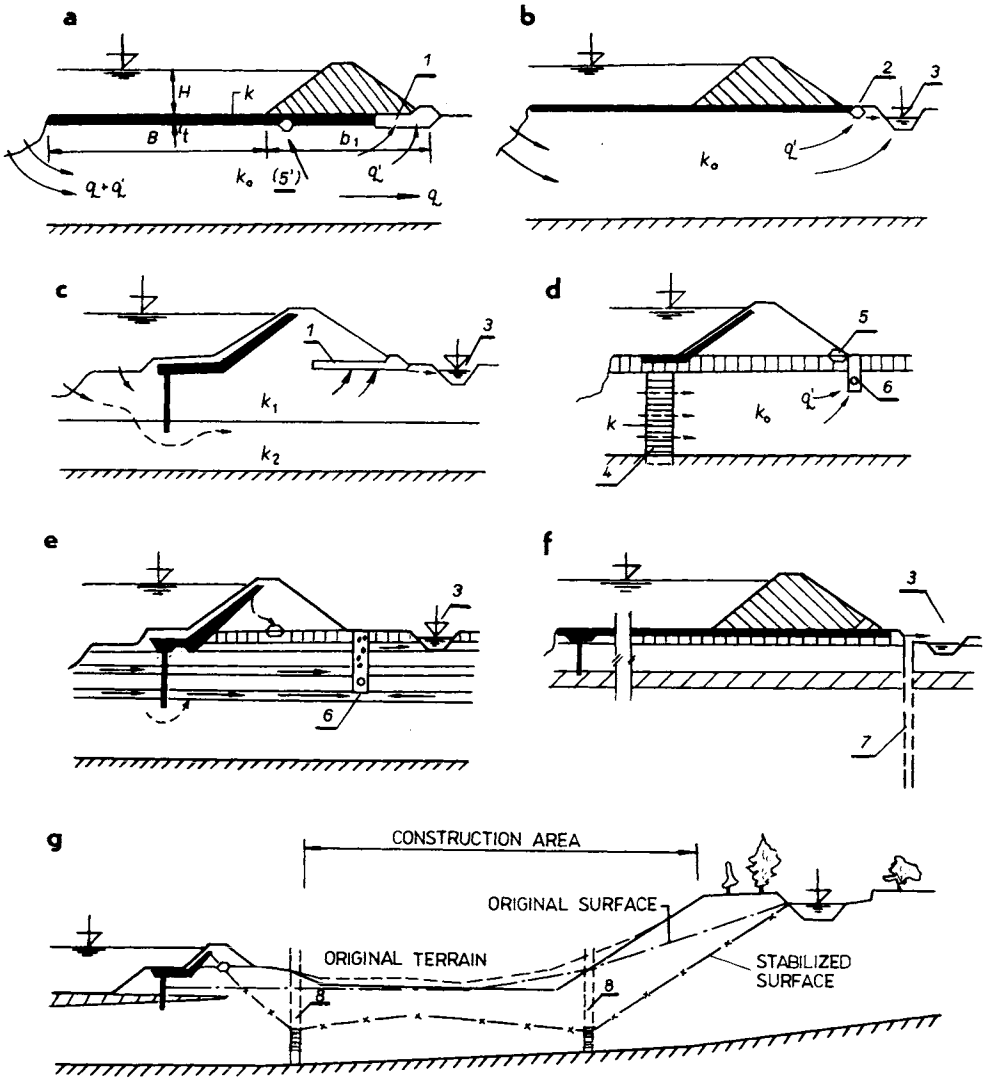

Fig. 6.21. Different types and positions of drains. a — drainage blanket (1), b — pipe drain (2) and seepage channel (3), c, d, e, f — combination of various active and passive antiseepage measures, g — stabilizing drain; 1 — blanket, 2 — pipe, 3 — channel, 4 — sealing (grout curtain), 5 — rocky toe drain, 6 — cut-off with pipe, 7 — deep well, 8 — well in operation-stabilizing water surface.

Under field geological conditions, a value of $I_{al} = 0.8—0.1$ is obtained through eqn. (6.63).

Protective filters and drains should be investigated very carefully, especially in cases where they are designed to protect soils threatened by filtration deformation (Istomina 1957, Lubochkov 1962) as mentioned later (Sections 6.7 and 6.8).

Drainage elements can be designed for a given unit rate $\bar{q}$ by eqns. (2.163)—(2.195). According to Nelson-Skornyakov (1949), the mean drain parameters can be obtained by approximate formulae. The active length of the drain (l_d) will be

$$l_d \cong 0.211 \frac{q}{k}, \tag{6.64}$$

the exit height (step) in the trench

$$h_s \cong 0.207 \frac{q}{k}. \tag{6.65}$$

The flow rate from the bottom of the trench is expressed by equation

$$q_d = \frac{2q}{\pi} \cos^{-1} \frac{2q}{\pi(q + kl_0)} \tag{6.66}$$

in the case of a bilateral seepage, and half this value if single-sided inflow into a trench of width l_0 is considered.

The *pipe drain* can be calculated through the formulae of Averyanov (1949). His formulae are analogous with eqn. (6.66)

$$q = \frac{2\alpha_1}{1 + \alpha_x} \left[q_0 + \frac{kD(H_1 - h_0)}{l_1} \right], \tag{6.67}$$

in which q_0 is the water inflow from the protected area; α_1 and α_x coefficients depending of the flow region

$$\alpha_1 = \frac{1}{1 + \frac{h_0}{l_1} A}, \qquad \alpha_x = \frac{1}{1 + \frac{h_0}{x} A},$$

$$A = 1.47 \log \frac{1}{\sin \frac{\pi d}{2h_0}}.$$

In accordance with the drawing (Fig. 6.22), depths D_1, D_2 of the water-saturated area (flow region) have values

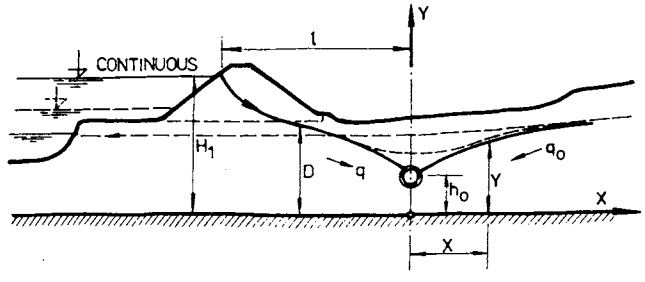

Fig. 6.22. Auxiliary calculation of a pipe drain after Averyanov scheme.

$$D_1 = \frac{H_1 - h_0}{2}, \qquad D_2 \cong h_0,$$

and the *ordinate of the phreatic line* can be obtained as

$$y = h_0 + \frac{1-\alpha_1}{1+\alpha_2}(H_1 - h_0) + \frac{\alpha_x + \alpha_1}{\alpha_x(1+\alpha_1)} \frac{q_0 x}{kD_2}. \tag{6.68}$$

Equations (6.67) and (6.68) have been used for designing the protective measures in many towns in Czechoslovakia (along the river Váh), and good agreement between calculation and experience has been observed. The difference between calculated and observed values has not exceeded 30%.

The drainage blanket can be calculated by means of the formulae deduced by Schneebeli (1966) given in Chapter 2 (eqns. 2.183—2.192). In some cases, the use of the Girinskiĭ (1947) solution with his potential of a multiple layer (Fig. 6.23) has many advantages.

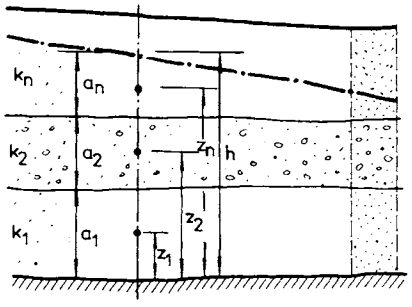

Fig. 6.23. Scheme for determining the Girinskiĭ potential.

His formula expressing the *potential* of n layers

$$\Phi = -\int_0^h k(h-z)\,\mathrm{d}z \cong -\sum_{i=1}^{i=n} k_i a_i (h - z_i), \tag{6.69}$$

for a homogeneous artesian horizon is very simple,

$$\Phi_1 = -\frac{kh^2}{2} \tag{6.70}$$

and equals that by Dupuit mentioned above.

The seepage in the vicinity of a river depends on the potential of the river and that of the drain circumference. The first can be expressed as follows

$$-\Phi_r = Q\frac{K'}{2K}, \tag{6.71}$$

in which the values of full elliptic integrals depend on the

$$\frac{L}{l_1}=\frac{4}{\pi}\left[K\varepsilon(\varphi_0, \lambda)-EF(\varphi_0, \lambda)\right], \tag{6.72}$$

there K, K', E are the full elliptic integrals with modulus λ and complementary modulus $\lambda'=\sqrt{1-\lambda^2}$, $\varepsilon(\varphi_0, \lambda)$, $F(\varphi_0, \lambda)$ are incomplete elliptic integrals with modulus and argument

$$\varphi_0=\sin^{-1}\frac{\sqrt{\frac{K-E}{E}}}{\lambda}. \tag{6.73}$$

These values should be substituted into eqn. (6.71) allowing us to obtain the seepage

$$Q=-\varkappa\Phi_r,\ \varkappa=\frac{\pi}{\tan h^{-1}\sqrt{\frac{l_1-r_0}{l_1+r_0}}}. \tag{6.74}$$

To the inflow rate, the unit inflow q_1 with length l_1 can be added; the total rate will be

$$Q=\varkappa(-\Phi_r+\mu_1 q_1 l_1),\ \mu_1=\frac{1}{K(\lambda^2+1)}. \tag{6.75}$$

If we have all dimensions of the surface drain and the required lengths (L_1, l_1), the complementary modulus λ' determines the equation

$$\lambda'=\sqrt{1-\lambda^2}=\frac{2l_1-L}{2l_1+L}, \tag{6.76}$$

which enables both the moduli of elliptic integrals K, K' and the value of coefficient $\varkappa$ to be obtained.

Reliefs and collecting wells are very different as regards structure. Perfect wells perforated round the whole circumference are simplest from the point of view of theory (Dupuit's conditions are fulfilled) and also from construction aspects. Theory and construction of perfect wells are well known to hydraulic engineers; it is not necessary to describe them. The remaining types of wells shown in Fig. 6.24 are distinguished by the perforation and by some details needed to increase inflow rate or relieve water pressure.

Besides these wells, sandy relief wells or (better) deep sandy drains should be mentioned as an efficient measure of uplift reduction. Perfect, partly perforated wells for pressure reduction and seepage control are the most common measure in engineering practice. One could list a number of advantages of a simple well (Fig. 6.24c) lacking wall perforation. If we have a well of 1.20—2.00 m in diameter, the protective filter can be made on the bottom where it can be constructed quite easily. The regenerative hydraulic process of the filter is simpler than for a well having the filter on its periphery (casing of the well).

Each of the wells mentioned above has another flow picture, but a number of

assumptions can sometimes be made. Provided that we know the well diameter ($2r_0$), the thickness of the water-bearing horizon and the form of the seepage line (the value of the height of the draw reduced by z_0), the quasi-perfect well quantity (yield), according to Babushkin (1955)

$$Q = \frac{2\pi k r_0 z_0}{\frac{\pi}{2} + 2\sin^{-1}\frac{r_0}{D+\sqrt{D^2+r_0^2}} + 0.515\frac{r_0}{D}\ln\frac{R_a}{4D}} \tag{6.77}$$

can be calculated, in which R_a is the radius of action of the well; $r_0/D \leqslant 1$ and $R_a/D \leqslant 10$. In this formula, the ratio $R_a : D$ seams to be overestimated.

In accordance with Muftakhov et al. (1963), the influence of different layer permeability coefficients (k_1, k_2) of two adjacent layers by an auxiliary value

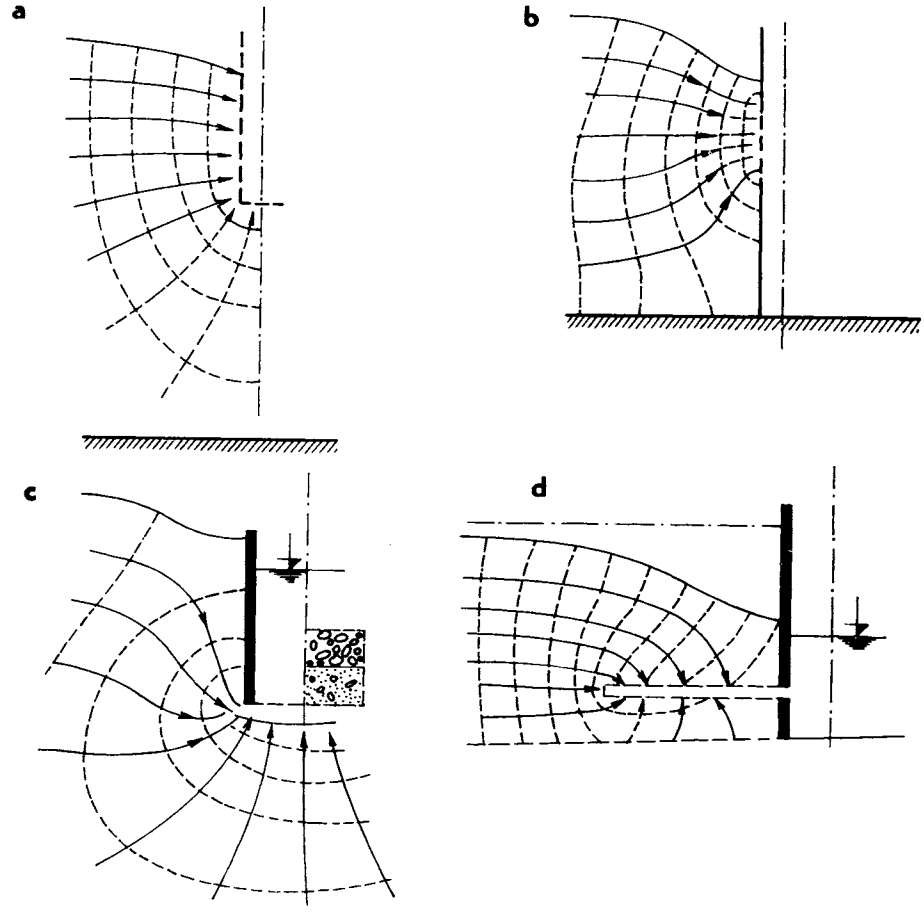

Fig. 6.24. Functional scheme of wells. a — "uncompleted well", b — confined well, c — with bottom filter, d — with radial pipe drain.

$\delta = k_1 - k_2/k_1 + k_2$ can be observed using this formula in the following form

$$Q = \pi k_1 D \left\{ \frac{h_d}{\ln R_a - \ln r_0} + \right.$$
$$\left. + \frac{2r_0}{\frac{\pi}{2} - \sin^{-1}\frac{r_0}{R_a} + 2\delta \sin^{-1}\frac{r_0}{D + \sqrt{D^2 + r_0^2}} + f_\delta\left(\frac{R_a}{D}, \frac{r_0}{D}\right)} \right\}, \qquad (6.78)$$

where D is the depth of the well bottom under the original groundwater level; h_d depth of the water table in the well under the groundwater level; k_1, k_2 permeability coefficients of the upper and lower layers; f_δ value of the dependence of $f_\delta(R_a/D, r_0/D)$ on r_0/D shown in Fig. 6.25. The diagram shows that in deep alluvial deposits at a ratio $r_0/D < 0.2$, the influence of the dependence $f_\delta(R_a/D, r_0/D_1)$ is not significant.

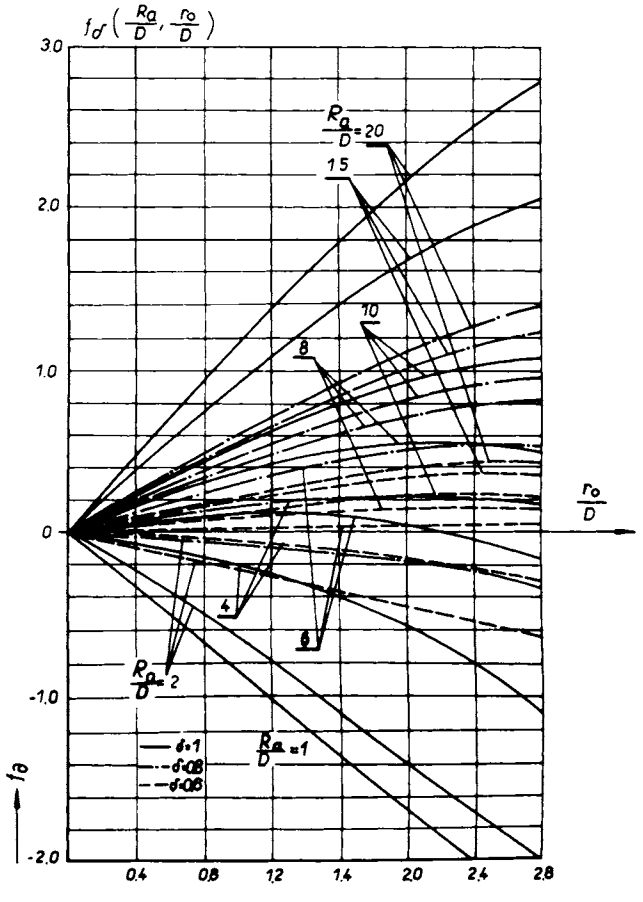

Fig. 6.25. Relationship $f_\delta\left(\frac{R_a}{D}, \frac{r_0}{D}\right)$ after Muftakhov et al. (1963).

It should be mentioned that in relief wells near levées, the value Q will change to a large extent. It will be influenced not only by the change of water level during a flood (groundwater table rise — D_w change) but by the change of magnitude R_a.

The time-dependent value ($R_{a,t}$) of radius R_a can be expressed by the equation

$$R_{a,t} = r_0 + 1.5\sqrt{at}, \tag{6.79}$$

in which $a = k\bar{H}/n_0$, t is the time of well operation (the operation usually starts at flood arrival t_0) at which the water level in the river bed rises above the groundwater table.

The pumping action should be synchronized with the water-table change as well as possible. If the head increases slightly above that by which the critical (flotation) gradient is given, the material will start to flow and piping or other soil instabilities will occur.

In accordance with Chapter 2 (Section 2.6), we obtain the drawdown in the well vicinity (on the surface of the filter mantle) during pumping, with rate Q, as follows

$$z_{cr,t} = \frac{Q}{2\pi k r_0}\left[1 - \Phi\left(\frac{r}{2\sqrt{at}}\right)\right]. \tag{6.80}$$

When remembering the critical drawdown (z_{cr}) at a distance $l = \varrho/2$ from the well, we get

$$z_{cr} = \frac{Q}{2\pi k}\left\{\frac{1}{r_0}\left[1 - \Phi\left(\frac{r}{2\sqrt{at}}\right)\right] - \frac{1}{\varrho}\left[1 - \Phi\frac{\varrho}{2\sqrt{at}}\right]\right\}. \tag{6.81}$$

By equating eqns. (6.80) and (6.81), we obtain the following expression

$$\frac{1}{r}\left[1 - \Phi\left(\frac{r}{2\sqrt{at}}\right)\right] = \left(1 - \frac{1}{\varepsilon}\right)\frac{1}{\varrho}\left[1 - \Phi\left(\frac{\varrho}{2\sqrt{at}}\right)\right],$$

in which the ratio z_{cr} and z, $\varepsilon = (z_{cr} - z)/z$ and the dependence $\alpha = f\left(\frac{r}{2(at)^{1/2}}\right)$ determine the critical time t_{cr}, at which we meet the drainage element in the whole system of protective measures.

Verigin (1962) solved eqn. (6.81) for many cases. After its evaluation for different values of ε and α, he found characteristic values $\varepsilon = 0.05$, $\alpha = 1$—1.64 and deduced several simple expressions for critical time

$$t_{cr} \leqq (1\text{—}2.66)\frac{\varrho^2}{a}$$

or

$$t_{cr} \leqq (4\text{—}10.7)\frac{l^2}{a}, \tag{6.82a}$$

for a thick layer and

$$t_{cr} = (1.6—2.4)\frac{l^2}{a} \tag{6.82b}$$

for a thin layer, where l is the distance of the well from the river bed; from the water inflow into the substratum (from infiltration line to well line).

6.6 Structure of Drains, Filters and Casing of Wells

Regardless of the function of a drain and a well as permeable elements designed for water drainage, we require that these elements protect the construction or foundation being charged and attached. This is the filter charge in the case of drains and casing in the case of wells. This may prevent the impregnation of coarse material with fine materials and clarify the water.

The filters should withstand chemical (corrosion) and mechanical degradation, textile filters should have long-term stability, particularly iron-steel filters. If the service life of a filter is limited, it is necessary to solve the problem by changing parts or through its overhaul.

The choice and design of a proper filter requires a knowledge of materials from various branches of science. It is impossible to deal with this subject in detail and therefore we shall mention only some aspects of the earth-filter design.

Filters or drains used to control seepage should satisfy two conflicting requirements.

(1) The size of the pores have to be small enough to prevent particles being carried from adjacent soil.
(2) The permeability should be high enough to allow rapid drainage of water entering the filter.

The following criteria have been found satisfactory for filters (Craig 1975):

$$\frac{(d_{15})_f}{(d_{85})_s} < 4 \text{ to } 5, \tag{6.83}$$

$$\frac{(d_{15})_f}{(d_{15})_s} > 4 \text{ to } 5, \tag{6.84}$$

$$\frac{(d_{50})_f}{(d_{50})_s} < 25, \tag{6.85}$$

in which f denotes "filter" and s denotes "adjacent soil". From eqn. (6.83), the requirement for preventing piping is given; eqns. (6.84) and (6.85) express the requirements which ensure that the filter permeability is high enough for drainage purposes.

Filters comprising two or more layers with different gradings can also be used, the finest layer being on the upstream side of the filter (of dam) on the downstream side (protecting the foundation). Such an arrangement is called a graded filter. In filter design it is also necessary to respect the flow direction. If the flow is, let us say, downward, each successive layer of material may be composed of particles so that the fine-sand layer is on the upper side followed by a layer of coarse material. It is necessary to consider the flow direction with respect to the contact between the protected soil and the filter layer (Fig. 6.26). The first flow direction (Fig. 6.26a) is favourable as regards stability; the flow direction causing uplift of the filter layer (Fig. 6.26b) is less favourable. A very dangerous case is that of coincidence of the

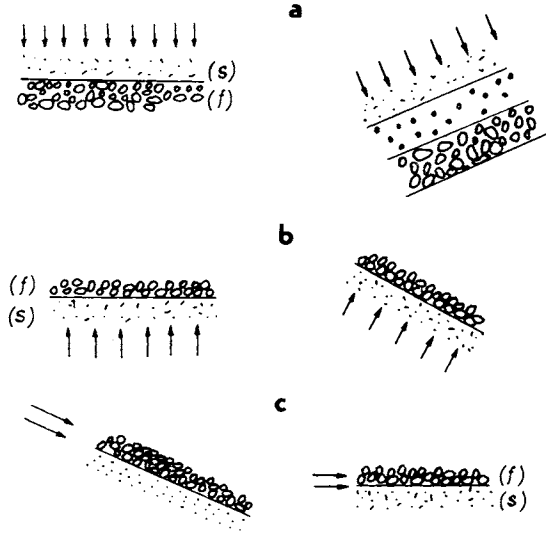

Fig. 6. 26. Soil contact position with respect to the flow direction. a — perpendicular down, b — perpendicular upward, c — along the contact.

flow and contact direction (6.26c), particularly so if the soil is in a loose state and when it shows a low uniformity (Fig. 6.27). The porosity should in general be lower than 0.37 ($n \leqq 37\,\%$). If the porosity is higher, the danger of filter damage is quite high if the flow direction is unfavourable.

The coefficient of permeability of the filter ($k^{(f)}$) may be higher than that of the protected soil ($k^{(s)}$) according to the relation

$$\frac{k^{(f)}}{k^{(s)}} \geqq 2\text{—}3.5$$

or

$$\frac{k^{(f)}}{k^{(s)}} = (2 + \sqrt[6]{c_u^f}). \tag{6.86a}$$

If all requirements are fulfilled, it is useful to investigate the allowed gradient (I_{at}) with respect to the grain size d_c — which can be carried away according to the following expression

$$I_{al} \leqq I_{cr} = \varphi_0 \sqrt{\frac{gn^{(f)} - d_c^2}{\nu k^{(f)}}}, \tag{6.86b}$$

in which

$$\varphi_0 = 0.6 \left(\frac{\gamma^{(f)}}{\gamma_w} - 1 \right) f^* \sin \left(30 + \frac{\vartheta}{8} \right).$$

Assuming an acceleration of $g = 981$ cm s^{-2}, the value f^* will be given by the following expression

$$f^* = 0.82 - 1.8n + 0.0062(C_u - C_{u,c}).$$

To determine the value f^*, the use of Abramov et al. (1964) diagrams can be recommended.

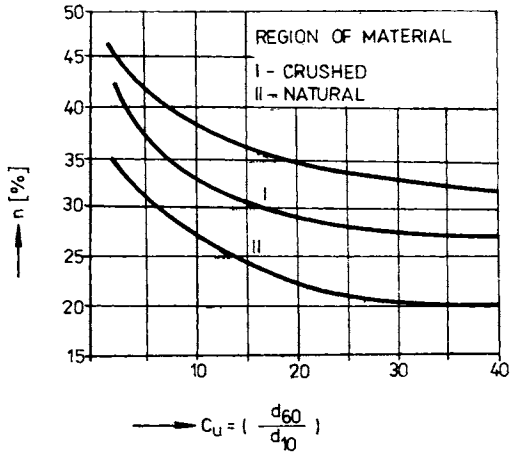

Fig. 6.27. Allowable porosity and uniformity.

The thickness of the filter layer $D^{(f)}$ depends particularly on two aspects, the grain size of the filter and technological aspects. The first rule, $D^{(f)} = (2—10)\, d_{max}$, can be easily fulfilled and thus the second requirement becomes important. The mechanical placing and compacting of the filter require a thickness $D^{(f)} \geqq$ 20—30 cm. The requirement of the allowed gradient should not be neglected. Approximate I_{al} values are given in Table 6.4.

Table 6.4. Orientation values of allowed gradients I_{al}

Type of drain	Surface (areal)		Strip		Prism or ripple		Well
Located	in the middle	at the toe	in the middle	at the toe	in the middle	at the toe	
Span of I_{al}	0.3—0.6	0.1—0.4	0.4—0.7	0.2—0.5	0.5—0.8	0.3—0.6	0.4—0.7
Average I_{al}	0.45	0.2	0.55	0.3	0.65	0.4	0.5

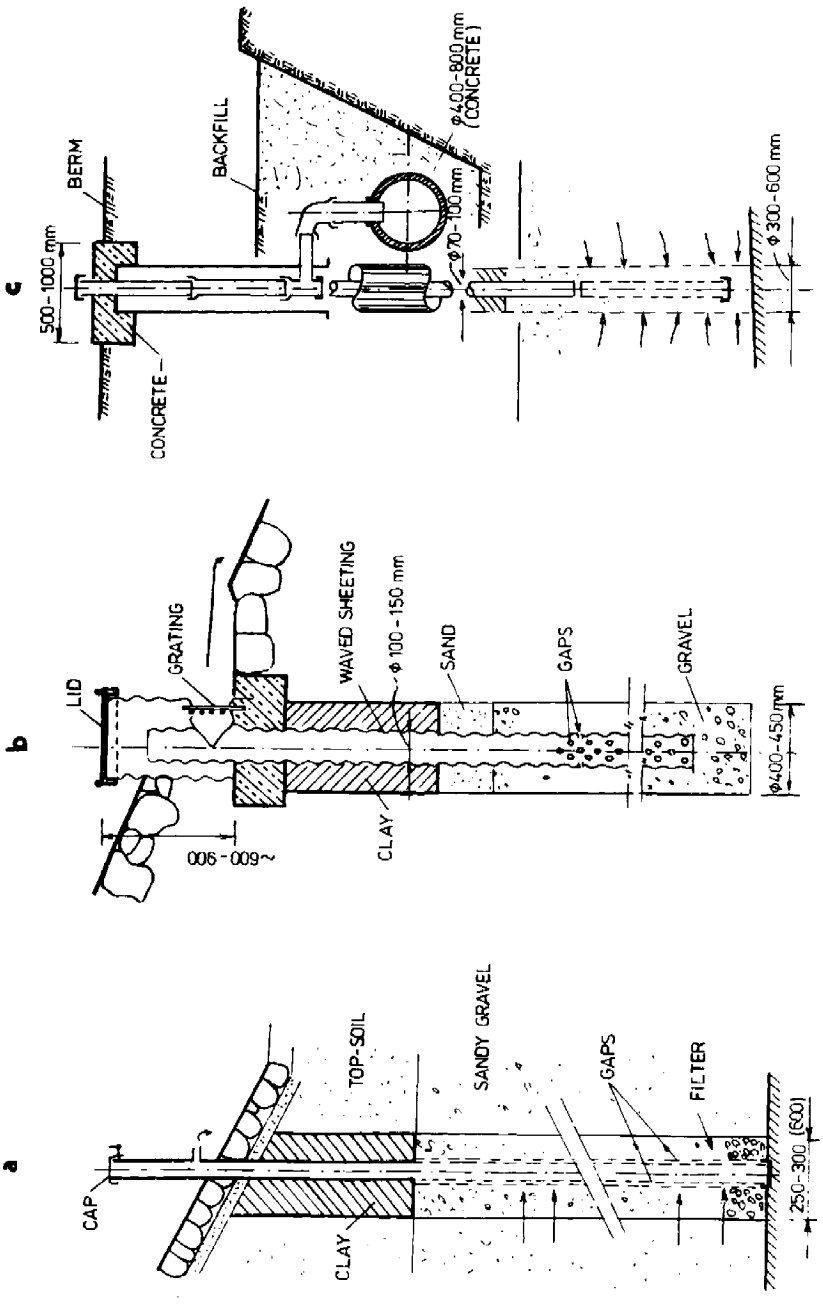

Fig. 6.28. Construction of wells. a — after CSN, b — after US Army Crops of Engineers, c — well with a syphon collecting the seepage water.

The construction and the casing of wells (Fig. 6.28) depend on the diameter and hydrogeological conditions, as well as the contractor's equipment. In Central Europe, quite simple perfect wells (Fig. 6.28a) with a steel pipe diameter 70—150 mm perforated in the lower end are employed. The casing of the well is formed by an earth filter. On the upper end there is an outlet pipe serving as an overflow.

In American practice, a kind of well made by the technique of boring (a bore hole 400—450 mm diameter) where a rocky casing is used in the lower part with a grooved pipe in the upper part (Fig. 6.28b). Grooved steel pipes perforated, with a large opening, and with a grill with a "spillway" are the most remarkable features of this kind of wells. Their advantage is their easy safety control. In the USSR, wickerwork wells (of round steel) welded into a round pipe form with an efficient casing having 70—75% useful openings on the circumference are also used. Their high efficiency — in comparison with normal perforated relief wells with 12—25% openings of the surface — has been stressed by the Russian specialist Abramov.

The third variation of well modification is characterized by a composed well profile (Fig. 6.28c), consisting of two perforated pipes and sections from different materials with a syphon leading the water into a concrete collector pipe of larger diameter (400—800 mm).

The function and efficiency of drains depend on many factors given by the intended purpose. When seepage is in question, we follow the growth of the amount of seepage by vertical (Fig. 6.29) and horizontal (Fig. 6.30) antiseepage measures as a consequence of the shortened seepage path. Despite this, the exit gradients are generally smaller in the protective layer, and therefore the decisive factor for safety of the subsoil should be controlled.

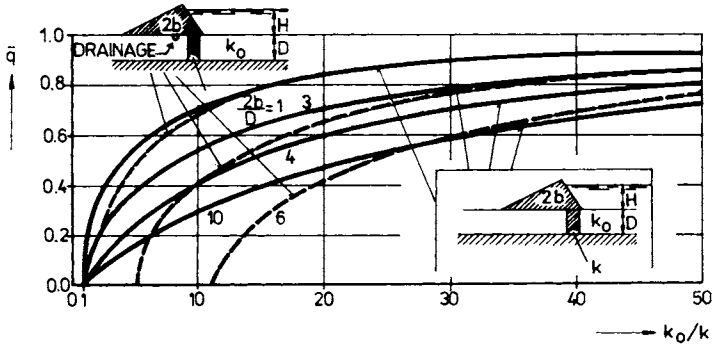

Fig. 6.29. Relationship $\bar{q} = f(k_0/k)$.

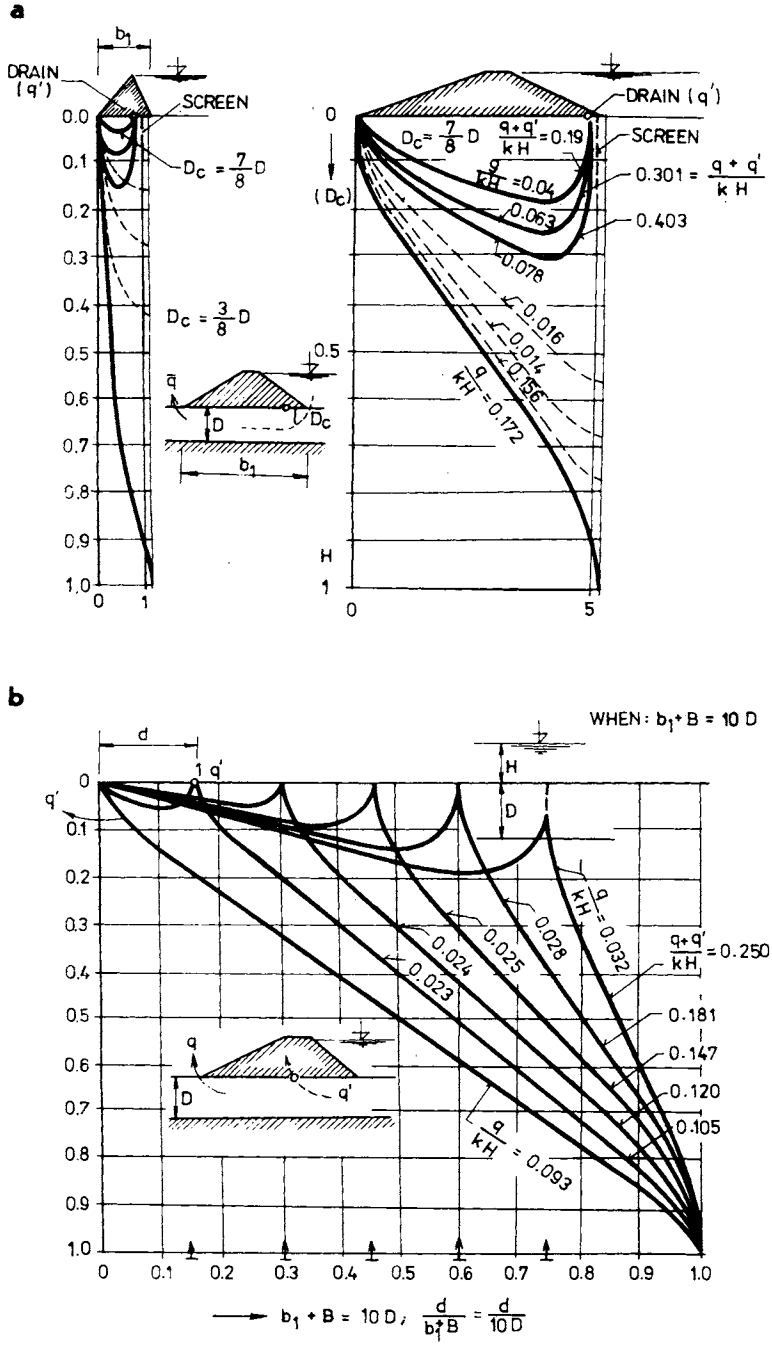

Fig. 6.30. Relationship q/kH and d, D_c, $b_1 + B$ of the drains. a — by vertical screen, b — by horizontal blanket.

The dependence represented by diagrams and the mathematical expression

$$I = \frac{H}{D} f_1\left(\frac{b_1}{D}, \frac{D_s}{D}, \frac{x}{D}\right) \tag{6.87}$$

provide complementary information about the efficiency of the drain mostly estimated according to the unit rate formula

$$\bar{q} = kHf_2\left(\frac{b_1}{D}, \frac{D_s}{D}\right). \tag{6.88}$$

The characteristic values in eqns. (6.87) and (6.88) can be rearranged into a new characteristic relation

$$\frac{I}{H/D} = \bar{q}f_3\left(\frac{b_1}{D}, \frac{D_s}{D}, \frac{x}{D}\right). \tag{6.89}$$

Equation (6.89) expresses a set of dependences giving a more complex picture of the flow region in the sub-base of the dam and its vicinity than old seepage indices (q) and many coefficients (of Bligh or Lane) characterizing the flow path or creep ratio which were once used by designers.

In special cases the uplift pressure can be quite influential on subsoil damage. This can be lowered in levées (Fig. 6.30a) quite efficiently by vertical sealing and an adequate kind of drain or by horizontal elements of active and passive measures (Fig. 6.30b). The active effect of drains is more remarkable in the case of an upstream position. In this position, the rock prisms, pipe, rock horizontal drain and similar surface drains can be located, but not a deep well. The relief wells are typical active antiseepage measures enabling the water pressure (artesian horizon) to be relieved at a great depth.

In flood periods, all kinds of strips, surface drains (of rock, pipe, ore trench) play an important control function. They can be connected to the automatic information system, as we shall consider in more detail in Chapter 7.

The efficiency of antiseepage measures depends on many factors and geological conditions. Cambefort (1967) has formulated the following conclusions on the basis of the following facts.

(1) The upstream blanket cannot be considered as an efficient antiseepage measure if the permeability coefficient of the subsoil exceeds $k = 1 \times 10^{-5}$ m s^{-1}. The blanket should be connected with some elements needed for reducing the uplift pressure and decreasing the exit gradients. These elements, however, increase the amount of seepage remarkably.
(2) With a heterogeneous pervious subsoil, the vertical sealing and drainage elements (all kinds of walls) are most efficient.
(3) In some cases, it is sufficient to make a grout curtain which reduces the permeability (k_0) by 10 to 20. The advantage is that a more remarkable reduction of the uplift results from using a blanket.

(4) The efficiency of the blanket is the largest in the case of a thin subsoil (D); in such cases the advantages of a wall are unequivocal.
(5) The advantages of walls as antiseepage measures are so convincing that they need no comparison with blankets.

Cambefort's *conclusions are in contradiction* with Middlebrooks' (1948) experiences and the theoretical work of Kratochvíl and Hálek (1959), who proved a *high efficiency of horizontal blankets* investigated in five cases (Fig. 6.31) where they assumed: an impermeable wall curtain which changes the value of k_0 in the ratio $k_0 : k = 100$; a more permeable curtain at $k_0 : k = 50$, then $k_0 : k = 30$ and finally a completely permeable curtain $k_0 : k = 1$.

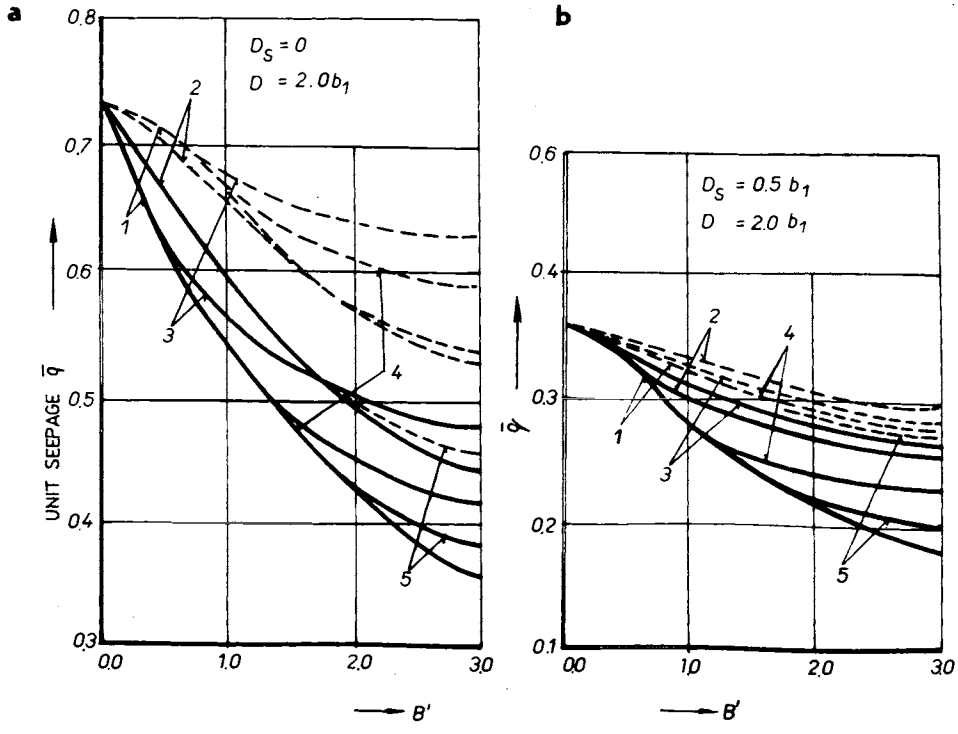

Fig. 6.31. Unit flow ($\bar{q}$) comparison for different sealing elements — after Kratochvíl and Hálek (1959). a — depth of the sealing $D_s = 0$, b — depth of the sealing $D_s = 0.5b_1$; 1—5 — different permeability relationships ($k_0 : k$) — see the text and literature mentioned above.

As shown in Fig. 6.31b, only a wall of sufficient depth is efficient. The conclusions of authors who considered the poor properties of vertical elements and the good properties of blankets, have been formulated as follows.

A wall reduces the blanket efficiency, a short wall shows no efficiency. If a permeable grout curtain is considered, the seepage losses increase with increasing

permeability, and in the case of a deep permeable subsoil only the efficiency of the blanket is evident. The influence of a crack in a blanket is obvious at a greater thickness of permeable subsoil; the damage of the wall influences the seepage to a smaller degree, while the blanket cannot function when damaged by cracks.

The authors did not investigate a multilayer heterogeneous subsoil or the case of an impermeable wall when the greatest advantages of vertical sealing elements are observed.

6.7 Computation of Seepage and Allowable Gradients According to Classical Theories of Water Flow

6.7.1 General Considerations and Calculation of Seepage

Classical methods of seepage computation are usually based on two principles; one is the flow-rate computation using Darcy's law as the basic formula which also leads to the basic equations of the potential theory. The second principle and the second step consists of the computation of critical gradients and critical velocities deduced by Terzaghi (1948) followed by calculation of water pressure and energy using Bernoulli's equation.

The *hydraulic gradients* are compared with *critical values* determined by water height H and critical flow path length L. These values give the calculated coefficient C of the flow-path length, which we shall consider further later.

These calculation steps were often taken full range. The conception of critical velocities and that of energy transfer based on the analysis of Bernoulli's equation were introduced in the fifties in the USSR and approximately at the same time in France, England and the USA where they were influenced by the theory of "fluidized bed", this being helpful when solving many stability problems met in the design of canal dams and levées.

The simplest theories based on *critical velocities* are those of Pavlovskiĭ (1922) and Patrashev (1952), whilst that of Istomina (1957) represents the method of critical-gradient computation with many new theoretical aspects disregarded by Lane (1935) in the sphere of field investigation and investigation of protective filters.

If we follow *Pavlovskiĭ's concept,* we can use his equation for critical velocities derived for grain and pore diameters (d or d_{17}), soil porosity (n), kinematic viscosity (ν) and "flow number" (N — which replaces Reynolds number). The formula for critical velocity has the following form

$$v_{cr} = \frac{1}{6.5}(0.74n + 0.23)\frac{\nu N}{d} \tag{6.90}$$

for sands with porosity $n = 40\%$, in water flow with $N = 50$ and $\nu = 0.013$ cm^2 s^{-1}.

Table 6.5. Values of creep ratio and coefficients C_B, C_L and C_k

Subsoil type	Observed		After Bligh C_B		After Lane C_L		C_k with respect to the depth of failure z_{cr}				
	Number	Height [m]	Real	Tabulated	Real	Tabulated	$z_{cr} \leqq 0{,}5H$	$1H$	$1.5H$	$2H$	$z_{cr} \geqq 3H$
Very fine sand	8	$\leqq 5$	7.93		5.18						
	8	6—14	6.61		4.22						
	$\Sigma = 16$	average	7.01	18	4.51	8.50	86	70	45	30	18
Medium sand	6	$\leqq 5$	9.24		3.05						
	7	5—17	5.38		3.47						
	$\Sigma = 13$	average	6.40	(15)	3.89	6.00	50	40	32	24	15
Coarse sand	7	$\leqq 5$	6.85		3.99						
	5	6—17	4.34		3.22						
	$\Sigma = 12$	average	5.17	12	3.45	5.00	35	26	18	14	10
Gravel	10	$\leqq 5$	5.95		3.73						
	10	6—17	4.73		2.97						
	$\Sigma = 20$	average	5.07	(10)	3.18	3.50	16	12	8	5	4
Gravel and sand	13	$\leqq 5$	5.92		4.11						
	8	5—9	4.07		2.78						
	$\Sigma = 21$	average	4.89	9	3.27	—	25	18	15	12	10
Boulders and gravel	8	$\leqq 5$	5.95		4.35						
	6	6—19	3.69		2.01						
	$\Sigma = 14$	average	4.30	—	2.67	2.50	8	6	4.5	4	2.5

C_k after laboratory experiments using soils having porosity $n \geqq 43\%$ by sands and $n \geqq 40$ by gravel.
Depth of critical path z_{cr} is related to the elevation (H) of the pool (river).

When calculating d as follows

$$d = 0.535 \sqrt[6]{C_u}\,\frac{n}{1-n}\,d_{17} = 0.535 \sqrt[6]{\frac{0.04}{0.015}}\,\frac{0.4}{1-0.4}\,0.02 = 0.008 \text{ cm},$$

then

$$v_{cr} = \frac{1}{6.5}(0.75 \times 0.4 + 0.23)\,\frac{0.013 \times 40}{0.008} = 6.6 \text{ cm s}^{-1}.$$

Sandy gravel of Danube deposits should remain stable up to a critical velocity of

$$v_{cr} = 0.053\,\frac{1}{0.025} = 2.1 \text{ cm s}^{-1}.$$

Calculations according to Patrashev give lower velocities which we obtain from his formula

$$v_{cr} = \frac{d}{n_0}\left(1 + \sqrt{1 + \frac{a_0 H_0}{d}\,k}\right), \tag{6.91}$$

and after evaluation of eqn. (6.91) for the given sandy gravel we obtain

$$v_{cr} = \frac{0.025}{0.4}\left(1 + \sqrt{1 + \frac{0.4 \times 2/3 \times 2.65(0.5 \times 1.0)0.15}{0.025}}\right) = 0.17 \text{ cm s}^{-1},$$

and the critical gradient (assuming laminar flow — according to Darcy)

$$I_{cr} = v_{cr}\,\frac{1}{k} = 0.17\,\frac{1}{0.15} = 1.15.$$

According to the *Istomina theory* (which cannot be analysed here in detail), it is necessary to take into account the coefficient of uniformity of soil (C_u). In our case — according to Istomina (1957) — we have

$C_u = 10$ corresponding to $I_{al} = 0.3$,
$C_u = 20$ corresponding to $I_{al} = 0.1$.

The allowable gradients are smaller than those calculated according to Patrashev.

Two facts can be stated after analysing the methods of v_{cr} and I_{cr} calculation. Firstly, the results obtained for the same soil by methods of different authors differ by 2—3 orders; for example, according to Pavlovskiĭ $v_{cr} = 6.6$ cm s^{-1}, but according to Goldstein we have $v_{cr} = 0.0027$ cm s^{-1}. Secondly, it can be seen that in the calculation of v_{cr} according to classical theories many aspects and influences are not respected.

The method of stability evaluation according to Blight and Lane using their coefficients (C_B and C_L) shown in Table 6.5 may be considered for a rough

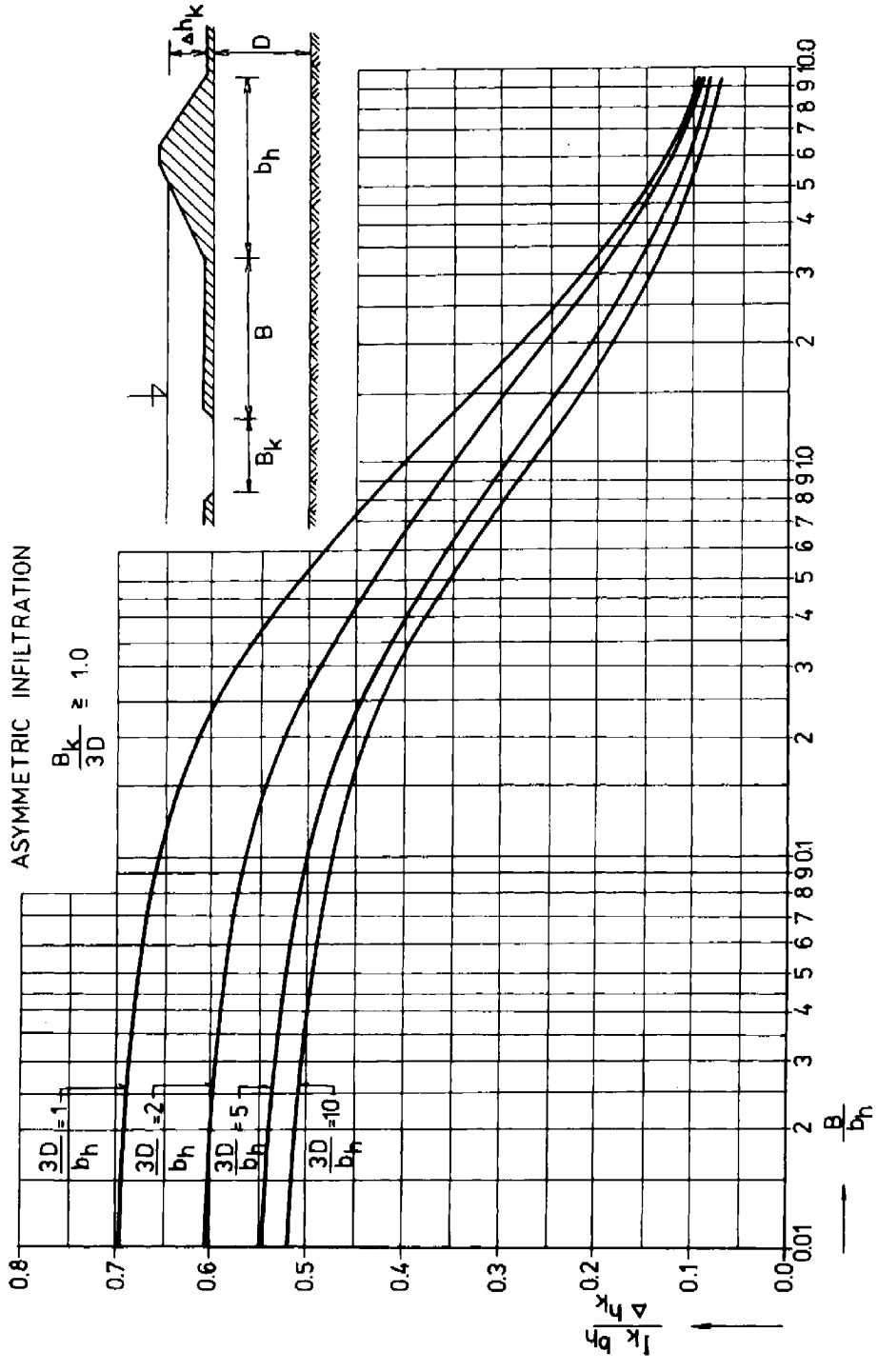

Fig. 6.32. Graph of the relationship (I_k, b_h) : $\Delta h_k = f(B : b_h)$ — infiltration conditions for asymmetric flow.

approximation and initial information which should be calculated more exactly using one of the new methods, discussed later. The coefficients C_B and C_L include rather different safety factors and do not consider the real state of the soil (n, m), nor the depth of the layer in question.

Some of these shortcomings are overcome in the new methods of *critical-gradient* calculations. Havlíček (1966) found the hydraulic gradient necessary for removal of a certain portion of fines (m) mixed with coarse material (gravel) assuming soil porosity (n_s) and unit weights γ_s and γ_d, and in the moment of attack by water of unit weight γ_w. His formulae

$$I_s = \frac{H}{L} = \gamma_d \frac{\gamma_s - \gamma_w}{\gamma_w} \frac{m}{n_s} = \frac{\gamma'}{\gamma_w} \frac{m}{n_s} \tag{6.92a}$$

or

$$I_s = \frac{\gamma}{\gamma_w} \frac{D}{z \pm D} \tan \Phi, \tag{6.92b}$$

where D denotes the layer thickness and z its depth, Φ angle of the soil friction (usually $\tan \Phi = 0.5$—0.7). After substituting in the values of the field, eqn. (6.92a)

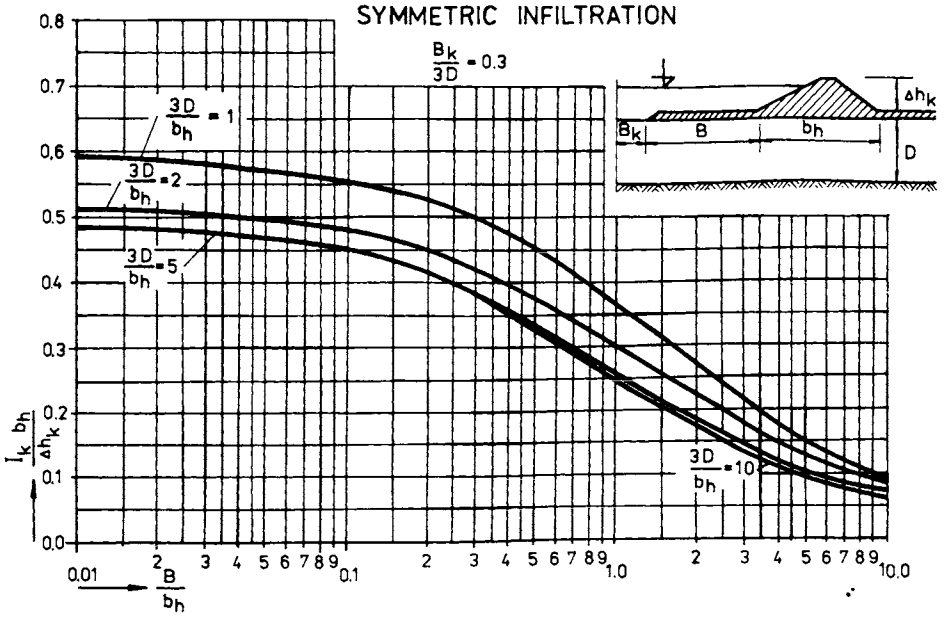

Fig. 6.33. Graph of the relationship ($I_k b_h$): $\Delta h_k = f(B : b_h)$ — infiltration conditions for symmetric flow after Hálek (1966).

gives $I_s = 0.55—0.8$ and eqn. (6.92b) gives $I_s = 0.125—0.20$. These values are more realistic under soil-deformation conditions than those by Patrashev.

It has been found that in the field, the real conditions are changed as a function of groundwater movement, rising and drawdown of the water table as well and also as a function of the operation of antiseepage elements as was proved in Chapter 2 and Section 6.6.

In practice, an appropriate diagram is found useful by for designer. The Manual (Hálek 1966) includes several such figures which can be used to determine gradient I_k such that the design criterion is satisfied. In the case of the design of the Danube levées, this was the *piping criterion-gradient* which can be expected near the toe of the embankment before the "piping" (boils) appears. The magnitude of I_k is affected particularly by the form of the structure (its width b_h) of the blanket (B), that of the river bed (B_k, b_k) water height (h_k) and permeable subsoil thickness (D). These values — denoted in Figs. 6.32 and 6.33 — helped in designing reliable antiseepage measures taking into account the design criteria (Δh_k, b_h, D, B_k or b_k) and observing the rule mentioned in Section 6.4 in accordance with eqns. (6.51)—(6.54). In this case, the following equations can be obtained

$$I_k = \frac{\Delta h_k}{\varkappa(B - b_h)} .$$

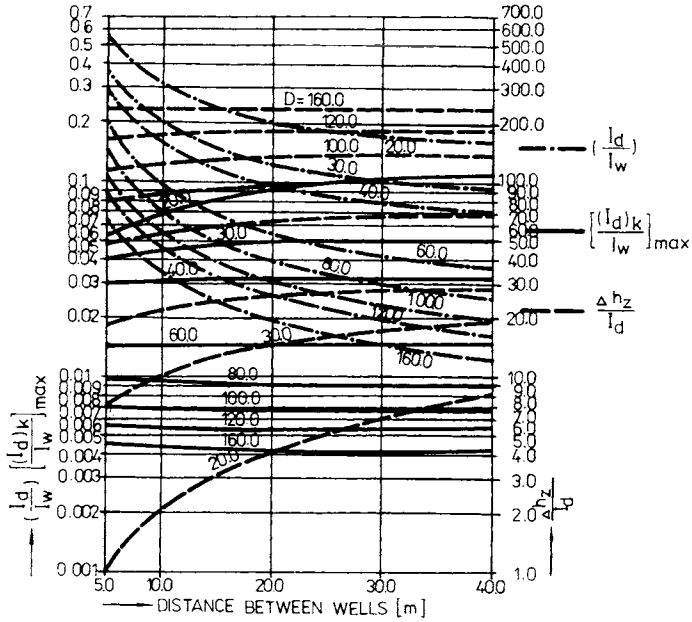

Fig. 6.34. Graph for active protection calculation.

Substituting

$$\frac{I_k b_h}{\Delta h_k} = g_r$$

we obtain

$$I_k = g_r \frac{\Delta h_k}{b_h}. \tag{6.93}$$

From the diagrams (Figs. 6.32 and 6.33), we can read off the value g_r corresponding to the relations $3D$: b_k and B_k : $3D$ or to the relation b_k : $3D$.

If *relief wells* are used on the downstream side with inflow into the seepage ditch (channel), then pressure gradients $(I_d)_k$ which determine the maximum rate of

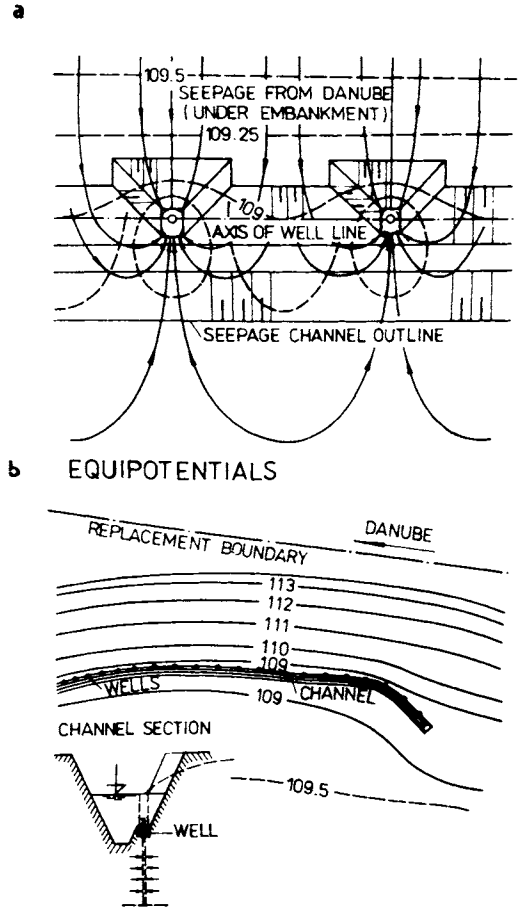

Fig. 6.35. Water flow and piezometric heights on the levée near Kosihy. a — flow lines, b — equipotentials (reduced scale) after Bartolčič (1968).

water inflow into the channel centrally between the wells and the mean value of the outlet gradient on the well casing along its height I_w can be obtained.

The parameter which should be determined is as follows

$$(I_d)_k : I_{w\,max}, \tag{6.94}$$

and in accordance with Fig. 6.34

$$\Delta h_z : I_d. \tag{6.95}$$

The solution of the flow-net and piezometric heights obtained by electrical analogy, showing the influence of the relief wells on the seepage pattern, are in Fig. 6.35.

6.7.2 The Use of Classical Stability Criteria

Observation of the states of flow and disturbance of stability of earths in levées sub-bases based on heterogeneous alluvial deposits having a permeability coefficient in the horizontal direction (k_h) considerably exceeding that in the vertical direction (k_v), has shown that we are very deficient in the design and judging of the passive protection elements, according to classical methods. It is not possible to use methods often used in the past, proceeding from the assumption (Table 6.5) of the *creep ratio* (CR) *after Bligh*, or of the critical gradients determined *after Lane*. Although the values of *their coefficients* (C_B and C_L) have been observed in natural conditions and enlarged by the safety factor (the recommended values are 1.2—3 times the observed values), the required seepage paths are short for the horizontal protective elements (blankets). In Table 6.5, we show the values after Bligh, $C_B = 4$ up to 18 (minimum 4), for boulder gravels and sands, and the value 18 for very fine sands and silts. After Lane, the values are $C_L = 1.6$—8.5 (for hard clays up to fine sands and silts). If we use these values, we get the allowable gradient of pressure $I = 0.1$—0.6 or $I = 0.05$—0.25. At the same time, in these values, the different influences of the flow velocity of water on the stability of coarse and fine soils are also included. Only thus is it possible to explain the fact that in gravels considerably greater pressure gradients are allowable than in sands.

Laboratory experiments and observations carried out on the Danube levées within the last decade have shown that in the above values several influences have not been taken into account, but which influence the stability of the sub-base. In particular, these are the depth of the threatened unstable stratum in which "piping" arises; the form and size of the grains; the contact of soils of different grain size (of different permeability) and thereby also of different resistance of the individual strata which have an influence on the gradient I given by the relation

$$I = \frac{H}{L} \quad \text{or} \quad I \doteq \frac{1}{C}, \quad \frac{L}{C} = H. \tag{6.96a}$$

It is more correct to take into account the differentiated resistances in the individual lengths (l) — in the different depths z_1, z_2 ... z_n.

If we introduce the relations

$$\frac{l_1}{C_1}+\frac{l_2}{C_2}+\frac{l_3}{C_3}+\ldots+\frac{l_n}{C_n}=H, \tag{6.96b}$$

$$l_1+l_2+l_3+\ldots+l_n=L,$$

we can obtain the correct calculation of the protection of the sub-base by a method similar to the known *method of Chugaev* (1965). Using values obtained by laboratory research and observation in natural conditions, we get the differentiated values of the coefficient $C=C_k$ for the *disturbed soils in the depth* z_{cr} under the foundation line as they are given in Table 6.5. By comparing the values C_L, C_B and C_k for small depths of stratum disturbed by filtration ($z_{cr} \leqq 3H$), we find that in laboratory tests, in the disturbance values of gradients and critical velocities were considerably smaller (C_k considerably greater) than Lane found in the observation of water flow in the sub-base of dams.

For completeness, we can state that in the experiments, the soils disturbed by filtration consisted of fine, coarse sands, gravels and gravel sands, with porosity $n=n_{cr}$. The conditions under which the values of the critical path were observed by Bligh and Lane for determining C_B, C_L are given currently in the literature (Davis 1952, Mallet and Pacquant 1951, Sherard et al. 1963).

In the observation of the *allowable gradients*, one can also use to advantage various Soviet methods, the best known of which are those of Istomina (1957), Lubochkov (1962), Bochever (1966), or the method of Zamarin et al. (1952). Information about older methods used in West Europe and the USA can be found in the monograph of Davidenkoff (1964). Many of these methods are based on the application of Prášil's method of a hydrodynamic network perfected by Khosla (1936) and Leliavsky (1957). Very often they also proceed from the revised method of Terzaghi (1948) who deduces the seepage force from the hydraulic gradient (I), unit weight of the water and its volume. In a homogeneous soil, the current flow of water is uniformly divided over the whole volume (column) of earth (with the depth D). For vertical flow, the following applies

$$\frac{\Delta h \gamma_w}{D}=I\gamma_w.$$

In Chapters 1 and 2, we often mentioned the application of this relation suitably adapted (eqn. 1.35). It is a relation most frequently used in engineering routine — especially in the case of the vertical flow of water and the equilibrium of forces in the vertical plane. From the derivation, it follows that in the original arrangement, it is a question of a relation applicable for laminar flow in which the kinetic energy of the watercourse is neglected, energy which cannot be neglected in the soil failures, as already proved in Chapter 1 (Section 1.9).

In practice, it is possible to use Terzaghi's equations after adequate expansion. The empirical relations and coefficients after Bligh or Lane can only be used for guidance. Since the method of judging, which uses the method of critical path — "the creep ratio", or *weighted creep ratio* — this is very simple, judging is very common. Up to the present, there is much controversy (Leliavsky 1957) as regards how to introduce the vertical path (s) and the horizontal length (l) of the seepage path into the magnitude of the total (computational) length L. In practice, the relative length $\lambda = s : l = 1 : 3.5$ up to $1 : 1.2$ or $1 : 1$ is considered equivalent. In reality, however, this relation may be $1 : 100$ up to $1 : 2$, according to the heterogeneity in natural conditions and other factors which, in levées, are often influenced by filtration disturbances (soil failures).

6.7.3 Dynamics of the Upstream Motion of Particles, attendant Phenomena and Levée-Subsoil Stability

Soil particles washed away from the subsoil by upstream water flow are also lifted by it. The *basic equilibrium* formula takes into account the lifted weight ($W' = G - U$) and hydrodynamic water pressure $F_w = (\pi/4)\, C_D \varrho_w\, (v^2/2)\, d_s^2$. This can be written as

$$\frac{\pi}{6} d_s^3 (\varrho_s - \varrho_w) = \frac{\pi}{8} C_D \varrho_w v^2 d_s^2. \tag{6.97}$$

Provided that velocity v is increasing above the equilibrium velocity, the grain will be carried out from the boil opening; in the case where it is reducing, the rise of the grain will cease in accordance with the principles given in Chapter 1 (Section 1.9, eqns. 1.37—1.43).

The exact expression of this state (taking into account the motion and acceleration of the particle) is more complicated. Considering particle acceleration, the following equation is valid

$$\frac{1}{6} \varrho_s \pi d_s^3 \frac{\mathrm{d}\bar{v}_s}{\mathrm{d}t} = \frac{1}{6} \pi d_s^3 g (\varrho_s - \varrho_w) - 2 C_D \pi \varrho_w d_s^2 |v_s|^2 \frac{\bar{v}_s}{|v_s|} -$$

$$- \frac{1}{6} \pi d_s^3 \,\mathbf{grad}\, p - \frac{1}{6} m_w \varrho_w \pi d_s^3 \frac{\mathrm{d}\bar{w}}{\mathrm{d}t}. \tag{6.98}$$

The left side of eqn. (6.98) represents the acceleration of the particle, the first member on the right side expresses the lifted weight of the particle, the second member represents the resistance of the medium to motion, the third member represents the pressure gradient and the fourth member represents the acceleration related to water — m_w denoting the virtual mass of water ($m_w = 0.5$ in the case of ideal fluid).

The difference between the velocity of water (w) and that of solid particles (v_s) depends on this mass and on the porosity number, given by the relation

$$\frac{e}{1-e}=\frac{3}{4}\left(\frac{v_s}{v_s-w}\right)^3. \tag{6.99}$$

This difference determines the fluctuating velocity component (v') and dispersed part of energy. Approximate relations

$$\frac{1}{2}\varrho_w v'^2=\frac{1}{2}\varrho_w(v_s-w)^2, \tag{6.100}$$

$$\varepsilon_1\cong\frac{(\bar{v}^2)^{3/2}}{d_s} \tag{6.101}$$

can be used for calculations.

Pulsation as an accompanying phenomenon of boils depends on the square of velocity fluctuation components, and thus

$$[v'_x-u'_x]^2. \tag{6.102}$$

The *dynamics of boils* are manifested not only by pressure pulsation but also by "explosions" which are associated with the action of air expelled from the pores of the soil. Air bubles with sand particles are encountered in the case of boils and pipings close to levées *during flood periods* in some river valleys (the Danube, Mississippi). These phenomena have been investigated by many scientists, for instance, Terzaghi (1948), Middlebrooks (1953), Leva et al. (1956), who have been studying them in association with soil instability and fluidized bed problems.

Seepage water pressure (P) and flow rate (Q) are the main characteristics providing information (Fig. 6.36) about changes and subsoil stability. If the dependence $P=f(Q)$ is linear (Fig. 6.36a) the soil is not disturbed (stable). If the seepage water penetrates into the pore channels closed by small pressures, these channels will be open at a pressure of ΔP_t, and the rate will increase from a value of Q_e to Q_{mf} without damaging the soil structure.

If rate Q is increased to a limit proportional to the pressure gradient (ΔP depending on the soil density), the flow rate and volume of porous media considered will also increase. Some of the particles move and by this movement part of the pressure ($\Delta P_s-\Delta P_t$) will be employed to overcome the friction between the particles. The remainder will be employed to transport water. At this moment (Fig. 6.36b), the expansion of the layer considered begins. This is the start of fluidization or liquefaction. These two phenomena — the first known to chemical engineering and the second to civil (hydraulic) engineering — have the same physical and chemical basis.

The basis of the *piping phenomenon* is a bit different: there is usually no volume increase. The change occurs in the pore channels only when fine particles are carried away. After that, the pressure increases to a value of P_c. At this point, the

pressure (P) is temporarily reduced, but nevertheless the flow rate increases (Fig. 6.36c). Now, the tortuosity of the pore channels decreases; their axes are more and more linear and the flow resistance decreases. This is a state of the internal damage of soil which causes an increased flow rate in the pores (Q_p). In the neighbouring soil, a linear conditioned seepage process can take place. Thus two or three flow regimes exist, changeable in time and space, evidenced by the appearance of pressure pulsation (Fig. 6.36d). These pressure pulsations and flow-rate changes manifested in the case of water and sand erruptions are symptomatic for soil deformations and for instability of territory near levées threatened by piping phenomena and hydraulic fracturing during a flood. It is typical that the unit flow rate, in such a region showing seepage deformation, is always higher than that in regions where the soil remains undisturbed.

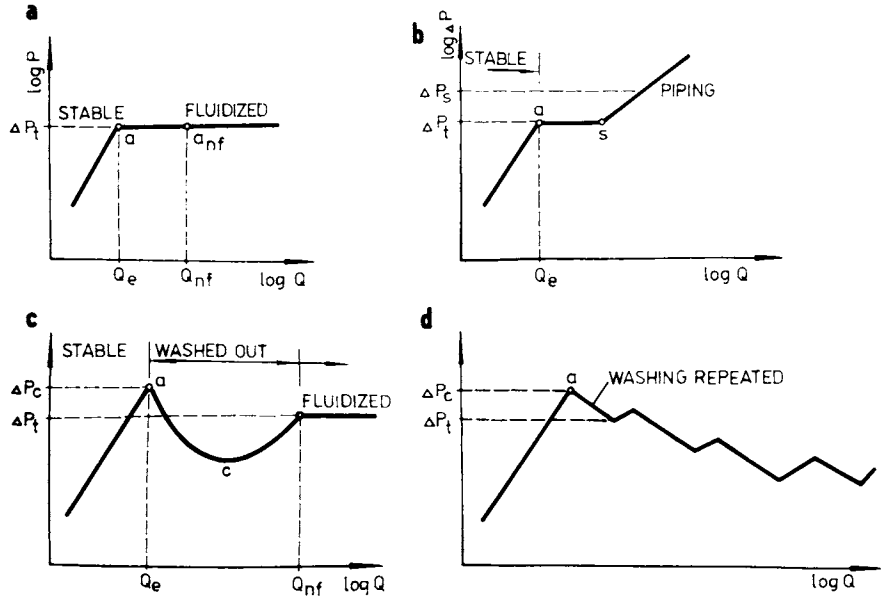

Fig. 6.36. Relationship between pressures (P) and rate of seepage Q log $P=f(\log Q)$ for stable and unstable soil deformations. a — stable and fluidized bed, b — transient phase from stable soil to piping damage, c — continuous damaging of the soil, d — damaging and washing repeated after Leva et al. (1956).

According to Leva et al. (1956), the decisive feature of the *soil instability* (porous media) is in the limiting seepage of *fluidization* expressed by his equation

$$Q_{mf}=0.005g\,\frac{\varrho_w}{\eta}\,(\varrho_s-\varrho_w)\,\Phi_s^2\,\frac{n_{mf}^3}{(1-n_{mf})}\,d_s^2. \tag{6.103}$$

This equation can be compared with eqn. (1.36b) derived for the incipient velocity in Chapter 1 (Section 1.9), by the help of the Kozeny—Carman equation. Leva denotes by n_{mf} such a minimum porosity which is the condition for the fluidization process, Φ_s is the shape factor; d_s the mean diameter derived from the grain-size distribution curve for grain groups ($\bar{d}_1$, $\bar{d}_2$, $\bar{d}_3$ ... $\bar{d}_n$) in the leg x if

$$d_s = \frac{1}{\Sigma x}(\bar{d}_1 x_1 + \bar{d}_2 x_2 + \bar{d}_3 x_3 + \ldots + \bar{d}_n x_n).$$

The remaining symbols are as before. The expression

$$\Phi_s^2 \frac{n_{mf}^3}{1 - n_{mf}} = \Phi_F^* \tag{6.104}$$

represents a fluidization factor whose values are given in Table 6.6.

Table 6.6. Values of the fluidization factor Φ_F^* (after Leva et al. 1956)

Sand description	Φ_F^* (for grain size d_s)[mm]	
	0.05 to 0.25	0.25 to 0.50
Uniform, well graded	0.23—0.10	0.10—0.08
Crushed	0.18—0.12	0.12—0.07

Substituting in average values of the most common sandy soils, a limiting unit flow rate can be calculated by means of the formula

$$q'_{mf} = 1.58 \times 10^{-4} \frac{d_s^{1.82}}{\gamma_s^{0.88}} \left(\frac{\gamma_s - \gamma_w}{\gamma_w}\right)^{0.94} \quad [\mathrm{l\,s^{-1}\,m^{-2}}]. \tag{6.105}$$

At a given seepage q, the case with which sand enters the fluidized state (state of liquefaction) is proportional to the weight of grains; it is to the size of diameter d_s. A sandy layer can pass into the liquified state at a unit flow rate of $q = 0.01\ \mathrm{l\,s^{-1}\,m^{-2}}$. This flow rate is observed in the Danube valley for instance, during fairly large floods over a distance of several kilometers between the towns of Šamorín and Štúrovo in Czechoslovakia.

6.8 Stability of Soil and its Resistance Characteristics

6.8.1 Resistance Constant K and Drag Coefficient C_D

Equation (6.103) derived from Leva represents the similarity and set up of the equations we introduced in Chapter 1 (eqns. 1.35—1.39 or 2.26—2.28), in which the resistances given by the structure of the porous media by the form of the porous

canals (α_s^2) and by the form of the grains (after Kozeny—Carman K_{KC}) by the value of the product $\alpha_s^2 K_{KC} \cong 200$ were taken into account. In the relations we derived there the influence of the porosity is evaluated, while in Leva there is more emphasis on evaluation of the influence of the grain shape.

The *influence of grain shape* [indicated after the original symbolization (Peter 1972b) by the symbol S_T], pore shape (α_s), tortuosity of porous canals (T_k) and other structural characteristics is more marked when we use eqn. (1.43) of Chapter 1 to express the characteristic of the modified Euler's number Eu used and the *global characteristic* of the quadratic resistances K_2^* in the relation

$$2\mathrm{Eu}\,\frac{R_H}{lT_k} = K_2^* \tag{6.106}$$

adapted for the equilibrium conditions for the moment of failure in which we find the hydraulic gradient I_{ro}. Using the relations for the hydraulic radius R_H — given in Chapter 2 — we obtain the equation* for expressing the value of the global resistance K_2^* — respecting grain characteristic (d_s) and pores opening (n_{eff}), its surface (a) and tortuosity (T_k)

$$K_2^* \cong g\,\frac{n_{eff}^3}{(1-n)}\,\frac{d_s}{T_k}\,\frac{I_{ro}}{q^{*2}}\,. \tag{6.107}$$

The values of the structural characteristics of resistances conditioning the *magnitude of resistances* of the flow and the conditions of stability are given in Table 6.7. From this it follows that rounded grains resist water least. By further analysis, we observe that a porous medium created by the freely inserted rounded grains is least stable. From this, it also follows that the drain on the downstream base of the dam found in old canals and levées, contributes not only to the mechanical stability of the levée body, but also to the hydraulic resistance of the toe of the embankment (earthfill) which is hydrodynamically under most load, as follows from Fig. 2.5 and from eqns. (2.79)—(2.90). Crushed materials proved good for securing the stability of the terrain along the levées.

If we consider the pressure on the individual rounded grains (with shape factor Φ_s) exposed to flowing water, as we see in more detail, we find that the magnitude

Table 6.7. Values of head (H) necessary for deformation of the soil strata

Path located	Through the contact (1)	Through the sand (2)	Contact (3)	Through the gravel (4)
Value of H	28—64%	100%	57—78%	8—23%

* Modifying the eqn. for pressure drop $\frac{\Delta p}{l}$ and $gI_{ro}\,\frac{n_{eff}^3}{T_k(1-n)}\,\frac{d_s}{q^{*2}a} = f_2\left(\frac{\mathrm{Re_M}}{2}\right)$.

of the pressure on one grain $F_{w,1}$ can be expressed in terms of quadratic resistances by the equation

$$F_{w,1} = C_{D,1} \Phi_s \frac{\gamma_w v^2}{2g} \frac{\pi}{4} d_s^2. \tag{6.108}$$

In the *transition region*, for movement of water of length l, a part pressure Δp is necessary. This expresses the pressure gradient which, in this region (Re = 3—300), can be determined approximately by means of the relation

$$\frac{\Delta p}{l} = \frac{C_{D,1}}{n^z} \Phi_s \frac{\gamma_w}{2g} \frac{v^{1.25}}{d_s^{1.25}}$$

If we replace this equation by the expression (eqn. 1.39) for the *incipient velocity* (v_0), we can write the equation

$$\frac{n^{4.5}(1-n)}{C_{D,1}} \frac{\gamma_s - \gamma_w}{0.1\gamma_w} = \frac{v_0^{1.5}}{d_s^{1.25}} = \frac{\gamma_s - \gamma_w}{f_0^*}, \tag{6.110}$$

$$\frac{n^{4.5}(1-n)}{C_{D,1}} \frac{1}{0.1\gamma_w} = \frac{1}{f_0^*}.$$

Since the *drag coefficient* $C_{D,1}$ depends on the shape of the grains, the friction coefficient is derived from the Reynolds number and from the porosity, and thus the *modified friction coefficient* f_0^* is dependent on these structural characteristics of the soil. To particular pair of values Re and n, there corresponds a particular point on the curve $f_0^* = f(\mathrm{Re}, n)$ for a constant shape factor. If we consider the value $\gamma_s - \gamma_w$ (given by Archimedes principle) as constant, then we can easily express the left-hand side of eqn. (6.110). To this dependence, we add the ratio $v_0^{1.5} : d^{1.25}$ determining the equilibrium (the incipient) velocities for the different grain sizes d. On the logarithmic graph, the relation between the resistances and the above equilibrium ratio represents a straight-line dependence.

By joining two such graphs for which the values are common $(\gamma_s - \gamma_w) : f_0^*$ (on the same scale), we obtain the resultant graph (Fig. 6.37) from which, after some adjustments, it is possible to determine the incipient velocity v_0 for the given flow conditions — determined by the pressure gradients, grain size (d) and soil porosity (n).

The difference between the simple relations derived in Chapter 1 (eqns. 1.36—1.40) is that the earlier relations have a validity in the laminar region (Re = 0.5—3) whereas relation (eqn. 6.110) applies to the transition region. With them it is possible to judge the stability of the uniform coarse sands and eventually of the gravels, if in their case liquefaction can occur, the origin of which is set at the value of the incipient velocity v_0, as stated in Section 1.9.

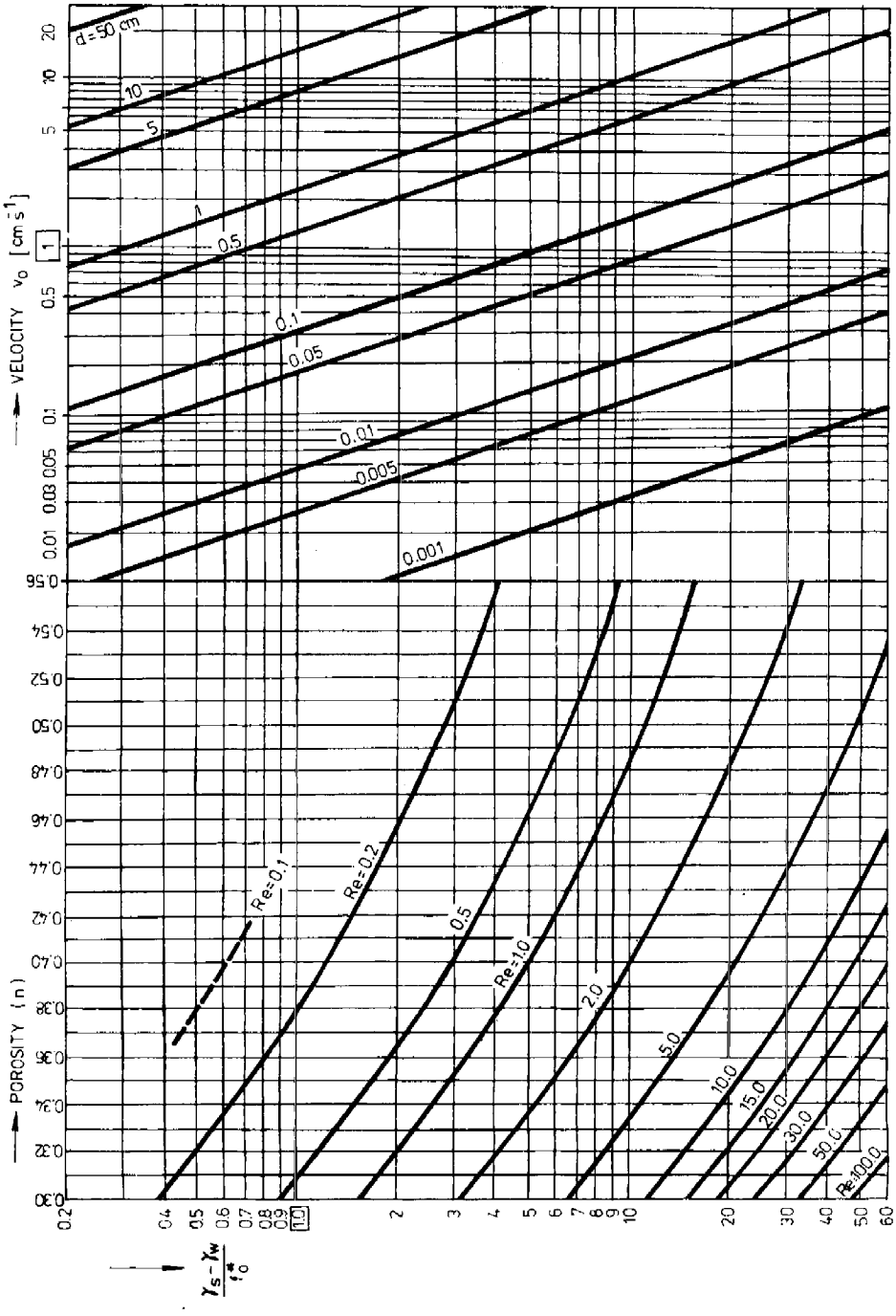

Fig. 6.37. Graph for determining the incipient velocity (v_0).

6.8.2 Reynolds Number (Re) and Archimedean Number (Ar)

In agreement with the research of the stability of cohesionless soils, proceeding from the knowledge stated in Section 1.9 and broadened with some theoretical aspects elaborated by Richardson (1957), we can use the specially adapted two-parameter structural equations (eqns. 2.36, 2.37) given in Chapter 2 for the creeping (fluidization) movement characterized by *Reynolds number* Re_{mf}. When we assumed this number to be equal to the value of Reynolds number in Stokes' (settling velocity) movement, where $v_{mf} = v_s$ and $\mathrm{Re}_{mf} = \mathrm{Re}_s$, the equilibrium equation for vertical flow may be written thus

$$\mathrm{Ar} = \frac{g}{\nu^2}\frac{\varrho_s - \varrho_w}{\varrho_w} d^3 = \alpha_s^2 K_1 \mathrm{Re}_s \frac{1-n}{n^3} + c^2 K_2 \mathrm{Re}_s^{\xi_1} \frac{(1-n)^{\xi_2}}{n^3}. \qquad (6.111)$$

According to previous explanations, on the right-hand side, we substitute

$$\mathrm{Re}_s = \frac{\mathrm{d}v_s}{\nu}, \quad \alpha_s^2 K_1 = (5.5\text{—}6.4)^2 \times (5\text{—}6) = 150 \text{ to } 246, \qquad (6.112)$$

$$c^2 K_2 = 1.75 \text{ to } 3.0, \quad \xi_1 = 1.4 \text{ to } 2, \quad \xi_2 = 0.1\text{—}0.5.$$

If we want to examine the influence of the velocity of water in the soil and the influence of porosity upon the stability of earth also expressed by the ratio of the "fall" (settling) velocity (v_s) and fluidization velocity at the onset of *liquefaction*, it is suitable to introduce certain associated characteristics supplemented by absolute values for the coefficients characterizing the flow resistances. By introducing Reynolds number for the fluidization velocity Re_{mf}, it is possible to obtain the equation

$$\mathrm{Ar} = \frac{g}{\nu^2}\frac{\varrho_s - \varrho_w}{\varrho_w} d^3 = 180\, \mathrm{Re}_{mf} \frac{1-n}{n^3} + 2.9\, \mathrm{Re}_{mf}^{1.9} \frac{(1-n)^{0.1}}{n^3}. \qquad (6.113)$$

In a detailed investigation, it would be desirable to examine the losses of the pressure $\Delta p/l$ for the laminar region and for the quadratic region of flow. In the laminar region, it is possible to write

$$\left(\frac{\Delta p}{l}\right)_1 = C_1 \frac{9}{4} \frac{(1-n)^2}{n^3} \eta_w \frac{v}{d^2}. \qquad (6.114)$$

In the turbulent region it will be

$$\left(\frac{\Delta p}{l}\right)_2 = C_2 \frac{3}{2} \frac{1-n}{n^3} \varrho_w \frac{v^2}{d}. \qquad (6.115)$$

6.8.3 Dimensionless Characteristics

To generalize our knowledge, it is suitable, in judging stability, to investigate the dimensionless characteristics which are introduced into the computation. Usually we have twelve soil and water characteristics, from which it is possible to arrange the following function

$$\mathrm{f}\left\{\left(\frac{g(\varrho_s-\varrho_w)}{18\eta_w v}\,d^2\right),\left(\frac{\varrho_w v d}{\eta_w}\right),\left(\frac{n}{n_{min}}\right),\left(\frac{d}{d_c}\right),\left(\frac{l}{d}\right),\left(\frac{P_c}{P}\right),\left(\frac{d_v}{D}\right)\right\}. \quad (6.116)$$

In real conditions in the sub-base and the body of levées and canal embankments, the separate members of our function have the following values

$$\frac{g(\varrho_s-\varrho_w)}{18\eta_w v}\,d^2=\frac{v_s}{v}=G_s\cong 0.1 \text{ to } 10{,}000 \text{ gravity parameter} \quad (6.117)$$

$\frac{\varrho_w v d}{\eta_w}=0.2$ to 200 — Reynolds number,

$\frac{n}{n_{min}}=\varepsilon_n=1$ to 2 — soil loosening, (6.118)

$\frac{d}{d_c}=\delta_s=1$ to 100 — heterogeneity parameter, (6.119)

$\frac{d_v}{D}=1\times10^5$ to 1×10^8 — ratio of gravitation and water diffusion,

$\frac{l}{d}$ — relative path of failure,

$\frac{P_c}{P}=1:1$ to 100 — relative pressure (capillary potential to water potential)

but also

$$\frac{P_c}{P}=0.$$

If we compare the values of the given dimensionless characteristics, we find that the *first four characteristics* and the relative pressure will *influence stability most.* Besides this, the relative path of failure will apply. As regards the relative path of failure, it is only possible to say that the most dangerous are seen to be the unstable strata near the surface of the ground. The damage found at depths $z\cong 3H$ (in the threefold part of the water height) are not at all dangerous.

The diffusion movement in general does not influence the stability of the soils during the seepage. Still smaller is the influence of the Van der Waals forces which

we never take into account. The inertial forces (F_i) have a special position: they are sometimes taken into account in the ratio to the gravity forces

$$\frac{F_i}{F_g} = \frac{2}{gd}\left(\frac{v}{n}\right)^2 .$$

At other times, we introduce them with the inverted value of the parameter $\varkappa_F$ into eqn. (1.43). The value of this parameter may be determined informatively by means of Table 1.8. To this value it is further possible to add that $\varkappa_F$ does not become interesting until the damage has developed ($v \geqq 5 \times 10^{-3}$ m s^{-1}).

If we were to analyse the stability conditions further, we would find that porosity enters the computation with the highest exponent and for this reason in the stability and gravitation parameters, it plays the highest role in the hydrodynamic load of the sub-base — at a certain water flow velocity of the water.

6.8.4 Total Pressure P_t

If we assume laminar flow, the force acting on the individual grains is given by the relation

$$F_l = 3\pi\eta_w \, dv.$$

Equilibrium with rounded grains of diameter d occurs if

$$\frac{1}{6}\pi d^3 g(\varrho_s - \varrho_w) = 3\pi\eta_w v d. \tag{6.120}$$

This means that the so-called Stokes' force produce on the grains a pressure P. If the grains are laid in a stratum of earth with porosity n, then stability may be secured, when the total pressure $P_t > P_s$ can be resisted. Computing all these pressures, we obtain the following equations (for rounded grains)

$$P_t = K_{KC}\frac{36(1-n)^2}{n^3 d^2}\eta_w v \frac{\pi d^3}{6(1-n)} = K_{KC}\frac{1-n}{n^3} 6\pi\eta_w v d. \tag{6.121}$$

When we substitute into eqn. (6.121) the expression for force F_l, then we can write for the *total pressure* P_t the expression

$$P_t = 2K_{KC}\frac{1-n}{n^3} F_l = 2K_{KC}\frac{1-n}{n^3} P_s. \tag{6.122}$$

Further, we substitute in the given relations average values of Kozeny—Carman constants (for simplicity, we usually use $K_{KC} = 5$) and values of average porosity (n) of the soil, in which we assume different sizes of rounded grains and therefore also different Archimedean number (Ar) in eqn. (6.111) or (6.114). If we further take into account the critical relations for the individual flow regions, then — as it is known from the fluidization technique (Aérov and Todes 1968) and arranged in

Table 6.8 — we can compute the ratio of the setting velocity (v_s) to the *minimal fluidization velocity* (v_f), Fig. 6.38. From the technical point of view, we can identify v_f with the velocity v_0 — at the onset of liquefaction (at the beginning of the expansion and disturbance of the sandy layer). This phenomenon has already been explained in Section 1.9.

Table 6.8. Values of porosity n_{mf} at the onset of fluidization of sands

Sand description	Grain diameter [mm]		
	0.06 to 0.25	0.25 to 0.50	0.50 to 2.00
From river deposit $C_u = 5—15$	45—42%	42—40%	40—38%
Alluvial sand, uniform	52—45%	45—42%	42—39%
Crushed granite	60—51%	51—45%	45—42%

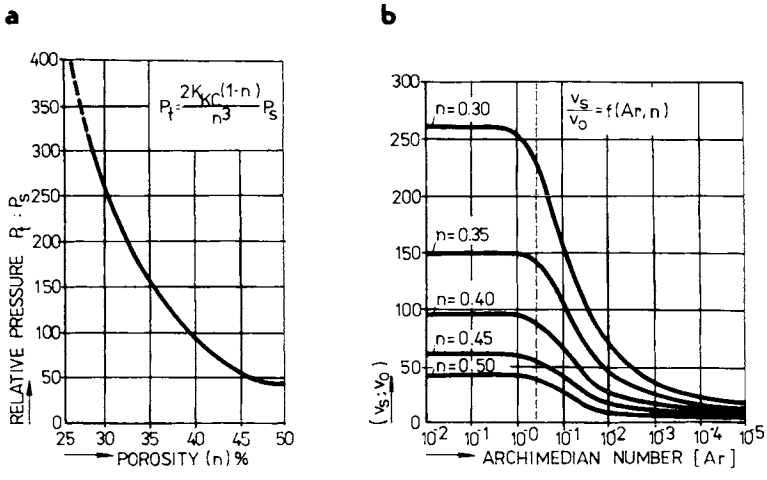

Fig. 6.38. Dependence of relative pressures $P_t : P_s$ and relative velocities $v_s : v_0$ on the porosity (n) of sands. a — pressures, b — velocities.

We get the graph illustrated in Fig. 6.38a showing the relationship $P_c : P_s = f(n)$. By a graphical elaboration of the values we obtain by using eqn. (6.114) with regard to the dependences between the Archimedean number and the Reynolds number, we get the graph illustrated in Fig. 6.38b.

If we now compare the values given in Chapter 1 (Table 1.7) for fine sands ($Ar < 1$) damaged in laminar flow, we get approximately equal values $v_s : v_0$ ($\cong 150$ for $n = 35\%$). This agreement confirms the fact that both the theories advanced by us are correct. For the case of sands, we may use both processes of stability computation indicated. The conditions of stability are closely connected with the

changeable (accidental) conditions of water flow, which is in turn considerably conditioned by the grain distribution (by microscopic conditions, also including porosity) and by the distribution of the individual strata of earth (in the macro level). Thus in the last three decades, methods of judging in which the conditions of movement of water and particles are taken as stochastic phenomena have been developed. Theories of this kind, elaborated as principles long ago (Scheidegger 1960), currently meet with difficulties connected with fundamental shortcomings of a statistical material which does not allow all the characteristics of soils and water movement, to be determined with sufficient reliability. Such determination is necessary for reliable elaboration of the computing programme by means of probability methods (Bear 1978).

6.8.5 Microscopic Level of Transport Phenomena

Let us consider pore interiors when water passes through them with increased velocity. To do so, let us focus our attention on a capillary tube with a diameter D_p and on small sphere with diameter d_s which represents a grain of the soil (Fig. 6.39). In the pore leg considered, the following forces are in action

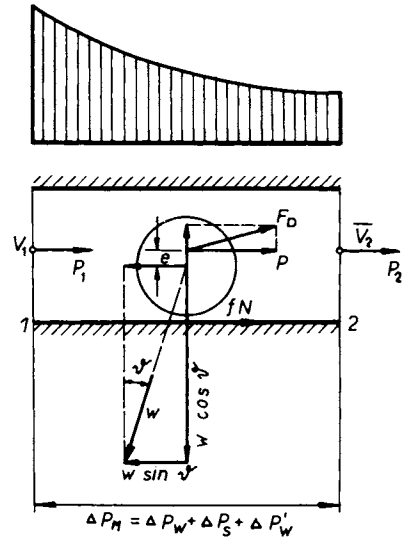

Fig. 6.39. Forces and pressures acting on a sphere.

$$W' = \frac{\pi}{6} d_s^3(\varrho_s - \varrho_w)$$ raised weight of the particle,

$$W \sin \vartheta = P + fN$$
$$W \cos \vartheta = L + N$$ weight components,

$$Pe = \frac{d_s}{2} fN \qquad \text{rotating moment,}$$

$$L = C_L S_s \frac{\varrho_w v^2}{2} \qquad \text{lifting force,}$$

$$F'_D = C_D S_s \frac{\varrho_w v^2}{2} \qquad \text{drag force,} \qquad (6.123a)$$

$$F_D = \sqrt{P^2 + L^2} \cong (\Delta P_s) \frac{\pi}{4} D_r^2 \qquad \text{resulting drag force.} \qquad (6.123b)$$

Here f is the friction coefficient; e distance of the force F_D from the centre of gravity of the sphere; P_s pressure required for traction of the grain determined by pressure drop P_M in the length of the leg considered (Δl); P_w pressure for the water movement; P'_w pressure required for the change in water flow caused by the presence of the sphere. Denoting the initial pressure P_1 and the final pressure P_2, we obtain

$$P_M = P_1 - P_2,$$

$$P_s = P_M - (P_w - P'_w). \qquad (6.124)$$

Assuming that the slope angle of the channel is ϑ, it can be proved that at the equilibrium pressure which leads to the equation

$$\tan \vartheta \geqq \left| \frac{f(d_s + 2e)}{2e} \right|, \qquad (6.125)$$

the sphere will rotate about its own axis without lateral shift unless pressure P is changed. If the pressure increases, the ball sphere moves ahead, if the pressure is reduced the ball sphere drops.

Drag (P) and *lifting force* (L) should satisfy the conditioned equation which gives the relation between drag (C_D) and lift (C_L) coefficients

$$\frac{P}{L} = \frac{C_D}{C_L} = \frac{G \sin \vartheta - fN}{G \cos \vartheta - N}. \qquad (6.126)$$

In the limiting position,

$$F_D = G \sin \vartheta_0 = P \qquad (\text{increasing } \vartheta \to N = 0),$$

$$\frac{C_D}{C_L} \leqq \tan \vartheta \qquad (\text{the grain is lifted}).$$

If $\vartheta < \vartheta_0$, then

$$f = \frac{W \sin \vartheta - C_D S_s \frac{\varrho_w v^2}{2}}{W \cos \vartheta - C_L S_s \frac{\varrho_w v^2}{2}}. \qquad (6.127)$$

The values of coefficients C_D and C_L depend on the Reynolc' number (Re), grain diameter (d_s) and pore diameter (D_p). It can be written

$$C_D = f_1\left(\mathrm{Re}, \frac{d_s}{D_p}\right) \cong \mathrm{f(Re)}, \tag{6.128a}$$

$$C_L = f_2\left(\mathrm{Re}, \frac{d_s}{D_p}\right). \tag{6.128b}$$

The real values of these coefficients were investigated in a hydraulics laboratory, at first for the case of the pipe hydraulics, and in the last thirty years more work was done on the aspects of field and theoretical conditions. Many investigators (e.g. Garde 1969) present the values found in width limits under various conditions. To engineering practice, the values of Kruyer, who studied the conditions of drag forces at a ratio $d_s : D_p = 0.79$ and obtained $C_D = 0.5—50$ at $C_L = 1/2\ C_D$, are of interest.

For stability, the calculation concept should be noted. The motion of grains in a pore channel influences many other forces; for instance, that of mutual attraction, Brown effect, etc., which can usually be disregarded in the field. The inertial forces and *total energy* (E) of motion expressed by equation

$$E = E_1 + E_2 = m\pi^2 N^2 \left[\frac{7}{10}(D_p^2 + d_s^2) - D_p d_s\right], \tag{6.129}$$

and given by translation motion (E_1) and rotation (E_2) in turbulent flow with frequency N, can seldom be ignored.

6.9 Filtration Deformations and their Origin

6.9.1 Theoretical Aspects and Laboratory Experiments

If we follow the physical conditions and the process of the origin of filtration deformation as an manifestation of instability, we see that these are in general more complicated than they appeared in the diagram in Fig. 6.39. *Heterogeneous earths* (Fig. 6.40-1a) by filtration deformations are primarily affected. Here the contact between the gravels and sands are usually disturbed first. These do not resist the water flow that is much faster than it is tolerable for sands (Fig. 6.40-1b). By washing away of the grains at the contact, the soil strength here is decreased and its deformation properties are changed. There occurs a gradual deformation not only of a hydraulic type and also usually a physical type (Fig. 6.40-2), mainly on the contact of different soils (Fig. 6.40-2a—f).

As already stated in Chapters 1 and 2, in fine sands the filtration deformations are connected with a volume change (Fig. 6.41). This change is expressed by the values of porosity n and e.

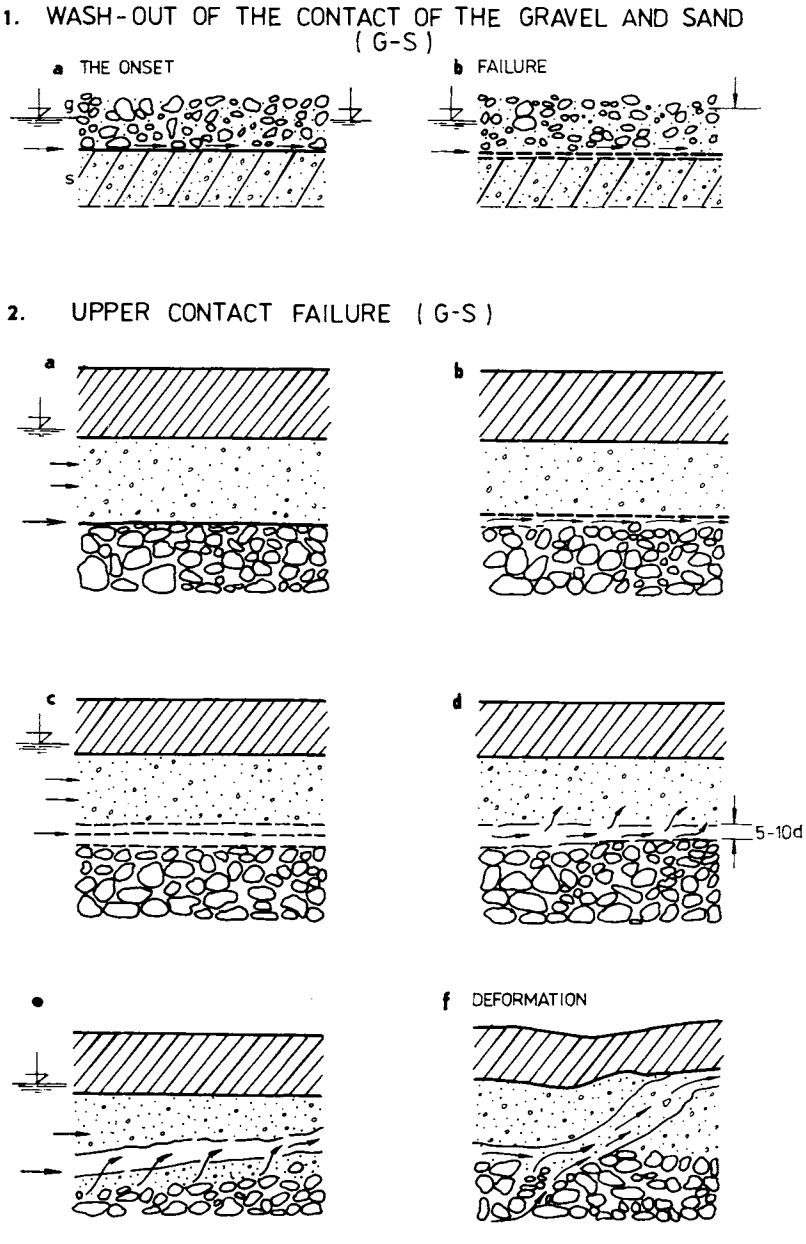

Fig. 6.40. Process of damage of the cohesionsless earth on the contact. Ia — contact gravel—sand, 1b — failure on the contact, 2a — three layer contacts, 2b — privileged path on the contact, 2c — wash-out of the contact, 2d — damage process, 2e — channeling of the sand layer, 2f — disturbance of the gravel-sand layer and deformation of the upper (loam) layer.

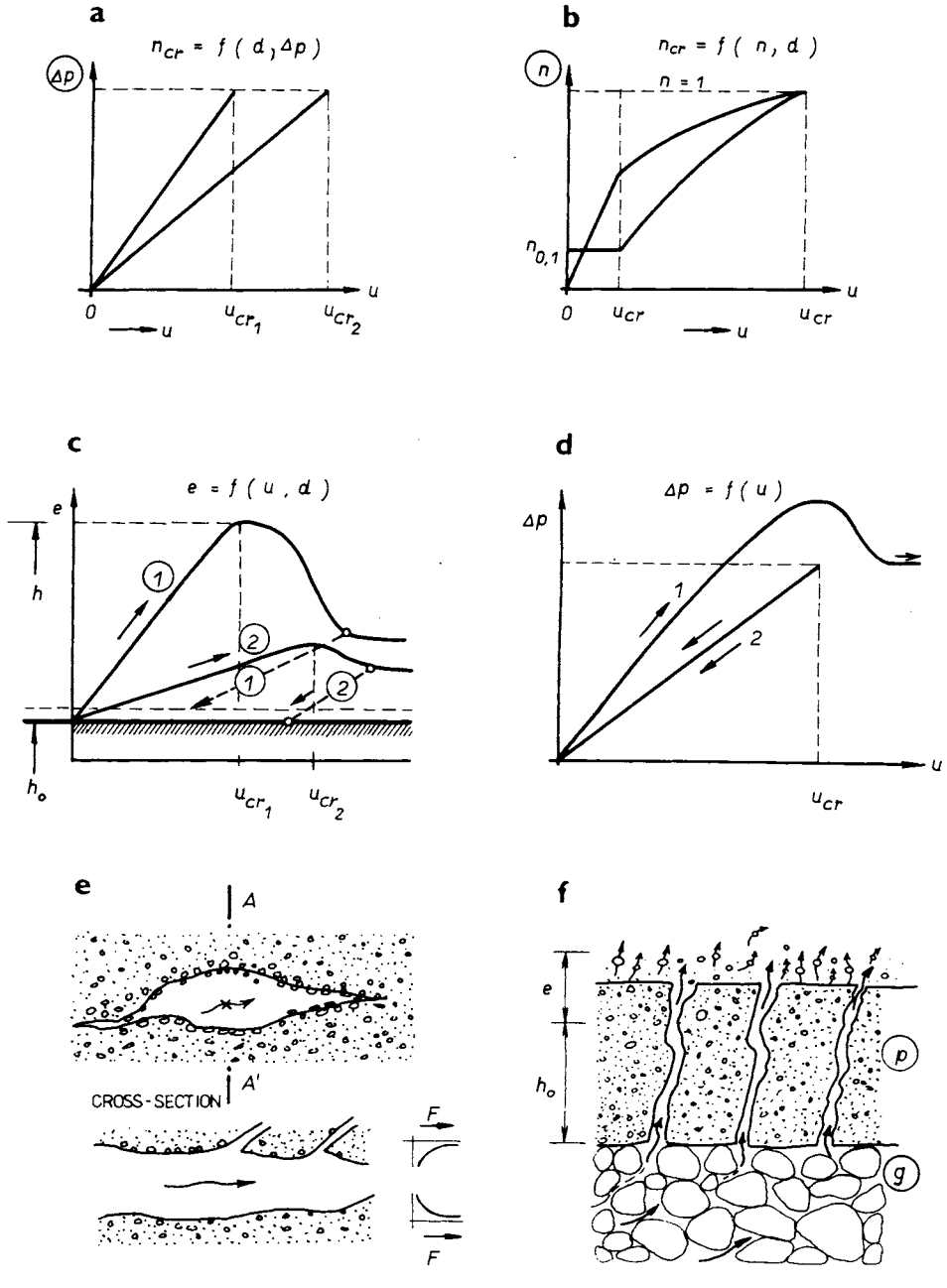

Fig. 6.41. Changes in the pressures and changes in the volume of sands in the critical regions (a—d), e, f — cavity and channeling of sand.

When we follow the development in the *disturbance* of soil and attendant *changes in the pressures and velocities* (Fig. 6.41a), we see that in the sands the velocities (u) increase proportionally with pressures (Δp). Darcy's assumptions are fulfilled. At the same time, it is characteristic that at a particular value of Δp, the change in the velocity is greater (u_{c2}) for a coarse-grained soil than for fine earth. Further it is characteristic that the given linear or quadratic relations apply only when the porosity does not change (Fig. 6.41b) $n_{0.1}$ = constant. In small grains (d = 0.01—0.2 mm) $\Delta p/n_0 = f(u)$ is valid. In coarse-grained sands and gravels will be applied: $\Delta p/h_0 = f(u^2)$. For an unloaded stratum of sands, it is characteristic that at a particular velocity the stratum begins to expand. Its thickness h_0 is increased by the value of the expansion e, whilst this one depends on the velocity and on the size of the grains: $e = f(u, d)$. This value is greater (1) in fine earths than in coarse-grained earths (2) (Fig. 6.41c). The expansion is a reversible process in most cases (Fig. 6.41d).

In some cases the soil cannot follow the pressures and velocity changes and there a tearing of the soil occurs with a decrease in the pressure. Here, we are talking of a phenomenon called also *hydraulic fracturing* in which a formation of fissures and later of cannals occurs (Fig. 6.41e, f). For *homogeneous sandy* strata approximately horizontal canals are characteristic. For thin strata of sand lying upon a stratum of gravel, vertical canals can be observed very often (Fig. 6.41f).

Part of the given phenomena belongs to the region of *fluidization*, which we have mentioned several times. If we take Reynolds number (Re) as a characteristic of the water flow and the characteristic of resistance against the washing out of particles in the vertical direction (v) the *Archimedean number* (Ar) (characteristic of the gravitation) remembering that this resistance changes with soil porosity (n) exponentially, then we can write a general relation between the given characteristics thus

$$K_F \, \mathrm{Re} = \mathrm{Ar}^y n^z. \tag{6.130}$$

Further, it is possible to introduce into eqn. (6.130) a modified factor of the fluid stratum ($f_{F,M}$) expressed by the relation

$$f_{F,M} = \frac{4gd(\varrho_s - \varrho_w)}{3\varrho_w v_f^2} n^z. \tag{6.131}$$

In the laminar region for rounded grains, we have

$$\frac{24}{\mathrm{Re}} = \frac{4gd(\varrho_s - \varrho_w)}{3\varrho_w v_f^2} n^z, \tag{6.132}$$

$$f_1\left(\mathrm{Re}, \frac{4gd(\varrho_s - \varrho_w)}{3\varrho_w v_f}, n^{z_1}\right) = 0. \tag{6.133}$$

In the turbulent region

$$\mathrm{Ar} = \frac{3}{4} C_{D,1} \, \mathrm{Re}^2,$$

$$f_2\left(\mathrm{Re}^2, \frac{4gd(\varrho_s-\varrho_w)}{3\varrho_w v_f^{\xi}}, n^{z_2}\right)=0. \tag{6.134}$$

The factor K_F (eqn. 6.130) has the value 12.5—14 and the exponent $z=3.5$—4.7 (5), as it follows from Table 6.9.

Table 6.9. Values of exponents ζ and z for various Re_ζ and Ar numbers

Region	Characteristic value		Exponents
I	$\mathrm{Re}_c < 0.2$	$18\,\mathrm{Re}_\zeta^{\zeta} = \mathrm{Ar}$	$\zeta = 1$; $z = 5$
II/1	$0.2 < \mathrm{Re}_c < 3$	$13.9\,\mathrm{Re}_\zeta = \mathrm{Ar}$	$\zeta = 1.0$ —1.4; $z = 4.5$
II/2	$3 < \mathrm{Re}_c < 20$	$14\,\mathrm{Re}_\zeta^{1.4} = \mathrm{Ar}$	$\zeta = 1.4$ —1.5; $z = 4.0$
II/3	$100 < \mathrm{Re}_c < 300$	$12.5\,\mathrm{Re}_\zeta^{\zeta} = \mathrm{Ar}$	$\zeta = 1.75$—1.9; $z = 3$
III	$\mathrm{Re}_c > 2000$	$0.6\,\mathrm{Re}_\zeta^{2} = \mathrm{Ar}$	$\zeta = 2$; $z = 2.5$

If we observe the expressions given (eqn. 6.130—6.134), we see that we can introduce into them the settling velocity, as it was done by Aérov and Todes (1968). Thus it is possible to obtain the relation $v_s = f(v_f, n)$ according to Fig. 6.42a, b, as well as further dependences between the expansion (e) and the velocity (v_f) and p (Fig. 6.42c, d).

The theoretical experimental relation

$$\mathrm{Ar}^y n^z = f(\mathrm{Re}) \tag{6.135}$$

illustrated in Fig. 6.42e, serves well for judging the dangers of disturbances in the fine soils (sands) and sandy gravels. It enables us to calculate more precisely just what technical action is necessary to secure the stability of the soils by compaction.

The given dependences (eqns. 6.111, 6.114 and 6.131—6.134) confirm the fact that by compaction of fine and medium-grain sands their stability is increased (their permeability is decreased) essentially more markedly than for gravels. To secure the stability of soils in the body and in the sub-base of levées, it is important to devote more attention especially to the compaction of sands.

As already mentioned, one of the most appropriate aids for judging the danger of the *filtration deformation* are the grain-size distribution curves. From the coefficient of uniformity of the soil (C_u) and the coefficient of curvature (C_c) as well as the so-called effective diameters d_{10} and d_{60} (Fig. 6.43) the danger can be determined. As regards the last two parameters we should often consider them to be markedly different in size from the value of effective diameter d_{eff} which is determined by means of eqn. (2.20) or (2.21)

$$d_{\mathrm{eff}} = \frac{2}{3}\frac{n_{\mathrm{eff}}}{1-n}\, d_s. \tag{6.136}$$

Alternatively we can deduce it from the hydraulic radium R_H (Fig. 6.43) which is

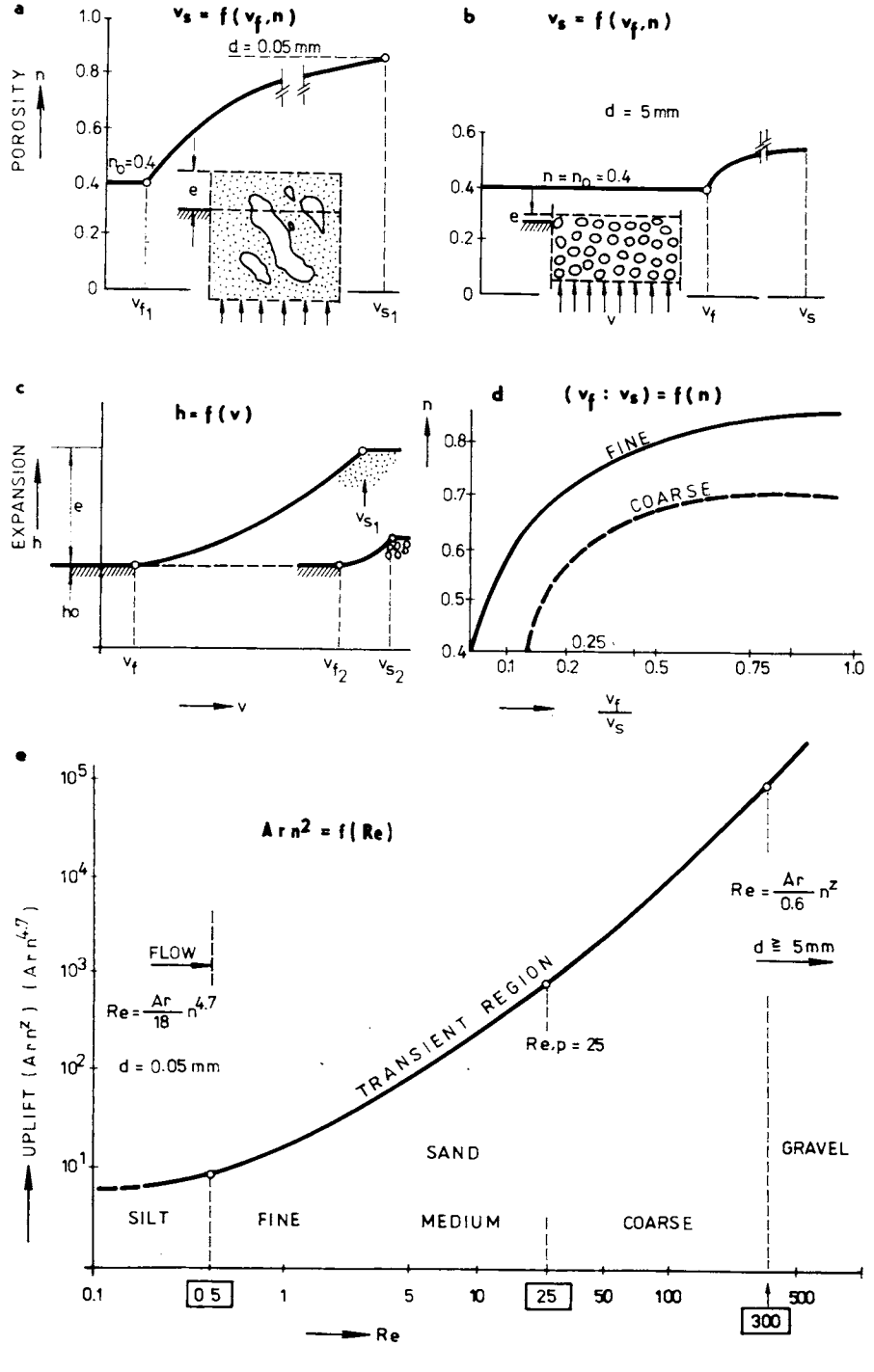
a
$v_s = f(v_f, n)$
d = 0.05 mm
POROSITY n
n_0=0.4
e
v_{f_1}
v_{s_1}
b
$v_s = f(v_f, n)$
d = 5 mm
$n = n_0 = 0.4$
e
v_f
v_s
v
c
h = f(v)
EXPANSION h
e
h_0
v_{s_1}
v_f
v_{f_2}
v_{s_2}
v
d
$(v_f : v_s) = f(n)$
n
FINE
COARSE
0.25
$\frac{v_f}{v_s}$
e
$Ar\,n^2 = f(Re)$
UPLIFT $(Ar\,n^z)$ $(Ar\,n^{4.7})$
FLOW
$Re = \frac{Ar}{18} n^{4.7}$
d = 0.05 mm
TRANSIENT REGION
Re,p = 25
$Re = \frac{Ar}{0.6} n^z$
d ≧ 5 mm
SILT
FINE
SAND
MEDIUM
COARSE
GRAVEL
0.5
25
300
Re

the only way when dealing with crushed material and flat grains which have a different *hydraulic radius* (Fig. 6.43a, b) in every plane and another value of effective diameter. In Fig. 6.43c, d these differences for a heterogeneous soil are evident.

It is not difficult to see that as regards stability, an *earth composition* is unfavourable, when the *particle size distribution* curve is not continuous. In the lower third a certain fraction is lacking. In the soils from the Danube and Jamuna valleys, it is ordinarily the fraction $d_c = 0.2—1.5$ mm. The ratio of diameter of the grain (d_c) which can be carried to diameter d_s varies widely; depending on the characteristic grain of the solid skeleton (d_s). It is often $d_s : d_c = 20—50$ (up to 100 and more).

Beside these "microscopic" indications, expressed by *heterogeneity* (δ_s) the filtration deformations have certain effects in the region of the mega scale, in actual terrain. Best known are the regions of the filtration deformation in the levées of the Mississippi valley in the USA, in the Danube valley, in the Jamuna valley in India, and near the river Niger in Africa. Here, however, the consequences of the unfavourable composition of the sub-base are not seen to be more marked, because there are no continuous levées.

Fig. 6.42. Consequences of sand expansion and relations between the characteristics of water flow (Re) and stability of earth (Ar, n); relationship between uplift (Ar) and Reynolds number (Re). a — fine expansion and its cavities, b — coarse sand (gravel) expansion and loosening, c — relationship expansion ($e \rightarrow h$) and velocities, d — dependence for relation of velocities v_f (in fluidization stage) to v_s (settling velocity) on the porosity (n) of fine and coarse sand, e — dependence of the uplift characteristic (Ar, n^z) on the critical Reynolds number (Re) for different soils (silt, sand and gravel).

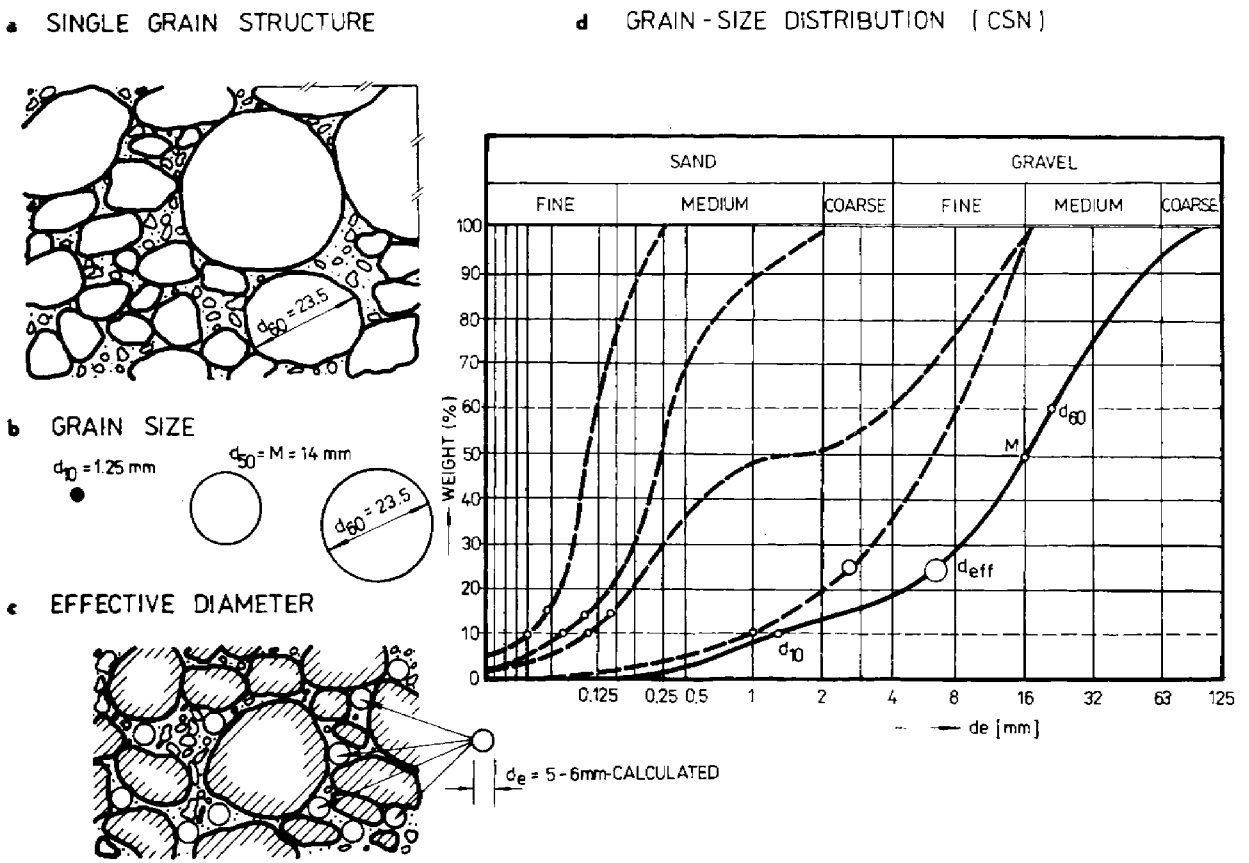

Fig. 6.43. Grain-size distribution. a — composition of grains, b — characteristic diameters d_{10}, d_{50}, d_{60}, c — effective diameter d_{eff}, d — indication of the characteristic diameters on the curve of grain-size distribution.

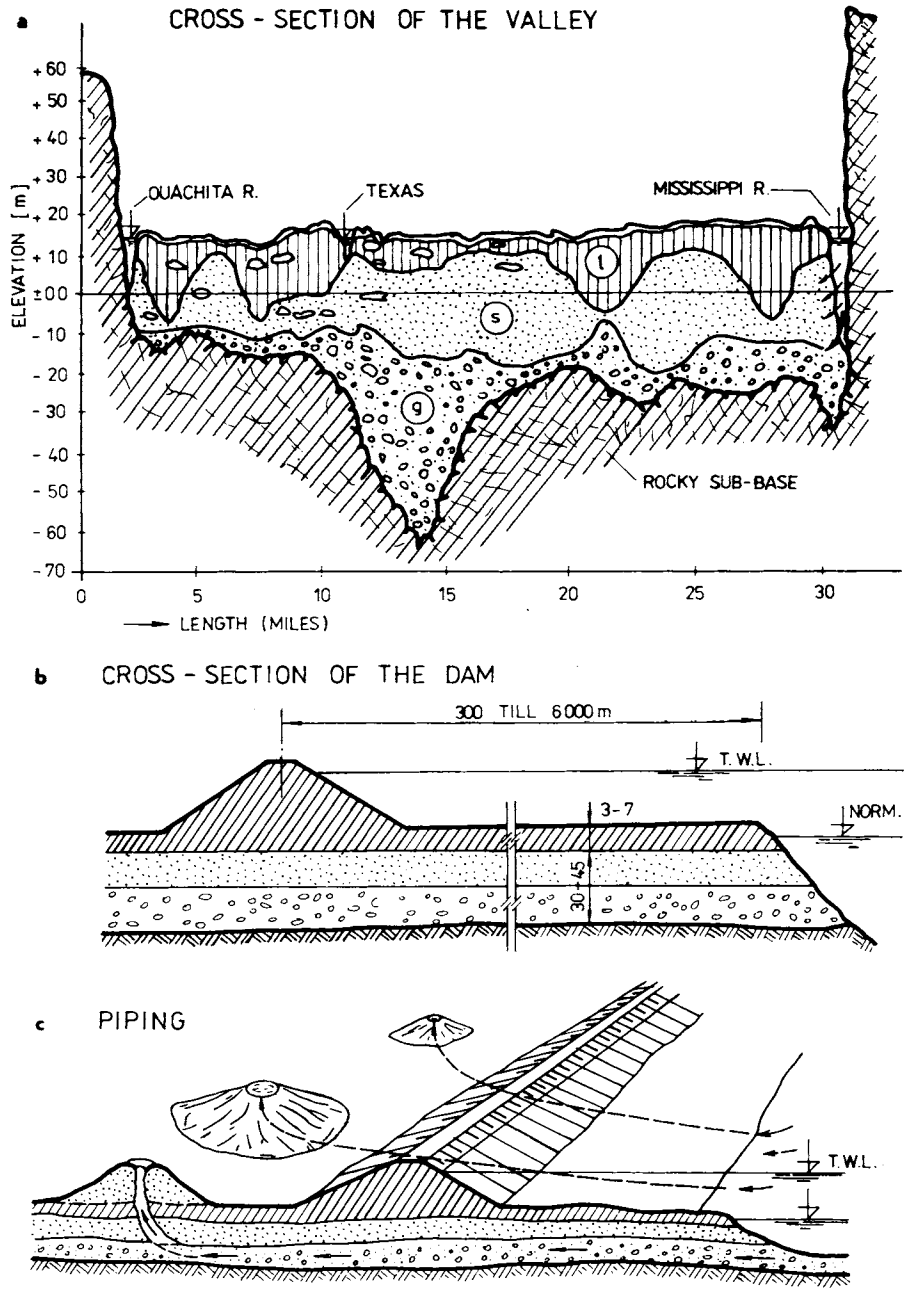

Fig. 6.44. Territory affected by filtration deformations in the Mississippi valley. a — geological profile of the territory with alluvial deposits, b — transverse section through the levée, c — distribution of soils and position of pipings.

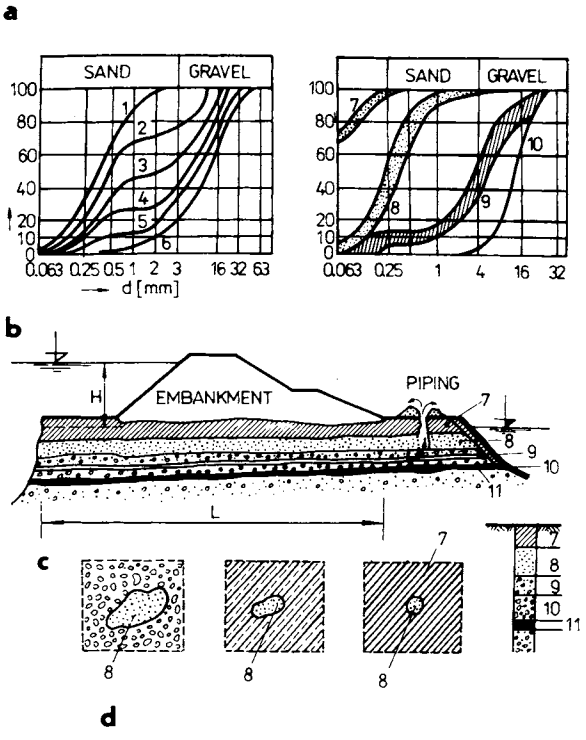

Fig. 6.45. Pipings near the Danube levées. a — grain-size distribution, b — embankment and lay-out of the layer, c — cross-section of the channel — in gravel, sand and loam layer — and exit of piping, d — piping in the nature (near the levée); 1—6 cohesionless soils, 7 — loam, 8 — sands transported by water, 9, 10 — damaged soils, 11 — clay layer.

6.9.2 Observations in the Field

In the Mississippi valley (Fig. 6.44) the well known *piping problem* has existed for the last 80 years (Harza 1935, Middlebrooks 1948, Matthes 1951, Turnbull and Mansur 1961). In the typical composition of alluvial deposits — rocky base covered with a layer of very permeable gravels ($k = 2 \times 10^{-4}$—4×10^{-3} m s^{-1}), less permeable sands and little permeable clays, there are the right conditions for fast penetration of the flood wave beneath the levées into the protected territory where the pipings arises (Fig. 6.44c). Sherard (Technical Memorandum USBR 1953) insists on the characteristic phenomenon of this deformation: "A concentrated leak occurring through and under the embankment."

The pipings in the Danube levées (Fig. 6.45) are connected with geological conditions (Fig. 6.46) similar to those of pipings near the Mississippi River, while in several places the sand is concentrated in the upper strata (damaged gravels and sands).

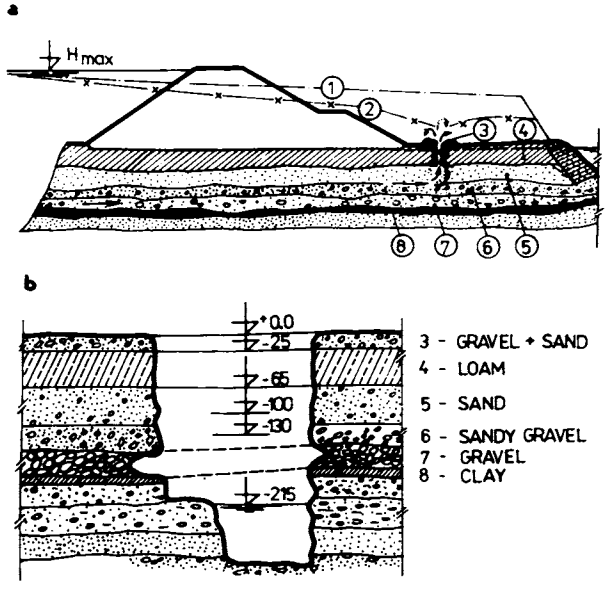

Fig. 6.46. Composition of soils influencing the occurrence of pipings near the Danube. a — piping and sand-boiling, b — lay-out of the layers; 1 — pressure (energy) line before piping occurrence, 2 — pressure line after piping occurrence, 3 — piping in the loam layer (4), 5—7 — damaged layers, 8 — clay layer.

The unfavourable fact consists in the *stratification* of Alluvium; under water bearing strata lies an impermeable stratum which contributes to the growth of the pressure gradient in the vertical direction. The unfavourable stability conditions also influence the unfavourable geological conditions along the river (Fig. 6.47), because the impermeable sub-base of the Neogene clays falls in the geological fractures near the village of Palkovičovo to great depths (300—400 m) and then rises again to the surface and thus narrow the flow profile of the groundwaters

moving along the Danube, up to a thousandth of the area which has a permeable sub-base in the 1820th river km.

In the narrowed profile — between the 1780th to 1790th river km during the great flood of 1965 as many as 100 pipings were found over the 1 km length of the levées.

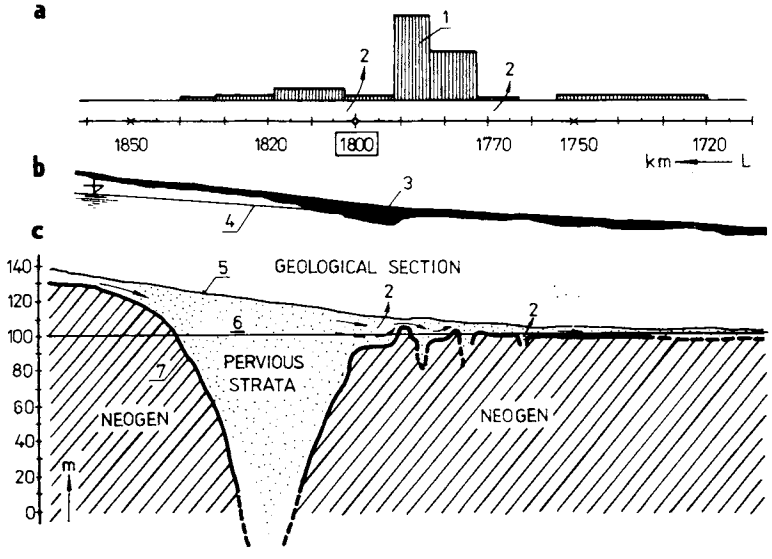

Fig. 6.47. Piping distribution and longitudinal geological profile of the Danube in the territory of Czechoslovakia. a — piping distribution along the river, b — thickness of the loam overburden, c — position of pervious strata; 1 — number of piping occurrence, 2 — location of dam failures, 3 — changeable overburden layer thickness, 4 — G.W.L., 5 — surface of the territory, 6 — alluvial (pervious) strata, 7 — Neogene clays.

Table 6.10. Orientation values of critical porosity n_{cr} = f(Re, Fr)

Value Fr	Critical porosity n_{cr} for Reynolds number of							
	0.2	1.0	2.0	10.0	20	50	80	100
0.01	0.65							
0.05		0.64						
0.10			0.62					
0.20				0.52				
0.50					0.50			
1.0						0.48	0.46	
2.0								0.45

We can state the filtration deformations are caused by *unfavourable field conditions* characterized by poor levée subsoil and river-bed subsoil which give rise to a *large water height* (H), increased *velocities* (u, v), *flow rate* (q) and *pressures* (p) within a short distance from the area threatened during the flood (Fig. 6.48).

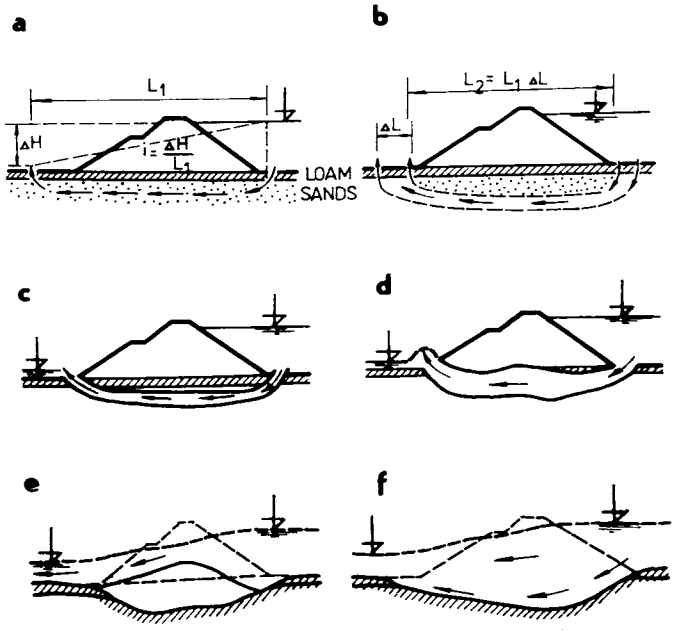

Fig. 6.48. Mean stages of the failure: seepage-channel and break. a — leakage through the subsoil sands, b — privileged path, c — channeling, d — channel grows, e — dam sinks, f — dam break.

The high porosity (n, n_{cr}), the unfavourable grain size distribution (C_u, C_c) and other factors mentioned above allow water inflow into the subsoil and underflow of the levée (first stage). In the second stage, the soil particles are washed away and transported from the upper side to the downstream toe. In the third stage, a continuous channel on the contact surface of loam and sands (or gravel) is formed. After that the channel grows in size and picks up the soil of the sub-base and of the levée body (fourth stage). In this way, the disaster stage becomes obvious. It begins in the sinking and its final stage is when the soil mass is carried away by water (Table 10).

This process of the evolution of *filtration damage* was observed in the laboratory (Fig. 6.49) and the contact failure was investigated in the field in the case of the earth cut in the Danube valley (Fig. 6.50).

The *soil failure* in the form of a channel has its origin near the downstream toe of the structure (Fig. 6.51) where the sand boils (1) first appear and then appear a regressive channeling with ejection shaft, transportation channel and evolution zone. The water stream also brings the water-soil mixture and transports it to the sand boil.

The patterns of the damage phenomena near the levée in the Mississippi valley, Jamuna valley (Fig. 6.52) and in the Danube valley are similar. The signs are heavy concentrated seepage flow which breaks through the impervious strata at the downstream toe of the embankment slope and a channel rapidly develops under

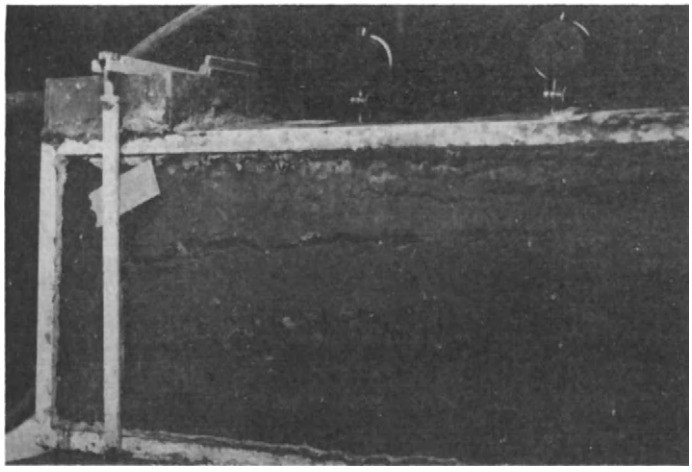

Fig. 6.49. Creation of a deformation of the soil model.

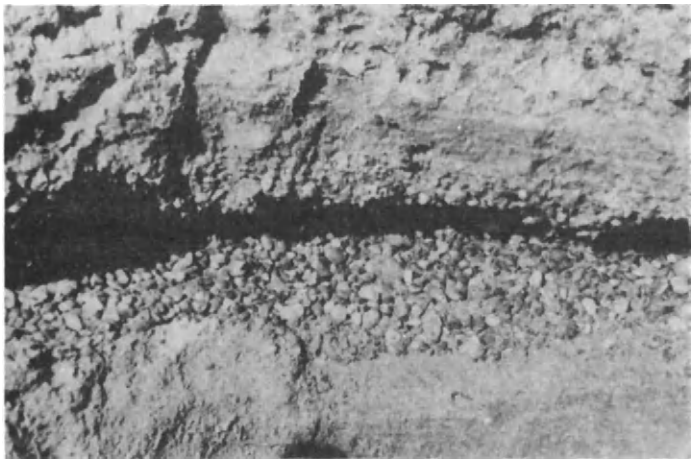

Fig. 6.50. Damage of sandy gravel in nature.

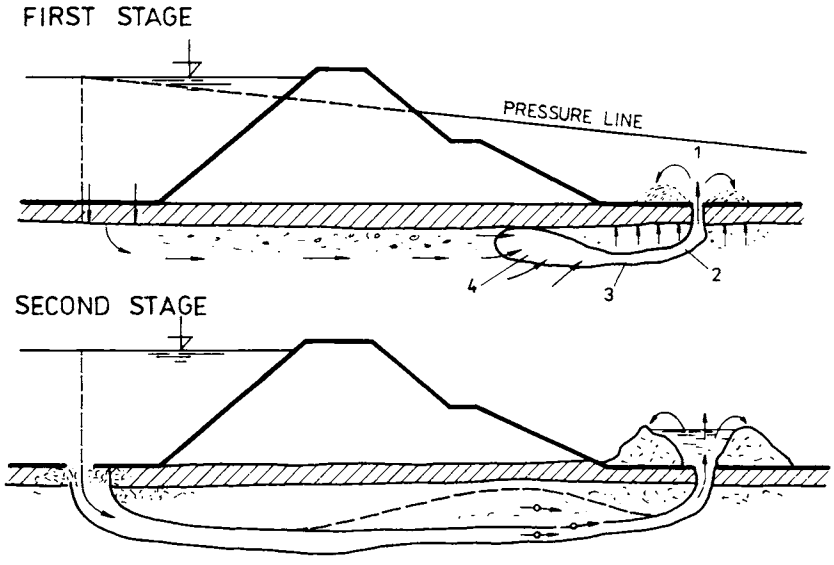

Fig. 6.51. Regressive channeling and boils near the levée toe. 1 — sand boil, 2, 3 — channel conduct, 4 — cavity.

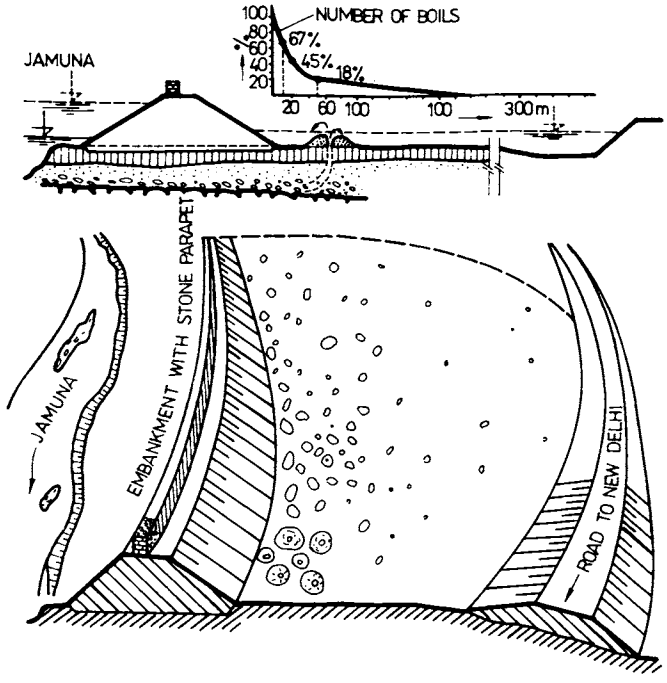

Fig. 6.52. Sand boils near the levée of the Jamuna river (India).

the embankment showing the stages mentioned above. *Boils* near the toe initially and overtopping of the structure finally are common characteristics of the *damage and disaster*. Middlebrooks (1948) divided the failure phenomena according to two forms of underseepage: underseepage in the form of large boils developing a pipe under the embankment, and underseepage in the form of pin boils destroying the stability of the toe and the slope stability. The instability of the slope is caused by loss in toe stability.

The root of the *instability problem* and mass energy transfer is the same in both cases. The source of failure is in the upper side of the embankment where the potential energy is accumulated, but the conditions of damage are created in the downstream toe and in the subsoil of the structure whose foundation makes channeling possible.

6.9.3 Underseepage and Boils Theory

Hydraulic analysis of piping phenomena (Fig. 6.53) leads to the conclusion that the mean attack of the water is concentrated at the toe. Creation of *channels* brings the action of the damage to the middle and then to the downstream toe. This

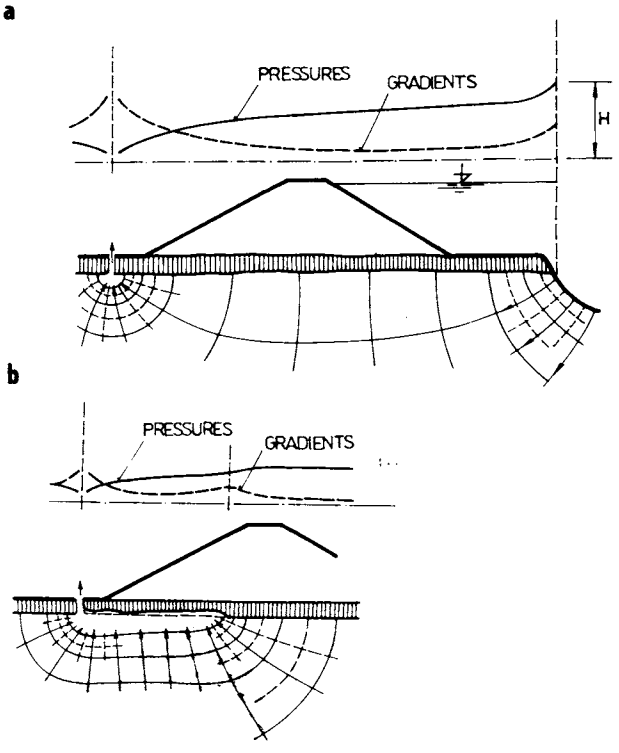

Fig. 6.53. Water pressure, gradients and flow net in the vicinity of the channel and the shaft. a — onset, b — progressive failure.

follows from the basic equations given in Chapter 1 and app ied by deduction of eqns. (6.16)—(6.21). By equating eqn. (6.21c) with Darcy's equation for the pressure gradient we can write

$$I_p = \frac{H\gamma_w}{\pi} \frac{1}{\sqrt{x^2 - b^2}} \quad \text{or} \quad I = \frac{h}{\pi} \frac{1}{\sqrt{x^2 - b_1^2}}. \tag{6.137}$$

Expressing the seepage force in the form

$$F_w = \gamma_w I V$$

for $V = 1$ (unit volume)
and using the value for gradient $I = I_{cr} = 1$, we get

$$1 = \frac{h}{\pi} \frac{1}{\sqrt{x^2 - b_1^2}}, \tag{6.138}$$

$$x^2 - b_1^2 = \left(\frac{h}{\pi}\right)^2, \quad x^2 - \left(\frac{h}{\pi}\right)^2 = b_1^2,$$

$$\frac{x^2}{b_1^2} - \frac{h^2}{b_1^2 \pi^2} = 1. \tag{6.139}$$

The gradients are divided according a hyperbolic law. The gradients (I) and velocities decrease with distance (d)

$$I = \mathrm{f}(d),$$

$$v = \mathrm{f}(d),$$

where $d = x - b_1$ is the difference between point x in consideration and the width of the footing bottom (b_1).

For the *seepage rate* of water flowing towards a circular boil opening, having radius r_0 at a distance r from the boil axis, determined by pressure gradient $\mathrm{d}h/\varrho_w \,\mathrm{d}r$, we can write

$$q = \pi r^2 k \frac{\mathrm{d}h}{\varrho_w \,\mathrm{d}r}. \tag{6.140}$$

Since height difference $\Delta h = h - h_1 \rightarrow h = p/\gamma_w$, we have

$$\int \mathrm{d}p = \frac{q\gamma_w}{\pi k} \int \frac{\mathrm{d}r}{r^2}$$

or

$$\int_{h_1}^{h} \mathrm{d}h = \frac{q}{\pi k} \int_{r_0}^{r} \frac{\mathrm{d}r}{r^2},$$

$$h = \frac{q}{\pi k} \left(\frac{1}{r_0} - \frac{1}{r}\right), \tag{6.141}$$

or the limit of the flow region $h \to h_0$ (by $r \to \infty$) will be

$$h_0 = \frac{q}{\pi k} \frac{1}{r_0}. \tag{6.142}$$

Using eqns. (6.131) and (6.132), we obtain

$$\frac{q}{\pi k} = \frac{h}{\frac{1}{r_0} - \frac{1}{r}} = h_0 r_0,$$

$$h = h_0 r_0 \left(\frac{1}{r_0} - \frac{1}{r}\right),$$

$$h = h_0 \left(1 - \frac{r_0}{r}\right). \tag{6.143}$$

Equating eqn. (6.142) with Darcy's equation, we obtain the *gradient* dependent on radii r_0 and r and water height (h_0); we thus obtain the following equations

$$q = kIS = kI\pi r^2,$$

$$I = \frac{q}{k\pi r^2},$$

$$I = \frac{h_0 r_0}{r^2} = \left(\frac{r_0}{r}\right)^2 \frac{h_0}{r_0}, \tag{6.144}$$

$$I = \mathrm{f}\left(\frac{r_0}{r}, \frac{h_0}{r_0}\right).$$

To be able to draw the *hyperbolic function*, we can introduce a parameter $f_1 = r_0/r$ and auxiliary ordinates

$$\begin{aligned} \bar{x} &= x \cos \alpha - y \sin \alpha, \\ \bar{y} &= x \cos \alpha + y \cos \alpha \end{aligned} \tag{6.145}$$

and thus we get from eqn. (6.143)

$$h = h_0(1 - f_1). \tag{6.146a}$$

For a special case: $\alpha = 45°$; $\cos 45° = \sin 45° = 1/\sqrt{2}$; $h_0 = 1$, we get

$$\frac{r_0}{r \frac{1}{\sqrt{2}} - f_1 \frac{1}{\sqrt{2}}} = r \frac{1}{\sqrt{2}} - f_1 \frac{1}{\sqrt{2}},$$

$$1 = \frac{r^2}{2r_0} - \frac{f_1^2}{2r_0}. \tag{6.147}$$

Equation (6.147) represents a hyperbola with axis of equal length by turning

through 45°. It is denoted $\eta = 2r_0/2r_0 = 1$. Introducing the symbol $f_2 = (1 - f_1)$ into eqn. (6.146), we get the pressure height at a distance r by a relation r_0/r, as

$$h = h_0 f_2. \tag{6.148}$$

If we introduce parameters $f_1^2 = f_3$ and $f_4 = h_0/r_0$, we are in the position to express the gradients in this way

$$I = f_3 f_4, \tag{6.149}$$

and to obtain the picture (Fig. 6.54) enabling us to determine the critical height h_0 and critical gradients I_{cr}. If we assume that $I_{cr} = 1$, from eqn. (6.144) it follows that

$$1 = \frac{h_0 r_0}{r^2}, \qquad r^2 = h_0 r_0. \tag{6.146b}$$

A large *boil opening* (r_0) due to a large water height (h_0) causes damage at a large distance. Through eqn. (6.143) we get the critical piezometric height

$$h_{cr} = h_0 \left(1 - \frac{r_0}{\sqrt{r_0 h_0}}\right) = h_0 - \sqrt{h_0 r_0}. \tag{6.150}$$

Using the conclusions of Havlíček (1966), we can deduce further theoretical relations for pressures P on the border of a boil, which passes through the top soil having a thickness h_p and permeability coefficient k_p at a large distance from the boil opening where $r = \infty$, $h = h_0$

$$P = h_p \gamma_w \left(1 + \frac{2kh_0}{r_0 k_p}\right). \tag{6.151}$$

If we put appropriate values into eqn. (6.142), we get the parameter of piezometric height at the border of the inflow zone h_0 and round the opening h_{01} by the use of the following equations

$$h_0 = \frac{r_0 I_p k_p}{2k} = \frac{r_0}{2}\frac{k_p}{k}\frac{\gamma'}{\gamma_w} \cong \frac{r_0}{2}\frac{k_p}{k}, \tag{6.152}$$

$$h_{01} = \frac{r_0 \gamma'}{2\gamma_w}. \tag{6.153}$$

Taking into consideration the case where $k_p \cong k$ and $\gamma' \cong \gamma_w$, we conclude that at the border of the zone, a smaller gradient is needed to cause damage as on the boil opening. In this limit zone the contact between sands and topsoil (loam, clay, for example) is under chief threat.

Besides this *contact path*, many other paths of damage are possible. A critical path was investigated in a multilayer soil system (Fig. 6.54e). The *layers of different permeability* and different flow resistances are: loam (L), sand (S) and gravel (G) and the paths pass through *sand* (1), the second (2) the *contact* between *sand* and *gravel*, the third (3) the *contact loam sand* and the fourth (4) was directed through the *gravel*. The heights H necessary to cause failure on the given path were evaluated in Table 6.7.

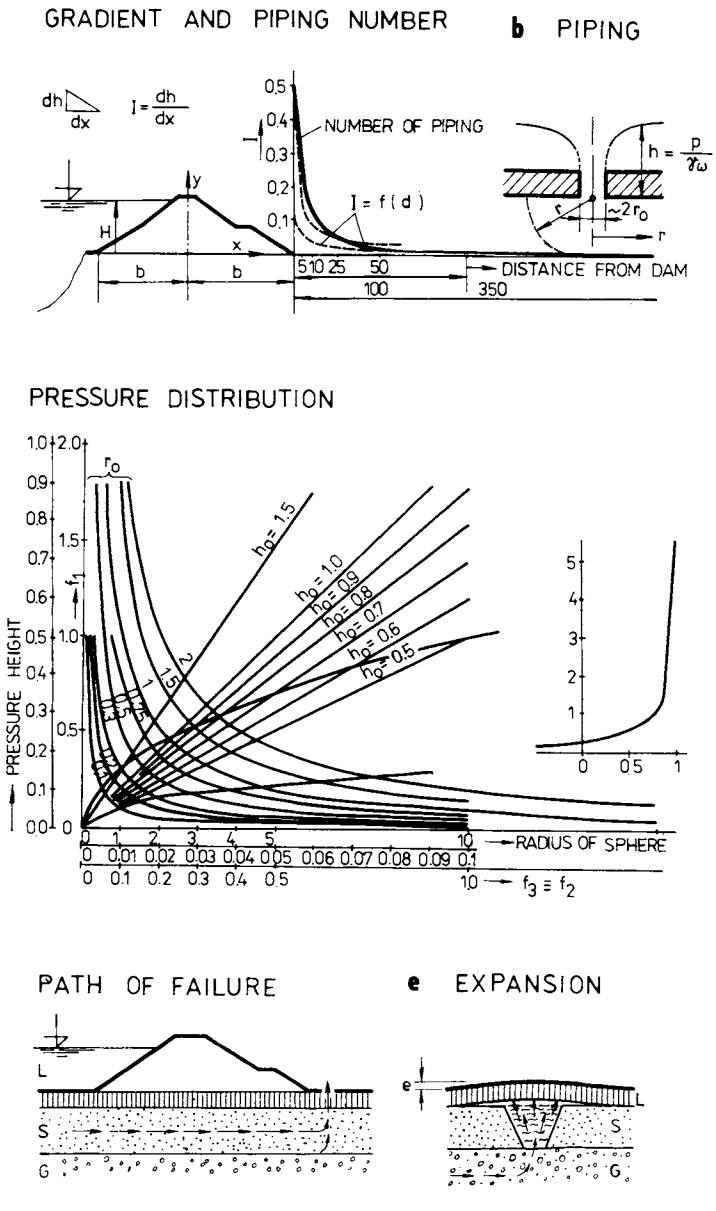

Fig. 6.54. Relationship of the height and boil diameter and critical path of failure. a, b — mean characteristics of the piping phenomenon (I — gradient, r_o — boil opening, $r(d)$ — distance from the boil axis, h_o, h — water height), c — dependence of piping characteristics on the pressure height, d — paths of failure in layered subsoil (L — loam, S — sand, G — gravel), e — expansion of sand layer and its consequence.

At first sight the small resistance of the gravel layer can be surprising. This layer was deepest, and the ground level and loam sand layer present (Fig. 6.54c, d) — two more resistant layers — remaining (L and S) intact. This can be explained by the fact that the resistance to flow of the gravel is small and thus the pressure height was remarkable in its tendency to strike the sand and loam by an upstream flow behind the downstream toe of the structure. In such cases expansion takes place. There is less tendency to liquefaction and the pressure is quite small. The *cavity between sand and loam layer* facilitates the ejection and transport of fines assumed in filtration deformations.

The flow rate is always greater in the gravel layer than in sand and so most damage is expected in the gravel.

By the *evolution of soil damage* in a heterogeneous soil profile, pressure migration takes place in the perpendicular direction (Fig. 6.55). To pass through the less permeable top layer (usually silty loam), an elevated pressure gradient (in relation to the sand and gravel layers) is needed. However, the flood-raised water level in front of the embankment assumes an elevated water pressure in the first, second and third stages of damage evolution. In stage (II) of perforation, the validity of Bernoulli's equation becomes evident. Energy turns into velocity and Newton's law governs the motion of water as well as that of solid particles carried away by the water stream.

Two phenomena, ignored by scientists investigating filtration deformations, may be mentioned in connection with the solution of this problem. It is the role of expansion which relieves the damaging process of the soil and that of air bubbles in the pores. In regions with filtration deformations in embankment subsoil, the expansion of sands and sandy layers may have a value of some centimeters, mainly if we are dealing with a special problem termed by Terzaghi *piping with heave.*

Air bubbles give warning of soil damage. If the seepage exceeds normal, bubbles are "incorporated" in the three-phase system: it blocks some pores. Two phases (solid particles and air) are stabil; only the water moves. In the initial stage of damage the situation changes, the air bubbles start to move with water and some instant later the solid particles move. The soil skeleton, consisting of solid particles, is broken and the three-phase system is unstable in part (by piping) or completely (by liquefaction).

Expansion is necessary for *liquefaction*, also facilitated by a great porosity. After Leva et al. (1956), a minimal porosity (n_{mf}) depending on grain size, grain shape and grain-size distribution is basic requirement for liquefaction (fluidization) and piping. Bearing values of the porosity n_{mf} are conditioned which facilitate the fluidization of sands (Table 6.8) if $n_{mf} = n_{cr}$.

The investigations in the field show that sand grains have a spherical shape in regions of damage. They are always rounded and smooth and they are coated by a thin film of clay suspension, which forms its surface. It is slippery and does mot influence the cohesion. Such coated grains are easy moved and can be washed

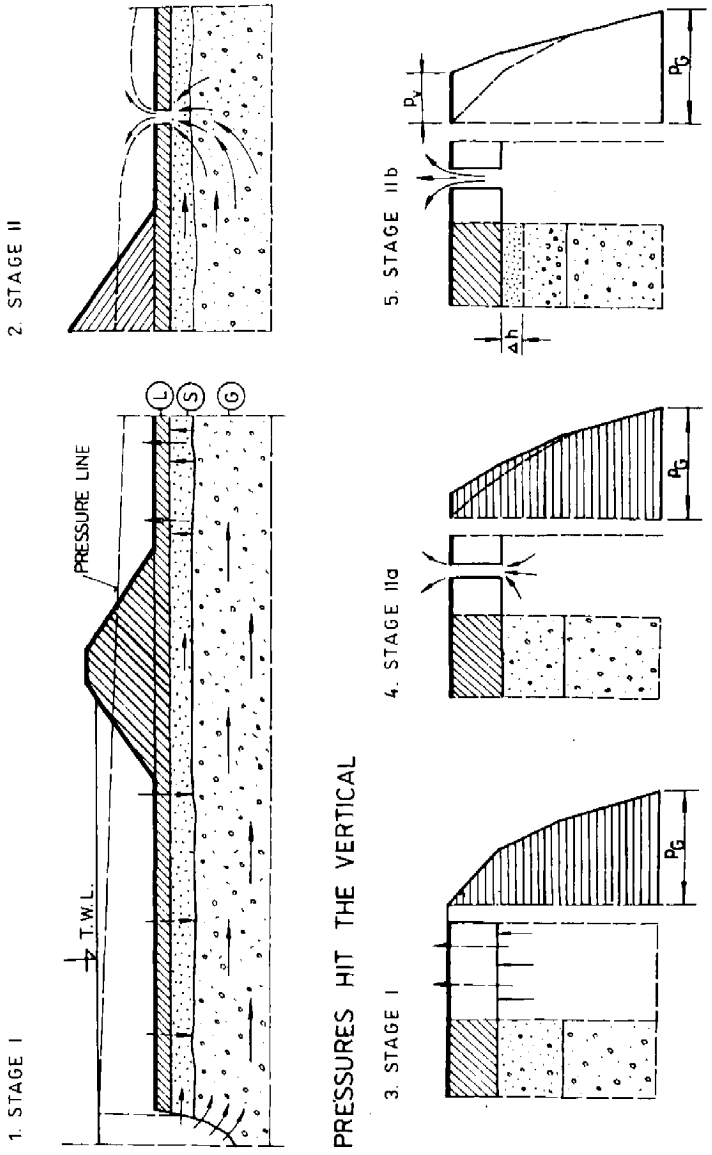

Fig. 6.55. Change of the pressure line and pressure distribution under failure conditions. a — the beginning of the failure, b — continuous damaging of the layers.

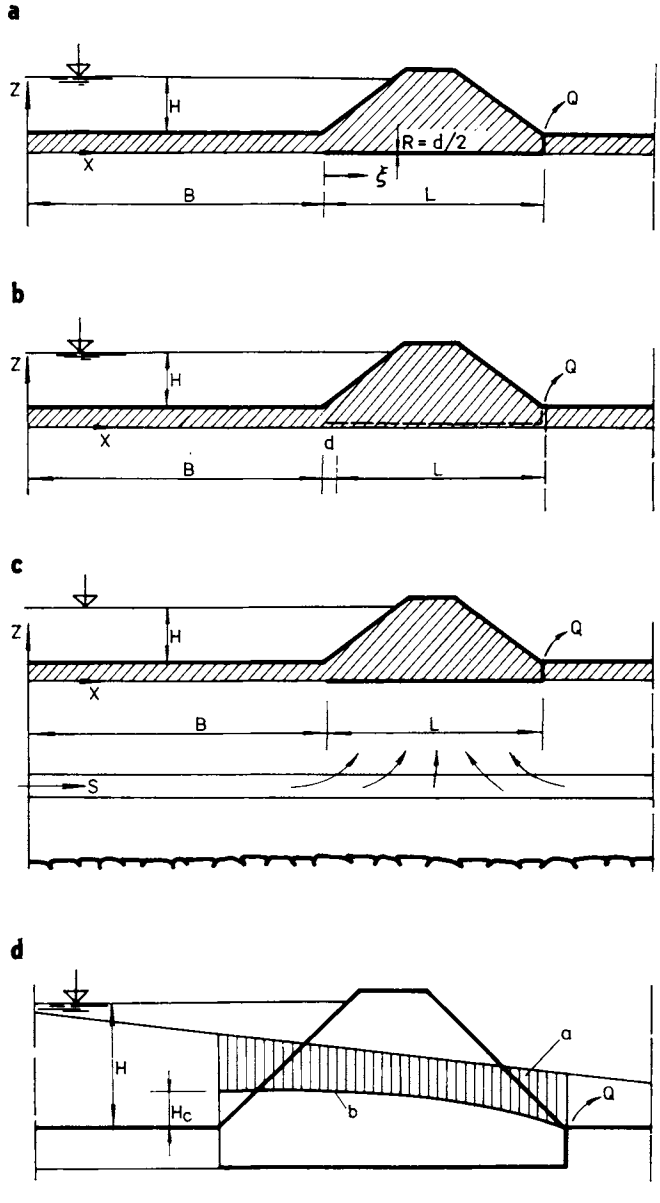

Fig. 6.56. Different kinds of privileged path — after Hálek (1967). a — transversal privileged path and piping at the toe, b — longitudinal path, c — privileged layer (s), connected with privileged path in the dam (contact) foundation, d — pressures along the privileged path.

ashore most easy. For crushed material (rocks), the requirement for grain mobility is a porosity 5—20% greater than for alluvial deposits. The crushed material resists water attack much better than natural sands and gravels.

On the subject of filtration deformation, we could mention the theory of a *privileged path* of Hálek (1967). This privileged path has its origin in the contact between top soil and subsoil, where a channel of diameter d is generated (Fig. 6.56). The seepage and water pressure tend from the upstream side to the downstream toe of the embankments. From a given amount of seepage Q, a velocity potential φ originates. This potential depends on channel diameter (d), the length of the privileged path (L), and the length of the blanket (B); it can be evaluated through the theoretical expression

$$\varphi = \frac{Q}{\pi L}\left(\ln\frac{2L}{d}\sqrt{\frac{2}{3}-\frac{1}{2}\ln\frac{4B+3L}{4B+L}}\right), \tag{6.154}$$

and thus

$$Q = \frac{\pi k L H}{\ln\dfrac{2L}{d}\sqrt{\dfrac{2}{3}-\dfrac{1}{2}\ln\dfrac{4B+3L}{4B+L}}}. \tag{6.155}$$

Substituting in the value of permeability coefficient measured in the field ($k = 10^{-3}$ to 10^{-2} m s^{-1}) and other parameters (L, H, B) which can be measured on the Danube levées, such a privileged path (some cm to dm in diameter) can yield $Q = 0.01$—0.100 m^3 s^{-1}. It far exceeds the critical value Q_{mf} given by Leva et al. (1956) as a limit seepage rate conditioned by fluidization (liquefaction).

It follows that the field conditions characterized by privileged-path generation should be viewed as a region with remarkable filtration deformation.

6.9.4 Soil Stability — Laboratory Tests

The results of research carried out in the Soil Mechanics Laboratory in Czechoslovakia enable us to correct the conceptions of Leva et al. (1956) concerning the process of disturbance of cohesionless soils composed of two different elements (sandy gravels) having different grain shapes, during repeated washing and increase in pressure gradients (Fig. 6.57). If we want to complete the graph of the *disturbance process* — indicated by Leva in Fig. 6.36d, we see that in the washing (the washing away of the sandy fill from the skeleton) of the gravels, the resistances in the soil decrease up to one tenth of the original value (I_{max}). The resistance changes are indirectly proportional to the flow velocity. At the same time, it is not possible to ignore the influence of the earth porosity (different value of n). The compact layer of soil (low porosity) guarantees, however, a marked increase in soil resistance only under the *initial hydrodynamic load* to the boundary

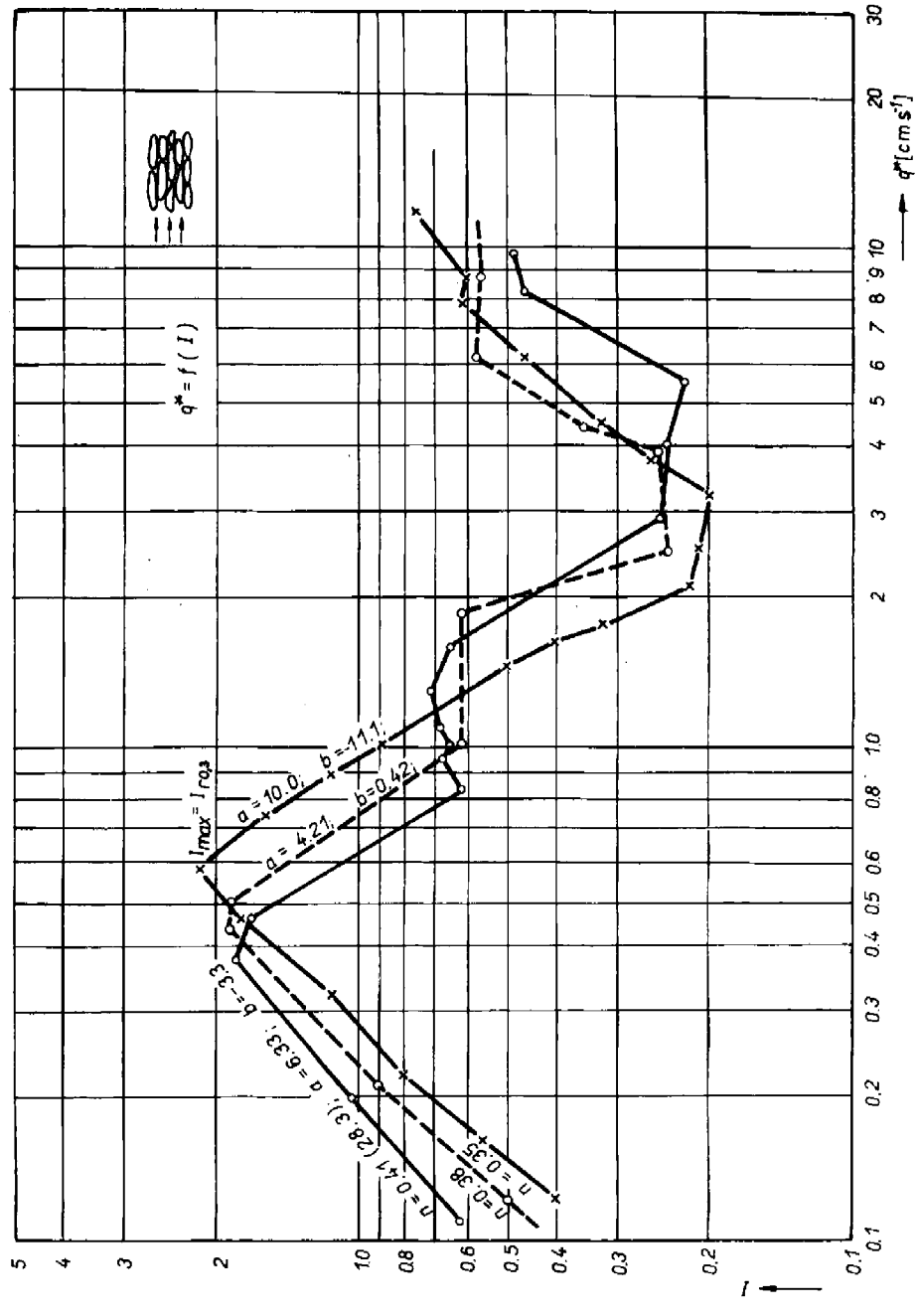

Fig. 6.57. Changes in the pressures of the flow for increase of velocity and deformation — for flat grains in a lying position.

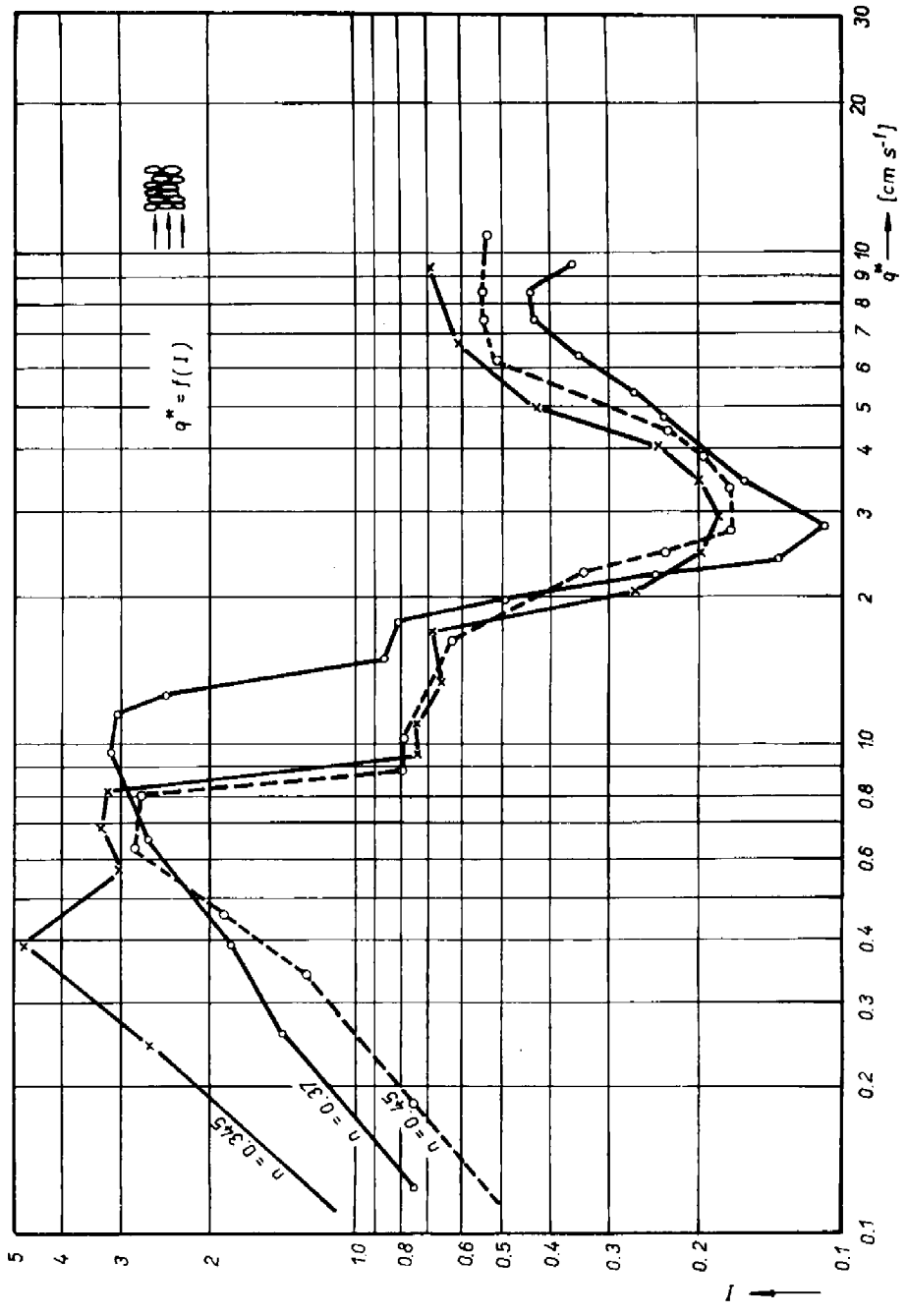

Fig. 6.58. Resistance of flow of flat standing grains.

of the disturbance. If such a soil is disturbed, it becomes permanently less resistant than under the initial load. Further, one should also notice that the resistance to disturbance by a current of water is also influenced by grain orientation.

Flat grains arranged upright (in the vertical direction) perpendicular to the water flow (Fig. 6.58) generally showed 2—2.5 times greater resistance to the *washing away* (disturbance) than flat grains lying on a flat surface. At the same time, the difference between the resistances (I_{max} : I_{min}) at the boundary of the disturbance was up to 30 times greater.

Similar conclusions are reached when the resistances of porous artificially created media are observed, the *skeleton* consisting of spherical, cubic, prismatic, or irregular angular shapes (grains of crushed rocks).

One series of experiments involved investigating the influence of the admixture of sands which formed the fill of the pores in the skeleton of the above-mentioned grains having the size of the median: $M = d = 20$ mm (rounded grains), $M = 20$—25 mm (cubic grains), $M = 18$—35 mm (flat grains laid vertically on the water flow), and $M = 15$—25 mm for the grains of crushed rocks. In laboratory experiments there was found the *hydraulic gradient* (I_{ro}) in a failure and the average velocity of water flow $\bar{u}$ determined from the fictive (discharge) velocity q^* — by means of the relation

$$\bar{u}^* = q^* : n_{eff}.$$

This value was used for determining the value of the factor of *hydraulic friction* f_H^* from the expression

$$f_H^* = 7925 R_H \frac{I_{ro}}{\bar{u}^{*2}}. \tag{6.156}$$

Further auxiliary values were determined by means of the relations already mentioned

$$d_{eff} = \frac{2}{3} \frac{n_{eff}}{1-n} d = 4R_H \qquad \text{for the skeleton,}$$

$$R_H = k_s \frac{n_{eff}}{1-n} d = \alpha \frac{n_{eff}}{1-n}.$$

The porosity of the granular material was $n_0 = 36$—38%. The sand-filler diameter $d = 0.05$—0.5 mm (4) ($\bar{d} = 0.2$ mm). The pores were filled in with sand in the proportion:

(15—50%) spherical grains,
(10—30%) cubic and flat rounded grains,
(15—60%) grains of crushed rocks.

The *critical-destruction gradient* $I_{ro} = 0.05$—0.92 at the mean discharge velocity $q^* = 0.26$ to $1.2\ \mathrm{cm\ s^{-1}}$, and a velocity $\bar{u}^* = 1.0$—$7.6\ \mathrm{cm\ s^{-1}}$ was found. If we assume that the grains of the diameter $d_c = 0.1$—4 mm were carried out, we obtain from the well known formula for Reynolds number

$$\mathrm{Re}_c = \frac{d_c \bar{u}^*}{\nu}$$

values of $\mathrm{Re}_c = 1.3$—12 and from the diagram, we can find the value of $f_H^* = 1.8$—26.

The function $f_H^* = f(\mathrm{Re}_c)$ plotted in Fig. 6.59 shows that for spherical grains the amount of sand-filler influences the hydraulic friction factor f_H^* and the stability of sand much more less than for crushed grains. With increasing quantity of the filler the stability of sand increased two to three times in the spherical and flat rounded grains and five times for the crushed material.

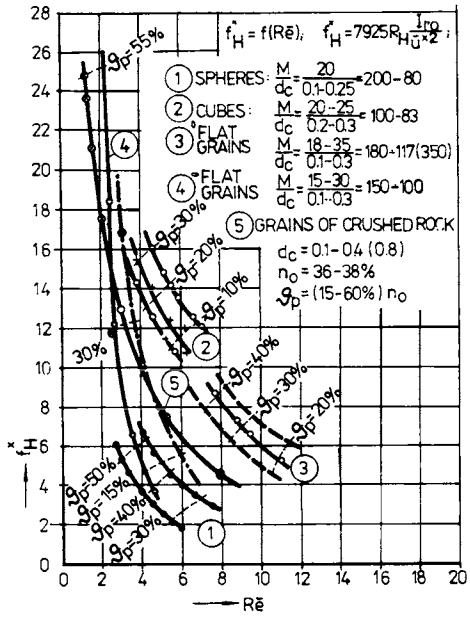

Fig. 6.59. Hydraulic friction factor as a function of Reynolds number (Re) for various forms of grains and various proportions of sands.

Interesting results can be met with in observing the values of drag coefficient C_D derived from the drag force F_D. According to facts already stated, it is possible to write for this force the expression (Peter 1972b)

$$F_D = C_0' \frac{\varrho_w u^2}{2} \pi d^2 = C_0 \left(1 + \frac{\delta}{r}\right) \left(\frac{\varrho_w \pi r^2}{2} u^2\right). \qquad (6.157)$$

The *simple expression* for the drag coefficient is

$$C_D = C_0 \left[1 + \frac{\delta_0}{Re^{0.5}}\right]^2 \tag{6.158}$$

and also

$$C_D = \frac{K_D}{Re_s^x}, \tag{6.159}$$

where K_D is the constant of dynamic resistance taking into account the grain shape; Re_s Reynolds number with respect to the fall velocity; x exponent depending on the flow velocity of water. All these values can be determined by experiments.

Using some hundreds of tests to determine these factors, we can obtain a system of equations in the form

$$\log C_D = \log K_{D,i} - x \log Re_{s,i} \tag{6.160}$$

with equilibrium condition $C_D = f_H^*$.

In this way the following *drag coefficient equations* have been deduced

$$C_D = \frac{30.6}{Re_s^{0.680}} \quad \text{for spherical grains,} \tag{6.161}$$

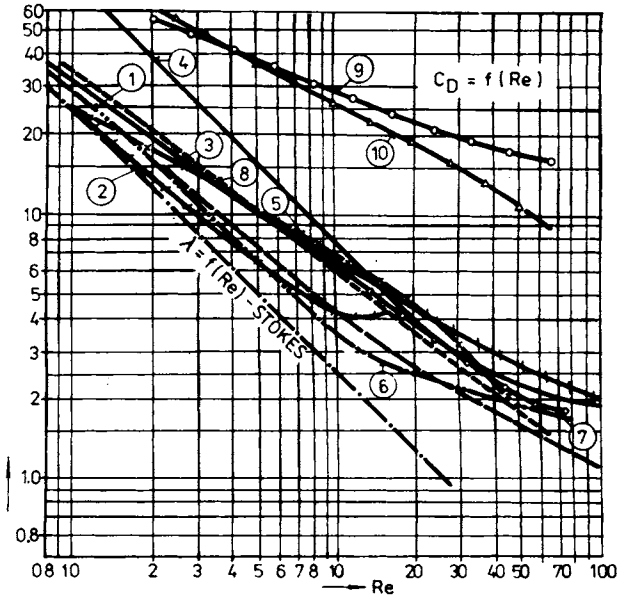

Fig. 6.60. The relationship $C_D = f(Re)$ after various authors. 1 — McDonald, 2 — Oseen, 3 — Kliatscho, 4 — Vanoni et al., 5 — Serafini, 6 — Gilbert and Davis, 7—10 — Peter: spheres, flat lying grains, standing grains, crushed rock.

$$C_D = \frac{34.7}{Re_s^{0.765}} \quad \text{for flat, lying grains,} \tag{6.162a}$$

$$C_D = \frac{69.1}{Re_s^{0.358}} \quad \text{for flat grains arranged upright,} \tag{6.162b}$$

$$C_D = \frac{85}{Re_s^{0.518}} \quad \text{for crushed rock grains.} \tag{6.163}$$

The values of *drag coefficient* C_D calculated thus plotted *against Reynolds number* are shown in Fig. 6.60, where values of this coefficient determined by means of other formulae are also shown. An analysis of these curves leads to the conclusion that nearly all the formulae used for determining the dynamic resistance of the grains have been deduced according to theory and by means of laboratory (or tunnel) tests made with spherical or flat rounded grains with the long axis lying along the flow direction. The resistance of porous media composed of crushed grains (curve 10) and flat grains in a disadvantageous position (arranged upright) to the flow direction (curve 9) has been given little attention till now.

To avoid piping, it is important to build a barrier or *break wall* against mass transfer. Such a role may be fulfilled by crushed materials, or porous media with disadvantageously oriented flat grains, which provide a high resistance to sand particles carried by water. In sandy soils (homogeneous porous media), the safety depends on the grain size, porosity and the conditions of expansion which play an important role in the mode of the mass and hydrodynamic pressure transfer.

6.9.5 Dam-failure Analysis

Several interesting conclusions, important to engineering routine, can be deduced from the analysis of earths and geological conditions, of stratigraphy of the strata of earths of different permeability and different resistances to deformation — in deformed levées (dam failures). The conditions of deformation can be examined at the site of the breakage of the levée near Kľúčovec, near Žitavská Tôň and near the village of Patince (Fig. 6.61) in the Danube valley, at the frontier between Czechoslovakia and Hungary (in the territory of Slovakia). It was shown that the *danger of deformation of soils* depends upon the hydrodynamic pressure, on the geological conditions and on the critical path.

Contact between loose sands and gravel can lead to very dangerous situations in a heterogeneous soil profile, since gravel allows a high flow velocity with low pressure losses.

In the first case near Kľúčovec, the water stream carried out the fine sands through the gravel pores. In the second case, the water stream and water pressure led to sand-layer *expansion and liquefaction.* Laboratory experiments show that the mutual combination of this damage and layer breakage is possible: the result of hundreds of experiments in laboratory and field. Trials were performed with the

intention of investigating the mechanism of damage evolution caused by seepage and sudden water-pressure increase. The most interesting seem to be experiments with layered permeable strata and a dam model attacked by seepage water. The level of this high water increased successively until soil damage appeared. In a series of these (108) experiments — performed in the laboratory — damage occurrences were as follows:

28	damage caused by contact suffusion	26.0%
20	fluidized bed observed	18.5%
22	simultaneous suffusion and fluidization	20.4%
16	damage caused by high water pressure	14.8%
10	damage caused by suffusion and water pressure	9.3%
12	other damage (cavity, layer-break, etc.)	11.0%
108	total	

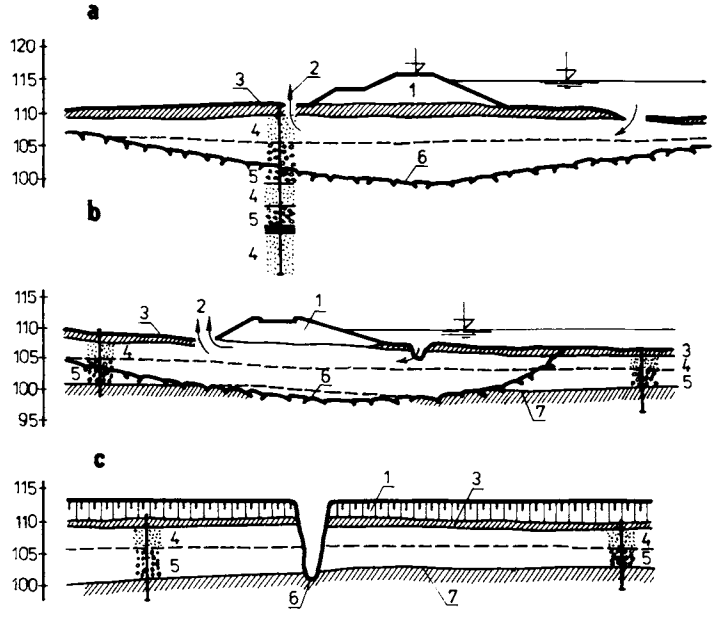

Fig. 6.61. Failure of the levée. a — in the vicinity of Kľúčovec, b — at Patince, c — cross-section perpendicular to the break; 1 — levée, 2 — piping (boil), 3 — loam, 4 — loose sand, 5 — sandy gravel, 6 — bottom of the wash out, 7 — Neocene.

The damage occurred at an average hydraulic gradient from $\bar{I}=0.07$ (as minimum) to a maximum $\bar{I}=1.35$. Separating the gradient into horizontal (I_h) and vertical (I_v) components, we obtain: min $I_h=0.1$, max $I_h=1.32$ (3.5 exception) and min $I_v=0.06$ max $I_{v\,max}=8.2$, respectively (Fig. 6.62). For the number of

pipings (y) in the field, an equation in the form

$$y = ax^b \, e^{cx} \tag{6.164}$$

could be deduced. With absolute values, the following equation was obtained

$$y = 13\,000x^{2.78} \, e^{-9.45x}. \tag{6.165}$$

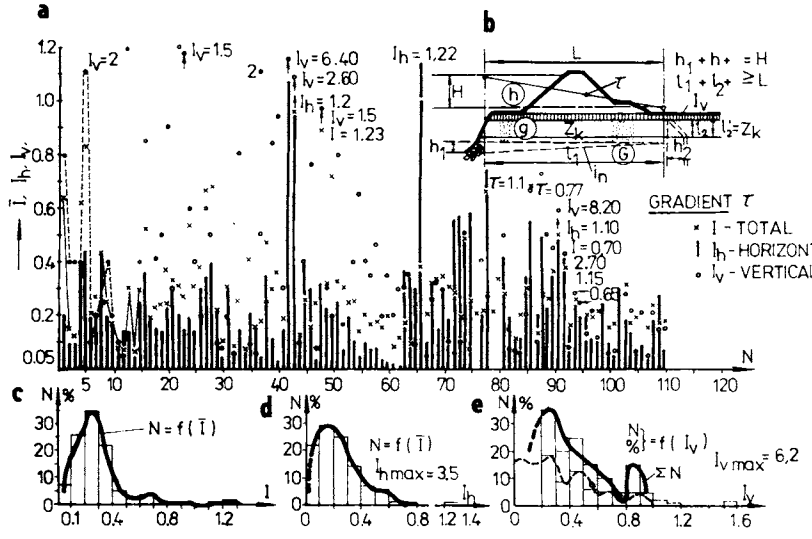

Fig. 6.62. Dependence $N = f(I)$ for various gradients. a — for $N = f(I)$ on the whole, b — scheme for the denotation of data, c — dependence $N = f(I)$, d — $N = f(I_h)$ for the contact suffusion, e — $N = f(I_c)$ for the fluidization (liquefaction).

Evaluating this equation, we get the probability of damage occurrences ($y = N$) for the given gradient $I = x$. By means of these data, the length of the impervious blanket, or of other antiseepage measures designed for soil-stability protection can be calculated. In the region considered, a blanket of about 200 m length was needed. However, in this case, it seems to be more convenient to change the soil quality (by means of compaction of the sand, etc.) than to move some million cubic meters of earth towards the river-bed.

6.9.6 Soil Characteristics and Water Stream Resistance

In Section 1.9 it was stated that the main *factors of resistance to piping* are: grain size (d), (d_c), pore size (d_0), density of soil particles (ϱ_s) and of water (ϱ_w), shape factor (Φ_s), soil porosity (n, Φ_n), tortuosity (T_k), stream velocity (u), superficial velocity (q^*), fall velocity of grain (v_s), gravity constant (g) and heterogeneity (δ_s). The function dependence can be written

$$f(d, d_c, d_0, \varrho_s, \varrho_w, g, q^*, \Phi_s, \Phi_n, T_k, v_s, \delta \quad (6.166a)$$

or by means of *Archimedean number* (Ar), *Reynolds number* (Re), *gravity parameter* (G_s), *constant of resistance* (K), and the *drag coefficient* (C_D) (Peter 1973)

$$f(\mathrm{Ar}, G_s, K, \mathrm{Re_M}, \mathrm{Re_C}, \mathrm{Re_s}, \Phi_n, C_D, \delta_s). \quad (6.166b)$$

The pressure drop Δp ($=\gamma_w h_z$) at a length (l) can be expressed

$$\gamma_w \frac{h_z}{l} = \gamma_w I = C_D \Phi_n \Phi_s \frac{\gamma_w v^2}{2g d_a}. \quad (6.167)$$

The pressure acting on one spherical grain of diameter d_a is (in accordance with eqn. 6.108)

$$F_{D,1} = C_{D,1} \Phi_s \frac{\gamma_w v^2}{2g} \frac{\pi}{4} d_a^2.$$

At the stage of *suffusion* the *seepage force* can be expressed by

$$F_D = \gamma_w f_H \Phi_n \delta_s^{0.5} \mathrm{Re}_c^{*\xi} \quad (6.168)$$

and in loose sand

$$F_D = \gamma_w f_H \Phi_n \delta_s \mathrm{Re}_c^{*\xi}. \quad (6.169)$$

The soil *resistance* in the state of suffusion can be calculated

$$W = \frac{31}{e^2} \gamma_w K S_g G_s^{*\xi}. \quad (6.170)$$

In expanded sand it is

$$W = \frac{15.5}{e} \gamma_w K S_g G_s^{*\xi}. \quad (6.171)$$

In the eqns. (6.168—6.171) we put in the values of the hydraulic friction (f_H) depending on the modified Reynolds number $\mathrm{Re_M}$

$$\mathrm{Re_M} = \frac{2}{3} \frac{n}{1-n} \frac{\mathrm{d}q^*}{\nu}.$$

The Reynolds number adapted to the grain diameter (d_c) — which is carried out is

$$\mathrm{Re}_c^* = \mathrm{Re}_c - \frac{3}{3-\xi} \mathrm{Re_M^{-0.2}} \quad (6.172)$$

if $\mathrm{Re}_c \geq 3$.

The gravity parameter G_s^* gives the relation

$$G_s^* = \frac{v_s}{q^*}. \quad (6.173)$$

The exponent ξ in eqns. (6.168—6.171) has the value: $\xi = 1$ in the laminar region, $\xi = 2$ in the turbulent region and $\xi = 1.1$ to 1.9 in the transient region of flow. It can be determined through the Table 6.9. In the same way, the constant K (which varies within the range $K = 4.5$—22) can be determined. The shape factor S_g (the values are $S_g = 1$—3) and the factor Φ_n — depending on the porosity (n) or (e) must be determined in the field, while the value of the coefficient of hydraulic friction (f_H) can be taken from the graph constructed from experimental data.

Finally, we can form the relation between the resistance of the soil (W^*) and the seepage force of the percolating water (F_D) in the given region and we get the degree of *filtration stability* SF

$$\mathrm{SF} = \frac{15.5 S_g K G_s^{*\xi}}{f_H \Phi_n e \delta_s \mathrm{Re}_c^{\xi}} \qquad \text{for sands.} \tag{6.174}$$

For sandy gravel we get the value of filtration stability

$$\mathrm{SF} = \frac{31 S_g K G_s^{*\xi}}{f_H \Phi_n e^2 \delta_s^{0.5} \mathrm{Re}_c^{\xi}} . \tag{6.175}$$

In the Danube valley grain size distribution curves can be used for soil stability computation. It is necessary to know the porosity (n), the depth (position below the ground surface — z) of the layer threatened by seepage water during the flood. For such a situation the safety factor of the sandy soil can be evaluated approximately

$$\mathrm{SF} = 0.25(3.906 + 0.342z - 0.005z^2)\left(\frac{n_{cr}}{n}\right)^4 . \tag{6.176}$$

Using the formulae, in eqns. (6.168)—(6.176), the conditions and assumptions made in its deduction must be borne in mind (Peter 1973).

6.10 Remarks Concerning Antiseepage Elements and Protection of the Sub-base

The *antiseepage elements* of levées have essentially a different character from the sealing of canal levées and the sealing of large dams. While the sealing of canals and dams must be secured, as far as possible, by a perfect sealing of the profile — to prevent the water losses—a completely watertight closing of the flowing profile of a river against floods of the territory we are protecting is not desirable. In general, certain interaction is desirable between the groundwater of the protected territory and the seepage water which escape from the river-bed into the adjacent pervious strata, and during a flood proceed against the normal flow of the groundwater. In the dry season, they proceed towards the river. From this point of view, the fundamental requirement for the antiseepage elements of the levées is often met, and so these elements must be arranged such that constant communication between

the ground and seepage waters within certain allowable limits is permitted of the elements of an active protection, it is required that they catch and eventually drain away a part of the seepage waters escaping from a river into the protected territory, at the period of high water within the levées.

From the afore said, it is clear that we distinguish:

(a) antiseepage elements of *passive protection*,

(b) antiseepage elements of *active protection*.

The first measures prevent excessive seepage and thereby keep it within desirable limits, the second regulate it actively, since they drain away part of the water.

As we have already emphasized (several times), the old generally levées packed passive antiseepage elements. Active protection elements occurred only sporadically and even then they lacked the necessary dimensions. In such levées then, there often occurred various kinds of filtration deformations, which we have already mentioned in this chapter.

6.10.1 Elements of Passive Protection

In levées, the following *antiseepage measures* are most often prepared (Fig. 6.63).

(1) horizontal earth blankets in front of the levée,
(2) horizontal blankets of artificial materials,
(3) antiseepage caskets (small water-filled reservoirs behind the levée),
(4) slurry trench cut-offs,
(5) diaphragm walls,
(6) grout curtains,
(7) curtains formed by depth vibration of earths.

In the first two cases (Fig. 6.63-1), *the horizontal protection elements* have the main purpose of lengthening the seepage path ($L_1 \ldots L_4$) (Fig. 6.63-2) and thus decreasing the velocity of water movement, and also the amount of seepage (q), as explained several times in Chapter 2 and Section 6.7.

Among the antiseepage protective elements, *antiseepage caskets* have a special position (Fig. 6.63-3). In these, the gradients of the seepage waters are decreased primarily by the fact that the pressure height H_1 is decreased by H_c given by the pressure of water in the casket; ΔH_2 is smaller than originally ΔH_1. On the levées of the Danube, such banks are usually 1.0—1.5 m high, whereby the hydraulic gradient is decreased by 20—30%.

Slurry trench cut-offs (Fig. 6.63-4) are considered to be some of the most progressive protection elements against seepage waters — particularly in cases where the subsoil is heterogeneous; when strata of sandy soils alternate with gravels. They are useful particularly when the gravels in the sub-base are disturbed by piping phenomena (suffusion) and if under this gravel the strata are mechanical-

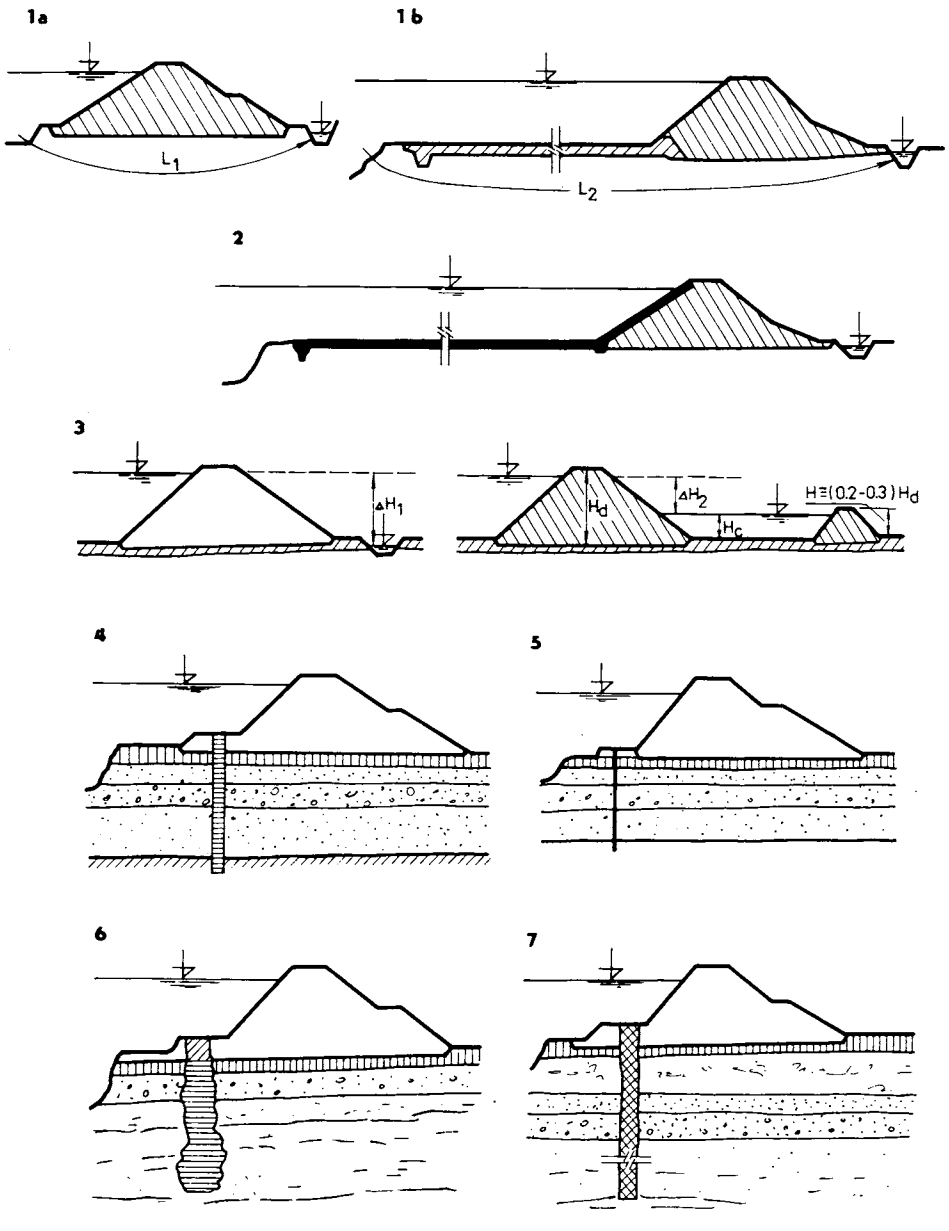

Fig. 6.63. Elements of passive protection. 1b—earth (natural) blanket, 2—asphalt-concrete (from artificial materials) blanket, 3 — pressure casket, 4 — slurry trench wall made of concrete and laid in a trench, 5 — diaphragm wall, 6 — grout curtain, 7 — curtain formed by depth vibration.

ly stable. The wall is then bound with such a stable stratum, eventually with the impervious sub-base.

In the past, the task of the antiseepage elements was performed by different kinds of *diaphragm walls* (Fig. 6.63-5), which usually reached to a depth of 5—8 m using wooden walls, and to a depth of 10—12 m using steel walls. These walls have two disadvantages: they increase considerably the gradients under the wall and they penetrate very hard into the gravels. In cases where the wall is driven among boulders, there easily arise openings in it, so-called "windows". Seepages concentrate at the "windows", and the water has a high velocity in which the fine particles of the soils are washed out.

The *grout curtains* (Fig. 6.63-6) decrease the seepage because the injection matter fills part of the earth pores, and thereby the permeability is decreased (the permeability coefficient is decreased). In the formation of a cement *grout curtain in gravels*, the permeability coefficient (k) of the gravel is decreased from one tenth to one thousandth of the original value. On average, a decrease in the value of k, is reached of 1/20 to 1/50 of the original value of the permeability coefficient. In sandy soil, the injection procedure meets with several problems. Usually it is necessary to select special chemical ingredients, or to use a suitable chemical treatment directly.

Within the last two decades, *depth vibration* has been used several times for packing the sub-base. Here, we are generally concerned with decreasing the permeability of the earth, by the fact that fine particles penetrate into the pores of the skeleton formed by the gravel grains.

Good experience with depth *vibration and vibroflotation* is reported chiefly by experts from FRG, Austria and Switzerland. Two West German companies (Johann Keller and Dr. Bauer) have had hundreds of successful cases over the last 30 years, in all continents. Among the best known done by Keller, are those using depth vibration in the levées of the Danube near Vienna (Fig. 6.64) where both an increase in the impermeability of the levées and of their subsoil was attained, and also an increase in their total stability. The detailed research of these levées was carried out by Prof. H. Borowicka who has also described them in detail (Borowicka 1968).

The technological experience with depth vibration is described in the German company literature (Bauer 1969), in various experts' accounts (Richart 1972). From the published reports it follows that using depth vibration correctly, it is possible to obtain a decrease in permeability from 1/5 to 1/50 of the original value. In the laboratory tests carried out at the Technical University at Karlsruhe (FRG) and in Bratislava (Czechoslovakia), they currently obtained in gravel a decrease in permeability coefficient k from 1/10 to 1/30 of the original value, if during the vibration no fine sands were added. With the addition of fine earths, in the course of compaction of the earth, the effect was ordinarily about twice as large. From the tests, it followed that in evaluating the influence of vibration on the permeability of

earth, it is possible to proceed from the change in porosity (n) given by the *reduction factor*

$$\Phi_{k,r} = k_1 : k_2 = (n_1 : n_2)^{3.5} \text{ to } (n_1 : n_2)^{4.5}. \tag{6.177}$$

This relation may also be used judging the efficiency of the depth vibration in nature. For example, in using depth vibration for packing a sandy gravel sub-base of a small sediment reservoir near the town of Zürich (1962) in Switzerland, the porosity of the freely laid sandy gravel changed from the value $n \cong 42\%$ to the value $n = 20\%$, which gives the value of the reduction factor

$$\Phi_{k,r} = (42 : 20)^4 \text{ to } (42 : 20)^{4.5} = 19.3 \text{ to } 28$$

which agrees well with the data found by the company Schafir-Mugglin by measurements in the field, in 1962.

Concerning the extent of compaction and thereby also the dimensions of the packing curtain formed by the depth vibration, a marked *effect of the vibration* of

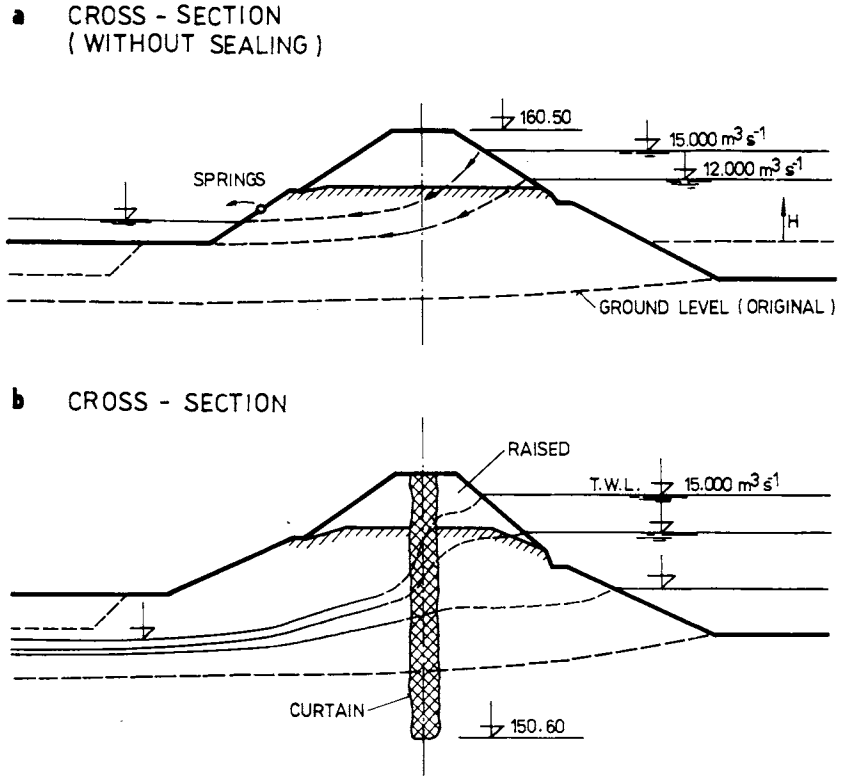

Fig. 6.64. Cross-section of the levée near Vienna. a — profile of the raised levée without vibration screen, b — with vibration screen.

the gravel is evident to a distance of 3—4 diameters of the vibrator used. For the dimensions and efficiency of depth vibrators which have a diameter of the head $\Phi = 240$ to 350 mm, it is possible to assume the thickness of the curtain to be 1.80—2.80 m.

In these cases, depth vibration was used to pack depths of 10—12 m. However, the company literature mentioned, describes possibilities of depth vibration to depths twice to three times greater: depths reached are 25—35 m.

Theoretical examination of the given problems shows (Fig. 6.65) that depth vibrated screen walls are an appropriate antiseepage measure, in which the degraded stratum of gravels is easily interrupted, and the seepage is limited, the stability of the sub-base being increaed. At high water levels, 4—5 m, which usually encountered with levées, a screen desirable; it reaches a depth of $D = (1.5—2.5)\,H$ (with an average of $2H$). On such a screen the gradient is usually $I = 3—4$ and below it $I = 1.2—1.5$. In the conditions indicated, it is possible to assume that the earth worked up by vibration, will remain stable, just as the sands under its lower end.

As an advantage of a vibrated screen is that it can be filled and strengthened, if for any reasons this is necessary.

The *classical elements* of passive protection mentioned at the beginning under numbers 1 to 6 were theoretically validated and evaluated at the beginning of this chapter (Sections 6.1—6.4); as regards their practicality, we should state that despite progress in the technology of levées, horizontal clay blankets, which have been well tested, are often used further as antiseepage elements, particularly when there are homogeneous strata of alluvial deposits, whose water-bearing part is characterized by a permeability coefficient $k = 1 \times 10^{-5}$ to 1×10^{-3} m s^{-1} and when the ratio of permeability coefficient in the horizontal (k_h) and vertical (k_v) directions does not exceed $k_h : k_v = 10$ to 20. For more heterogeneity, it is advantageous to interrupt the horizontal strata of gravel by a vertical sealing element.

Horizontal blankets formed from asphalt concrete (about 6—15 cm thick) are, in comparison with clay blankets (50—120 cm thick), generally more expensive. The blankets made from artificial plastic foil appear to be appropriate elements of passive protection for temporary use (during a flood) and as a part of different reconstruction building structures.

Antiseepage-antipressure *caskets* belong to the most economical elements of protection. When considering the principles applied in the design of caskets which are filled by water during a flood and in states of high water in a river, they are generally only considered in homogeneous levées (filled with loams or clayey soils and loess wind-borne material) where the heel is soaked during a flood, and thereby the stability of the whole levée is decreased. This is one of the main causes for which, at the present time, antiseepage caskets are designed.

Slurry trench cut-offs are antiseepage elements which saw increased use in

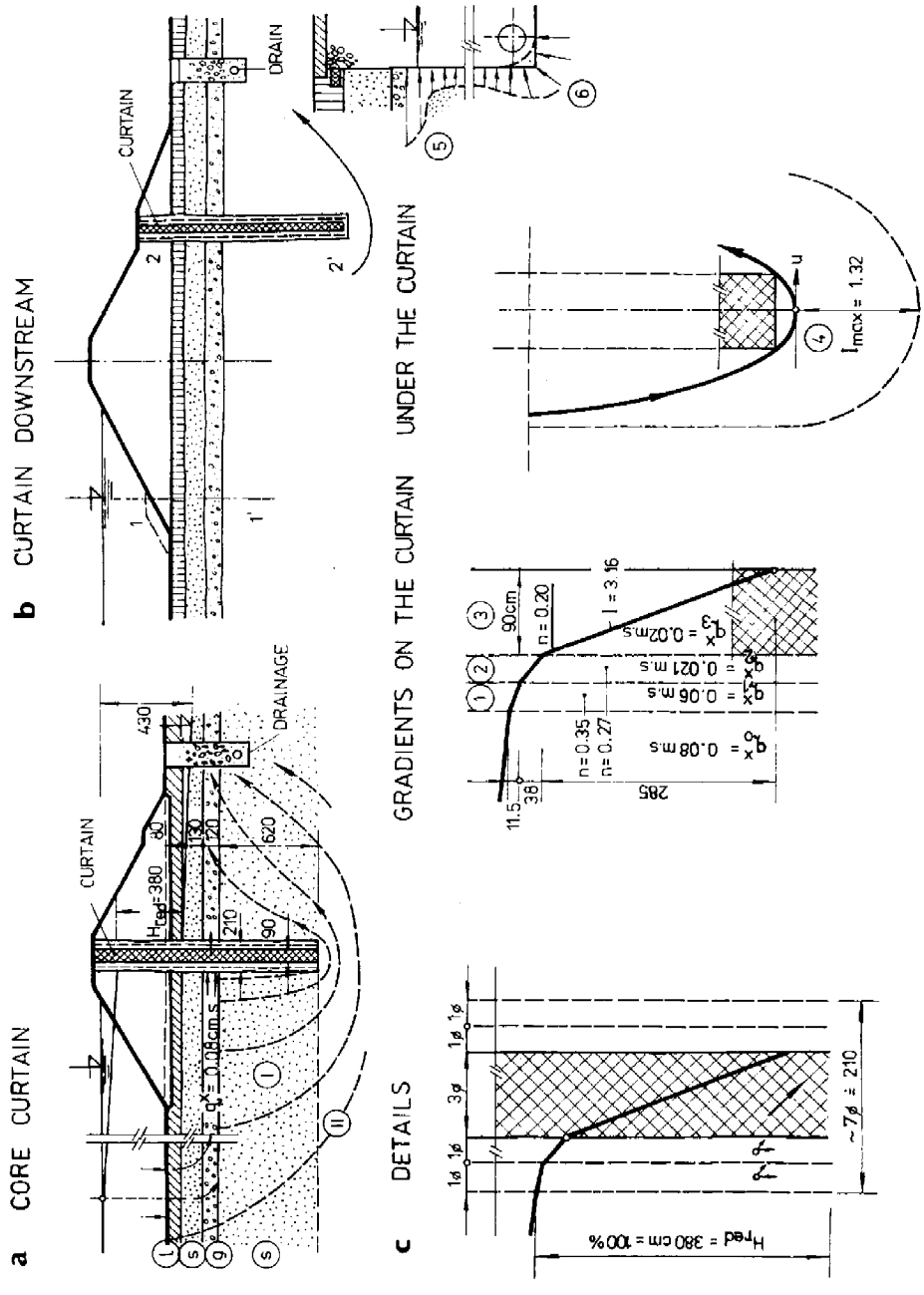

Fig. 6.65. Results of the theoretical investigation into the division of gradients on a vibrated wall. a — in the middle of a levée, b — at the downstream heel, c — gradients.

northern Italy (the Po valley), at the end of the fifties, for protection against seepage. Over two decades, they have become the most widely used vertical packing elements for the protection of levée sub-bases, by virtue of the large progress in mechanical equipment and technical processes. Efficient machines were first developed by Italian companies and Spanish-French (ICOS-Veder, RODIO-Marconi), French (SOLETANCHE), English (KILLY) and German (SALZGITTER, ETMO) companies in the West and GOSSTROĬ in the USSR. Today more than 100 patents exist for machine equipment, and different special technologies have been developed, to allow adaptation to local geological conditions and requirements of protection such that other technologies (drilling technique and injection technique) are generally unable to compete in performance or expense with slurry trench cut-offs made of concrete. The walls can attain a depth of 50—60 m (or more). For protecting levée sub-bases, the walls are made so that ordinarily they attain depths most often 10—12 m — exceptionally more than 20—30 m. Their advantage is that if correctly designed, they resist the hydrodynamic load well. With hydraulic gradients $I = 10—15$ (exceptionally 30), they remain stable. One disadvantage is that in the case of incomplete binding with the sub-base, large hydrodynamic tensions occur under the end.

Diaphragm wooden walls had already failed in competition with other antiseepage elements half a century ago, being ineffective. In the USA, they were replaced 40 years ago in several constructions by *steel diaphragm walls*. Unfortunately these are subject to corrosion, and today they are only rarely able to compete with concrete walls.

Grout curtains which, up to the present, have kept their leading position in the construction of large dams (Cambefort 1961b, 1967) have not found any wider application. Some experiments in protection of the sub-base of the Danube levées using grout curtains built up in their upstream toe were not successful for several reasons. They have the disadvantage that alluvial deposits which have to be tightened by injections lay great claims to mechanical equipment. It is difficult to prescribe an appropriate composition of the injection blend and find the technological procedures of the injection (the height of the general aspect of the strata and the direction of the process). Another disadvantage is that in territory which shows instability caused by seepage water, it is also difficult to secure the stability of the grout curtain which has to stabilize the territory (the sub-base of the levée). This fact was shown markedly in two experimental sections of the Danube levées in the region of Palkovičovo—Komárno, where such a curtain (6—8 m deep) was completely damaged hydraulically over eight years (Bažant 1967).

The difficulties which occur in the *injection of* layered *alluvial deposits* are explained in the literature (Brauns and Blinde 1978).

Some evaluation of the traditional and new elements of seepage protection can be found in the Proceedings of the International Congresses of the Soil Mechanics

ICSMFE (Paris 1961), of European Conferences (ECSMFE — Budapest 1973, Brighton 1979 and the International Conference ICOLD — Mexico 1976).

6.10.2 Elements of Active Protection

Active protection is secured above all *by drainage*, relief wells, ditches and filters, and if necessary a whole system of protection in which the elements mentioned are suitably arranged together.

The most perfect systems of active protection elements were constructed some decades ago in the USA on the levées of the Mississippi and Missouri Rivers. The system mainly concerned *filters and drainage* from the selected natural stone of gravels and sands, out of which earth-works of wells and *flat blankets and drainage*, pipe drains of stone material and recently also of glass laminated fibres were formed. For strengthening the *drainage ditches*, stone floors are being replaced by an appropriate *prefabricated pavement*, eventually by precast elements. These are laid in an appropriate profile — most often as a trapezium. The advantage of prefabricated material is that it requires less work, the time saving being due to the use of mechanical tools.

The advantages of the wide usage of machines in the formation of elements of active protection are shown chiefly in the vertical elements of protection. Among them are chiefly walls which diminish the uplift pressure, and drainage wells and sand piles in which, up till recently manual procedures were extensively used. New building machines and various kinds of artificial materials markedly contribute towards the simplification of technical procedures and towards shortening the building term.

During the last three decades which have elapsed from the time when Terzaghi, Rice, Arthur and others (3rd Congress ICOLD, Stockholm 1948) theoretically validated the functions of the passive and active elements of protection, various methods of research have been developed (Finn and Pickering 1971); as have computation methods (Hunt 1971, Irmay 1971, Ibad-Zadze and Shteinman 1972) which allow an increase in the security of levées and their sub-bases threatened by damage due to the hydrodynamic load of soils. Some theoretical approaches were explained in Chapter 2, and in Sections 6.5 and 6.6, and the hydraulic aspects of the elements of the passive and active protection measures against the seepages were emphasized. It should by remembered that elements of active protection also play an important role in securing the total stability of levée sub-bases, from the point of view of reducing the uplift pressure and pore pressures, the acceleration of the consolidation of soil and also from the point of view of improving their mechanical characteristics.

Nearly all materials built-in elements of the active protection of the sub-base have a greater shear strength than the earths which are protected and some are also able to transfer the tension stress, whereby the resistance of the sub-base is

increased not only against hydraulic, but also against mechanical damage. This applies to a larger extent to vertical elements of active protection such as wells, sand piles, sand drains with reinforced earth and gravel-sand walls. The last construction solution is used mainly where there is danger of sliding and movements of land slides and creep or flow. In this regard, vertical elements have the priority of protection which, from the mechanical point of view, have the function of passive protection, and they have the advantage of attaining great depths.

6.10.3 Protection of Earth against Mechanical Load

The protection of earth (in the body and sub-base of levées) against mechanical load, and methods of increasing resistance against this tension were theoretically explained in part in Chapters 1 and 3. There, we devoted our attention mainly to ways of increasing the resistance, in which the earth shear strength was increased in the body or sub-base of the levées, by building in soils which have favourable characteristics as regards *mechanical resistance.* The problem was solved by appropriate use of cohesionless soils: and the ways of increasing this resistance and the new characteristics were indicated. At the same time, we were dealing with ways of improving conditions connected with the compaction of soils.

Recently, there has been a transition towards methods and construction adaptations in which the earths mentioned are replaced in use by *artificial building material.* We use materials which enable us to replace the shear strength which is secured in the earths by friction — by strength tension or a combination of several building materials suitably adapted (as regards form and position). Hence, for a long time a need has been felt for replacing the earth filters which require much work and are very expensive, and thus they slow down the process of building. During the course of operation, they are in very delicate position in the levées, on which the whole safety of the construction often depends.

Experiments to solve this very sensitive element problem by use of *ceramic filters and protective strata of ceramic materials* have not solved satisfactorily the problem of decreasing the amount of work, the expanse and the increase in security against damage. Often expensive elements are needed, which usually have the disadvantage that they are inelastic. In large deformations, they are easily damaged.

Considering the aspects mentioned before, the various kinds of *technical textiles* which enable the protection of the construction, or of the sub-base and an increase in the strength seem to have more advantage, particularly in the following cases.

(1) In the construction of *various kinds of filters* and their parts
   — in soil packing (clay, plastic core),
   — horizontal drainage blankets,
   — in wells they partly replace the casing fittings, rock screening and the filter,
   — in sandy drains they form the cover of this protective structure.

(2) In the *formation of contacts* between different kinds *of earth* (protection of the contact of sands and sandy earths against washing away).
(3) In *contacts between concrete* objects *and earths* — protection of the contact.
(4) In the formation of passage — *strengthening strata* — protection of the sub-base in the tightening elements.
(5) In the establishment of *consolidation layers* and drillings.
(6) In securing organic (vegetation) *strengthening of the slopes* and of the territory in the downstream part (toe) of the levée threatened by piping (pin and boils).

The advantage appears to be in the fact that the manufacture of machines and new technological processes have in view the use of these new artificial materials and new protective elements. For example, we can mention the progressive equipment of the Swedish Company LINDEN-ALIMAK which has developed an efficient equipment Alidrain which can be mounted a suitable type of excavator.

Alimak's ADS drain stitcher consists of a mast (height 12—24 m), or set of conduits, through which a specially designed steel mandrel travels. The mandrel, completely enclosing the Alidrain, is then guided into the soil between equally spaced sets of rollers. The Alidrain is fed through the mandrel from a storage reel mounted on the mast. The mast is easily raised and lowered by a hydraulic cylinder on the carrier.

The installation rate varies between 0.4 and 0.8 m s^{-1}, depending on the soil and site conditions. However, the actual job results indicate a high production progress per rig shift (by courtesy of LINDEN-ALIMAK 1978).

We cannot analyse in detail this new development or protective elements in technology and progressive mechanization equipment, so we will simply mention the artificial materials used for this purpose. These are primarily *polyethylene, polyamide, polyester,* polyolefine and polypropylene fibres. We mentioned some of these materials in Chapter 1, when dealing with protection membranes used in the packings and tightening foils.

These fibres are used either as fabric (threads, woven crosswise), or as unwoven textile (eventually appropriately combined) and as knitted materials characterized by eyes (usually bigger) formed by knitting. Remembering that in our cases, we require the textiles to allow water passage, and to stop the particles of soil carried by it, then we can state that the variable distance of the threads, or the size of the eyes, replaces the size of the pores which in the soil is given by the grain size (particle) of the soil. The difference here is that in *artificial fibres* transitory profiles, such as their mechanical properties, can be arranged to a greater precision than in the earths (natural materials). This fact is often mentioned as one of the advantages of artificial protective fibres; there is also the chief advantage which is mainly technological (they are not dependent on weather, type of earth, and "uncontrollable" deformity properties).

As regards the advantages just mentioned which are most valuable to engineering contractors, the manufacture of artificial fibres and fabrics in Europe, Japan and the USA has spread very widely within the last few years. West European companies manufacturing artificial fabrics, today offer protective textiles under different Trade Marks. The best known are: GOUDERAK (protective fabric — England), NICOLN (Holland), SOLETANCHE-COLAS (France), SODOCA (unwoven textile — France), FIBERTEX (Denmark), COLBOND, COLBACH and STABELONKA (FRG), POLYPELT (Austria), TERAM and PARAVEB (different kinds of fabrics and coatings — England). In the USA, the best unwoven protective textile TYPAR has a wide range of use. In Czechoslovakia, several kinds of polypropylene textiles are on sale; they are sewn into sheets with dimensions 4.5×50 m up to 4.5×100 m. These show very good mechanical and deformable qualities.

At the hydroelectric structures on the Váh in Czechoslovakia, there are experimentally built-in protective textiles with the Trade Mark TATRATEX. Dam builders are greatly interested in them, as are the builders of hydroelectric stations on the Danube and the Dyje, because it was shown that in using these textiles, the productivity of work increased in the building of protective strata as much as twice, in contrast with situations where protective layers of soil had been used. In none of the cases mentioned, on the dams of the Váh or Dyje, however, have direct financial savings been achieved. Nevertheless, technical textiles are more effective as a protection than the classical methods (with earth protective filters and with transitory strata), if all effects are considered; generally a shortened term of construction results.

So far, we have no reliable comparison of the length of duration of these protective textiles, with protective elements formed from soils and ceramic materials. At the present time, we depend mostly on data given by their manufacturers; these, however, often seem to be too optimistic. Even if the length of duration of the textiles used as filters and protective strata is shorter than the length of duration of earth filters and protective elements, one can assume that they will gradually widely replace graded soils, selection of which is slow. This applies chiefly to the protection and interim measures taken on levées during floods, when the saving of time is the prime objective in securing protection (stability).

Concerning the *protection against mechanical damage* and excessive deformations in levées founded on insufficiently consolidated river deposits (very often in the building of levées), the trend in constructing these types of levées worldwide shows that there is a tendency to remove unconsolidated soils by excavation only when vital, and otherwise to take measures for accelerating the consolidation and stabilizing of the sub-base. The peculiar problem of consolidation and the securing of stability of the sub-base is being solved similarly in regions of permafrost.

The design of the dam and dykes of the Long Spruce project in Canada is an

example of this tendency. A typical section of the mean dyke (3—9.1 m height) consists of a homogeneous, semi-pervious sand-fill with crushed rock and rip-rap protection of the slope and crest. The foundation materials are excavated to a depth such that the predicted settlement does not exceed 1.5 m. Consequently, the embankments are super-elevated by 1.5 m, to eliminate or minimize future maintenance associated with settlements. A *network of sand drains* (Fig. 6.66) is

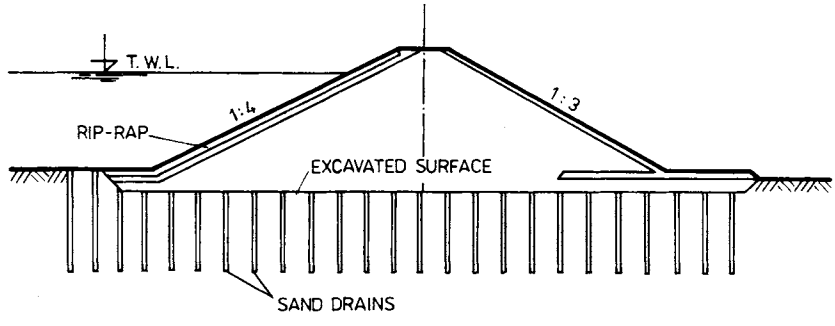

Fig. 6.66. Typical cross-section of a dyke with sand drains — Long Spruce scheme (ICOLD, 1976).

provided to relieve the high pressures which develop in the water trapped in the thawing soil. Sand drains of 0.30 m diameter and above 4.5 m (15 ft) in depth will have a total length of 18.290 linear meters. More detailed information can be found in McConnel, Proceedings of the 12th ICOLD, Mexico, G.P.6, pp. 533—555 (ICOLD, 1976).

Chapter 7
MEASUREMENTS AND OBSERVATION OF DAMS AND LEVÉES

Measurements and observation of dams and levées are very important during operation, having particular relevance to maintenance. Possibly they are more important for these structures than for any other type of hydrotechnical structure. In most cases, the significance of measurement results is emphasized by these main conditions: lower degree of project perfection (mainly for levées) in comparison with other structures; worse geological conditions (they are often founded directly on non-consolidated alluvial fluvial accumulation); lack of acquaintance with these conditions (knowledge of levées subsoil built 35—50 years ago is insufficient). Usually the quality of insufficiently protected subsoil is made still worse. Because of the relatively small height of dams and levées, these problems are generally underestimated in comparison with those of large dams and also in comparison with the problems of hydroelectric power plants, where operators (generally electrical engineers) monitor closely every construction defect.

More important than economy, the preservation and safety of the environment of dams and levées requires careful observations.

7.1 General Requirements and Methods

Measurements on completed structures have to provide information about the properties of the earth work and its basic static and hydraulic behaviour. Depending on the purpose, we may distinguish:

(a) check measurements — for checking deformations, stresses, seepage, uplift pressures, changes of soil properties, etc.;
(b) design measurements — to achieve the most economic design for the dam or its various elements (filter, drainage ...);
(c) study measurements — for getting more detailed information about the behaviour of the embankment and its relation to the land and other structures.

Measurements and observations may be visual (direct) or instrumental. Instrumental measurements are widespread nowadays because they allow objective data to be obtained for checking the behaviour of dams and levées or for design. The

greatest advantages of instrumental measurements can be obtained, especially with automatic devices, on levées, which can extend some tens or hundreds of kilometers: to ensure adequate monitoring, a staff of some hundred people is needed.

To examine the problems mentioned in Chapters 1—6, the methods and validities of our measurements must be known. Thus we shall consider:

— general aspects of surveying — geodetic and physical methods;
— experimental methods and measuring equipment;
— the results obtained in particular cases;
— the inspection and devices for a large canal and levée scheme.

General surveying techniques consist principally of levelling, triangulation, and photogrammetry.

Optical levelling is used to determine the relative displacement of the observed points, and therefore, by repeated levelling, we obtain the setting and deformation of the structure.

Laser levelling plays the same role as optical levelling, but with greater accuracy.

Levelling involves tracking a set of fixed reference points, suitably located according to surveying principles. The principle here is essentially the same as that employed in other engineering measurements, except that the techniques employed (bench marks, direction finders) must be adapted to the specific conditions. Accuracy must be higher generally than in ordinary field surveying. Czechoslovak standards require an accuracy of ± 0.5—0.3 mm, with an average error of $m = \pm 0.5$—0.10 mm. If a back-check shows a deviation greater than ± 0.10 mm, measurements are repeated.

In Czechoslovakia, optical levelling is carried out on all important canal embankments and on levées of the river Danube. Hydrostatic levelling, widespread in concrete-dam surveying, has only a small field of application in embankment observation.

Triangulation, a method for determining the relative displacement of points, is based on measuring horizontal and vertical angles, which change if any displacement takes place.

The height (v) of a point may be calculated using the equation:

$$v = s \tan \varepsilon + i + O. \tag{7.1}$$

The largest change (Δv) between two points measured is given by the equation:

$$\Delta v = \Delta v_1 + (1 + \tan^2 \varepsilon) \frac{s}{\varrho''} \Delta\varepsilon + \Delta s \tan \varepsilon\,, \tag{7.2}$$

where ε is the elevation angle; s distance between instrument (transit) and point observed; i height of instrument; O correction factor for refraction and Earth's curvature; Δv_1 height difference in the line of the instrument (horizontal) due to the change of its position.

In practical measurements, the horizontal is determined by precision levelling. If measurements are made with a precision $\varepsilon = \pm 1°$, then $\tan \varepsilon \cong 0$, and hence

$$\Delta v = \frac{\Delta \varepsilon''}{\varrho''} s. \tag{7.3}$$

The horizontal displacement of a point P can be determined using the equation

$$q_1 = \frac{s_1 \Delta \alpha_1}{\varrho''} \quad \text{or} \quad q_2 = \frac{s_2 \Delta \alpha_2}{\varrho''}, \tag{7.4}$$

where s_1, s_2 are the distances between point P and instrument, and $\Delta \alpha_1$, $\Delta \alpha_2$ are angular differences.

The mean height error

$$m_{\Delta v} = \frac{\Delta \varepsilon''}{\varrho''} m_s + \frac{s}{\varrho''} m \tag{7.5a}$$

and the mean point displacement error

$$m_2 = \frac{\Delta \alpha''}{\varrho''} m_s + \frac{s}{\varrho''} m_{\Delta \alpha''}. \tag{7.5b}$$

In the *photogrammetric method*, the displacement of tracking points is measured on an optical model created by observing a stereographic projection of two slides of the object under investigation. This displacement may be measured either on a time or space scale.

If the time scale is adopted, the displacement of a tracking point is determined by the coordinates defined by the relationship, referring to Fig. 7.1,

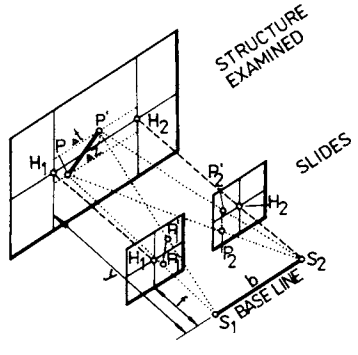

Fig. 7.1. Determining of sliding by photogrammetry.

$$\Delta x = (x_1 - x_0) m_s; \qquad \Delta z = (z_1 - z_0) m_s, \tag{7.6}$$

where x_0 and z_0 are photographic coordinates for the initial (basic) measurement, x_1 and z_1 are photographic coordinates for n-th measurement, m_s is the photographic scale.

For a real spatial base line, the displacement may be calculated using the equations

$$\Delta y = bc\,\frac{p_0 - p_1}{p_0 p_1} = \frac{bc}{p_0 p_1}\,(p_{s2} - p_{s1}), \tag{7.7a}$$

$$\Delta x = b\left(\frac{x_1}{p_1} - \frac{x_0}{p_0}\right) = \frac{b}{p_1}\left(p_{s1} + x_0\,\frac{p_{s2} - p_{s1}}{p_0}\right), \tag{7.7b}$$

$$\Delta z = b\left(\frac{z_1}{p_1} - \frac{z_0}{p_0}\right) = \frac{b}{p_1}\left(q_{s1} + z_0\,\frac{q_{s2} - q_{s1}}{p_0}\right), \tag{7.7c}$$

where b is the photographic base line; c constant; p_0 horizontal (absolute) parallax of a point in the initial measurement; p absolute parallax of the same point in the subsequent measurement; p_{s1} deformation parallaxes on the left slide; p_{s2} deformation parallaxes on the right slide.

The accuracy of this measurement depends on the deformation parallax of the instrument used, which is given (for the Zeiss 18/18 apparatus) by the factor

$$m_p = \pm 0.003\text{—}0.005 \text{ mm}.$$

Photogrammetric methods are also employed to advantage for measuring the deformation of canal dams and levées. The method is particularly suited for determining embankment deformations in a dam body which can be detected on its surface.

Since the aim of measurement is to provide information, it is necessary to perform a basic measurement before any operation of the structure — immediately after it is filled. Late and inaccurately performed measurements can result in the following observations.

The most widespread surveying technique, triangulation, can be effective if the following conditions are fulfilled.

(1) An extended system of check points is set up at a distance sufficiently great to eliminate the influence of the soil deformation due to the thrust of the dam, the pressure of the water, and the swelling of the soil due to permeation by water. To provide a fixed point, a separation of 300—500 m is usually needed. In unfavourable conditions, as with canal-embankment construction in the Váh valley in Czechoslovakia, a heave of the ground surface caused by the swelling of silty soil of 10—15 cm can be reached. Deformation of this scale cannot be neglected.

(2) The triangulation network fixes the positions of the theodolites, by which the reference points on the work are observed together. These theodolite stations must be perfectly steady and founded on firm ground.

(3) The use of instruments of the highest precision (such as Zeiss and Wild T-instruments) is recommended.

(4) The measurements should be taken under similar atmospheric conditions; the distortion due to refraction errors is then minimized.

Following these recommendations, a triangulation accuracy of ± 0.5 mm can be attained in all cases of measurement for canal embankment and levées deformation. In contrast, using the photogrammetric method, an accuracy of ± 3—5 mm is obtained, which can be sufficient in some cases mentioned above (land slides and other slope deformations), and here other advantages of photogrammetry can come into play.

In all cases of check and study measurements, the properties of the soil in the sub-base and that incorporated into the dam body must be taken into account. Displacement of the soil can take the form of slip of the surface or well below the ground surface. The observation point must be set on the surface or at a suitable depth, depending on the observed phenomenon.

The simplest and easiest way to gauge the performance of an earth dam is to determine surface movement. Such determination requires that a series of measuring points are located on the surface of the embankment at established locations. Periodic checks of these locations using level, transit and chain will indicate total settlement and lateral and longitudinal movement. The equipment will reveal loss of free board resulting from slow solid creep allowing enough time to make repairs. However, data secured from an installation of this type are sometimes not valuable means of determining improvements in design and construction practices. This is because it is impossible to ascertain whether movement is deep-seated or superficial, and because the magnitude of motion is very often within the limit of error of the measuring method.

In such cases, special and more detailed measurement has to be made. It can be useful to install special devices enabling us to observe the whole profile of the dam, considering a cross-section where different pick-ups can be placed. It can be useful to collect a complex series of values giving an idea of the variation of load and displacement with time and to separate consolidation of the soil mass in the embankment from settlement of the foundation.

To collect more data on consolidation, many different devices have been advocated during the last 30 years — in the USA (BUREC), France (Soletanche, Télémac), England (SR of Uni), Holland (Philips), Denmark (DISA-Elektronik), Switzerland and also the USSR, Hungary and Czechoslovakia. Many are multipurpose instruments as well as being specialist instruments, and this enables the measurement of all deformation characteristics. With the data from such instruments as tensometers, pressure gauges, pore-pressure measuring instruments, extensometers — measuring displacements and stresses in space, the behaviour of the structure can be observed.

In this way, geodetic methods (triangulation and levelling) remain as principal measurements, and physical, geoelectrical and geophysical methods also have the

role of check and study measurements performed more frequently, or automatically during the operation.

7.2 Measurement of Displacements of the Soil and Earthworks

The oldest methods used for measuring displacement of dams and levées are geodetic methods, and allowed the periodic survey of chosen stable profiles. Nowadays, these methods have been replaced or supplemented by methods of observation of reference marks. The instrumentation consists of metal rods usually attached to the top of the substratum, and sliding in a tube (bitumen-packed). These mark rods are put into inspection shafts and are some ten meters (10—30 to 80 m) in length. A second rod fixed to the overburden at the base of the filter records the settling at that point. The measurements are made by levelling.

Telescopic tubes were introduced in the USA by BUREC in the forties, and consist of plates with tubes passing through the centre. Any number of plates desired can be arranged on the same vertical. The tubes are connected to each other by tubes of slightly larger diameter, in which they slide. Measurements are made by means of a "torpedo" provided with two pawls, which is lowered to the bottom of the hole. When this device is raised, the successive engagement of the pawls with the lower edges of the short tubes enables the levels of the different plates to be noted. The plates are usually spaced 1.5 meters apart, enabling a number of points to be observed.

Such telescopic tubes have been installed not only in the USA but also in almost all European countries for observing the displacement of canals and levées. At present, this method of observation cannot be considered to be effective or accurate enough. New electronics, sonic and laser-equipped devices give ready and accurate results (Danel, Schodl et al., LDA Symposium, Copenhagen, 1975).

Nowadays, an attempt is being made to provide the dam with control elements which, giving information continuously on the actual behaviour of the structure, make it possible to know the variations with regards to the assumed hypothesis. In canal dams and levées, settlement and displacement in the vicinity of the embankment are in question. Even with best quality levée subsoil, both vertical and horizontal displacement very often occur (Fig. 7.2). In canal embankments (Fig. 7.2a), the settlement line will not be coherent as is shown by results from measurements (Fig. 7.2b) on the gallery of the head-race canal at the power station of Morge in France (1964—1965), where the settlement under the embankments reached more than 22 cm on the axis of the embankment, while on the axis of the canal it was only 8 cm (Coulomb and Moreau 1967).

Some instruments and probes allowing the investigation of vertical displacement and sliding movement will now be mentioned.

For deformation readings on the surface and at separate points in the layers at small depths under the ground surface (less than 3—4 m) in earth dams, simple contact feeler transducers have proved successful (Fig. 7.3). The contact feeler (1) in the transducer presses against the surface of the observation point (steel, cast

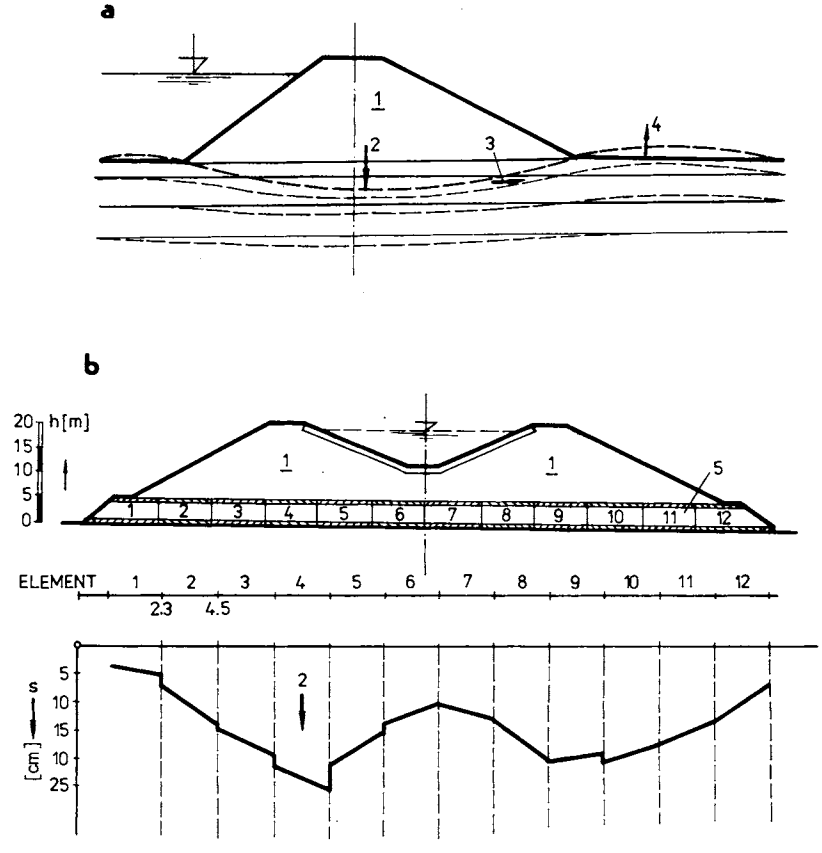

Fig. 7.2. Settlement and horizontal movement caused by embankment. a — levée on soft subsoil, b — canal dams and its settlement; 1 — embankment, 2 — settlement, 3 — horizontal movement, 4 — heave, 5 — gallery.

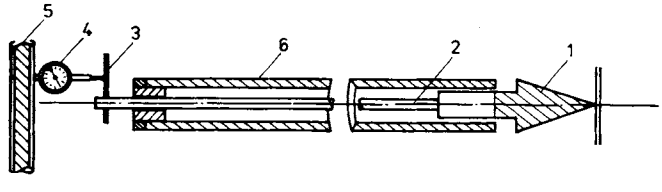

Fig. 7.3. Tube with measuring point. 1 — point, 2 — pole, 3 — arm, 4 — measuring gauge, 5 — rigid bim, 6 — plastic tube.

iron or brass plate), whose vertical motion is trasferred to a stiff bar (2), against the arm (3) of which the stiff measuring bridge (5) and dial indicator (4) rest. The stiff bar slides in a PVC protection pipe (6) of diameter 25 mm. The dial indicator (4) is attached to the measuring bridge by means of magnetic holders. The dial indicator, which measures displacement with an accuracy ± 0.01 mm, allows measurement of point displacement with an accuracy of ± 0.1 to ± 0.025 mm. This accuracy is much better than that of the telescopic pipe BUREC. However, the simple measuring device mentioned above can be used only in the short term.

Cambefort (1972) introduces a special procedure for investigating the movements of an earth mass by electric carottage using a sonde (electrode) of a cylindrical metal probe (Fig. 7.4), which is lowered into a given earth mass. If this electrode passes through a surface of a slip, an anomalous step on the diagram of carottage will show Fig. 7.4b, as a consequence of the diminution of electrical resistance.

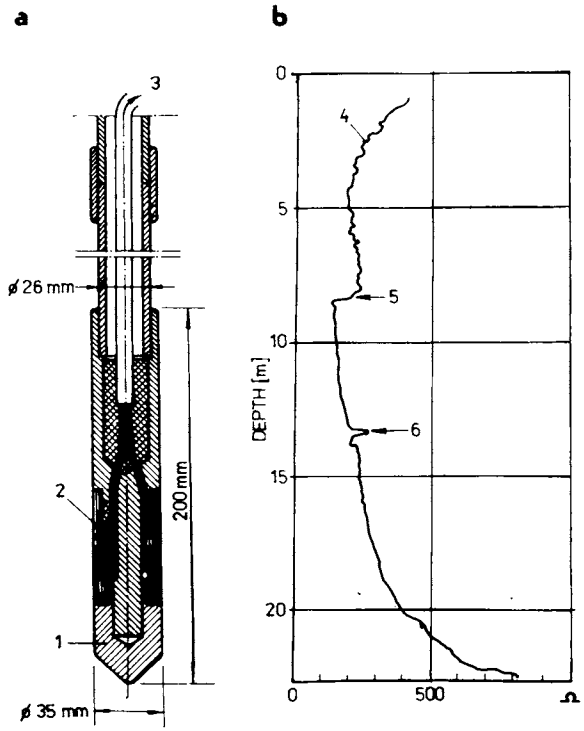

Fig. 7.4. The probe of Sederblom and diagram of electric "carottage". a — probe detail, b — electrical resistance depending on the depth; 1 — contact point with soil, 2 — ring isolation, 3 — connected with Wheatstone bridge, 4 — the curve $\Omega = f(D)$, 5 — failure surface, 6 — sand layer.

In Terzaghi's lectures (1974), some interesting results from displacement measurements can be found. Wilson (1974) describes an excellent example of measurement of a fill-activated landslide in California where an old levée (founded on various sedimentary formations) was reconstructed. In the past, in the Por-

tuguese Bend area on the Pacific Ocean coast, scattered volcanic ash has been deposited by volcanic activity and has settled down through the water. The road embankments and other structures constructed in the fifties suffered a tremendous movement up to two centimeters a day, mainly in periods of rainfall. Such a large displacement can be observed by geodetic methods, and also by optical levelling, triangulation, and photogrammetry.

The measurement of settlement and horizontal displacement of the Atchafalaya levée (Fig. 7.5) in Louisiana (USA) is an example where the vertical and horizontal displacements are related to the profile of the embankment and indirectly to the stress-strain conditions. It was apparent during construction (1964) that the crest of the embankment was settling downwards and that the adjacent slopes were deflecting outwards away from the fill. The soil profile consists of about 13.5 m (40 ft) of soft peat and organic clay above a layer (28 m) of soft medium clay which

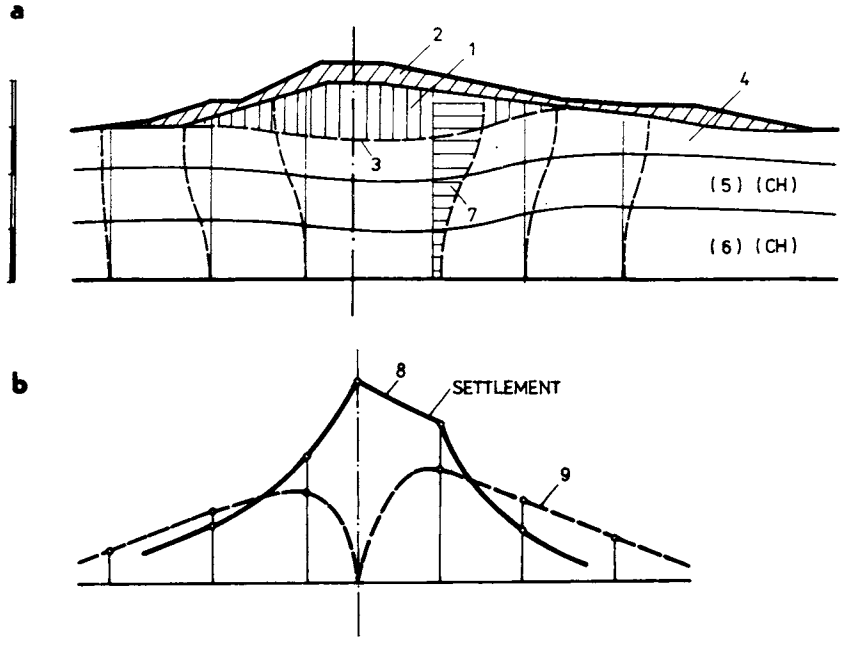

Fig. 7.5. Atchafalaya levée — scheme of displacement. a — scheme of the structure and subsoil layers, b — displacements; 1 — existing levée, 2 — new fill, 3 — settlement line, 4 — flat and soft organic clay, 5 — soft to medium clay, 6 — medium clay, 7 — vertical stresses acting in the vertical level, 8 — values of vertical displacement, 9 — horizontal displacement.

occurs progressively in the lower portion of the peat and soft organic clay. The total horizontal and vertical movements that developed in the first 18 months following construction reached a maximum value of 1 m (settlement) on the dam axis, and more than 0.5 m under the slope portion (horizontal movement). It was probably

more than 60% of the height of the embankment and over 25% of the thickness of clay and peat layer. The movements reduce more or less linearly, at a rate which indicates zero displacement at a distance of about 150—160 m (500 ft) from the dyke. At the end of 6 months, the movements were sufficiently large that vertical cracks developed in the embankment itself and at the toe of the embankment. This example shows that lateral movements resulting from the construction of relatively shallow embankments on soft ground can create problems. Thus the design of such embankments is extremely difficult, as was concluded by Wilson (1974).

To increase the storage capacity of *Lake Zumpango* — in the northwest part of the valley of Mexico — an earth levée of 6.50 m in height was built. The foundation consists of an upper layer of stiff silty sand, with a thickness of 1—2.5 m underlain by a soft clay layer 2.0—4.0 m thick. The clay layer has a natural water content up to 400%, and so has a very low shear strength. Because theoretical methods do not take into account the interaction between the upper stiff layer and the soft clay, the construction of a test embankment (Fig. 7.6) was decided upon. The instrumentation of the structure allowed the measurement of settlement, compression and extension. The soft clay layer extruded laterally. Because of the layer of stiff silty sand, there was no lateral extension or spreading of the test embankment itself. On the contrary, the settlement of the central portion of the embankment, caused by the extrusion of the soft clayey layer, resulted in inward movement of the embankment. Unequal tension in the subsoil layer caused some cracks on the slope of the embankment.

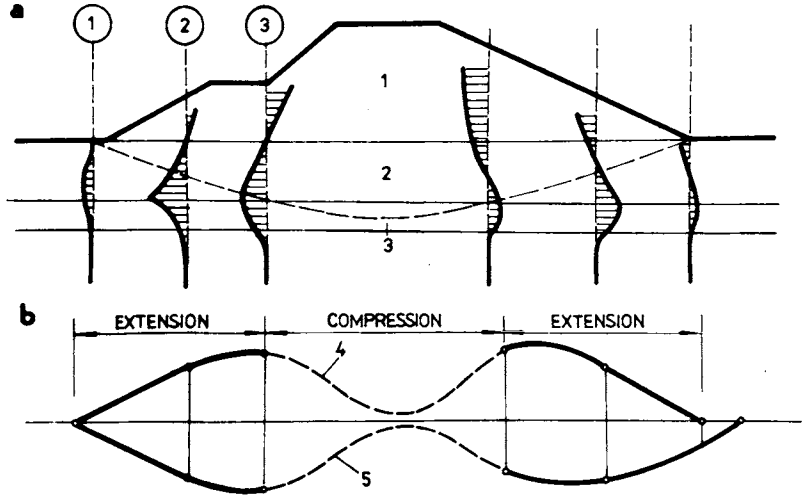

Fig. 7.6. Zumpango test embankment and its tension. a — scheme of the structure and subsoil layers, b — movements; 1 — embankment, 2 — shift silty sand, 3 — soft clay, 4 — inward movement of surface, 5 — outward movement of soft clay.

The measurement of displacement at various points near a levée in California, which failed in 1964, showed that a small hydraulic fill and artesian pressure can cause instability in terrain some hundred meters distant from an embankment.

Three examples are given here to show that the strength and deformation characteristics of the materials composing the dam and subsoil influence the displacements of individual layers and that of the whole territory. Thus the relative displacement at the zone boundary should always be taken into account in analysis, when a large divergence of deformation characteristics is present. It is not exceptional for stress redistribution to take place in the subsoil and in the body of an embankment consisting of diverse soils. Consequently, a zone which appears in conventional analysis to be unstable, changes into a stable zone and vice versa (Matsui 1976). The failure of the levée in California, mentioned above, can be cited as an example (Wilson 1974).

7.3 Measurements of Stresses and Pore Pressures

Pressure-measuring instruments were first used during dam construction. The construction (Fig. 7.7) of such instruments presented certain difficulties in that they themselves constitute a disturbing factor in the medium under pressure. In the

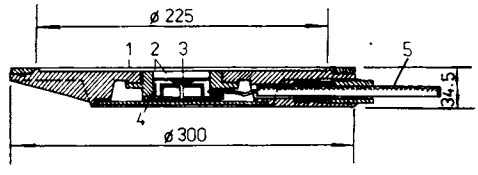

Fig. 7.7. Pressure gauge for determining soil pressure. 1 — membrane, 2, 3 — transducer.

fifties, many instruments appeared from such sources as Swedenborg, Klejlman, Johansen, Civil Engineering Department, BUREC USA, etc. Nowadays, stresses are usually recorded using pressure cells. This sort of pick-up cell (Fig. 7.8) senses the stresses translated hydraulically (by oil) to a membrane, via this transducer (electromagnetic of electric), and thence to a reading or recording instrument. The pressure gauge senses stresses via a membrane and usually a bridge of strip strain gauges.

Another system of pick-up is *the electrical pressure cistern,* based on capacity variation of condensers with a dielectric, is very often found in Scandinavian countries today. The capacity measurements are made with a Wheatstone bridge constructed by Philips in Holland.

Uplift pressures in foundations are determined by means of specially constructed bore holes, from which manometer pipes lead to the surface — above the crest or dam slope (Fig. 7.9), so that the measurement of the water level in them can be

made, and thence the magnitude of uplift determined. Water pressures (uplifts) at various elevations can be measured by simple piezometric tubes (Fig. 7.10) or by double piezometers. The height of the water level in the tube, as a measure of uplift, can be determined by means of Rangun's whistle or some other pick-up, as we shall mention later (Section 7.5).

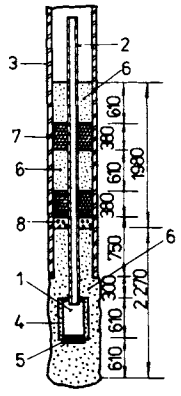

Fig. 7.8. Open piezometric gauge. 1 — chamber, 2 — tube, 3 — casing, 4 — Norton's reference tube, 5 — rubber stopper, 6 — sand, 7 — bentonite, 8 — modified sand.

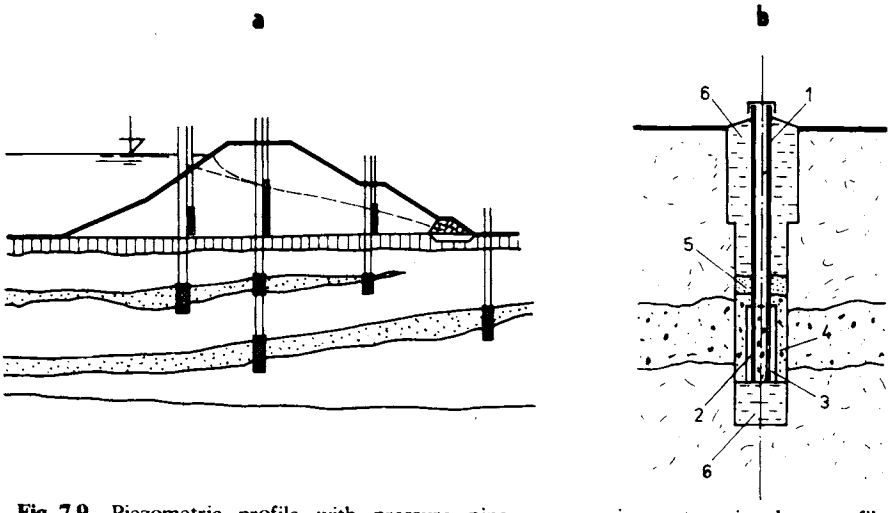

Fig. 7.9. Piezometric profile with pressure pipes. a — piezometers in dam profile, b — stand-pipe measuring pressures in a layer; 1 — tube, 2 — perforation, 3 — porous tube, 4 — fine gravel, 5 — sand, 6 — clay.

Measurements of pore pressures in fine-grained soils are based on a variety of principles. These are three methods most frequently employed, namely hydraulic (with water, mercury or oil as the usual media), resonance (water acting upon a cell containing a vibrating string) and magnetoelectric.

Hydraulic-transducer piezometers (Fig. 7.11) are based on the same principle as the previous type, except that the water level (pressure) is not transduced in the probe itself, but is transferred to the measuring instrument via pipes. This allows the piezometer probe to be put into the soil (the dam body), while the actual readings may be made at some distance.

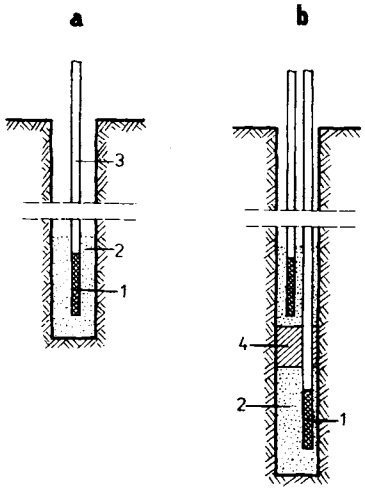

Fig. 7.10. Single- and double-tube piezometers. a — single tube, b — double tube; 1 — perforated section of tube, 2 — sand, 3 — tube (∅ 20 to 30 mm), 4 — seal horizon (clay stopper).

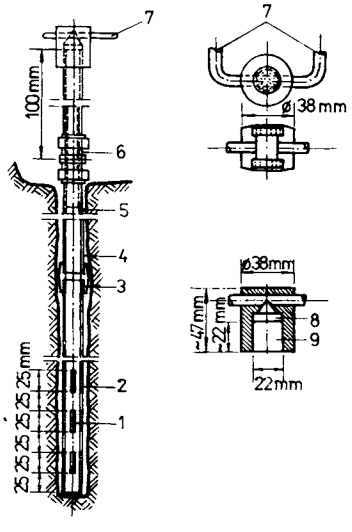

Fig. 7.11. Hydraulic-transducer piezometer. 1 — perforated end, 2 — loose earth fill, 3 — coupling, 4 — clay stopper, 5 — plastic tube, 6 — elastic coupling, 7 — plastic tube, 8 — recess for sealing ring, 9 — hole for inserting the joining piece.

The Télémac string probe (Fig. 7.12) can be mounted directly into the dam body or its foundation. The pick-up cell (1) is inserted into a bore hole, filled in with sand (2) and insulated with clay (3), through which a cable (4) is taken to the recording instrument. Water expelled from the soil whose pore pressure is to be determined percolates through sand and porous disc (5) to the pressure cell (7) containing a taught string (6). This string is excited and its vibrations are transferred to the receiver containing an identical string stretched by a known force. Stress (pore pressure) in the soil at the measuring point is then determined by the resonance of this string.

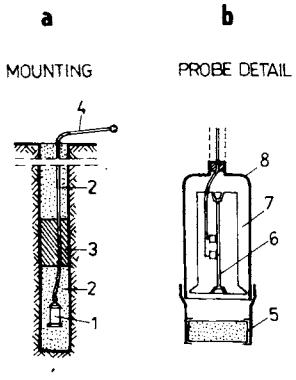

Fig. 7.12. The Télémac pore-pressure pick-up. a — method of mounting, b — probe detail; 1 — pressure cell, 2 — sand, 3 — clay stopper, 4 — cable (to recording apparatus), 5 — porous disc, 6 — string, 7 — pressure cell, 8 — case.

The US Bureau of Reclamation membrane pick-up (Fig. 7.13a) resembles the Télémac in appearance, but it contains a membrane sensor instead of string, and this membrane is mounted perpendicular to the longer axis of the probe. Water pressure acts upon the membrane which activates a contact closing an electric circuit. By a stream of air of known pressure, led into the chamber through lengthwise holes, this contact may be broken. This break will take place when the

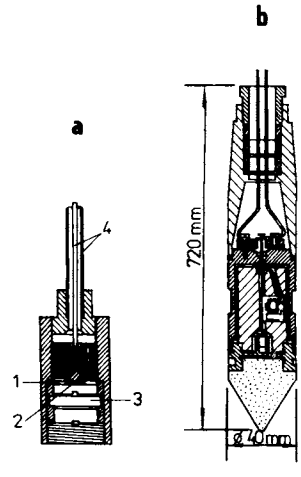

Fig. 7.13. Pore-pressure "heads". a — Bureau of Reclamation, b — Maihak; 1 — membrane, 2 — contact, 3 — porous disc, 4 — copper tubes.

pressure of the air stream equals that of the pore pressure being measured. For this reason, such a pick-up is sometimes called an electric-conversion pneumatic pressure pick-up — as we shall mention again.

Maihak's string pick-up (Fig. 7.13b) is based on the same principle as the Télémac pick-up, but has a solid porous tip instead of a plate (disc), which in the preceding types involves certain mechanical disadvantages, such as bending.

While in the USA and Asia (India), BUREC instrumentation is most commonly used for dams, Maihaks's and the Télémac apparatus can be found in operation in Europe, with good results. The USSR has developed its own instrumentation for measuring stresses and pore pressures in dams and levées and this is also used in Czechoslovakia, Poland and Rumania, as well as the pressure gauge and piezometers named above.

Alimak's BAT piezometer introduced in recent years (LINDEN-ALIMAK, 1978) has two separate parts: the piezometer and measuring unit (sensor equipment). The piezometer-filter section has a ceramic filter through which pore water communicates with the nipple (Fig. 7.14). The filter tip is screwed into a galvanized pipe, which is driven down into the ground to a predetermined depth. It has no sensitive parts: the air can be eliminated from the pores of the ceramic filter without danger. To measure the pore pressure, a sensor is lowered down into the pipe until it reaches the nipple of the filter tip. A stabilized value of pore water pressure (A) is measured when the sensor sleeve fits over the nipple of the tip. When the sensor is lifted, so that it no longer fits over the nipple, a value (C) of the water column in the connecting pipe is measured. If the water column in the connecting pipe is B, the value of pore pressure (u) is

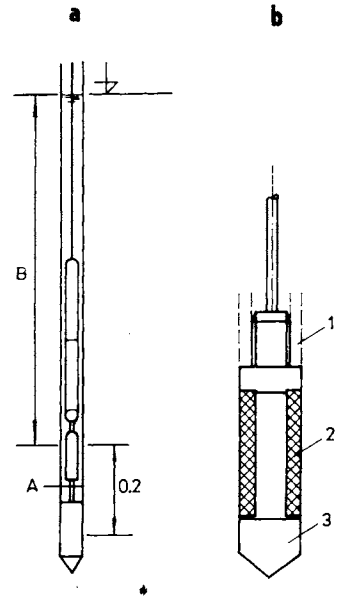

Fig. 7.14. Alimak's BAT piezometer. a — arrangement of the stable part, b — detail of the probe; 1 — stainless nipple, 2 — ceramic filter, 3 — thermoplastic tip.

$$u = A + B - C + 0.2\ \text{m} \quad [\text{m}]. \tag{7.8}$$

A digital read-out gives an immediate reading. Accuracy is ± 1 cm for the water column.

The advantage of this piezometer lies in the simplicity of its frame and its mode of use. A single measuring unit handles hundreds of filter tips.

It is difficult to describe every sort of apparatus (permanent and portable) used in measuring stresses and pore pressures, developed since the 1930s, when US BUREC installed the first in certain earth dams in the USA. It can be said that the first attempt to get direct information about stress-strain conditions was made on large dams. Little attention was paid to canal dams, and levées, since small earth works were ignored in this respect. Designers and constructors explained: results from instruments indicate that most embankment consolidation is accomplished during the construction period. However, they forgot that, in contrast, the foundation may be consolidated for some time after construction is completed. In the construction of levées, we very often come across unconsolidated soils in the substratum of the structure. Such a substratum has to be checked out in all directions.

In canal-dam construction, we must keep two things in mind. Pore-pressure studies have shown that the pressure developed in impervious materials during construction usually exceeds any pressure developed thereafter. However, in the case of a failure of the lining sealing membrane, the connection of canal water with a layer line of low permeability (silty loam) can lead to pore pressure increases. This fact about water pressure can change the stability conditions. Such a leg of the dam or levée substratum has to be checked by pore-pressure measurement.

The pore pressures of the dam itself are to a large extent in the hands of the designer and constructor. They have to modify the construction method to reduce pore pressure as much as possible. The limiting moisture allowable during construction and the extent of pore pressure has to be anticipated (Chapter 3).

7.4 Hydraulic Measurements and Special Types of Observation

For observing the behaviour of dams and levées, hydraulic measurements have primary importance. Above all, this means flow measurements and filtration observation, and connected water losses. In canals, we observe the influence of filtration on the regime of underground water. Besides this, in some cases the influence of filtration water on the stability of earth in the body and subsoil of dams is observed. This was mentioned in Chapters 1 and 6. All data usually refer to water levels in rivers or canals. This level is usually measured by means of limnographs (Fig. 7.15). Further, in large waterway and power-station canals, two kinds of

measurements are often made: those of the hydrodynamic effects of waves, caused by wind, vessels or specialized canal operations (sudden closing of turbines — shock waves), and measurements of ice effects on the stability of the lining or pavement.

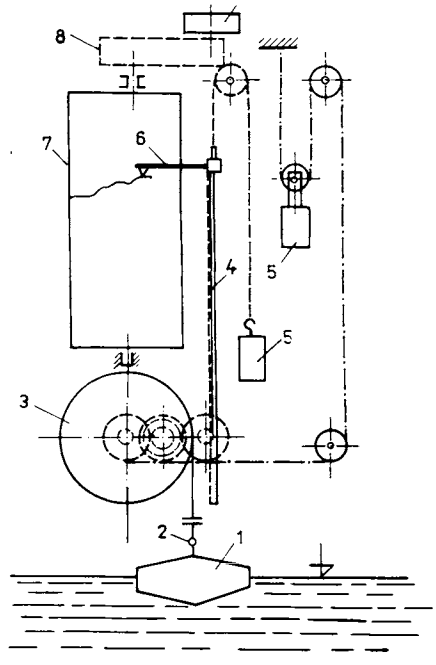

Fig. 7.15. Water-level registration by means of Holzschauer instrument. 1 — float, 2 — transmission of nickel, 3 — wheelwork, 4 — lath with cog-wheel, 5 — weight, 6 — control stick with plotter, 7 — drum, 8 — transmission to the drum, 9 — clock.

General principles of hydraulic measurements are partially described in certain basic literature (Davis and De Wiest 1966). Some special aspects of underground water effects are described by Harr (1962). A work by Yakshchin (1962) summarizes the experiences of designers in the USSR in cases when more attention is paid to territorial stability than to measurements of water losses. The works of Turnbull and Mansur (1954 and 1961) are amongst the best known concerning hydraulic problems of levées on big rivers. In these works we find a summary of American experience, gained during construction of antiseepage measures on the Mississippi River, under conditions of severe defects in the levée subsoil. Work by Czechoslovakian (Bažant and Hálek 1968) and Hungarian (Ihring and Lászloffy 1954, Kézdi 1967) specialists, which describe experiences in measurement and observation of the Danube levées, have similar characteristics.

As regards the methodical approach to observation of water-level efects during flood, the work of Gyalokay (1956) is interesting. He observed for an intermediate land levée, the possibility of expressing the influence of a rise in water level on the groundwater level in territory adjacent to the river Danube. Radchenko (1976)

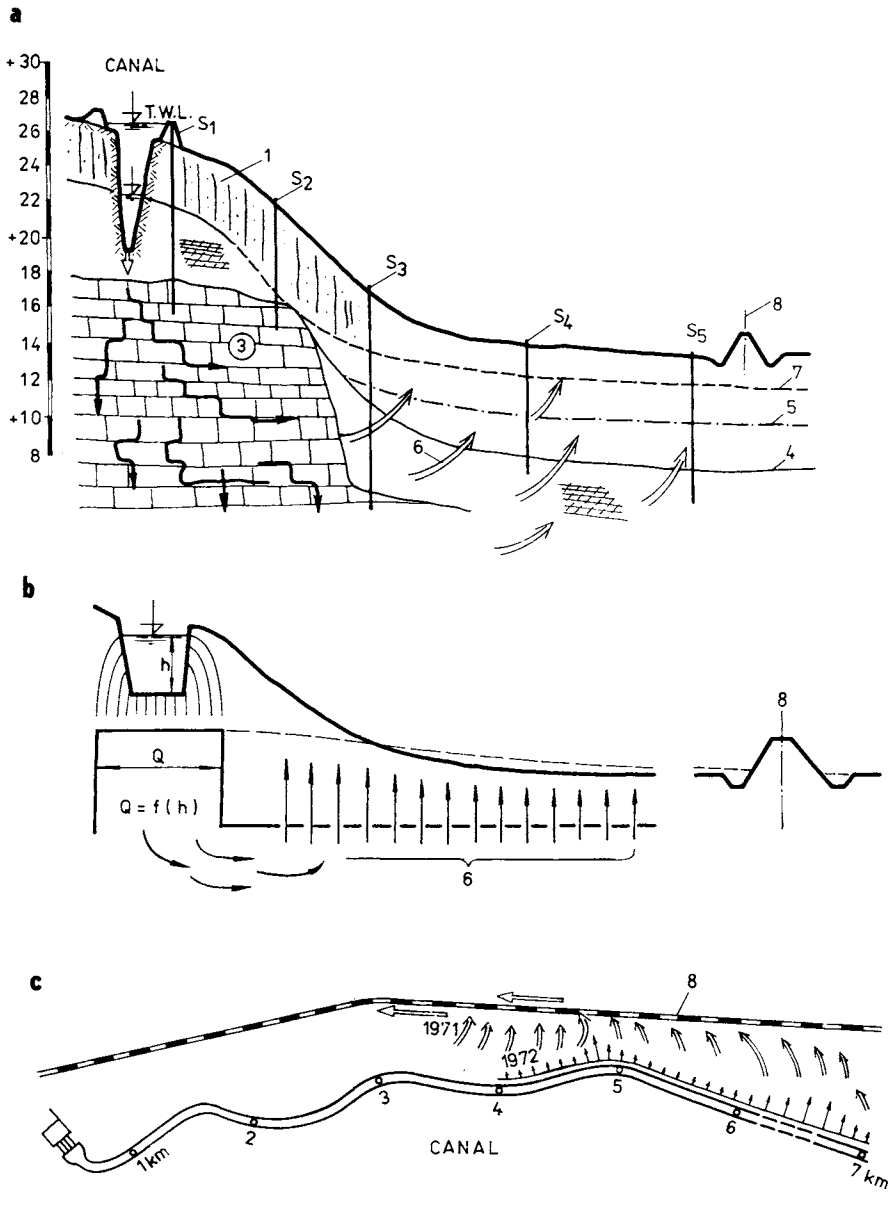

Fig. 7.16. The influence of the canal water on groundwater level in the vicinity. a — geological conditions, b — calculating scheme, c — the location scheme; 1 — overburden, 2 — soils of low permeability, 3 — lime stone, 4 — soil interface, 5 — original water level, 6 — water-pressure direction, 7 — raising water level, 8 — railway; $S_1 \ldots S_5$ observed bore-holes piezometers (adjustment after Gazdaru et al. 1974).

used experimental-theoretical methods instead of direct measuring methods. He observed the influence of the Danube embankment on the capacity of water sources (pump wells, built along levées). Whose capacity increases filtration water, gathered in channels built along the levées.

One of the frequent problems in which direct and indirect hydraulic measurement methods are applied, is that of filling the permeable ground layers with water, which infiltrates from the canal (Fig. 7.16). This problem is typical in the main for irrigation canals, where the profiles are not packed for the above-mentioned reasons. When raising the water level (h) in the canal, the gradient of water filtration also increases. In places where the canal bottom approaches a series of strata of permeable rock (calcite) in the subsoil, fissures can lead to short-circuiting to the water-bearing subsoil. The level of the groundwater rises until it reaches the surface, where it can endanger land and buildings. In the above-mentioned case, a railway (8) was thus endangered.

A similar case, described in the literature (Gazdaru et al. 1974), was an irrigation canal, built on a slope which conducted $Q = 80\ m^3\ s^{-1}$ of water. Water filtration amounted to $0.37—1.26\ m^3\ s^{-1}$, i.e. $0.05—0.17\ m^3\ s^{-1}\ km^{-1}$, and that is 0.46—1.58 % of the water flow in the canal. Therefore, the problem here was not one of water losses, but one of danger to the landscape. Landslides resulted, the railway was endangered, and the environment was damaged.

This case concerns the question of water-level measurement in bore holes, filtration checking measurements, and determination of permeability and filtration intensity I_s, the value of which

$$I_s = f(h),$$

determines the quantity through water head h.

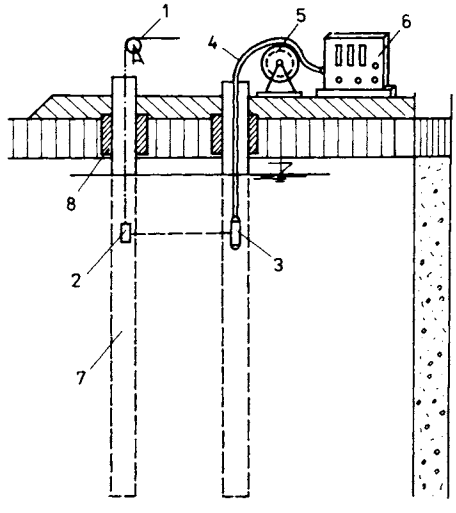

Fig. 7.17. The application of nucleonic principles of measurement (isotope method) in the field. 1 — hanging of tracer, 2 — radioisotope (^{60}Co), 3 — G-M detector, 4 — cable, 5 — windless, 6 — nuclear counter, 7 — perforated tube, 8 — sealing.

This example of measurement and observation is given because it is a very simple case, where the simplest devices, simple measurement (bore-hole observation), and water-level measurement enable us to gather information on any undesirable effect, and to propose methods for removing the imperfections. In this case, the

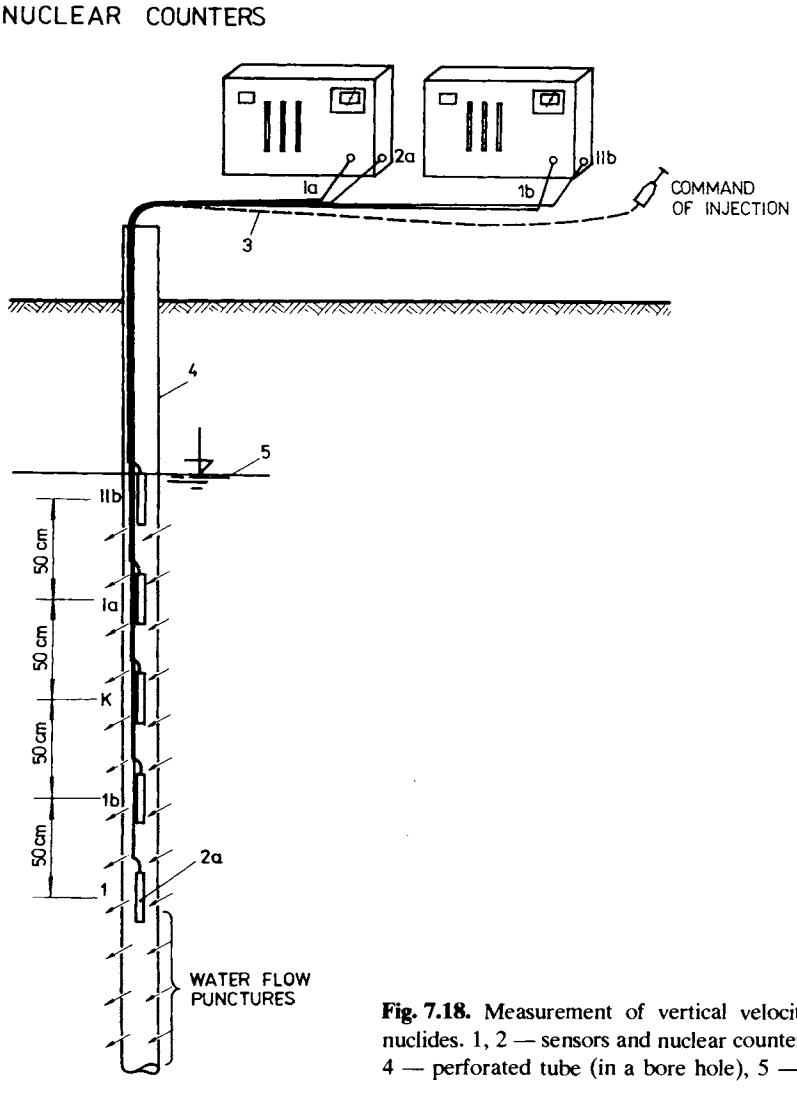

Fig. 7.18. Measurement of vertical velocities by means of nuclides. 1, 2 — sensors and nuclear counter, 3 — to injector, 4 — perforated tube (in a bore hole), 5 — water table.

paths of groundwater motion, obtained by a theoretical-empirical method, were also depicted.

At present, we also know many methods for direct and indirect measurement of hydraulic quantities, which make the determination of underground water flow

possible both in the body of embankments, and in the subsoil. Geophysical methods of measurement have been relatively well tested in embankments and levées in Czechoslovakia (Fig. 7.17). Methods of water labelling by means of radionuclides have also been tested. Usually the so-called single-well method, allows the determination of the horizontal velocity of water motion, as well as the vertical velocity. Vertical rate of flow is determined by means of the continuity equation (motion) of labelled water in a vertical direction. By means of this method, it is possible to determine the flow direction, and indirectly the active ground porosity. This is advantageous as regards time economy, and the simple methods and use of portable injection, transduction and detection devices are also advantageous (Fig. 7.18).

Table 7.1. Summary of equipment to level and water motion velocity pick-up

No.	Equipment		Purpose	Principle
	Designation	Specification		
1	Limnograph	GR-38 (USSR)	Level measurement	Float — clock — — work-drum
2	Limnograph	Metra 501	Level measurement	Float — clock — work — perforated tape
3	Level gauge	Holzschrauer	Level measurement	Float — toothed lath-drum
4	Level gauge	UDH 2	Level measurement in bore hole	Ultrasound reflection from water surface
5	Current meter	GR-21 (USSR)	Velocity measurement	Screw — revolution measurement
6	Current meter	GR-55	Velocity measurement in bore hole	Screw — revolution counter — filament lamp
7	Radiometer	RD-JS	Water-motion-velocity measurement	Gamma-emitter pulse measurement
8	Thermal probe	VÚVH (CSSR)	Velocity measurement	Thermistors — Wheatstone bridge — voltmeter
9	Drainage flow meter	SEV NIIGIM (USSR)	Flow-rate (q) measurement	Microscrew
10	Measurement of solid particles	VITUKI (Hungary)	Turbidity measurement	Am-241 emitter detector
11	Geophone	VITUKI	Flow-rate measurement	—
12	Wave motion pick-up	VITUKI	Wave spectrum pick-up	Float — potentiometer

We can observe the velocity of underground water motion by means of a simple current meter (Hálek and Rybnikář 1963).

In earth dams, older geodetic methods and methods of marking by means of chemical solutions and colouring substances are widely used in general.

Just as geodetical measurement — precise levelling — is fundamental to deformation measurement, the measurement of water level is fundamental to hydraulic-measuring methods. Most water-level transducers probably exist for that reason. The number of patented water-level transducers in the year 1978 reached over 200 in Europe and over 20 in Czechoslovakia. The catalogue of products for the eastern countries shows 16 water-level pick-ups. Some of these and other devices for hydraulic measurements are shown in Table 7.1.

In dams with jacket concrete or asphaltic/concrete sealing, special hydraulic measurements must be carried out. We can determine the permeability by means of special modified permeability meters, while the water losses are determined so that in the sealing element we form a system of channels — usually in the slope and near the base. These are directed towards the measuring point, where we measure the rate of flow quantities.

7.5 Stable Instrumentation and Telecontrol of Instruments

The large extent (especially in very long embankments) of canal embankments and levées, the large number of measuring points or observation objects, an ever increasing number of observed values, the use of repeated and continuous control, the requirement of speedy information and its readibility all lead to the fact that the classical methods of dam observation by means of portable instruments — geodetic methods — are fast be coming redundant. Modern replacement methods consist mainly of indirect measurement and telemetring, as well as automatic and semi-automatic measuring processes. It is characteristic for these measuring processes, that the measured quantity is read out at the observed point. This quantity is transduced to the appropriate electrical quantity and the signal is taken to the measuring point, which can be remote from the observed point. We can take the signals from several points to one point, the measurement centre, or connect it to various pick-ups, which read out various quantities (deformations, tensions, pore pressures, water levels, etc.). For reading out and registering several signals at one point, it is necessary to elaborate the collective measurement and observation projects.

These projects, designed in Czechoslovakia, the USSR, France, FRG and other European countries, usually anticipate the measurements of these phenomena, which give a view of the load state and earth-body response to these loads:

(a) state of water level in the river;
(b) stress magnitude on selected profiles (where the stress can reach critical values);
(c) displacements (deformations) of points in the embankment body;
(d) displacements of points in the subsoil — subsoil settlement;
(e) displacements of points on the outline — on the embankment slopes (slope deformation);
(f) displacements of points at joints with concrete objects — joint observation;
(g) ice pressure, pressure effects of wind-produced or other waves;
(h) water level (underground and filtration water) in bore holes;
(i) volume of filtration water;
(j) quantity of solid particles, displaced by water — these are settled in sedimentation vessels.

Comparing the above-mentioned amount of information required with the amount and quality of information observed in sample earth dams equipped with measuring devices 30 years ago (Drouhin et al. 1948), we can see that today we require much more information as far as the number (3—5 times more per kilometer) and accuracy of observed quantities, are concerned.

Thus, within the framework of a general discussion on canal dams and levées, we cannot discuss measuring methods and particular instruments in detail: we must limit ourselves to simply noting the measuring systems, and we also give brief descriptions of some of the most used measuring pick-ups, instruments and devices.

In the diagram (Fig. 7.19) is shown a summary of measuring instruments and recorder sets. It especially concerns the three levels of measurement, which differ from direct displacement measurement in precise levelling and other traditional measuring methods.

Indirect measurements — the ten above-mentioned quantities may all be observed indirectly, but the advantages of these measuring methods are only demonstrated in some of them. At present, the methods of measuring water level and displacement magnitude — settlement of embankment and subsoil — are those most complete. The magnetic-electrical principle, which makes possible the transfer of a measured quantity to a distance of some tens of meter, up to 120—150 meters, with an accuracy of 1—5 mm, is suitable as a way of measurement and transfer of a measured quantity from the sensor to the recorder.

Grading instruments (which have a measuring angle range of 5—6° up to some tens of degrees with a measuring accuracy of 1—2′ down to some tens of seconds) make possible the sensing of deformation and deviation from the required direction (from slanting slopes and others similar).

In Table 7.2, we summarize the sensors used in indirect measurements in Czechoslovakia. Some comments on the quantities measured are given.

Relative displacements are measured by means of extensometers and different types of dilatometers. The transfer of quantities measured by means of these

Table 7.2. Summary of pick-ups used in indirect measurement

No.	Pick-up		Object and range of measurement			Remarks on installation
	Designation	Principle	Object	Range	Accuracy	
1	Magnetic rod probe (HSS-74)	Magnetic	Relative displacement	to 20 m	± 1 mm	PE tubing in trench
2	Magnetic drawing probe (HST-74)	Contact connecting	Horizontal control points	up to 120 m	± 5 mm	Tubing and drawing device
3	Magnetic hanging probe (MSZ-74)	Magnetic	Settlement in bore holes over each other	80 m	± 3—5 mm	Builded in bore hole (casing)
4	Magnetic probe with float (MSH-74)		Water level		± 3 mm	Piezometric bore hole
5	Inclinometric cart	Resistance tensometer	Slope deformation	± 30°	± 1′	On the slope surface
6	Inclinometer		Deflection	±6°	± 10′	In the bore-hole casing
7	Depth mark	Resistance (inductive) transmitter	Relative displacement	0—80 mm	± 1%	In bore hole
8	Extensometer — rod	Transmitter	Point displacement	0—40 mm	± 1%	Casing
9	Extensometer — magnet	Magnetic	Point displacement in embankment	200 m	± 20 mm	In tube

No.	Pick-up		Object and range of measurement			Remarks on installation
	Designation	Principle	Object	Range	Accuracy	
10	Resistance extensometer	Resistance transmitter	Displacement of two points	0—200 mm	± 1%	In trench in embankment
11	Dilatometer — outer	Resistance	Joint gaping	0—10 mm	± 1%	In the surface
12	Dilatometer — inner	Inductive		0—40 mm	± 1.5%	In embankment
13	Electrolytic pendulum	Electrolytic	Deflection	0—50 mm	± 0.5%	In vessel
14	Float water level	Resistance inductive	Settlement difference	± 20 mm	± 1%	Two vessels and tubing
15	Pore-pressure gauge	Télémac	Pore pressures	to 120 m	± 3 mm	After producer instructions
16	Pore-pressure gauge	Maihak		to 150 m	± 2 mm	
17	Manometer with transmitter	Resistance	Uplift water under pressure	10 m	± 250 mm	In tube
18	Pneumatic equipment	Pneumatic	Free level	10 m	± 250 mm	Tubing
19	Filtration gauge with float	Resistance transmitter	Water volume (q)	5 l s^{-1}	± 1%	Vessel and overflow
20	Signalling element - magnetic switch	Magnetic contact	Displacement	to 3000 m	± 10 mm	On the structure or pick-up

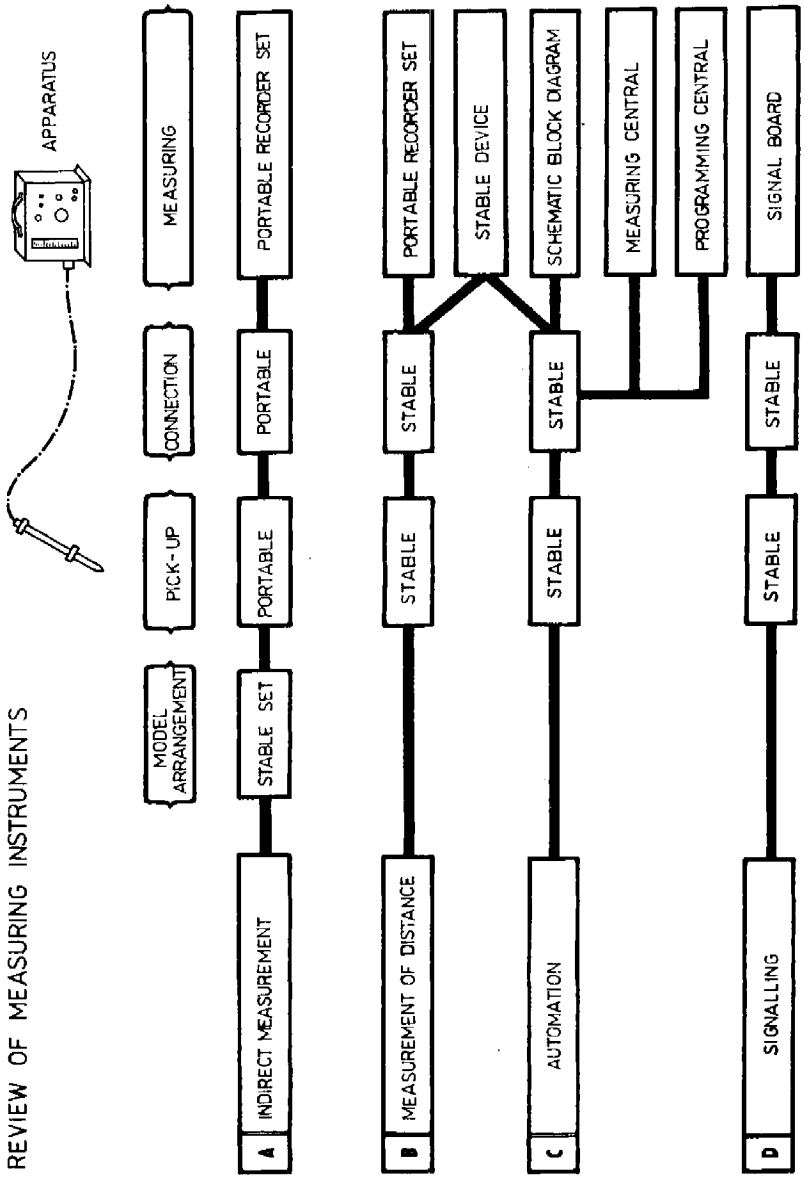

Fig. 7.19. Categories of measurements and apparatus arrangement.

sensors meets with certain difficulties as do the installation of wiring and instruments, which are placed in an excavated earth trench. It is very difficult to protect them from damage. The transfer of measured quantities (by the electromagnetic or resistance principle) is often influenced by the relatively great clearance of sensor dead travel (retardation) which makes the measurement inaccurate.

The same problems occur in different types of grading instruments, especially those which measure *settlement difference.*

Direct measurements — uplift and water-level measurement is based on the manometric (pneumatic) principle, which does not allow long-distance transfer of a measured quantity.

Measurement of seepage quantity based on the principle of volume measurement or float-position registration requires the connection of an electrical circuit, which enables telemetric registration.

In many instances, the purpose of *signalling devices* is to give a warning against a certain significant (usually "critical") value of the measured quantity. This warning is usually made by means of contactless switching.

Measuring instruments which make telecontrol possible use proper *compensating bridges* for indirect measurement. They connect the pick-up with a resistance transmitter, and they make possible the read-out of the resistance value (of the measured quantity) on a suitably adjustment segmented circular scale. In field measurements, we prefer portable instruments, powered by battery.

Registration instruments which are used for different types of measurements, are suitably adjusted with regard to the sort of quantity observed, its magnitude, and the distance of the registration instrument from the pick-up point, as much as the special conditions, to which the instrument is exposed.

An effort to concentrate the measuring instruments at one centre is characteristic of measurement on canal dams and levées. Corresponding suitably transformed signals lead to this centre (usually transferred by electrical mains) and they are carried to display for read-out and for registration.

In the last decade, in all countries with progressive measuring techniques (USSR, England, Denmark, France, Holland, FRG, USA and others), we can witness the automation of observed quantity pick-up and the observing of some sections of dams by means of automatic centres, manned in the past by hundreds of watchmen. The developed Czechoslovak electrotechnical industry has made possible the production of efficient and accurate measuring instrument: a summary is shown in Table 7.3.

At present, some tens of particular quantity pick-up devices (deformation, stress, filtration quantity and others) have been developed in the world — mainly in West Europe, the USA and the USSR. These devices give information on the body of dams and their subsoil behaviour. Well known companies like Hottinger—Baldwin

Table 7.3. Summary of measuring instruments

No.	Measuring instrument	Purpose	Application
1	Compensating Bridge VÚIS MK-75	Indirect measuring and telemetering	Pick-ups with resistance transmitter
2	Indicating Instrument ZEPAX	Telemetering	Pick-ups with resistance and inductive transmitter
3	Point Recorder ZEPAKORD	Continuous telemetering at 1—6 measuring points	Pick-ups with resistance and inductive transmitter
4	Compensating Recorder ZEPAREX	Continuous telemetering at 2—6 measuring points	Pick-ups with resistance and inductive transmitter
5	Digital Voltmeter MT 100	Telemetering	Pick-ups with inductive transmitter
6	Function Block (Digital Voltmeter MT 101 + Voltage Converter MT 101B)	Telemetering	Pick-ups with resistance transmitter
7	Digital Measuring Centre MT 143	Automatic measuring	Pick-ups with resistance and inductive transmitter
8	Analogue-Digital Measuring System ADIMES	Automatic measuring and information	Pick-ups with resistance and inductive transmitter
9	Digital Voltmeter TESLA FAD 010	Telemetering	Pick-ups with inductive transmitter
10	Measuring Centre TESLA EMU 102	Automatic measuring at 100 measuring points	Pick-ups with inductive and resistance transmitter
11	Measuring Centre TESLA EMU 160	Automatic measuring with large number of data inputs (100—1000)	Pick-ups with inductive and resistance transmitter
12	Function Block for Pneumatic Measuring in Piezometers	Liquid-level telemetering	Uplift bore holes
13	Long-Time Delay Program Relay TMP 31	Program switching of measuring circuit. Cycle length: 2, 5, 15 min; 3, 7, 24 h	
14	Signal System type VÚIS	Switching of signal element light signalling	
15	Transistor Relay R5841 + Signal Lights	Switching of signal element VÚIS or magnetic pick-up light signalling	

Input	Output	Power	Accuracy
Variation of resistance	Read-out from the circular scale 100%	Battery 3 V	± 1%
dc current, variation of resistance	Pointer indication on the scale	Mains 220 V	± 1.5%
dc voltage, variation of resistance	Analogue recording and pointer indication on the scale	Mains 220 V 50 Hz	± 1.5%
dc voltage, variation of resistance	Analogue recording and pointer indication on the scale	Mains 220 V 50 Hz	± 0.5%
dc voltage 1 mV—15 V	Digital read-out from the display unit	Mains 220 V 50 Hz	±0.03%
Variation of resistance	Digital read-out from the display unit	Mains 220 V 50 Hz	± 0.04%
dc voltage, variation of resistance	Digital read-out from the display unit, printed record, punched tape	Mains 220 V 50 Hz	± 0.04%
dc voltage, variation of resistance	Digital read-out from the display unit, printed and graphic record, punched tape	Mains 220 V 50 Hz	± 0.04%
0.1—1000 V, 5 measuring ranges	Digital read-out from the display unit	Mains 220 V (127 V), 50 Hz	± 0.02% ± 1 digit
dc voltage, variation of resistance	Digital read-out from the display unit, printed record, punched tape	Mains 220 V (127 V), 50 Hz	± 0.02% ± 1 digit
dc voltage, variation of resistance	Digital read-out from the display unit, printed record, punched tape	Mains 220 V (127 V), 50 Hz	± 0.02% ± 1 digit
Pressure of water column = air pressure of 0—0.1 MPa	Depends on the measuring instrument	Mains 220 V 50 Hz	± 2.5%
—	Impulse length: min. 2%, max. 98% of cycle length	Mains 220 V	± 1.5% of cycle length
—	—	Battery 3 V or 4.5 V	—
—	—	Mains 220 V 50—60 Hz	—

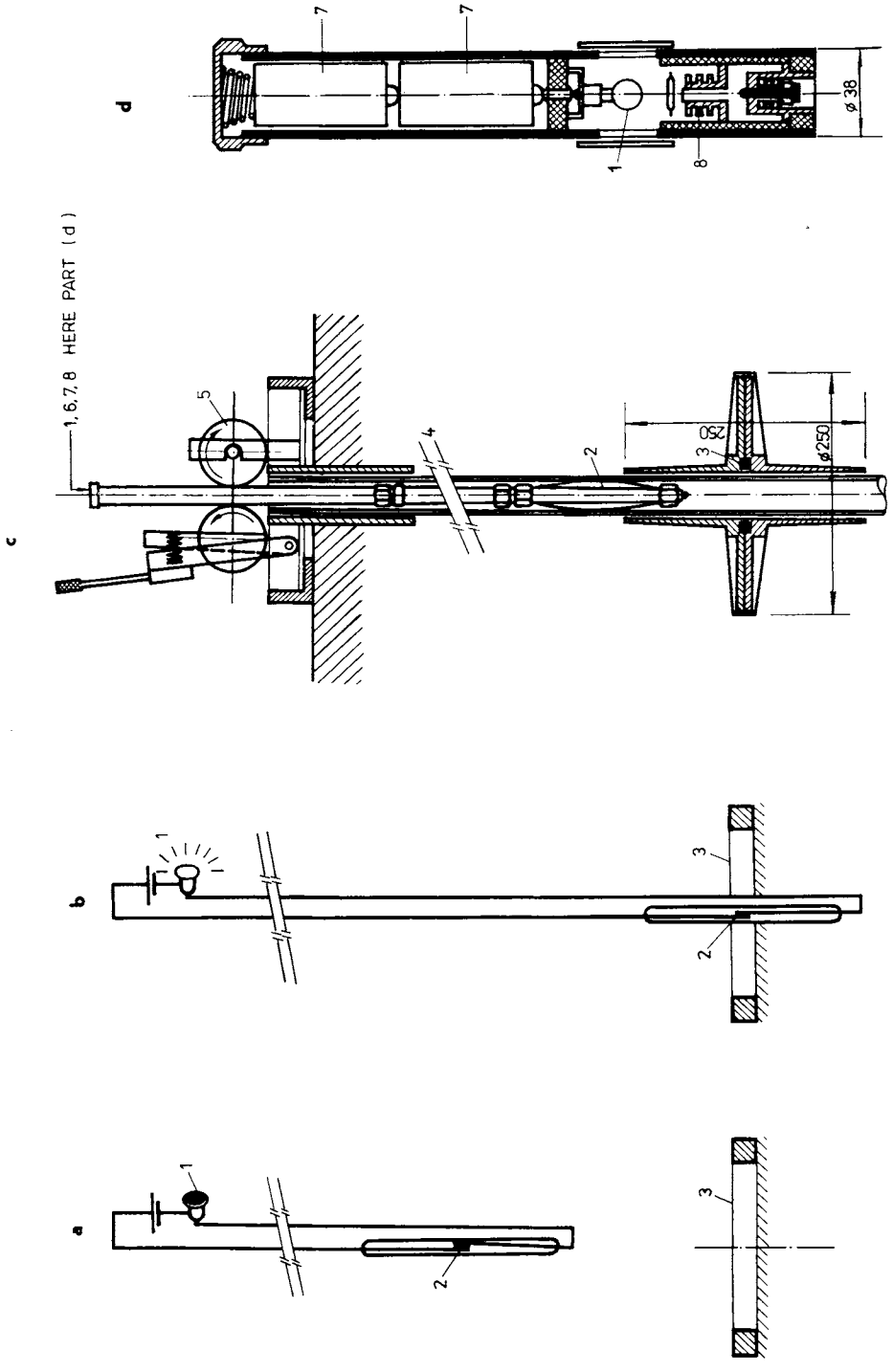
d
7
7
ø 38
1
8
c
1, 6, 7, 8 HERE PART (d)
5
4
2
3
250
ø250
b
1
3
2
a
1
2
3

Messtechnik (FRG), Robertson (Great Britain), Philips (Holland) and others offer catalogues describing these devices and their range of use. Engineers in practice cannot generally master the operation of individual devices in detail, but they must know the principles on which some instruments are based. Thus they should acquire the experience to know to expect from a particular devices.

The basic scheme of a *magnetic probe* (Fig. 7.20) shows the measurement principle. In the general position (Fig. 7.20a), the circuit is not closed. It is closed by means of a reed contact (2), when it reaches the magnetic field of a ring magnet (3) (Fig. 7.20b). A filament signal lamp lights. The next part of this figure shows the functional unit with the ring magnet (3), built into the body or subsoil of the dam whose settlement we are observing. Probe (2), placed on a pressure bar (4) of known length, slides into the circuit of the ring magnet (3) by means of discs (5) provided that the filament lamp (1) placed in the signalling head (6) is alight. The filament lamp is the light source for signalling, and two battery cells are the source of electric current. In addition, there is a transistorized voltage amplifier (8) as well as other elements in the cylindrical head, which provide for the substantial signalling function of the head.

In the probe, which can reach to a depth of 20—30 m, we can spread but many control points (rings), the positions of which are measured. These rings may be at variable distances from each other (usually 1—5 meters). The PE casing has a diameter 34/25 mm, the length of pressure rodding (set of rods) elements is 2 m. The mass of rodding and the corresponding head is approximately 10.0 kg (with a rodding length of 20 m).

We can also use the magnetic probe for horizontal distance measurement, in this case the drawing-out capacity of the probe usually being advantageous. By extending the probe, we can increase the distance between the farthest control point (ring) and the head (up to 40—50 m).

The inclinometer is the next device, and is well proven in measuring slope differences (slope-surface deformation and others). The beam with its weight acts as a multipurpose element. In deformation measurement on an embankment slope (Fig. 7.21), an inclinometrical element hung on a cable (3) is mounted onto a cart (2), which is lowered down the slope by means of a winch (4) beyond which its own measuring equipment (5) is placed (Fig. 7.21a). Pendulum motion pick-up, which reacts to any slope-surface unevenness, is effected by means of tensometric strips (6), which are adhered to the steel beam (Fig. 7.21b).

Fig. 7.20. Magnetic probe. a — initial position, b — measuring position, c — construction and transmission of vertical movement, d — head of the instrument; 1 — lamp, 2 — contact, 3 — ring magnet, 4 — pressure bar, 5 — friction disc, 6 — signalling head, 7 — battery, 8 — amplifier.

Relations between the slope angle α and the coordinates (x, y), which give the position of point B (Fig. 7.21c), are simple; we can write

$$x_B = a_B \cos \alpha - e_B \sin \alpha,$$
$$y_B = a_B \sin \alpha + e_B \cos \alpha. \tag{7.9}$$

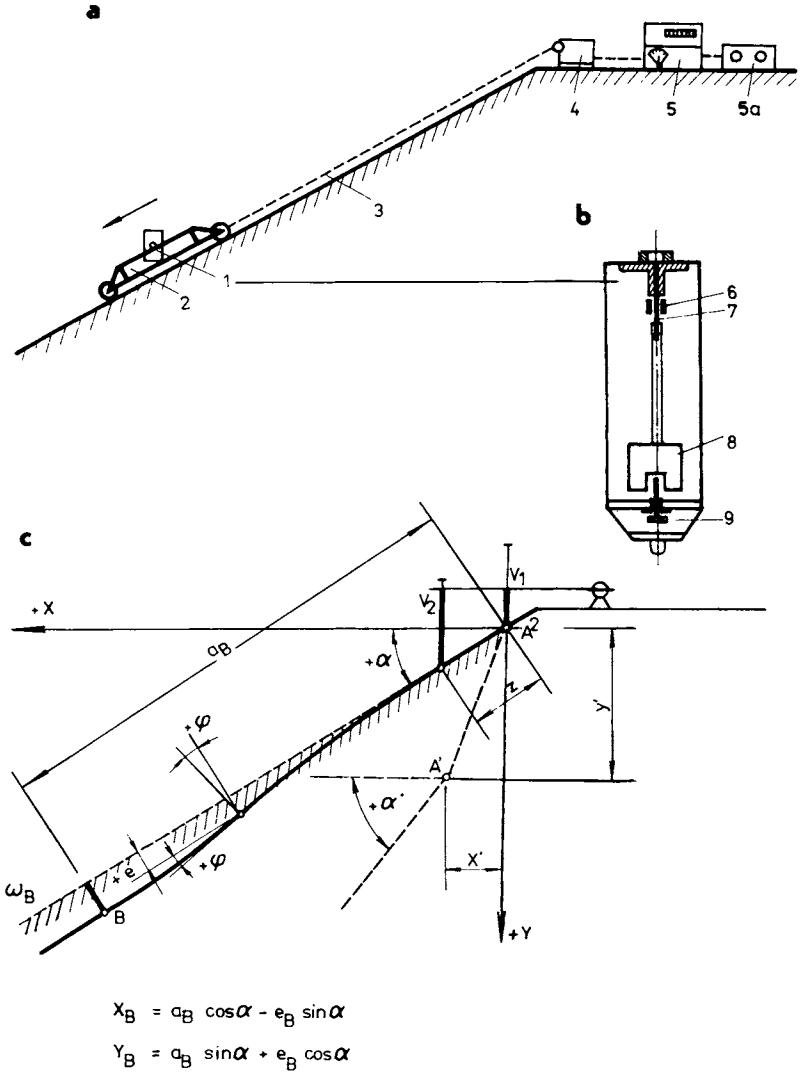

$$X_B = a_B \cos\alpha - e_B \sin\alpha$$
$$Y_B = a_B \sin\alpha + e_B \cos\alpha$$

Fig. 7.21. Inclinometer. a — location of devices, b — mean measurements element, c — relationship between slope of earth structure and position of instrument (carriage); 1 — measurement device, 2 — carriage, 3 — hanging cable, 4 — roll up, 5 — measuring equipment, 6—9 — pendulum with tensometric strip and functioning organs.

When the inclinometric element is used for the measurement of casing (or wall) deflection from the vertical, then the deflection φ, given by the ratio of horizontal deciation Δx to height Δh, is measured directly, by means of the relation

$$\varphi = \frac{dx}{dz} \cong \frac{\Delta x}{\Delta h}.$$

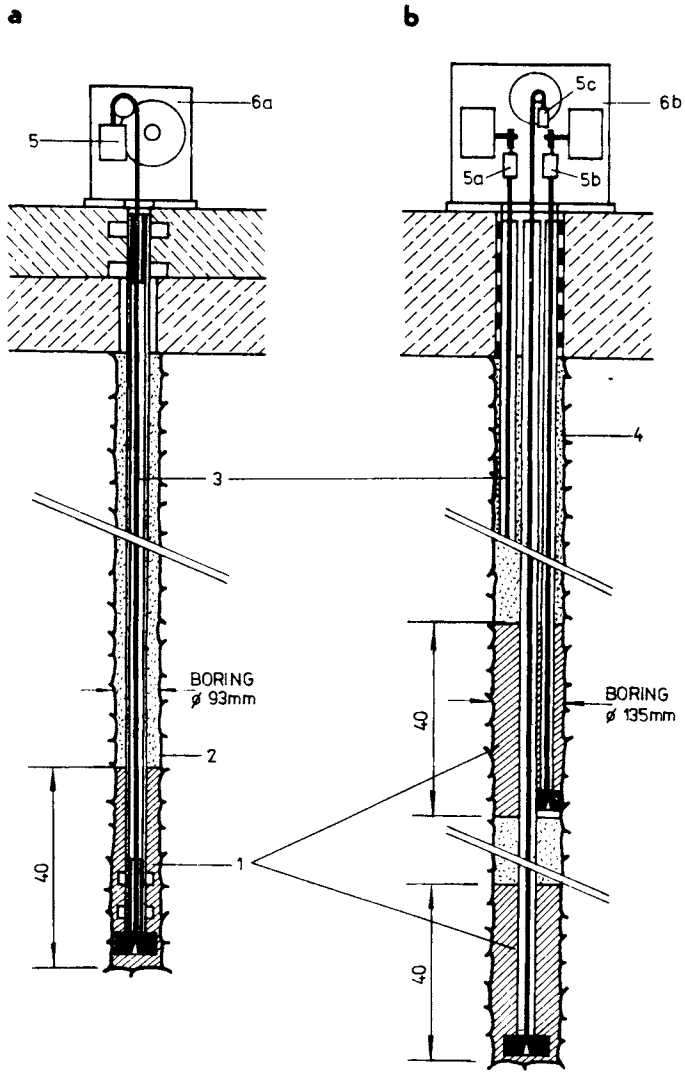

Fig. 7.22. Deep mark. a — with one weight, b — with three weights; 1 — concrete, 2 — soil, 3 — wire, 4 — three PVC tubes, 5 — weight, 6 — measurement head.

Deflection at a general point P will be

$$x_P = \int_0^{h_P} \frac{dx}{dz} dz \cong \Delta h \sum_{i=0}^{i=h} \varphi_i + x_0, \tag{7.10}$$

where x is the value of absolute displacement of the casing in the horizontal direction, φ_i the deflection, read out for two inclinometer positions

$$\varphi_i = \frac{1}{2}(\varphi_i - \varphi_i^{180°}). \tag{7.11}$$

If n is the number of divisions on the measuring equipment, d value of one division (or digit) and k constant, which gives the angle corresponding to one division (determined by calibration), then the total deviation will have the value

$$\varphi = ndk. \tag{7.12}$$

A depth mark (Fig. 7.22) allows earth-settlement (deformation, compression) measurement by determination of the difference between a fixed concrete setting in a bore hole and a stable measuring head filler. This equipment makes possible the replacement of telescopic tubes, which are used in canal dam and levée construction in Europe, following the American organization "The Bureau of Reclamation". Depth-mark (HZ-74) measurement is much more precise and it has the great advantage of the possibility of telemetering by means of an inductive or resistance transmitter, connected to the pick-up.

Extensometers of many different types usually make use of the pick-up and measurement principles as explained for the above-mentioned measuring equipment. They are mainly differentiated according to measured length transfer or differences in the distances of observed points.

Rod and draw-bar extensometers are differentiated from the concisely described depth mark, mainly in the lower and upper parts. In the lower part (in the bore hole) they are gripped by an anchor, and in the chuck head they are tensioned by a spring and not by a weight as for the depth mark.

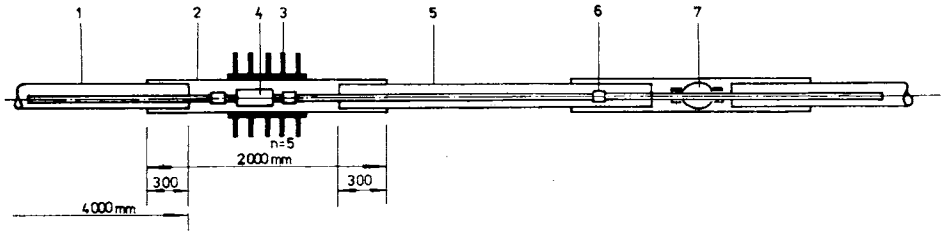

Fig. 7.23. Magnetic extensometer. 1 — steel pipe (∅ 83 mm), 2 — PVC pipe (90/80), 3 — control point, 4 — sensor, 5 — steel pipe, 6 — junction of measuring unit, 7 — distance element.

The magnetic extensometer (Fig. 7.23) is specified to pick up the deformation characteristics of earth built into the embankment body and the subsoil. In a dam, it is located in a horizontal position, where it lies in a steel dilatation casing (1), which carries a polyethylene tube (2) with control point (ring 3). Inside is the rodding (set of rods) with the pick-up (4). Inside at the control point, the ring magnet is located. By a change in control-point position relative to that of the stable pick-up, the magnetic field is displaced. At the same time the reed contacts, influenced by the field, are closed. The given resistance change is proportional to the displacement magnitude. The pick-up range is 200 mm, or n times 200 mm when the extensometer has n measuring discs.

The resistance extensometer is more complicated in construction. Its operation is based on the resistance principle and the circular resistance transmitter is exploited as the pick-up for this extensometer. Changes in point positions (in the form of grillages placed in the earth) are transferred to the end points of the pick-up by means of rodding. In general, it is more complicated than the magnetic extensometer; its advantage lies in its possible use in the pick-up of vertical displacements (settlement) and displacements in other directions, as well as the great ease of pick-up automation and all measurement programming (read-out interval programming).

In spite of this fact, dam constructors in West Europe usually give preference to magnetic extensometers, while in the USA and Mexico resistance extensometers are more popular (ICOLD 1976).

The dilatometer with telecontrol serves for relative (mutual) displacement measurement of two parts of a construction, separated from each other by a joint, created during construction of the object or during its dislocation caused by irregular settlement, etc. It has a dial indicator connected to a circular resistance transmitter, so that the longitudinal displacement of the indicator contact pin is transmitted to rotary motion of the transmitter axis (Fig. 7.24). The displacement range ($p = 10$ mm) accords with the scale range of 270°. The transmitter axis diameter (d), on which tin-bronze wire ($\Phi = 0.3$ mm) is coiled, is given by the relation

$$d = \frac{4p}{3\pi} - \Phi = \frac{4 \times 10}{3\pi} - 0.3 = 3.9 \text{ mm}.$$

The diameter of the dilatometer is 90 mm. Its case is 200 mm long. The measurement accuracy is ± 0.1 mm. It now replaces the commonly used dilatometric cramps, established on two neighbouring parts of a concrete object. Their distance is determined by means of a dilatometric wedge. Here the disadvantage is that with the inverted syphon and other concrete-object dilatations, a direct read-out can only be carried out with great difficulty and direct instrument registration would be impossible.

A float filtration ratemeter (Fig. 7.25) makes possible automatic telemetring of filtration flows, which pass through a certain measuring profile and so replaces the previously used simple measuring overflow device or the various types of tipping (dumping) vessels for flow-volume measurement. In this case, the flow is ascertained by means of a glass float placed in one of the seepage measuring chambers.

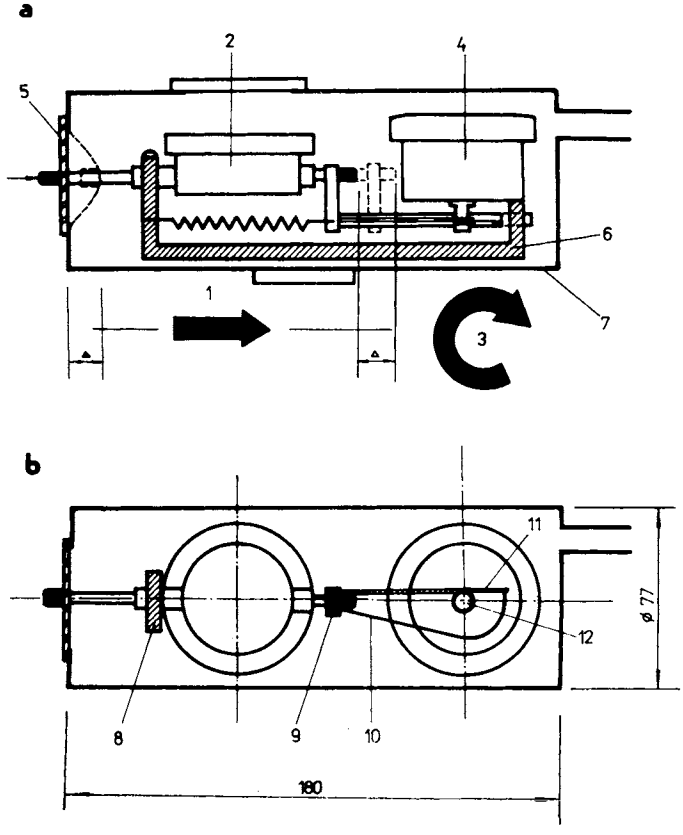

Fig. 7.24. Dilatometer. a — longitudinal section, b — sight on its down face; 1 — movement direction, 2 — indicator, 3 — turn direction, 4 — sender, 5 — membrane, 6 — beam, 7 — watertight shelter, 8 — fastening of the indicator, 9 — fastening of the spring, 10 — spring, 11, 12 — gearings.

The float is mechanically connected to an electrical pick-up adjusted to telemeter displacement measurement. Measurement and conversion of the measured quantity are based on the resistance or inductive principle, with long-distance signalling being realized by means of an electromagnetic switch.

The filtration ratemeter gives the flow-rate measurement to $q = 5 \times 10^{-3}$ m^3 s^{-1} with an accuracy $\pm 1\%$ of the flow-rate value; for values less than $q =$

$3—4 \times 10^{-4}$ m^3 s^{-1}, the measuring accuracy falls to perhaps one tenth. Evaluation of the quantity is made by means of a dependence graph

$$q = f(h),$$

which is designed and calibrated especially for each pick-up and for each measuring profile.

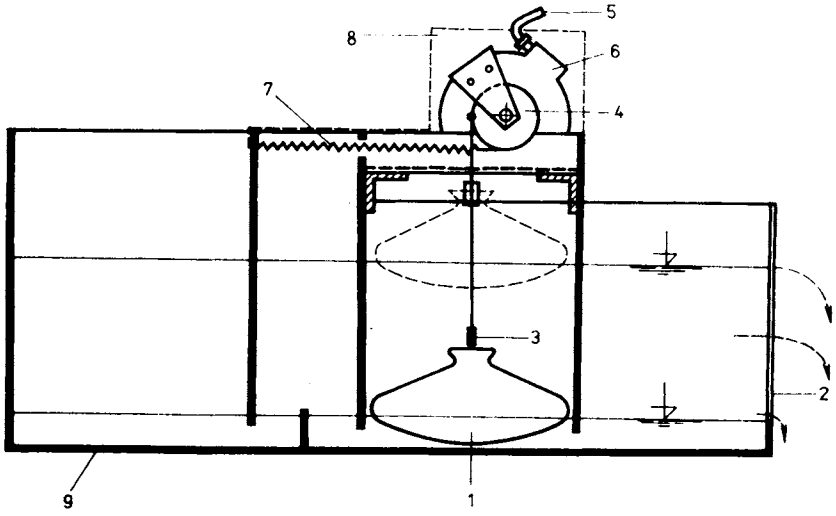

Fig. 7.25. Seepage-quantity measurement device. 1 — float, 2 — three-angle overflow, 3 — light pick-up, 4 — wave of the sender, 5 — cable, 6 — transmitter, 7 — spring, 8 — shelter, 9 — casing.

Centralized water-level measurement in the probes is exceptionally important in measurements and observations on canal embankments and levées, because the probes, to be used as uplift meters (on a level with the layer under pressure), and the piezometers usually compose the basic diagnostic elements, and they are therefore always present in any larger construction. On great lengths of embankment, these are hundreds or thousands. Ten thousand piezometers altogether are proposed for the various Danube constructions (dams, weir, power house, territory, etc.).

With this great number of individual objects, automatic water-level measurement has fundamental importance. The pick-up of values and their transfer are based on several principles. Most common are: pneumatic, electromagnetic, resistance and inductive principles. In recent years, ultrasound and laser technique has been applied here.

In Czechoslovakia, mainly pneumatic equipment, developed in the Research Institute for Building, Bratislava—Brno is under design. In this type of

measurement, the water pressure in the bore hole is balanced by air pressure in a tube immersed in water. The air pressure at the moment of pressure balance is measured; at this instant the excess air supply begins to bubble through the water. With simple long-distance read-out, the control points on the manometer scale are switched over. The corresponding air pressure in the system is read-out on the manometer scale and thus the water level in the probe is determined.

For this purpose the electric measuring point selector switch with a time-delay relay, which makes the read-out and registration of values on the digital voltmeter possible, is used at automatic measurement.

In contrast to these advantages (telecontrol, automatic transfer and read-out, simplicity), there is one fundamental disadvantage, namely the low accuracy of water-level measurement. The stated accuracy of ±100—250 mm is sometimes inadequate — mainly for canal embankments.

The next device, designed for water-level measurement is *the ultrasound digital level gauge* UDH 2 developed at the Research Institute of Mechanization and Automation in Nové Mesto nad Váhom. The level gauge probe is located at the bottom of the dam, river or bore hole, where we wish to measure the level. The water-level measuring method is based on the transformation of an ultrasonic wave, increasing the time interval of the pulse. The principle is shown in Fig. 7.26.

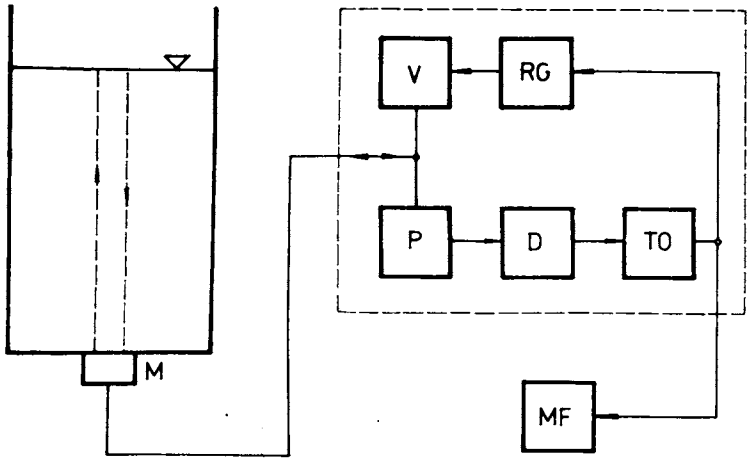

Fig. 7.26. Ultrasound-level gauge UDH 2. M — transducer, P — receiver, D — detector, TO — shaping circuit, RG — relaxation generator, V — transmitting generator, MF — frequency meter.

The pulse transmitted from the transducer (probe) M is aimed at the water surface and after reflection and a time interval t impinges back on the transducer M. After processing by electronic circuits (receiver P, detector D, shaping circuit TO,

relaxation generator RG), this pulse starts the transmitting generator V, which transmits a pulse to the water surface through the transducer M. The recurrence frequency of the pulse is given by the sum of the pulse travel time in water and the delay time in the electronic circuits (negligible compared to the water travel time). The pulsy frequency, given numerically by the frequency meter MF, and its inversely proportional to the water level.

The level-gauge supply voltage is 220 V, 50 Hz, with a measuring accuracy of ± 1 cm. The probe-box lead length is a maximum of 30 m, the box-scaler (MF) distance can be up to 1000 m. We can connect the level-gauge evaluation box, by means of the measuring point selector switch, to four probes and thus we can measure the level at four points. The measuring range is 0.1—10 m.

The float gauge developed at the Department of Geotechnics at the Faculty of Civil Engineering in Bratislava is designed for measurement of water level in bore holes, displaced by no more than 1 meter.

The principle of operation of this gauge is shown in Fig. 7.27. A permanent magnet (PM) placed in the float (P) moves in sympathy with the water level and it connects the magnetic reed contacts MC displaced within PVC waterproof tube. The separation of the contacts is 1 cm and therefore two contacts are connected for

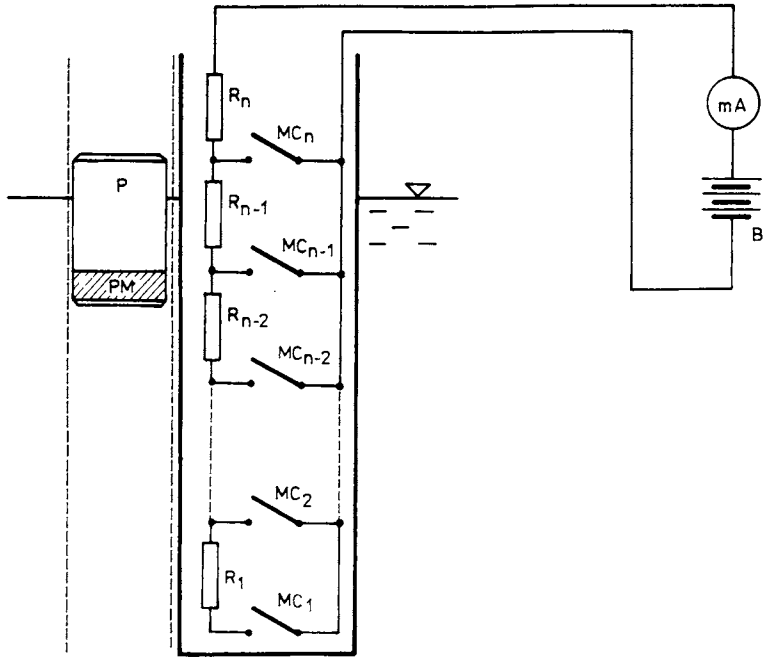

Fig. 7.27. Float-level gauge with reed contacts. P — sensor, PM — permanent magnet, MC — reed contacts, $R_1 \ldots R_n$ resistances.

each magnet position. The problem of obtaining no deflection on the milliammeter when any of contacts are disconnected by a defect (implying a water level out of the measuring range) is almost eliminated by this. Even when two contacts are always connected, for example, MC_{n-2} and MC_{n-1}, here the milliammeter deflection is the same as if just one was connected (in our case MC_{n-1}).

In order for this equipment to be linear, i.e. the electric current and deflection of the instrument increase linearly with increasing water level, the resistances R_1—R_n must be different. We can determine their values from the relation

$$R_j = \frac{U}{I_j} - \sum_{i=j+1}^{i=n} R_i, \tag{7.13}$$

where U is the battery voltage, I_j currents chosen for different water levels (for example, for a water level of 1 cm $I_1 = 0.01$ mA; for 2 cm $I_2 = 0.02$ mA; for 10 cm $I_{10} = 0.1$ mA; for 100 cm $I_{100} = 1$ mA).

Because of its simplicity, and the fail-safe feature of its double contacts, the above float gauge is reliable, accurate (accuracy ± 0.5 cm) and not very costly. It may be modified easily for optical or acoustic signalling of any dangerous water-level rise (Lichner 1976).

7.6 Soil Testing and Control

Surveys of canal embankments and levées must take into account knowledge of geological conditions in the substratum and of the quality of material incorporated in the embankment, which can vary with the conditions of operation, as stated in Chapter 1. To safeguard the structure, it is very often necessary to investigate the soil properties after an appropriate time delay, mainly in suspicious cases — if the structure has to be reconstructed, strengthened, etc.

Some tools and devices enabling the investigation of natural soil properties, subgrade compaction, levée and embankment control, should be mentioned here.

A disposable sampler has a sort of compact pole with a handle designed for taking samples of soil to depths of about 3—4 meters. It may be used for vertical sampling from the ground or horizontal sampling in the side of test pits, slopes of embankment, larger diameter wells and other openings. Special types of such samplers have a saw-tooth cutting end for easier driving. The SOILTEST sampler (A-43) can take a sample 30 cm long or more which can be inspected readily through the cut-away side of the tube. This soil sample allows detailed investigation in the field or laboratory. The soil can be preliminarily identified and allocated to the appropriate group — after visual and manual procedures in the field — as mentioned in Chapter 1.

The volumeter is used for fast measurement of the field density of soil in an undisturbed condition. It has a cylinder of calibrated volume (0—30 cm^3) and

a marked piston-reading with an accuracy to 0.05 cm^3. This simple instrument is a valuable tool for civil engineers and dam contractors.

The speedy moisture tester enables direct determination of density and moisture content from only one weighing. By using values of density and moisture content, other parameters such as unit weight of soil, its porosity, etc., can be calculated by soil specialists (Sections 1.3—1.6).

The penetrometer and standard penetration test is a widely used aid in ground exploration where soil near levées is menaced by failure. A split-barrel sampler (Fig. 7.28) 30 to 60 mm (standard 50.8 mm) in diameter, is driven into the sand at the bottom of a bore hole by means of a 63.6 kg mass falling freely through a distance of 760 mm (standard). After an initial drive of 150 mm, the number of blows required to drive the sampler through a depth of 305 mm is determined. This number is called the standard penetration resistance (N) and has been correlated empirically with the relative density of the sand. Tests should be carried out at intervals of 760 mm within the significant depth. More details of the test are given in British Standard (BS 1377), Czechoslovak Standard (CSN 731 821) and others.

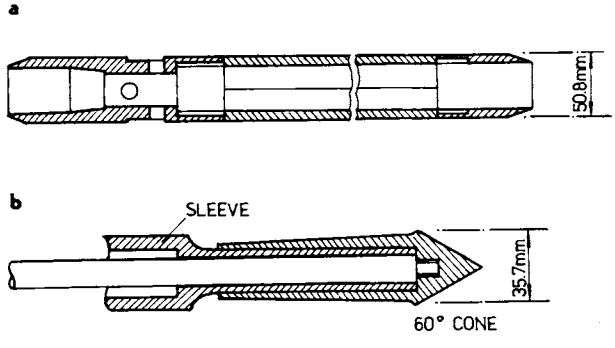

Fig. 7.28. Sampler and penetration test device. a — split-barrel sampler, b — Dutch cone.

The average N value for each bore hole is determined and the lowest average should be used in design or in calculation of the required safety factor. For fine sands and non-plastic silts below the water table the measured N value, if greater than 15, is reduced to N' where

$$N' = 15 + \frac{1}{2}(N - 15). \tag{7.14}$$

After Peck (Craig 1974), an approximate correlation between standard penetration resistance and shear-strength parameter Φ' can be determined (Fig. 7.29).

In the penetration tests, the effective overburden pressure (neglected by Terzaghi and Peck 1948) has to be taken into account because of its influence on bearing capacity and its resistance to hydrodynamic loading, mentioned in Chapters 1 and 6. The relationship between standard penetration resistance and

effective overburden pressure was analysed by Gibbs and Holtz (1957) (Fig. 7.30) and showed the important influence of this pressure on the value of N for a given relative density.

The Dutch cone — used in the Dutch Cone Test — is a penetrometer having an apex angle of 60°, and 35.7 mm in diameter (area 10 cm^2). The cone is attached to rods running inside a sleeve and can be pushed independently into the sand by means of a hydraulic jack, no boring being required. The cone is pushed a distance of 500 mm into the sand at a rate of 10 mm s^{-1} and the load measured by use of a pressure gauge. The load divided by the end area is termed the cone penetration resistance (C_r). It allows us to calculate the compressibility constant C as a function of the constant C_r and effective overburden pressure (σ_0')

$$C = 1.5 \frac{C_r}{\sigma_0'}. \tag{7.15}$$

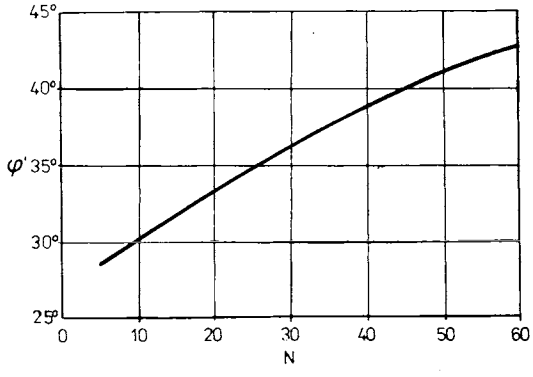

Fig. 7.29. Relationship between standard penetration resistance (measured for N number of blows) and shear strength Φ — after Peck and Thornburn (1953).

This can be recorded automatically by some special Dutch penetrometers equipped with a band recorder registering depth and load applied.

The torquevane, for determination of shear strength in cohesive soils, is used as a supplementary testing device in test pits, dam bodies and the subsoils of embankments.

The SOILTEST *pocket penetrometer* (Model OL-700) indicates the unconfined compressive strengths of soils. It has a direct-reading scale (in kp per cm^2). From the readings, the value of cohesion can also be determined.

The proving *ring penetrometer* is used for obtaining the compaction and penetration resistance of soils in shallow surveys.

The portable *SOILTEST X-Y recorder* set which automatically records axial deformation and load consists basically of a multirange sensitive load cell, strain pick-up and improved X-Y recorder. Its use facilitates continuous and simultaneous measurement of stress and strain with automatic recording of data, whether of

long or short duration. Load is sensed by the load cell which utilizes a linear variable differential transformer to measure the deflection of its beam resulting from compression loads. This deflection is translated into a proportional electrical signal, indicated on the y-axis of the recorder.

The strain is transduced into an electrical signal by the displacement of the probe shaft in the strain pick-up. The strain is indicated on the X axis of the recorder. As stress and strain develop, the recording pen is driven across the graph paper to give a continuous and exact plot of the relationship of load versus deformation.

The complete set, included in the standard stress-strain X-Y recorder set, are the following: X-Y Recorder with pen assemblies, pad of graph paper, load cell, strain transducer, necessary cables and connectors and operating instructions. The apparatus works with a 400—10,000 Hz excitation frequency and 2—6 volts as excitation voltage.

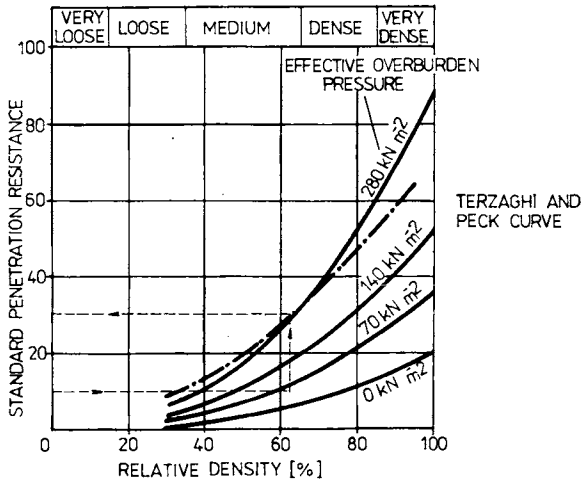

Fig. 7.30. Relationship between standard penetration resistance and effective overburden pressure — after Gibbs and Holtz (1957) and Craig (1974), respectively.

The most efficient survey and research instrument adopted for use on canal embankments and levées in cases where preliminary exploration during the period of design and construction was neglected, seems to be the *SOILTEST Stratameter* (R-50).

This instrument consists of: Transmitter Unit (power supply) — output voltage up to 750 volts, power output 75 to 112.5 watts; current enabling range selection by six push-buttons (0.01—0.15 amps) taken from battery (2 gel cells rechargeable, 6 volts) and Receiver Unit with measuring range of 0.005 ohms to 1000 ohms resistivity, 1 to 10,000 millivolts in 3 decades attached to 4 mercury batteries (5-AA cells, 1.4 volts). It is used to give a profile of sub-surface conditions, showing depth to bedrock and changes in soil strata and indicating differences in soils at the test site. It is also used to determine the depth of the water table and to

find discontinuities typical for a region beset by soil failures (piping, hydraulic fracturing, etc.).

The electrical earth resistivity system surveys the sub-surface down to 150 m. It advantages are: exploration of the strata proceeds very rapidly; the simple procedure of the survey is also cheaper than traditional investigation by bore-hole methods.

In Czechoslovakia, an older resistivity system of investigation was used twenty years ago as a preliminary survey for localing sand and gravel deposits, determining depth to bedrock and finding fracture lines in bedrock in the Danube and Váh valleys, as well as the Vltava valley. The greatest employment of electrical resistivity surveys was made from 1962 to 1964, when a strip of land more than 100 km long and over 1 km wide near the Danube levées was investigated. This was always in conjunction with bore-hole techniques, which gave much more detailed information (Jakubec and Tichý 1964).

The new multi-propose instruments from Soiltest, Inc. Evanston offered recently (SOILTEST, 1978), work faster and more accurately when used in appropriate conditions. In investigation of river deposits, a sample gravel detector may furnish reliable data for the design and maintenance of embankments.

In Austria and Hungary, *the seismic method* was used to determine the geological conditions necessary for planning, in the construction and reconstruction of levées in the Danube valley. Meanwhile, in France both electrical resistivity and seismic methods were used with good results in deposit investigation — reducing the number of test bores needed. In all cases with ground exploration of canal embankments (in the Rhône and Rhine valleys), important savings in time and test casts were made.

We should mention here the good results achieved with the use of the *Nuclear Density Meter* (Nuclear Chicago) in the Mississippi valley in the USA and in Czechoslovakia in the Danube valley — exploring the embankments of levées and their subsoil over sixty years. The investigation carried out for the Danube scheme design showed a low density (large porosity) of soil at a depth 1.2—4.5 m below the ground surface in sand and sandy-gravel strata where most of the piping phenomena during the flood in 1965 were observed.

As regards a dam itself, other instruments were used in connection with the hydraulic development of the Bas—Rhône and large dams in France (Delattre 1959, Sherard et al. 1963).

Telelevels give the vertical displacement of determined points inside the rock-work mass of the dam.

Radio-probes indicate and measure the horizontal movement of a number of marks along measurement lines inside the dam.

Hydraulic tellers, using the same measurement lines as radio-probes, provide for measurement of vertical displacement of the marks already used for the radio-probes.

Such equipment requires the placing of concrete recesses in the middle of the earthwork, and the of making beds of material of studied granulometry for laying the pipes. This causes a good deal of interference with the work of placing the material in the dam.

A short outline of the portable set and stable instrumentation used during dam construction shows the possibility of exploring and surveying not only the performance of the structure and its sub-base, but also the behaviour of the earthwork and land in its vicinity during operation. This is especially important for levées, which are sometimes out of operation for long periods. During these periods, the structure or its sub-base can be damaged by animals, vegetation or man. The abrupt arrival of a flood can lead to a dangerous situation which in the past was controlled by hundreds to thousands of guards and workers "mobilizied" to safeguard "the protective line" (embankment, seepage canal, drainage, etc.). In the "flood backyard" — every 15—20 kilometers — a supply of material (steel beams, wood, sand, gravel, many thousands of bags, pipes, etc.) — was prepared for use in the battle for levées (for support). All the stores — made with this old conception of control — were concentrated for a "passive battle" against water — to counterbalance the water load (sand, bags filled with sand, basins filled with water) on the downstream side of the embankment.

Testing the soil in the embankment body and its sub-base and preparing an active battle — making additional perforations for overburden and drainage into the subsoil — provide a new way of preventing damage. To analyse the situation quickly, extensive and rapid measurements of uplift and pore pressure are needed. The subsoil of levées contains layers of permeable soil with a cover of clay or a silty layer with high pore pressure. This can be spread and dissipated by bore holes or by a simple penetrometer, having the role of a control tool.

Such an active concept of soil testing and control is a better solution for aid during a flood than the old concept with its costly backyard. It saves money and man power.

7.7 Water-resource Information in a River Basin and the Location of Instruments

The aim of abandoning the old control system based on an imperfect network of objects (limnograph, ombrograph and discharge measurement on the river made by observers, who also had the duty of observing the groundwater level for canal dams and levées) leads not only to the use of new measurement methods and new instruments, on-lined briefly, but also to a new information system. The new scheme of control is characterized by the use of measurement at a distance, by the location of the instruments over the whole catchment area — mainly near a hydraulic structure where power-stations and energy canals play a special role

CANALS AND INFORMATION SYSTEM

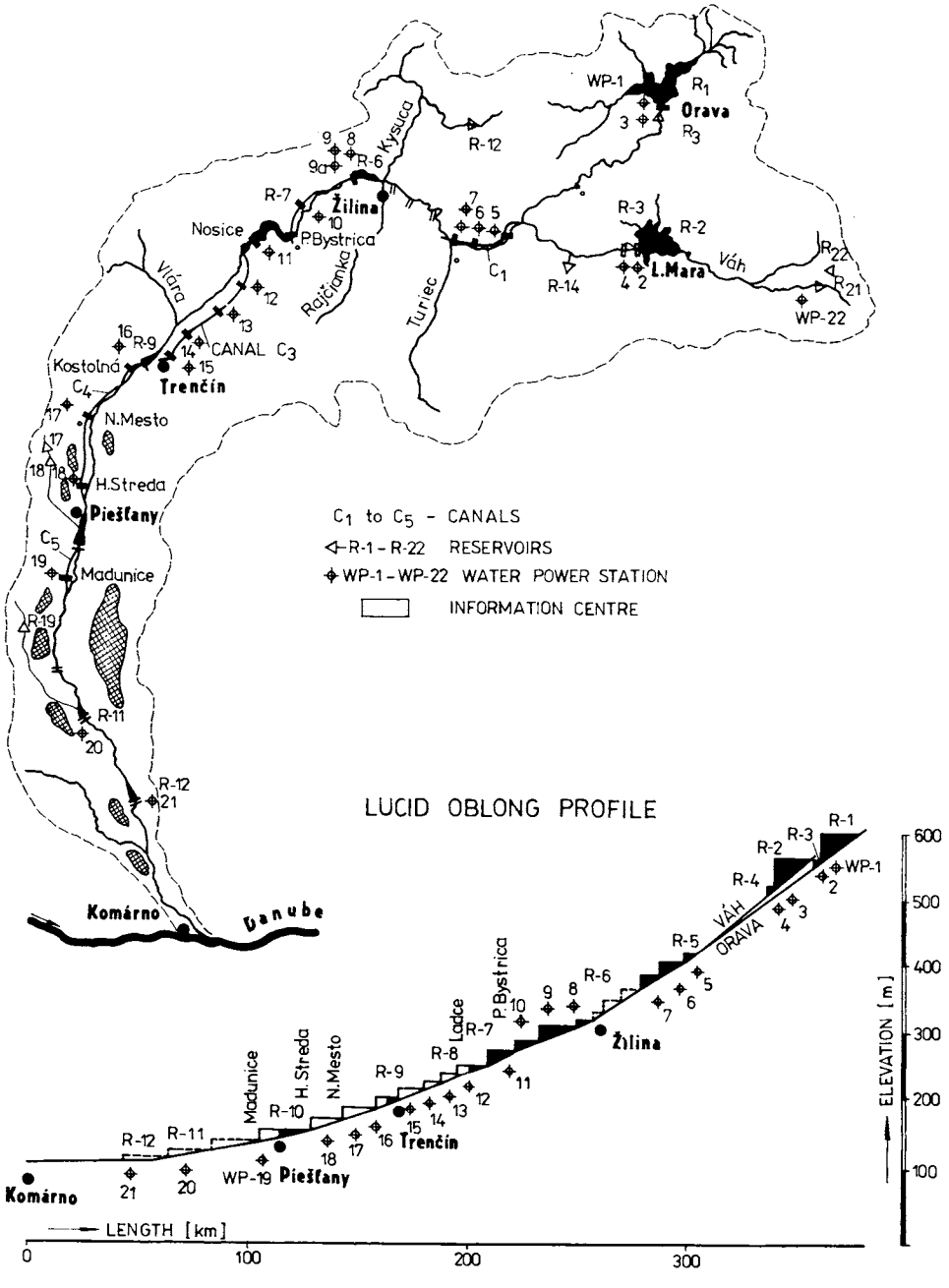

Fig. 7.31. The canals and hydraulic structures in the Váh valley.

— and by the concentration of information (measurement recorder) in a control centre equipped with a computer.

Two examples of information transfer from Czechoslovak territory will be mentioned here. First, an outline of the new information system on the river Váh (catchment area 10,640 square kilometers) will be given. Then, the project of measurement and observation on the Danube scheme will be described with respect to two main centres (Bratislava and Budapest) and a special information control centre.

In Váh valley mainly the new information system of the water sources will be analysed, meanwhile in the Danube project the measurement instruments and its location with respect to the canal dam and levées will be described.

In the present *the control system in the river Váh*, and its tributaries consists of canals with a total length of dams more than 200 kilometers. The levées above 360 kilometers in length protecting the territory of catchment area are in operation here. The catchment area is controlled by two mean and 8 small reservoirs built for safeguarding of hydraulic energy in 19 hydroelectric stations. (Fig. 7.31).

A dense network of limnographs and ombrographs built during thirty years (116 stations in total), worked accurate enough, but the information transfer was slow. And so, in the time of great rainfall sometimes the flood was in the valley earlier as the information itself. All hydraulic structures in the Váh valley were menaced; the dams in the first place.

In last ten years a new system was designed. Here there are 147 ombrographs and 152 limnographs in the catchment area and near the canal, levées and other hydraulic structures with additional 42 observed points, where also the snow cover can be measured and evaluated.

In the water resources centre (Central Board of Water Resources System) there is the informative and warning service concentrated and so the possibility to keep the antiflood precautions and to make all measurement is given. But the means needed for the levée protection from damage are nearly the same as for twenty years. The situation is more complicated in the period of extreme discharge, because the requirements of many water users (not only that of energetics) must be respected. In the first place the safety of dams, of land and of the cities and population must be respected. It is necessary to make appropriate decision very quickly — respecting the situation in the catchment area and this one of hydraulic structures. The first part of the system is a monitory instrumentation containing 56 sense organs (Fig. 7.32) distributed in controlled area to give the information about the water situation. In the 23 stations the atmospheric precipitations quite near the flow are measured. Three stations are located of the main flow (Peter et al. 1978).

The secondary intercom system (I.C./2) has conveyance counters equipped with measured value receivers (2), recorders (3), and displays (4), which are joined to the long-term memory (M) and to the signalling (5). The central intercom system (Fig. 7.33) P.V. in Piešťany is additionally equipped with a perforator [6].

An information system, equipped with this modern device, ensures:
(a) safeguard against flood;
(b) optimum operational regime for water structures at low discharges;
(c) the provision of co-operation with the hydroenergetic intercom system;
(d) flow pollution minimization (below industrial centres);
(e) collection of data for short- and long-term predictions of the water-reserve situation in the river basin;

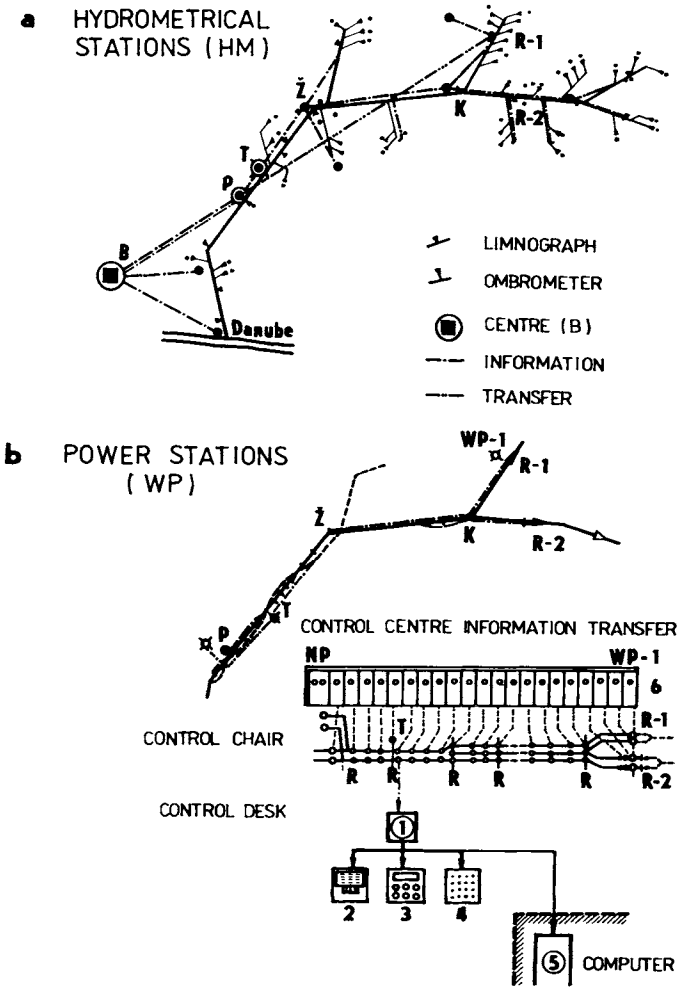

Fig. 7.32. Váh canal scheme and its control. a — control stations in the Váh valley and connection with the centre in Bratislava, b — Váh reservoirs and power-stations and its control; 1 — receiver of measured values, 2 — recording by electric typewriter, 3 — display, 4 — signalling, 5 — computer, 6 — automatic "service" and signalling.

(f) information to water users and the general public (sport, fishing) about the water resources.

In addition, the new information system has to ensure co-operation with the modern power-engineering system and also equipment systems for hydraulic structures.

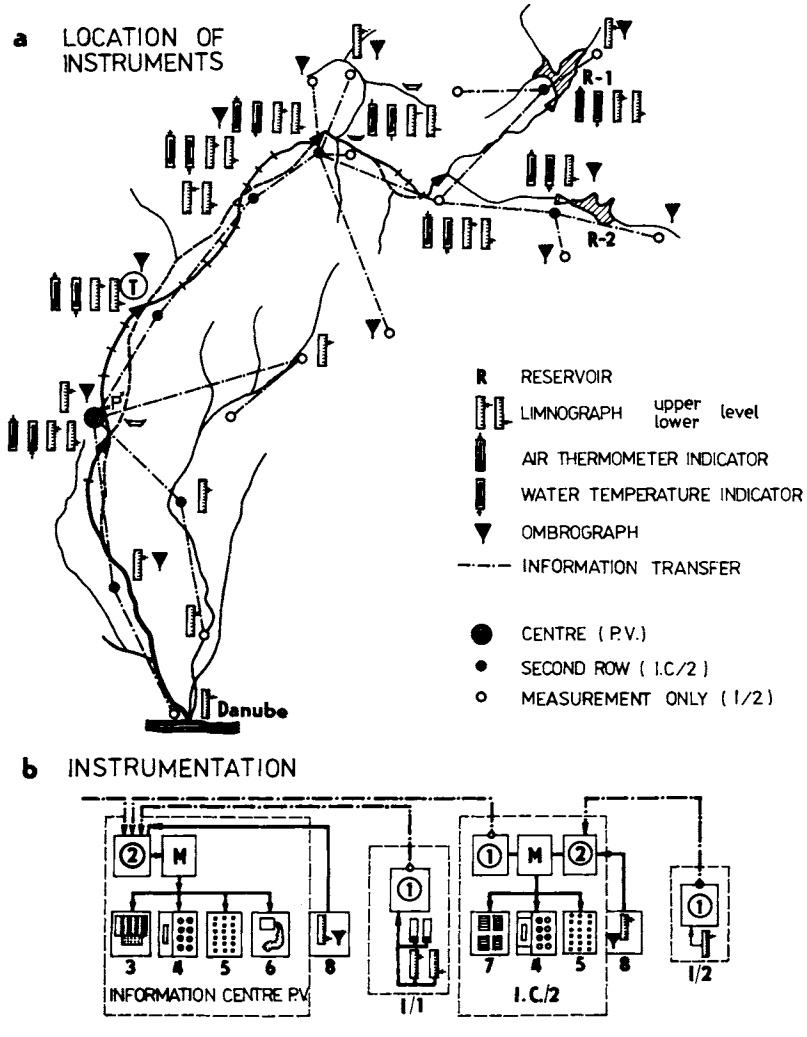

Fig. 7.33. The new information system, sense organs location and instrumentation of information centres. P.V. — basic information and control centre, I.C./2 — secondary centre, I/1 — measuring and transmitting station (of several values), I/2 — registration and transmitter of signal measured values; M — memory circuit; 1 — transmitter, 2 — receiver, 3 — recorder with electric typewriter, 4 — display, 5 — signalling, 6 — shorten values recording, 8 — point measurement (not automatic).

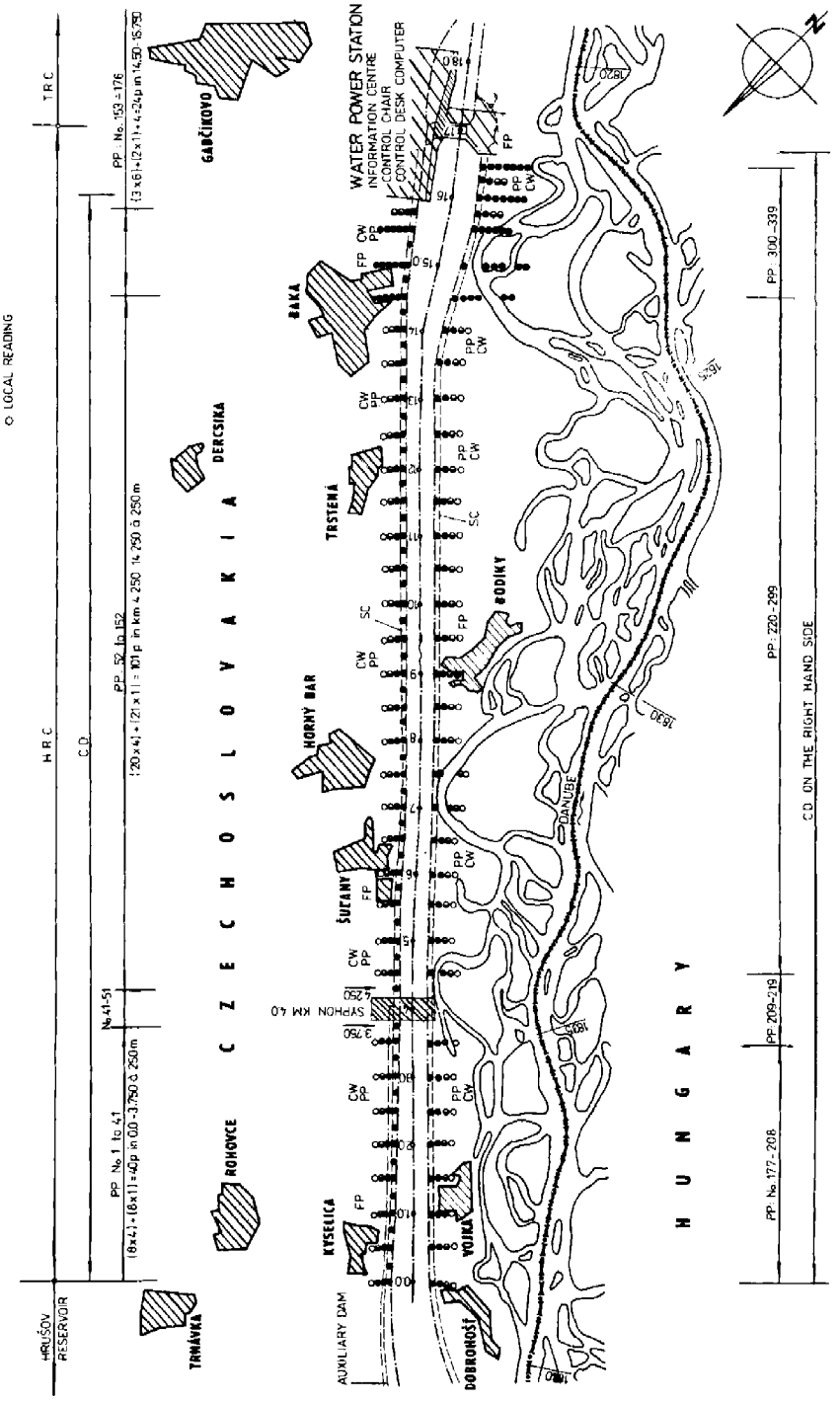

Fig. 7.34. Location of the Danube head-race canal (HRC) and lay-out of instruments along the dams.

The water-resource system on the river Váh has a relatively extensive information system. The basic hydrometeorological system, more than 50 years old, still serves to give general information to the population and basic information about precipitation and water levels. Registration of readings from the instruments incorporated in the embankments was not included in this mean control system, despite wide demand from users and the population at large. It serves almost exclusively the requirements of energetics. Water resources connected with the operation of dams and the functioning of heavy industry, intensive land use (irrigation), supply of utility and drinking water, recreation, sport and other water uses, employ a third information system, which presents a very source of information of water resources but little about the hydraulic structures.

Despite twenty-years' improvement of this information and control system, further limitations in reliability can be seen in the transfer of information. The main limitations are:

(a) those caused by changes developed in water-resource systems in the regime of outflows, and in the relation between water resources and the natural medium and also the structures;
(b) insufficient registration of water resources (characteristics of flows) and information about the behaviour of dams;
(c) insufficient registration of events and places of low safety;
(d) imperfections in technical equipment for the operation devices in hydraulic and sanitary technical structures;
(e) inadequacy in the network of information points (sensing organs);
(f) inadequate interconnection of the three information systems mentioned above.

These imperfections in the system must be overcome by observers and officer of manager.

7.8 Inspection and Measurement Devices on Canal Embankments and Levées

A number of instruments and apparatus will be put to use in inspecting the behaviour of the structures on the Danube (Fig. 7.34) project. Embankments and levées will be observed not only during construction and filling, but also in any follow up which may occur in the course of time.

The principal measurements are connected with topometrical calculation done by precision levelling and triangulation from a series of fixed points outside the zone of influence of canal embankments and other hydraulic structures.

The Danube project, most of which is a project of measurement and regional survey concerning canal embankments and levées on Czechoslovak and Hungarian

territory with a total length of more than 300 km earthworks, has a complex control system. The structures will be monitored at 920 cross-sections, in which over 8000 probes — sensors — will be operational. Canal embankments and levées will be subjected to a regular schedule of measurement: water level, load (tension), pressure (uplift, pore pressure), and among these observation of displacement (Sections 7.2—7.5): these will be the results of the four centres (Bratislava, Gabčíkovo, Nagymaros and Budapest, respectively). The number of measurements and the transfer of information are given in Table 7.4. It is shown that near the dykes of the Danube reservoir — RD(H) near Bratislava — more than a thousand sensors will operate and the same amount of information can be obtained from the head-race canal (HRC), which also reaches the centre in Gabčíkovo. At Nagymaros (near Budapest) it is mainly data (of levées) acquired from the Danube tributaries (including the Váh) which are processed.

Table 7.4. Number of measurements and information transfer

Location \ Information transfer	Local reading	Local centre	Local centre plus long distance transfer	Long distance transfer only	Sum
Gabčíkovo: RD	589	89	142	212	1032
HRC	436	148	113	284	981
WP + Centre	680	350	192	76	1298
TRC	119	—	48	36	203
In centre Gabčíkovo	1824	587	495	608	3514
Nagymaros: DJ	144	4	24	38	210
DH	192	—	34	47	273
D	395	—	83	79	557
JZ	249	—	42	57	348
KO	193	—	37	57	287
JV	506	—	100	90	696
BV	284	—	55	81	420
Danube tributaries					
BV + D	606	—	103	128	837
For Nagymaros	2569	4	478	577	3628
Total: G + N	4393	591	973	1185	7142

The control centre in Gabčíkovo, equipped with a computer and many control devices, will have the following functions:

(a) data acquisition (water levels, pressures, etc.) from embankment sensors;
(b) data validation;
(c) data processing computation of theoretical effects and their conclusions;
(d) data storage (measured values and computed data are saved for future retrieval and research purposes);

(e) management of phone or tele-transmission of messages to remote installations (data, warnings, alarms, for internal malfunctions, etc.);
(f) management of recording onto cassette magnetic-tape, if this is to be effected locally. Transcription for data bank storage on standard;
(g) management of verbal communication with maintenance operator (visualization); execution test instruction, etc.

The hydroelectric plant in Gabčíkovo (CG) will be a leading station (Figs. 7.34, 7.35) for the operation of the whole Danube water-resource scheme and a centre for automation research. Almost all data will be derived from the water level in the reservoir and in the head-race canal which will be visualized in Gabčíkovo (G). Here there will be display for more than 200 automatic displacement sensors (Table 7.4). Water level, pore pressure and displacement data will be printed and stored successively. The mean data will come from hardware providing an information flow from the embankment and its model to the computer (on-line) and data-processing centre.

The location of sensors (probes) in the embankment profiles can be shown as in Fig. 7.35 representing a cross-section of reservoir (R) and its embankment with the bore holes included the profile. Control organs (pipe-lines and seepage channels) can be seen here, as well as a control well (CW) which has to prevent the leakage of groundwater seeping through the sandy gravel (alluvial) deposits, while the first-named organs control the seepage water percolating through the embankment body. Piezometric probes (PP) have to record the groundwater level (pressure). A levelling point (LP) allows investigation of the displacement of the embankment and surroundings, referred to fixed points (FP). No stress measurement is provided because it is negligible since it is small — these is no danger of mechanical failure.

The location of instruments along canal embankments and in levées is much the same (Figs. 7.34, 7.36). They are arranged within the profiles, such that the sensor can be read at hand, or at a distance. A different way of reading is to install three, four or even five sensors in a measurement profile. In the lower part of the structure on a length 0.0—4.5 km and 4.5—13.5 km, there are five instruments on one profile; from 13.5—18.0 km there are four sensors (for bore holes) and from 18.0 to 25.0 km only three. This disposition takes the magnitude of danger and maintenance by surveyors into account. Here the subsoil stability of the structure was noted as a priority; concrete structures were also respected.

The weir and hydroelectric station with its information centre, control seat and main computer, governing the measurements and management of communication with the maintenance operator has the maximum number of installations in its vicinity (39 different sensors) as mentioned previously (Table 7.5).

The reliability of measurements depends on the reliability of instruments themselves and of the type of model for the structures put into the deterministic model constructed by the designer. The warning and alarm system derives its action

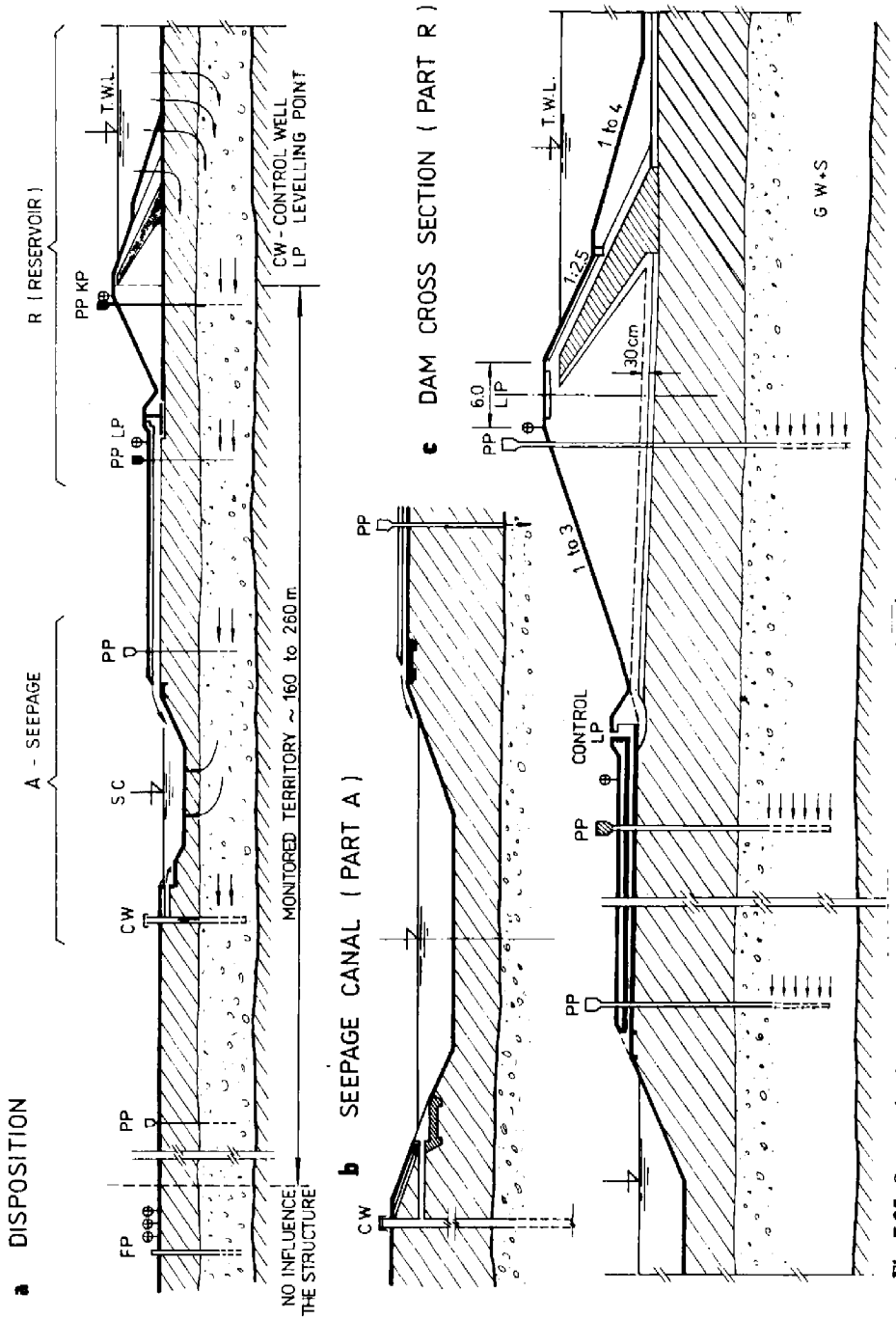

Fig. 7.35. Sensors in the cross-section of the Danube valley. a — the piezometer and wells near the structure, b — seepage canal and control of the territory, c — control of the dam and control points position.

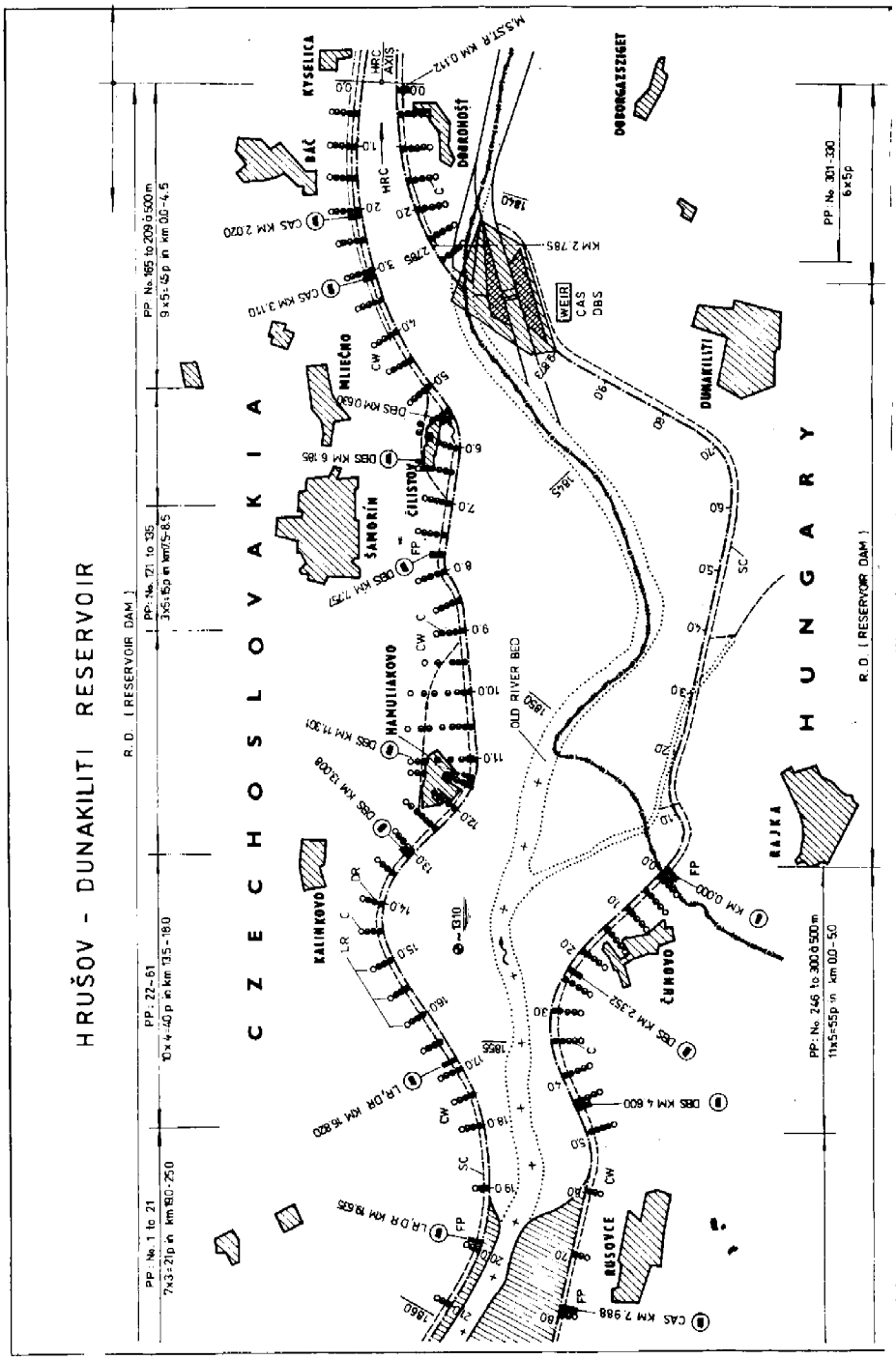

Fig. 7.36. The Hrušov-Dunakiliti reservoir control system. CAS — canal auxiliary (concrete) structure, DBS — dam auxiliary (concrete) structure, CW — control well, PP — piezometric probes, LR — local reading, DR — distance reading, FP — fix point.

Table 7.5. List of measurements, instrument (probe) numbers and measurement locations on the Danube scheme (Bratislava—Budapest)

Location	1	2	3	4	5	6	7	8	9	10	11	12	13	14	15	16	17	18	19	20	21	22	23	24	25	Remarks
G – RD (H)	–	–	–	36	206	126	–	97	330	100	3	4	14	15	13	–	–	–	20	–	–	–	–	–	–	See Fig. 7.36
G – HRC	–	–	–	30	192	–	–	54	339	192	–	2	23	17	19	–	–	6	–	50	–	10	3	–	–	See Fig. 7.34
G – WP + Centre	24	20	20	–	36	300	120	–	72	60	–	2	3	2	3	–	6	1	10	10	30	76	40	160	200	
G – TRC	–	–	–	12	67	–	–	71	66	30	–	1	–	–	–	–	–	–	–	–	–	–	–	–	–	
$\sum$ G	24	20	20	78	501	426	120	222	807	382	3	9	40	34	35	–	6	7	30	60	30	86	43	160	200	Reading Br. + G.
N: L-DJ	–	–	–	6	58	–	–	22	56	20	–	2	8	10	8	–	–	–	–	–	–	–	–	–	–	
L-DH	–	–	–	9	69	–	–	37	96	30	–	2	5	7	5	8	–	–	–	–	–	–	–	–	–	
L-D	–	–	–	15	144	–	–	48	244	60	–	1	7	9	7	4	–	–	–	–	–	–	–	–	–	
L-JZ	–	–	–	9	90	–	–	35	128	30	–	–	11	13	11	–	–	–	–	–	–	–	–	–	–	
L-KO	–	–	–	9	59	–	–	24	78	100	–	2	5	1	1	20	–	–	–	–	–	–	–	–	–	
L-KV	–	–	–	18	150	–	–	59	296	60	–	1	13	16	13	–	–	–	–	–	–	–	–	–	–	
L-BV	–	–	–	15	120	–	–	48	180	80	–	1	16	9	16	–	–	–	–	–	–	–	–	–	–	
L-BV + D	–	–	–	21	240	–	–	82	322	30	–	4	16	14	16	–	–	–	–	–	–	–	–	–	–	
$\sum$ N	–	–	–	102	930	–	–	355	1410	410	–	13	81	79	77	32	–	–	–	–	–	–	–	–	–	Reading G + N.
$\sum$ (G + N) total	24	20	20	180	1431	426	120	577	2217	792	3	22	121	113	112	32	6	7	30	60	30	86	43	160	200	Control Br. – Bu.

Type of measurement : 1 to 10 several kind of levelling (displacement), 11–14 water-level measurements, 15–17 flow-rate measurements, 18–20 pore-pressure and uplift measurements, 21, 22 extensometers, 23–25 geodetic measurements.

from the critical height of water in the canal and that of groundwater, which is related to fixed points in the surrounding territory obtained mainly by geodesy.

In canal embankments and their vicinity, several kinds of geodetic measurements are carried out (Table 7.5). Triangulation and optical levelling are the basic measurements which were performed as design measurements before embankment construction, besides those check measurements assumed both in the construction stage and in the period of canal operation. The fixed reference points are located at a distance of 200—260 m (160 m minimum) from the axis of the embankment or levée. Bench marks, direction finders and several probes (usually in bore holes) between these points and the axis are arranged on a measurement profile, the line of which is perpendicular to the embankment axis. Thus, the water-level gauge (piezometer), dilatometer, extensometer and fixed reference points are arranged by HRC.

In a dyke profile, where seepage water is controlled not only by longitudinal (gravel drains) but also transverse drains, this sort of measuring profile is complemented by a measuring shaft, pipe-line water collector and seepage channel with a deep control and observation well (1000 mm in diameter). Measurement in both canal embankments and levées have almost the same scheme of location for instruments on the downstream side of the embankment, but the quantities to be controlled and the period of observation and long-distance information transfer, data validation, data processing (computation) and storage are different. For canal embankments an automatic, digital, on-like control, performed periodically, is provided. Meanwhile, dykes (levées) have to be controlled mainly during flood periods. The displacements of the structure and leakage into it and into its subsoil have to be monitored to create a continuous (during the flood) streamlined flow-line of information, processing and storage as well as off-line updating of a data base. To this end, a visual display unit and a printer for the data needed for an alarm are being considered for the information and computer centre in Gabčíkovo.

In the project, a variety of measurements in the Danube valley on the Czechoslovak experiences of flood damage from the years 1954, 1965, 1971 and those of the Danube levée disaster in 1965 were taken into account. At the time of the reconstruction of these structures (in the years 1966 to 1976), partial account was taken of the fact that the damage was initiated in the subsoil. Therefore, three types of passive antiseepage measures were performed on the upstream side of the levée: a slurry trench at the toe (3.5—4.5 m deep or more, 26 km in length), a deep slurry trench, filled in with loam and cement concrete forming a wall 14.5—27 m in depth and 32 km in length, and a horizontal silty clay blanket (120—260 m wide, over 40 km in length) as mentioned in Chapters 4 and 6.

The first and second methods of subsoil protection showed many disadvantages during 5 to 8 years of operation, because piping phenomena in sandy gravels and

liquefaction of sands are only partially reduced. Because of this fact, a new lay-out of antiseepage measures was designed. It (Fig. 7.37a) consists of pasive and active methods of subsoil protection at the toe. The protective drainage (Fig. 7.37b) near the gravel toe of the levée, is equipped with detecting elements which, give a warning signal when the water level exceeds the danger mark. Combination of the

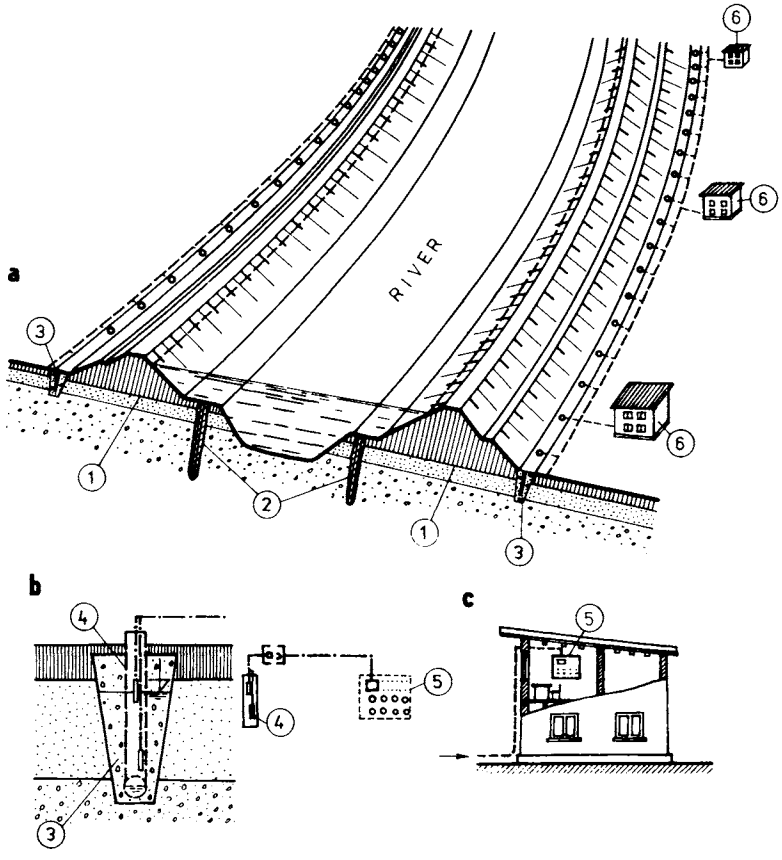

Fig. 7.37. The subsoil protection and control. a — complete scheme, b — protective drain, c — watch-house; 1 — canal embankment, 2 — antiseepage element (slurry trench wall), 3 — protective drain, 4 — exploratory boring with electric contacts, 5 — control desk, 6 — watch-house.

hydraulic and electric systems, connected to the answering (reply) set and the control desk in the control centre (Fig. 7.37c) enables a watch to be kept on any dangerous situation arising along the levée. It allows an alarm to be sounded, and precautions to be taken, required to ensure the safety of the structure and the whole territory.

REFERENCES

ABRAMOV, S. K., KUZNETSOVA, N. A., MUFTAKHOV, A. Zh. (1964), Simplified Calculation Methods of Two Lineal Drainages (in Russian), Izd. literatury po stroiteľstvu, Moscow
(АБРАМОВ, С. К., КУЗНЕЦОВА, Н. А., МУФТАХОВ, А. Ж. (1964), Пластовые дренажи в строительстве, Изд. литературы по строительству, Москва).

AÉROV, M. É., TODES, O. M. (1968), Hydraulic and Thermal Basis of Operation of the Apparatus with a Steady Fluidized Bed (in Russian), Izd. Khimiya, Leningrad
(АЭРОВ, М. Э., ТОДЕС, О. М. (1968), Гидравлические и тепловые основы работы аппаратов со стационарным и кипящим зернистым слоем, Изд. Химия, Ленинград).

AKHUTIN, A. N. (1951), Volga—Don Canal (in Russian), Izd. Pravda, Moscow
(АХУТИН, А. Н. (1951), Волго-Донской канал, Изд. Правда, Москва).

AMBRASEYS, N. N. (1960), Über die Berechnung von erdbebensicheren Erddämmen, VDI-Nachrichten **102,** 26, 1241—1243.

AVERYANOV, S. F. (1949), Rough estimation of the role of filtration in the zone of curve shaped bed (in Russian), Doklady Akad. Nauk SSSR **69,** 3—24
(АВЕРЬЯНОВ, С. Ф. (1949), Приближенная оценка роли фильтрации в зоне криволинейной каймы, Доклады АН СССР **69,** 3—24).

BABUSHKIN, V. D. (1955), Methods of the Shaft Wells Calculations (in Russian), VNII-VODGEO, Moscow
(БАБУШКИН, В. Д. (1955), Методы расчета шахтных коллоидов, ВНИИ-ВОДГЕО, Москва).

BARTOLČIČ, M. (1968), Forecasting of groundwater regime of the Žitný ostrov (in Slovak), Research report, Water Research Institute, Bratislava
(Prognóza režimu spodných vôd Žitného ostrova, Výskumná správa, Výskumný ústav vodohospodársky, Bratislava).

BAUER, K. (1969), Gründung und Bodenverdichtung mit Tiefenrüttlern, Frankfurt.

BAŽANT, Z. (1967), Some questions of filtration stability violation in gravelly sand foundation of the levées (in Czech), Vodohospodársky časopis **15,** 2, 82—93
(Některé otázky porušování filtrační stability ve štěrkopísčitém podloží říčních hrází, Vodohospodársky časopis **15,** 2, 82—93).

BAŽANT, Z., HÁLEK, V. (1968), Some theoretical questions of antiseepage measure designs against water losses from rivers and water reservoirs in the Danube valley (in Czech), Proc. Technical University, Brno, 73—87
(Některé teoretické otázky projektování ochranných opatření proti vlivu průsaku z řek a vodních nádrží Podunajské nížiny, Sborník VUT, Brno, 73—87).

BEAR, J. (1978), Relations between microscopic and macroscopic description in porous media, Proc. Symp. Scale Effects, IAIHR, Thesaloniki, 1—32.

BELL, F. G. (1977), How aggregates affect concrete quality, Civil Engineering **47,** July/Aug., 39—43.

BERÁNEK, J., SOKOL, D. (1961), Fluidization Technics (in Czech), State publishers of technical literature, Prague (Fluidizační technika, SNTL, Praha).

BERTRAM, G. E. (1967), Experience with seepage control measures in earth dams, Proc. Ninth Int. Congress ICOLD, Istanbul, **3,** 24—29.

BISHOP, A. W. (1954), The use of pore-pressure coefficient in practice, Geotechnique (G.B.) **4,** 14—18.
— (1955), The use of the slip circle in the stability analysis of earth slopes, Geotechnique (G. B.) **5,** 7—17.
BISHOP, A. W., BJERRUM, L. (1960), The relevance of the triaxial test to the solution of stability problems, Research Conference, Boulder, Colorado.
BOCHEVER, F. M. (1966), Evaluating the performance of shore embankments with consideration given to imperfection of river beds (in Russian), VNII-VODGEO, Moscow, 218—226
(БОЧЕВЕР, Ф. М. (1966), Оценка производительности береговых водозаборов с учетом несовершенства речных русел, ВНИИ-ВОДГЕО, Москва, 218—226).
BORELI, M. (1978), Hétérogénéité des milieux poreux et effet d'echelle, Proc. Symp. Scale Effects, IAIHR, Thesaloniki, 33—70.
BOROWICKA, H. (1968), Hochwasserdam am linken Donauufer, Mitteilungen der Technischen Hochschule Wien, Heft 19.
BOUWARD, H. (1960), Barrages mobiles et prises d'eau, Eyrolles, Paris.
BOUWER, H. (1965), Theoretical aspects of seepage from open channel, Proc. ASCE, HY 3, 37—59.
BRAUNS, J., BLINDE, A. (1978), The role of stratification in the penetration of grouts through fluvial sediments, Proc. Symp. Scale Effects, IAIHR, Thesaloniki, 71—89.
BULATOV, G. YA. (1968), To the evaluation of the seepage resistance of heterogeneous grained low cohesion soils (in Russian), Trudy LPI im. M. I. Kalinina (Leningrad), 292, 96—100
(БУЛАТОВ, Г. Я. (1968), К оценке фильтрационной прочности разнозернистых малосвязных грунтов, Труды ЛПИ им. М. И. Калинина (Ленинград), 292, 96—100).
CAMBEFORT, H. (1961a), Recherche des écoulements d'eau privilégiés et prélèvements intacts de sols cohérents hetérogènes, Proc. Fifth Int. Conf. SMFE, Paris, 23—27.
— (1961b), L'injection et ses problèmes, Bull. Techn. Suisse Romaine, Sep., 36—42.
— (1964), Injection des sols, Eyrolles, Paris.
— (1967), Lutte contre les effets des écoulements sous les barrages, Proc. Ninth Congress ICOLD, Istanbul, 81—97.
— (1972), Géotechnique de l'ingénieur, Reconnaissance des sols, Eyrolles, Paris.
CAQUOT, A., KÉRISEL, J. (1956), Traité de méchanique des sols, Gauthier—Villars, Paris.
CARMAN, P. C. (1956), Flow of Gases through Porous Media, Butterworths, London.
CASAGRANDE, A. (1959), An unsolved problem of embankment stability on soft ground, Proc. First Panamerican Conf. SMFE, Mexico, 721—746.
— (1974), Role of the "calculated risk" in earthwork and foundation engineering, Terzaghi Lectures 1963—1972, ASCE, New York, 72—121.
CASAGRANDE, A., RIVARD, P. J. (1959), Strength of highly plastic clays in Norvegian Geotechnical Institute, Harvard Soil Mechanics System, No. 60. Harvard Univ., Cambridge, Mass.
CHARNYI, I. A. (1951), Groundwater (in Russian), Gostekhizdat, Moscow
(ЧУГАЕВ, Р. Р. (1965), О расчетах фильтрационной прочности основания плотин, Гид-
CHUGAEV, R. R. (1965), Calculation of seepage resistance of the dam foundations (in Russian), Gidrotekhnicheskoe stroiteĭstvo **35,** 2, 34—37
(ЧУГАЕВ, Р. Р. (1965), О расчетах фильтрационной прочности основания плотин, Гидротехническое строительство **35,** 2, 34—37).
CLOUGH, R. W., WOODWARD, R. I. (1967), Analysis of embankment stresses and deformations, Proc. ASCE, SM 4, 523—536.
COMOLET, R. (1969), Mécanique des fluides, Tome 1 — Statique et dynamique, Masson, Paris.
Construction Industry International (CII) (1977), Scrapers hit French canal target, CII House (London), 6, 48—54.
COULOMB, R., MOREAU, J. (1967), Achèvement et mise en service du réservoire Seine, Construction (Paris), 3, 281—291.
CRAIG, R. F. (1974), Soil Mechanics, Van Nostrand Reinhold, New York.

DACHLER, R. (1936), Grundwasserströmung, Springer-Verlag, Wien.
DARCY, H. (1856), Les fontaines publiques de la ville de Dijon, Paris.
DAVIDENKOFF, R. V. (1964), Deiche und Erddämme, Werner-Verlag, Düsseldorf.
DAVIS, C. V. (1952), Handbook of Applied Hydraulics, McGraw-Hill, Toronto.
DAVIS, S. N., DE WIEST, R. J. W. (1966), Hydrology, McMillan, London.
DE BEER-LOUISBERG, E. (1961), Définition des coefficients de sécurité, Proc. Fifth Int. Conf. SMFE, Paris, 541—555.
DELATTRE, P. (1959), The Rhône dévelopment — Montélimar, Travaux (Paris), 2, 124—128.
DEMMER, W., GROLITSCH, E. (1968), Bodenuntersuchungen und ihre Auswertung für den Damm Freistritz. Österreichische Zeitschrift, 10, 656—662.
DESAI, CH. S., ABEL, J. F. (1972), Introduction to the Finite Element Method, Van Nostrand Reinhold, New York.
DRACOS, Th. (1978), Time behaviour and time scales of groundwater flow, Proc. Symp. Scale Effects, IAIHR, Thesaloniki, 71—80.
DROUHIN, M. et al. (1948), Méthodes de recherches et instruments pour mesurer les efforts et les déformations dans les barrages en terre et en béton, Proc. Third Int. Congress ICOLD, Stockholm, 9.1—9.15.
DUNCAN, J. M., CHANG, C. Y. (1970), Nonlinear analysis of stress and strain in soils, Proc. ASCE, SM 4, 1629—1654.
EHRENBERG, J. (1936), Standfestigkeitsberechnung von Staudämmen, Proc. Second Int. Congress ICOLD, Washington, 72—78.
EISENSTEIN, Z. (1974), Application of finite element method to analysis of earth dams, Seminar on Soil Mechanics, Rio de Janeiro.
ESCANDE, L. (1943), Hydraulique générale, L'Ecole Polytechnique de Toulouse.
FELLENIUS, W. (1927), Erdstatische Berechnung mit Reibung und Kohäsion, W. Ernst, Berlin.
— (1936), Calculation of the stability of earth dams, Proc. Second Int. Congress ICOLD, Washington, 445—453.
FINN, L. D., PICKERING, D. J. (1971), Sand liquefaction investigation, Proc. ASCE, SM 4, 639—659.
FLORIN, V. A. (1948), Theory of Soil Mass Compaction, Gos. izd. stroit. lit., Moscow
(ФЛОРИН, В. А. (1948), Теория уплотнения земляных масс, Гос. изд. строит. лит., Москва).
FORCHHEIMER, P. H. (1914), Hydraulik, B. G. Teubner-Verlag, Leipzig.
FRANKE, E. (1972), Grundsätze für die Beweisung von dichten Deckwerken, Der Bauingenieur **47**, 47—53.
FREY, Z. B. (1963), Development and evaluation of soil bearing capacity, Foundations of structures, US Army WES, Vickburg, Miss.
FRÖHLICH, K. O. (1955), General theory of the stability of slopes, Geotechnique (G. B.) **5**, 37—43.
FÜHRBÖTER, A. (1966), Der Druckschlag auf Deichböschungen, Mitteilungen des Franzius Instituts, Technische Universität Hannover, Heft 28.
GARDE, J. R. (1969), Variation of the drag coefficient of the sphere rolling along a boundary, La Houille Blanche, 7, 727—732.
GAZDARU, A., KELLNER, P., GEORGE, D. (1974), The leakage of water — an irrigation canal and its accompanments (in Rumanian), Studii de geotehnică, fundații si constructii hidrotehnice **18**, 197—230
(Exfiltrațiile dintr — un canal de aducțiune pentru irigații acestora, Studii de geotechnică, fundații si constructii hidrotehnice **18**, 197—230).
GAZIEV, E. (1977), Problems associated with special types of fill dams, Discussion, Proc. Twelfth Int. Congress ICOLD, Mexico, 52—54.
GEIER, F. H., MORRISON, W. R. (1968), Burried Asphalt Membrane Canal Lining, US Gov. Print. Oft., Washington.

GIBBS, H. J., HOLTZ, W. G. (1957), Research on determining the density of sand by spoon penetration testing, Proc. Fourth Int. Conf. SMFE, London, SM 4, 53—62.

GIRINSKIĬ, N. K. (1947), Some problems of groundwater dynamics (in Russian), Proc. GIG, 9, Moscow (Гиринский, Н. К. (1947), Некоторые вопросы динамики подземных вод, Сб. ГИГ, 9, Москва).

GUBIN, F. F. (1950), Hydroelectric Power Stations (in Russian), Gosénergoizdat, Moscow (Губин, Ф. Ф. (1950), Гидроэлектрические станции, Госэнергоиздат, Москва).

GULOTI, P. et al. (1970), Control of sediment flow into subsurface drains, Proc. ASCE, IR 5, 437—449.

GYALOKAY, M. (1956), Destination of groundwater inflow into Žitný ostrov region by water balance method (in Slovak), Vodohospodársky časopis **4,** 2, 134—142
(Určovanie prítoku podzemných vôd do územia Žitného ostrova metódou vodnej bilancie, Vodohospodársky časopis **4,** 2, 134—142).

HÁLEK, V. (1963), The HYDRAL electric network analyser (in Czech), Proc. Technical University, Brno, 2 (Síťový elektrický analysátor HYDRAL, Sborník VUT, Brno, 2).

— (1966), On the mechanism of river bank infiltration in the soil profile composed of some soil layer (in Czech), Vodohospodársky časopis **14,** 4, 312—321 (O mechanismu nestacionární břehové infiltrace do půdního profilu složeného z několika vrstev zeminy, Vodohospodársky časopis **14,** 4, 312—321).

— (1967), On the generation of privileged ways in the sub-base of levées (in Czech), Proc. Sci. Conf., Brno, 127—134 (Poznámky k vzniku privilegovaných cest v podloží ochranných hrází, Sborník vědecké konference, Brno, 127—234).

HÁLEK, V., RYBNIKÁŘ, J. (1963), Hydrotechnical Research (in Czech), State publishers of technical literature, Prague
(Hydrotechnický výskum, SNTL, Praha).

HÁLEK, V., ŠVEC, J. (1979), Groundwater Hydraulics, Academia, Prague.

HAMMAD, H. Y. (1960), Seepage losses from parallel canal systems, Proc. ASCE, EM 4, 43—50.

HANSEN-BRINCH, J., LUNDGREN, H. (1960), Hauptprobleme der Bodenmechanik, Springer-Verlag, Berlin.

HANUŠKIN, J. (1924), Waterwork cooperative on the River Ondava (in Slovak), Chronicle of the Cooperative, Trebišov, 86—87
(Vodné družstvo na Ondave, Kronika družstva Trebišov, 86—87).

HARPAZ, Y. et al. (1963), The place of isotope methods in groundwater research. Proc. Symp. Radioisotopes in Hydrology, Tokyo, 175—192.

HARPER, J. F. (1970), Viscous drag in steady potential flow past a buble, Chem. Eng. Sci. **25,** 342—343.

HARR, E. (1962), Groundwater and Seepage, McGraw-Hill, New York.

HARZA, L. (1935), Uplift and seepage under dams constructed on sand, Proc. ASCE, HY 4, 1342—1357.

HAVLÍČEK, J. (1964), The relation of resistance of soils against shear depending on its effective stress (in Czech), in: Selected Theoretical Problems of Earth Dam Constructions, SAV Publishers, Bratislava, 103—116 (Závislost odporu zemin proti usmyknutí na jejich efektivním napětí, v: Vybrané teoretické problémy stavby zemných hrádzí, Vydavateľstvo SAV, Bratislava, 103—116).

— (1966), The causes of the Danube levées disaster near Čičov (in Czech), Vodní hospodářství, 8, 341—347 (Příčiny protržení dunajské hráze u Čičova, Vodní hospodářství, 8, 341—347).

HEINRICH, G., DESOYER, K. (1955), Hydromechanische Grundlagen für Grundwasserströmungen, Ingenieur Archiv.

HOBST, L. (1962), Evolutionary Structures of Waterworks (in Czech), State publishers of technical literature, Prague
(Vývojové konstrukce vodních staveb, SNTL, Praha).

HODGSON, M. (1977), Waterproofing concrete, Civil Engineering **47,** July/Aug., 47—49.

HOFFMANN, W. (1968), Besondere Mitteilungen zur Frage der Beständigkeit der Dichtungen der Erddämme, Technische Hochschule, Dresden.

HOLLAND, C. R., ROTHWELL, E. (1977), Model studies of fabric dust filtration (Flow characteristics), Filtration and Separation, 2, 30—32.

HOUGH, B. K. (1957), Basic Soil Engineering, Roland Press, New York.

HUARD de la MARRE, P. (1958), Résolution des problèmes d'infiltration à la surface libre, Eyrolles, Paris.

HUNT, B. W. (1971), Vertical recharge of unconfined aquifer, Proc. ASCE, HY 7, 1007—1030.

HVORSLEV, M. J. (1949), Time lag in the observation of groundwater wells and pressures, US Army WES, Vickburg, Miss.

— (1951), Time lag and soil permeability in groundwater observatories, US Army WES, Vickburg, Miss.

IBAD-ZADZE, YU. A., SHTEINMAN, B. S. (1972), The field steady of sand motion through porous medium. Proc. IAIHR-ISSS, Ontario, 173—205.

ICOLD (1976), Twelfth International Congress on Large Dams — Transactions, Mexico City, March 29—April 2, Mexico.

— (1977), Committee on Analysis and Design of Dams: Finite Element Method in Analysis and Design of Dams, Bulletin 30, Paris.

IHRING, D., LÁSZLOFFY, W. (1954), Danube flow of July 1954 (in Hungarian), Offprint of Rev. Hung. Technics, 11
(A Duna juliusi árvize, Különnyomat a Magyar Technika, 11).

IRMAY, S. (1958), On the theoretical derivation of Darcy and Forchheimer formulas. Amer. Geophys. Union **39,** 702—707.

— (1967), On the meaning of the Dupuit and Pavlovsky approximations in aquifer flow, Journal of Water Resources **5,** 2, 5—12.

— (1971), The mechanics of entrainment of solid particles in turbulent channel flow, Proc. Int. Symp. Two-Phase Systems, Haifa, 23—27.

ISTOMINA, V. S. (1957), Seepage Stability of Soils (in Russian), Gos. izd. po stroit. i arkh., Moscow
(ИСТОМИНА, В. С. (1957), Фильтрационная устойчивость грунтов, Гос. изд. по строит. и арх., Москва).

IZBASH, S. V., KHALDRE, KH. I. (1959), Hydraulics of the River Bed Overpass (in Russian), Gosénergoizdat, Moscow
(ИЗБАШ, С. В., ХАЛДРЕ, Х. И. (1959), Гидравлика перекрытия русел рек, Госэнергоиздат, Москва).

JAKUBEC, L. (1966), Piping registrated near the Danube levées during the flood in the year 1965 (in Slovak), Reports of the Geological Institute, Bratislava, 1—86
(Vývery zaznamenané v podunajských ochranných hrádzach počas povodne r. 1965, Správa IGHP, Bratislava, 1—86).

JAKUBEC, L., TICHÝ, Š. (1964), Danube scheme. Head-race canal and construction materials (in Slovak), Reports of the Geological Institute, Bratislava, 1—182
(Dunajské vodné dielo. Prívodný kanál a stavebné materiál, Správa IGHP, Bratislava, 1—182).

JANSEN, R. B. et al. (1976), Problems of hydraulic fill dams, Proc. Twelfth Int. Congress ICOLD, Mexico, 337—361.

JEPPSON, R. W. (1968), Seepage from channels through layered porous medium, Water Research (USA) **4,** 2, 435—445.

JÜRGENSON, L. (1934), The application of theories of elasticity and plasticity to foundation problems, Journal Boston SCE.

KÉZDI, Á. (1967), Stabilized Earth Roads (in Hungarian), Akadémiai Kiadó, Budapest (Stabilizát földutak, Akadémiai Kiadó, Budapest).

— (1974), Handbook of Soil Mechanics, Akadémiai Kiadó, Budapest; Elsevier, Amsterdam.
— (1976), Handbuch der Bodenmechanik. IV. Anwendung der Bodenmechanik in der Praxis, Akadémiai Kiadó, Budapest; VEB Verlag für Bauwesen, Berlin.
KHOSLA, A. N. (1936), Design of weirs on permeable foundations, Central Board of Irrigation and Power, 12—15.
KIRKHAM, D. (1964a), Physical artificies and formulas for approximating water table fall, Proc. Soil Sci. Soc. Amer. **28,** 585—590.
— (1964b), Exact theory for the shape of the free water surface, Journal of Geophysical Research, June, 2537—2545.
KOLÁŘ, V. et al. (1975), Berechnung von Flächen- und Raumtragwerken nach der Methode der finiten Elemente, Springer-Verlag, Wien.
KOPACZ, J. (1961), Distribution des constraints à la rupture, forme de la surface de glissement et hauteur théoretique des talus, Proc. Fifth Int. Conf. SMFE, Paris, 641—651.
KOROLEV, A. A. (1956), Canals of the Hydropower Plants, Gosénergoizdat, Moscow (КОРОЛЕВ, А. А. (1956), Каналы гидроэлектрических станций, Госэнергоиздат, Москва).
KOSTER, J. (1975), Push Towns in Canals, Hydraulic Laboratory, Delft.
KOSTYAKOV, A. N. (1951), Principles of Irrigation Systems, Selkhozizdat, Moscow (КОСТЯКОВ, А. Н. (1951), Основы мелиорации, Сельхозиздат, Москва).
KOZENY, J. (1927), Theorie und Berechnung der Wasserströmung, Wasserkraft und Wasserwirtschaft (Wien), 5, 37—43.
— (1953), Hydraulik — ihre Grundlagen und praktische Anwendung, Springer-Verlag, Wien.
KRATOCHVÍL, J. (1978), Mathematical modelling of stress and strain of multiphase heterogeneous porous media on the solution by finite elements method (in Czech), Vodohospodársky časopis **26,** 3, 118—126
(Matematické modelování problémů deformací a napětí mnohofázového porovitého prostředí a jeho řešení metodou konečných prvků, Vodohospodársky časopis **26,** 3, 118—126).
KRATOCHVÍL, J., HANSLIAN, J. (1969), Stresses and displacements solution for fill dams (in Czech), Inženýrské stavby **17,** 1, 7—10
(Řešení napětí a přetvoření sypaných hrází, Inženýrské stavby **17,** 1, 7—10).
KRATOCHVÍL, S. (1961a), The sealing of earth and rock dams (in Czech), Inženýrské stavby **9,** 10, 312—328
(Tesnění zemních a kamenitých přehrad, Inženýrské stavby **9,** 10, 312—328).
— (1961b), Water Reservoirs and Dams (in Czech), ČSAV Publishers, Prague (Vodní nádrže a přehrady, Nakladatelství ČSAV, Praha).
— (1965), Evolution of asphaltic concrete sealing of large dams (in Czech), Inženýrské stavby **13,** 10, 326—331 (Vývoj těsnení přehradních hrází asfaltovým betonem, Inženýrské stavby **13,** 10, 326—331).
— (1968a), Sealings and slope protection of large canal structures (in Czech), Inženýrské stavby **16,** 7, 246—252 (Utěsnení a ochrana velkých kanálů asfaltovým betonem, Inženýrské stavby **16,** 7, 246—252).
— (1968b), Sealing and strengthening of big canals by asphaltic concrete (in Czech), Inženýrské stavby **16,** 11, 465—470 (Utěsnění a spevnění velkých kanálů asfaltovým betonem, Inženýrské stavby **16,** 11, 465—470).
— (1969), The wind waves parameters on water reservoir (in Czech), Vodohospodársky časopis **17,** 4, 413—425 (Parametry větrových vln na přehradní nádrži, Vodohospodársky časopis **17,** 4, 413—425).
— (1974a) Beitrag zur Frage der Asphaltbetondichtung im Wasserbau, Wissenschaftliche Zeitschrift der Hochschule Weimar, 3, 151—159.
— (1974b) The design of asphalt concrete aporn of the head-race canal of the water power plant Gabčíkovo—Danube scheme (in Czech), Hydroconsult, Bratislava (Návrh asfalto-betonového

plášťového těsnění přívodního kanálu vodní elektrárny Gabčíkovo — vodního díla Dunaj, Hydroconsult, Bratislava).

— (1975), The use of the asphalt concrete sealing in the technology of the hydraulic structure in Gabčíkovo (in Czech), Communication for Hydroconsult, Bratislava (Použití asfalto-betonového těsnění při výstavbě hydrotechnických staveb v Gabčíkově, Sdělení pro Hydroconsult, Bratislava).

— (1976), Periodical wave transformation by transition from deep water to a shallow water (in Czech), Vodohospodársky časopis **24,** 6, 592—611 (Transformace periodické vlny při přechodě hluboké vody na mělkou vodu, Vodohospodársky časopis **24,** 6, 592—611).

— (1977), Water impact on slopes (in Czech), Vodohospodársky časopis **25,** 1, 27—42 (Vodní úder na svahy, Vodohospodársky časopis **25,** 1, 27—42).

— (1979), Waves developed by a vessel in a limited nonflowing water, Vodohospodársky časopis **27,** 4, 359—377 (Vlny vyvolané plavidlem na omezené neproudící vodě, Vodohospodársky časopis **27,** 4, 359—377).

KRATOCHVÍL, S., HÁLEK, V. (1959), The effect of sealing elements of hydraulic structures founded on permeable subsoil (in Czech), Proc. Technical University, Brno, 3—4
(Účinnost těsnících prvků hydrotechnických staveb, Sborník VUT, Brno, 3—4).

LAMBE, T. W. (1960), The engineering behaviour of compacted clays, Proc. ASCE, SM 5, 43—52.

LAMBE, T. W., WHITMAN, R. V. (1969), Soil Mechanics, Wiley, New York.

LANE, E. W. (1935), Security from underseepage, Proc. ASCE, EM 4, 1269—1274.

LEATHERWOOD, F. N., PETERSON, D. F. (1954), Hydraulic head loss at the interface between uniform sands of different size, Trans. Amer. Geophys. Union **35,** Aug., 588—594.

LEĬBENZON, L. S. (1953), Ground Hydraulics of Water, Oil and Gas, Izd. Akad. Nauk SSSR, Moscow (Лейбензон, Л. С. (1953), Подземная гидравлика воды, нефти и газа, Изд. АН СССР, Москва).

LELIAVSKY, S. (1957), Irrigation and Hydraulics, Wiley, New York.

LEVA, M. et al. (1956), La prévision du débit de la fluidisation dans les solides granulaires, Génie chimique **75,** 33—42.

LICHNER, L. (1976), The use of magnetic counter for unit weight measurement (in Polish), Pomiary i automatika, 3, 104—105
(Stosowanie magnetycznych czujnikow do merżenia ciężaru objętościowego, Pomiary i automatika, 3, 104—105).

LINDEN-ALIMAK, AG (1978), A new method of sounding soil strata, Skellefteå, 7.

LINDQUIST, E. G. (1933), On the flow of water through porous soil, Proc. First Int. Congress ICOLD, Stockholm, 123—128.

LOBDELL, H. L. (1969), Rate of constructing embankments of soft ground, Proc. ASCE, SM 5, 61—68.

LUBOCHKOV, I. A. (1962), Suffosion-resistant noncohesive soils, Izv. VNIIG **71,** 61—90
(Лубочков, И. А. (1962), Несуффозионные несвязные грунты, Изв. ВНИИГ **71,** 61—90).

LUDEWIG, M. (1974), Konstruktive Grundlagen für die bituminöse Aussendichtung in der DDR, Wissenschaftliche Zeitschrift der Hochschule Weimar, 160—164.

LUDEWIG, M., THIEME, J. (1978), Die Sicherheit der Böschungen bei bituminösen Aussenhautdichtungen in Wasserbau, Wissenschaftliche Zeitschrift der Technischen Hochschule Dresden, 151—163.

MALLET, CH., PACQUANT, J. (1951). Les barrages en terre, Eyrolles, Paris.

MARSAL, R. J., ALBERO, J. A. (1976), Performance of dams built in Mexico, Proc. Twelfth Int. Congress ICOLD, Mexico, 791—798.

MARTIN, C. S. (1971), Behaviour of porous bed near flow singularity, Proc. ASCE, SM 2, 393—415.

MARTIN, H. C. (1966), Introduction to Matrix Methods of Structural Analysis, McGraw-Hill, New York.

MASLOV, M. M. (1958), Problem of heigh earth dam density in condition of seismic activity, Proc. Sixth Int. Congress ICOLD, New York, 468—472.

MATSUI, J. (1976), Measurement of relative displacement, Proc. Twelfth Int. Congress ICOLD, Mexico, 895—918.

MATTHES, G. H. (1951), Paradoxes of the Mississippi, W. H. Freeman, San Francisco.

MENCL, V. et al. (1965), Three questions on the stability of slopes, Proc. Sixth Int. Conf. SMFE, Montreal, 512—516.

MIDDLEBROOKS, T. A. (1948), Seepage control for large earth dams, Proc. Third Int. Congress ICOLD, Stockholm, 10.1—10.16.

— (1953), Earth-dam practice in the United States, Proc. ASCE, SM 3, 695—728.

MIDDLEBROOKS, T. A., JERRIS, W. H. (1947), Relief wells for dams and levées, Proc. ASCE, HY 4, 1321—1334.

MISTÉTH, E. (1967), Basic principles for structural design by probability theory (in Hungarian), Mélyépitéstudományi Szemle, 7, 225—235; 8, 326—336
(Müszaki létesimények erötani számításának a valósziüségelméleten nyogvó alapelvei, Mélyépitéstudományi Szemle, 7, 225—235; 8, 326—336).

MORGENSTERN, N. R. (1963), Stability charts for earth slopes during rapid drawdown, Geotechnique (G.B.) **13**, 121—131.

MORGENSTERN, N. R., PRICE, V. E. (1967), A numerical method for solving the equations of stability of general slip surfaces, Computer Journal **9**, 388—396.

MUFTAKHOV, A. ZH. et al. (1963), To the Problem of Layer and Well Drainage Calculations, Gosstroïizdat, Moscow
(МУФТАКОВ, А. Ж. и др. (1963), К вопросу о расчетах пластовых и колодцевых дренажей, Госстройиздат, Москва).

MUSKAT, M. (1946), The Flow of Homogeneous Fluids through Porous Media, McGraw-Hill, New York.

— (1949), Physical Principles of Oil Production, McGraw-Hill, New York.

MYSLIVEC, A. (1964), Problems of choice of impermeable clay cores in earth and rock-fill dams (in Czech), in: Selected Theoretical Problems of Earth Dam Constructions, SAV Publishers, Bratislava, 163—172 (Problémy při volbě těsnících zemin vrstvy v zemních a kamenitých hrázích, v: Vybrané teoretické problémy stavby zemných hrádzí, Vydavateľstvo SAV, Bratislava, 163—172).

— (1968), Soil Mechanics (in Czech), State publishers for technical literature, Prague (Mechanika zemin, SNTL, Praha).

NAPETVARIDZE, S. G. (1959), Resistivity of Hydraulic Structures to Earthquake (in Russian), Gosstroïizdat, Moscow
(НАПЕТВАРИДЗЕ, С. Г. (1959), Сейсмостойкость гидротехнических сооружений, Госстройиздат, Москва).

NELSON, R. W., REISENAUER, A. E. (1963), Application of radioactive tracers in scientific groundwater hydrology, Proc. Symp. Radioisotopes in Hydrology, Tokyo, 207—230.

NELSON-SKORNYAKOV, F. B. (1949), Seepage in Homogeneous Porous Media, Stroïizdat, Moscow
(НЕЛЬСОН-СКОРНЯКОВ, Ф. Б. (1949), Фильтрация в однородной среде, Стройиздат, Москва).

NOORTGEDACHT, D. A., REE, G. J. (1964), Die Absperrung und Überwachung der Zuidersee, Informationsdienst der Niederlande, Den Haag.

NOSOVA, O. N. (1972), Calculation of Sandy Soils Yield (in Russian), Gosénergoizdat, Moscow
(НОСОВА, О. Н. (1972), Расчет водоотдачи песчаных грунтов, Госэнергоиздат, Москва).

NUMEROV, N. S. (1947), Calculation of seepage of the horizontal drain (in Russian), Izv. VNIIG **34**
(НУМЕРОВ, Н. С. (1947), Фильтрационные расчеты горизонтального дренажа, Изв. ВНИИГ **34**).

— (1951), On the inflow of groundwater to a rectilinear ditch (in Russian), Izv. VNIIG **46**
(НУМЕРОВ, Н. С. (1951), О притоке грунтовых вод к прямоугольной траншее, Изв. ВНИИГ **46**).

NUMEROV, N. S., ARAVIN, V. I. (1955), Calculation of Hydraulic Structures of Seepage (in Russian), Gosstroïizdat, Moscow
(НУМЕРОВ, Н. С., АРАВИН, В. И. (1955), Фильтрационные расчеты гидротехнических сооружений, Госстройиздат, Москва).

PACCARD, T. A. (1977), Seepage prevention with impermeable membranes, Civil Engineering **47,** May/June, 28—32.

PATRASHEV, A. N. (1952), Hydromechanics (in Russian), Stroïizdat, Moscow
(ПАТРАШЕВ, А. Н. (1952), Гидромеханика, Стройиздат, Москва).

PAVLOVSKII, N. N. (1922), Theory of Groundwater Motion under the Hydraulic Structures (in Russian), Politekhnicheskiĭ Institut, Leningrad, 2
(ПАВЛОВСКИЙ, Н. Н. (1922), Теория движения грунтовых вод под гидротехническими сооружениями, Политехнический институт, Ленинград, 2).

— (1930), Unsteady Motions of Groundwater (in Russian), Gosizdat, Moscow
(ПАВЛОВСКИЙ, Н. Н. (1930), Неравномерное движение грунтовых вод, Госиздат, Москва).

— (1931), Seepage through Earth Dams (in Russian), Klub uchennykh, Leningrad
(ПАВЛОВСКИЙ, Н. Н. (1931), О фильтрации воды через земляные плотины, Клуб ученных, Ленинград).

PECK, R. B., THORNBURN, T. H. (1953), Foundation Engineering, Wiley, New York.

PETER, P. (1964a) Consolidation and pore pressures in fine-grained soils of earth works (in Slovak), Stavebnícky časopis **12,** 10, 602—622 (Konsolidácia a pórové tlaky v súdržných zeminách zemných konštrukcií, Stavebnícky časopis **12,** 10, 602—622).

— (1964b), Some problems of Danube hydraulic structures foundation (in Slovak), Inženýrské stavby **12,** 8, 425—432 (Niektoré problémy zakladania vodných diel na Dunaji, Inženýrské stavby **12,** 8, 425—432).

— (1965), Water movement on the contact of soils of different permeability and its influence on the stability or organic soil slope protecting layer (in Slovak), Vodní hospodářství, 12, 9—13 (Pohyb vody na styku zemín rôznej priepustnosti a jeho vplyv na stabilitu humusovitého opevnenia svahu, Vodní hospodářství, 12, 9—13).

— (1972a), The filtration stability of cohesionless soils (in Slovak), DSc. Thesis, Technical University, Bratislava (Stabilita nesúdržných zemín, Doktorská práca, SVŠT, Bratislava).

— (1972b), Degree of filtration stability of cohesionless soils — destination by help of dimensionless characteristics, (in Slovak), Stavebnícky časopis **20,** 10, 721—738 (Určovanie stupňa filtračnej stability nesúdržných zemín pomocou bezrozmerných charakteristík, Stavebnícky časopis **20,** 10, 721—738).

— (1973), The relations between the form of grains and masstransfer resistances of porous media in the nature, Proc. RILEM Symp., Prague, E181—190.

— (1974a) The damages and failures caused by seepage in the levées vicinity of the Czechoslovak section of the Danube, Proc. SÉV, Moscow

— (ПЕТЕР, П. (1974a), Нарушения и аварии в следствие фильтрации при защитных дамбах на чехословацком участке Дуная, Сб. СЭВ, Москва).

— (1974b), Three theories of sand liquefaction and its application in the stability computation (in Slovak), Proc. Technical University, Bratislava 124—136 (Tri teórie stekutenia pieskov a ich aplikácia pri výpočte stability, Zborník SVŠT, Bratislava, 124—136).

— (1974c), Piping problem in the Danube valley in Czechoslovakia, Proc. Fourth Danube Eur. Conf. SMFE, Bled, 35—40.

— (1975), Water and water reservoirs for human needs in Czechoslovakia, Proc. Second Conf. IWRA, New Delhi, 117—124.

— (1976), Changes of seepage and uplift in 15 Czechoslovak dams during the operation period, Proc. Twelfth Int. Congress ICOLD, Mexico, 213—218.

— (1977), Changes in physical properties of soil during wetting and hydrodynamic loading, Proc. Fifth Danube Eur. Conf. SMFE, Bratislava, 257—271.

— (1979), Estimating the changes caused by the hydrodynamic loading of soils in dam foundations, Proc. Thirteenth Int. Congress ICOLD, New Delhi, 291—295.

PETER, P. et al. (1978), The river Váh system. Transfer of water resources information and its contraints, Proc. Second Conf. Water Resources Knowledge, Colorado, 857—862.

PETTERSON, K. E. (1955), The early history of circular sliding, Geotechnique (G.B.) **5**, 275—284.

POLKO, I., HOBST, E. (1978), Stability computations of canal embankment of Danube hydraulic works (in Slovak), Report of Hydroconsult, Bratislava
(Výpočty stability kanálových hrádzí vodného diela na Dunaji, Správa Hydroconsultu, Bratislava).

POLUBARINOVA-KOCHINA, P. YA. (1952), Theory of Groundwater Motion (in Russian), Gos. izd. tekhn.-teor. lit., Moscow
(Полубаринова-Кочина, П. Я. (1952), Теория движения грунтовых вод, Гос. изд. техн.-теор. лит., Москва).

POPOV, K. V. (1950), Hydraulic Structures, Gos. izd. s.-kh. lit., Moscow
(Попов, К. В. (1950), Гидротехнические сооружения, Гос. изд. с.-х. лит., Москва).

POST, P., LONDE, P. (1955), Der Erdstaudammbau — amerikanische Praxis (translated from French), Sager—Wörner, München.

RADČENKO, I. (1976), The influence of waterwork Gabčíkovo on the capacity and quality of water source Rusovce — Ostrovné lúčky (in Slovak), Research report, Institute of Hydrology and Hydraulics, Slovak Academy of Sciences, Bratislava
(Vplyv vodného diela Gabčíkovo na výdatnosť a kvalitu vodného zdroja Rusovce — Vodné lúčky, Výskumná správa, Ústav hydrológie a hydrauliky, Slovenská akadémia vied, Bratislava).

REINIUS, E. (1955), The stability of slopes of earth dams, Geotechnique (G.B.) **5**, 181—189.

RICHARDSON, E. G. (1957), The suspension of solids in turbulent stream, Proc. Roy. Soc. **162**, 583—597.

RICHARDSON, J. F., HENWOOD, G. A., ROWE, P. N. (1961), The drag on a half inch sphere in water, Symposium on Fluidisation, Westwinster, March 7, 1961, Transactions of the Institution of Chem. Engineering **39**.

RICHART, F. E. et al. (1970), Vibrations of Soils and Foundations, Prentice-Hall, New Jersey; Englewood Cliffs, London.

RINGHEIM, A. S. (1964), Experiences with the Bearpaw shales at the South Saskatchewan river dam, Proc. Eighth Int. Congress ICOLD, Edinburgh, 529—550.

RÖMISCH, K. (1969), Berechnungsverfahren zur praktischen Ermittlung der in einem Kanal durch ein fahrendes Schiff herforgerufenen maximalen Wasserspiegelschwankungen, Mitteilungen der Forschungsanstalt für Schiffahrt, Heft 24.

SCHEIDEGGER, A. E. (1960), The Physics of Flow through Porous Media, Univ. Toronto Press, Toronto.

SCHNEEBELI, G. (1966), Hydraulique souterraine, Eyrolles, Paris.

SCHNITTER, G., ZELLER, J. (1961), Geotechnical investigations of mixtures of bitumen clay or bentonite with sandy gravel, Proc. Seventh Int. Congress ICOLD, Rome, 88—94.

SCOTT, R. F. (1963), Principles of Soil Mechanics, Addison—Wesley, Reading.

SCOTT, R. F., SCHOUSTER, J. J. (1968), Soil Mechanics and Engineering, Addison—Wesley, New York.

SEED, H. (1966), A method for the earthquake-resistant design of earth dams, Proc. ASCE, SM 1, 13—41.

— (1973), Stability of Earth and Rockfill Dams during Earthquake, Wiley, London.

SEED, H. et al. (1973), Analysis of the slides in the San Fernando dam during the earthquake of February 9, 1971, Earthquake ERC, Univ. California, Report No. ERC 73/2, June.

SEMBENELLI, P. (1976), Behaviour of synthetic membranes on granular supports, Proc. Twelfth Int. Congress ICOLD, Mexico, 70—79.

SHERARD, J. L. et al. (1963), Earth and Earth Rock Dams, Wiley, New York.
— (1973), Piping in earth dams of dispersive clay, Proc. ASCE, SM 4, 542—568.
SKEMPTON, A. W. (1954), The pore pressure coefficient A and B, Geotechnique (G.B.) **4**, 143—147.
— (1964), Long-term stability of clay slopes, Geotechnique (G.B.) **14**, 77—78.
SMRČEK, F. (1958), Canal Construction of the Váh River (in Czech), State publishers of technical literature, Prague
(Stavba kanálu na Váhu, SNTL, Praha).
SOILTEST (1978), Subsurface Electrical Resistivity, Evaston, Ill.
SOKOLOVSKII, V. V. (1942), Statics of Noncohesive Soils (in Russian), Izd. Akad. Nauk SSSR, Moscow
(СОКОЛОВСКИЙ, В. В. (1942), Статика сыпучей среды, Изд. АН СССР, Москва).
STRIEGLER, W., WERNER, D. (1969), Dammbau in Theorie und Praxis, Verlag für Bauwesen, Berlin.
TAYLOR, D. W. (1948), Fundamentals of Soil Mechanics, Wiley, New York.
TERZAGHI, K. (1943), Theoretical Soil Mechanics, Wiley, New York.
— (1948), The most recent precautions to avoid the formation of piping, General report, Proc. Third Int. Congress ICOLD, Stockholm, 10.10—10.11.
— (1959), Soil mechanics in action, Civil Engineering **29**, Feb., 71—73.
Terzaghi Lectures: Collection of lectures, Published by ASCE, New York 1974.
TERZAGHI, K., PECK, R. B. (1948), Soil Mechanics in Engineering Practice, Wiley, New York.
TREBIN, C. F. (1959), Seepage of liquids and gases in porous media, Gostoptekhizdat, Moscow
(ТРЕБИН, Ц. Ф. (1959), Фильтрация жидкостей и газов в пористых средах, Гостоптехиздат, Москва).
TROLOPPE, D. H. (1957), The systematic arching to the stability analysis of embankments, Proc. Fourth Int. Conf. SMFE, London, 382—386.
TSCHEBOTARIOFF, G. P. (1949), Large scale earth pressure tests, BUREC.
— (1956), Soil Mechanics, Foundations and Earth Structures, McGraw-Hill, New York.
TURNBULL, J. W., MANSUR, C. I. (1954), Relief well system for dams and levées, Proc. ASCE, HY 3, 842—861.
— , — (1961), Design of control measures for dams and levées, Proc. ASCE, HY 4, 1540—1568.
UGINCHUS, A. A. (1953), Canals and its Structures (in Russian), Gos. izd. lit. po stroit. i arkh., Moscow
(УГИНЧУС, А. А. (1953), Каналы и сооружения на них, Гос. изд. лит. по строит. и арх., Москва).
— (1960), Calculation of Seepage through Earth Dams (in Russian), Gosénergoizdat, Moscow
(УГИНЧУС, А. А. (1960), Расчет фильтрации через земляные плотины, Госэнерфоиздат, Москва).
USSR Standard (1975), Technical conditions of water ways calculation on see and river structures and slopes, SN 92—75
(ГОСТ (1975), Технические условия определения волновых воздействий на морские и речные сооружения и берега, СН 92—75).
VAN ASBECK, W. F. (1968), Bitumen im Wasserbau, Verlag Hüthig und Dreyer, Mainz.
VAN DER WEELE, I. P. H. (1968), DELTA Plan, Amsterdam.
VEDERNIKOV, V. V. (1932), Seepage from Canals (in Russian), Gosstroïizdat, Moscow
(ВЕДЕРНИКОВ, В. В. (1932), Фильтрация из каналов, Госстройиздат, Москва).
VERIGIN, N. N. (1962), Methods for determining seepage properties of rocks, Gos. izd. lit. po stroit. i arkh., Moscow
(ВЕРИГИН, Н. Н. (1962), Методы определения фильтрационных свойств горных пород, Гос. изд. лит. по строит. и арх., Москва).
VOLKER, E. (1969), Nonlinear flow in porous media by finite elements, Proc. ASCE, HY 6, 2093—2114.

VOSHCHININ, A. P. (1959), Methodology of seepage calculations in earth dams design (in Russian), Trudy Gidroproekta (Moscow) **2**, 57—77
(Вощинин, А. П. (1959), Методика фильтрационных расчетов при проектировании земляных плотин, Труды Гидропроекта (Москва) **2**, 57—77).

WAGNER, A. A. (1957), The use the unified soil classification system by the Bureau of Reclamation, Proc. Fourth Int. Conf. SMFE, London, 27—36.

WALTERS, R. C. S. (1971), Dam Geology, 2nd edn., Butterworths, London.

WARD, J. C. (1966), Turbulent flow in porous media, Proc. ASCE, HY 4, 412—421.

WILSON, D. (1974), Observational data on movements related to slope instability, Terzaghi Lectures 1963—1972, ASCE, New York, 287—310.

WITTMANN, L. (1978), Phenomena and parameters of two-component soil, Proc. Symp. Scale Effects, IAIHR, Thesaloniki, 1.67—1.80.

World Water — River Management Information (1978), Public confidence eroding as Rhine solution cludes engineers, May, 36—38.

YAKSHCHIN, N. N. (1962), Middle Donets—Donbass canal, Bull. NTI Gidroproekta (Moscow), 14, 3—31.
(Якщин, Н. Н. (1962), Канал Средний Донец—Донбасс, Бюл. НТИ Гидропроекта (Москва), 14, 3—31.

ZAMARIN, É. A. et al. (1952), Design of Hydraulic Structures (in Russian), Izd. Énergiya, Moscow (Замарин, Э. А. и др. (1952), Проектирование гидротехнических сооружений, Изд. Энергия, Москва).

ZIENKIEWICZ, O. C., MAYER, P., CHEUNG, Y. K. (1966), Solution of anisotropic seepage by finite element, Proc. ASCE, EM 1, 186—204.

ZIENKIEWICZ, O. C. et al. (1970), The Finite Elements Method in Structural and Continuum Mechanics, McGraw-Hill, London.

AUTHOR INDEX

SUBJECT INDEX